University of California, San Diego

Department of Structural Engineering

Test Report

Report No. TR-2002/04

Performance of Lifelines Subjected to Lateral Spreading: Japan Blast Test Results

by

Scott A. Ashford

Associate Professor of Geotechnical Engineering

Teerawut Juirnarongrit

Graduate Student Researcher

Department of Structural Engineering

University of California, San Diego

July 2002

ACKNOWLEDGMENTS

TABLE OF CONTENT

LIST OF TABLES

LIST OF FIGURES

xii

1   Introduction

Two full-scale experiments using controlled blasting were conducted in November and December 2001 in the Port of Tokachi on Hokkaido Island, Japan, (Figure 1.1 and Figure 1.2) to study the performance of lifeline facilities subjected to the lateral spreading. This research project was the joint collaboration between the University of California San Diego and several Japanese organizations. This overall research effort was lead by Dr. Takehiro Sugano of the Port and Airport Research Institute (PARI). The primary objective of the test was to assess the performance of quay walls subjected to the lateral spreading using controlled blasting. The diagram of the overall test is presented in Figure 1.3. One quay wall was of traditional design and new seismic design criteria was applied to the other. Each wall supported approximately 7.5 meters of hydraulic fill which was susceptible to liquefaction. The ground surface behind the traditionally designed quay walls was gently sloped. Since the test area was so large, it enabled researchers to include additional experiments in the zone of liquefaction and lateral spreading without interfering with the primary objective of the quay wall test. The University of California, San Diego, together with Waseda University lead by Professor Masanori Hamada, collaborated with other Japanese researchers to install the lifeline specimens in the zone of lateral spreading through the PEER Lifelines Program with support from Caltrans, Pacific Gas & Electric and the California Energy Commission.

In all, UCSD installed 6 test specimens. The pile specimens in the experiment program consisted of a single pile, a 4-pile group, and a 9-pile group. In addition, two natural gas pipelines and one electrical conduit were installed. Two were installed at approximately 1 meter below the ground surface and perpendicular to the direction of flow. The other gas pipeline with 22 m long was installed parallel to the direction of the flow.   The schematic diagram of location of test specimens is presented in Figure 1.3. Apart from the UCSD, many organizations and universities/institutes cooperated in this research are summarized in Table 1.1. The example of some experiments are: a study of group of single piles and geomembrane behaviors subjected to lateral spreading as well

as a study of soil behavior during the lateral spreading by the Waseda University (WU); a study of the influence of improvement depth on the degree of settlement induced by liquefaction by the University of California, Berkeley (UCB); and an uplift experiment on buried structures due to soil liquefaction by Japan Gas Association. However, this report will present only the details of research carried out by the UCSD.

This report summarizes the general test information as well as the UCSD test results. Data from other researchers will be available in reports by others. It is anticipated that subsequent analyses, as well as data by others, will be presented in future reports.

Table 1.1 Participants in the Japan Lateral Spreading Test

Universities /Institutes	Industrial Participants
Port and Airport Research Institute	Japan Reclamation and Dredging Association
Civil Engineering Research Institute	Japan Association for Steel Piles
Waseda University	Japan Association for Marine Structures
University of Tokyo	Japan Gas Association
University of California, Berkeley	Tokyo Electric Power Company
University of California, San Diego	Kanden Kogyo
PEER	Sato Kogyo
	Caltrans
	Pacific Gas & Electric
	California Energy Commission

1.1   *Background*

Lateral spreading, which usually refers to global displacements of gently sloping ground due to liquefaction, is one of the primary earthquake hazards. In past earthquakes, lateral spreading has caused considerable damage to civil infrastructure including port facilities, buildings, bridges, and utilities. Good examples are the damage

of quay walls and buildings in the 1995 Kobe earthquake; damage of pile foundations in the 1964 Niigata earthquake; the damage of over 250 bridges and numerous embankments along the Alaskan Railroad and Highway during the 1964 earthquake; the damages of numerous water and gas lines that contributed to the a large destructive fire in the city in the 1906 earthquake; and the significant damage in the San Francisco area in 1989 Loma Prieta earthquake (Bartlett and Youd 1992b; Seed 1987; Youd and Hoose 1976; Bardet and Kapuskar 1993; Clough et al. 1994; and O' Rourke and Pease 1992). Therefore, it is extremely essential to understand the behavior of soil as well as structures during the lateral spreading in order to improve the current design method for structures and lifeline utilities to prevent the catastrophic failure for the future earthquakes. Meanwhile, most lateral spreading research to date has focused on small-scale centrifuge studies (e.g. Abdoun *et al.*, 1996), limited area 1-g shake table tests (e.g. Tokida et al., 1993), or case histories (e.g. Hamada and O'Rourke, 1992; O'Rourke, 1996). In addition, some full-scale has been carried out to study behavior of deep foundations in sand liquefied by controlled blasting (e.g. Ashford *et al.*, 2000), but these tests do not account for the global translations of the lateral spreading soil mass. In light of this, the full-scale instrumented lifeline components in a controlled lateral spreading test were carried out in order to understand the performance of lifelines and be able to implement the test results in engineering practice. The test results will be an invaluable source of data for further development of the empirical methods and/or complex numeral models to use to design lifeline facilities subjected to lateral spreading.

Specifically, the objectives of this research are to:

1. Conduct damage and performance assessments of a single pile, a 4-pile group, and a 9-pile group subjected to lateral spreading.

2. Conduct damage and performance assessments of the natural gas pipeline as well as electrical conduit subjected to lateral spreading.

3. From instrumentation in the piles and pipelines, evaluate loading conditions on the structures during the lateral spreading.

4.	Utilize developing numeral platforms within PEER (OPENSEES) to analyze the behavior of test results, as well as utilize simpler models and empirical methods derived from past earthquakes.

By accomplishing these objectives we will be able to assess current design procedures and provide recommendations for the cost effective design of lifeline facilities subjected to lateral spreading. Using the detailed information obtained from this unique full-scale experiment, improved performance of pipelines and pile foundations during seismic events can be expected once these recommendations are implemented.

Port of Tokachi, Obihiro, Hakkaido Island , Japan
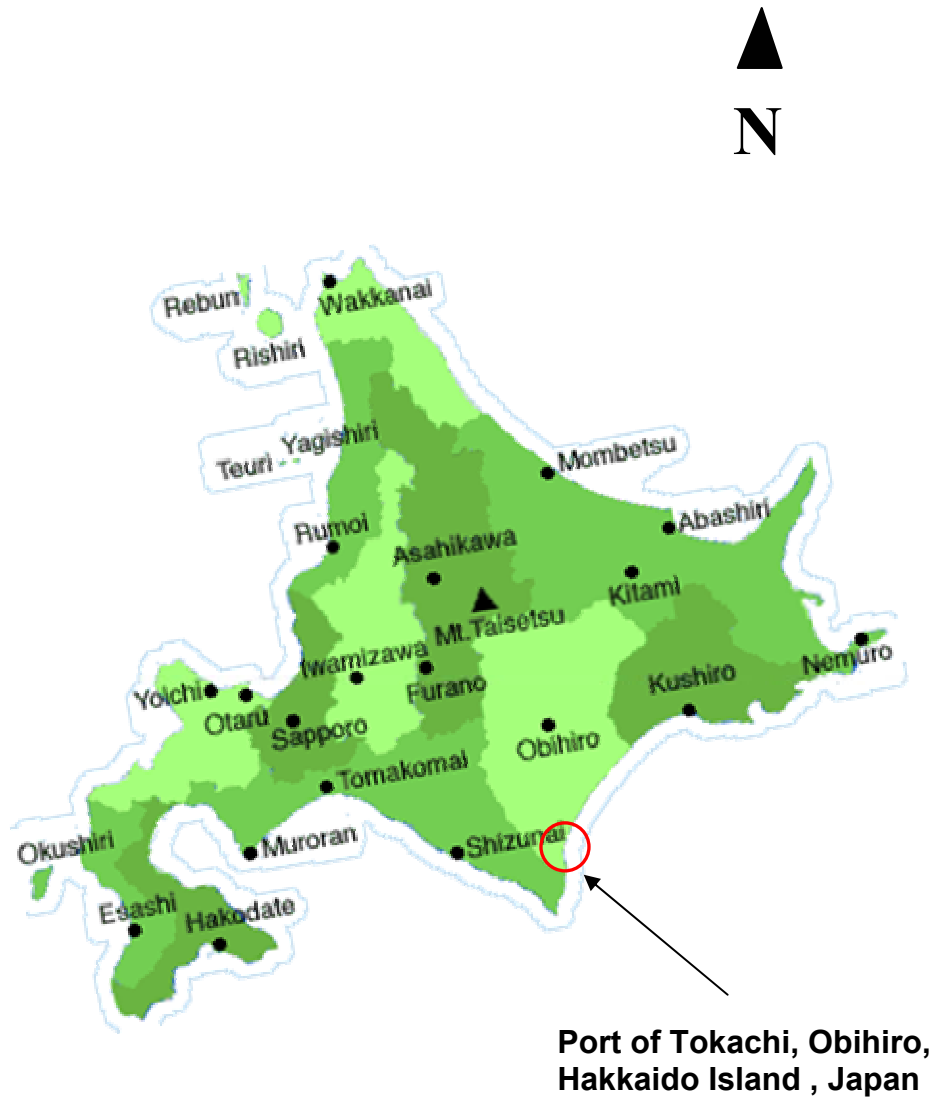
Figure 1.1   Site Location

Figure 1.2   Aerial View of Japan Blast Test Project Site
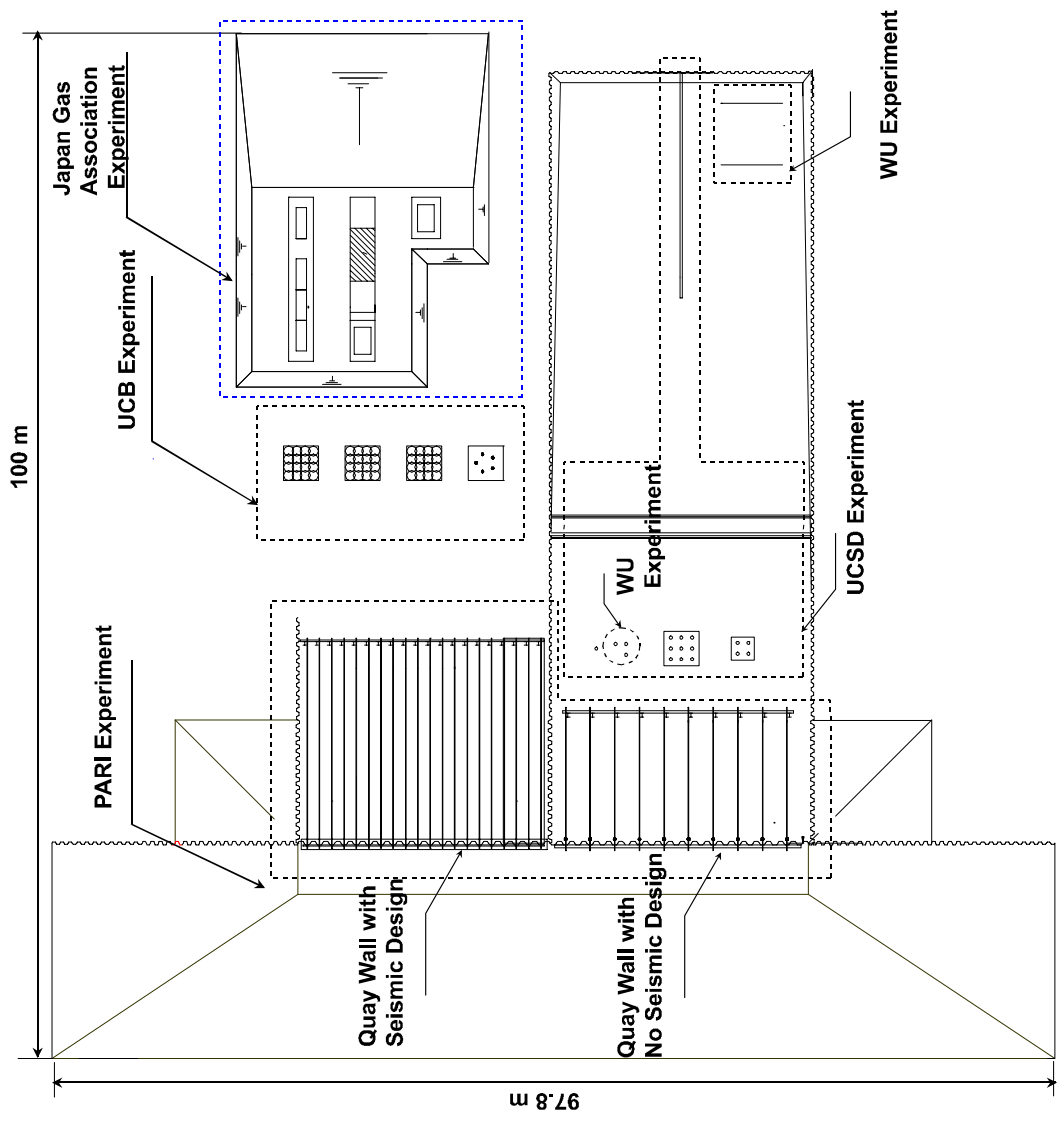
Figure 1.3 Schematic Diagram of Overall Japan Blast Test

2 Site Characterization and Pilot Lateral Spreading Studies

In this chapter, the results from extensive subsurface investigation programs of the test site are presented. These include geotechnical information from several boring logs conducted in the test area, grain size distributions, and index properties. Furthermore, the details regarding the pilot studies of lateral spreading test at the area adjacent to the actual test site are also provided.

2.1 Site Conditions

The site was located at the Port of Tokachi, on Hokaido Island, Japan. The test site for full-scale lateral spreading experiment was approximately 100 m by 100 m area. This location was chosen to be a test site because (1) the soil condition was susceptible to liquefaction and (2) the area of the site was large enough to perform the full-scale lateral spreading test. The test site was a recent man-made land and the construction was completed just a few years ago. The land was built by hydraulically placing fill without any improvement technique; therefore, the soil was very loose and highly susceptible to liquefaction.

Subsurface soil exploration program was carried out in many areas throughout the test site to characterize the soil condition as presented in Figure 2.1. The soil condition consisted of a 7.5 m thick of hydraulic fill underlain by a very dense gravel layer of a natural soil. The hydraulic fill generally consisted of a 4-m of very loose silty sand layer with uncorrected SPT-N values ranging from 1 to 5. This was underlain by a 3.5-m layer of very soft lean to fat clay with sand. Uncorrected SPT blow counts ranged from 0 to 2 blows per foot in this layer. Soil boring logs at various locations are given in Figure 2.2 through Figure 2.8. Soil properties for each borehole are summarized in Table 2.1 through Table 2.7. Soil profiles across sections A-A, and B-B are presented in Figure 2.9 and Figure 2.10, respectively. The water table varies from 0.5 m to 1 m below the ground surface. Figure 2.11 through Figure 2.14 presented the grain size distribution of the hydraulic fill of individual boreholes plotted together with the Japanese standard

8

curves for liquefaction potential evaluation. It is clearly seen that most soil of this test site fell into the zone of highly susceptible to liquefaction, therefore this test site was appropriate for conducting the full-scale lateral spreading test. Uncorrected SPT-N values profiles are presented in Figure 2.15. In addition, shear wave and P-wave velocity profiles are given in Figure 2.16. Cone penetration tests were also conducted in several locations, but the data are not available at this time. They will be incorporated in the final report.

2.2 Pilot Studies

Prior to perform the full-scale lateral spreading test, two pilot studies were carried out to verify the site configuration as well as the amount and locations of charges to be used. This was to ensure that the soil can be successfully liquefied and the amount of global translation of the soil satisfies the requirement. The locations of each pilot test are presented in Figure 2.17.

The first pilot test was carried out in August 2001 about 50 m behind the actual test site as presented in Figure 2.17. According to a discussion with Japanese researchers, the results of the first pilot test did not achieve the goal because the maximum horizontal movement was only 20 cm. One of the explanations was that the layout of the pilot test site was somewhat different from that of actual test because there was no excavation for a waterway in front of the test embankment. Therefore, the movement of the soil was impeded by the soil in front of it. With the actual site configuration, the horizontal movement was expected to be much greater than the results obtained from the first pilot test.

The second pilot study was carried out on September 14, 2002 with the modification of the site configuration to be as close as possible to the actual site configuration. The configuration of the second pilot test was scaled to 1/3 of the actual site configuration. Layout of the second pilot test is presented in Figure 2.18. Overviews of the pilot test site are shown in Figure 2.19 and Figure 2.20. Blast holes were spaced at 6.0 m on centers in the regular grid pattern as denoted by M1 to M10. Explosives were

installed in each borehole at depths of 3m and 6m below the ground surface. The amount of charge was 3 kg for each depth. Several pore pressure transducers were installed in various locations as denoted by PWP1 to PWP6 to measure an increase in pore water pressure after the blasting. K1 to K17 were the survey points. The explosive at the back corner of the embankment (M10) was detonated initially and preceded one after the other towards the water the way (M1).

Figure 2.21 and Figure 2.22 show the excess pore pressures at multiple depths measured during the test together with effective vertical stress. Table 2.8 summarizes the excess pore water pressure ratios from each transducer. The excess pore pressure ratios were generally over 50%. Two of them were close to 100%. Sand boils were observed in several places which confirmed that the soil was successfully liquefied. Figure 2.23 shows the vector displacements and contour of settlement after the completion of the test. The results indicate that the maximum soil movement was about 50 cm, and the sheet pile moved more than 70 cm. Figure 2.24 through Figure 2.27 present the site condition after the blast, as well as the evidence of liquefaction. The magnitude of these movements, as well as qualitative evidence of liquefaction satisfied the researcher's goal and it was expected to induce more movement from the actual full-scale lateral spreading test. The success of the second pilot test led the research team to advance to the full-scale lateral spreading experiment.

Table 2.1　Summary of Soil Properties for Borehole A-4

BH	Sample No.	Depth (m) From	Depth (m) To	SPT N-Values	wn (%)	Gs	Soil Composition (%) Gravel	Sand	Silt	Clay	Cu	Cc	LL	PL	PI	USCS	Soil Description
A-4	P1	0.00	0.20	-	9.3	2.67	16.5	76.7	6.8	0.0	3.8	0.6	NP	NP	NP	SP-SM	Poorly graded SAND w/ silt and gravel
	P2-1	1.00	1.40	1	33.6	2.74	0.0	64.8	26.2	9.0	37.9	5.6	NP	NP	NP	SM	Silty SAND
	P2-2	1.00	1.40	-	63.4	2.74	0.0	21.0	66.8	12.2	-	-	45.0	22.7	22.3	CL	Lean CLAY w/ sand
	P3	2.00	2.35	3	21.5	2.72	0.0	85.6	12.3	2.1	4.0	2.2	NP	NP	NP	SM	Silty SAND
	P4	3.00	3.30	3	45.6	2.68	0.0	45.9	44.1	10.0	47.6	2.4	45.1	21.2	23.9	CL	Sandy CLAY
	P5	4.00	4.40	2	40.3	2.66	0.0	57.9	29.6	12.5	111.3	1.6	38.9	19.2	19.7	SC	Clayey SAND
	P6-1	5.00	5.35	2	54.2	2.73	0.0	8.7	64.3	27.0	-	-	48.7	22.7	26.0	CL	Lean CLAY
	P6-2	5.00	5.35	-	62.8	2.71	0.0	1.6	50.9	47.5	-	-	60.2	27.9	32.3	CH	Fat CLAY
	P7-1	6.00	6.30	28	53.4	2.69	0.0	14.2	65.8	20.0	-	-	51.4	22.0	29.4	CH	Fat CLAY
	P7-2	6.00	6.30	-	27.1	2.69	0.0	83.4	12.8	3.8	7.8	4.2	NP	NP	NP	SM	Silty SAND

Table 2.2　Summary of Soil Properties for Borehole A-5

BH	Sample No.	Depth (m) From	Depth (m) To	SPT N-Values	wn (%)	Gs	Soil Composition (%) Gravel	Sand	Silt	Clay	Cu	Cc	LL	PL	PI	USCS	Soil Description
A-5	P1	0.00	0.20	-	16.9	2.67	40.9	57.5	1.6	0.0	42.1	0.1	NP	NP	NP	SW	Well-graded SAND w/ gravel
	P2	1.00	1.30	4	12.9	2.66	16.0	72.1	7.9	4.0	5.3	1.3	NP	NP	NP	SW-SM	Well-graded SAND w/ silt and gravel
	P3	2.00	2.40	1	23.3	2.69	3.7	86.8	6.7	2.8	2.1	1.2	NP	NP	NP	SW-SM	Well-graded SAND w/ silt
	P4	3.00	3.46	1	29.9	2.70	24.0	56.9	12.6	6.5	29.3	10.6	NP	NP	NP	SM	Silty SAND w/ gravel
	P5	4.00	4.45	0	70.6	2.65	0.0	12.3	70.7	17.0	-	-	52.0	24.9	27.1	CH	Fat CLAY
	P6	5.00	5.45	0	71.9	2.78	0.0	18.9	67.1	14.0	-	-	54.3	25.2	29.2	CH	Fat CLAY w/ sand
	P7	6.00	6.45	0	80.8	2.67	0.0	7.0	73.5	19.5	-	-	65.1	27.7	37.4	CH	Fat CLAY
	P8	7.00	7.35	1	61.5	2.66	0.0	8.6	69.4	22.0	-	-	47.8	22.6	25.2	CL	Lean CLAY
	P9	8.00	8.30	10	23.2	2.73	0.0	87.6	8.4	4.0	4.9	2.9	NP	NP	NP	SM	Silty SAND
	P10	9.00	9.30	41	24.4	2.73	16.5	67.8	10.9	4.8	30.2	7.1	NP	NP	NP	SM	Silty SAND w/ gravel
	P11	10.00	10.30	33	22.9	2.66	0.0	80.7	13.3	6.0	14.6	6.8	NP	NP	NP	SM	Silty SAND
	P12	11.00	11.30	44	19.2	2.74	3.3	77.6	12.1	7.0	37.3	12.1	NP	NP	NP	SM	Silty SAND

Note: wn = Natural Water Content, Gs = Specific Gravity, Cu = Coefficient of Uniformity, Cc = Coefficient of Gradation, LL = Liquid Limit, PL = Plastic Limit, PI = Plastic Index, USCS = Unified Soil Classification System

11

Table 2.3 Summary of Soil Properties for Borehole B-1

BH	Sample No.	Depth (m) From	To	SPT N-Values	wn (%)	Gs	Gravel	Sand	Silt	Clay	Cu	Cc	LL	PL	PI	USCS	Soil Description
B-1	P1	0.00	0.20	-	30.6	2.70	8.4	73.0	10.6	8.0	43.2	18.3	NP	NP	NP	SM	Silty SAND
	P2	1.00	1.30	5	15.1	2.74	9.8	79.4	8.3	2.5	3.8	1.1	NP	NP	NP	SW-SM	Well-graded SAND w/ silt
	P3	2.00	2.30	3	26.8	2.73	1.2	81.8	12.5	4.5	9.5	4.6	NP	NP	NP	SM	Silty SAND
	P4	3.00	3.35	2	25.7	2.77	6.9	74.4	14.1	4.6	12.7	6.1	NP	NP	NP	SM	Silty SAND
	P5	4.00	4.40	1	56.0	2.66	0.0	29.0	57.9	13.1	-	-	46.6	24.6	22.0	CL	Lean CLAY w/ sand
	P6	5.00	5.45	1	71.3	2.68	0.0	21.8	65.0	13.2	-	-	57.5	23.9	33.6	CH	Fat CLAY w/ sand
	P7	6.00	6.45	1	65.4	2.68	3.9	21.9	64.0	10.2	34.9	4.1	57.5	23.3	34.3	CH	Fat CLAY w/ sand
	P8	7.00	7.30	12	29.6	2.70	3.7	74.0	15.3	7.0	24.7	11.1	NP	NP	NP	SM	Silty SAND

Table 2.4 Summary of Soil Properties for Borehole B-3

BH	Sample No.	Depth (m) From	To	SPT N-Values	wn (%)	Gs	Gravel	Sand	Silt	Clay	Cu	Cc	LL	PL	PI	USCS	Soil Description
B-3	P1	0.00	0.20	-	18.0	2.73	2.9	81.7	11.4	4.0	12.4	5.8	NP	NP	NP	SM	Silty SAND
	P2	1.00	1.30	5	25.5	2.70	4.1	77.9	13.0	5.0	10.2	4.9	NP	NP	NP	SM	Silty SAND
	P3	2.00	2.30	2	28.4	2.75	2.4	78.3	15.8	3.5	7.4	3.4	NP	NP	NP	SM	Silty SAND
	P4	3.00	3.45	1	28.6	2.71	0.0	77.2	18.8	4.0	13.0	6.3	NP	NP	NP	SM	Silty SAND
	P5	4.00	4.45	0	31.2	2.71	0.0	77.2	16.8	6.0	21.9	10.1	NP	NP	NP	SM	Silty SAND
	P6	5.00	5.45	1	49.8	2.71	0.0	44.8	38.2	17.0	-	-	39.6	19.4	20.1	CL	Sandy lean CLAY
	P7	6.00	6.30	2	76.5	2.70	0.0	3.6	78.4	18.0	-	-	66.5	29.9	36.6	CH	Fat CLAY
	P8	7.00	7.30	1	64.7	2.70	0.0	4.6	54.4	41.0	-	-	60.9	27.3	33.6	CH	Fat CLAY
	P9	8.00	8.30	21	25.4	2.72	0.0	82.4	13.4	4.2	9.2	4.7	NP	NP	NP	SM	Silty SAND

Note: wn = Natural Water Content, Gs = Specific Gravity, Cu = Coefficient of Uniformity, Cc = Coefficient of Gradation, LL = Liquid Limit, PL = Plastic Limit, PI = Plastic Index, USCS = Unified Soil Classification System

Table 2.5   Summary of Soil Properties for Borehole B-4

BH	Sample No.	Depth (m) From	To	SPT N-Values	w_n (%)	G_s	Soil Composition (%) Gravel	Sand	Silt	Clay	C_u	C_c	LL	PL	PI	USCS	Soil Description
B-4	P1	0.00	0.20	-	20.0	2.69	8.0	74.1	13.9	4.0	13.4	5.5	NP	NP	NP	SM	Silty SAND
	P2	1.00	1.35	2	10.1	2.67	32.9	55.6	7.5	4.0	77.4	0.3	NP	NP	NP	SW-SM	Well-graded SAND w/ silt and gravel
	P3	2.00	2.30	2	49.7	2.70	0.0	46.7	45.3	8.0	29.5	1.5	NP	NP	NP	ML	Sandy SILT
	P4	3.00	3.45	1	43.3	2.70	17.6	51.9	20.0	10.5	109.3	16.7	NP	NP	NP	SM	Silty SAND w/ gravel
	P5	4.00	4.45	0	31.8	2.70	0.0	79.6	14.4	6.0	21.9	10.4	NP	NP	NP	SM	Silty SAND
	P6	5.00	5.30	1	53.8	2.69	0.0	41.8	40.2	18.0	-	-	46.7	22.1	24.6	CL	Sandy lean CLAY
	P7	6.00	6.30	1	54.9	2.70	0.0	31.9	52.1	16.0	-	-	46.0	21.5	24.5	CL	Sandy lean CLAY
	P8-1	7.00	7.20	1	69.0	2.72	0.0	1.2	50.8	48.0	-	-	66.0	30.0	36.1	CH	Fat CLAY
	P8-2	7.20	7.45	-	32.8	2.74	0.0	77.1	16.9	6.0	12.7	6.3	NP	NP	NP	SM	Silty SAND
	P9	11.00	11.30	44	21.3	2.72	0.0	76.6	16.9	6.5	16.7	8.1	NP	NP	NP	SM	Silty SAND

Table 2.6   Summary of Soil Properties for Borehole C-1

BH	Sample No.	Depth (m) From	To	SPT N-Values	w_n (%)	G_s	Soil Composition (%) Gravel	Sand	Silt	Clay	C_u	C_c	LL	PL	PI	USCS	Soil Description
C-1	P1	0.00	0.20	-	20.9	2.68	10.7	79.9	6.9	2.5	2.2	1.1	NP	NP	NP	SW-SM	Well-graded SAND w/ silt
	P2	1.00	1.30	8	20.9	2.68	16.0	71.5	8.5	4.0	6.6	2.2	NP	NP	NP	SM	Silty SAND w/ gravel
	P3	2.00	2.30	0	75.8	2.75	0.0	24.5	56.5	19.0	-	-	61.2	27.8	33.4	CH	Fat CLAY w/ sand
	P4	3.00	3.45	0	84.4	2.68	0.0	4.4	67.6	28.0	-	-	78.8	28.8	50.0	CH	Fat CLAY
	P5	4.00	4.45	0	78.5	2.67	0.0	7.6	62.4	30.0	-	-	66.3	26.5	39.9	CH	Fat CLAY
	P6	5.00	5.45	1	82.7	2.67	0.0	6.4	65.6	28.0	-	-	71.7	30.1	41.6	CH	Fat CLAY
	P7	6.00	6.45	0	83.9	2.72	0.0	11.9	58.1	30.0	-	-	68.2	26.2	42.0	CH	Fat CLAY
	P8	7.00	7.10	13	44.7	2.67	0.0	76.5	17.7	5.8	22.5	8.3	NP	NP	NP	SM	Silty SAND

Note: w_n = Natural Water Content, G_s = Specific Gravity, C_u = Coefficient of Uniformity, C_c = Coefficient of Gradation, LL = Liquid Limit, PL = Plastic Limit, PI = Plastic Index, USCS = Unified Soil Classification System

Table 2.7 Summary of Soil Properties for Borehole B-4

BH	Sample No.	Depth (m) From	To	SPT N-Values	w_n (%)	G_s	Gravel	Sand	Silt	Clay	C_u	C_c	LL	PL	PI	USCS	Soil Description
D-1	P1	0.00	0.20	-	14.8	2.72	31.6	61.7	4.7	2.0	23.7	0.1	NP	NP	NP	SW-SM	Well-graded SAND w/ silt and gravel
	P2	1.00	1.30	3	15.3	2.69	9.3	78.7	7.5	4.5	19.6	0.7	NP	NP	NP	SM	Silty SAND
	P3-1	2.00	2.35	1	20.0	2.65	12.6	74.4	10.0	3.0	32.7	0.9	NP	NP	NP	SM	Silty SAND
	P3-2	2.00	2.35	-	69.9	2.64	0.0	8.4	75.6	16.0	-	-	NP	NP	NP	ML	SILT
	P4	3.00	3.45	1	27.9	2.68	0.0	76.1	16.9	7.0	41.0	18.7	NP	NP	NP	SM	Silty SAND
	P5	4.00	4.40	2	31.1	2.76	0.0	79.5	15.5	5.0	18.1	8.6	NP	NP	NP	SM	Silty SAND
	P6	5.00	5.40	2	24.2	2.68	19.6	64.4	11.0	5.0	16.9	6.8	NP	NP	NP	SM	Silty SAND w/ gravel
	P7	6.00	6.30	2	30.4	2.68	2.7	66.5	17.8	13.0	-	-	29.7	20.0	9.7	SC	Clayey SAND
	P8	7.00	7.10	34	37.1	2.65	0.0	57.3	36.7	6.0	25.2	4.8	NP	NP	NP	SM	Silty SAND

Note: w_n = Natural Water Content, G_s = Specific Gravity, C_u = Coefficient of Uniformity, C_c = Coefficient of Gradation, LL = Liquid Limit, PL = Plastic Limit, PI = Plastic Index, USCS = Unified Soil Classification System

Table 2.8 Summary of Excess Pore Water Pressure Ratio, 2nd Pilot Test (Data from Sato Kogyo)

PPT No.	Depth (m)	Water Depth (m)	Effective Stress (kPa)	Excess Pore Pressure (kPa)	Ru (%)
PWT1	3.0	0.50	28.4	32.6	114.8
PWT2	5.5	0.50	48.0	45.0	93.8
PWT3	3.0	0.98	33.1	4.5	13.6
PWT4	6.0	0.98	56.6	38.0	67.1
PWT5	3.0	1.50	38.2	16.0	41.9
PWT6	6.0	1.50	61.7	34.5	55.9

Figure 2.1   Locations of Soil Borings (Data from PARI)

Soil Boring Log

Project Number	
Logger -	

Boring Number A-4
Sheet 1 **of** 1

UC San Diego

Project	Performance of Lifelines subjected to Lateral Spreading	**Ground Elevation**	+1.890 m
Location	Hiroo, Port of Tokachi, Japan	**Water Level Elevation**	+1.490 m
Drilling Method and Equipment	Rotary Wash Drilling, TDC-1	**Starting Date**	9/20/2001
Drilling Contractor	Tokyo Soil Research Co., Ltd.	**Finishing Date**	9/20/2001

Figure 2.2   Soil Boring Log for Borehole A-4 (Data from PARI)

Soil Boring Log

UC San Diego

Project Number	
Logger -	

Boring Number A-5
Sheet 1 **of** 1

Project	Performance of Lifelines subjected to Lateral Spreading	**Ground Elevation**	+3.020 m
Location	Hiroo, Port of Tokachi, Japan	**Water Level Elevation**	+2.620 m
Drilling Method and Equipment	Rotary Wash Drilling, TDC-1	**Starting Date**	8/24/2001
Drilling Contractor	Tokyo Soil Research Co., Ltd.	**Finishing Date**	8/25/2001

Sample Descritption

Soil Description

Gravel
Sand
Silt
Clay
Claystone

SPT N-Values
0 10 20 30 40 50 60

Comments

Depth (m) | Elevation (m) | Depth below Ground Surface (m) | Interval | Sample Number | Graphic

Very Loose, Dark Brown, Well-Graded SAND with Silt and Gravel to Silty SAND with Gravel (SW-SM, SM)

Very Soft, Dark Gray, Fat CLAY with Sand (CH)

Medium Dense, Dark Gray, Silty SAND (SM)

Dense, Dark Gray, Silty SAND (SM)

Hard, Dark Gray, CLAY
Dense to Very Dense, Dark Gray, GRAVEL with Sand

Dark Brown, Weathered Claystone

Sample intervals: P1 1.00, P2 1.30 2.00, P3 2.40 3.00, P4 3.45 4.00, P5 4.45 5.00, P6 5.45 6.00, P7 6.45 7.00, P8 7.35 8.00, P9 8.30 9.00, P10 9.30 10.00, P11 10.30 11.00, P12 11.30

Elevations: -0.58 / 3.60, -4.70 / 7.40, -5.90 / 8.60, -8.68 / 11.70, -8.98 / 12.00, -10.78 / 13.80, -12.16 / 15.18

SPT N-Values: 4, 0.8, 0.7, 0, 0, 0, 0.9, 10, 41, 33, 44, 41, 50/8, 50/19, 50/18

Figure 2.3   Soil Boring Log for Borehole A-5 (Data from PARI)

18

Soil Boring Log

UC San Diego	

Project Number	_____	**Boring Number**	**B-1**
Logger	-	**Sheet** 1 **of** 1	

Project	Performance of Lifelines subjected to Lateral Spreading	**Ground Elevation**	+2.710 m
Location	Hiroo, Port of Tokachi, Japan	**Water Level Elevation**	+2.410 m
Drilling Method and Equipment	Rotary Wash Drilling, TDC-1	**Starting Date**	9/20/2001
Drilling Contractor	Tokyo Soil Research Co., Ltd.	**Finishing Date**	9/20/2001

Sample Descritption

Soil Description

Gravel
Sand
Silt
Clay

Claystone

SPT N-Values

0 10 20 30 40 50 60

Comments

Depth (m)	Elevation (m)	Depth below Ground Surface (m)	Interval	Sample Number	Graphic
				P1	
1			1.00		
			1.30	P2	
2			2.00		
			2.30	P3	
3			3.00		
	-0.79	3.50	3.35	P4	
4			4.00		
			4.40	P5	
5			5.00		
			5.45	P6	
6			6.00		
			6.45	P7	
7	-4.29	7.00	7.00		
	-4.59	7.30	7.30	P8	
8					

Soil Descriptions:
- Very Loose, Dark Brown, Silty SAND (SM)
- Very Soft, Dark Gray, Lean to Fat CLAY with Sand (CL, CH)
- Medium Dense, Dark Gray, Silty SAND (SM)

SPT N-Values: 5, 3, 1.7, 0.8, 0.7, 0.7, 12

Figure 2.4   Soil Boring Log for Borehole B-1 (Data from PARI)

19

Figure 2.5   Soil Boring Log for Borehole B-3 (Data from PARI)

Soil Boring Log

Project Number		Boring Number	B-4
Logger	-	Sheet 1 of 1	

Project	Performance of Lifelines subjected to Lateral Spreading	Ground Elevation	+3.110 m
Location	Hiroo, Port of Tokachi, Japan	Water Level Elevation	+2.310 m
Drilling Method and Equipment	Rotary Wash Drilling, TDC-1	Starting Date	8/26/2001
Drilling Contractor	Tokyo Soil Research Co., Ltd.	Finishing Date	8/28/2001

Legend: Gravel, Sand, Silt, Clay, Claystone

SPT N-Values (0 10 20 30 40 50 60)

Depth (m)	Elevation (m)	Depth below Ground Surface (m)	Interval	Sample Number	Soil Description	SPT N-Value
				P1	Very Loose, Dark Brown, Silty Sand with Gravel (SM)	1.7
1			1.00	P2		
	+1.51	1.60	1.35			2
2			2.00	P3	Very Loose, Dark Gray, Silty Sand (SM)	
			2.30			
3			3.00	P4		0.7
			3.45			
4			4.00	P5		0
	-1.34	4.45	4.45		Very Soft, Dark Gray, Lean to Fat CLAY (CL, CH)	
5			5.00	P6		1
			5.30			
6			6.00	P7		1
			6.30			
7			7.00	P8-1		0.7
	-4.09	7.20		P8-2	Very Loose, Dark Gray, Silty SAND (SM)	
	-4.59	7.70	7.45		Very Dense, Dark Gray, GRAVEL	50/6
8						
9						50/2
10						50/3
	-7.29	10.40				
11			11.00	P9	Dense, Dark Gray, Silty SAND	44
	-8.59	11.70	11.30			
12					Dark Brown, Weathered Claystone	50/29
13						50/20
14						50/19
15	-12.05	15.16				50/16
16						

Comments

Figure 2.6   Soil Boring Log for Borehole B-4 (Data from PARI)

Soil Boring Log

Project Number _____ **Boring Number** C-1

Logger - _____ **Sheet** 1 **of** 1

UC San Diego

Project	Performance of Lifelines subjected to Lateral Spreading	
Location	Hiroo, Port of Tokachi, Japan	
Drilling Method and Equipment	Rotary Wash Drilling, TDC-1	
Drilling Contractor	Tokyo Soil Research Co., Ltd.	

Ground Elevation	+3.010 m
Water Level Elevation	+2.710 m
Starting Date	8/31/2001
Finishing Date	8/31/2001

Depth (m) | Elevation (m) | Depth below Ground Surface (m)

Sample Description: Interval | Sample Number | Graphic

Soil Description

Gravel   Claystone
Sand
Silt
Clay

SPT N-Values   0 10 20 30 40 50 60   Comments

Sample	Interval	Soil Description	SPT N
P1		Loose, Dark Brown, Silty SAND with gravel (SM)	
	1.00		
P2	1.30		8
	2.00	Very Soft, Dark Gray, Fat CLAY (CH)	
P3	2.30		
	3.00		
P4	3.45		0
	4.00		
P5	4.45		0
	5.00		
P6	5.45		0.7
	6.00		
P7	6.45		0
	7.00	Medium Dense, Dark Gray, Silty SAND (SM)	
P8	7.30		13

Elevation markers: +1.01 at 2.00; -3.79 at 6.80; -4.29 at 7.30

Figure 2.7   Soil Boring Log for Borehole C-1 (Data from PARI)

Soil Boring Log

Project Number		Boring Number	D-1
Logger	-	Sheet	1 of 1

Project	Performance of Lifelines subjected to Lateral Spreading	Ground Elevation	+3.09 m
Location	Hiroo, Port of Tokachi, Japan	Water Level Elevation	+2.710 m
Drilling Method and Equipment	Rotary Wash Drilling, TDC-1	Starting Date	8/31/2001
Drilling Contractor	Tokyo Soil Research Co., Ltd.	Finishing Date	8/31/2001

Soil Description legend: Gravel, Sand, Silt, Clay, Claystone

SPT N-Values: 0 10 20 30 40 50 60

Depth (m)	Elevation (m)	Depth below Ground Surface (m)	Interval	Sample Number	Soil Description	SPT N-Value
				P1	Very Loose, Dark Brown, Silty SAND with gravel (SM)	
1			1.00	P2		3
2	+0.99	2.10	1.30 / 2.00	P3-1		
	+0.49	2.60	2.30	P3-2	Very Soft, Dark Gray, SILT (ML)	0.9
3			3.00	P4	Very Loose, Dark Gray, Silty SAND (SM)	0.7
4			3.45 / 4.00			
5			4.45 / 5.00	P5		1.5
				P6		1.5
6			5.45 / 6.00			
7	-3.71	6.80	6.45	P7		2
	-4.21	7.30	7.00	P8	Dense, Dark Gray, Silty SAND (SM)	34
8			7.30			
9						

Figure 2.8   Soil Boring Log for Borehole D-1 (Data from PARI)

Figure 2.9   Soil Profile along A-A Line

Figure 2.10 Soil Profile along B-B Line

25
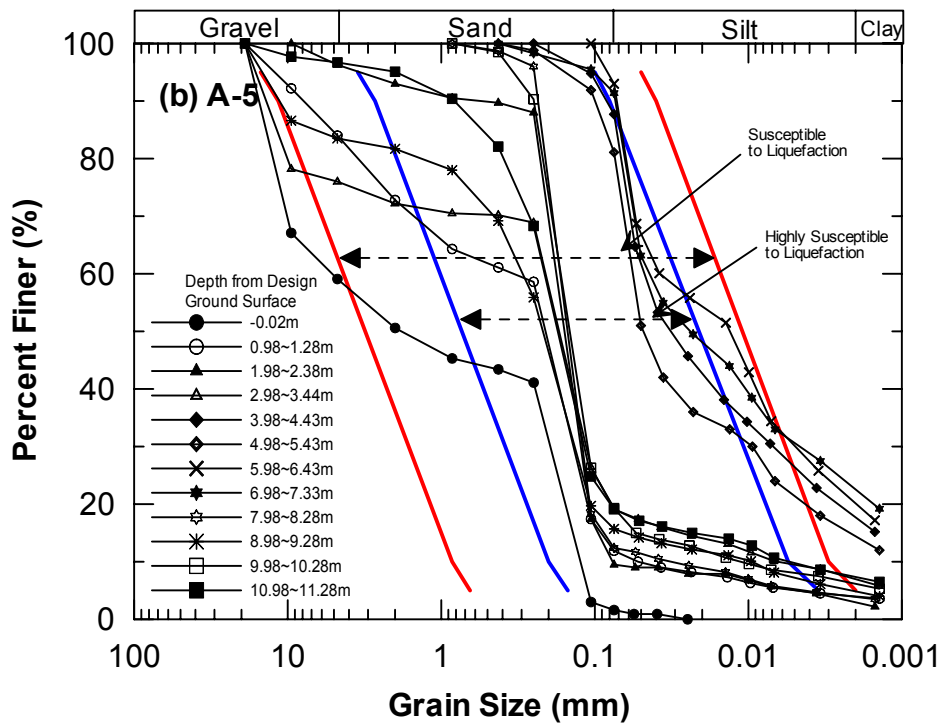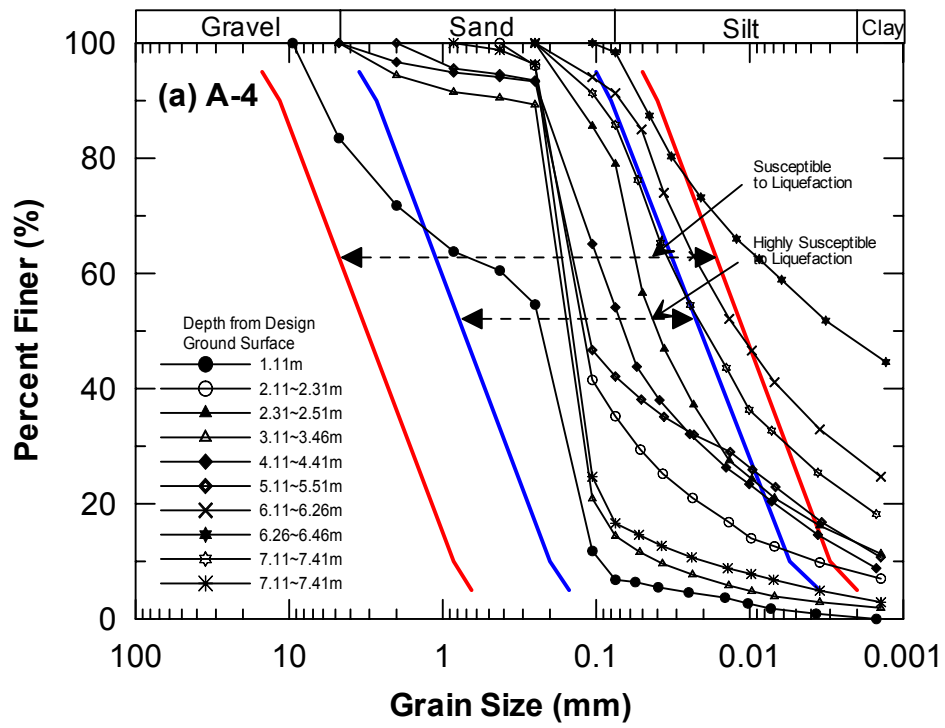
Figure 2.11 Grain Size Distribution for Boreholes (a) A-4 and (b) A-5 (Data from PARI)
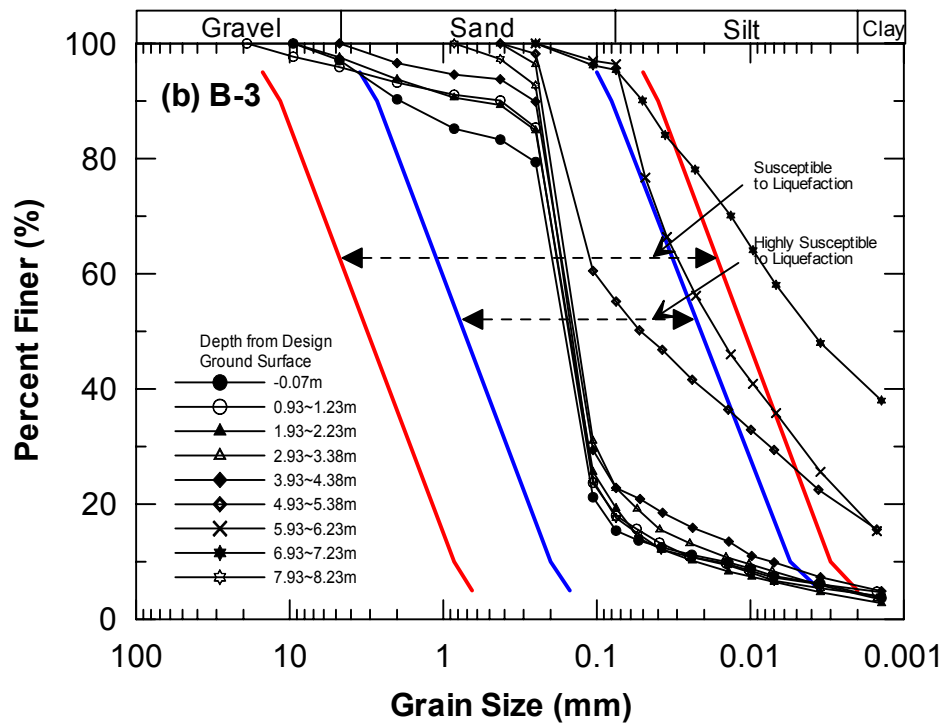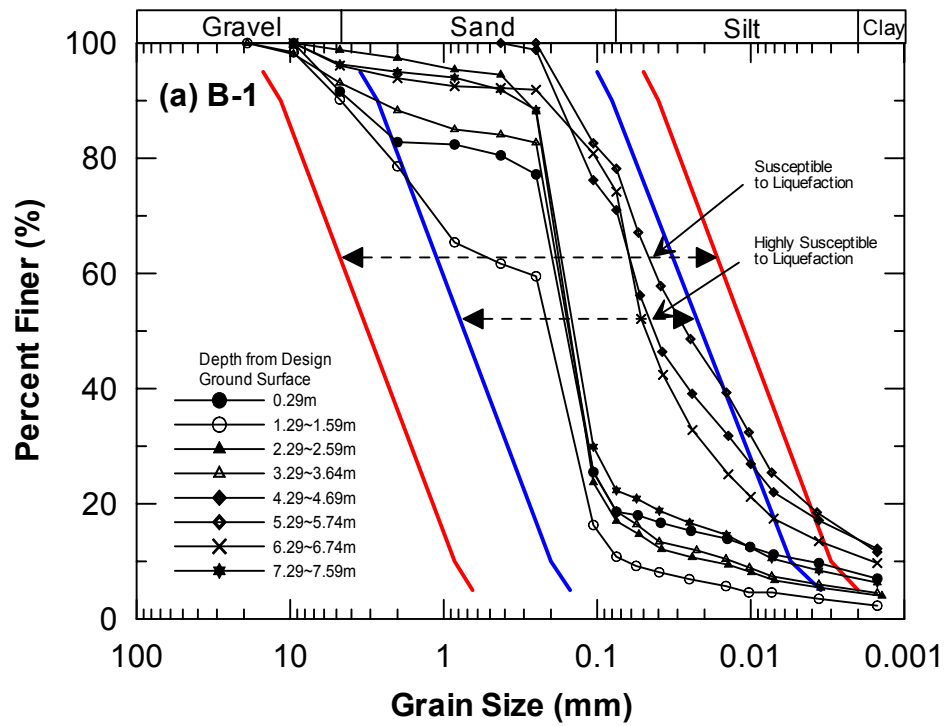
Figure 2.12   Grain Size Distribution for Boreholes (a) B-1 and (b) B-3 (Data from PARI)
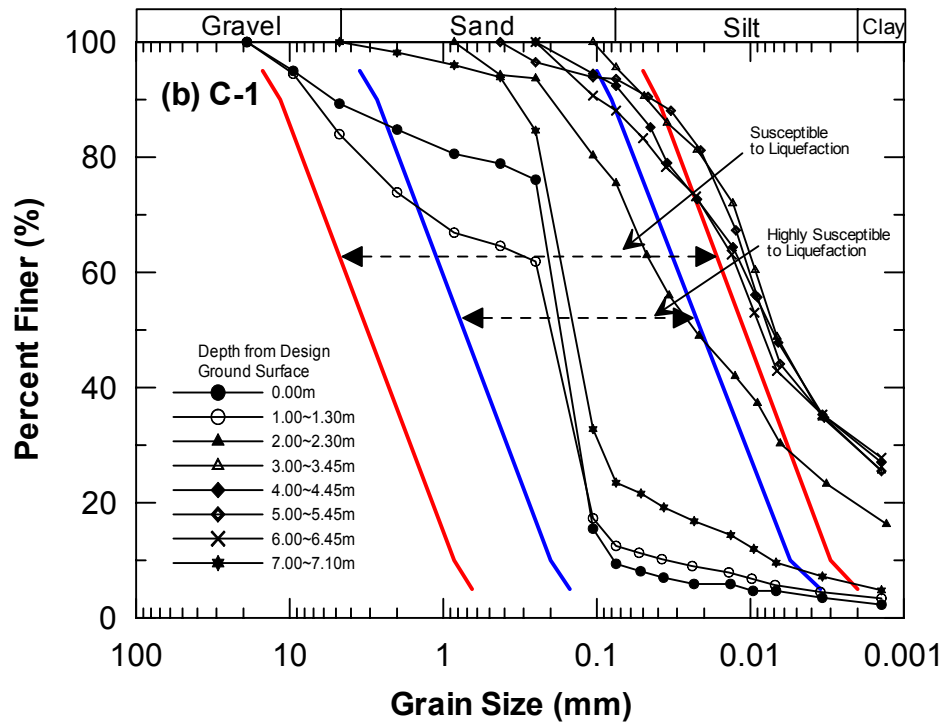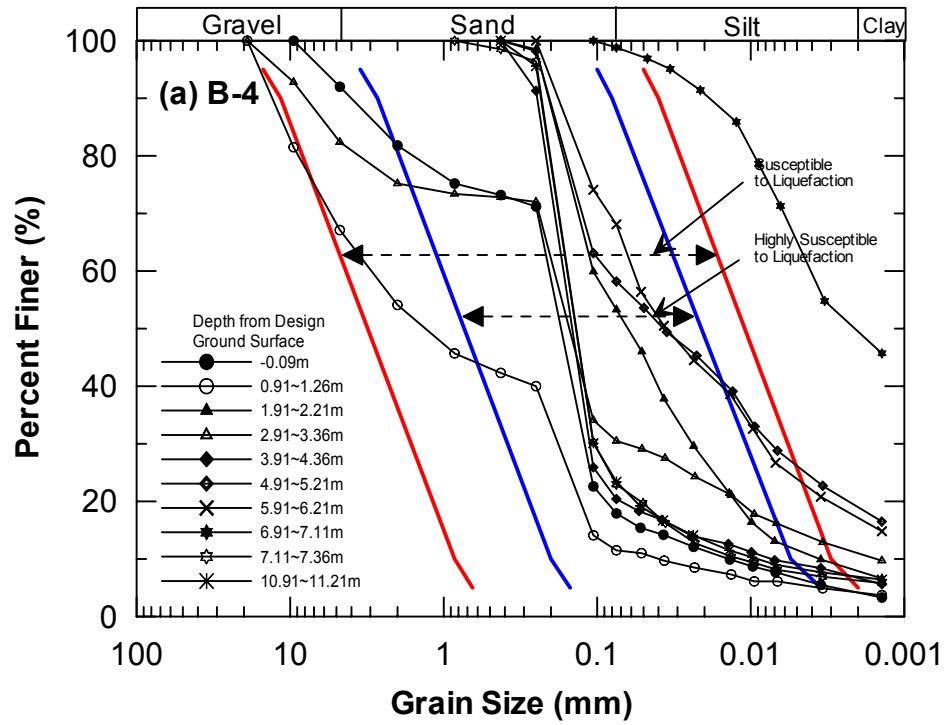
Figure 2.13   Grain Size Distribution for Boreholes (a) B-4 and (b) C-1 (Data from PARI)
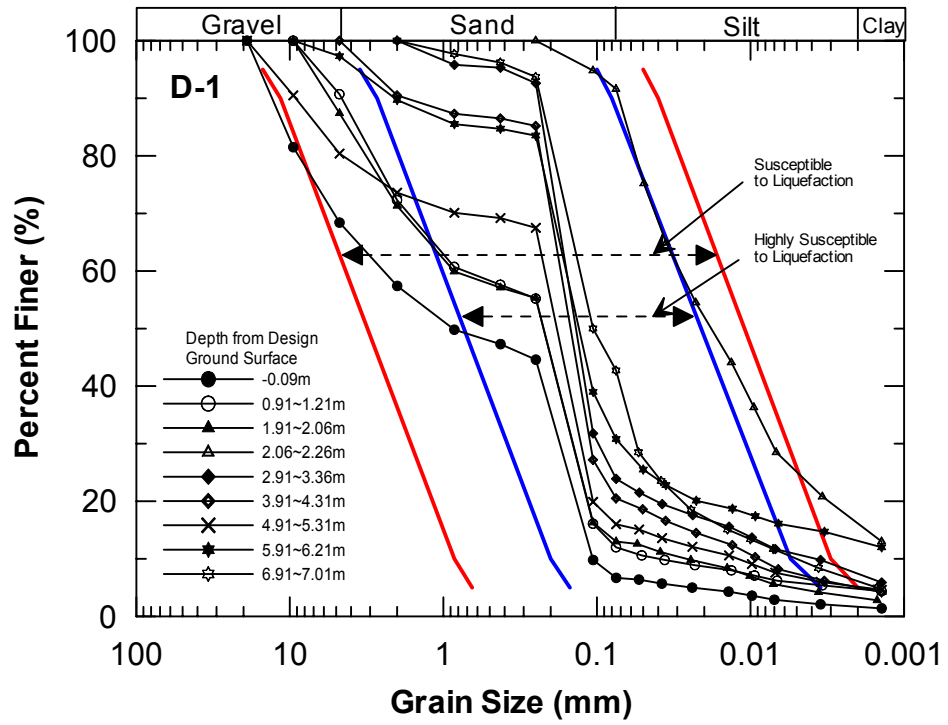
Figure 2.14   Grain Size Distribution for Borehole D-1 (Data from PARI)
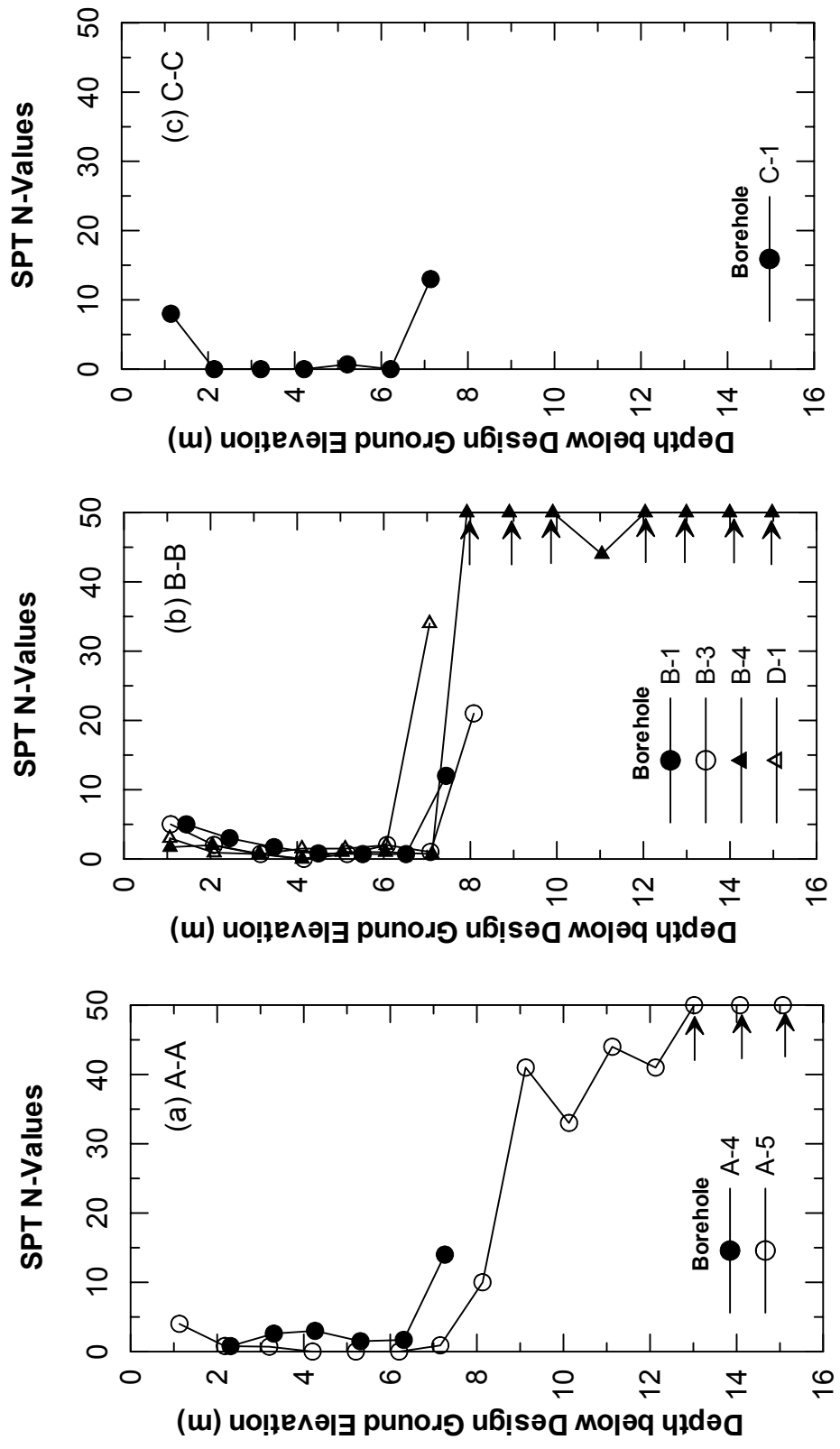
Figure 2.15   Profiles of Uncorrected SPT-N Values (Data from PARI)

30
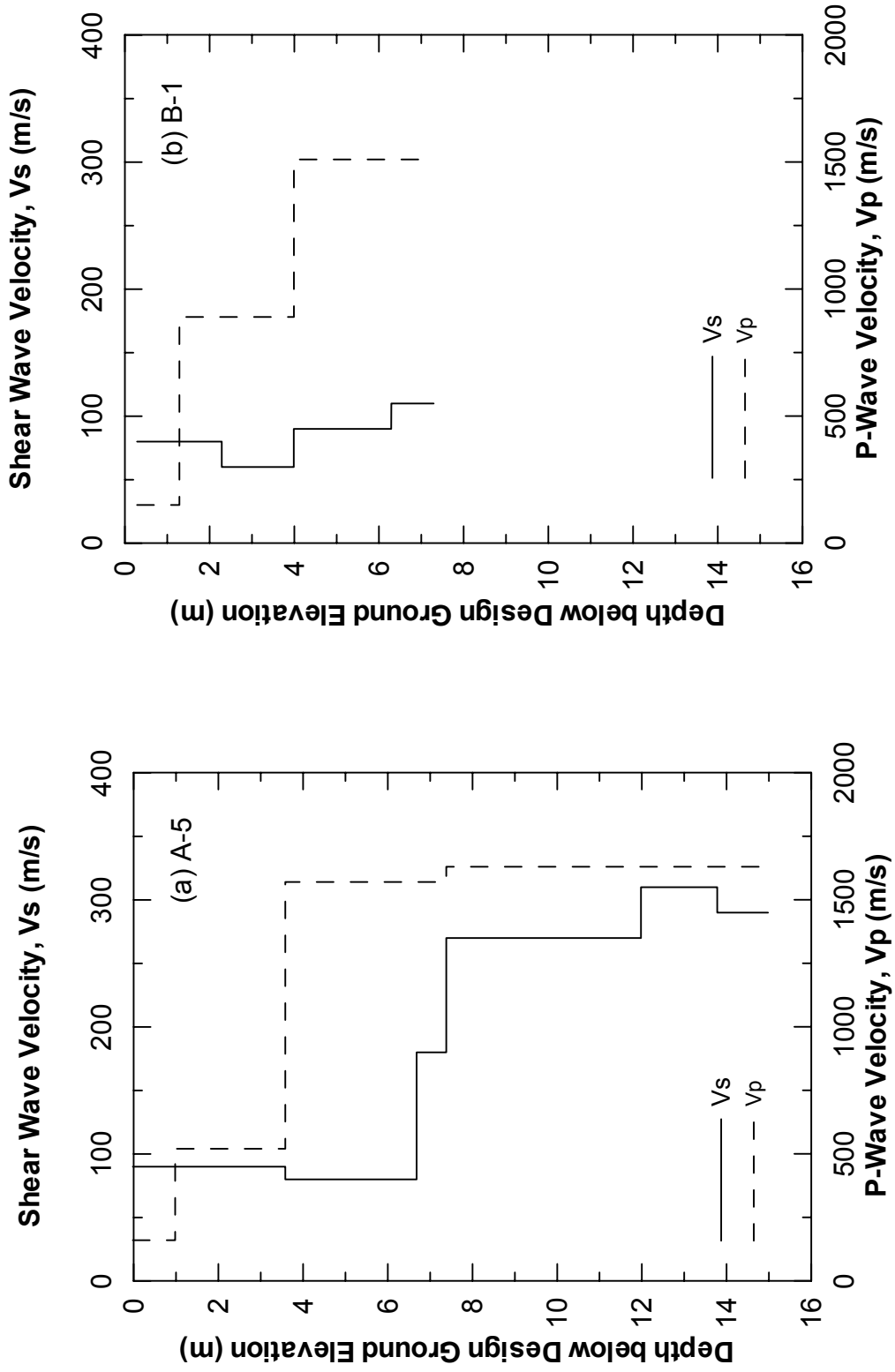
Figure 2.16 Shear Wave and P-Wave Velocity for (a) Borehole A-5 and (b) Borehole B-1(Data from PARI)
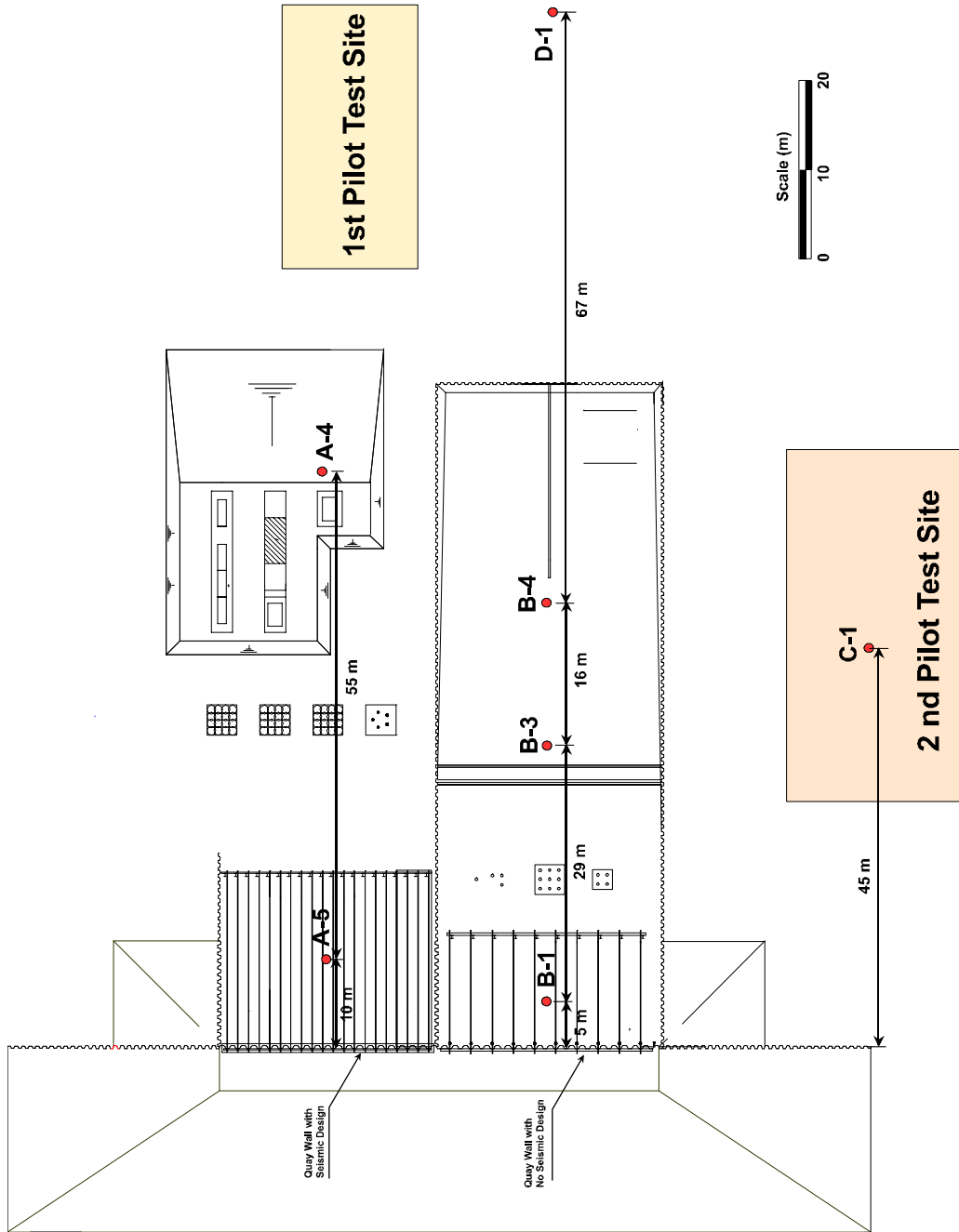
Figure 2.17 Layout of Pilot Test Sites
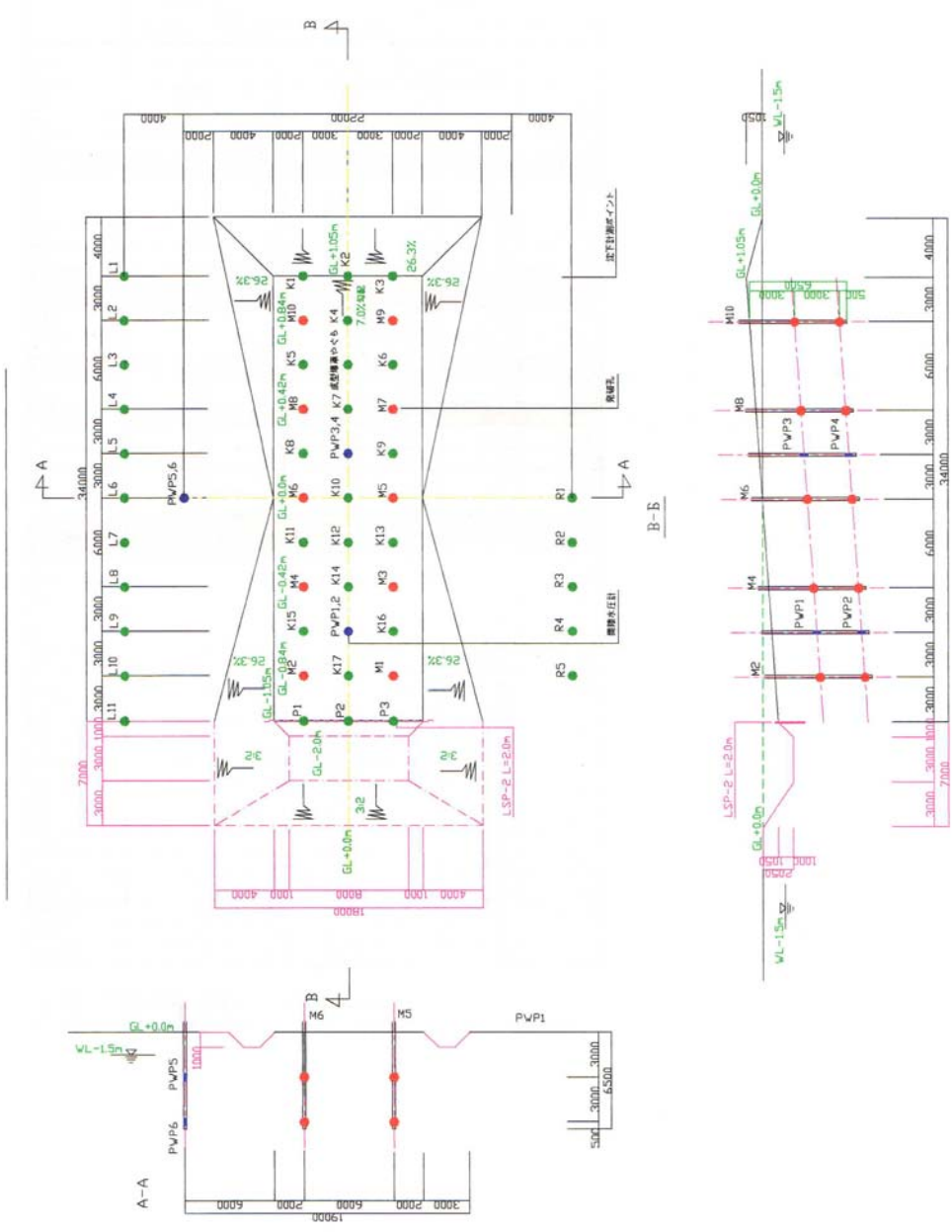
Figure 2.18 Site Layout for 2nd Lateral Spreading Pilot Test (Data from Sato Kogyo)

Figure 2.19   Overview of 2nd Lateral Spreading Pilot Test (Front View)

Figure 2.20   Overview of 2nd Lateral Spreading Pilot Test (Side View)
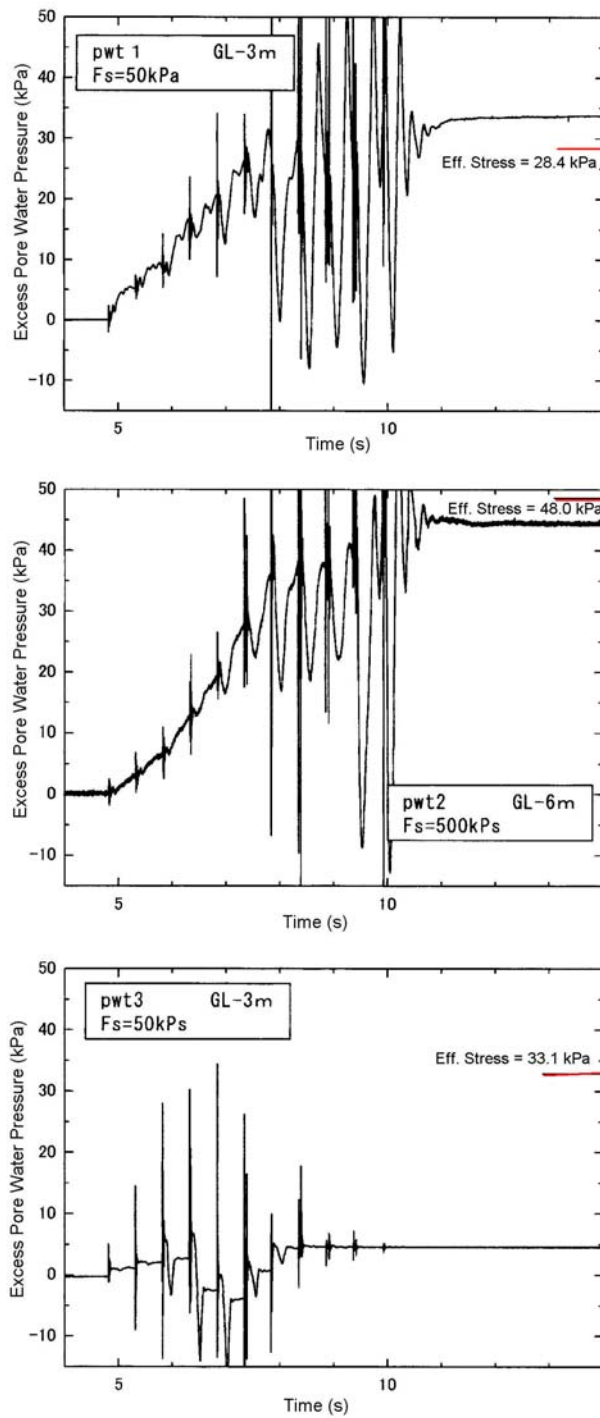
Figure 2.21 Excess Pore Water Pressure Data for 2nd Pilot Test (PWT1-PWT3), Data from Sato Kogyo

Figure 2.21   Excess Pore Water Pressure Data for 2nd Pilot Test (PWT1-PWT3), Data from Sato Kogyo
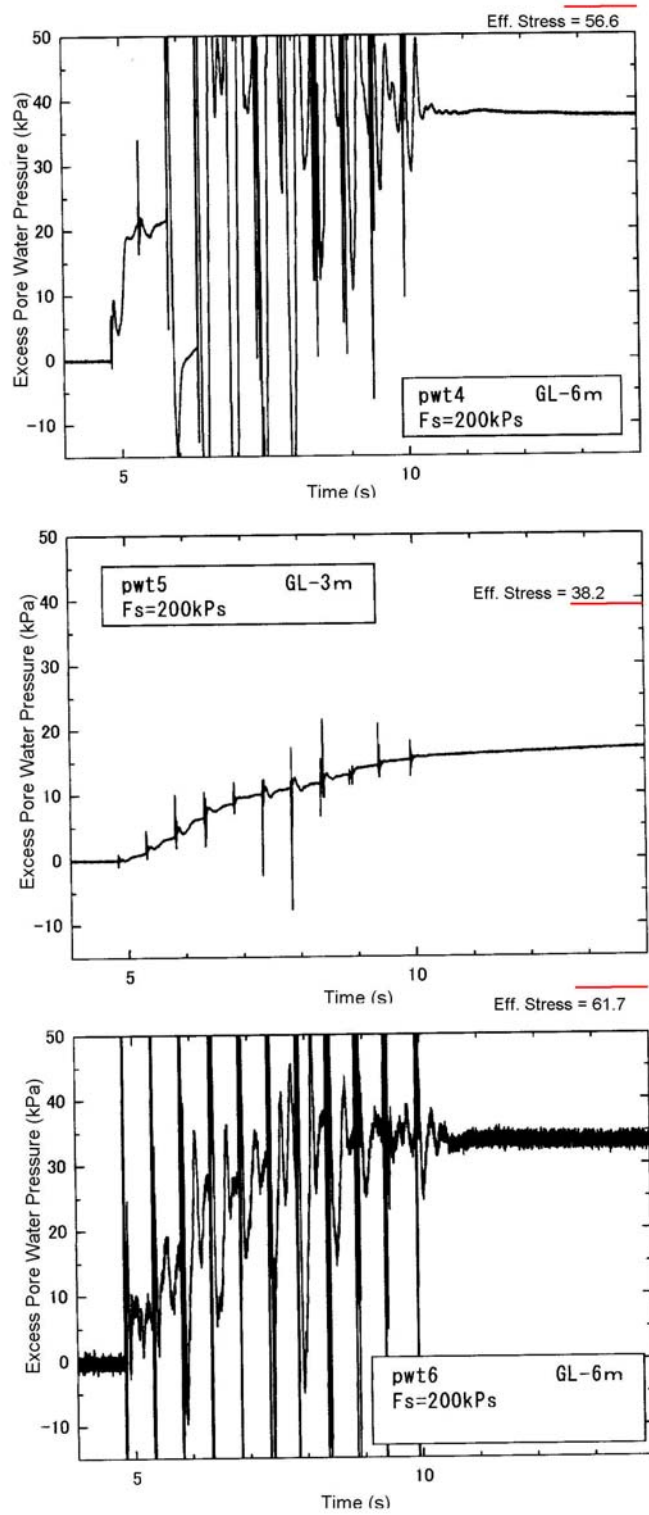
Figure 2.22   Excess Pore Water Pressure Data for 2nd Pilot Test (PWT4-PWT6) , Data from Sato Kogyo

Figure 2.23 Vector Displacements and Settlement Contour after Lateral Spreading, 2nd Pilot Test, Data from Sato Kogyo

37

Figure 2.24   Movement of Sheet Pile Wall following Blasting

Figure 2.25   Surface Cracks after the Blast

Figure 2.26   Tracing of Surface Cracks

Figure 2.27   Evidence of Liquefaction : Sand Boils

3 Test Set-Up of 1st Full-Scale Lateral Spreading Experiment

With the accomplishment in the pilot lateral spreading test, the construction of the actual test site for the first full-scale lateral spreading experiment was then launched in the late of August 2001 and completed in the early of November 2001. The details of the test site are discussed in this chapter. This is followed by the detailed instrumentation and installation procedure. Instrumentation employed to measure responses of soil and lifelines during the lateral spreading are described. The locations of blast holes, amount of charges used as well as the sequence of blasting are also given. Finally, the descriptions of data acquisition system employed in this test are provided.

3.1 Description of Test Site

The UCSD experiments on performance of lifelines subjected to lateral spreading were located in a zone of the unapplied seismic design quay wall where the large global translation of the soil was expected. A layout of the test site for the UCSD experiment is shown in Figure 3.1. Overviews of the site are presented in Figure 3.2 and Figure 3.3. The test site was approximately 25 m wide by 100 m long. The front face was bordered by a 25-m wide water way with the bottom located at elevation of -5.00 m. The water elevation was approximately +2.00 m on the test date. The sheet pile quay wall was driven to the elevation of -8.00 m and was anchored by the tie rods which were fixed to H-piles to prevent the movement of the quay wall. The quay wall retained 7.5 m of hydraulic fill with the design elevation at the ground surface of +3.00m. The UCSD pile specimens were located at 19.0 m away from the quay wall. Figure 3.4 shows the layout of UCSD pile foundations consisting of a single pile, a-4 pile group and a 9-pile group. A group of free head single piles of WU were also located in this region. The gas pipelines and electrical conduit were located across the test sites at 30 m and 32.2 m away from the quay wall. Both were installed at the elevation of +1.75 m. The ground surface started to gently elevate upwards at 25.2 m away from the quay wall with the

slope of 4% such that the elevation of the other end of the site was +5.00 m. The other gas pipeline was installed parallel to the direction of flow with the center of the pile being located at 1 m below the ground surface. The test site was surrounded by the sheet piles to tip elevations between -5.00 to -8.00m.

3.2   Description of Test Specimens

The foundation specimen's 318-mm diameter of steel pipe piles with wall thickness of 10.5 mm and a nominal length of 11.5 m were used to model foundation systems which included a single pile, 4-pile group and 9-pile group. The yield strength of these steel pipe piles was 400 MPa.   A total of 9 piles were instrumented with electrical strain gauges (i.e., 1 single pile, 2 piles for the 4-pile group, and 6 piles for the 9-pile group). The strain gauges were located at 0.6 m intervals on two opposite sides of the piles (i.e., upstream (front) and downstream (back) sides) to measure the bending moment along the pile as presented in Figure 3.5. In addition, two rosette strain gauges were attached to each pile to measure the shear force developed in each pile in the pile group during the lateral spread. One was attached at a depth of 1.9 m below the original pile head and the other one was attached just below the pile cap. A series of tiltmeters at various depths were also installed on one pile of each foundation system to use as backup data for strain gauges. The 75x40x5 steel channels with the yield strength of 400 MPa were welded to the steel pipe piles to protect the strain gauges from damage during the pile installation.

Gas pipelines were 500 mm in diameter with wall thickness of 6 mm. One of them was installed transversely across the test site which was perpendicular to the flow direction, denoted as pipeline type A and the other was installed parallel to the flow direction, denoted as pipeline type C. The length of the pipelines type A and C were approximately 25 m and 22 m, respectively. The electrical conduit denoted as pipeline type B was 268 mm diameter with a wall thickness of 6 mm, a length approximately of 25 m. It was installed transversely across the test site, 2m away from the pipeline type A. All of them were instrumented with electrical strain gauges along their lengths as

41

presented in Figure 3.6. The strain gauges along the sides of the pipeline type A and B were used to measure the bending moment of the pipelines subjected to horizontal movement from lateral spreading. This will be also valuable for back-calculating the soil pressure distribution along the pipelines. The strain gauges along the top of the pipelines, which measured the bending moment along the pipelines in the vertical direction, will be used to calculate the settlement of the pipelines. Apart from the strain gauges, a series of tiltmeters were also instrumented to use as a backup data for strain gauges. For the longitudinal gas pipeline (pipeline type C), the strain gauges were installed along the top, side, and bottom of the pipeline. The strain gauges along the side of the pipeline were utilized to measure axial force distribution along the pipeline type C subjected to drag force from a flow of the soil around it. The strain gauges along the top and bottom of the pipeline C will be used to calculate the settlement. A series of tiltmeters were installed at various locations to use for a backup of strain gauge data.

3.3   Pile Installation Procedure

A diesel driving machine was used to install the piles into the ground as presented in Figure 3.7. Most piles were driven full length into the ground corresponding to about 3.0 to 3.5 m into denser soils to generate the fixity at the pile tips. This was to ensure that the movement of the soil due to the lateral spreading can produce the bending moment along the pile and hence allow quantifying the distribution of the soil pressure acting on the pile from strain gauge data. At the end of pile installation, it was found that about 20% of strain gauges were lost during the installation. Figure 3.8 and Figure 3.9 present the elevation of piles after driving for a 4-pile group and a 9-pile group, respectively. As observed on the photographs, the piles were driven to different depths because a couple of them reached refusal, likely due to the presence of boulder at that particular depth.

After the completion of pile installation, excess pile lengths were cut. Then, the construction of pile caps was continued using standard of Caltrans. Figure 3.10 shows locations of pile tips together with the position of remaining strain gauges after cutting the piles. The depths of soil plug were also measured as indicated in the figure. The

details of the pile caps for the 4-pile group and the 9-pile group were given in Figure 3.11 and Figure 3.12. The piles were spaced at 3.5 pile diameter center-to-center corresponding to 1.113 m. The dimensions of pile caps of the 4-pile group and 9-pile group were 2.333 m x 2.333 m x 1m and 3.446 m x 3.446 m x 1 m, respectively. Figure 3.13 presents the sequence of construction of a pile cap. A summary of concrete strength for the pile caps at 7 and 28 days is given in Table 3.1.

3.4   Pipeline Installation Procedure

Figure 3.14 present the installation sequence of pipeline A and B, while Figure 3.15 presents the installation of pipeline C. Due to the Japanese regulation of transportation, the pipelines needed to be cut into a few segments and then were welded together at the test site. Steel plates were welded to the pipelines on both ends of the pipelines type A and B, and one end of pipeline type C. The ground was then excavated with the side slope of approximately 1:1 to a depth of 1.45 m below the ground elevation. Subsequently, the backfill material was placed and compacted to a required thickness of 0.20 m for the base layer using rammer and roller vibrator. The pipeline was then lifted up and set in place with an approximate depth of 1m below the ground surface. Then, both ends were anchored to the sheet pile wall using high strength bolts. Shims were used if necessary. This type of connection allowed for some rotation on both ends of the pipelines. Subsequently, the sand was backfilled with multiple compacted layers in accordance with Japanese Gas Association specification to achieve a compact dry density unit weight of 90% of the maximum dry unit weight determined in the laboratory by standard Proctor test (ASTM D-698). Based on the laboratory test results, the optimum dry density and optimum moisture contents of this backfill material was 14.7 kN/m^3 and 16.8%, respectively. For each layer, the field density tests were carried out at 3 random locations using the sand cone method (ASTM D-1556). The field density test results of each layer for location of pipeline A, B and pipeline C are summarized in Table 3.2 and Table 3.3, respectively. It shows that the density of compacted soil met the specification with the relative compaction (R) of more than 90%.

Apart from the strain gauges and tiltmeters, several instruments were also installed to capture the behavior of soil and lifelines in more details. These include pore pressure transducers, soil pressure cells, string-activated linear potentiometers, accelerometers, inclinometer casings, and Global Positioning System (GPS) units. The plan of instrumentation for the entire site is presented in Figure 3.17. The instrumentation plans nearby the pile foundation systems and pipelines are enlarged as illustrated in Figure 3.18 and Figure 3.19, respectively. The details of each instrument are described as the followings.

A total of 24 pore pressure transducers were installed at various locations and depths throughout the test site to measure the excess pore water pressure built up during the liquefaction. The transducers were installed nearby the test specimens as well as in the free field. The measured excess pore water pressure will be used to calculate the excess pore water pressure ratio to indicate the degree of liquefaction during the test.

For the 4-pile group and 9-pile group, soil pressure cells were installed at the front and back sides of the pile cap surfaces to measure the pressure distribution of the soil acting on both upstream and downstream sides. A total of 8 cells were employed for this test. The magnitude of resultant forces acting on both pile caps can be calculated based on the data from soil pressure cells. The locations of soil pressure cells are presented in Figure 3.20.

Three accelerometers were installed on the top of the pile caps and single pile to measure the horizontal acceleration responses during the test. The direction of accelerometers was set to be parallel to the flow direction. The tiltmeters were also attached adjacent to those accelerometer locations for measuring the pile head rotations.

To measure the profiles of soil displacement due to the lateral spreading, inclinometer casings were installed. First, the borehole was drilled to the stiff layer, and then the casing was lowered into the hole. After that, the inclinometer casing was adjusted until the direction of grooves was approximately parallel to the flow direction. Borehole was then backfilled with the sand. The sensor was lowered into the casing to measure the rotations along the casing before and after the test. Assuming that the

rotation and displacement at the tips of the casing were zero, the displacement profile of the soil can be calculated. Furthermore, three of displacement array fibers were also installed to measure the real-time displacement soil profiles.

The string-activated linear potentiometers were used to measure the relative displacement between two points of interest. For example, the potentiometer connected between inclinometer casing and pile cap indicates the relative movement between soil and the pile cap. The locations of linear potentiometers installed for this test are summarized in Figure 3.18

The GPS units were used to measure real-time the movement in longitudinal, transverse, and vertical direction. They were setup at several locations (i.e., on the pile caps, single piles, and ground surface) in order to capture the movement of piles as well as the soil during the test. The locations of GPS units are presented in Figure 3.17 through Figure 3.19.

3.5   Controlled Blast

As success in using the controlled blast to induce liquefaction of the soil in several tests in Japan as well as the full-scale lateral load tests at Treasure Island (Ashford *et al*. 2000), the same method was implemented to liquefy the soil at the test site and thus induce the lateral spreading. The blast holes were spaced at 6.0 m on centers in the regular grid pattern as presented in Figure 3.21. The charges were installed at depths of 3.5 m and 7.5 m below the ground surface (El +3.00m). The amount of charge varied from 2 kg nearby the pile specimens to 3-5 kg at other areas. It was done this way so as to prevent damage to a large number of instruments installed in the vicinity of pile specimens. The sequence of the blasting started from the back corner of the embankment (B1) and then proceeded successively towards the quay wall (B48). This was followed by the detonation of the secondary blast holes around the perimeter of the test site as denoted by C1-C14 and D1-D3. The purpose of these explosives was to loosen the soil in the vicinity of sheet pile to allow unrestricted flow of the soil in such region. Approximately 10 sec after a completion of primary and secondary blasting, the

additional explosives were used to break tie rods of the quay wall and allow the quay wall to move freely and thus create additional movement of the soil within the test area.

3.6 Data Acquisition System

A total of more than 400 channels were connected to the high speed data acquisition systems to collect and process the data during the test. The number of channels required for this test was more than the capacity of the UCSD data acquisition system, therefore an additional data acquisition system was rented from Tokyo Soil Research Company in Japan to satisfy the requirement. The UCSD data acquisition system was the SCXI system manufactured by National Instruments. It consisted of SCXI-1001 chassis, SCXI-1120, SCXI-1520, and SCXI-1121 modules together with SCXI-1320, SCXI-1321, and SCXI-1314 front mounting terminal blocks. The UCSD system had a capability to support up to 320 channels comprised of 280 channels of strain gauges and 40 channels of other instruments (i.e., accelerometers, linear potentiometers, and tiltmeters). The Japanese system was manufactured by Kyowa consisting of 150 strain gauge channels. Both systems started recording the data at the same time approximately 3 minutes before the blasting. The data were synchronized with other test participants at 116.76 seconds before the blast using the 5 volt signal as an indication. The data were acquired at sampling rate of 100 Hz for about 3 minutes following the blasting to capture all the important information during the test. The scan rate was then changed to 10 Hz and 0.1 Hz for the duration of about 2 hours and 24 hours, respectively to measure the decrease in excess pore water pressure with time.

Table 3.1   Summary of Concrete Strength for Pile Caps

Date of Casting	Date of Test	Concrete Age (Days)	Truck No.	Slump (cm)	Air (%)	Sample No.	f_c' (MPa)	$f_c'_{ave}$ (MPa)
10/15/02	10/22/02	7	1	7.0	4.3	1	29.3	29.5
						2	29.4	
						3	29.8	
			2	8.0	4.6	1	29.5	29.5
						2	29.7	
						3	29.7	
			3	7.0	4.4	1	28.6	29.0
						2	28.9	
						3	29.4	
10/15/02	11/12/02	28	1	7.0	4.3	1	36.7	36.7
						2	36.8	
						3	36.6	
			2	8.0	4.6	1	35.9	35.9
						2	35.5	
						3	36.2	
			3	7.0	4.4	1	36.1	36.2
						2	36.7	
						3	35.7	

Table 3.2   Summary of Field Density Test Results for Pipeline A and B

Location	Layer No.	Sample No.	Total Density (kN/m³)	Water Content (%)	Dry Density (kN/m³)	Relative Compaction, R (%)	Average Relative Compaction (%)
Pipeline A and B	Base	1	17.27	25.0	13.81	94.0	96.1
		2	17.75	24.9	14.21	96.7	
		3	17.74	23.8	14.33	97.5	
	1	1	16.87	17.8	14.31	97.4	96.3
		2	16.22	15.5	14.05	95.6	
		3	16.72	18.7	14.08	95.8	
	2	1	16.35	17.6	13.90	94.6	96.1
		2	17.37	19.4	14.55	99.0	
		3	15.89	14.2	13.91	94.6	
	3	1	15.92	15.6	13.77	93.7	94.1
		2	15.56	12.5	13.84	94.2	
		3	15.82	13.9	13.89	94.6	
	4	1	16.12	13.3	14.23	96.8	95.2
		2	15.43	13.3	13.62	92.7	
		3	16.13	14.3	14.11	96.0	
	5	1	15.82	15.0	13.76	93.7	95.6
		2	16.62	16.0	14.33	97.5	
		3	15.98	13.8	14.05	95.6	

Note: $R(\%) = \dfrac{\gamma_{d(field)}}{\gamma_{d(max-lab)}} x100\%$

$\gamma_{d(field)}$ = Field dry density

$\gamma_{d(max-lab)}$ = Maximum dry density measured in laboratory by standard Proctor test

Table 3.3   Summary of Field Density Test Results for Pipeline C

Location	Layer No.	Sample No.	Total Density (kN/m³)	Water Content (%)	Dry Density (kN/m³)	Relative Compaction, R (%)	Average Relative Compaction (%)
Pipeline C	Base	1	16.01	14.7	13.96	95.0	96.1
		2	16.57	16.0	14.28	97.2	
		3	16.17	14.7	14.10	96.0	
	1	1	16.34	14.4	14.28	97.2	97.2
		2	16.86	14.6	14.72	100.0	
		3	16.28	17.4	13.86	94.3	
	2	1	16.27	13.8	14.30	97.3	97.2
		2	15.90	14.7	13.86	94.3	
		3	16.76	14.1	14.69	100.0	
	3	1	16.33	14.4	14.28	97.2	95.9
		2	15.80	12.6	14.03	95.5	
		3	15.83	13.2	13.98	95.1	
	4	1	15.55	12.7	13.80	93.9	92.2
		2	15.09	12.9	13.36	90.9	
		3	15.35	14.0	13.47	91.7	
	5	1	16.00	14.4	13.99	95.2	95.8
		2	16.00	14.8	13.94	94.9	
		3	16.14	12.8	14.30	97.3	

Note: $R(\%) = \dfrac{\gamma_{d(field)}}{\gamma_{d(max-lab)}} x100\%$

$\gamma_{d(field)}$ = Field dry density

$\gamma_{d(max-lab)}$ = Maximum dry density measured in laboratory by standard Proctor test
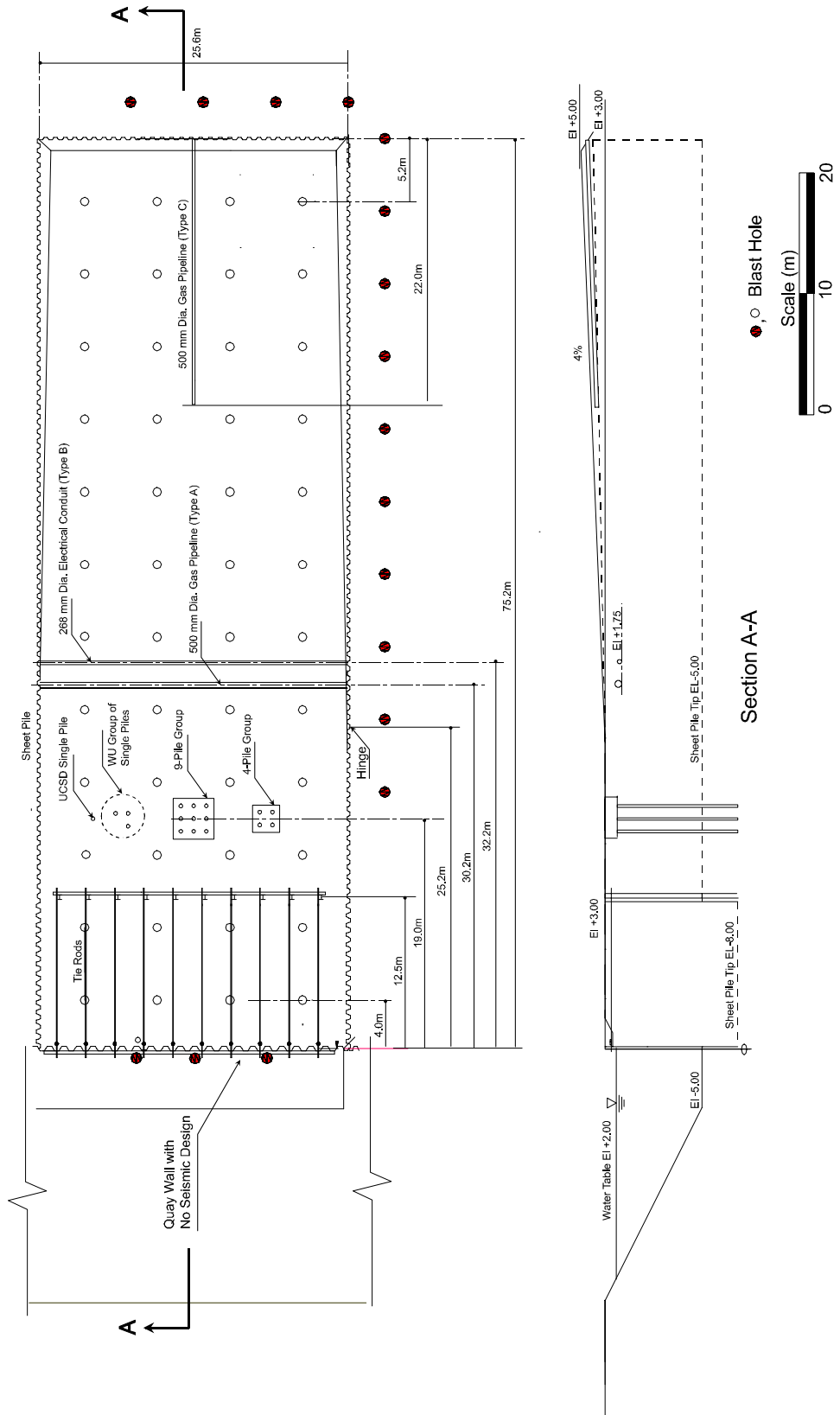
Figure 3.1   Schematic Diagram of Test Site

Figure 3.2   Overview of Test Site, 1st Japan Blast Test (Front View)

Figure 3.3   Overview of Test Site, 1st Japan Blast Test (Side View)
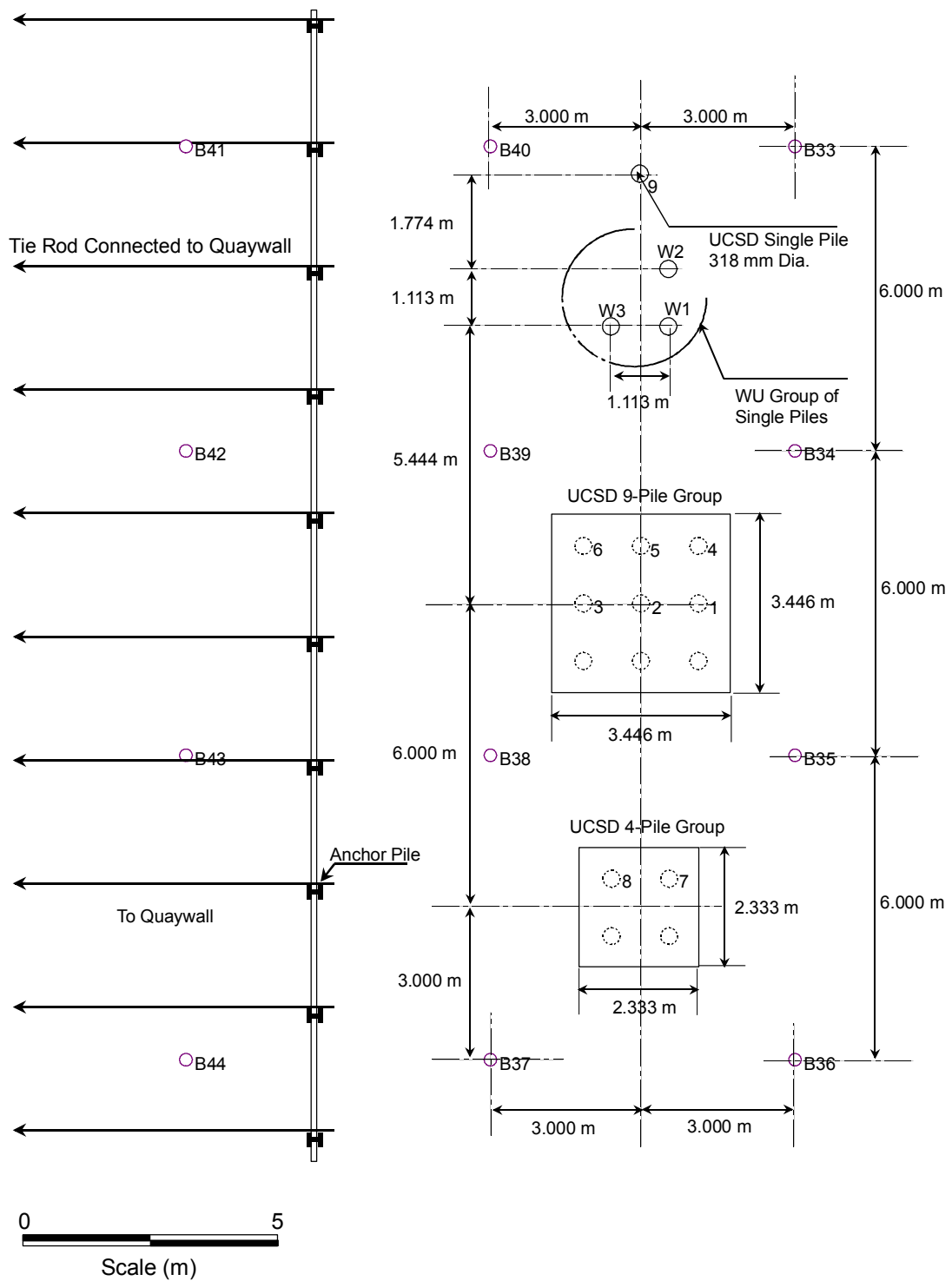
Figure 3.4 Schematic Diagram in Vicinity of UCSD Pile Specimens

Back Front

0.70 m

Instrumented Piles

⑨

Varying depth for each pile

Waseda University Experiment

W2

W3   W1

Shear
Strain Gauge

A   A

11.50 m

Tiltmeter

Instrumented Piles

⑥   ⑤   ④

③   ②   ①

○   ○   ○

Flow Direction

Bending
Strain Gauge

16 stain gauges@0.60m = 9.60 m

Channel 75x40x5

Instrumented Piles

⑧   ⑦

○   ○

1.20 m

318 mmO.D., 10.5 mm thick,
f_y = 400MPa

Channel 75x40x5

Flow Direction

Back   Front
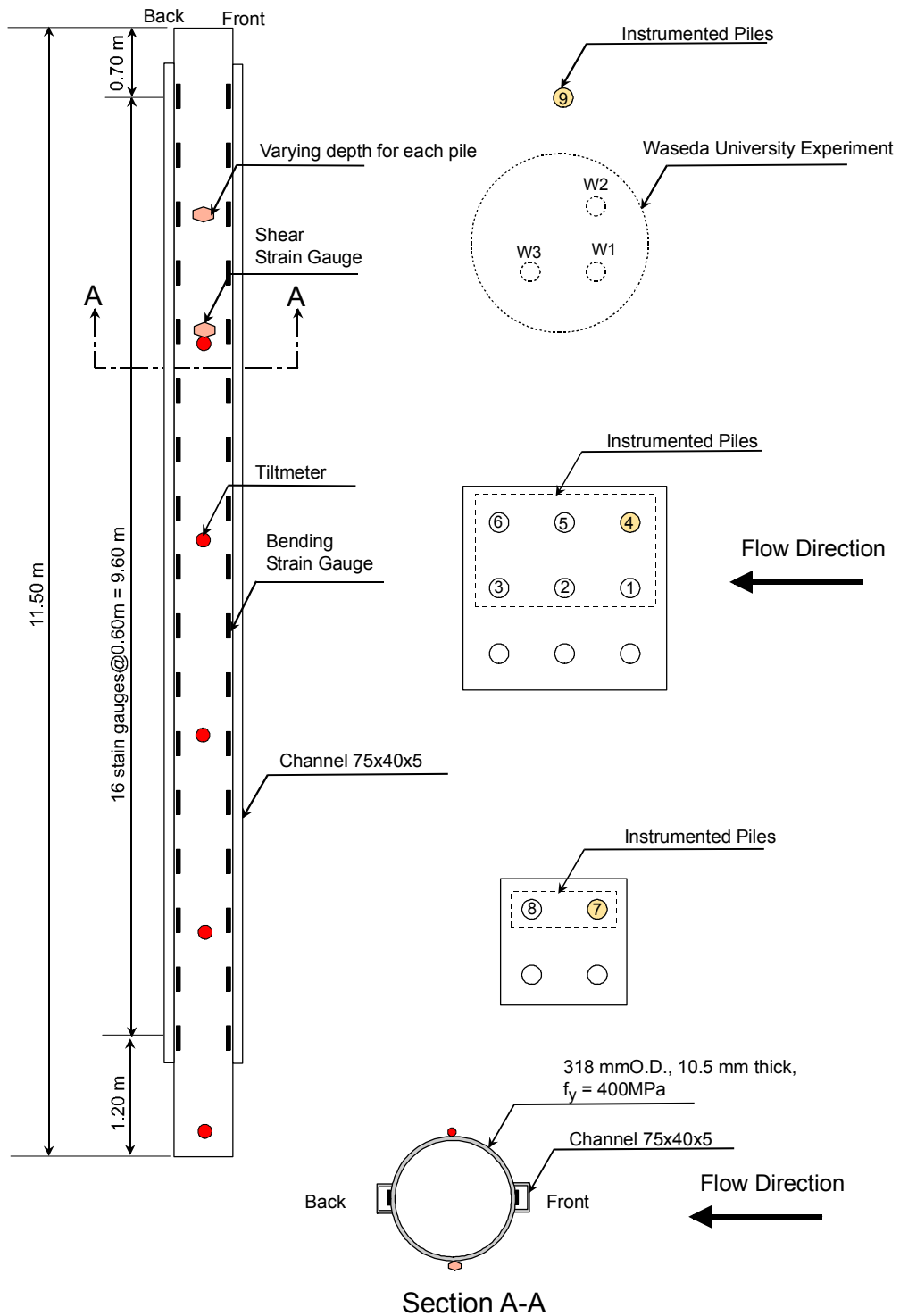
Section A-A

Note : Tiltmeters were installed only for pile No 4, 7 and 9.

Figure 3.5 Locations of Instruments for Steel Pipe Piles
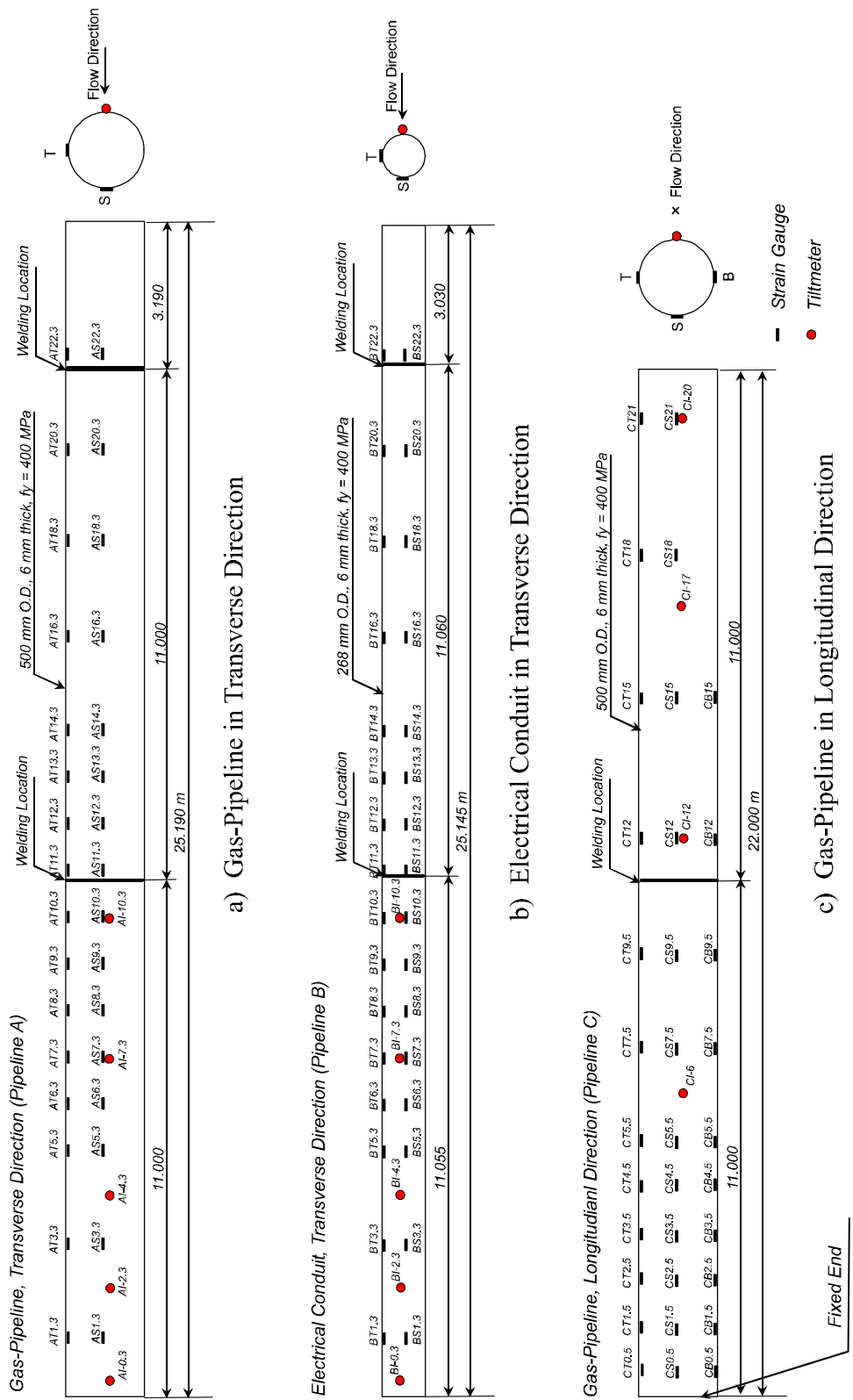
Figure 3.6   Locations of Instruments for (a) Gas-Pipeline in Transverse Direction, (b) Electrical Conduit in Transverse Direction, and (c) Gas-Pipeline in Longitudinal Direction

54

Figure 3.7   Installation of Pile a) Locating Pile to Specified Location , and b) During Pile Driving

Figure 3.8   Piles of 9-Pile Group after Completion of Installation

Figure 3.9   Piles of 4-Pile Group after Completion of Installation
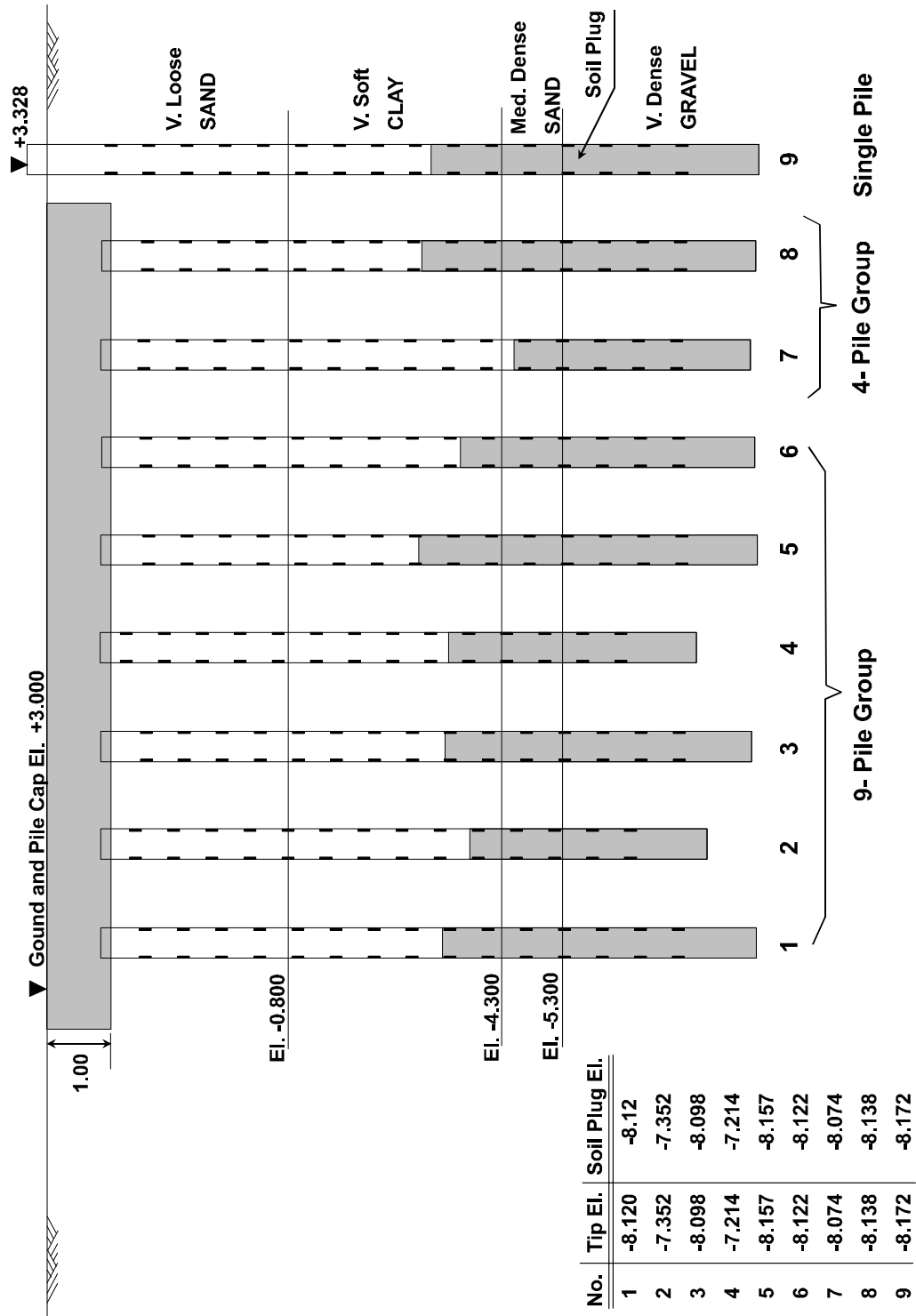
Figure 3.10   Locations of Strain Gauges sand Pile Tips after Pile Installation

▼ +3.328

▼ Gound and Pile Cap El. +3.000

1.00

El. -0.800

El. -4.300

El. -5.300

V. Loose SAND

V. Soft CLAY

Med. Dense SAND

Soil Plug

V. Dense GRAVEL

1   2   3   4   5   6   7   8   9

9- Pile Group

4- Pile Group

Single Pile

No.	Tip El.	Soil Plug El.
1	-8.120	-8.12
2	-7.352	-7.352
3	-8.098	-8.098
4	-7.214	-7.214
5	-8.157	-8.157
6	-8.122	-8.122
7	-8.074	-8.074
8	-8.138	-8.138
9	-8.172	-8.172

Units in millimeter.
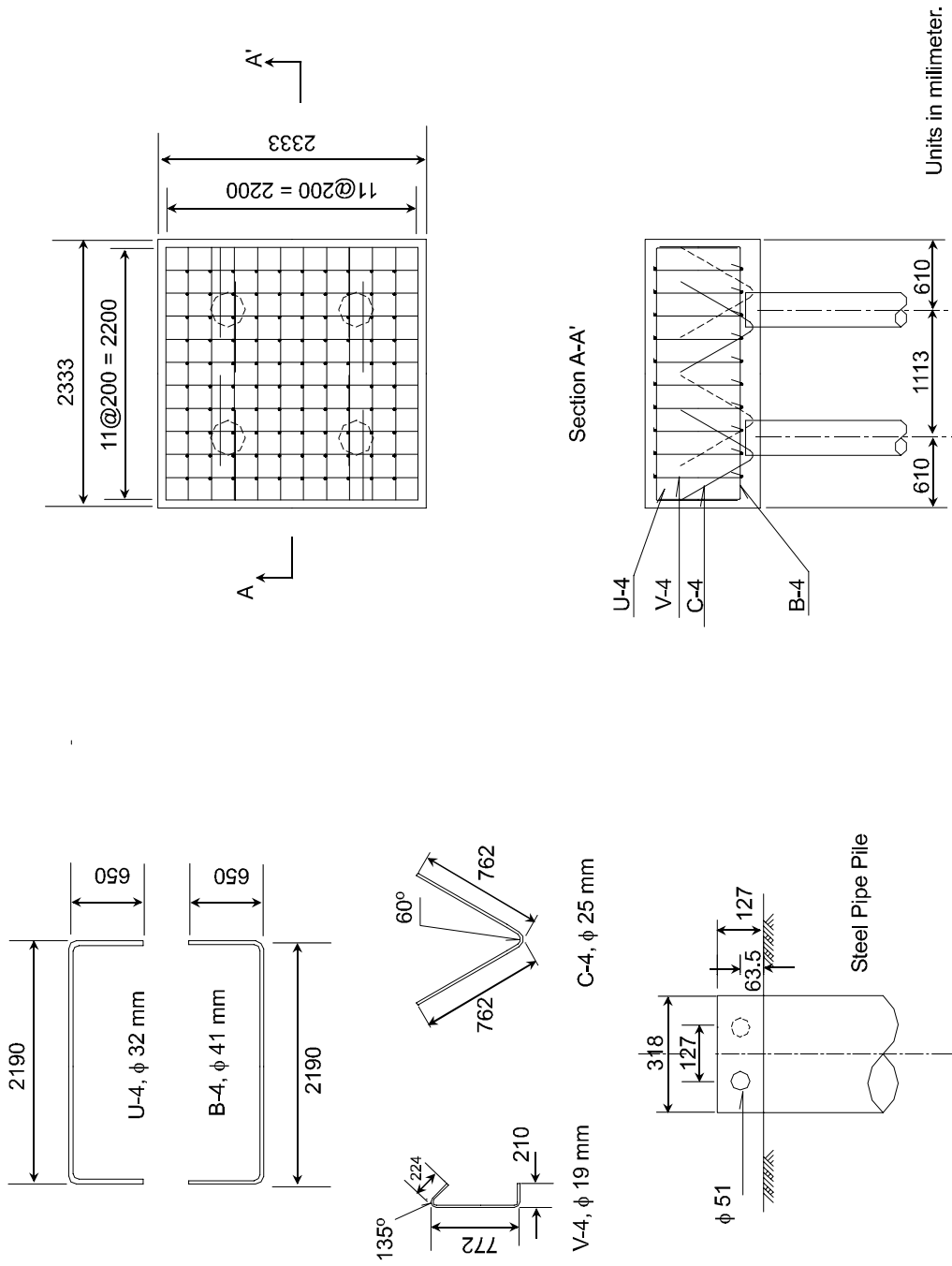
Figure 3.11   Details of Reinforcing Steel for Pile Cap of 4-Pile Group

58
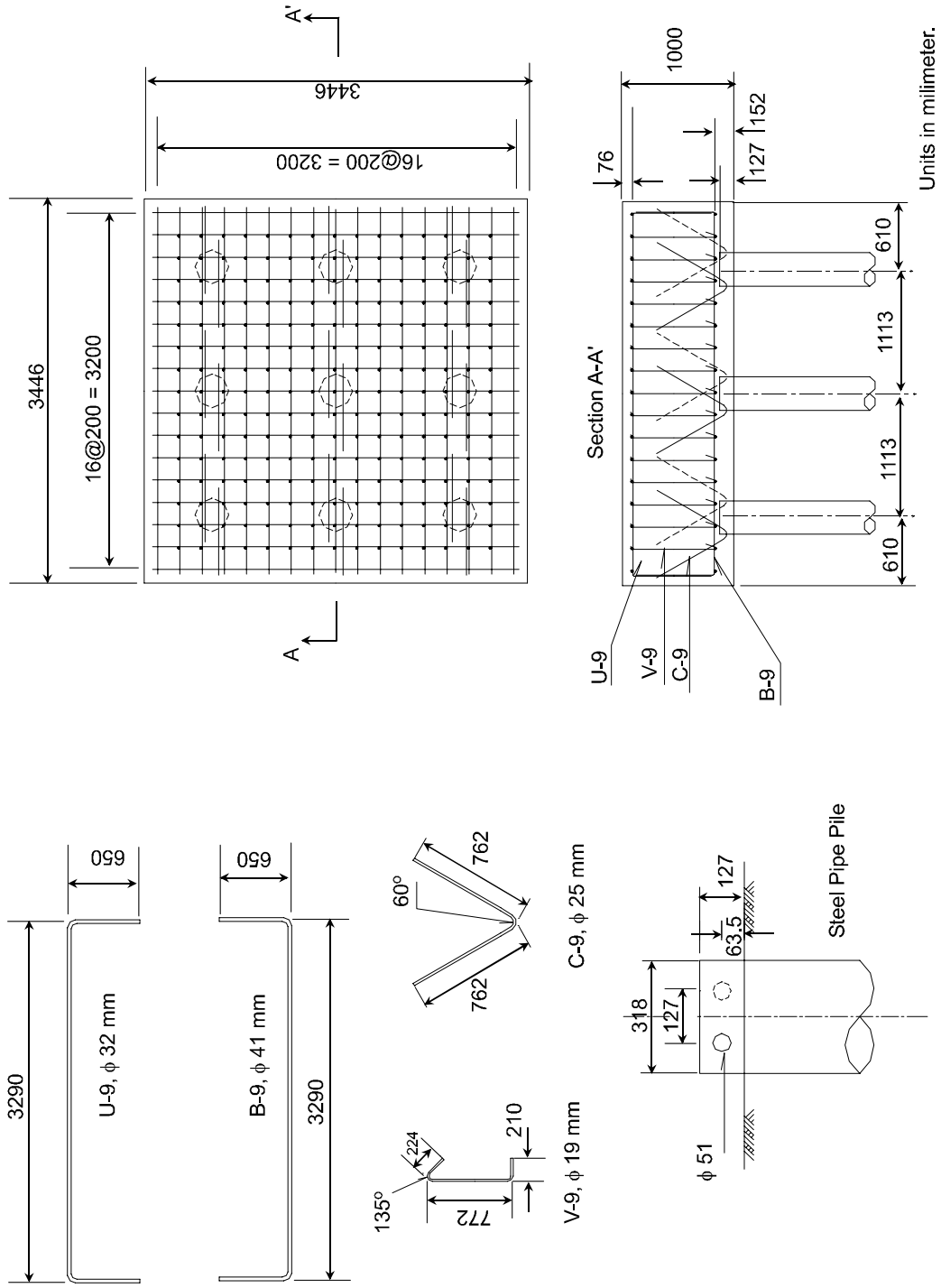
Figure 3.12   Details of Reinforcing Steel for Pile Cap of 9-Pile Group

59

1. Cutting Piles to Design Elevation

2. Cutting Holes for V-Hooks

3. Placement of 10 cm Gravel

4. Placement of 10 cm Lean Concrete

5. Installation of V-Hooks

6. Construction of Reinforcement

7. Construction of Formworks

8. Pile Cap after Concrete Work

Figure 3.13   Procedure for Construction of Pile Cap

1. Welding of pipeline together

2. Wedding of Connection Plate

3. Excavation for Pipeline AB Installation

4. Measurement of Cross Section

5. Compaction of Base Layer

6. Installation of Pipeline A

7. Installation of Pipeline B

8. Pipeline A and B in Place

Figure 3.14   Procedure in Construction of Pipeline Type A and B

9. Connection of Pipeline to Sheet Pile

10. Compaction of 1st Layer

11. Compaction of 2nd Later

12. Field Density Test of 2nd Layer

13. Compaction of 3rd Layer

14. Filed Density Test of 4th Layer

15. Sand Placement for 5th Layer

16. Completion of Installation

Figure 3.14   Procedure in Construction of Pipeline Type A and B (Cont'd)

1. Excavation for Installation of Pipeline C

2. Measurement of Cross Section

3. Compaction of Base Layer

4. Field Density Test for Base Layer

5. Installation of Pipeline Type C

6. Connection to Sheet Pile

7. Compaction of 1st Layer

8. Completion of Installation

Figure 3.15   Procedure in Construction of Pipeline Type C
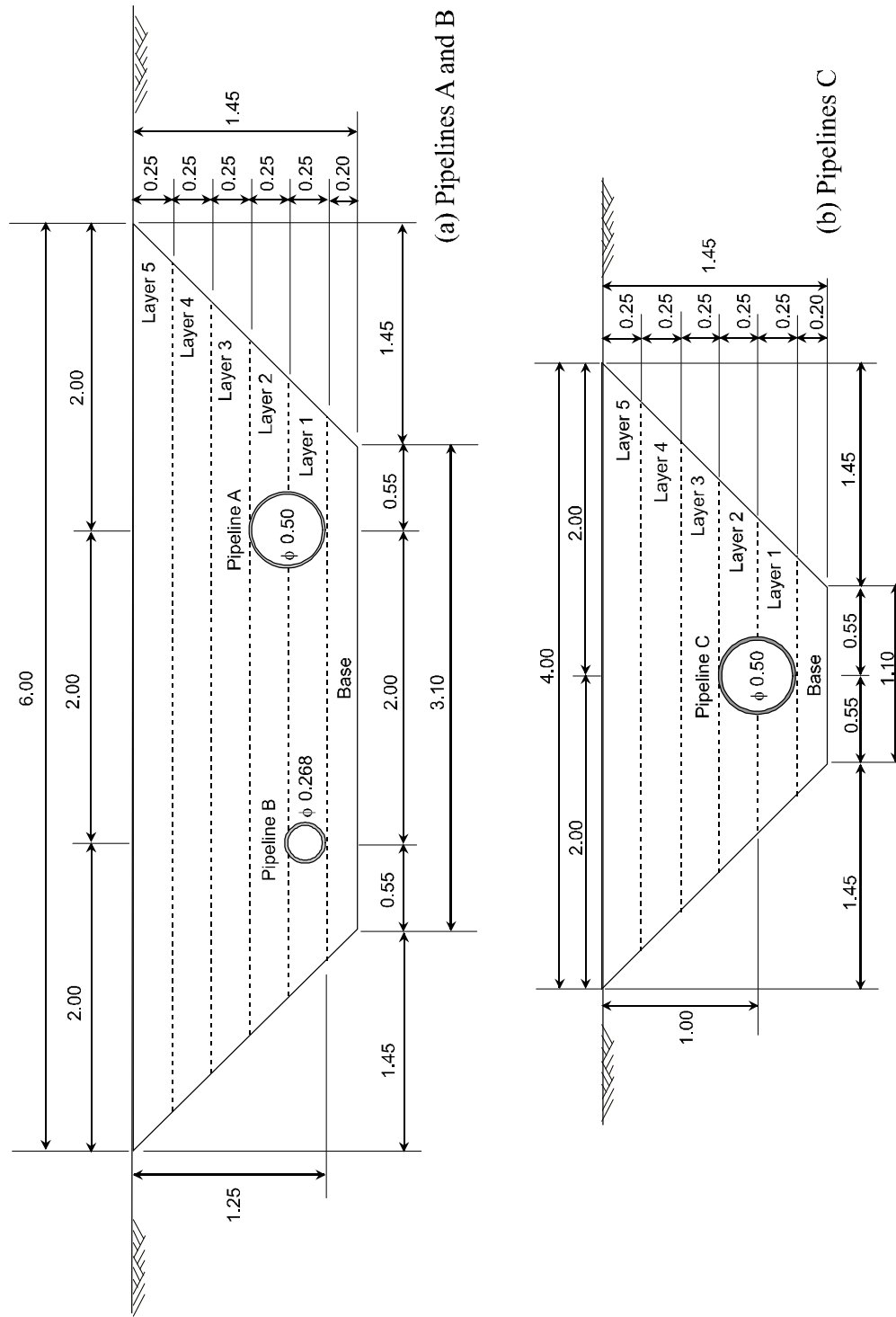
Figure 3.16   Cross Sections of Multiple Compacted Layers for (a) Pipeline A and B, and (b) Pipeline C

64
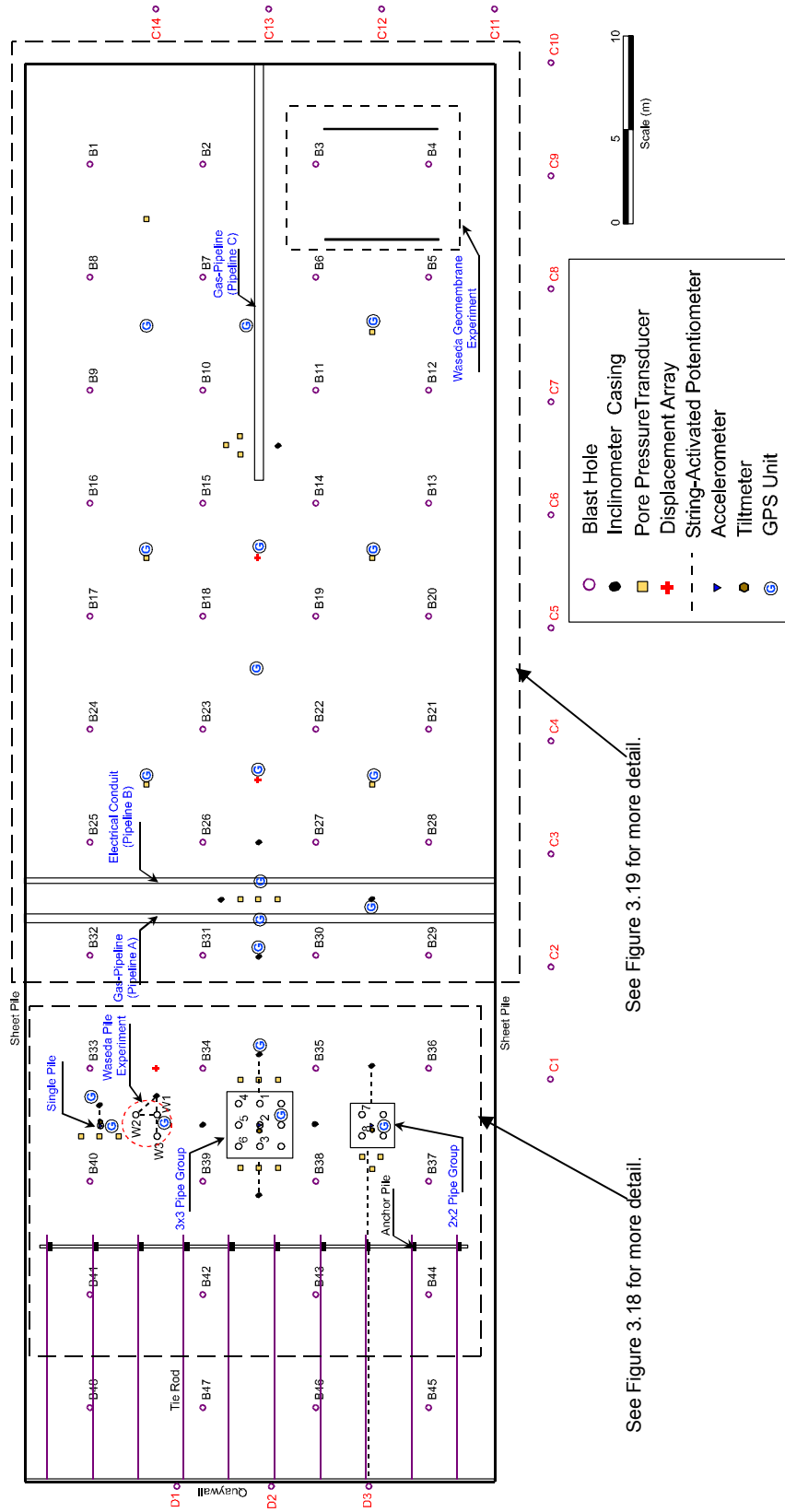
Figure 3.17 Schematic Diagram of Instruments at Test Site

65
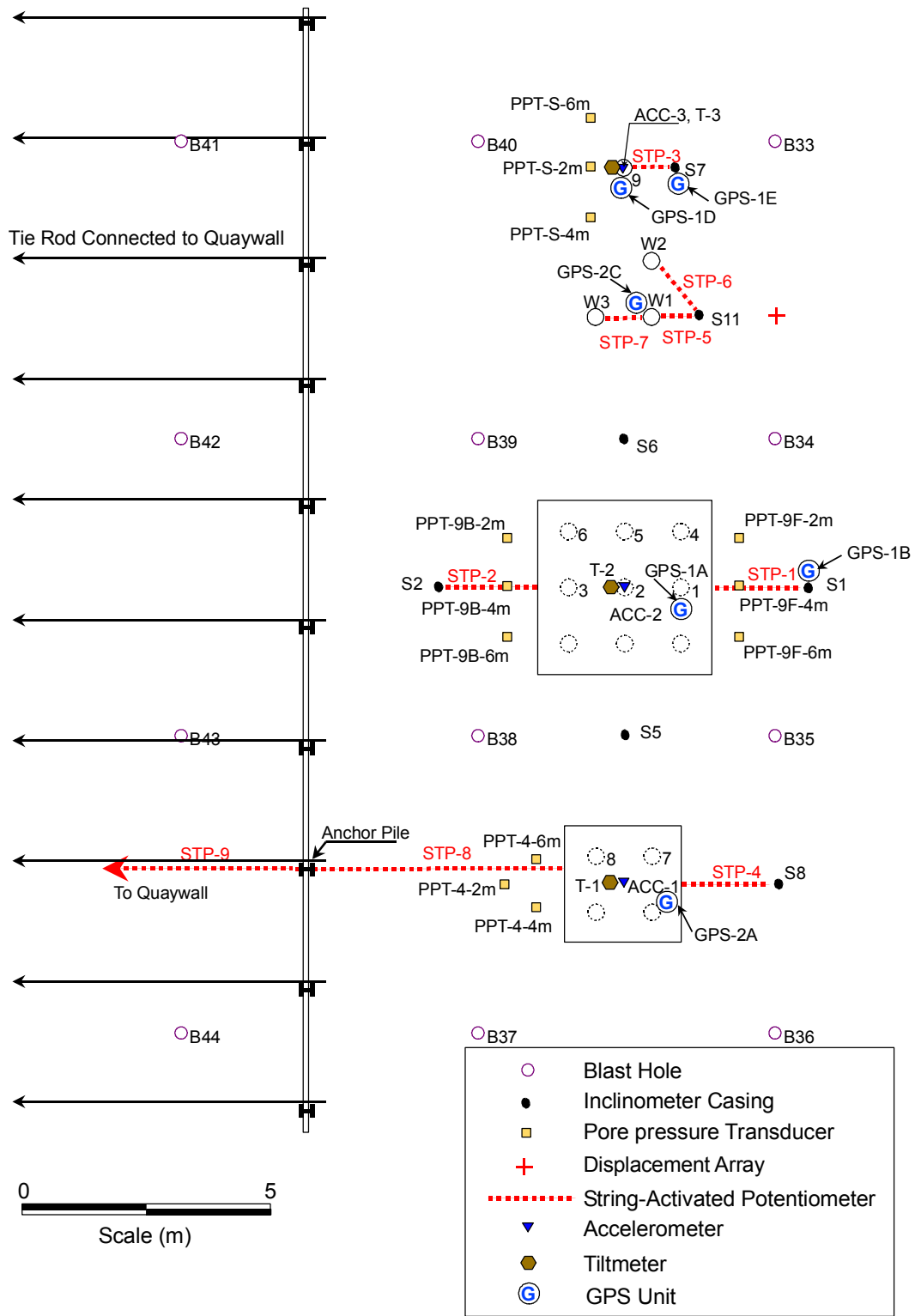
Figure 3.18   Schematic Diagram of Instruments nearby Pile Specimens
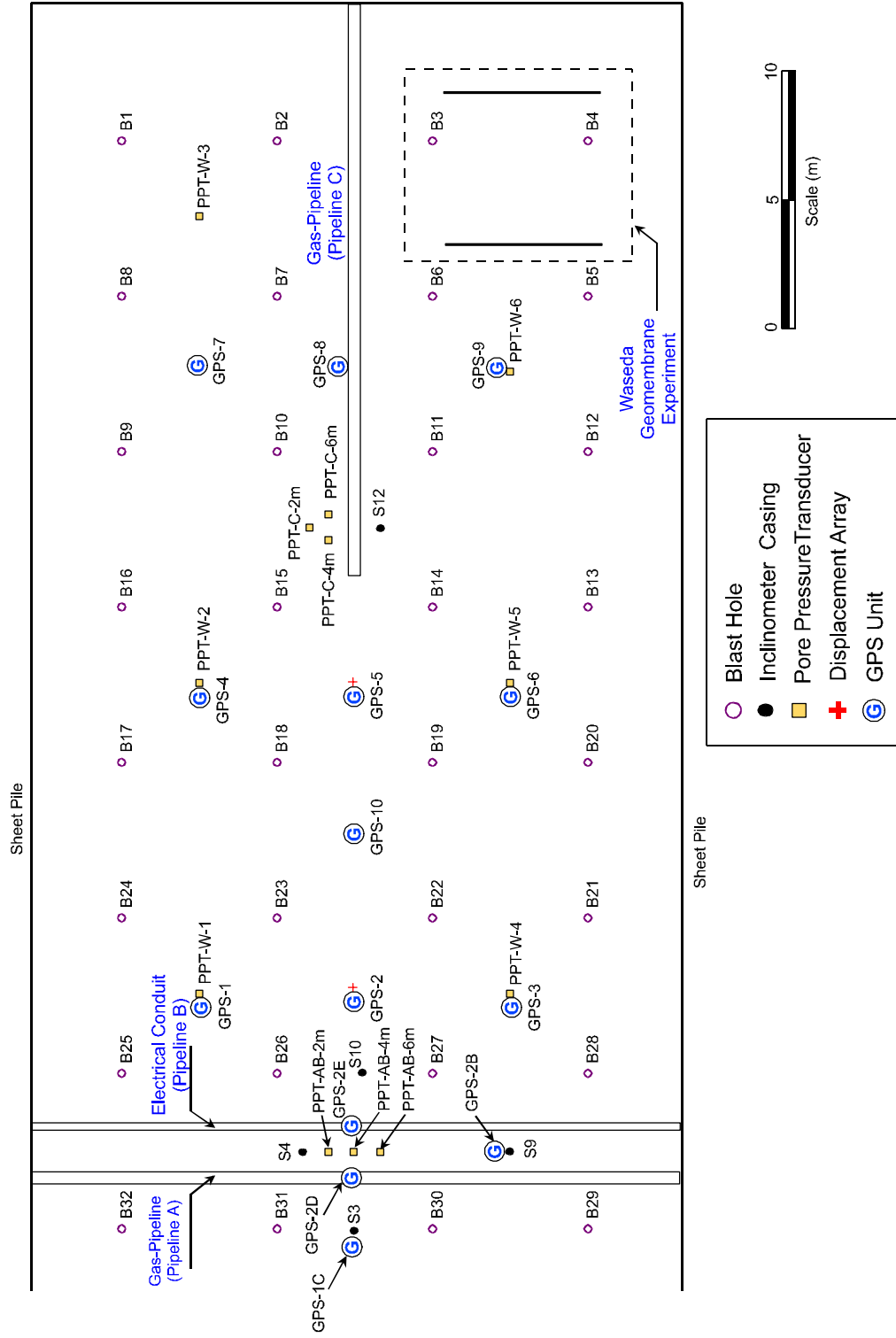
Figure 3.19 Schematic Diagram of Instruments nearby Pipelines

67
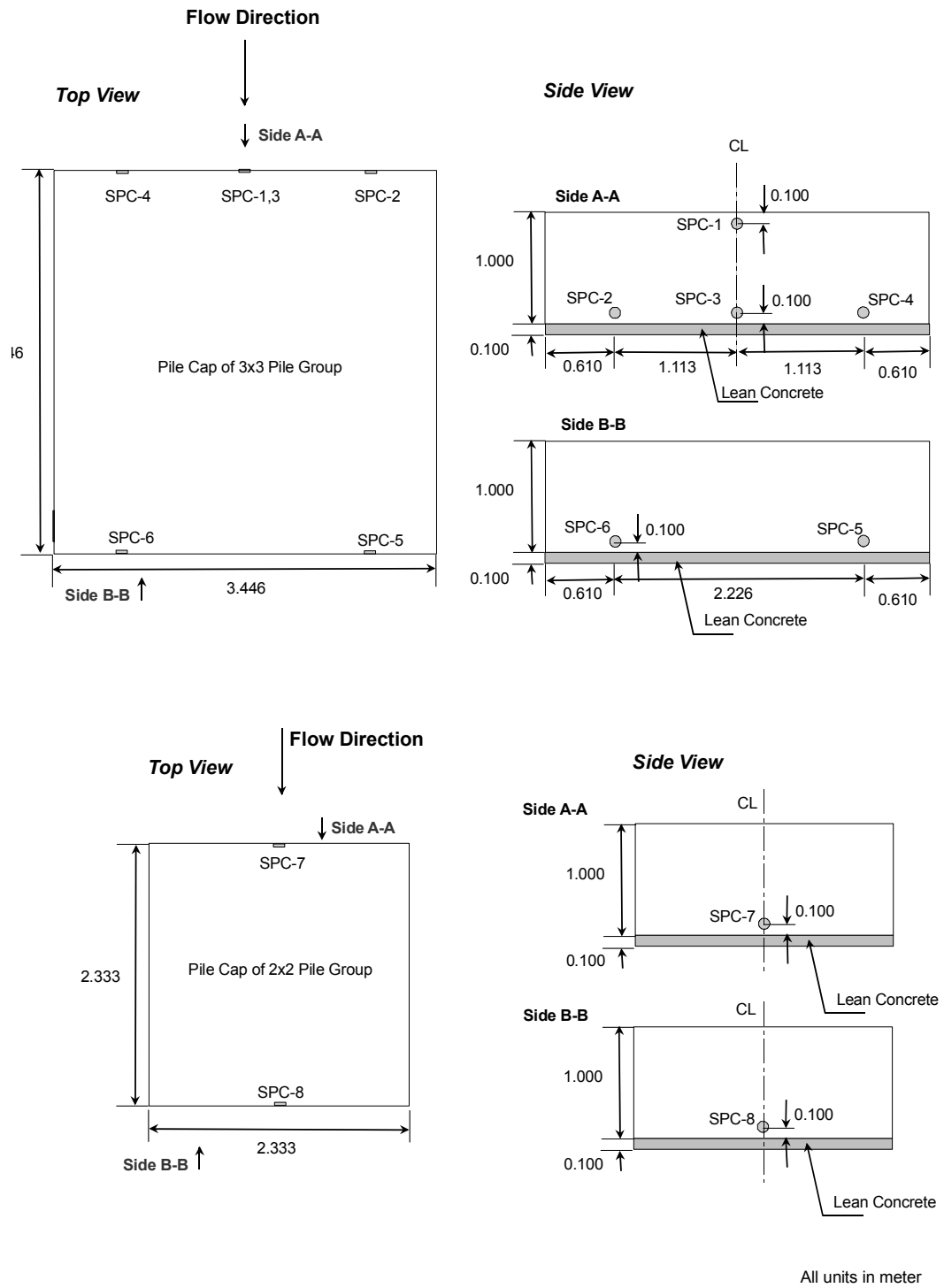
Figure 3.20   Location of Soil Pressure Cells
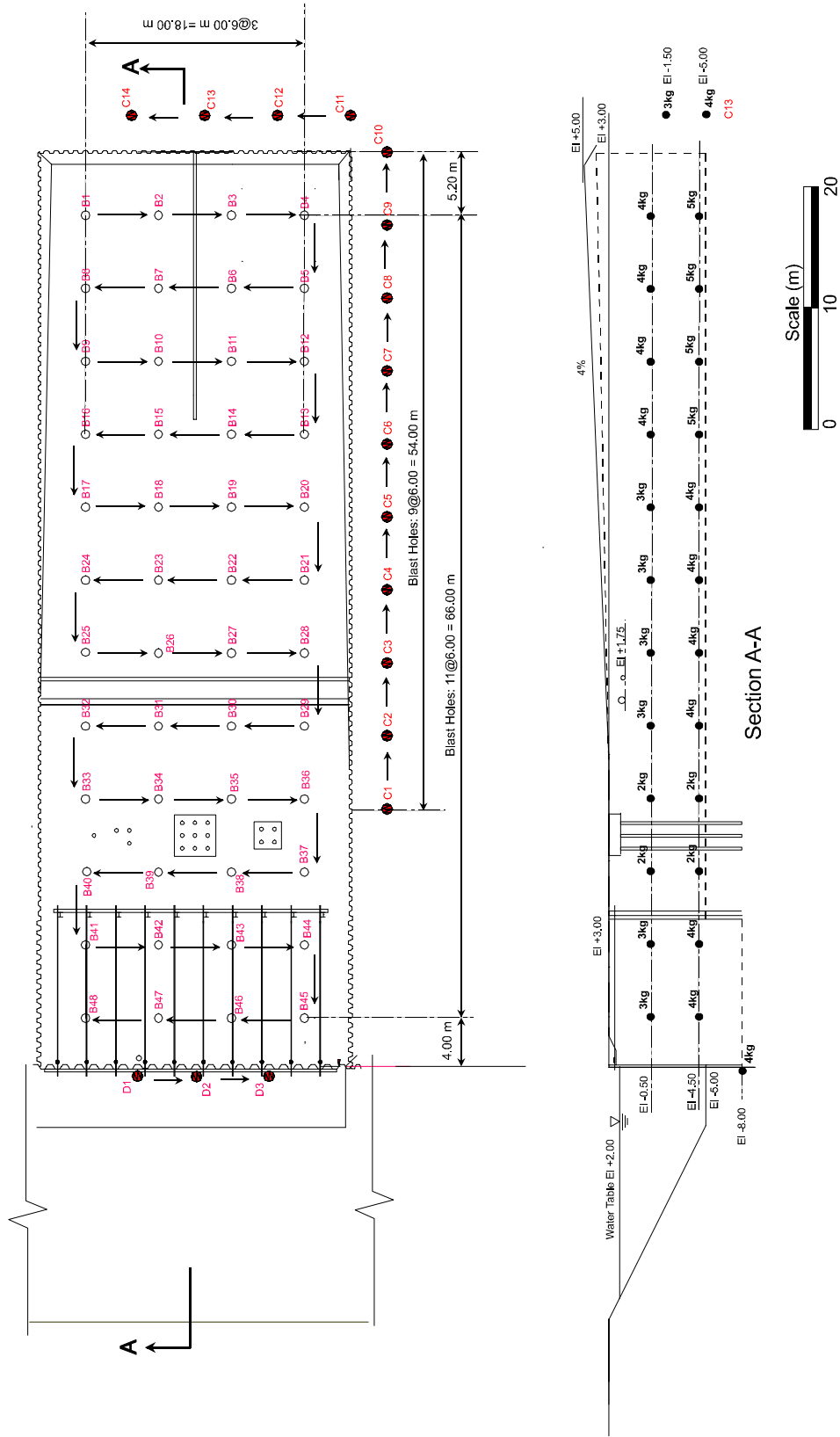
Figure 3.21   Locations of Blast holes and Blasting Sequence

4 Test Results of 1st Full-Scale Lateral Spreading Experiment

In this chapter, preliminary test results of the 1st full-scale lateral spreading experiment using controlled blasting are presented. For each test specimen, the results of strain gauges as well as the excess pore pressures nearby each specimen are presented and discussed. Then, the results of other instruments will be presented separately for comparison purposes. Furthermore, the overview of site condition after the test as well as the results of surveying after the test is described. It is noted that time at 0 second presented in each plot associated with the initiation of the blast.

4.1 Single Pile

The time-history of strain of a single pile at various depths are presented in Figure 4.1 and Figure 4.2. Figure 4.3 presents the strain profile at time of 70 seconds, which can be considered as the residual strain after the lateral spreading occurred. It is noted that most strain gauges on back side of the single pile, as well as a series of tiltmeters, were damaged during the pile installation. The test results indicate that the strains at depths between 0 and 4 meters were insignificant implying that the resultant force acting on the pile for the first 4 meters was negligible. This can be explained in a number of ways. One of possible explanations on this phenomenon is that after the soil was liquefied, it becomes to behave like viscous fluid material being able to flow around the pile without significant force acting on the pile on the first 4 m of loose sand. The soil resistance began to increase with depth for the next 3.5 m where very soft clay layer existed. The maximum strain occurred in a dense soil layer at depth about 9 m below the ground surface.

To determine the moment along the length of the pile, the section analysis was first performed to calculate the moment-curvature relationship of the steel pipe pile using UCFyber, a finite element program from section analysis. Assuming the bilinear stress-strain relationship for the steel, the moment-curvature relationship of the steel pipe pile is

presented in Figure 4.4. The pile curvatures were calculated from the strain gauge data using the following equation:

$$\phi = \frac{\varepsilon_t - \varepsilon_c}{h} \tag{4.1}$$

where ϕ is curvature, ε is strain, t and c denote tension and compression, respectively, and h is distance from both strain gauges. However, if one of both strain gauges was damaged, the following expression was used.

$$\phi = \frac{\varepsilon}{d} \tag{4.2}$$

where d is the distance of strain gauge from neutral axis.

The moment was calculated by multiplying the flexural rigidity of the pile with the curvature data. Figure 4.5 shows the moment distribution of the pile indicating that maximum moment was approximately 67% of yield moment of the section.

Figure 4.6 and Figure 4.7 present excess pore pressure ratio responses at different depths nearby the single pile for durations of 100 seconds and 1hour, respectively. The excess pore pressure ratios were calculated by assuming a total soil unit weight of 16 kN/m^3 and the water table at 1 m below the ground surface. It shows that the excess pore water pressure ratios had built up since the blast was initiated and reached the maximum values at about 30 seconds following the blast. Both transducers show excess pore pressure ratio reaching 100%. The excess pore pressure ratio fluctuated more as the blasting moved closer to the transducers. After the completion of blasting, the excess pore water pressure dissapated with time. The excess pore pressure ratio immediately after the completion of the blast ranged from 80% to 90%, and then dropped to about 50% to 60% one hour following blasting.

4.2   4-Pile Group

Two piles of a 4-pile group, denoted as No.7 and No.8, were instrumented with strain gauges. A series of tiltmeters were also installed along the length of the pile No.7.

Unfortunately, the tiltmeters were damaged during the pile installation because the sensors could not resist strong vibration during driving of the pile. Most of strain gauges on the back side of the pile No.7 were also damaged. The results of strain gauge of each pile at various depths are presented in Figure 4.8 through Figure 4.11. The residual strain profiles of pile No.7 and No.8 are presented in Figure 4.12 and Figure 4.13, respectively. For pile No.8, the strains on both sides along the pile were reasonably symmetric indicating the consistency of strain gauge data. The moment distribution of each pile was estimated as presented in the in Figure 4.14 and Figure 4.15. The shape of moment profile from the experiment agreed well with a typical analysis of a pile with fixed head condition showing that the results from the test were reasonable and appropriate for further analysis to estimate the pressure distribution of liquefiable soil on the pile. The maximum moment of both piles occurred in a dense soil layer at a depth of 9 m below the ground surface with ranging in magnitude from 180 to 245 kN-m for pile No.7 and No.8, respectively. The ratios of maximum moment to yield moment were 0.35 to 0.47 which were less than those occurred in the single pile.

The results from pore pressure transducers nearby the 4-pile group are presented in Figure 4.16 and Figure 4.17. The excess pore pressure ratios reached the peak at about 30 seconds after the blast detonated ranging in values from 80% to more than 100%. This indicates that the soil was liquefied in this neighborhood. The excess pore pressure ratio had dropped to between 50% and 100% just after the completion of the blast and proceeded to drop to between 40% and 65% one hour after the blast.

4.3   9- Pile Group

A total of 6 piles in a 9-pile group were instrumented with strain gauges. The results of strain gauges on each pile at different depths are presented in Figure 4.18 through Figure 4.29. Furthermore, the strain profile of each pile at the time about 70 seconds after the blast initiated is also presented in Figure 4.30 through Figure 4.35. It is noted that the strain gauge on the back side of the pile No. 4 as well as the tiltmeters were damaged during pile installation. Similar to the results of the 4-pile group, the strain

gauge profiles on the front and back sides of each pile were symmetric showing that the strain gauge data obtained from the test were reliable.

The moment distribution of each pile calculated from strain gauges data is presented in Figure 4.36 through Figure 4.41.   It is observed that the moment distribution of all piles in the group was more or less similar except for pile No. 2 and No.4 where the moments were smaller than the others. This is likely due to the fact that both piles were shorter in length and thus the degree of fixity into the dense soil layer was less, resulting in smaller moment developed in the piles. The maximum moment of the piles occurred at depths about 9m below the ground surface with ranging in magnitude from 60 to 230 kN-m, corresponding to about 12% to 44% of the yield moment.   The moment distributions occurred in the piles of the 9-pile group were comparatively similar to those measured in the 4-pile group. Data from GPS units which will present in later section also show that the movement of the 4-pile group and the 9-pile group were similar. These similar measurements of the pile groups support that the moment distribution occurred for both pile groups should also be comparable.

The results of excess pore pressure ratios nearby the 9-pile group at various depths are presented in Figure 4.42 through Figure 4.45.   The excess pore water pressure ratios started to build up immediately after the blast. The rate of increase in pore water pressure become more rapidly as the blast moved closer to the transducers. The increased in pore water pressure ratios proceeded to reach the maximum values at approximately 30 seconds after the blast and then continued to drop with time. Again, the results show that the soil in the vicinity of the 9-pile group was liquefied with the maximum excess pore pressure ratios exceeded 100%.   The excess pore pressure ratios dropped to between 50% and 90% one hour after the blast.

4.4   Gas Pipeline in Transverse Direction (Pipeline A)

The strain gauge data along transverse gas-pipeline (pipeline A) are presented in Figure 4.46 and Figure 4.47. The profiles of strain gauge on the top and the side of the pipeline are shown in Figure 4.48. Unlike the data of pile foundation systems, the strain

data of pipeline were somewhat irregular from what we expected (i.e., the maximum strain occurs at the mid span of the pipeline.). This is probably due to the fact that the pipeline was subjected to non-uniform soil pressure along its entire length produced by the compression wave from the blasting which likely to produce inconsistent pressure distribution by its nature. Due to the irregularity of strain gauge data, the moment distribution along the pipeline was not computed at this time, but will be further investigated once additional data from other researchers becomes available.

Figure 4.49 and Figure 4.50 present the data from pore pressure transducers installed between the middle of the pipeline A and B in multiple depths.   Similar characteristics of response of excess pore pressure ratio were observed as those transducers for the pile foundation systems.   However, the excess pore pressure ratio reached the maximum values at about 20 seconds, which was 10 seconds earlier than those transducers installed in the vicinity of pile foundation. This is because the blasting occurred in the vicinity of pipelines sooner than that of pile foundation system.   Both transducers show maximum excess pore pressure ratio exceeding 100% over 100 seconds showing that soil in this region was liquefied during the test.   The excess pore pressure ratio then dropped below 80% one hour following blasting.

4.5   Electrical Conduit in Transverse Direction (Pipeline B)

The strain data along a transverse electrical conduit are presented in Figure 4.51 and Figure 4.52. The profile of strain gauge on the top and the side of the pipeline are shown in Figure 4.53. The data are somewhat irregular similar to the results of pipeline A, and will require further analysis once more data is available.. The possible reason as mentioned in previous section can be applied to explain the irregularity of the results. It is observed that strain distribution along the side of the electrical conduit was larger than that of the gas-pipeline. This is because both pipelines had the same magnitude of movement (This refers to the GPS data which will mention in the later section of this chapter) which implied that the distribution of curvature was approximately no different;

therefore, larger diameter pipeline produced larger strain.   The excess pore pressure ratios nearby this pipeline were already discussed in the previous section.

4.6   Gas-Pipeline in Longitudinal Direction (Pipeline C)

The responses of strain gauges along longitudinal gas pipeline are presented in Figure 4.54 through Figure 4.56. The profiles of strain gauges on the top, side, and bottom of the pipeline are shown in Figure 4.57.   Again, the results were not the same as what we expected. The strain along the side where it was intended to measure the axial strain distribution should have the maximum strain at the support and zero strain at the end if the soil flowed parallel to the direction of the pipeline. However, the measured strain distribution shows that the maximum moment occurred at about the middle of the pipeline. This is because the actual blasting energy produced not only the movement parallel to the pipeline but also perpendicular to the pipeline. In this particular case, the movement mainly occurred in the direction perpendicular to the pipeline. This was observed from the evidence of a relative large movement of sheet pile wall on one side of the embankment as presented in Figure 4.58. The measurements from GPS data also confirmed that the movement in this vicinity was mainly perpendicular to the flow direction.

The excess pore pressure responses at various depths in the vicinity of the pipeline C are presented in Figure 4.59. The excess pore pressure built up immediately after the blast initiated and reached the maximum values at about 10 seconds. The maximum excess pore pressure ratios ranged from 80% to over 100 % showing that the soil nearby the pipeline was liquefied. Just after the blast ceased, the pore water pressure ratios decreased to between 60% and 80%. The ratios dropped to 35% to 60% one hour after the blast.

4.7   Results of Other Instruments

Other instruments that were installed far away from the test specimens or inappropriate to include in the above sections are discussed here. This includes the pore

pressure responses in the free field region, data from soil pressure cells, the accelerations and rotations of the pile head, soil displacement profiles from the inclinometer readings, relative movement between soil and lifeline utilities using linear potentiometers, and the real-time movements of lifeline utilities and near field from the GPS units. The details of test results are discussed below.

The excess pore pressure data distributed throughout free field region were presented in Figure 4.61 and Figure 4.64. The excess pore pressure ratio built up and reached their peaks at time between 5 to 15 seconds, depending on the locations of the transducers. The closer to the back corner of the embankment where the blasting was first initiated, the sooner reaching the maximum excess pore water pressure. Pore water pressure ratios obtained from all the transducers in the free field were relatively larger than those in the vicinity of pile specimens due to the larger amount of explosives used in this zone. The excess pore water pressure ratios exceeded 100%. One hour after the blast, the excess pore pressure ratios dropped to between 50% and 90%. Several sand boils were observed confirming that using the controlled blast could successfully induced the liquefaction throughout the test area.

The data of soil pressure cells on the pile caps of the 4-pile group and the 9-pile group are presented in Figure 4.65. The locations of soil pressure cells are given in the previous chapter. The data seems to be not consistent. The soil pressures acting on the pile caps appeared to be relatively small with the average magnitude of less than 5 kN/m^2.

The results from accelerometers and tiltmeters at the pile head are presented in Figure 4.66 and Figure 4.67, respectively. The acceleration at the pile head due to the effect of blasting decreased with increasing the foundation stiffness with the acceleration being highest for the single pile and lowest for the 9-pile group. The results from tiltmeters show that the pile head rotation of the single pile (free head condition) at the end of the test was approximately 2 degree, while the rotation of the 9-pile group (fixed head condition) was insignificant. It is noted that the tiltmeter installed on the 4-pile group was damaged.

Profiles of soil displacement obtained from the inclinometer readings after the completion of the blast test are presented in Figure 4.68 through Figure 4.78. The results indicated that the maximum movement of the soil occurred at the ground surface as expected. The displacements obtained from inclinometer data were slightly less than the actual soil displacement (i.e., compared to GPS data) because an absolutely fixed boundary condition at the tip of the casing was assumed to compute the soil displacement profile. In fact, some movement of inclinometer casings at the tips might occur resulting in underestimating the soil displacements. The summary of the movement at the ground surface of each location are summarized in Table 4.1. The movement of the soil ranged approximately from 18 to 41 cm with the average values of 30 cm. It is noted that the fiber optic displacement arrays which were installed to measure the real times soil displacement were all damaged due to the effect of blasting.

The results of string activated linear potentiometers are presented in Figure 4.79 through Figure 4.81. A summary of relative movement between two points of interest after the blast is given in Table 4.2. According to the measurements, it can be observed that the movement of single pile (No.9) and the soil in front of the pile is approximately the same, while the movements of the Waseda single piles were more than the soil. This might be due to the fact that the Waseda piles were sit just above the dense layer; while the UCSD pile was penetrated 3 meters into the dense layer. The Waseda piles were therefore likely to behave like a rigid pile in which the rotation and movement at the pile tip were expected. In contrast, the UCSD pile behaved more like a flexible pile where the rotation and the movement at the pile tip was insignificant. Therefore, the displacement at the pile head of the UCSD single pile was less than those of the Waseda piles. As expected, the soil in front of and behind the pile groups moved approximately 8 to 15 cm more than the pile groups. It is noted that there might be some small error on the measurements due to the uplift of slope inclinometer casing as remarked in Table 4.2.

The displacement time histories from GPS units installed at several locations on the ground surface as well as on lifeline utilities are presented in Figure 4.82 through Figure 4.97. The data of 4 Caltrans' GPS units loss during the critical blasting period due

to intermittent GPS antenna interference and wireless communications loss (Turner 2002). One of Waseda GPS units (GPS-5) out of 10 was not working during the test. Displacements in longitudinal, transverse, and vertical directions obtained from Caltrans' GPS units at one minutes and 22 hours following blasting are summarized in Table 4.3 and Table 4.4, respectively. No horizontal creep was observed over 22 hours following blasting. Most of the horizontal displacement associated with the lateral spreading took placed within tens of seconds following the blast. However, the data revealed that the maximum settlement of 10 cm was observed over an extended period of time as the pore water pressures dissipated. Ground surface displacements in the vicinity of embankment soil were monitored using WU's GPS units. A summary of the movements of the embankment soil at 30 minutes following the blast is given in Table 4.5. The vector displacements in horizontal plane throughout the test site are presented in Figure 4.98. The largest horizontal displacement was about 0.55 m occurring at a group of Waseda free head piles. The data from the GPS units in the vicinity of the pipelines show that the movements of the gas pipeline and electrical conduit were similar. Surprisingly, data from 2 GPS units showed a significant movement of an embankment soil perpendicular to the expected flow direction. This is because the soil in the applied seismic test site adjacent to the embankment soil was liquefied causing a significant decrease in lateral confinement in transverse direction comparatively to the flow direction where the soil was not liquefied yet.

The displacement measurements from GPS units were verified against linear potentiometer measurements in two locations. One of them was the relative displacement between the single pile (GPS-1D) and slope inclinometer casing S7 (GPS-1E). The other was the relative displacement between the 9-pile group and slope inclinometer casing S1. Table 4.1 presents comparisons of relative displacements obtained from GPS data and linear potentiometers data. Excellent agreement between measurements from GPS units and linear potentiometers were observed with the difference being within 1 cm, which is the accuracy typically associated with real time kinematics GPS methods. This confirmed the consistency of measurements using the GPS.

4.8   Overview of Site Condition after Testing

After the end of the test, the evidence of liquefaction (i.e., sand boils, water coming out from the ground, and ground settlement) were observed in many placed throughout the test area.   The sand boils were observed especially in the vicinity of blast holes and inclinometer casings where the water could escape from the ground easier than the other area due to appearance of gapping between soil and those casings.   Figure 4.99 through Figure 4.105 show general overviews of site condition after the test.

4.9   Survey of Movement after Testing

Prior to and after the test, the location of specimens, inclinometer casings, and many references on soil surface were measured to determine the relative movement of those in x, y, and z direction due to the global translation of the soil mass. Figure 4.107 presents the vector movement of soil and specimens as well as the settlement contour at the end of the test.

Table 4.1   Summary of Measured Soil Displacements at ground Surface from Inclinometer Results

Name	Displacement in A-Axis (m)	Displacement In B-Axis (m)	Total Vector (m)	Remarks
S1	-	-	-	Casing damaged.
S2	0.310	-0.059	0.315	
S3	0.233	-0.049	0.238	
S4	0.179	-0.031	0.182	
S5	0.413	-0.050	0.416	
S6	0.348	0.078	0.356	
S7	0.309	-0.057	0.314	
S8	0.242	-0.059	0.249	
S9	0.315	0.096	0.330	
S10	0.323	-0.021	0.324	
S11	0.307	0.025	0.308	
S12	0.236	0.165	0.288	

Table 4.2   Summary of Test Results from Linear Potentiometers

Name	Location	Relative movement (m)	Interpretation	Remarks
STP-1	9-pile group and Inc. S1 (upstream)	-0.096	Soil moved 96 mm more than pile.	
STP-2	9-pile group and Inc. S2 (downstream)	+0.144	Soil moved 144 mm more than pile.	
STP-3	Single pile and Inc. S7 (upstream)	+0.002	Soil and pile moved together.	
STP-4	4-pile group and Inc. S8 (upstream)	-0.080	Soil moved 80 mm more than pile.	S8 moved 0.3 m upward.
STP-5	Single pile (W1) and Inc. S11 (upstream)	+0.158	Pile moved 158 mm more than soil.	S11 moved 0.2 m upward.
STP-6	Single pile (W2) and Inc. S11 (upstream)	+0.074	Pile moved 74 mm more than soil.	S11 moved 0.2 m upward.
STP-7	Single pile (W1) and Single pile (W3)	+0.008	Both piles have the same movement.	
STP-8	4-pile group and anchor pile	+0.170	Anchor pile moved more than soil.	
STP-9	Anchor pile and quay wall	+0.347	Quay wall moved more than anchor pile.	

Note: Refer to Figure 3.18 for a better understanding of the relative movements.

Table 4.3   Summary of Caltrans' GPS Data, approximately 1 Minute Following Blasting

| Location | Displacement (m) | | | Horizontal Displacement (m) (x-y plane) | Angle to Flow Direction (Degree) |
	Longitudinal (x)	Transverse (y)	Vertical (z)		
1A					
1B					
1C	0.341	-0.023	-0.001	0.341	3.88
1D	0.364	0.005	0.006	0.364	-0.78
1E					
2A	0.214	-0.037	0.014	0.217	9.79
2B					
2C	0.552	-0.016	0.010	0.552	1.68
2D	0.367	-0.080	-0.011	0.376	12.36
2E	0.368	-0.093	-0.043	0.380	14.24

Table 4.4   Summary of Caltrans' GPS Data, approximately 22 Hours Following Blasting

| Location | Displacement (m) | | | Horizontal Displacement (m) (x-y plane) | Angle to Flow Direction (Degree) |
	Longitudinal (x)	Transverse (y)	Vertical (z)		
1A	0.176	-0.042	0.014	0.181	13.39
1B	0.282	-0.025	0.032	0.283	5.11
1C	0.331	-0.018	-0.090	0.332	3.08
1D	0.350	0.005	0.008	0.350	-0.86
1E	0.338	-0.003	0.026	0.338	0.51
2A	0.209	-0.035	0.005	0.212	9.42
2B	0.343	-0.088	-0.091	0.354	14.45
2C	0.547	-0.012	0.012	0.547	1.28
2D	0.362	-0.078	-0.111	0.371	12.18
2E	0.372	-0.096	-0.128	0.384	14.49

Table 4.5   Summary of WU s' GPS Data, approximately 30 Minutes Following Blasting

| Location | Displacement (m) | | | Horizontal Displacement (m) (x-y plane) | Angle to Flow Direction (Degree) |
	Longitudinal (x)	Transverse (y)	Vertical (z)		
1	0.332	-0.175	-0.072	0.375	27.79
2	0.389	-0.100	-0.045	0.402	14.41
3	0.347	-0.032	-0.005	0.348	5.27
4	0.314	-0.406	-0.246	0.513	52.28
5	--	--	--	--	--
6	0.337	-0.021	-0.171	0.338	3.56
7	-0.002	-0.590	-0.507	0.590	89.81
8	0	-0.302	-0.490	0.302	90.00
9	0.126	-0.001	-0.333	0.126	0.46
10	0.385	-0.169	-0.117	0.420	23.70

Table 4.6   Verification of GPS Measurements with Data from Potentiometers

GPS Location	Potentiometer Location	GPS Measurement (m)	Potentiometer Measurement (m)
GPS 1A - 1B	STP-1	0.106	0.096
GPS 1E -1D	STP-3	0.012	0.002
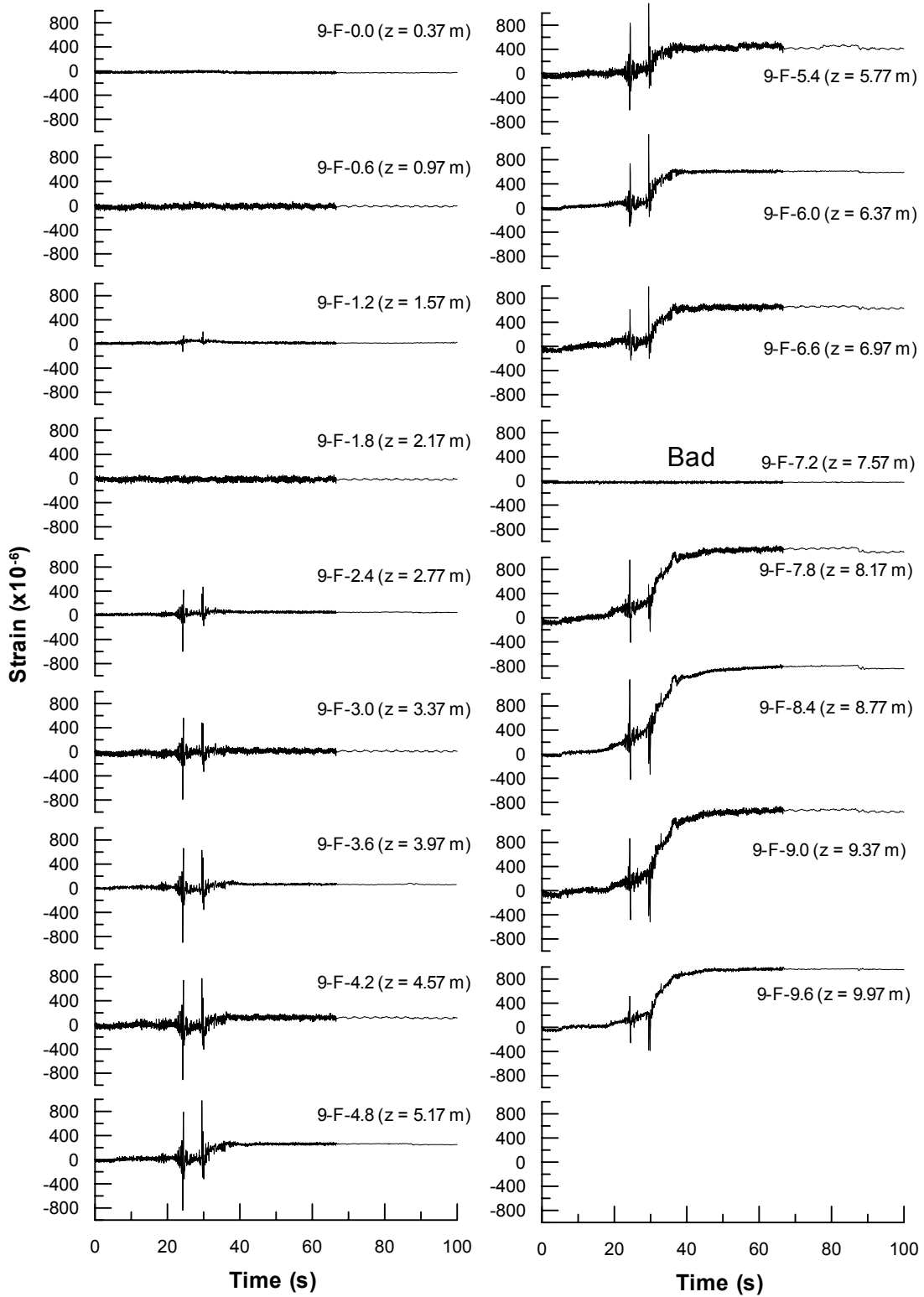
Figure 4.1　Strain Gauge Response along Single Pile (Pile No.9) at Front Side
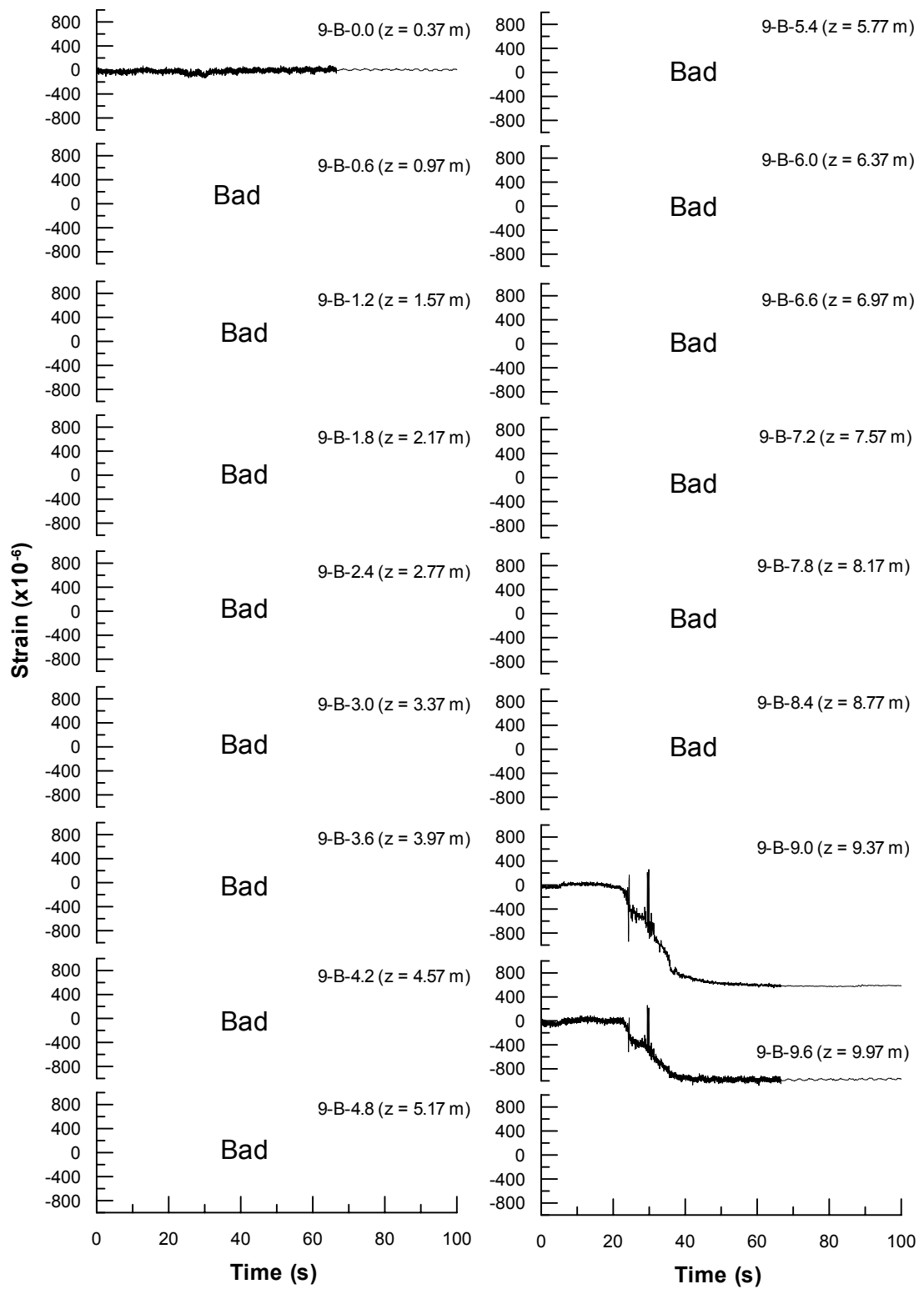
Figure 4.2   Strain Gauge Response along Single Pile (Pile No.9) at Back Side

Back   Front

9

Single Pile

Flow Direction

Front
Back

Strain (x10⁻⁶)

El +3.000

El +2.000

V. Loose
SAND

El -0.800

V. Soft
CLAY

9

El -4.300

Med. Dense
SAND

El -5.300

V. Dense
GRAVEL
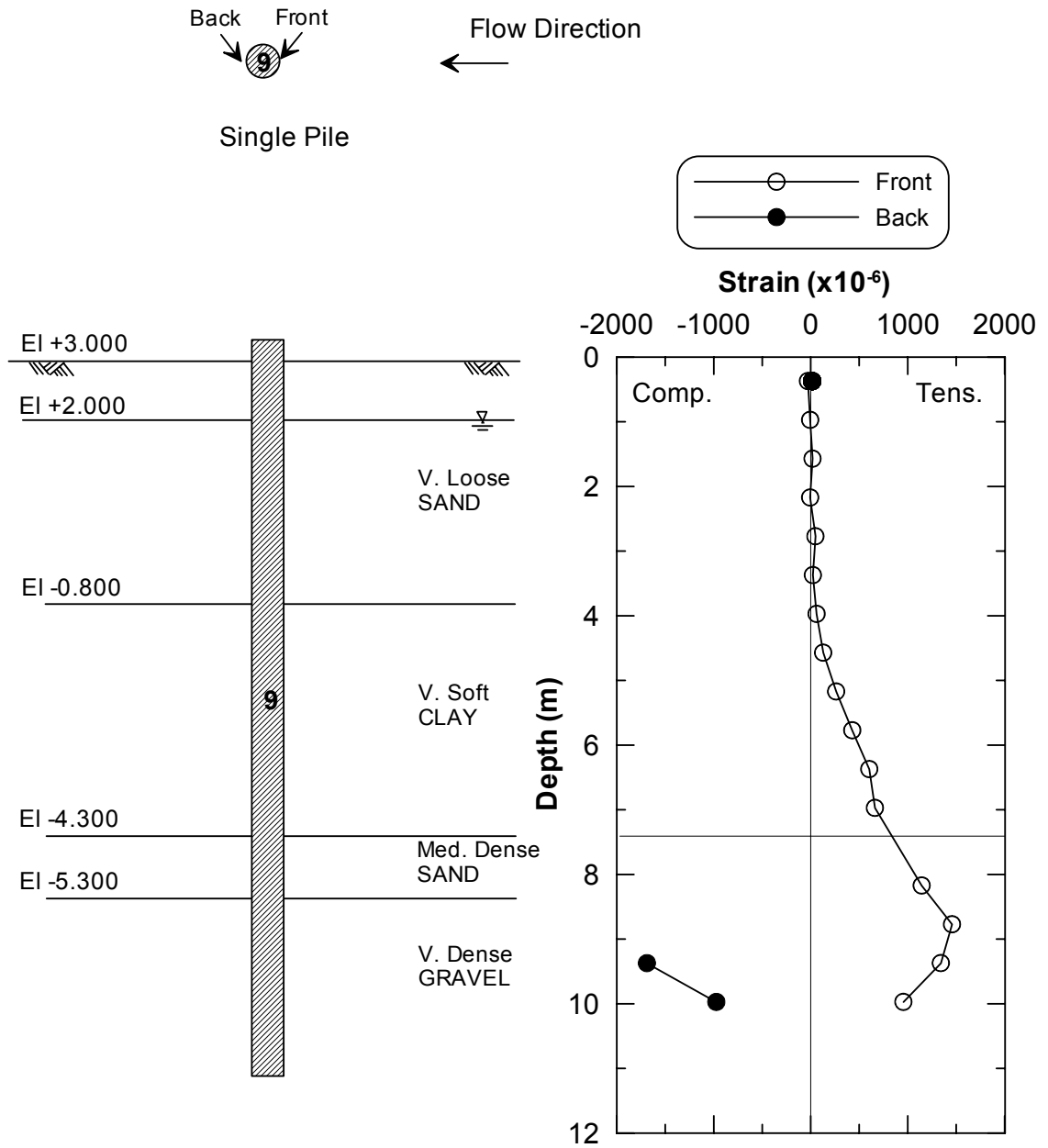
Figure 4.3   Profile of Residual Strain of Single Pile (Pile No.9) after Lateral Spreading
(t = 70s)

86
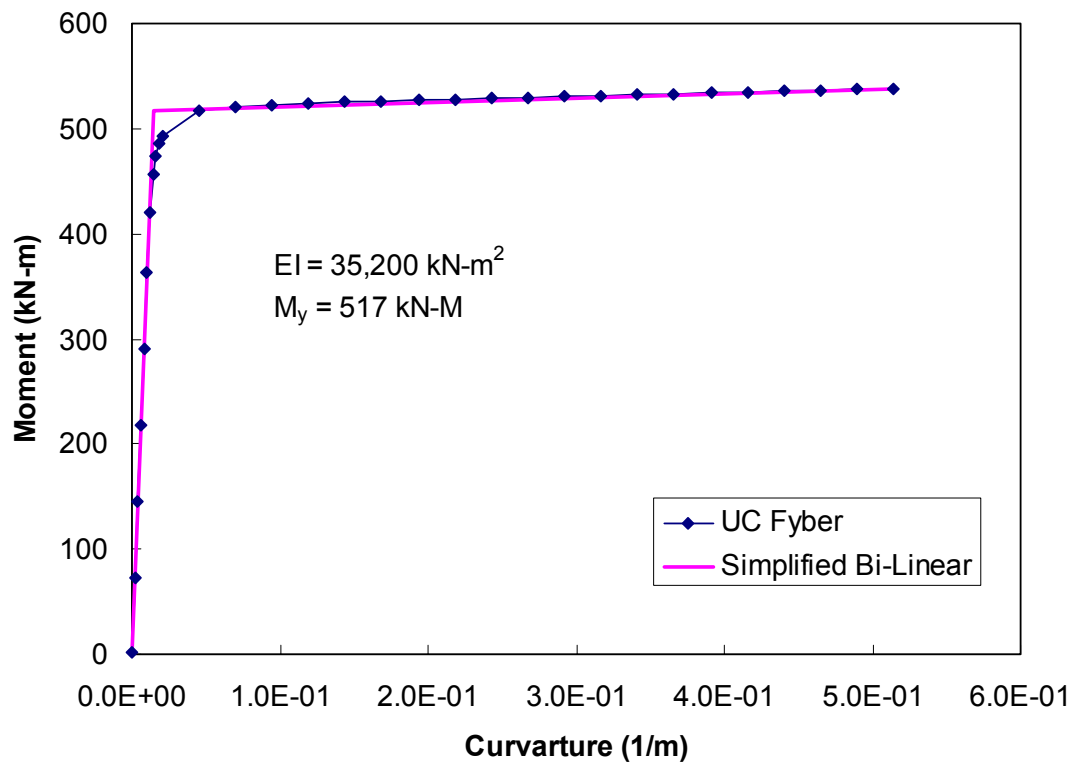
Figure 4.4   Moment-Curvature Relationship for Steel Pipe Pile

Back Front

Flow Direction

Single Pile

Moment (kN-m)
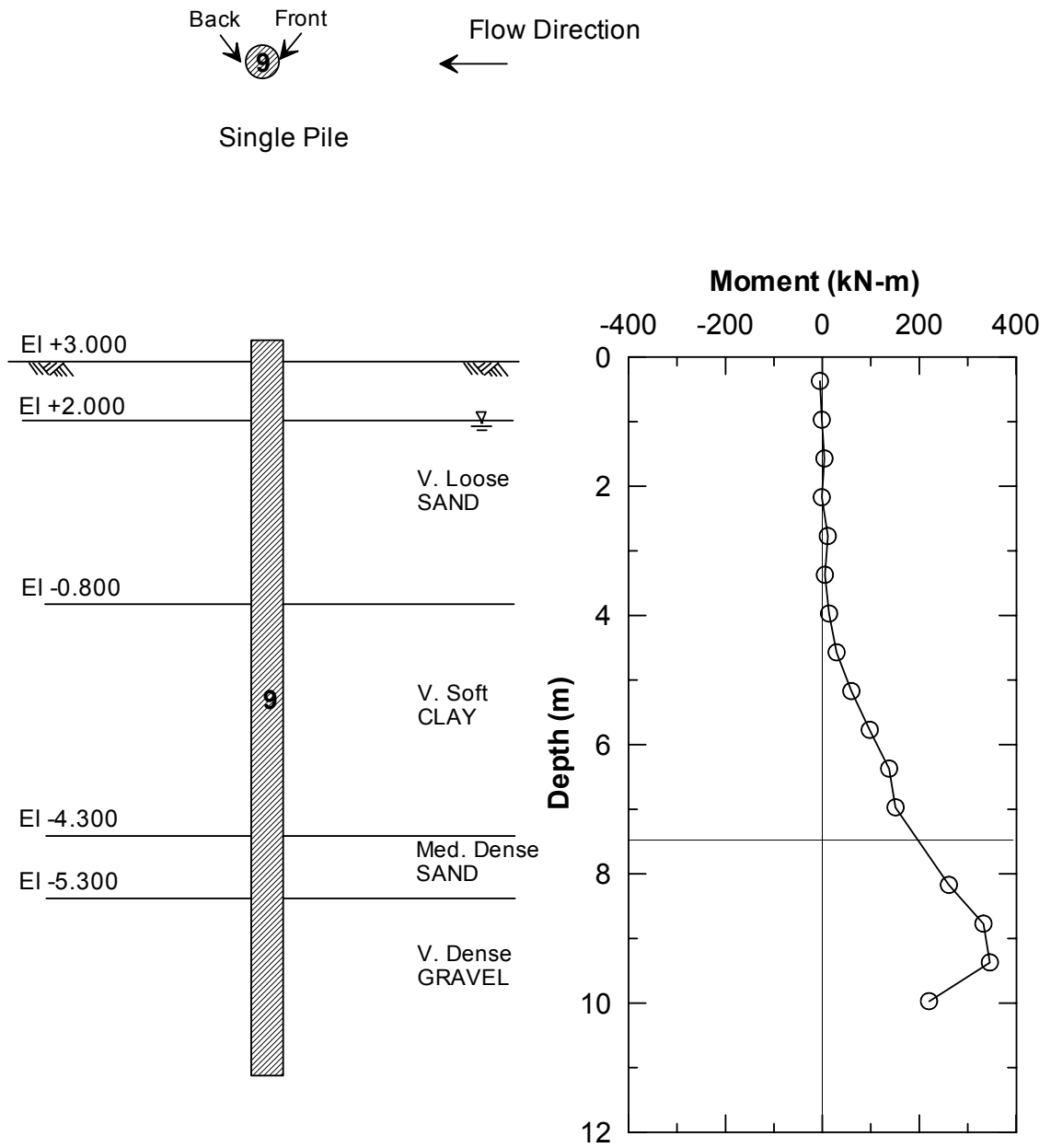
Figure 4.5   Moment Distribution along Single Pile (Pile No.9) after Lateral Spreading (t = 70s)
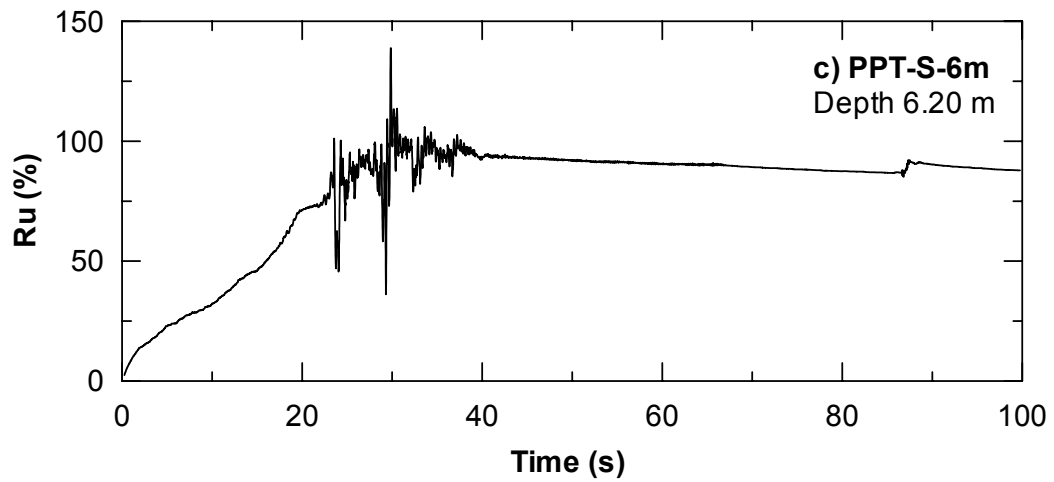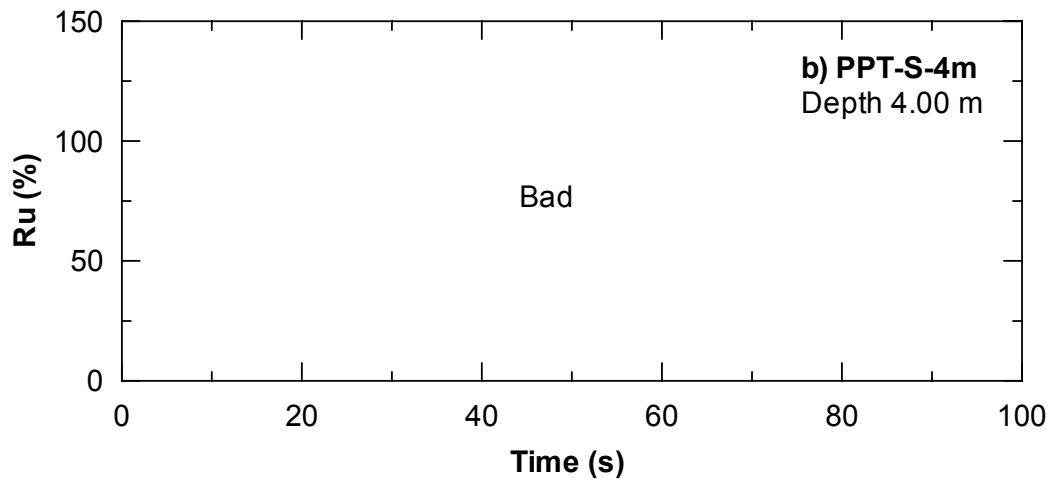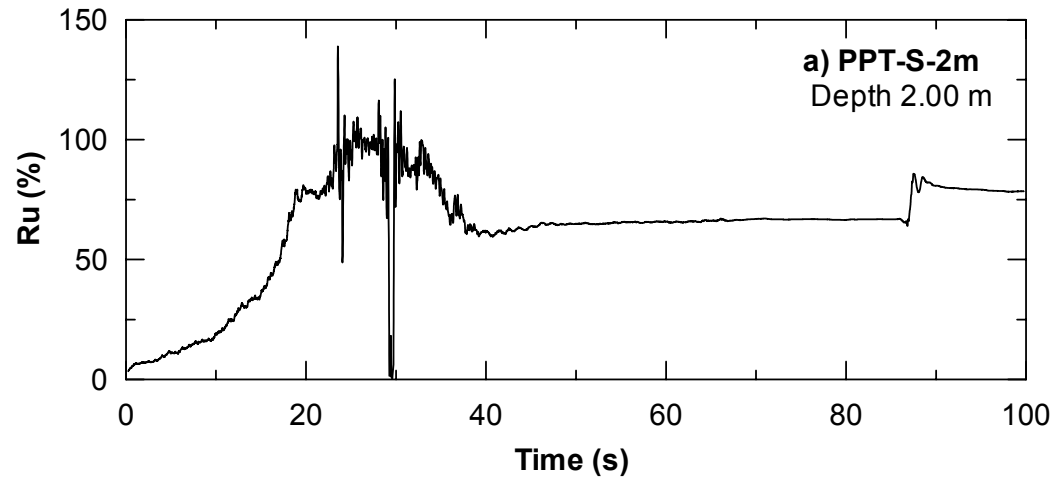
Figure 4.6   Excess Pore Water Pressure nearby Single Pile (a) PPT-S-2m, (b) PPT-S-4m, and (c) PPT-S-6m, 100s Duration
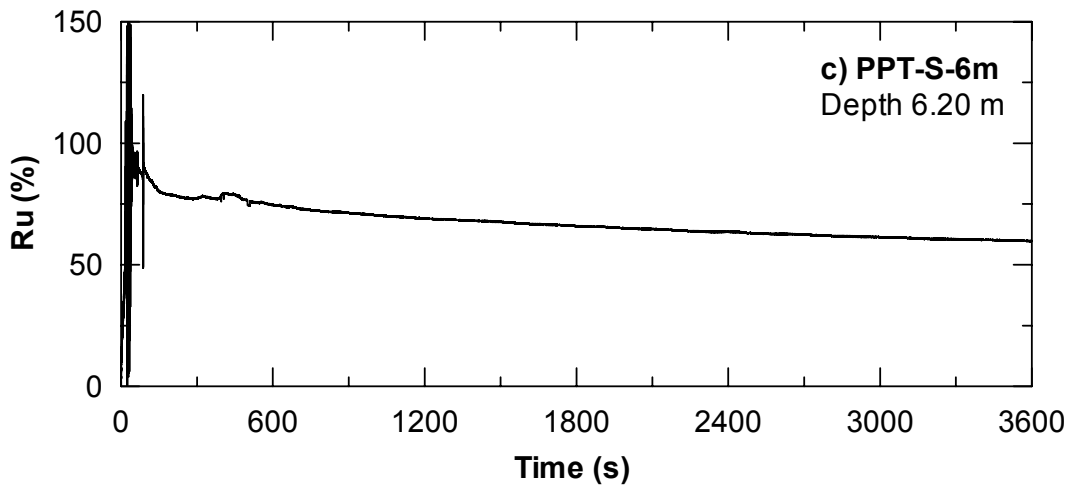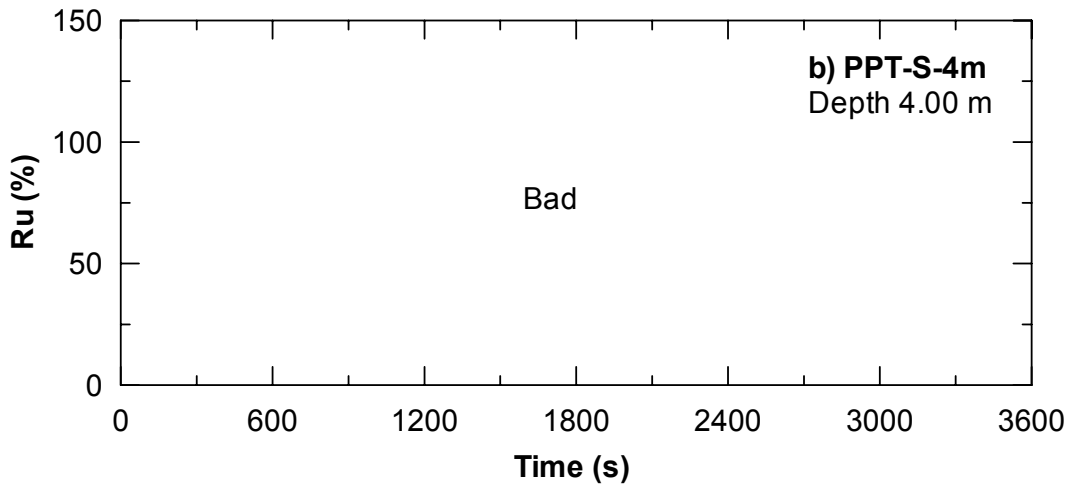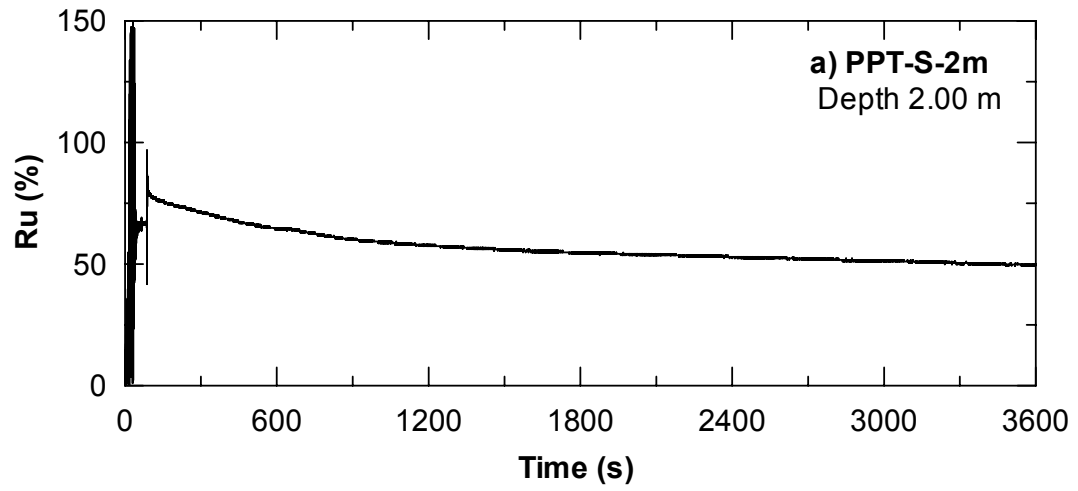
Figure 4.7   Excess Pore Water Pressure nearby Single Pile (a) PPT-S-2m, (b) PPT-S-4m, and (c) PPT-S-6m, 3600s Duration
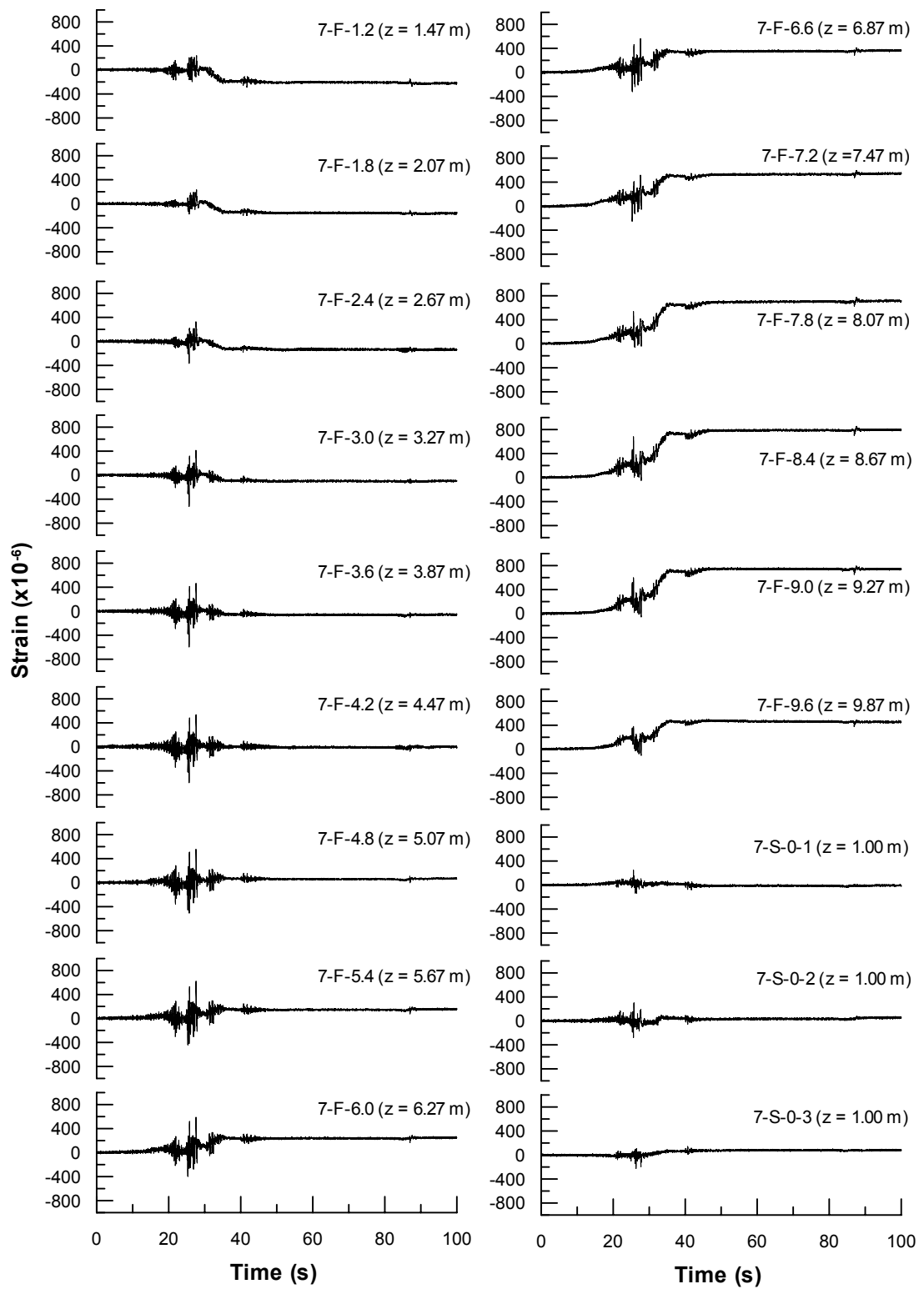
Figure 4.8   Strain Gauge Response along Pile No.7 (Front Side) of 4-Pile Group

91
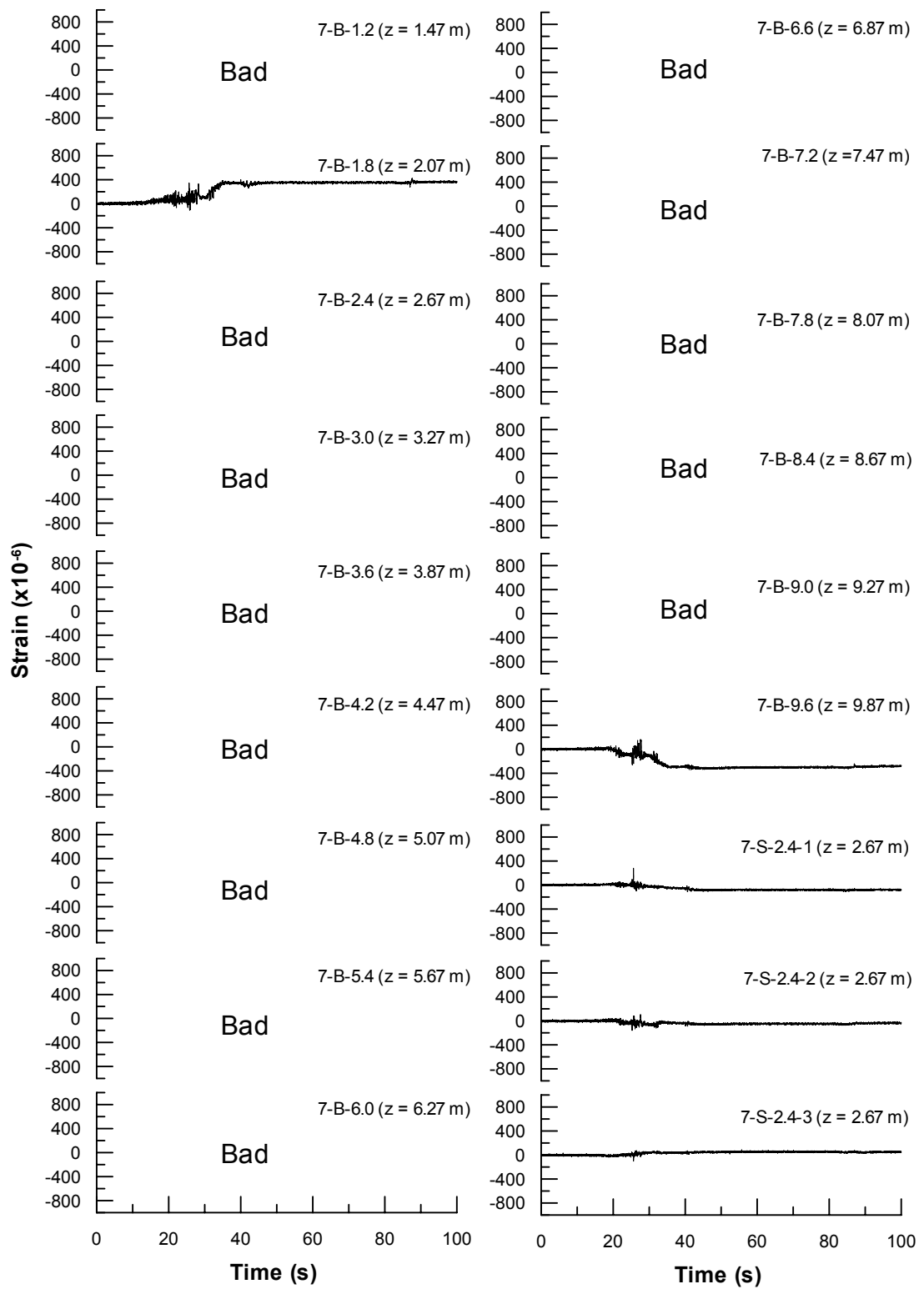
Figure 4.9   Strain Gauge Response along Pile No.7 (Back Side) of 4-Pile Group
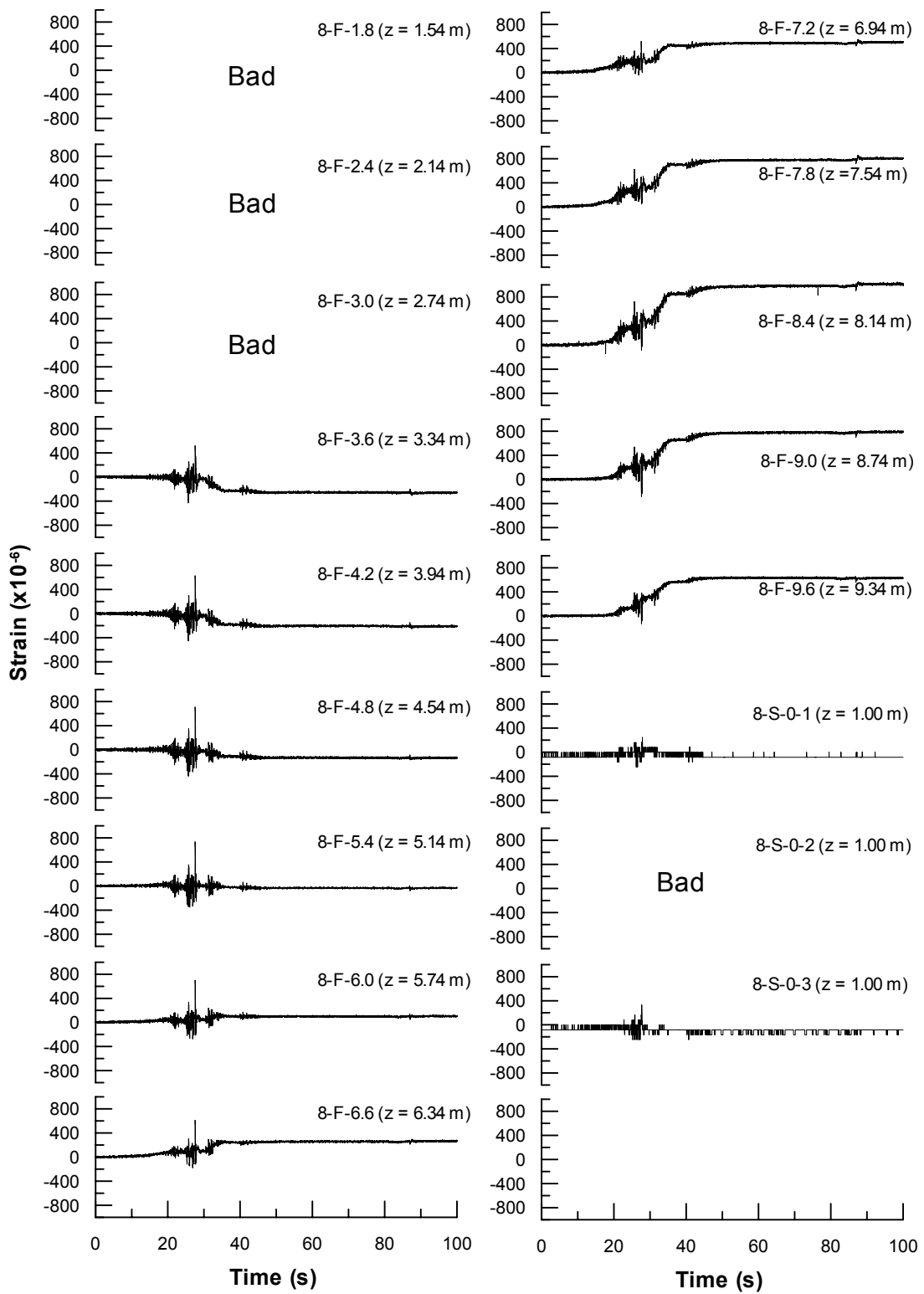
Figure 4.10   Strain Gauge Response along Pile No.8 (Front Side) of 4-Pile Group

93
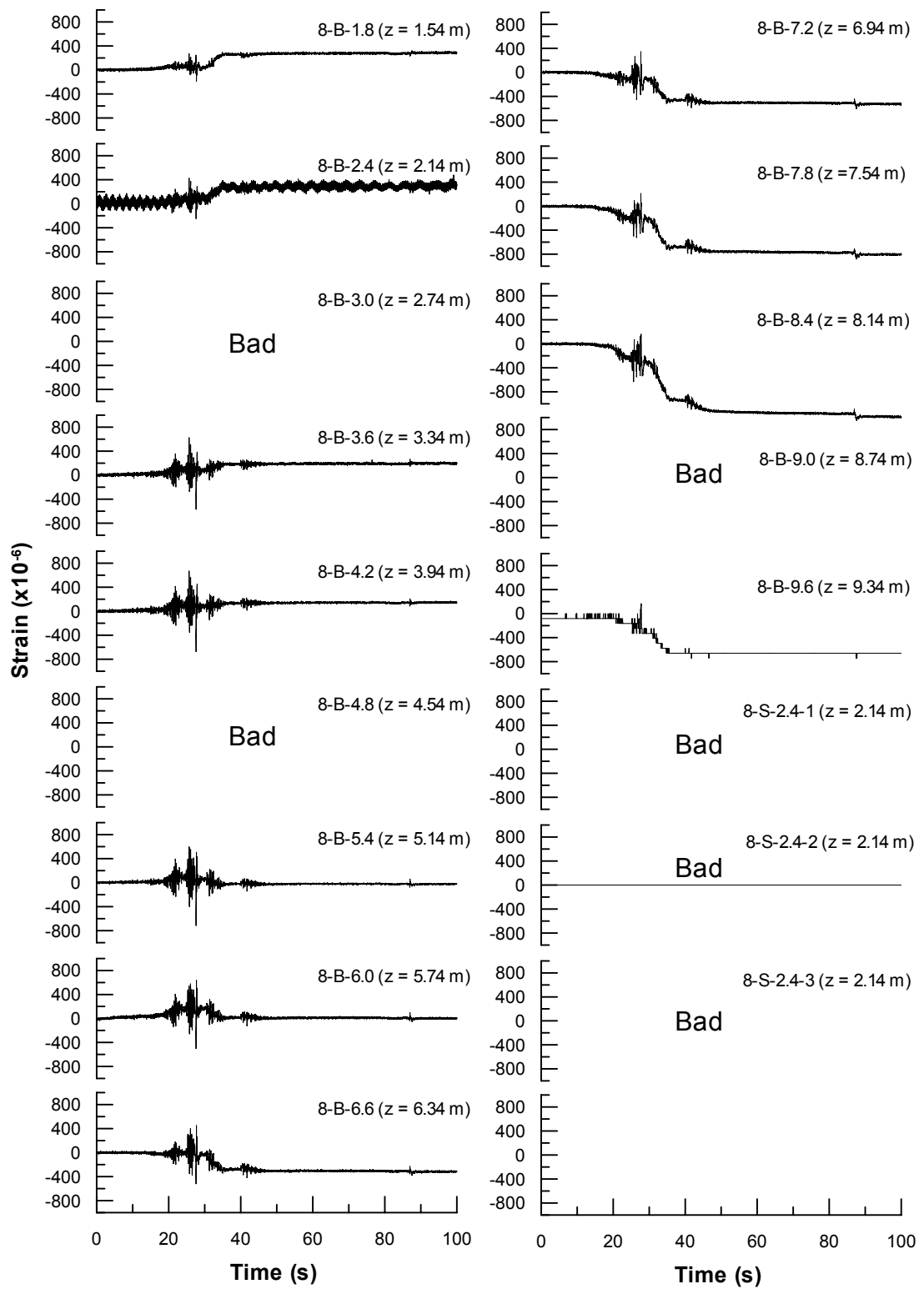
Figure 4.11   Strain Gauge Response along Pile No.8 (Back Side) of 4-Pile Group

94
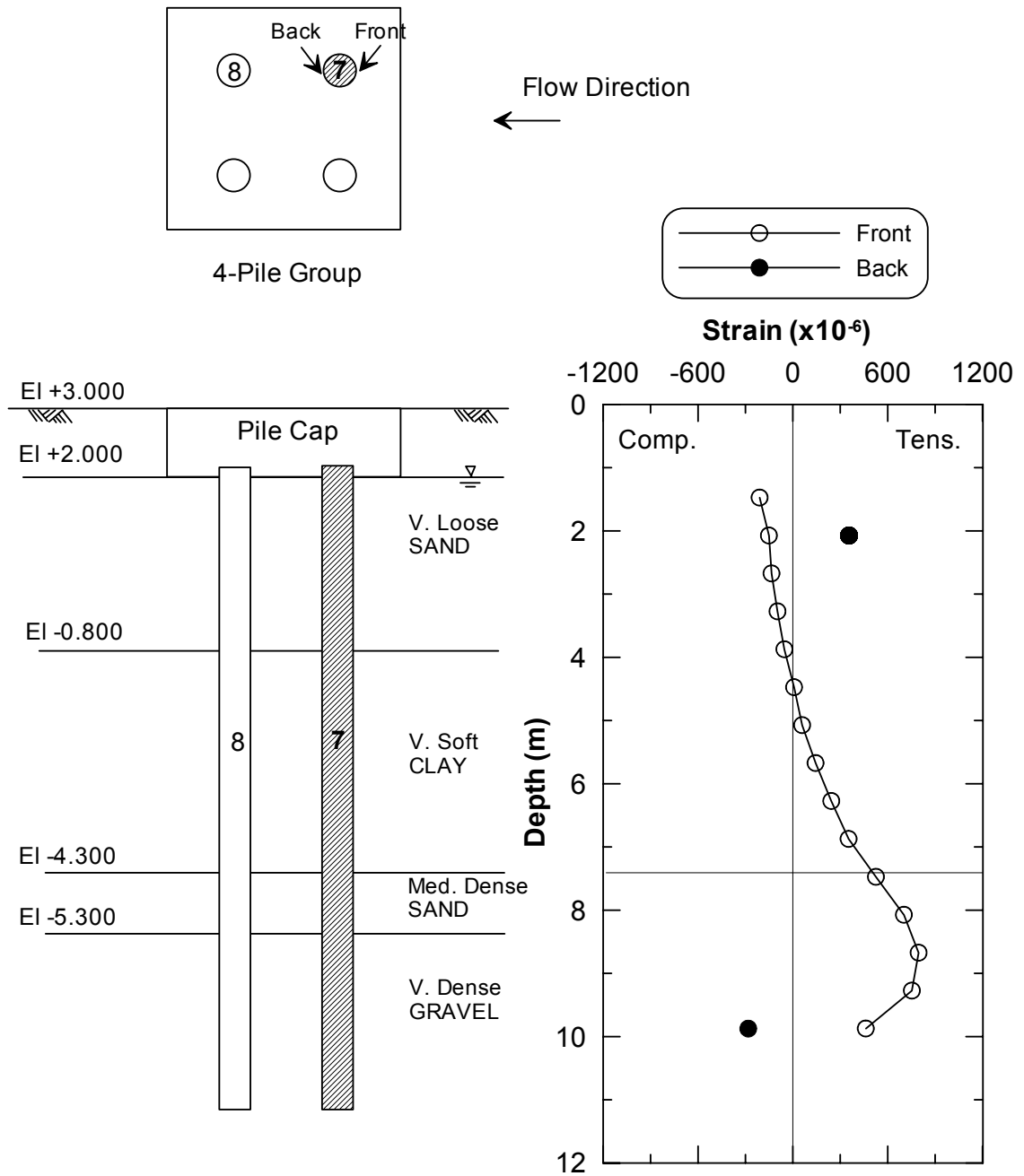
Figure 4.12　Profile of Residual Strain of Pile No.7 of 4-Pile Group after Lateral Spreading (t = 70s)
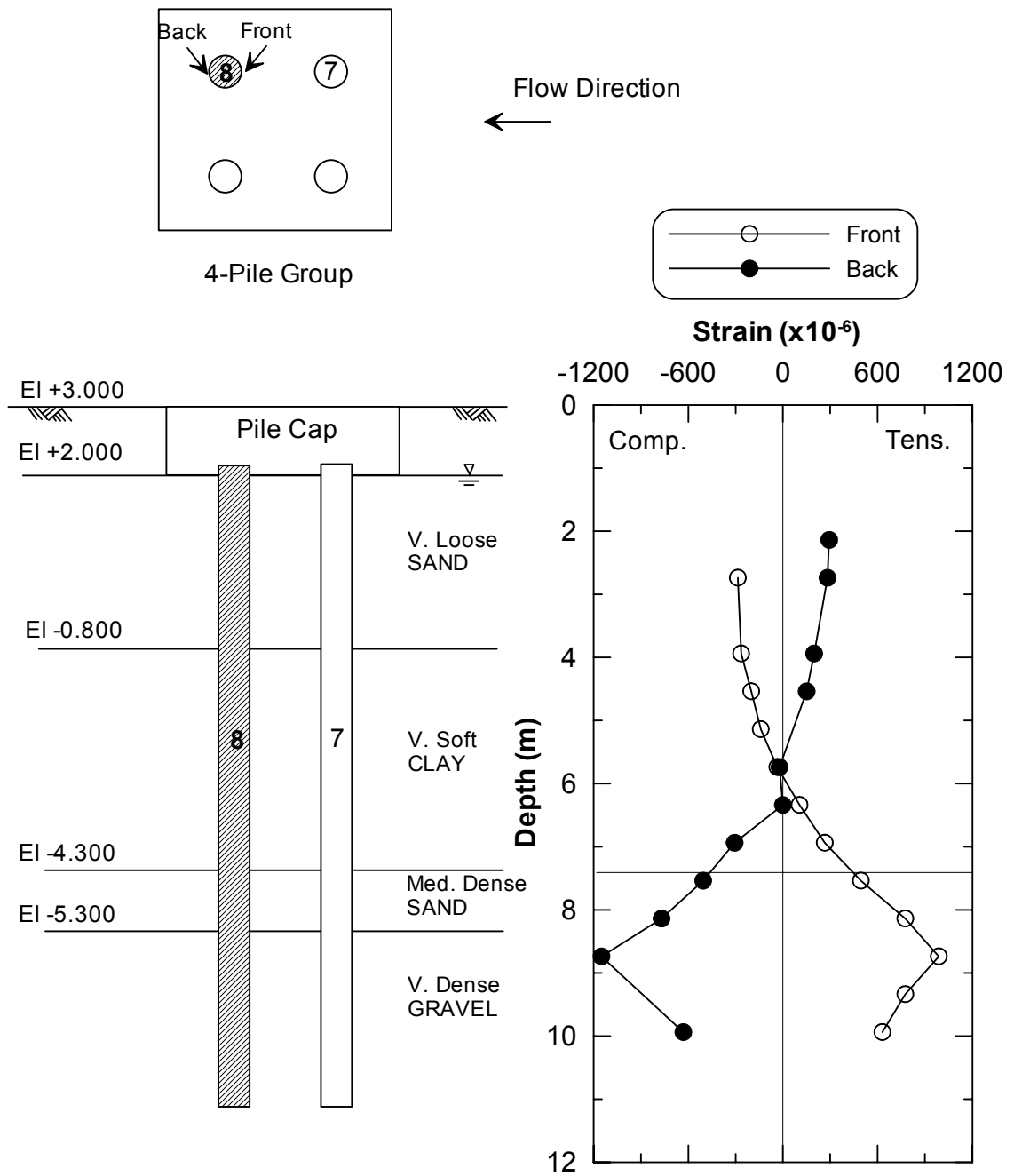
Figure 4.13   Profile of Residual Strain of Pile No.8 of 4-Pile Group after Lateral
Spreading (t = 70s)
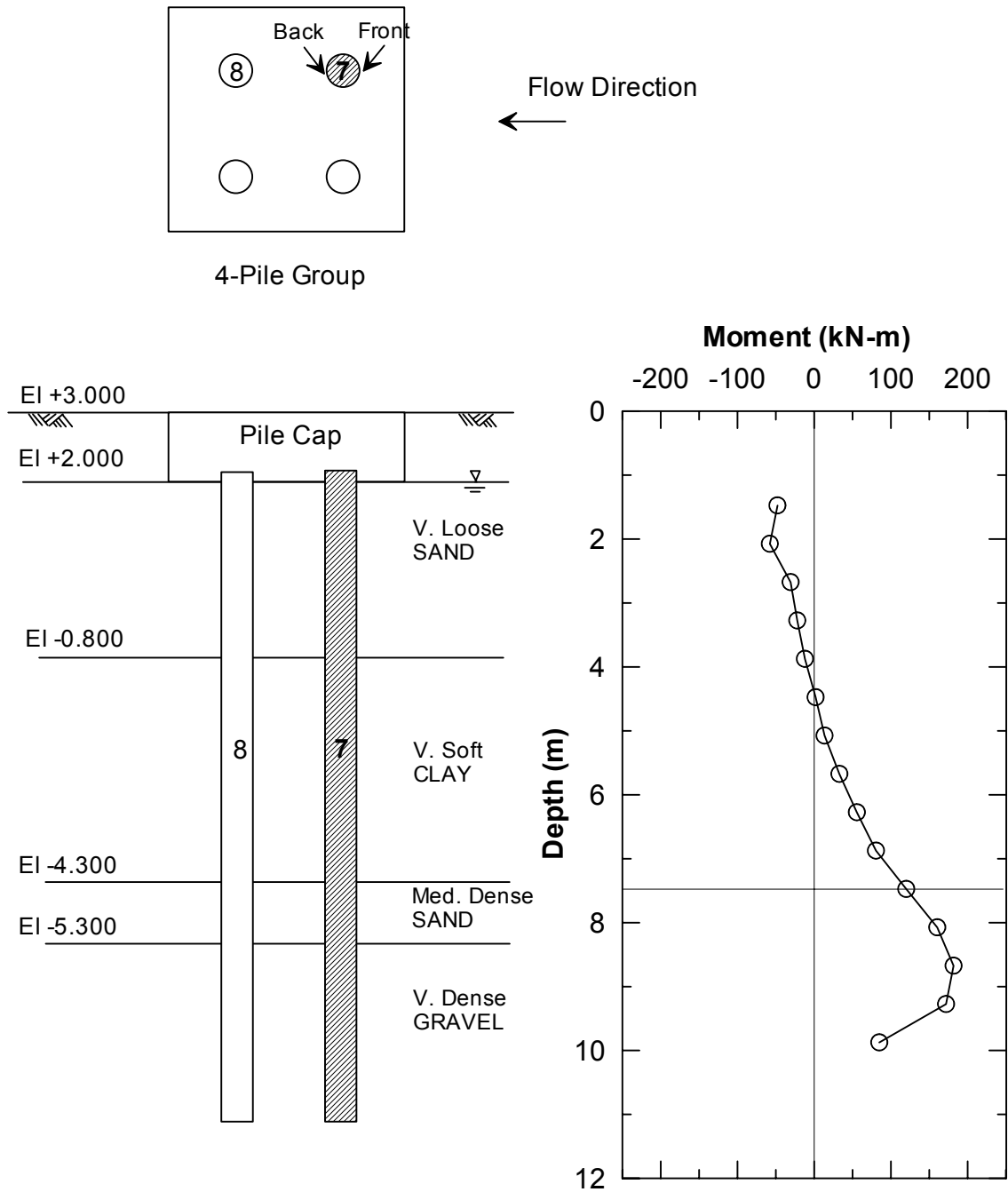
Figure 4.14   Moment Distribution along Pile No.7 of 4-Pile Group after Lateral Spreading (t = 70 s)
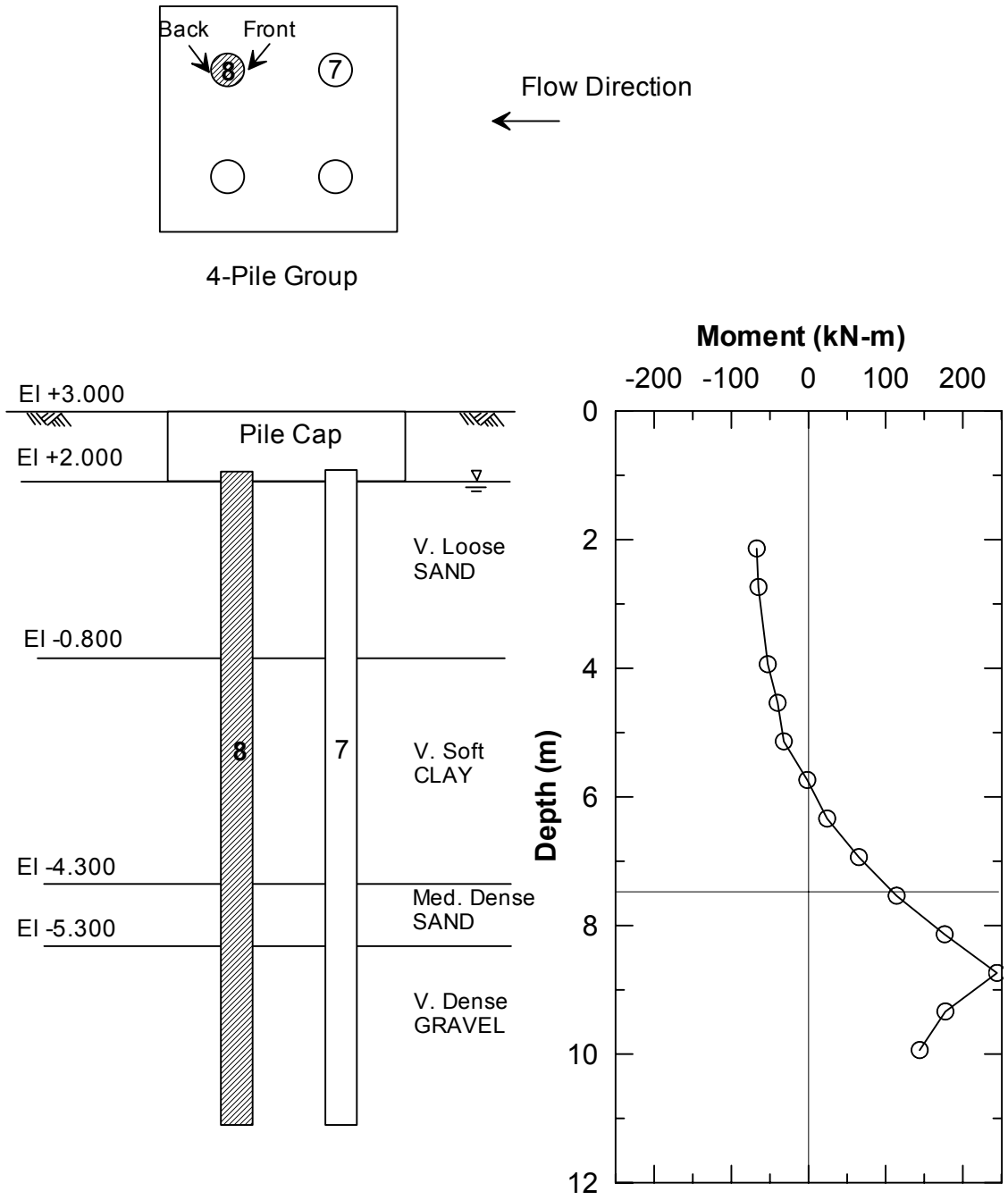
Figure 4.15   Moment Distribution along Pile No.8 of 4-Pile Group after Lateral Spreading (t = 70 s)
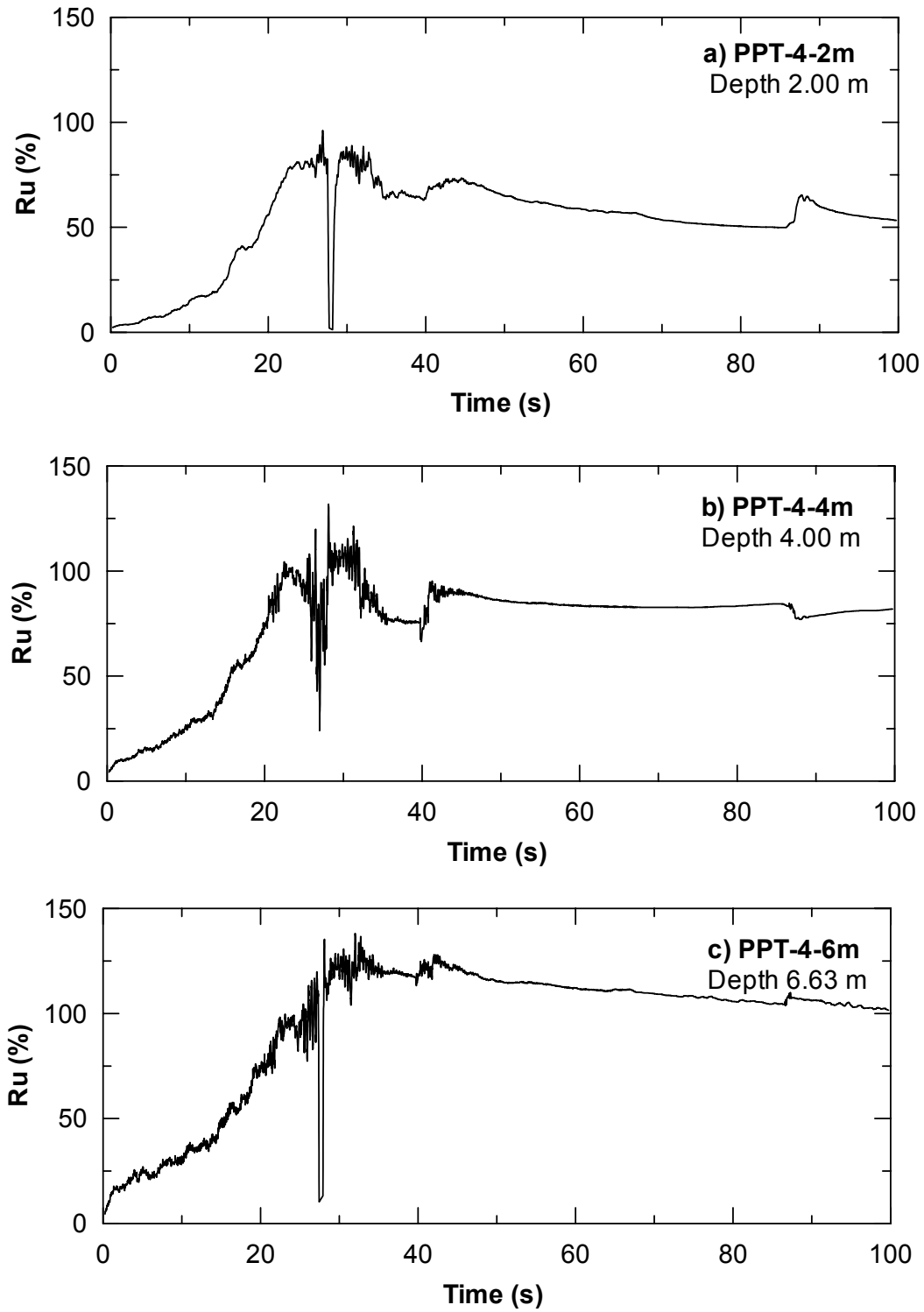
Figure 4.16   Excess Pore Water Pressure Ratio nearby 4-Pile Group (a) PPT-4-2m, (b) PPT-4-4m, and (c) PPT-4-6m, 100s Duration
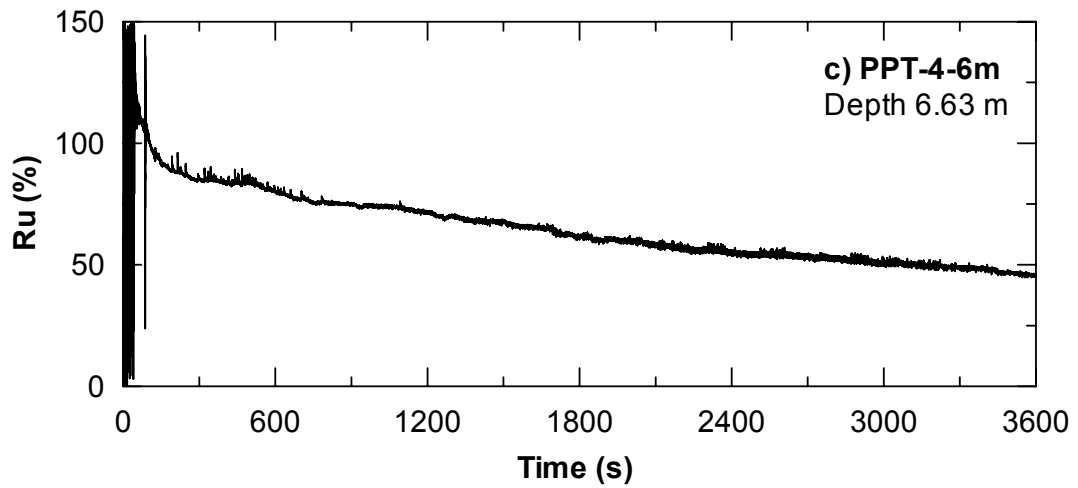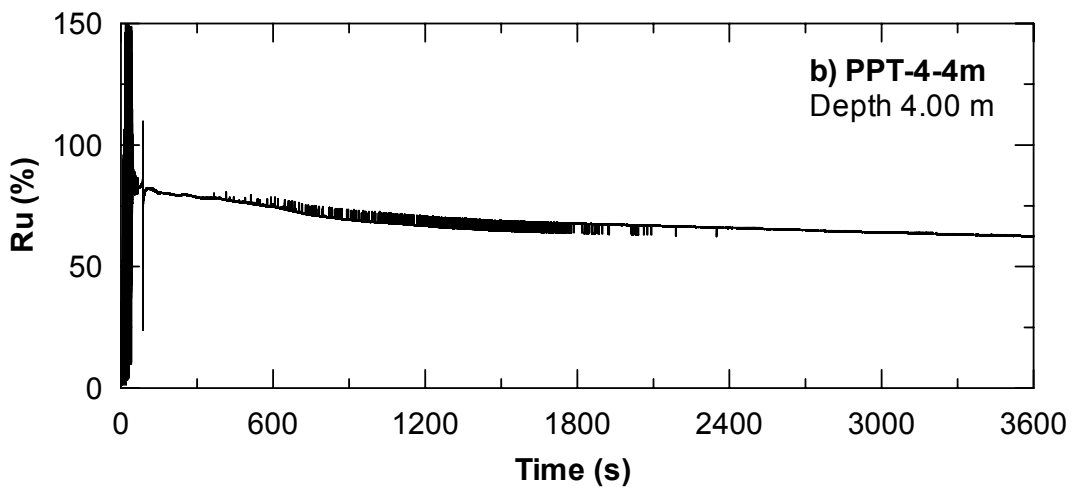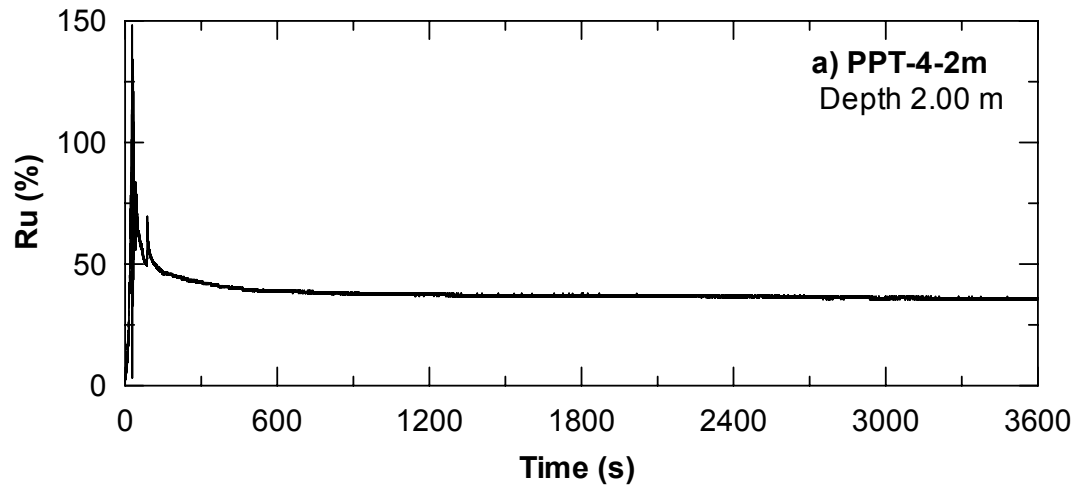
Figure 4.17 Excess Pore Water Pressure Ratio nearby 4-Pile Group (a) PPT-4-2 m, (b) PPT-4-4m, and (c) PPT-4-6m, 3600s Duration
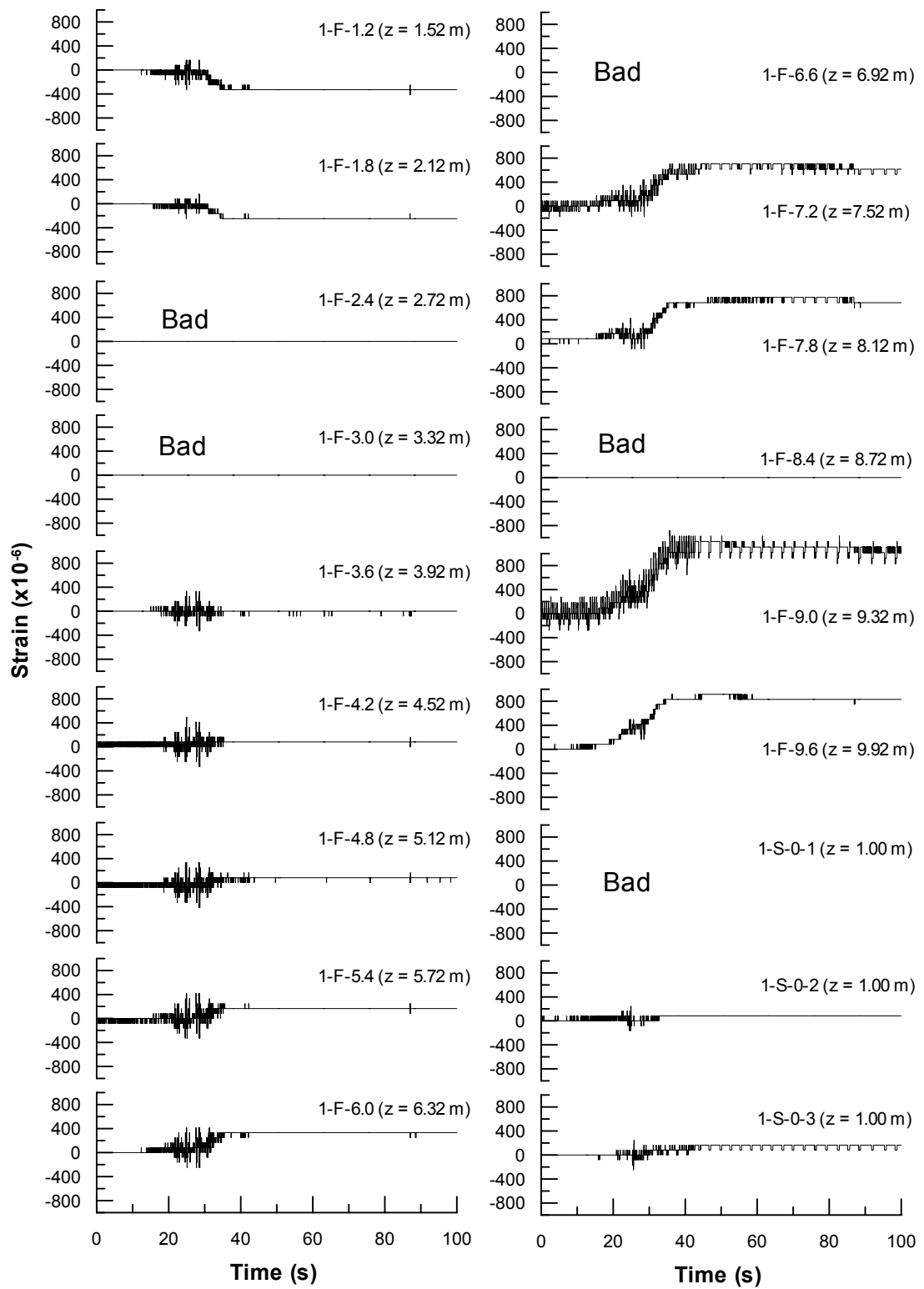
Figure 4.18   Strain Gauge Response along Pile No.1 (Front Side) of 9-Pile Group

101
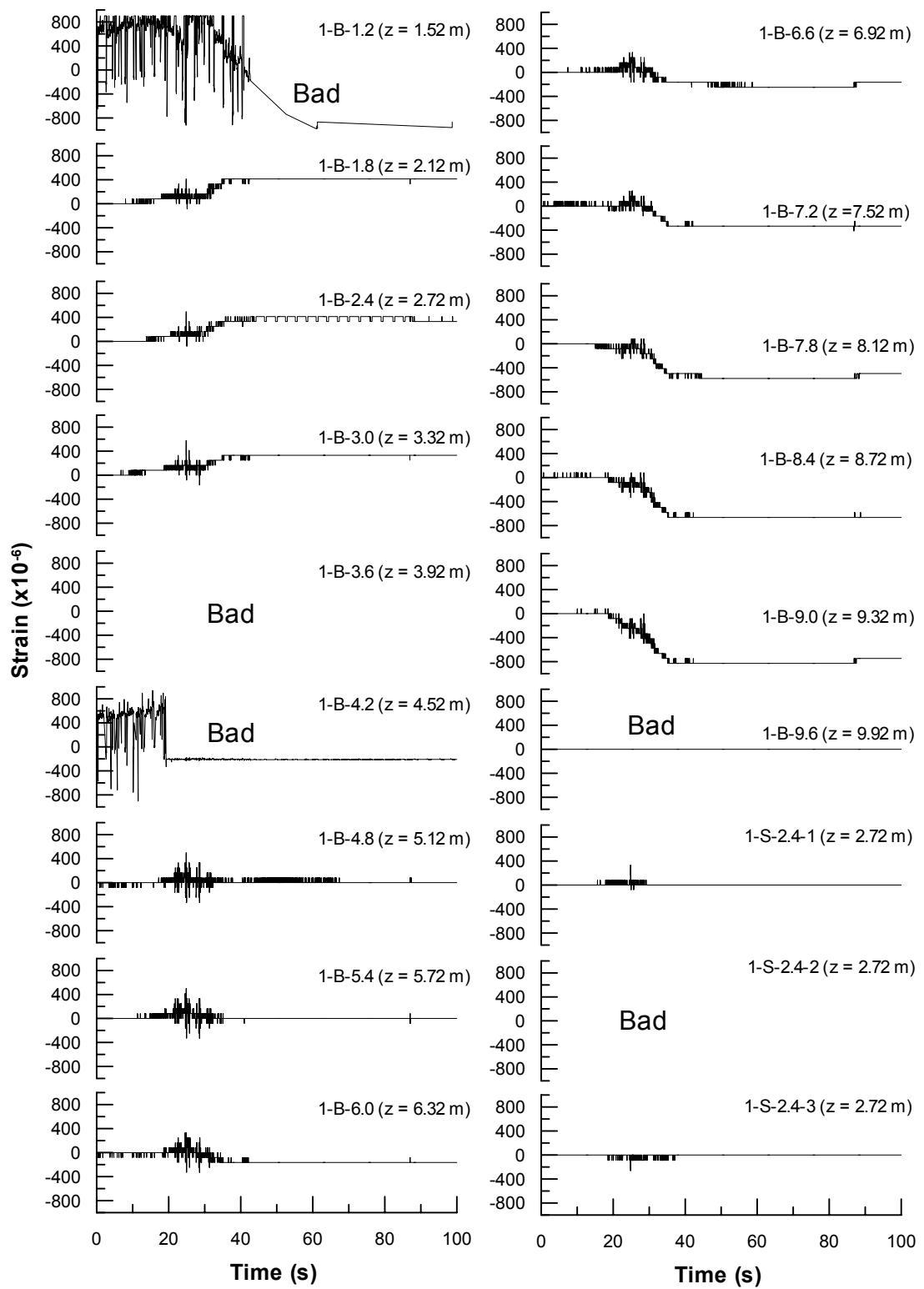
Figure 4.19   Strain Gauge Response along Pile No.1 (Back Side) of 9-Pile Group
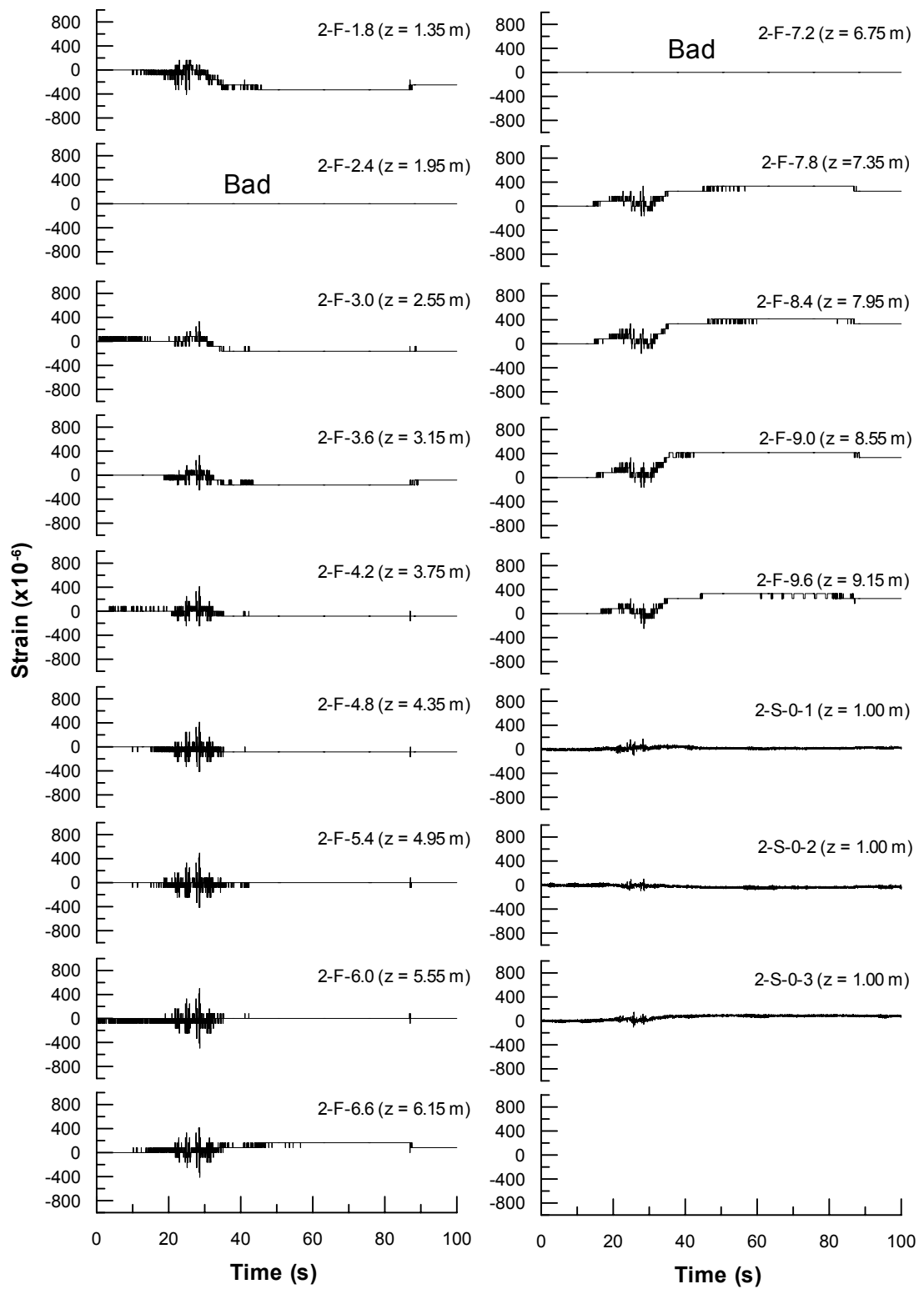
Figure 4.20   Strain Gauge Response along Pile No.2 (Front Side) of 9-Pile Group

103
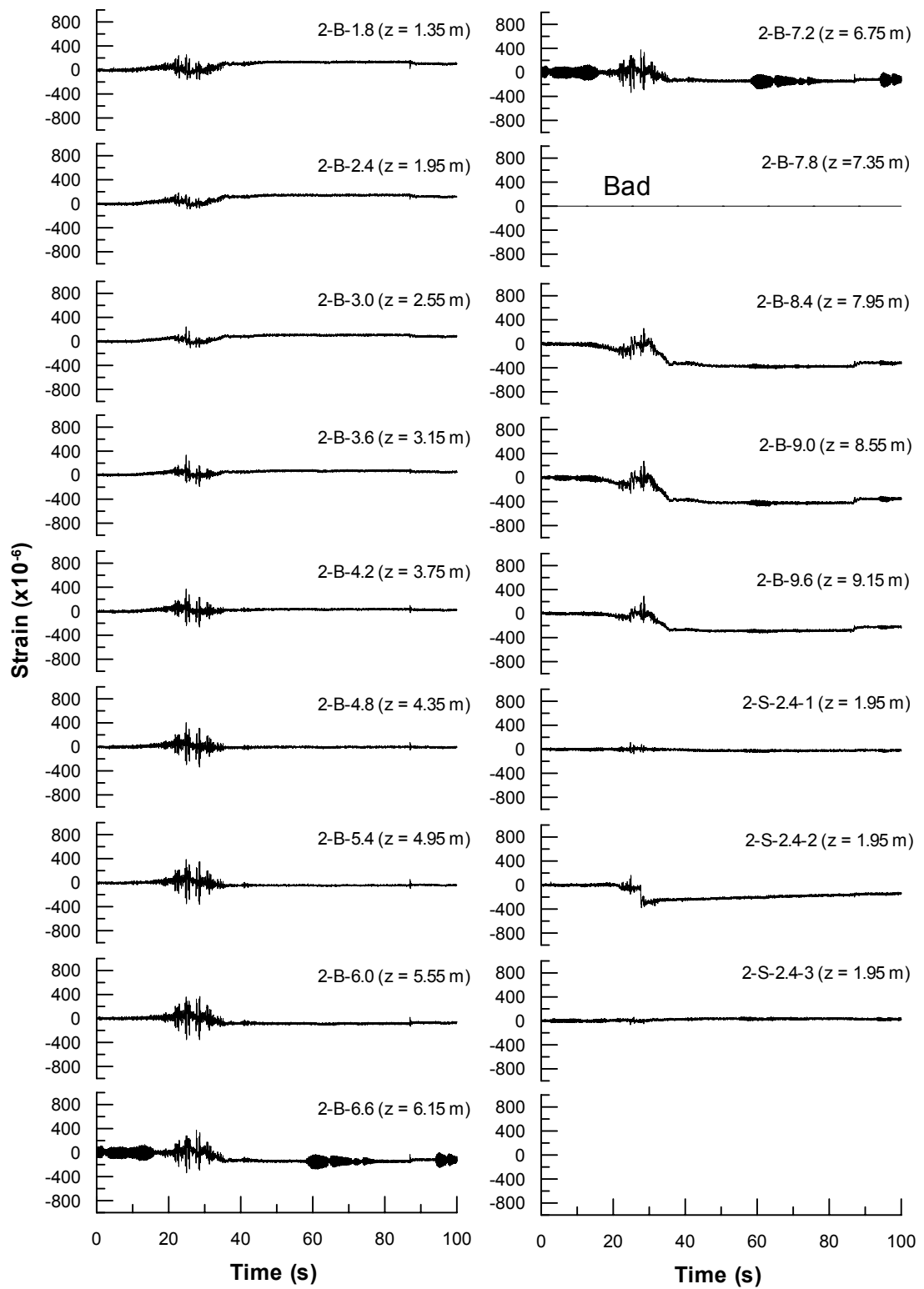
Figure 4.21   Strain Gauge Response along Pile No.2 (Back Side) of 9-Pile Group

104
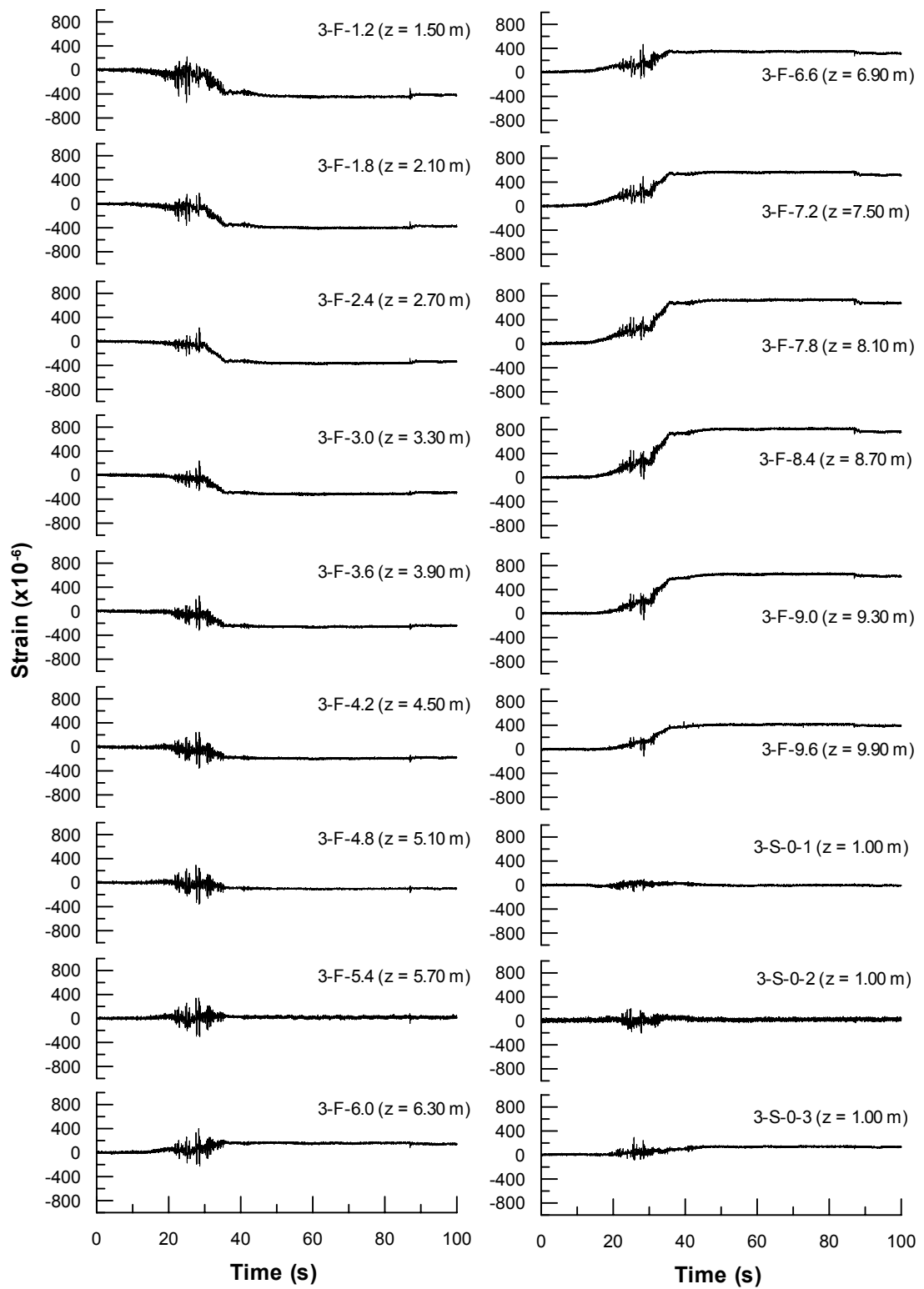
Figure 4.22   Strain Gauge Response along Pile No.3 (Front Side) of 9-Pile Group
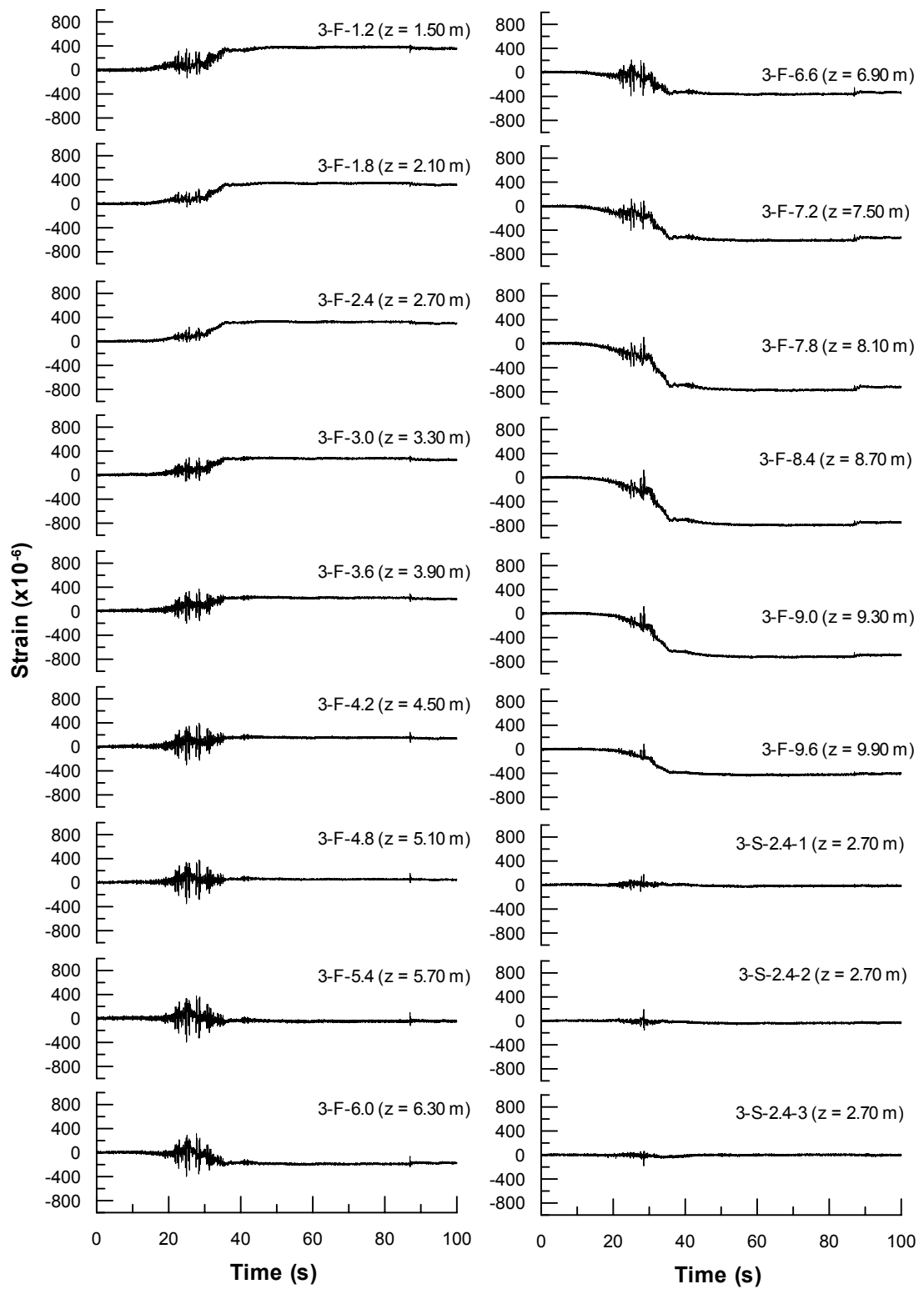
Figure 4.23   Strain Gauge Response along Pile No.3 (Back Side) of 9-Pile Group

106
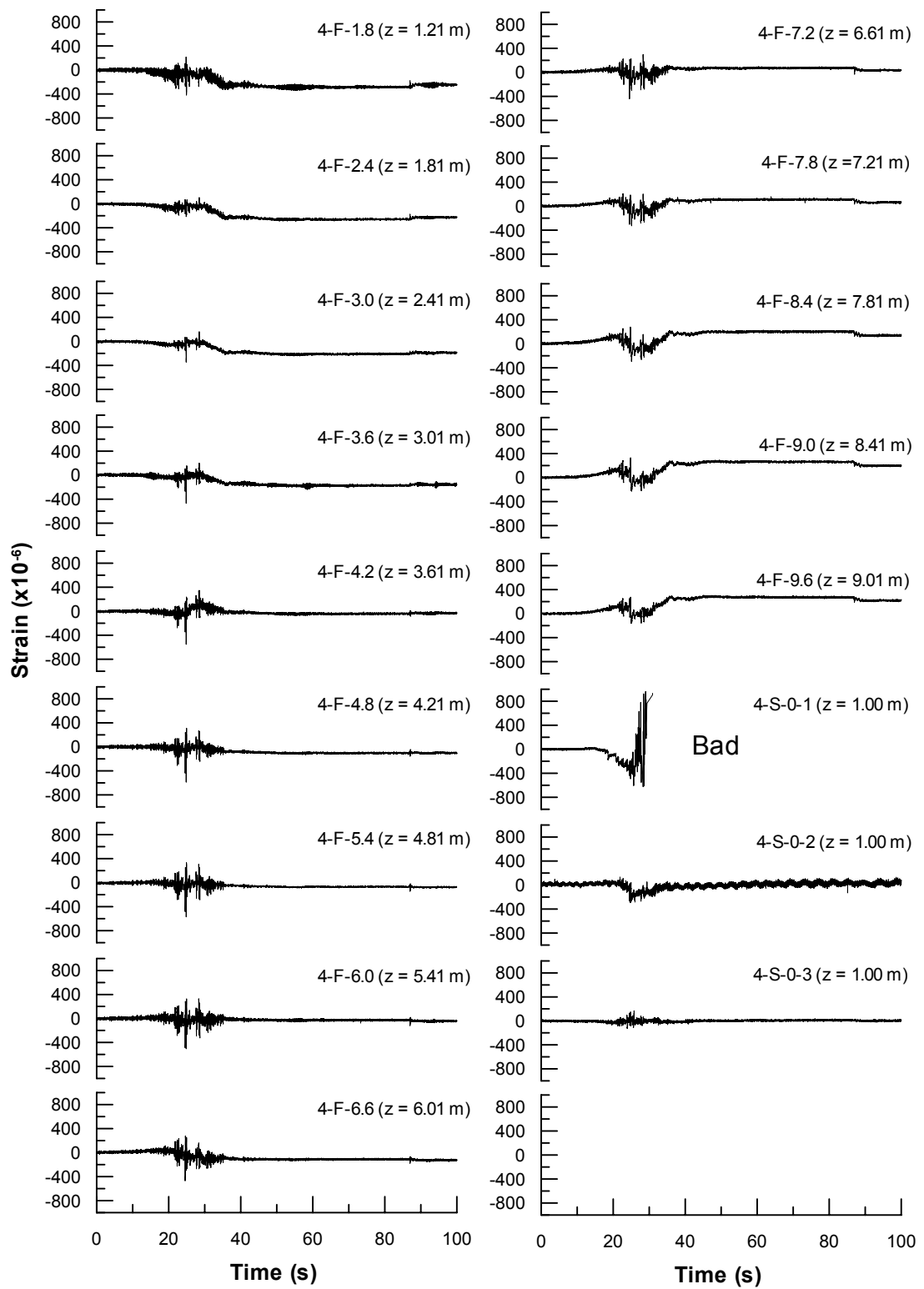
Figure 4.24   Strain Gauge Response along Pile No.4 (Front Side) of 9-Pile Group
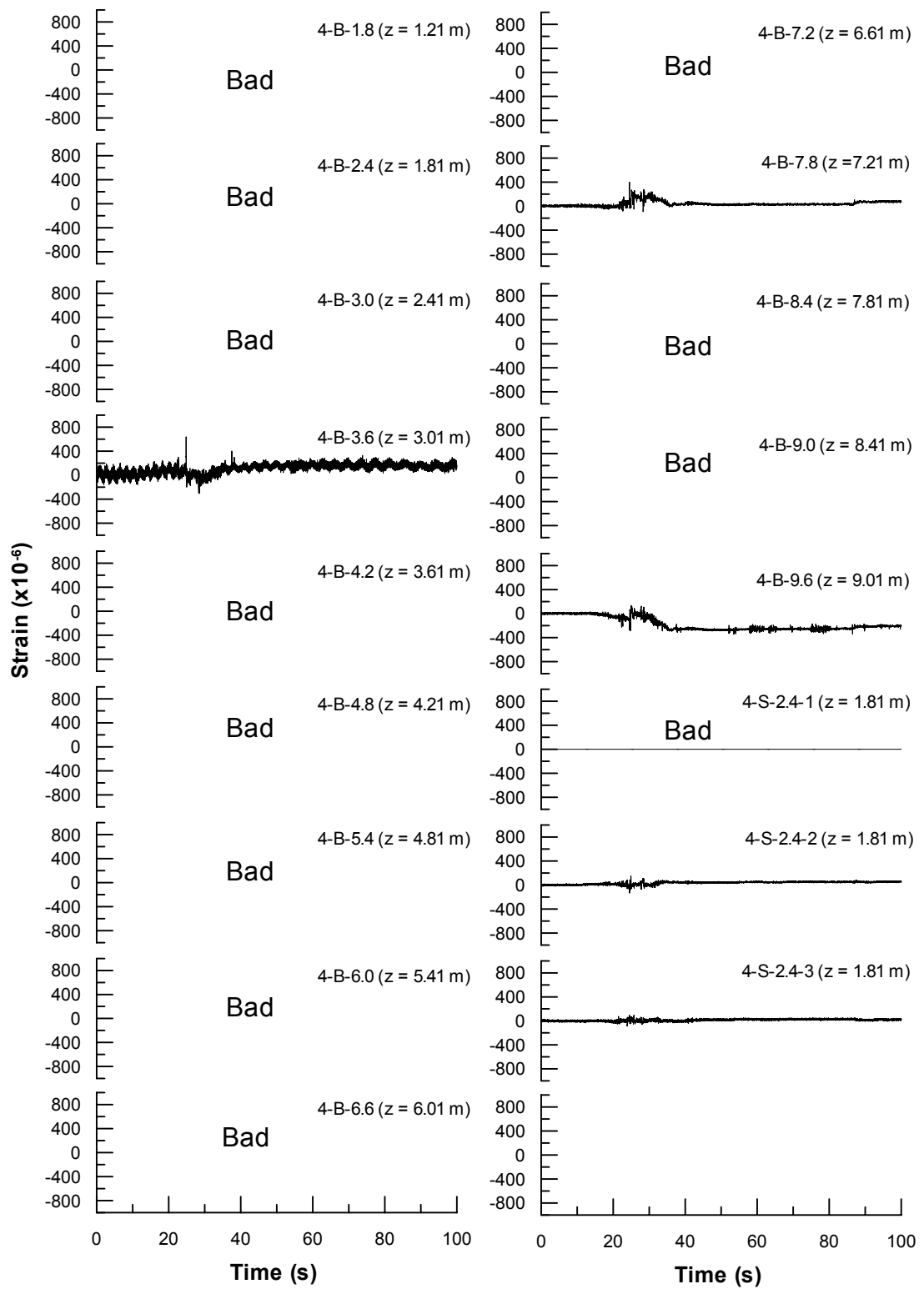
Figure 4.25   Strain Gauge Response along Pile No.4 (Back Side) of 9-Pile Group
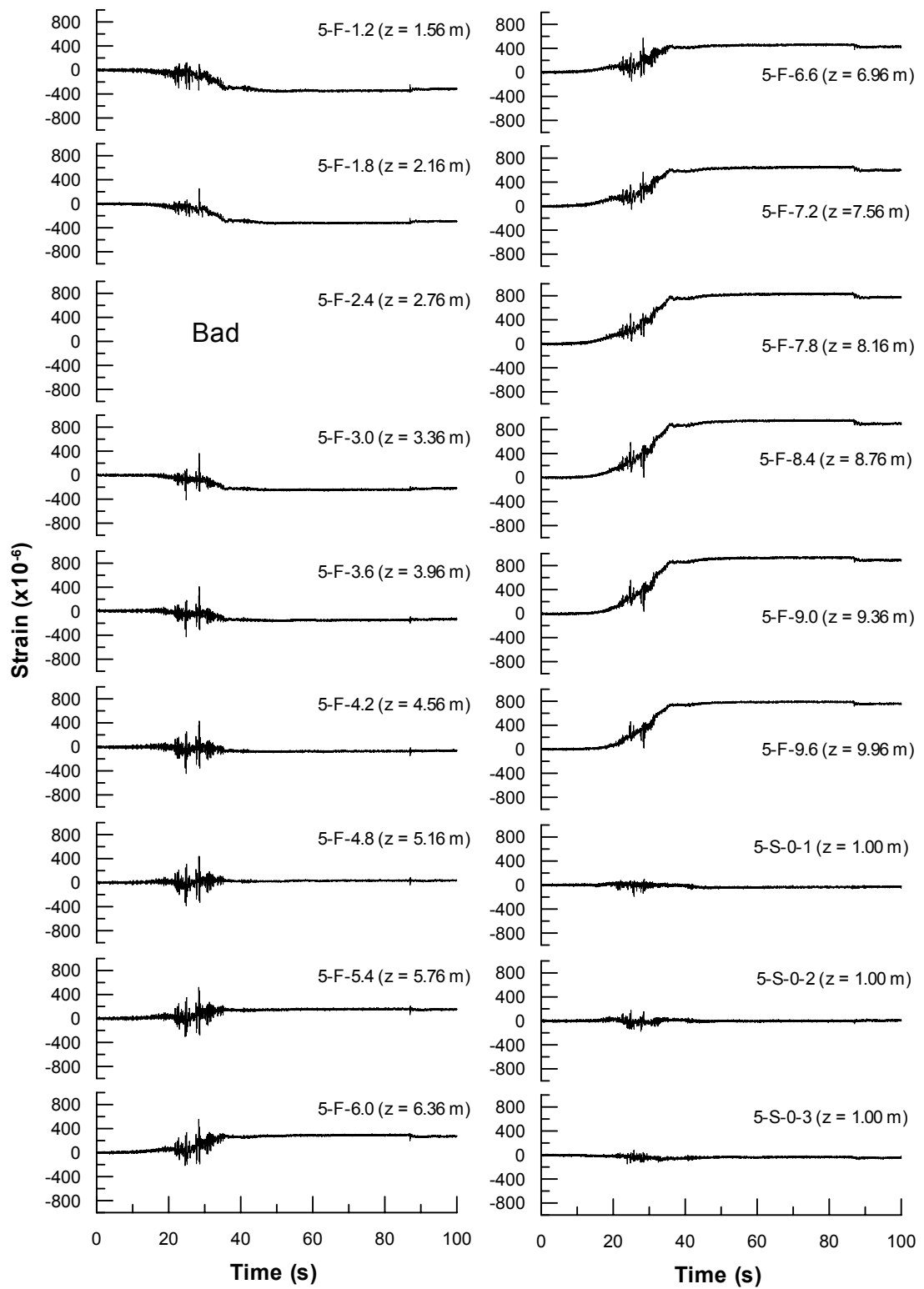
Figure 4.26   Strain Gauge Response along Pile No.5 (Front Side) of 9-Pile Group
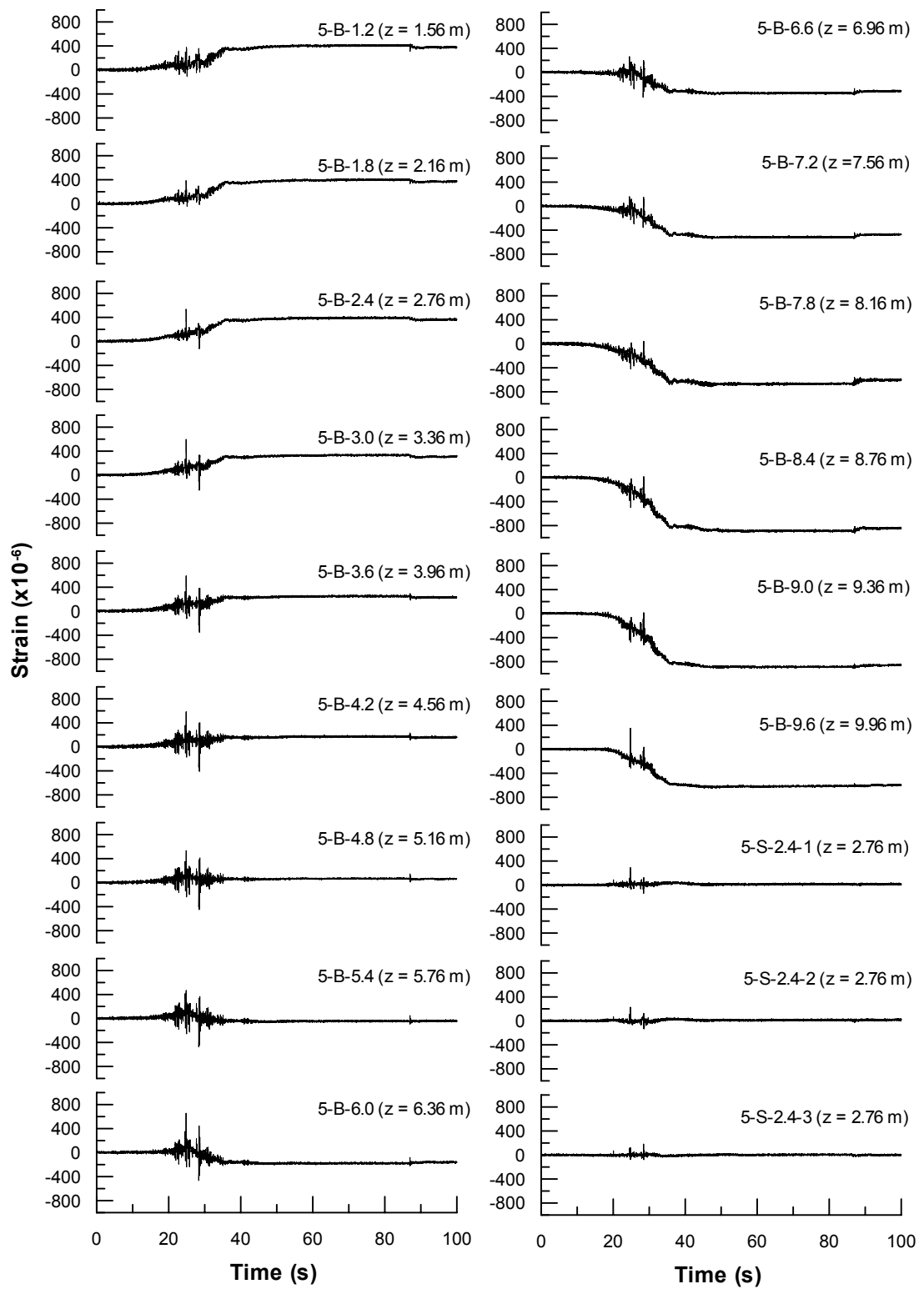
Figure 4.27   Strain Gauge Response along Pile No.5 (Back Side) of 9-Pile Group

110
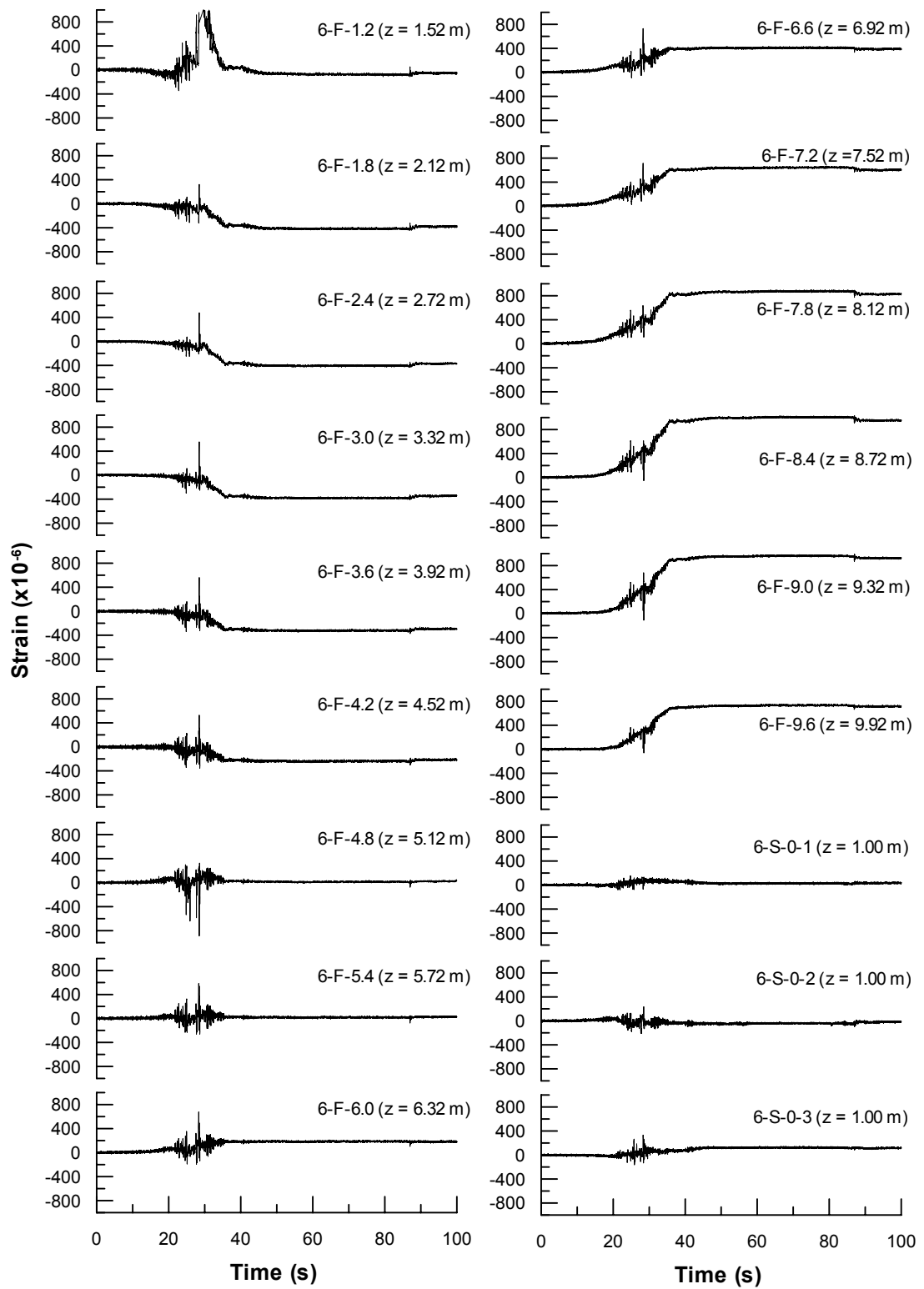
Figure 4.28   Strain Gauge Response along Pile No.6 (Front Side) of 9-Pile Group

111
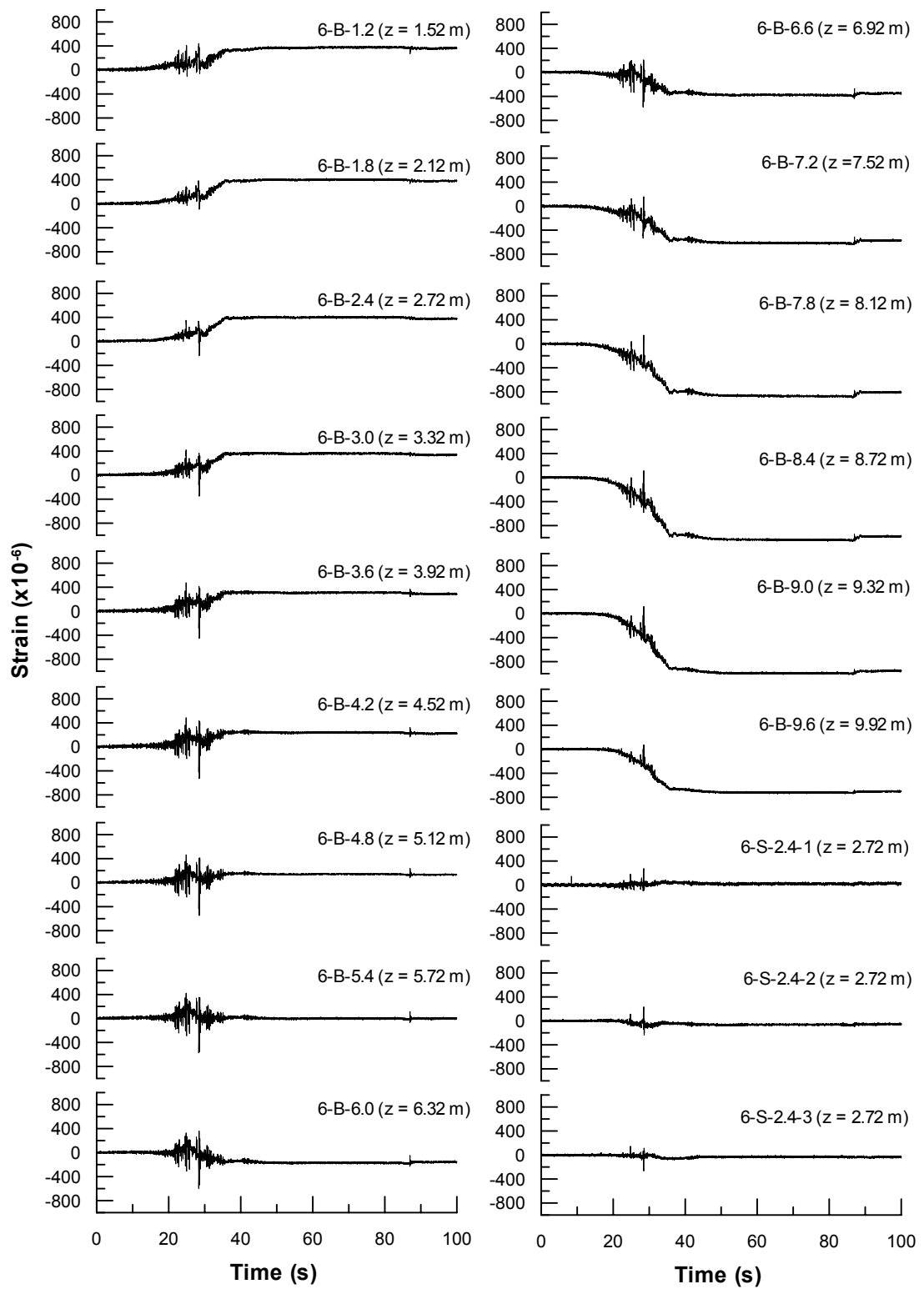
Figure 4.29   Strain Gauge Response along Pile No.6 (Back Side) of 9-Pile Group

112
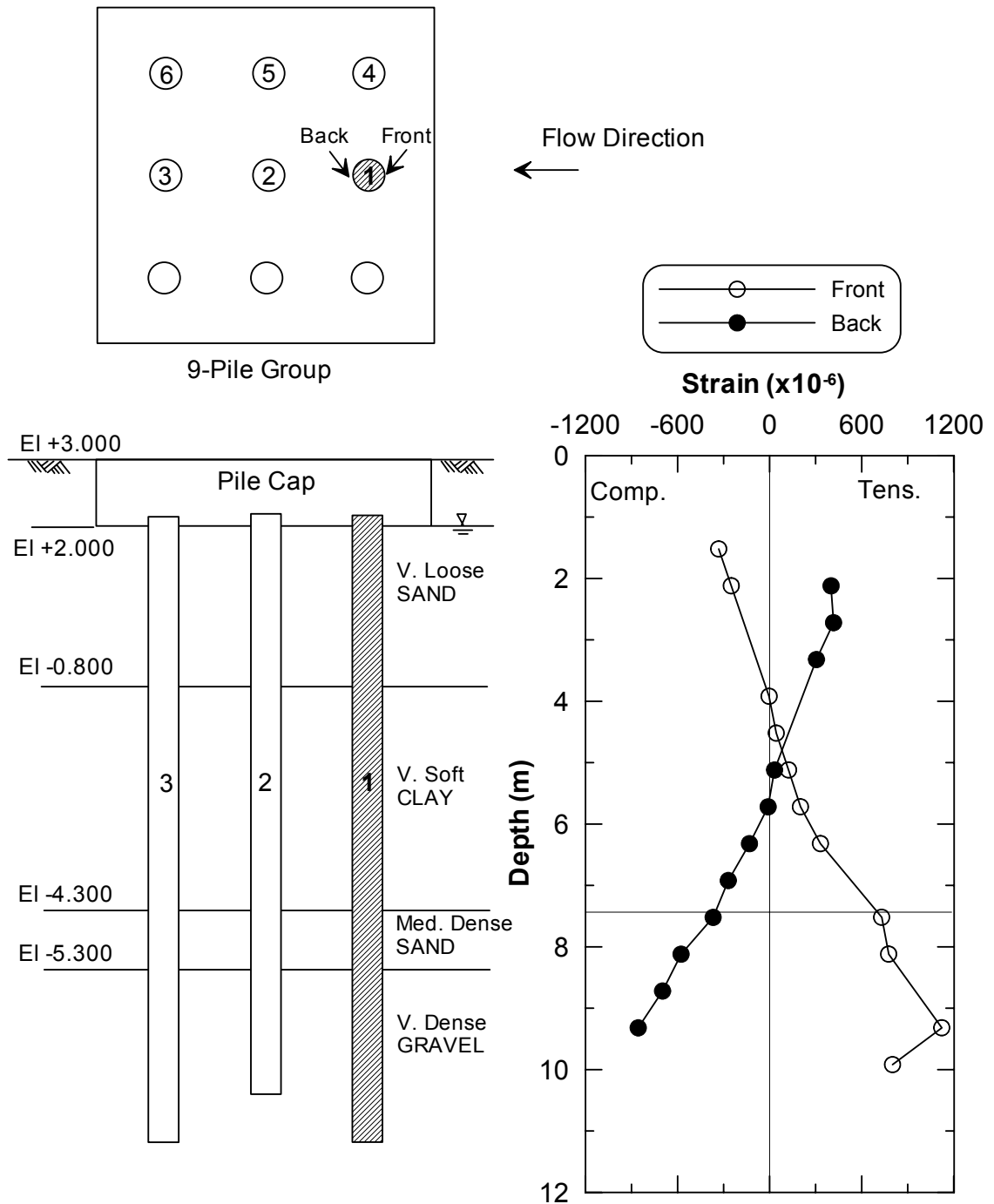
Figure 4.30   Profile of Residual Strain of Pile No.1 of 9-Pile Group after Lateral Spreading (t = 70s)
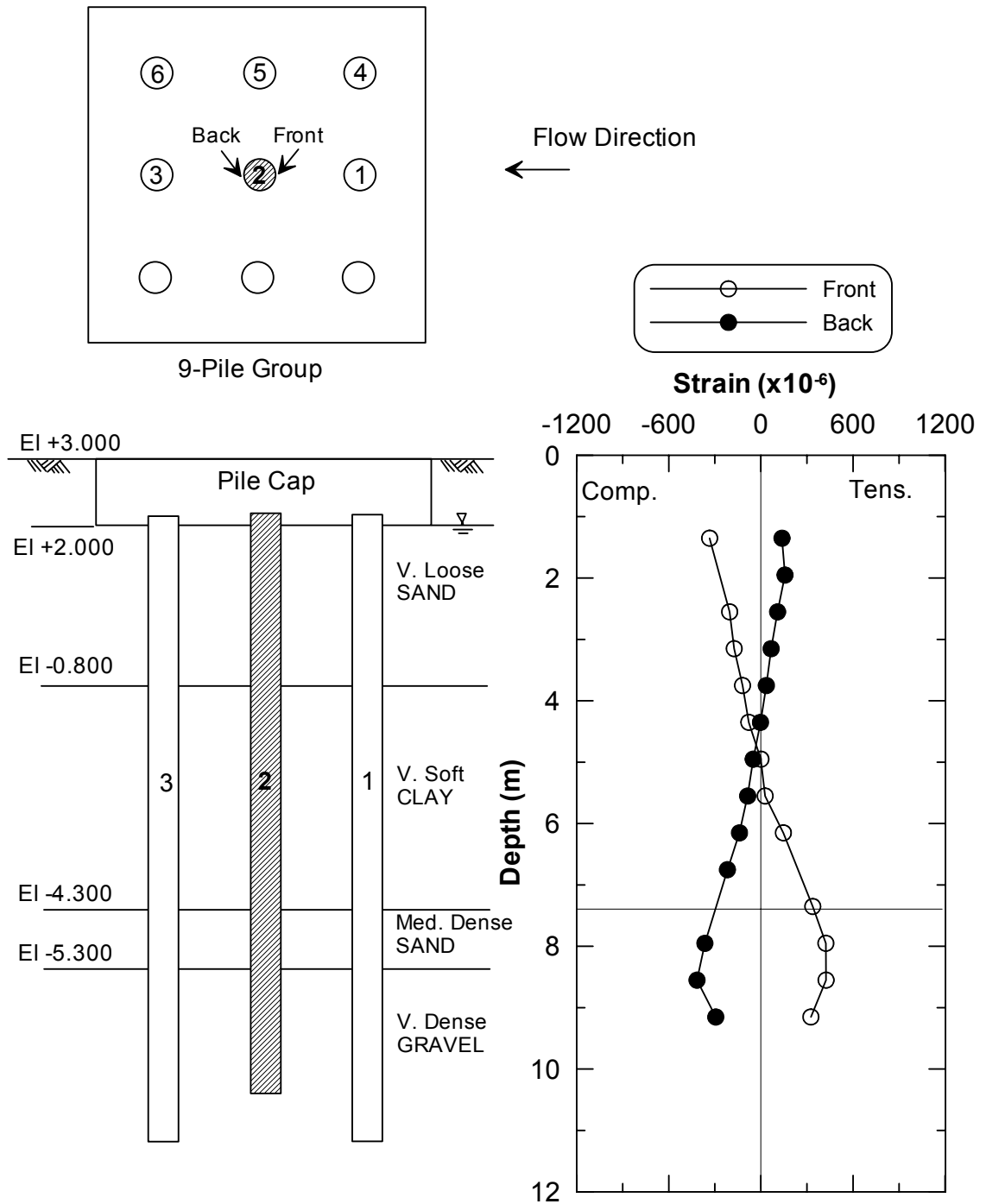
Figure 4.31   Profile of Residual Strain of Pile No.2 of 9-Pile Group after Lateral
Spreading (t = 70 s)
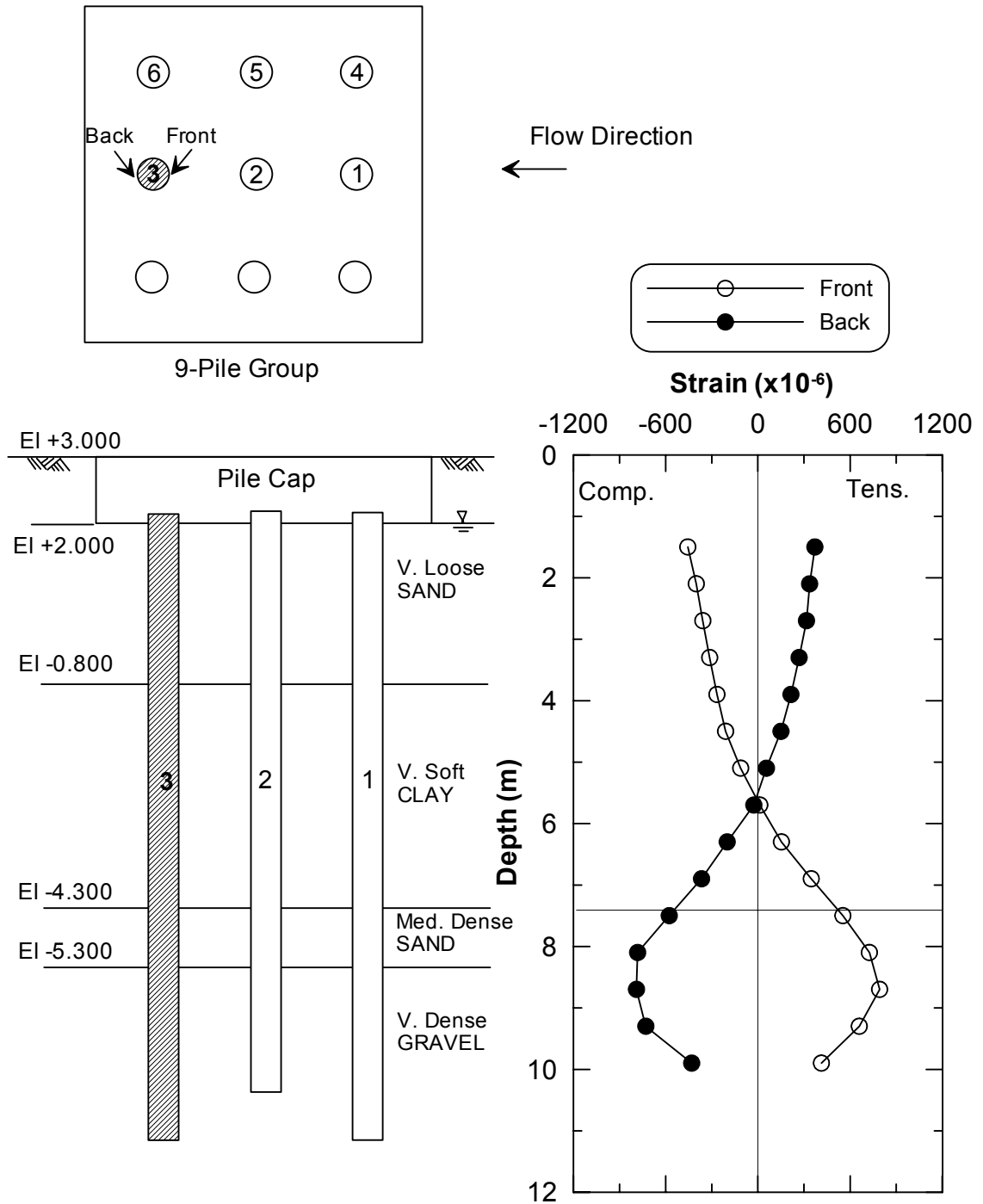
Figure 4.32 Profile of Residual Strain of Pile No.3 of 9-Pile Group after Lateral Spreading (t = 70 s)
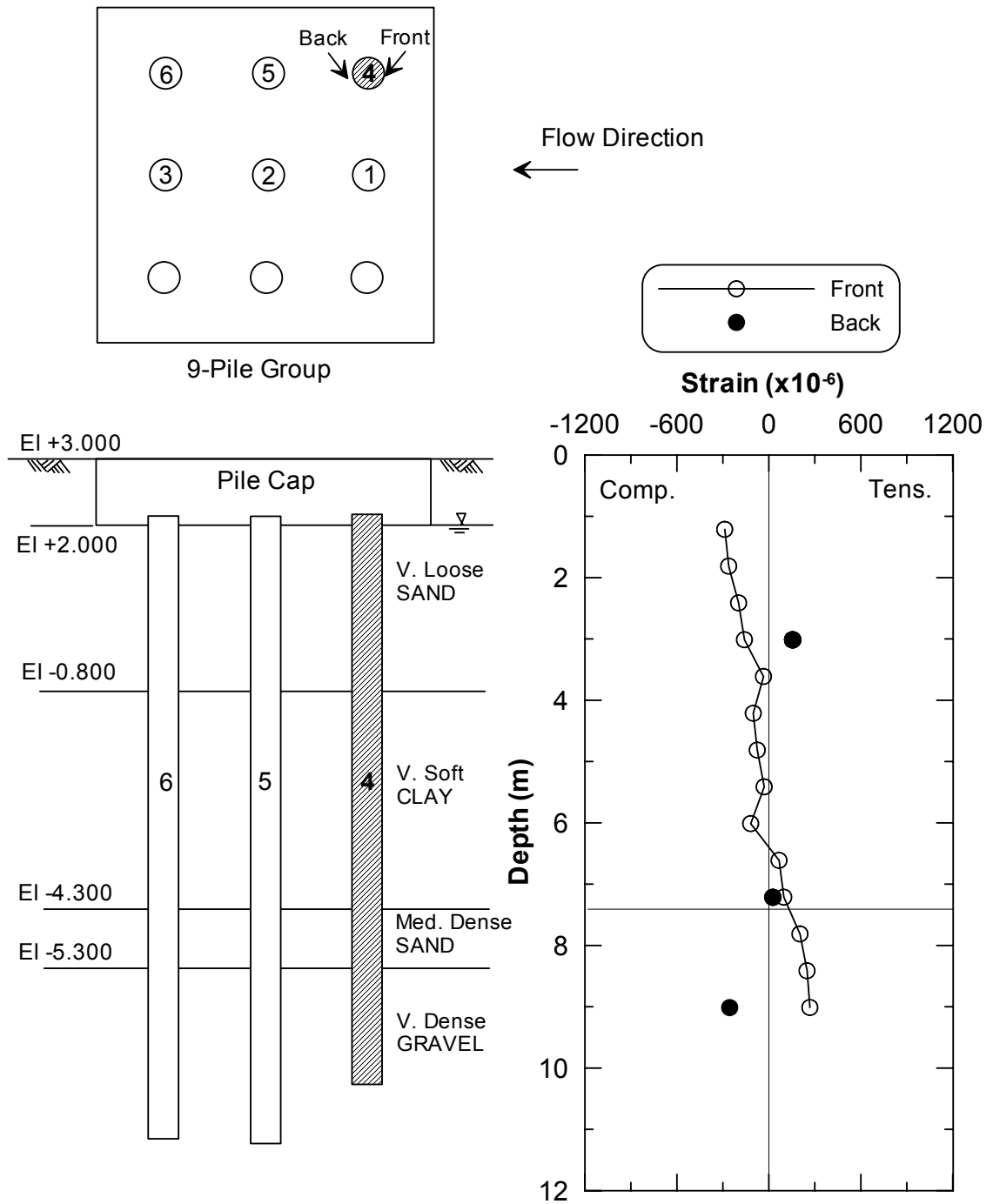
Figure 4.33   Profile of Residual Strain of Pile No.4 of 9-Pile Group after Lateral (t = 70 s)
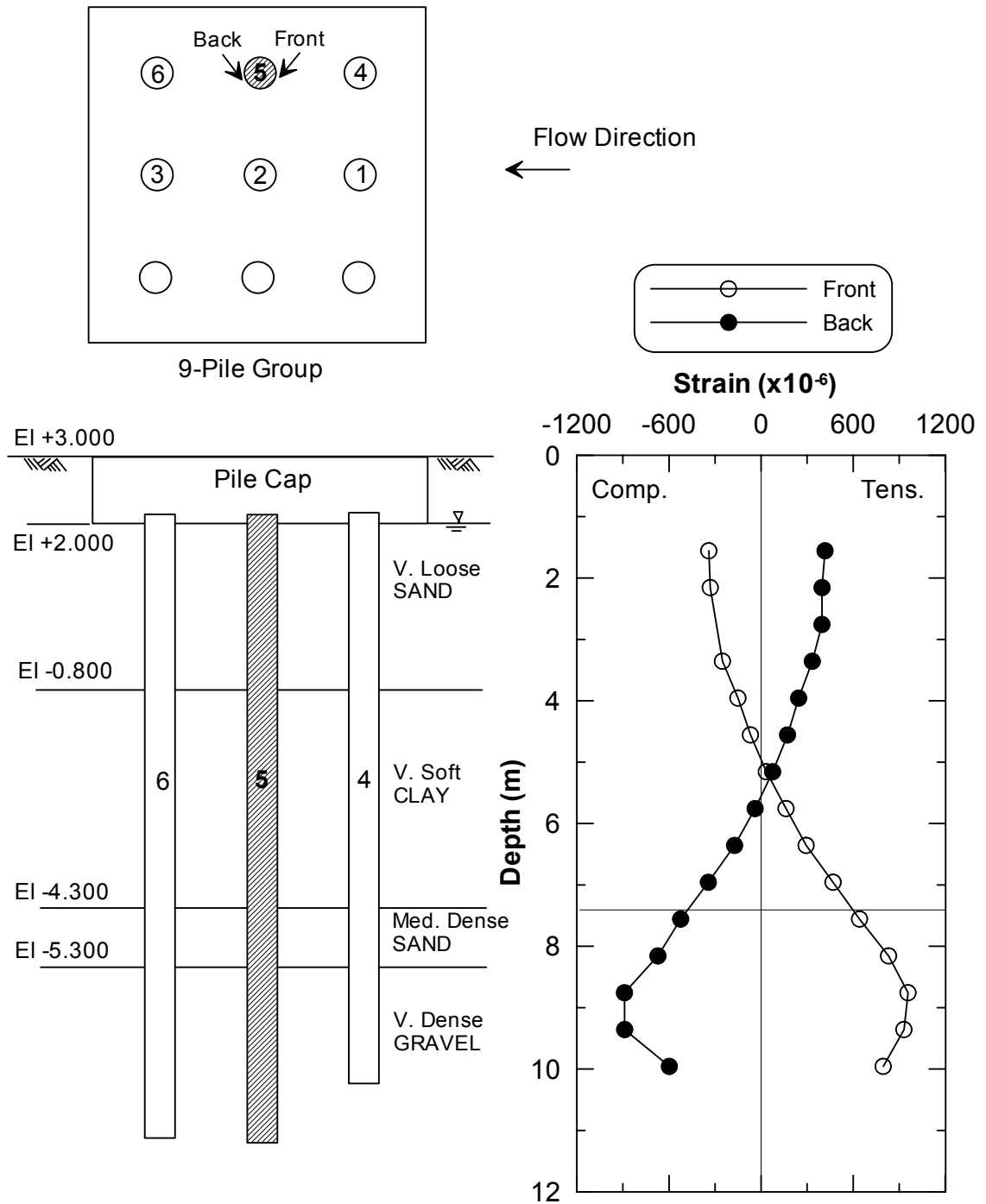
Figure 4.34 Profile of Residual Strain of Pile No.5 of 9-Pile Group after Lateral Spreading (t = 70 s)
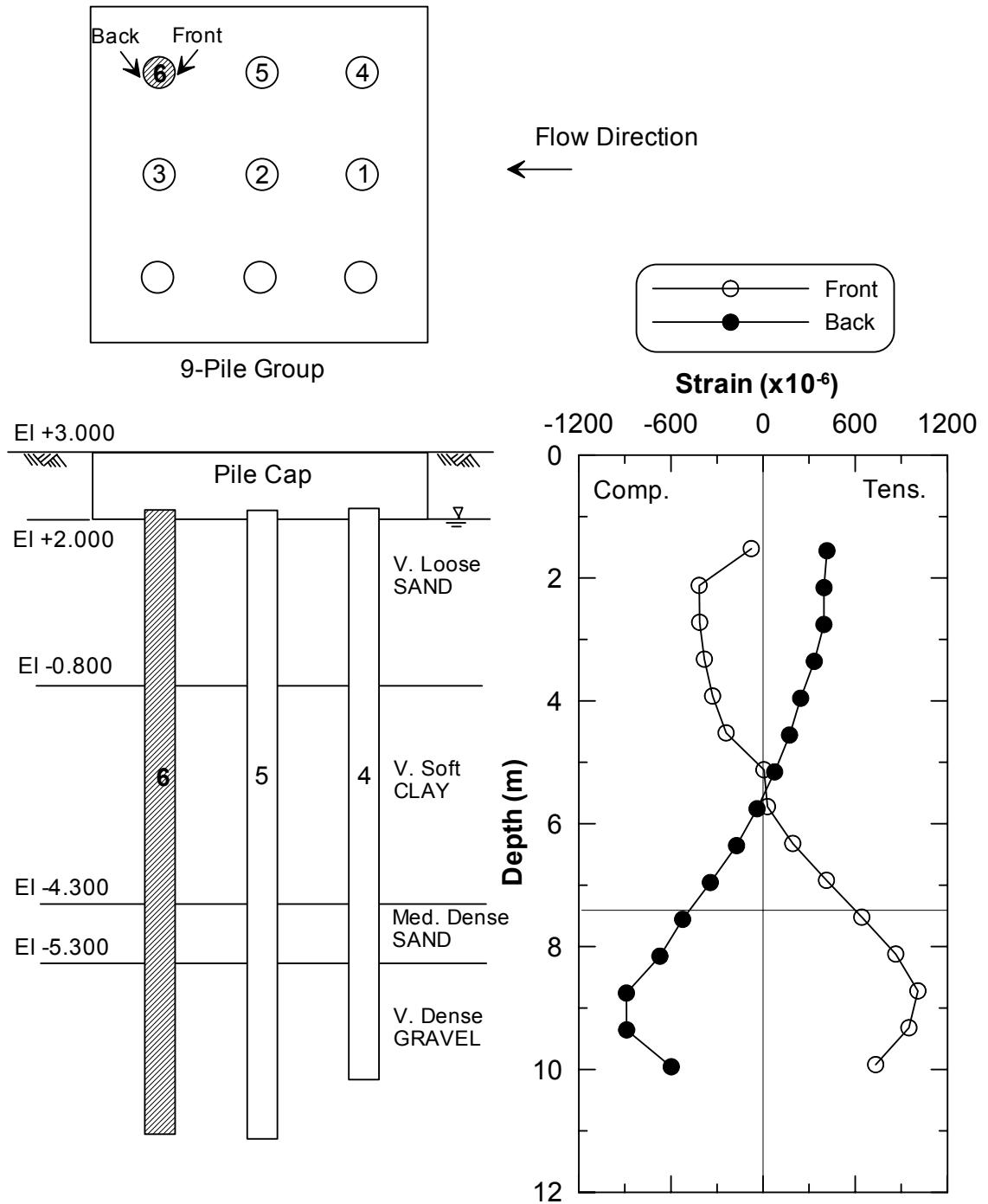
Figure 4.35   Profile of Residual Strain of Pile No.6 of 9-Pile Group after Lateral Spreading (t = 70 s)
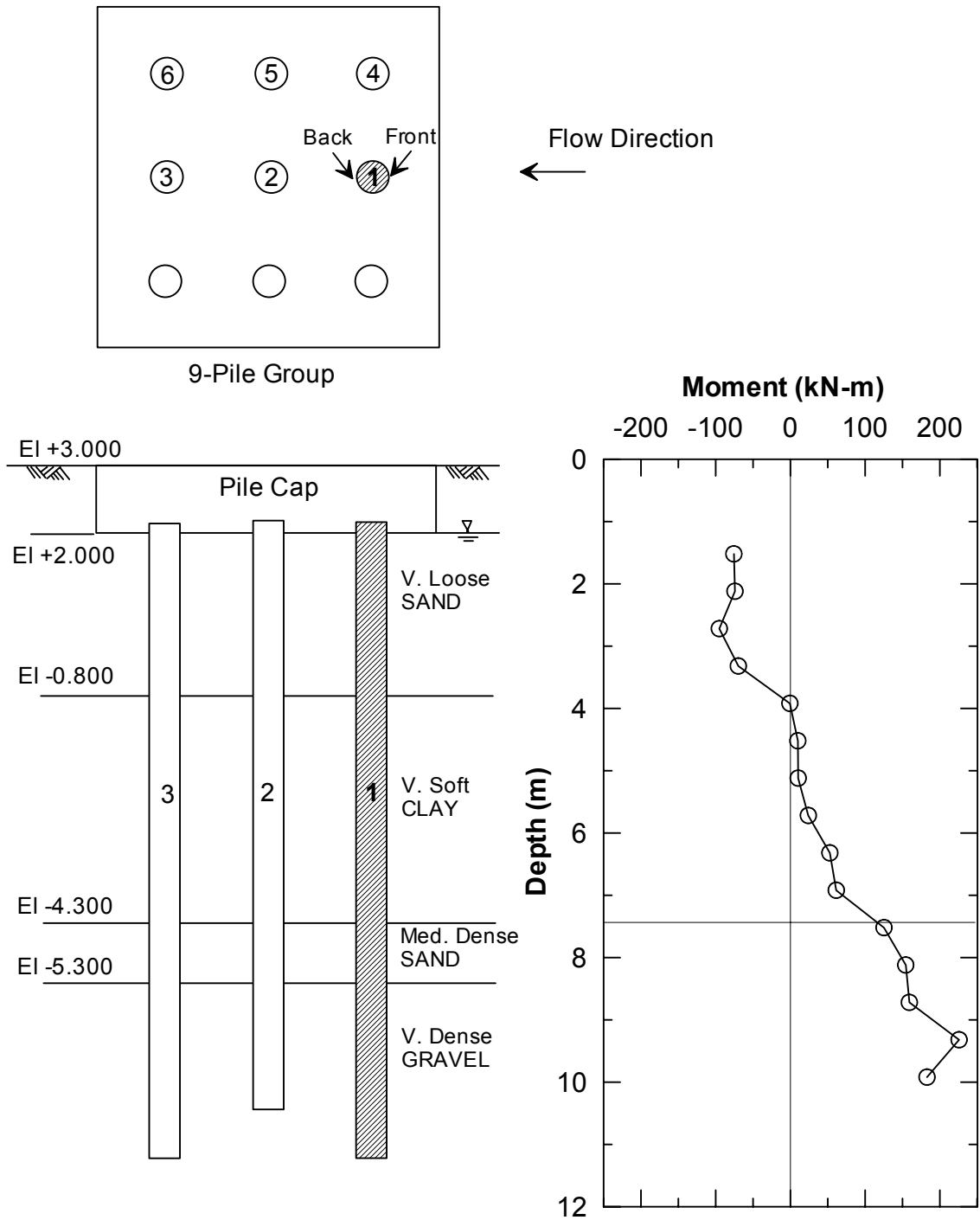
Figure 4.36   Moment Distribution along Pile No.1 of 9-Pile Group after Lateral Spreading (t = 70 s)
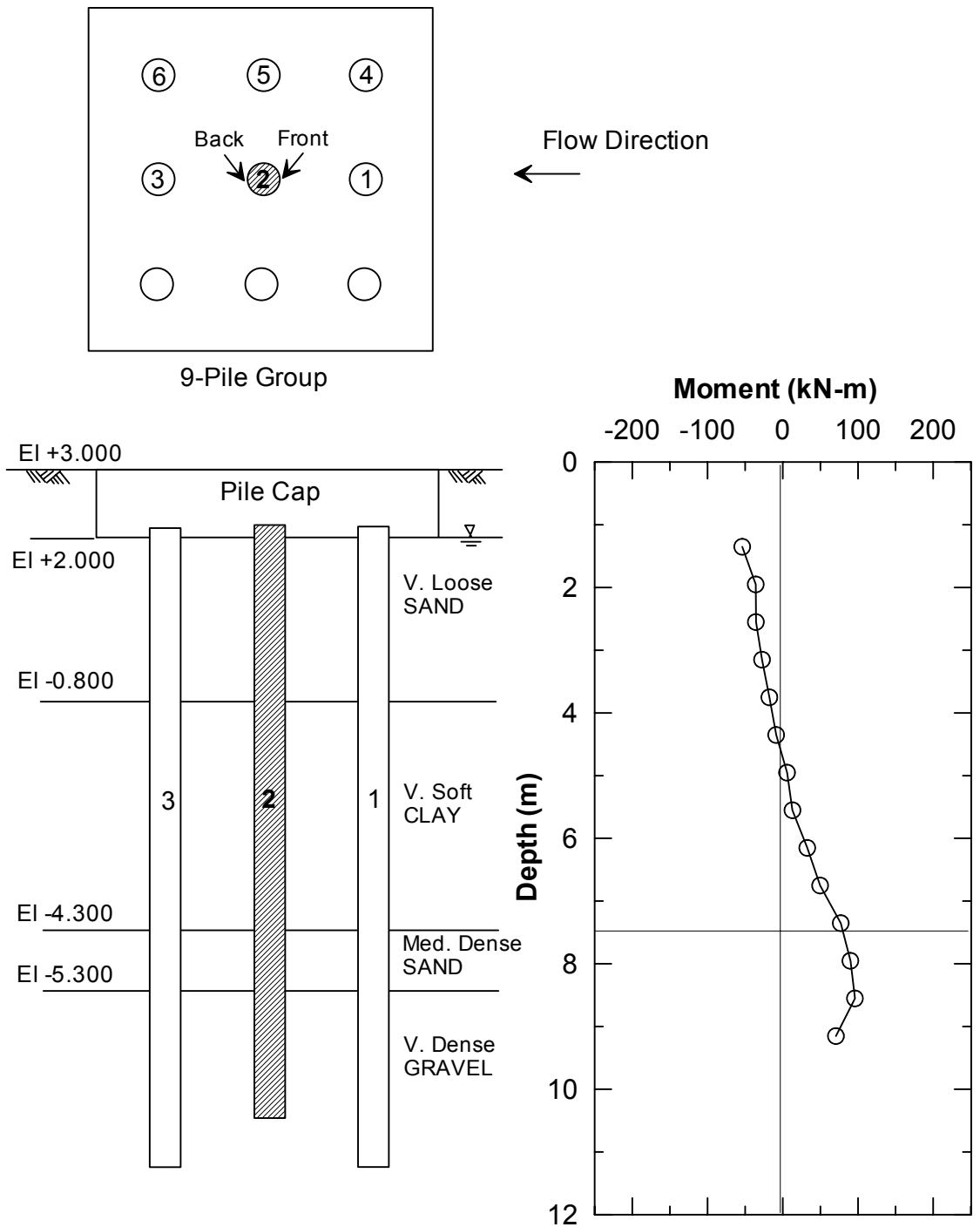
Figure 4.37 Moment Distribution along Pile No.2 of 9-Pile Group after Lateral Spreading (t = 70 s)
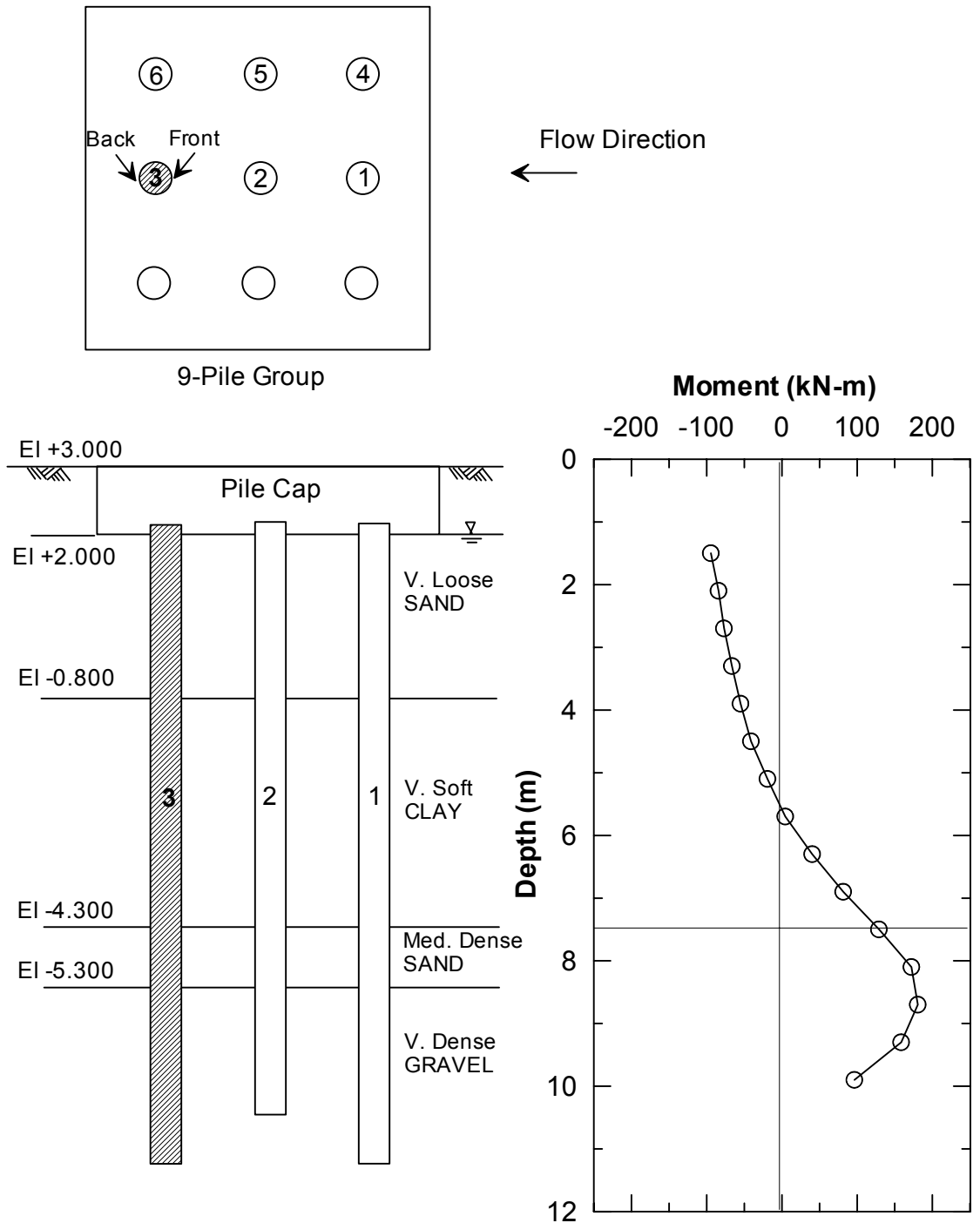
Figure 4.38   Moment Distribution along Pile No.3 of 9-Pile Group after Lateral Spreading (t = 70 s)
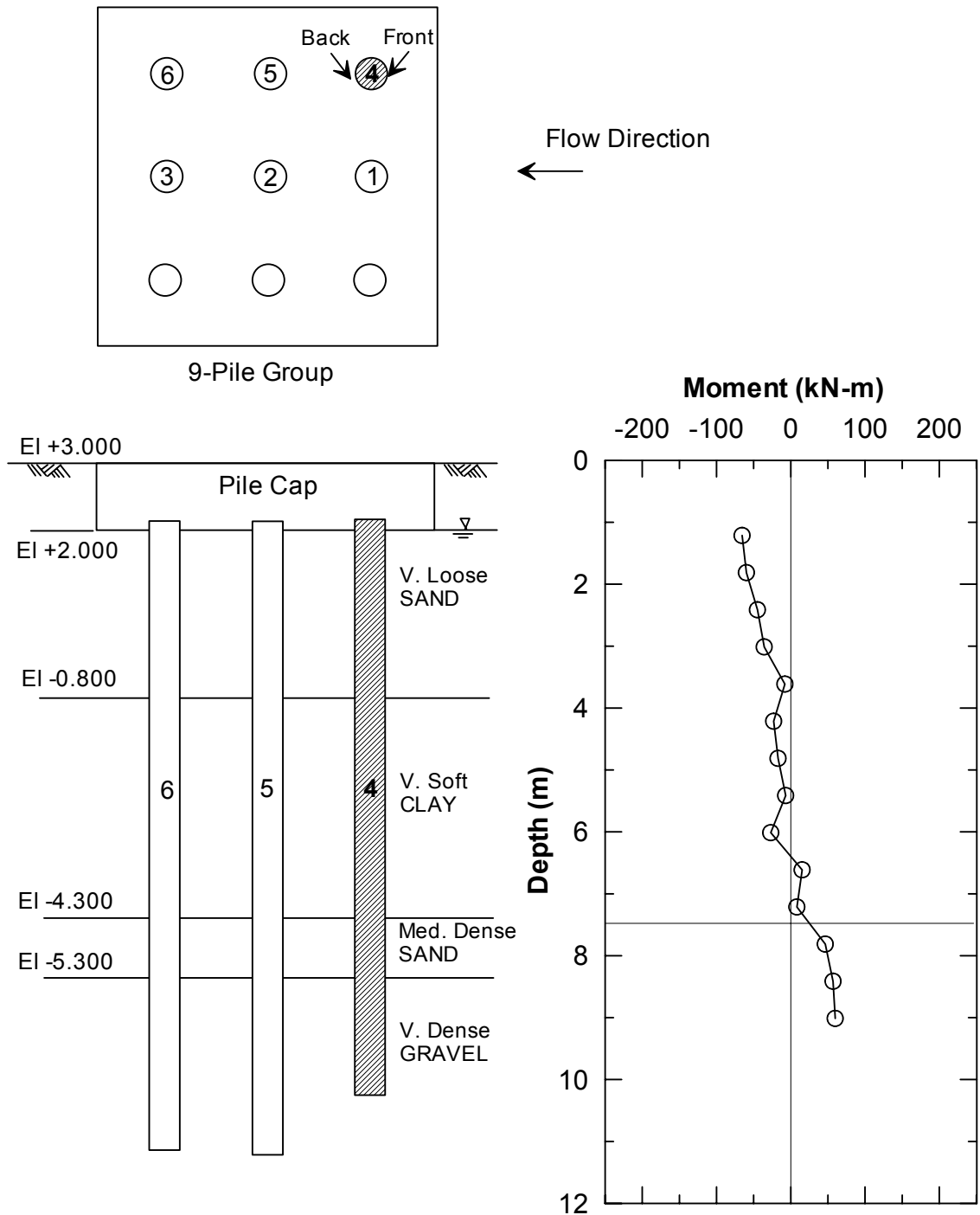
Figure 4.39   Moment Distribution along Pile No.4 of 9-Pile Group after Lateral Spreading (t = 70 s)
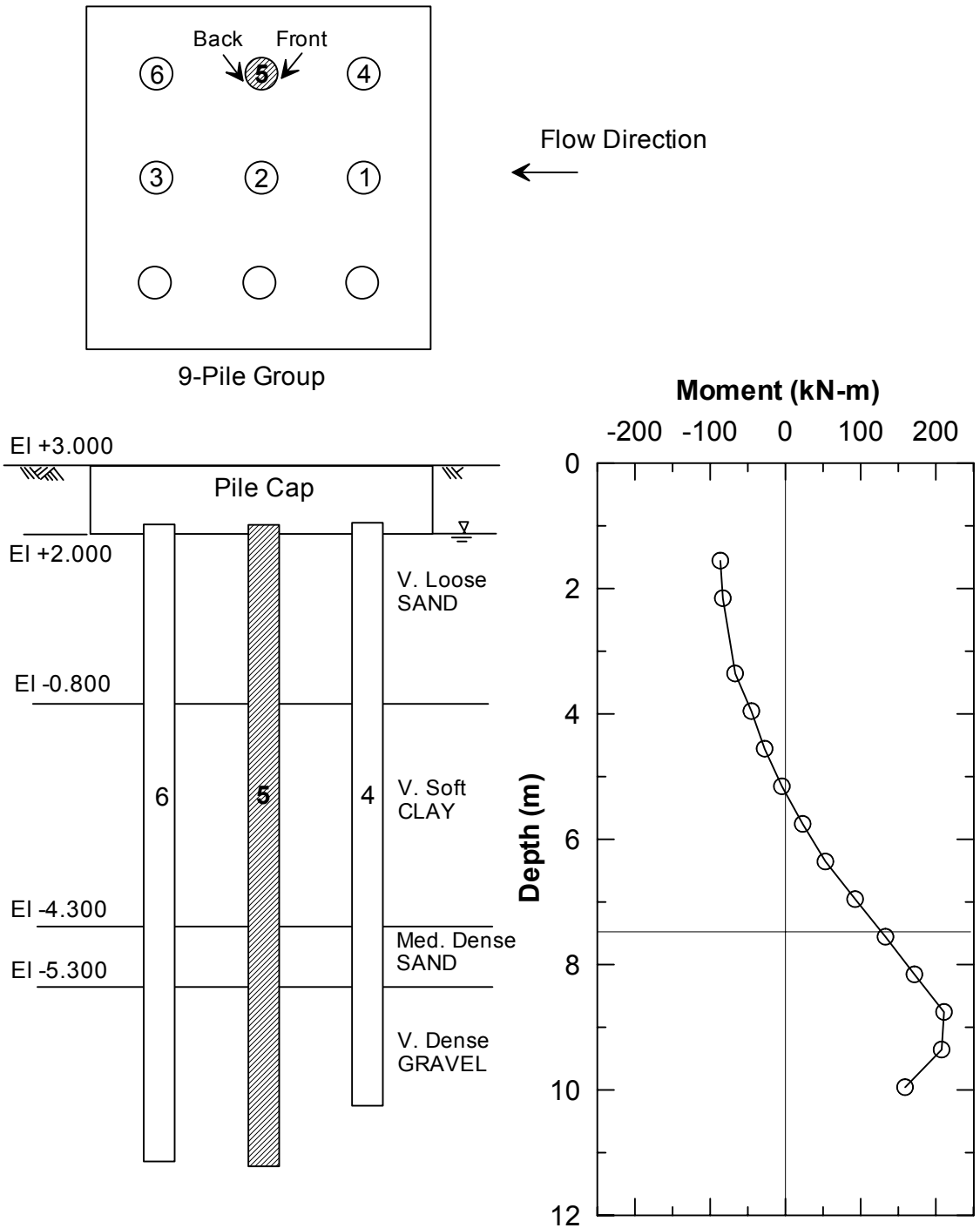
Figure 4.40   Moment Distribution along Pile No.5 of 9-Pile Group after Lateral Spreading (t = 70 s)
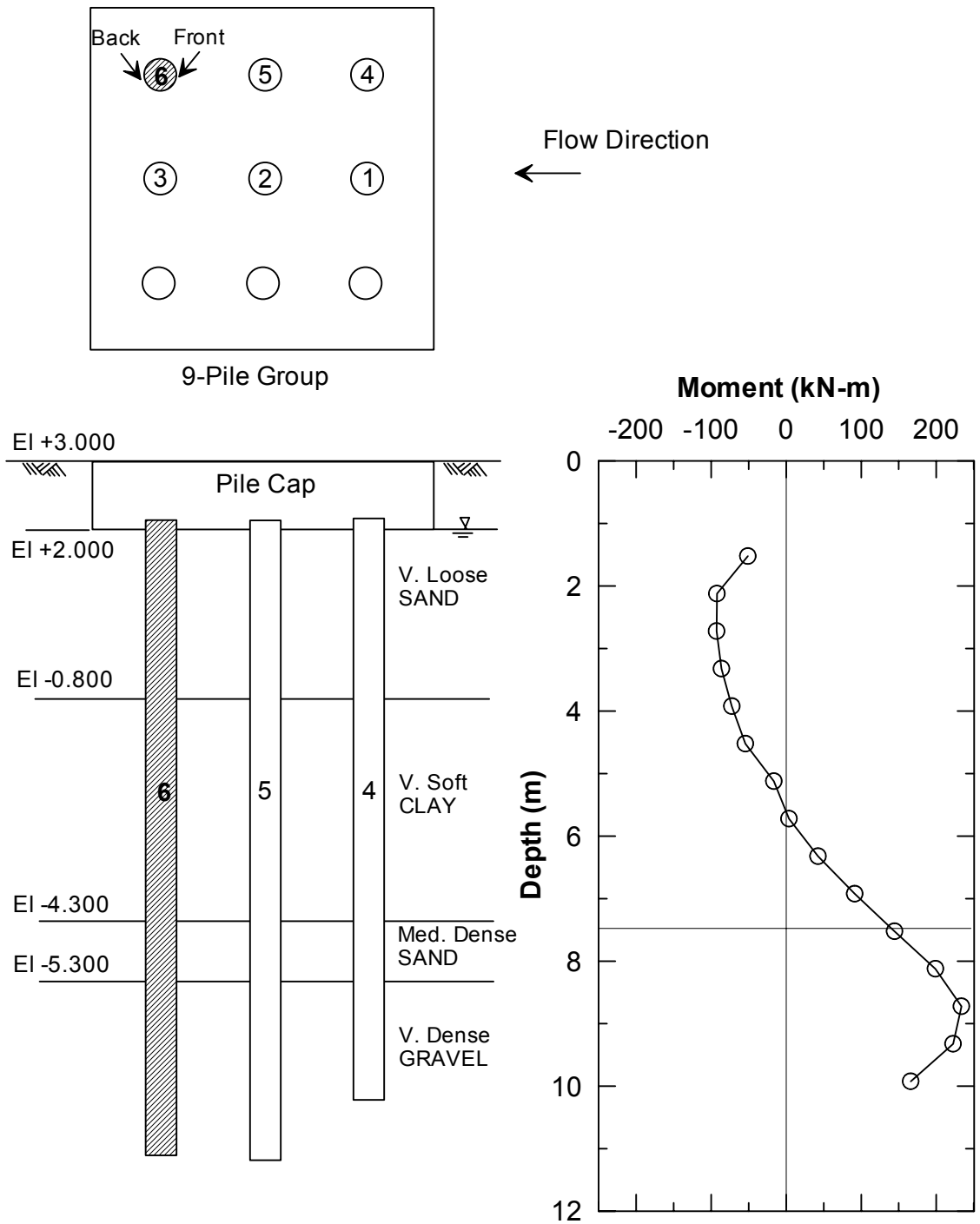
Figure 4.41   Moment Distribution along Pile No.6 of 9-Pile Group after Lateral Spreading (t = 70 s)
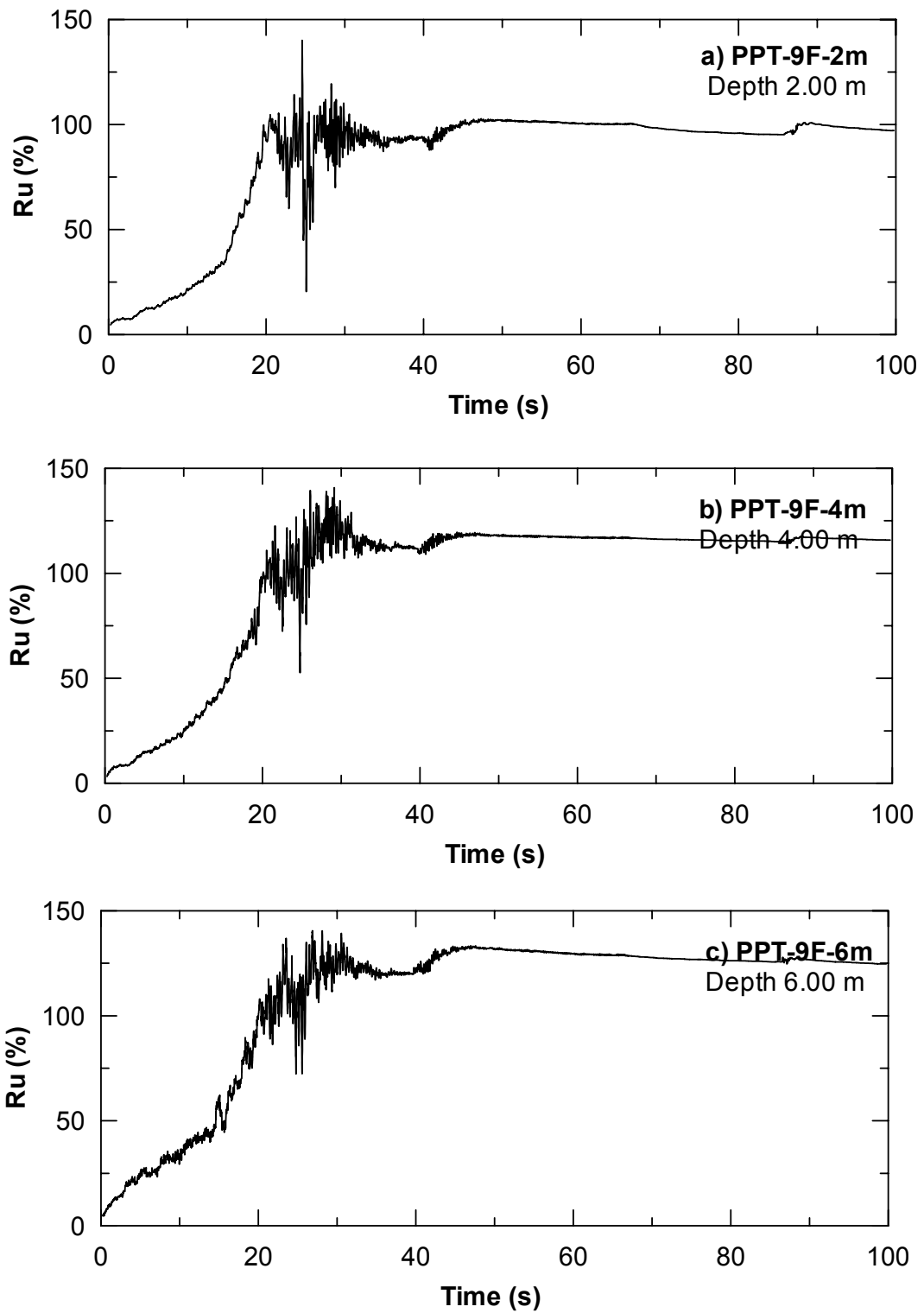
Figure 4.42   Excess Pore Water Pressure Ratio nearby 9-Pile Group (Front Side) (a) PPT-9F-2m, (b) PPT-9F-4m, and (c) PPT-9F-6m, 100s Duration
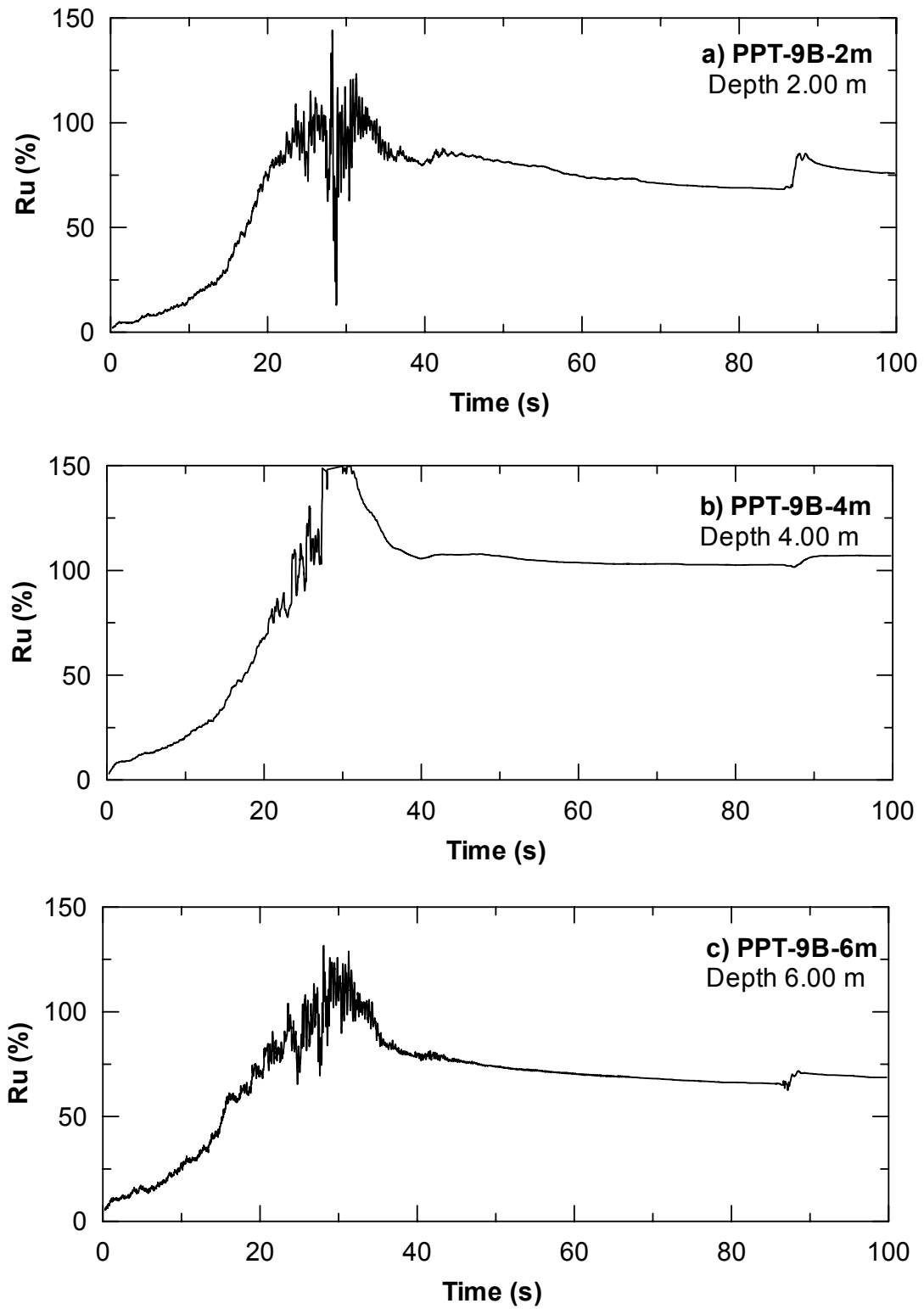
Figure 4.43 Excess Pore Water Pressure Ratio nearby 9-Pile Group (Back Side) (a) PPT-9F-2m, (b) PPT-9F-4m, and (c) PPT-9F-6m, 100s Duration
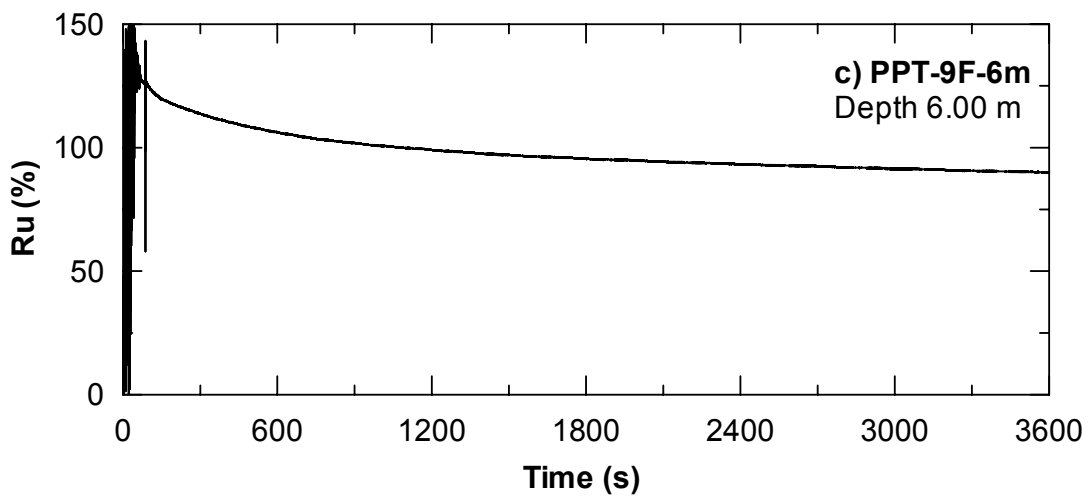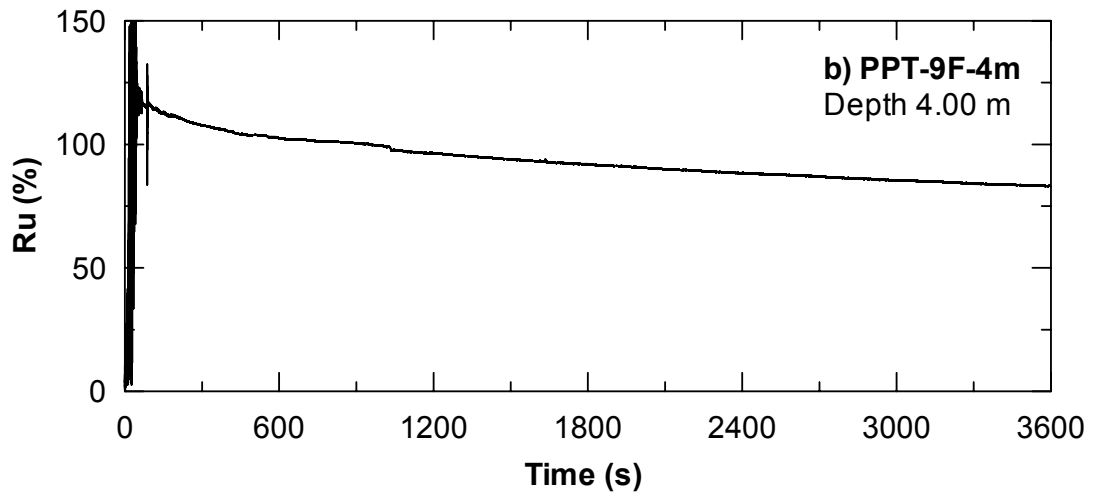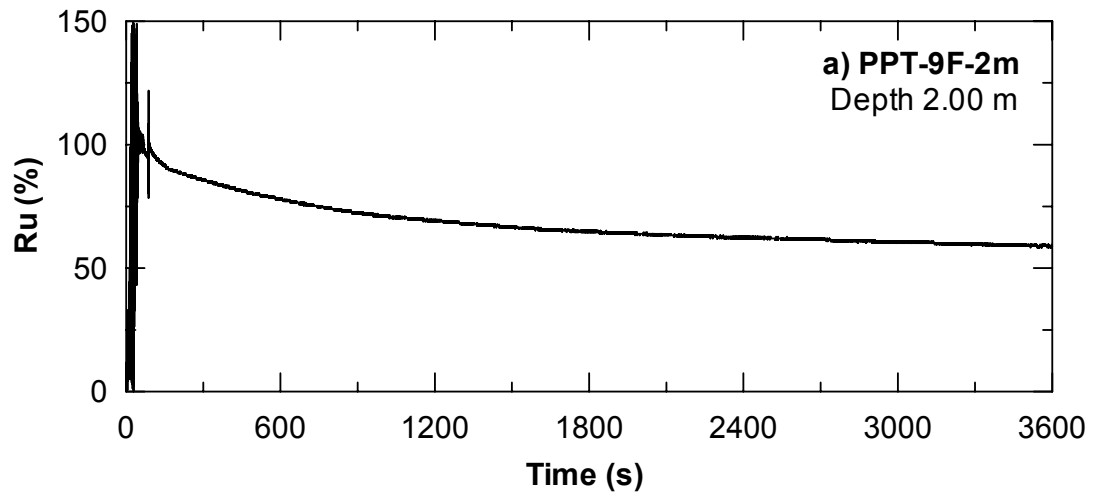
Figure 4.44   Excess Pore Water Pressure Ratio nearby 9-Pile Group (Front) (a) PPT-9F-2m, (b) PPT-9F-4m, and (c) PPT-9F-6m, 3600s Duration
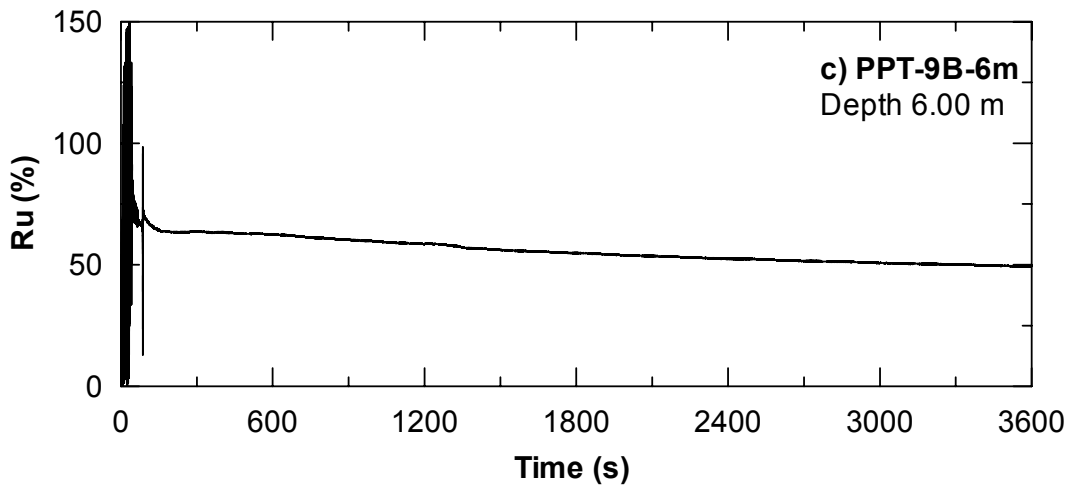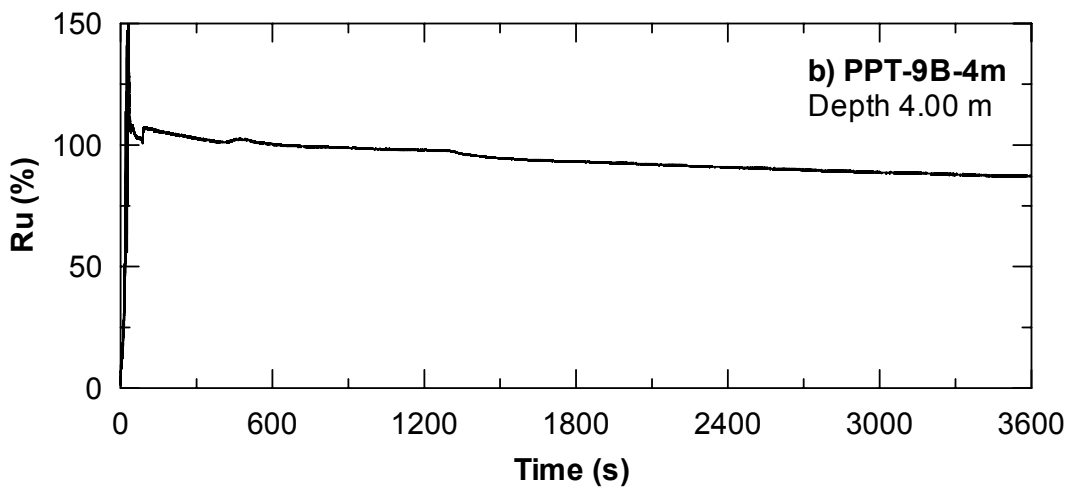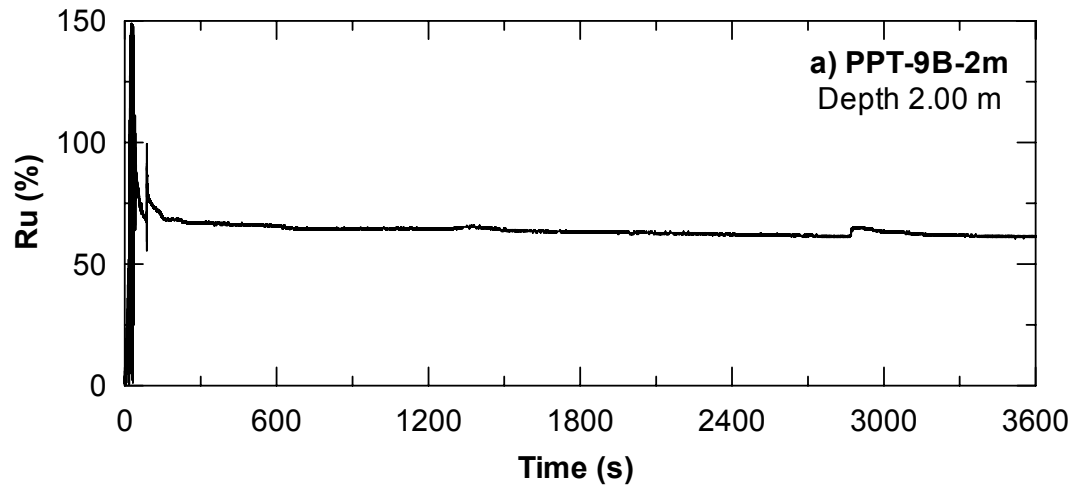
Figure 4.45   Excess Pore Water Pressure Ratio nearby 9-Pile Group (Back) (a) PPT-9B-2m, (b) PPT-9B-4m, and (c) PPT-9B-6m, 3600s Duration
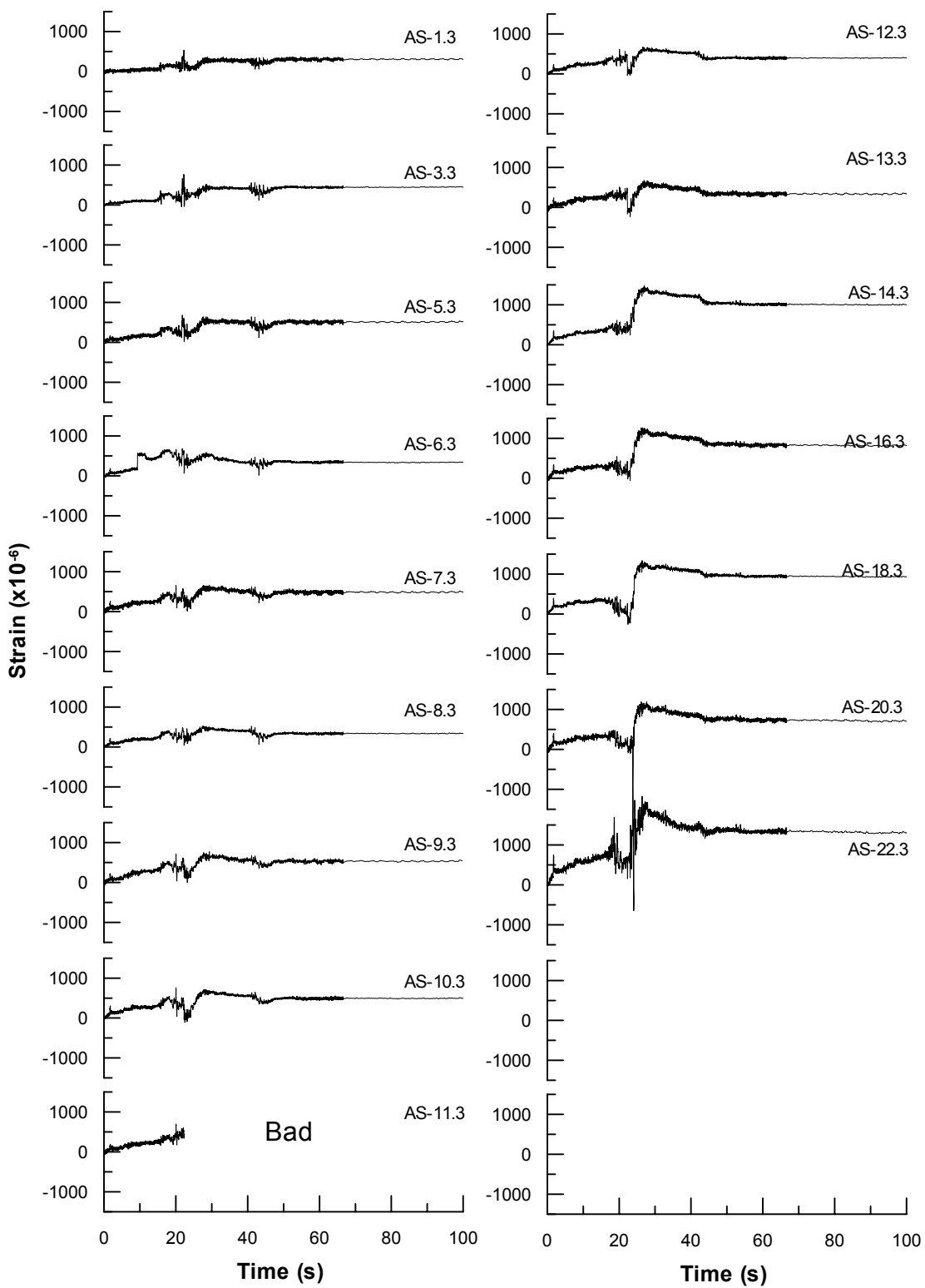
Figure 4.46   Strain Gauge Response along the Side of Transverse Gas-Pipeline
(Pipeline Type A)

129
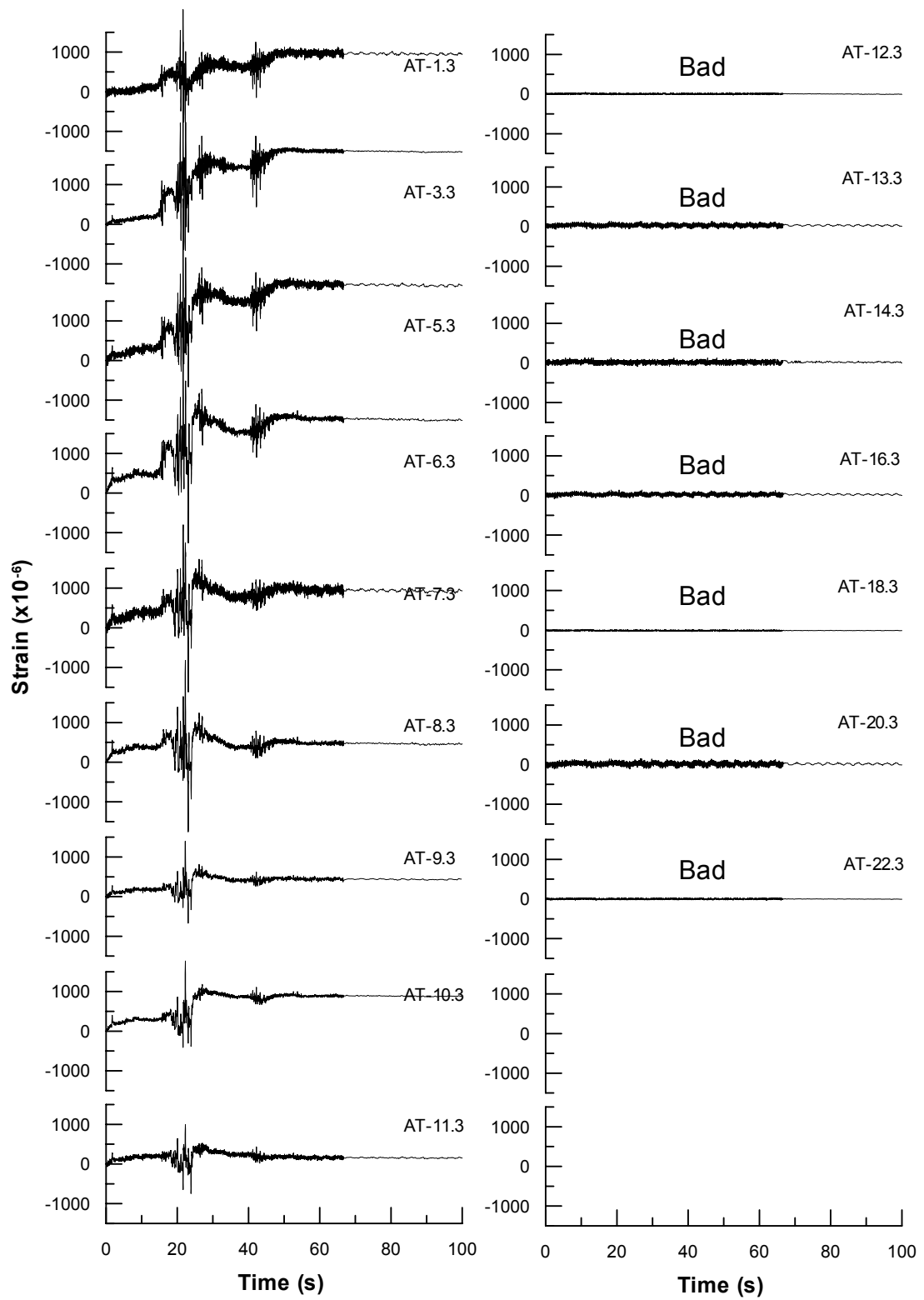
Figure 4.47   Strain Gauge Response along the Top of Transverse Gas-Pipeline (Pipeline Type A)
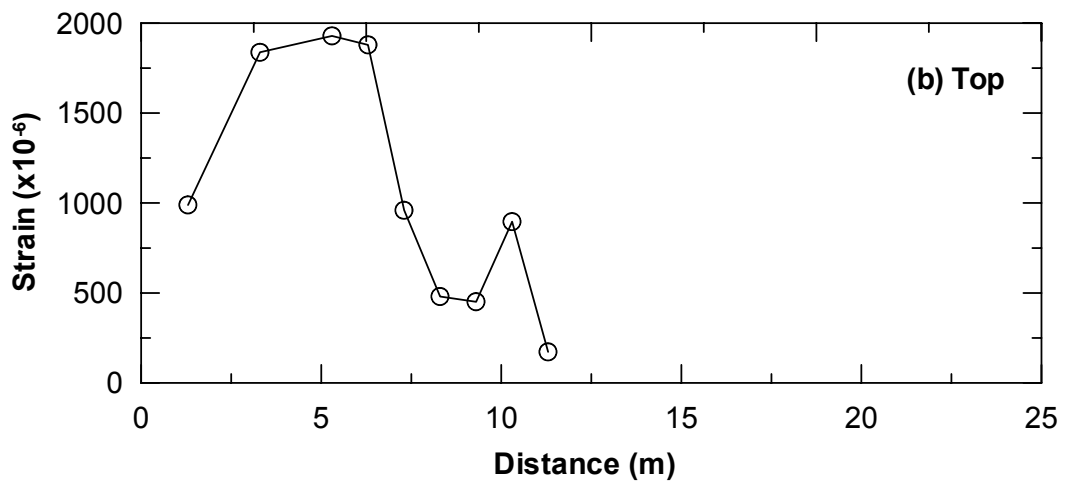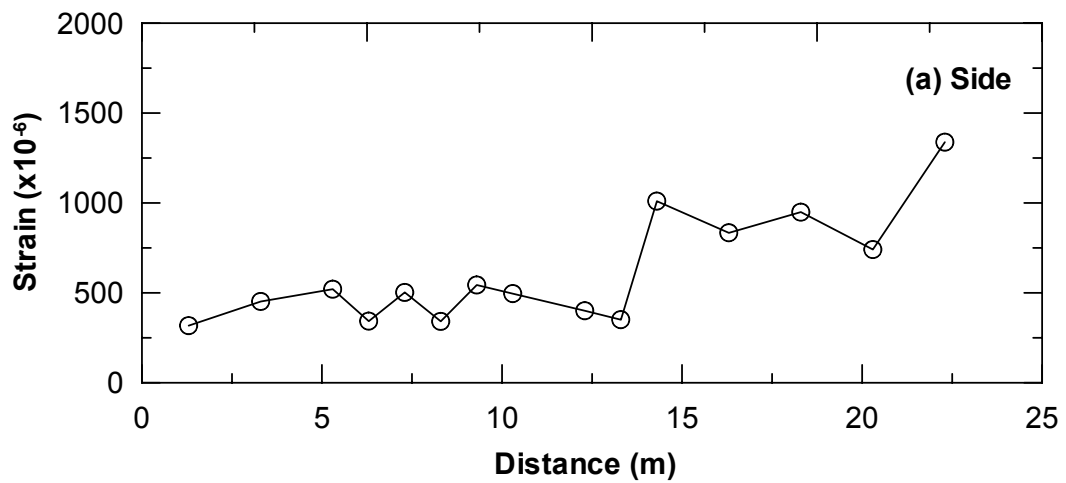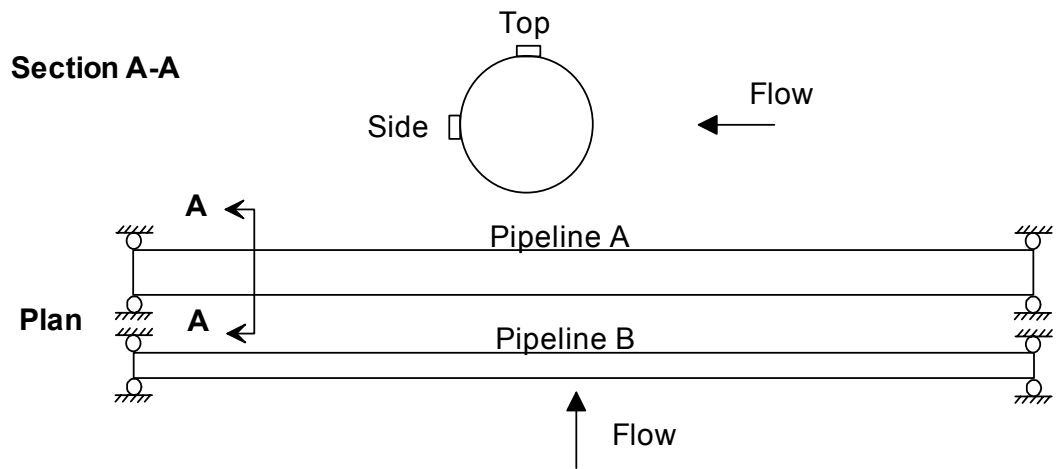
Figure 4.48   Profile of Residual Strain of Pipeline Type A (t = 70s) at (a) Side of
Pipeline, and (b) Top of Pipeline
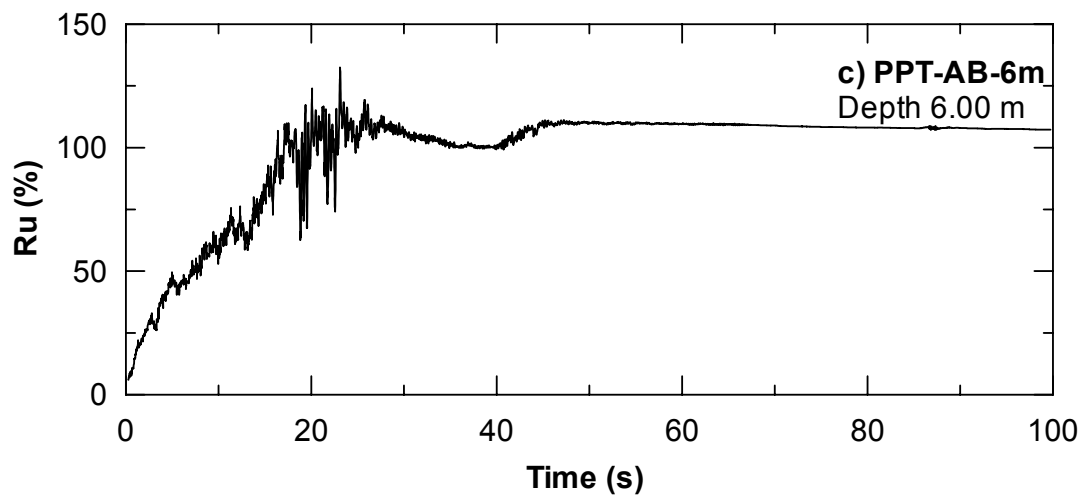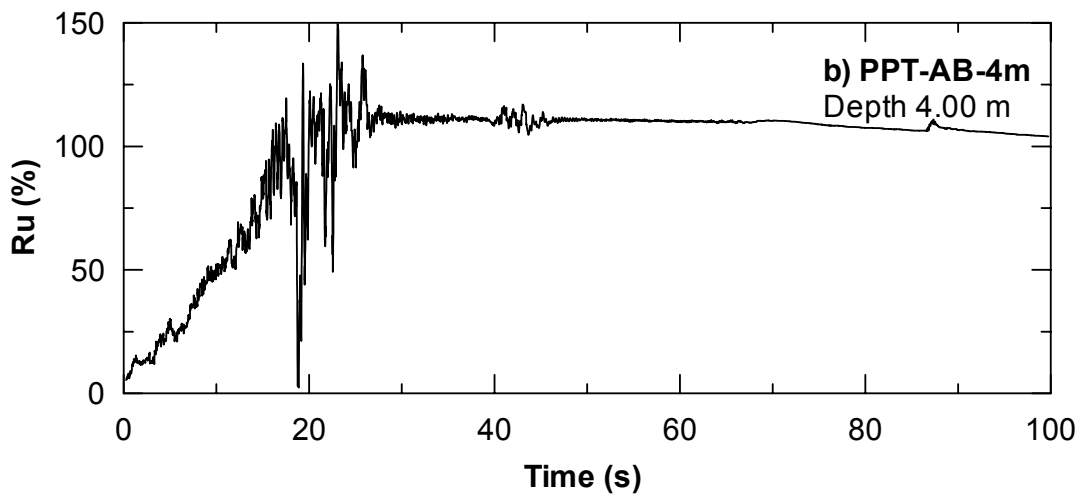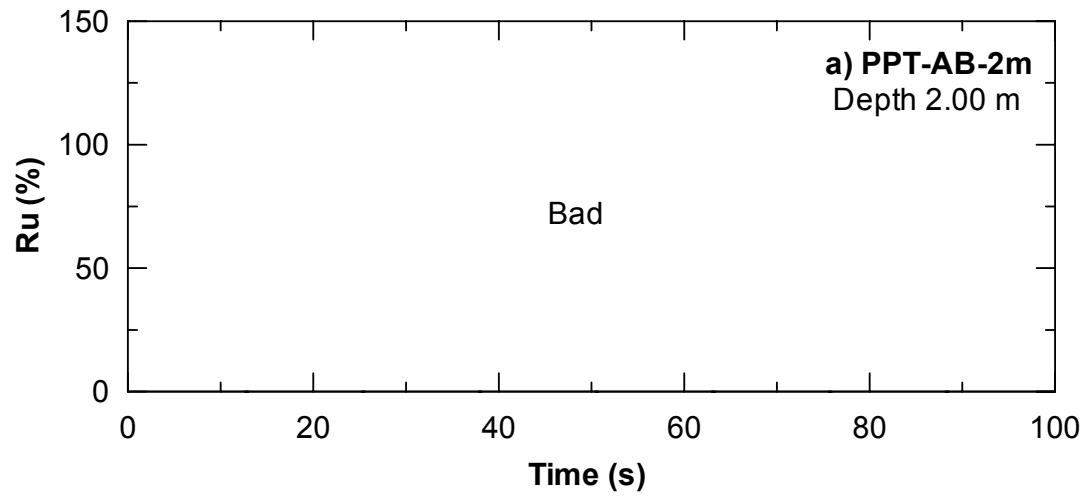
Figure 4.49   Excess Pore Water Pressure between Pipeline A and B (a) PPT-AB-2m,
(b) PPT-AB-4m, and (c) PPT-AB-6m, 100s Duration
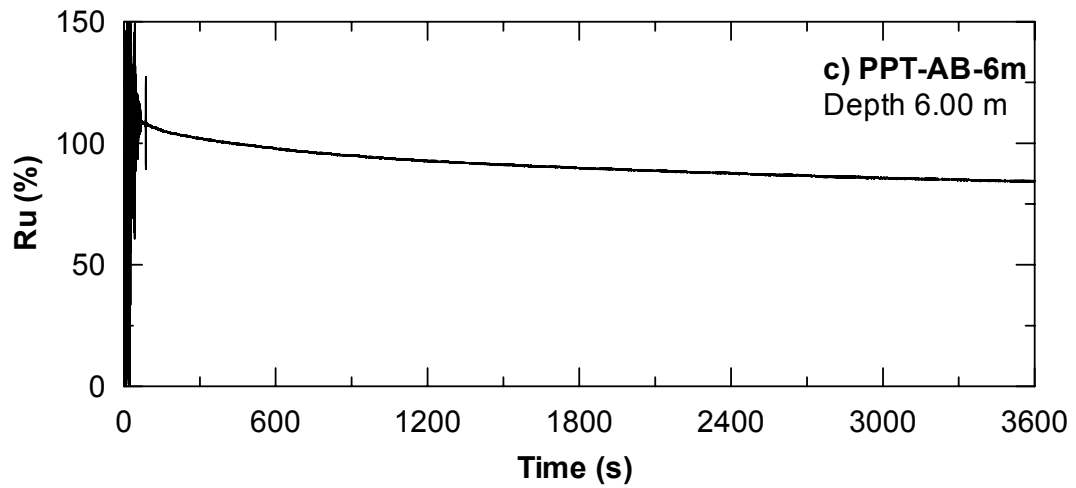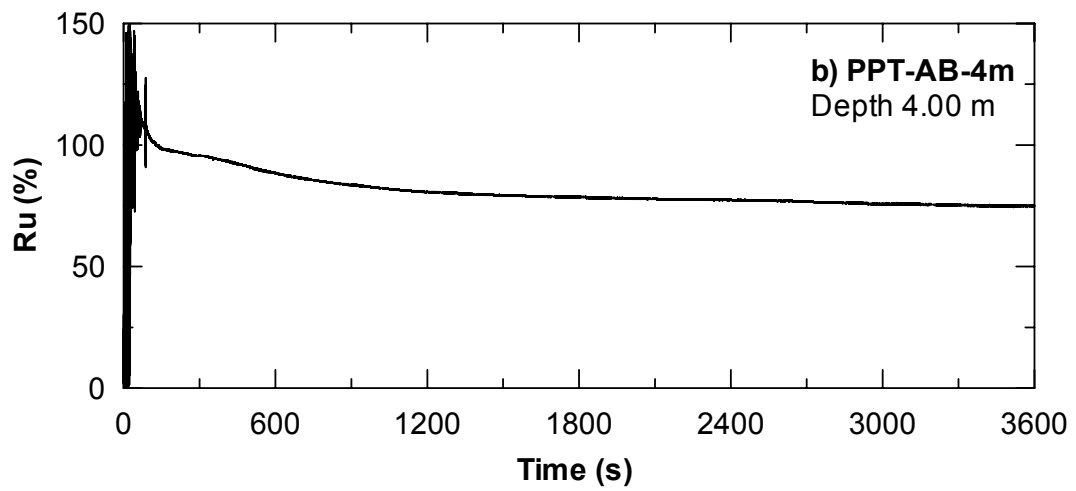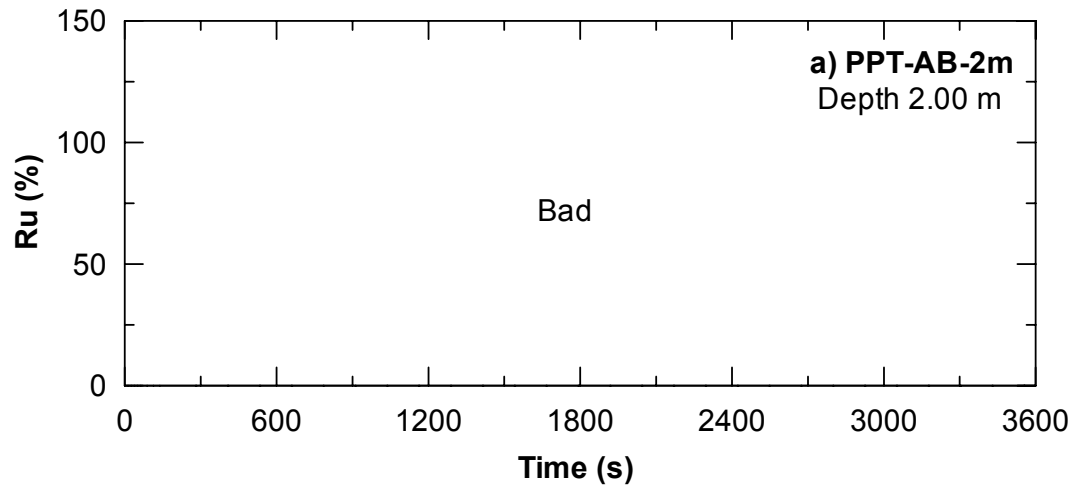
Figure 4.50   Excess Pore Water Pressure Ratio between Pipelines A and B at Depths
(a) 2.00 m, (b) 4.00 m, and (c) 6.00 m, 3600s Duration
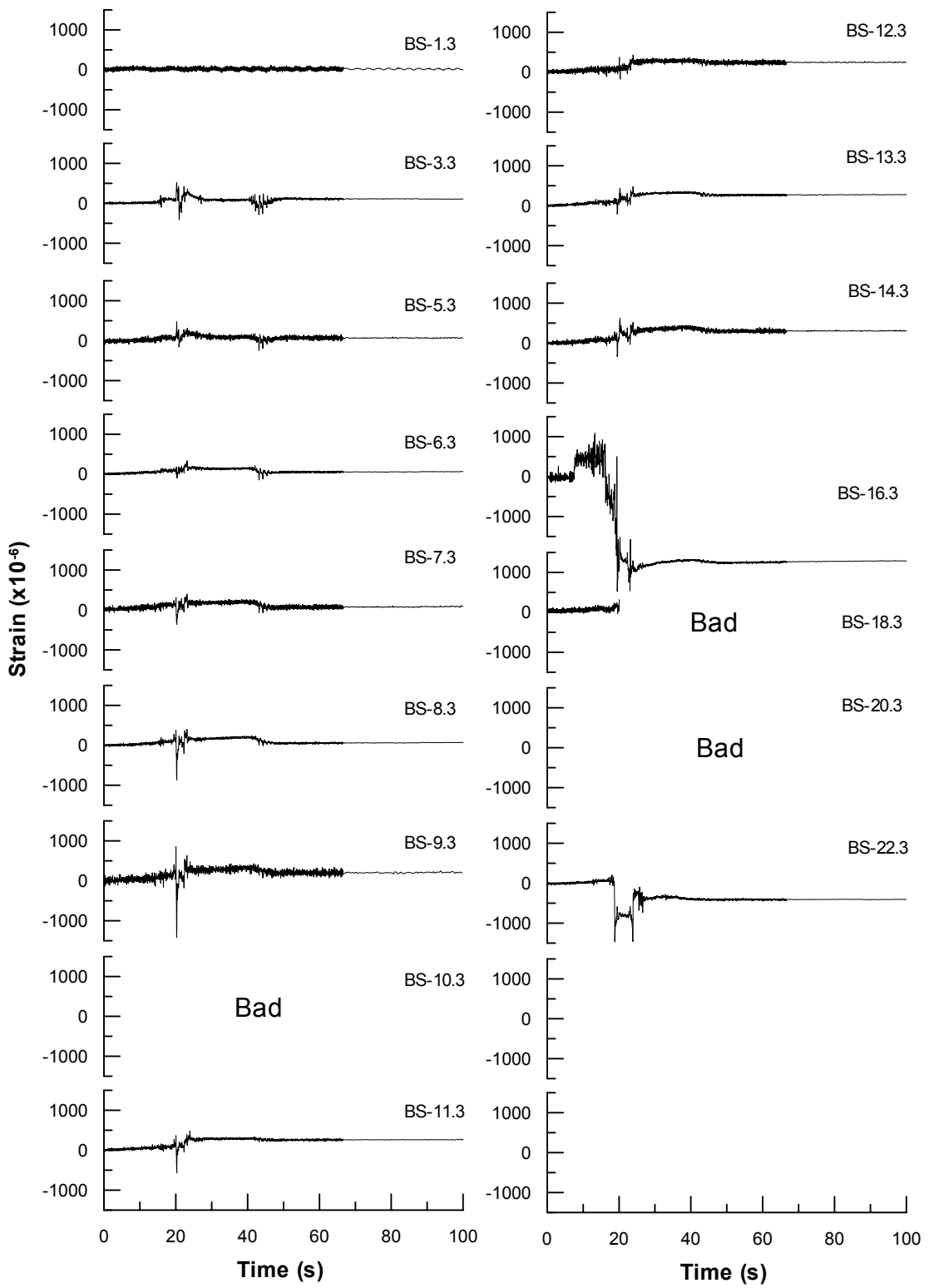
Figure 4.51   Strain Gauge Response along the Side of Transverse Electrical Conduit (Pipeline Type B)

134
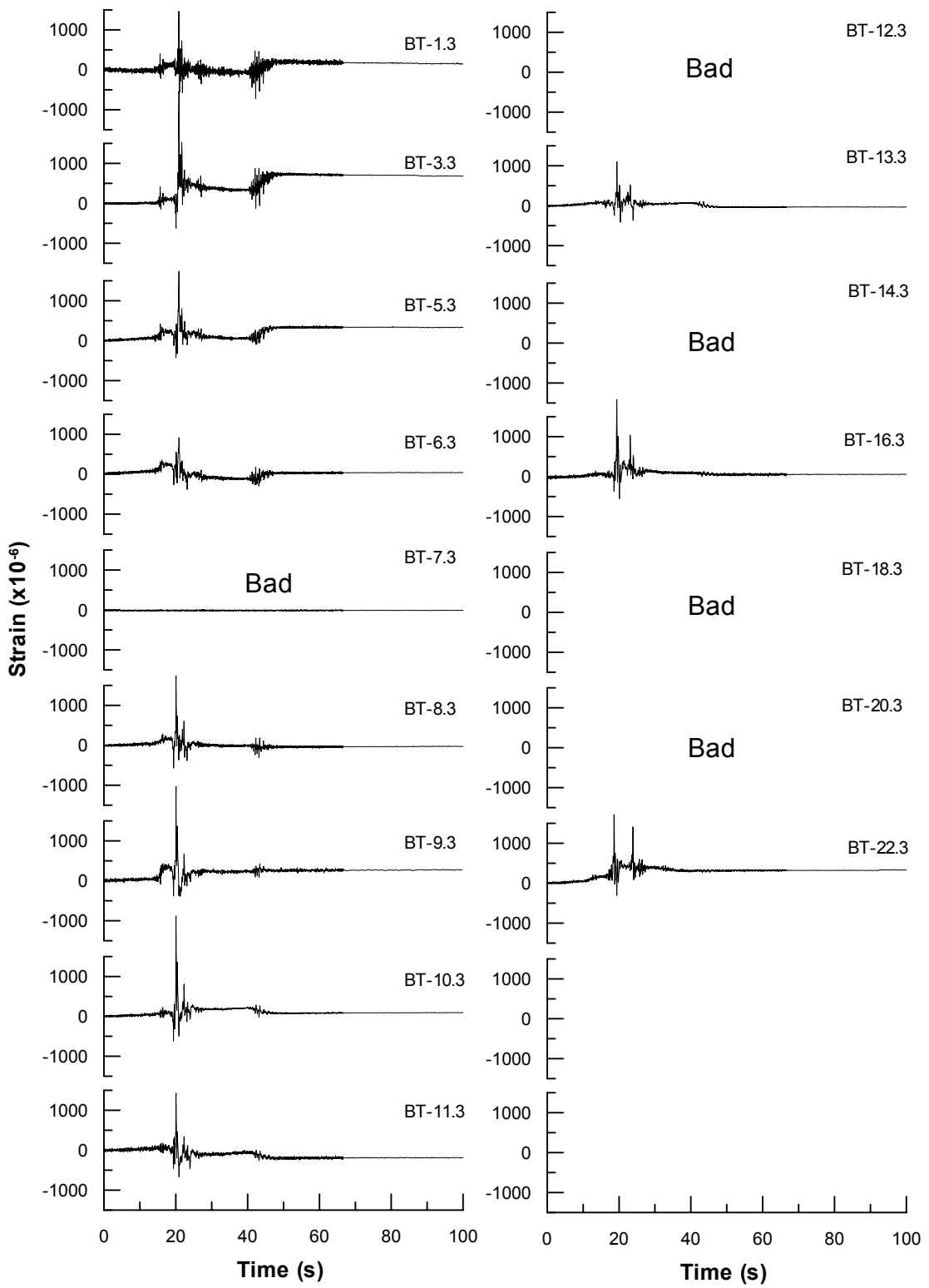
Figure 4.52   Strain Gauge Response along the Top of Transverse Electrical Conduit (Pipeline Type B)
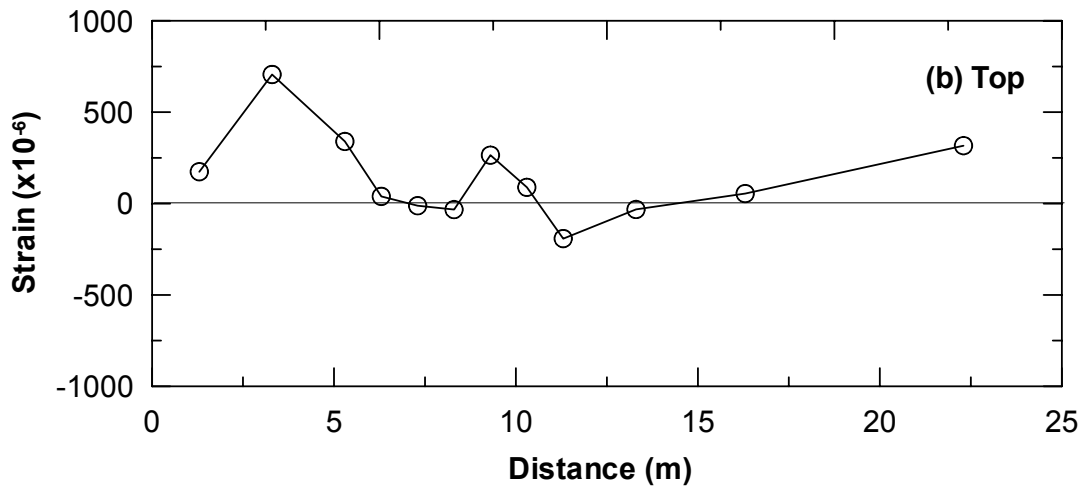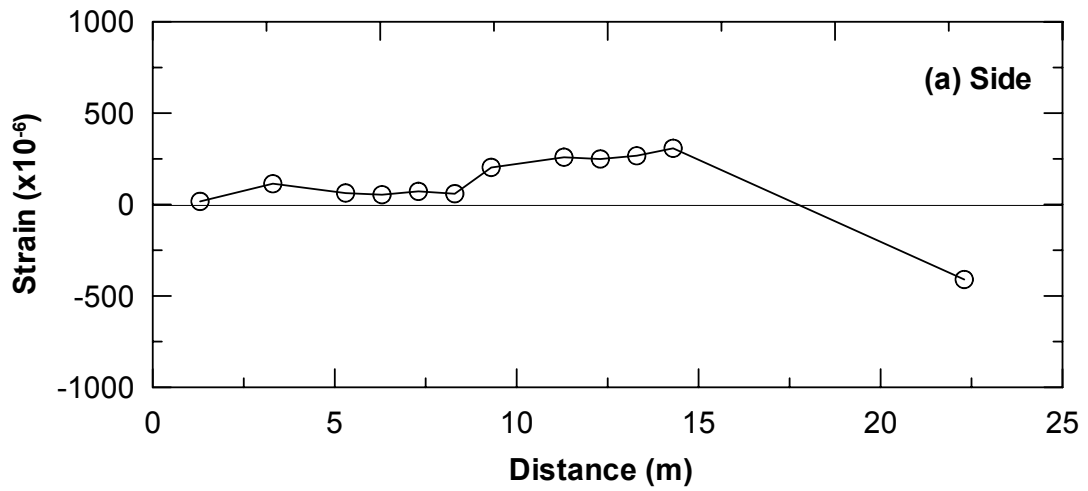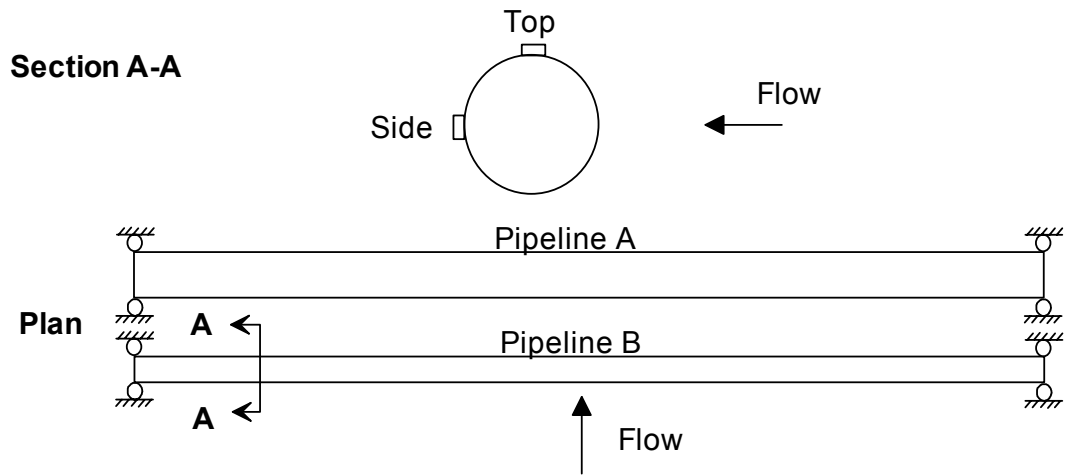
Figure 4.53   Profile of Residual Strain of Pipeline Type B (t = 70s) at (a) Side of Pipeline, and (b) Top of Pipeline
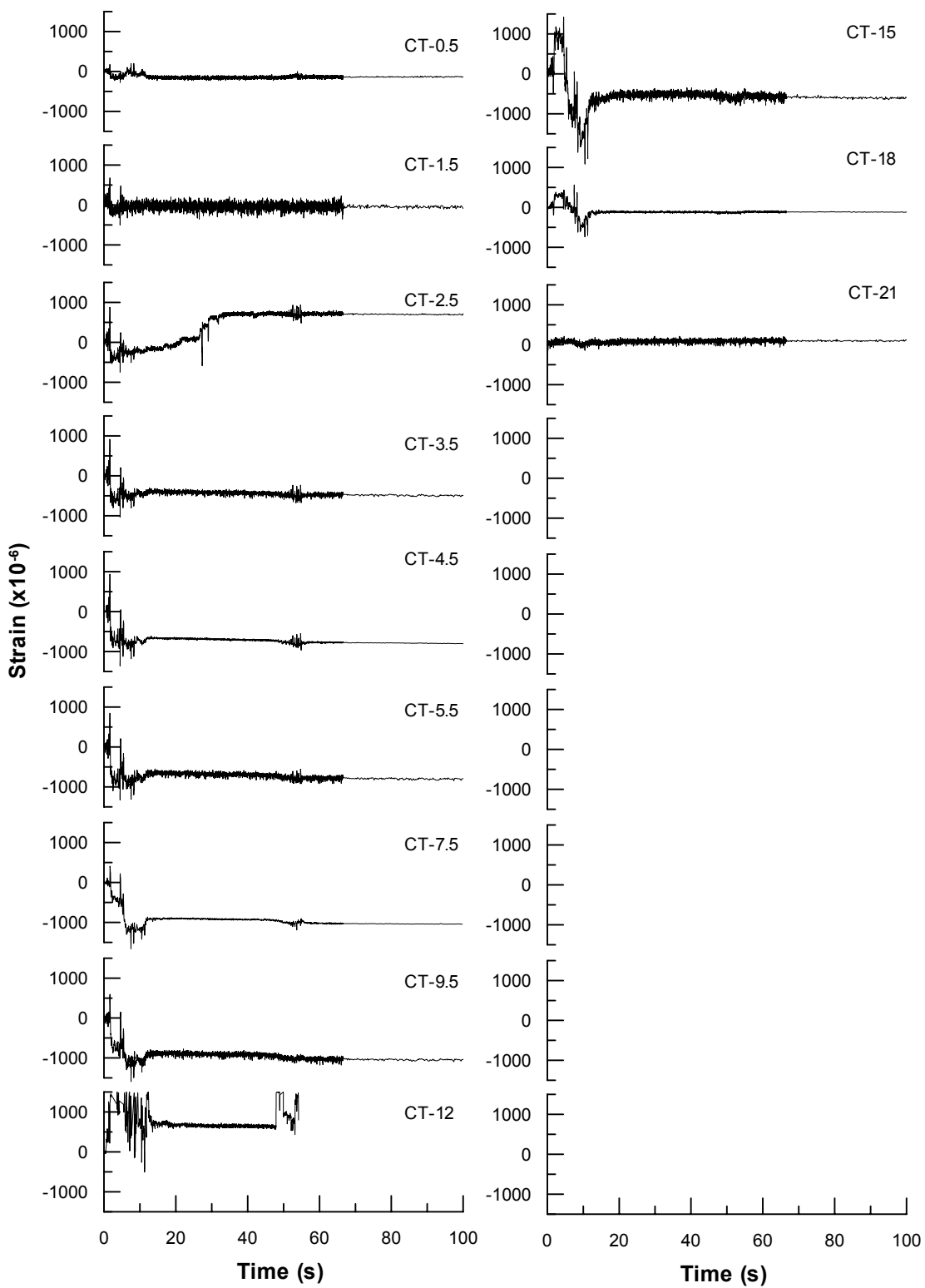
Figure 4.54   Strain Gauge Response along the Top of Longitudinal Gas Pipeline (Pipeline Type C)

137
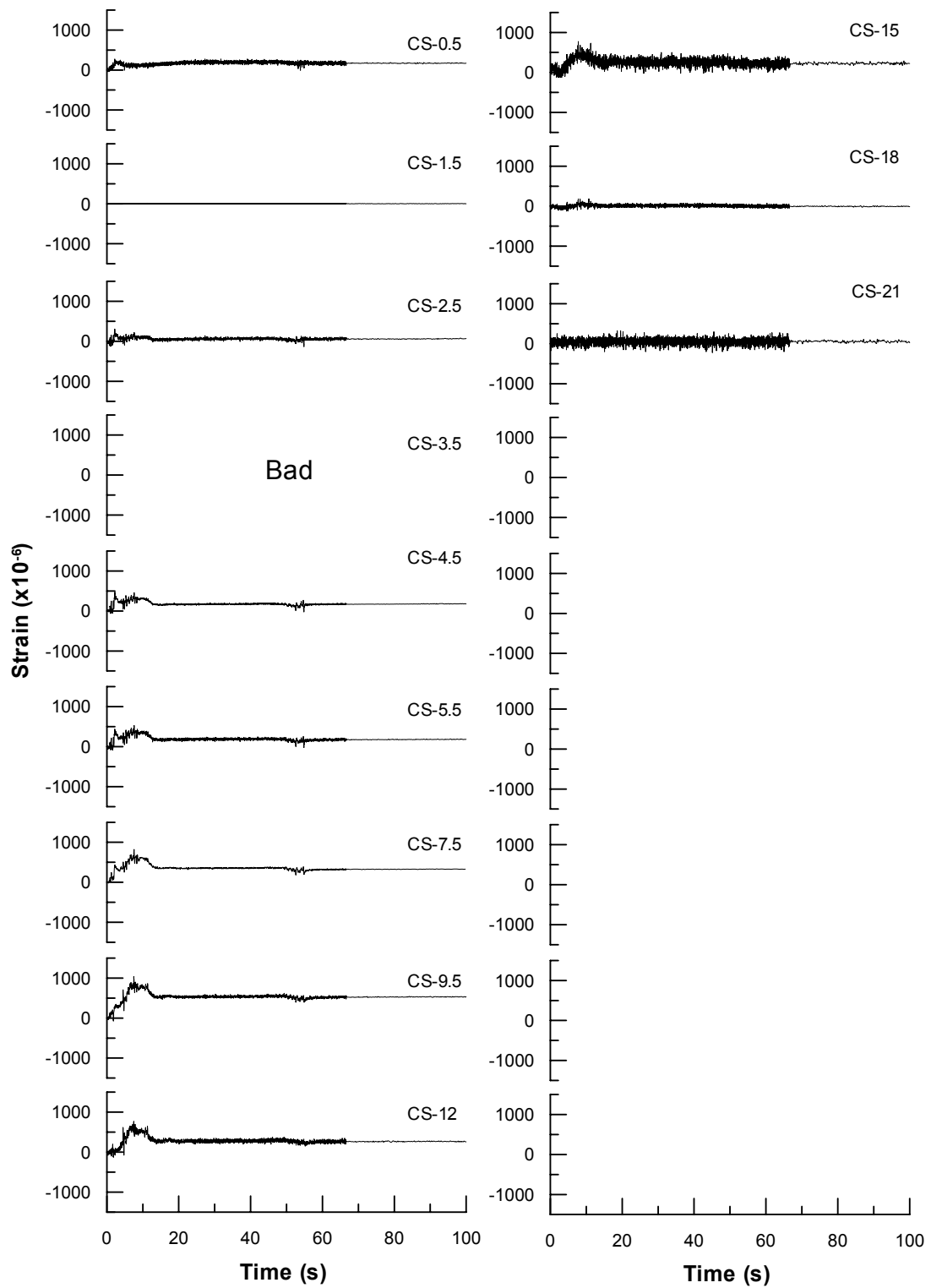
Figure 4.55   Strain Gauge Response along the Side of Longitudinal Gas Pipeline (Pipeline Type C)
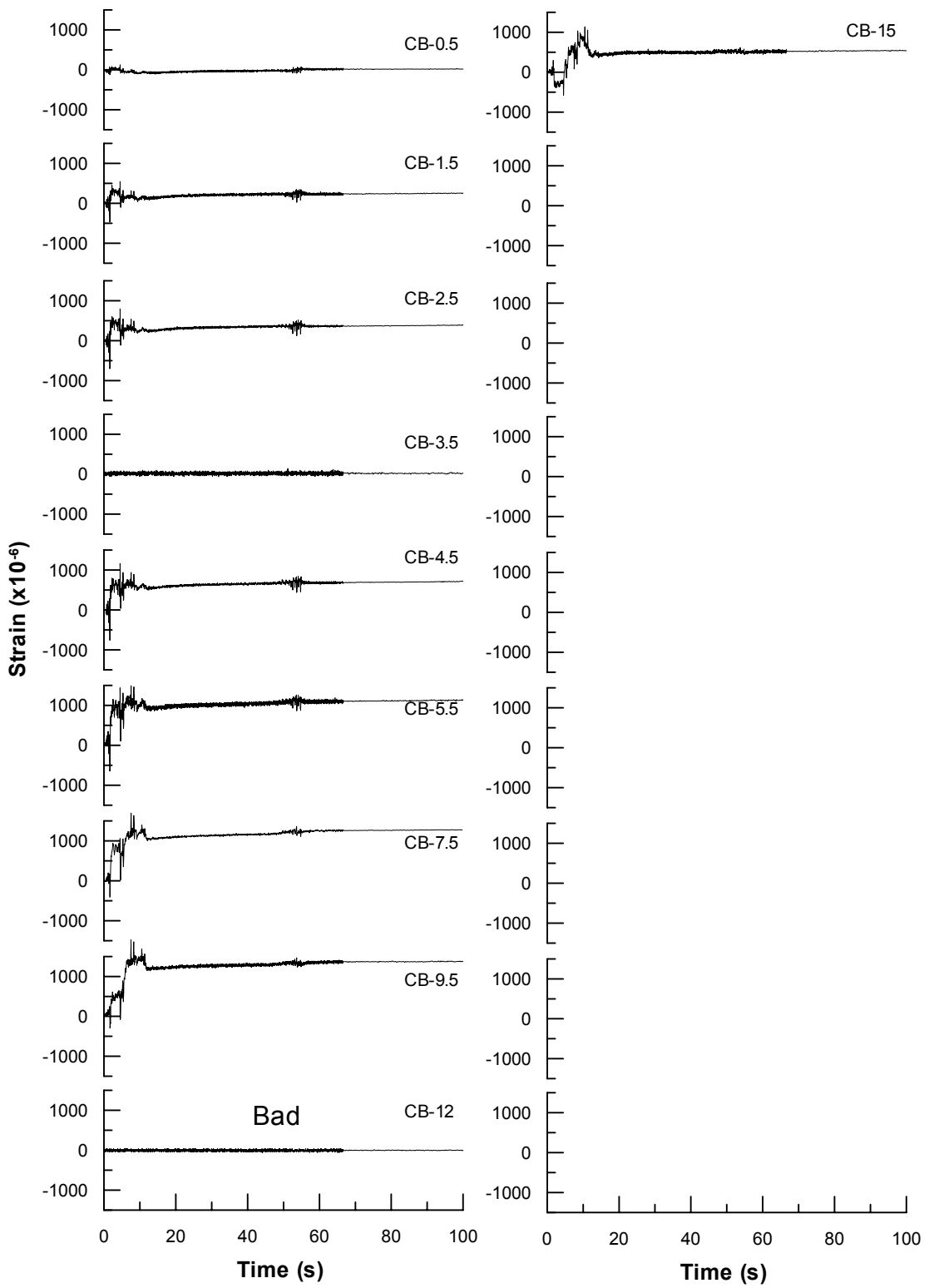
Figure 4.56   Strain Gauge Response along the Bottom of Longitudinal Gas Pipeline
(Pipeline Type C)
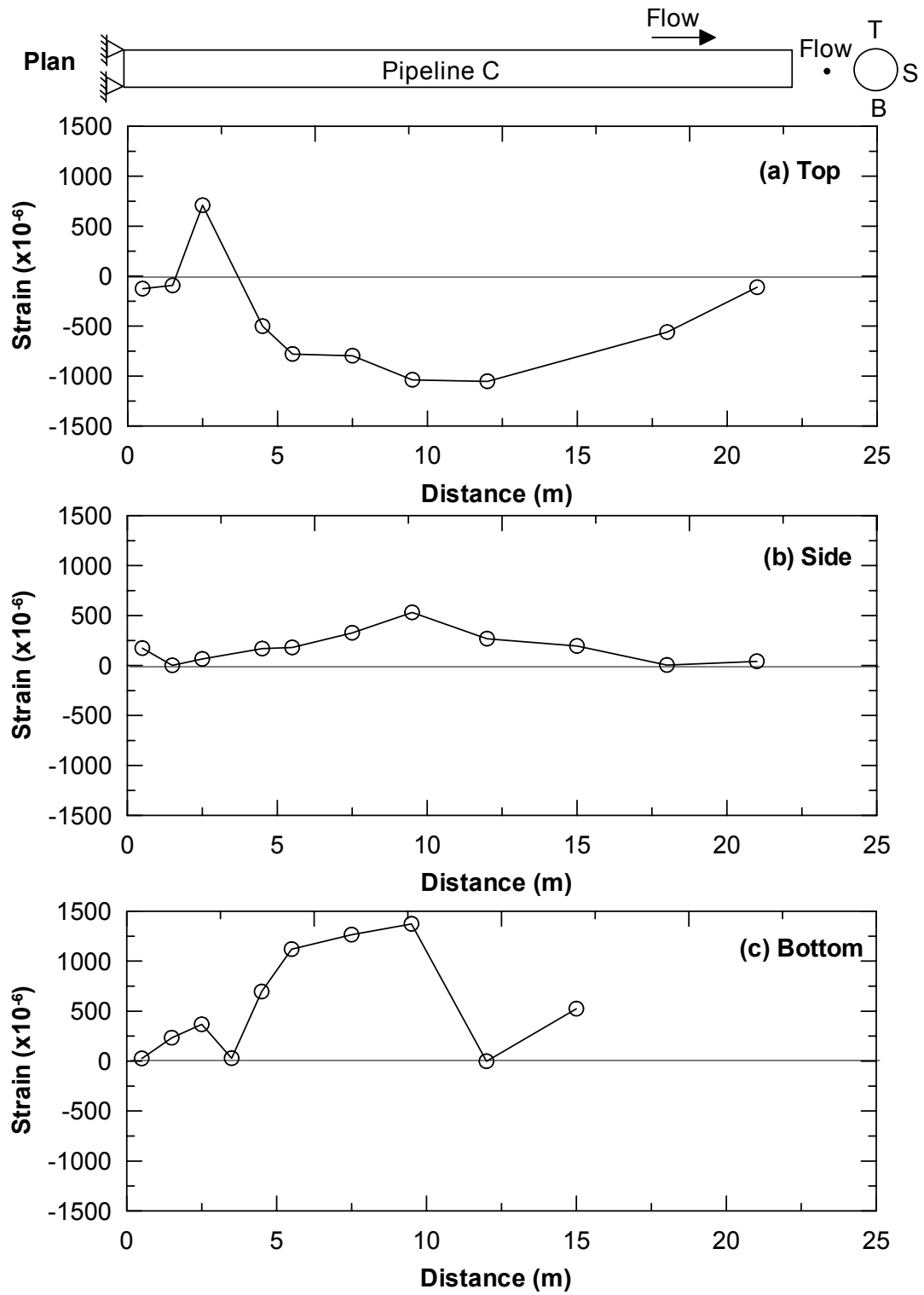
Figure 4.57   Profile of Residual Strain of Pipeline Type C (t = 70s) at (a) Top, (b)
Side, and (c) Bottom of Pipeline

Figure 4.58   Lateral Movement of Sheet Pile due to Effect of Blasting
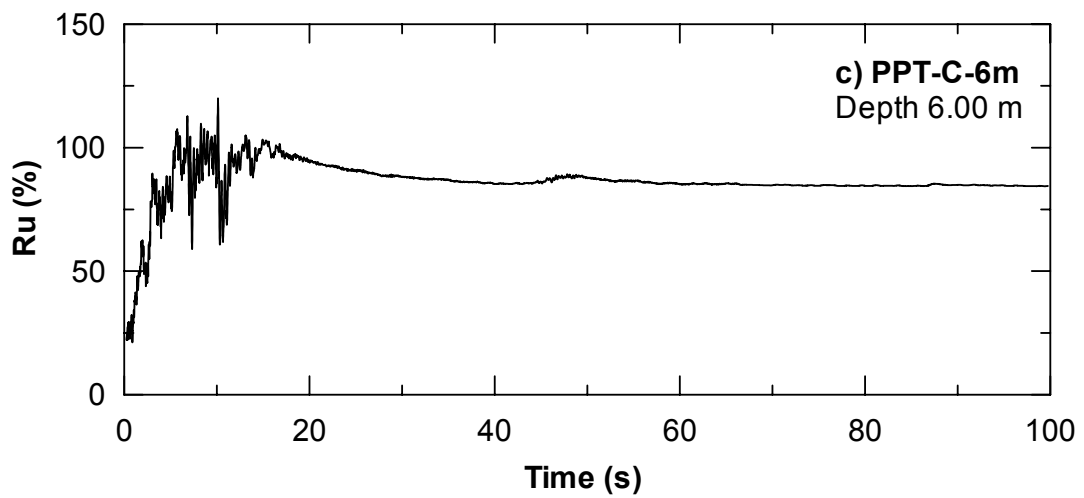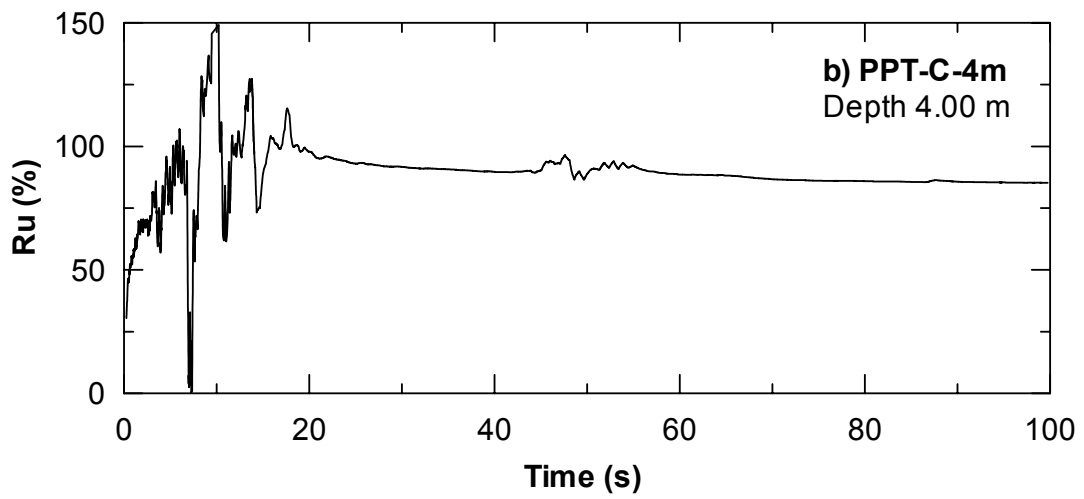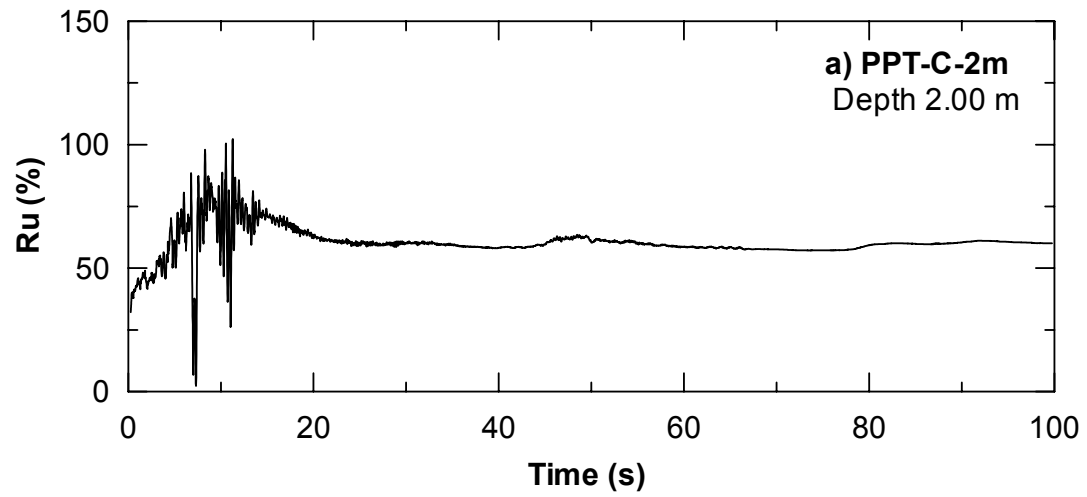
Figure 4.59 Excess Pore Water Pressure between Pipeline C (a) PPT-C-2m, (b) PPT-C-4m, and (c) PPT-C-6m, 100s Duration
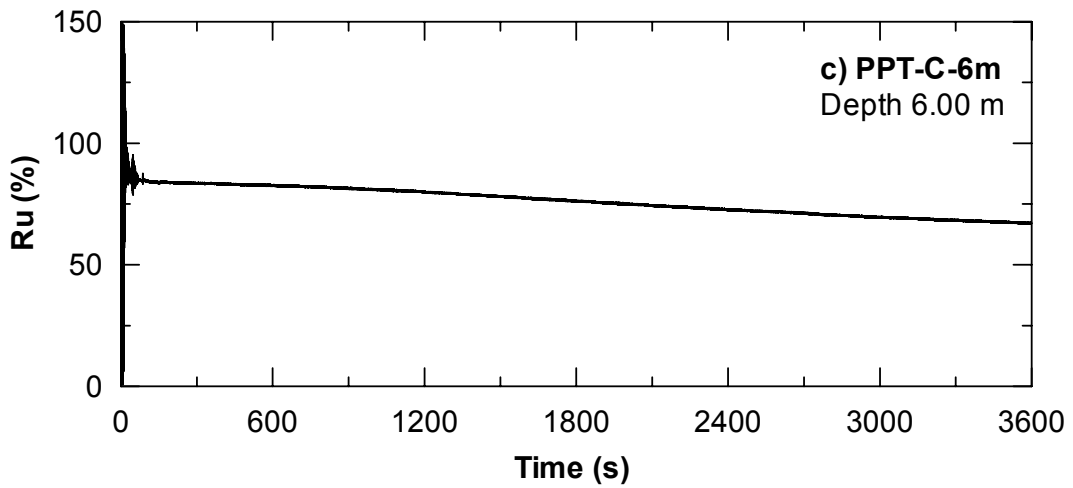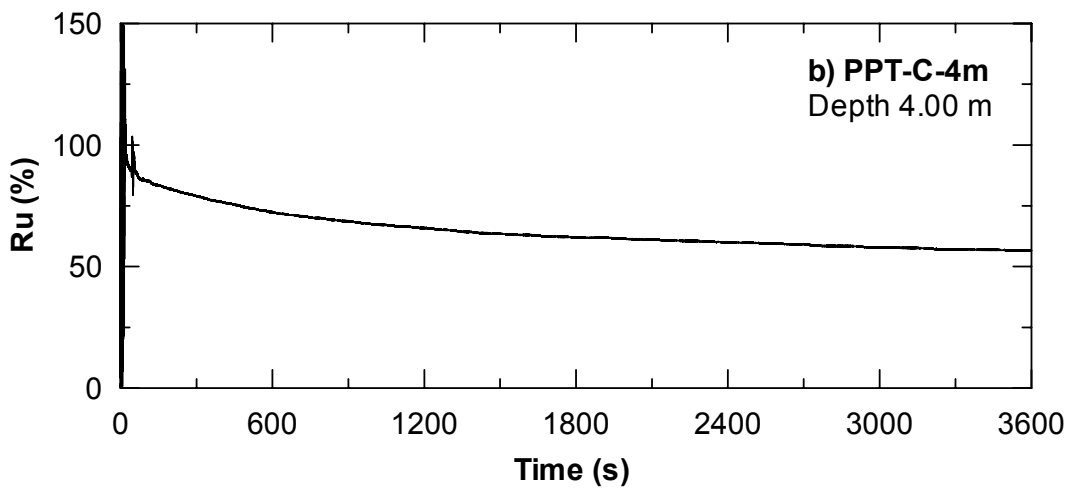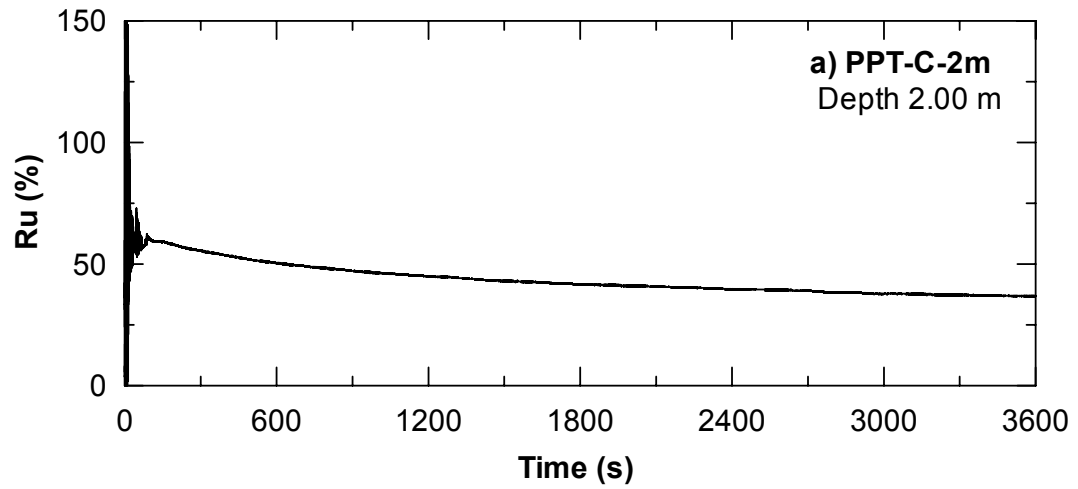
Figure 4.60   Excess Pore Water Pressure between Pipeline C (a) PPT-C-2m, (b) PPT-C-4m, and (c) PPT-C-6m, 3600 s Duration
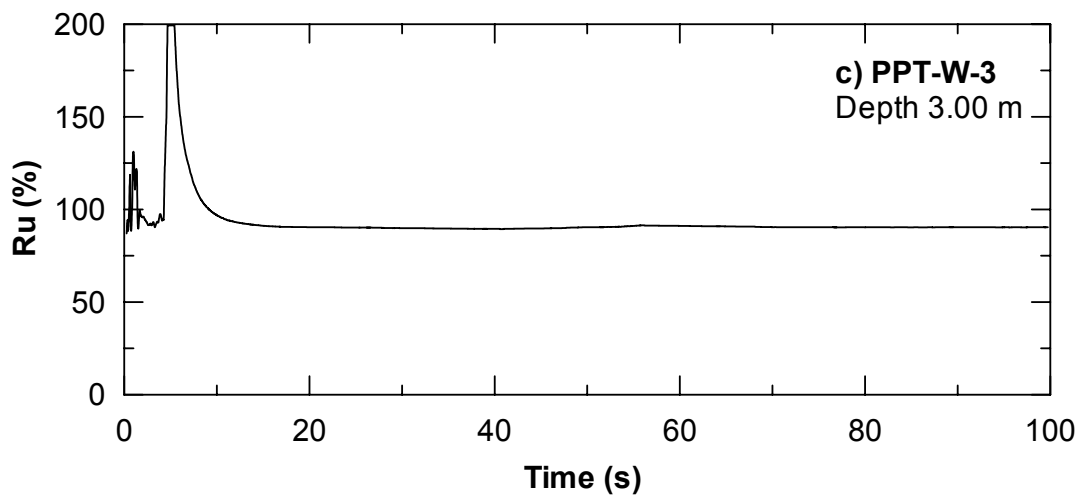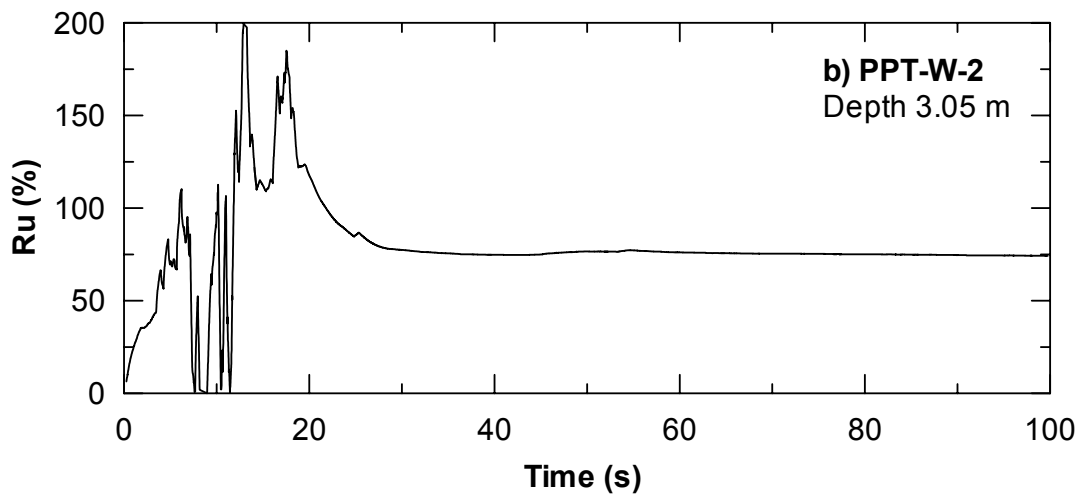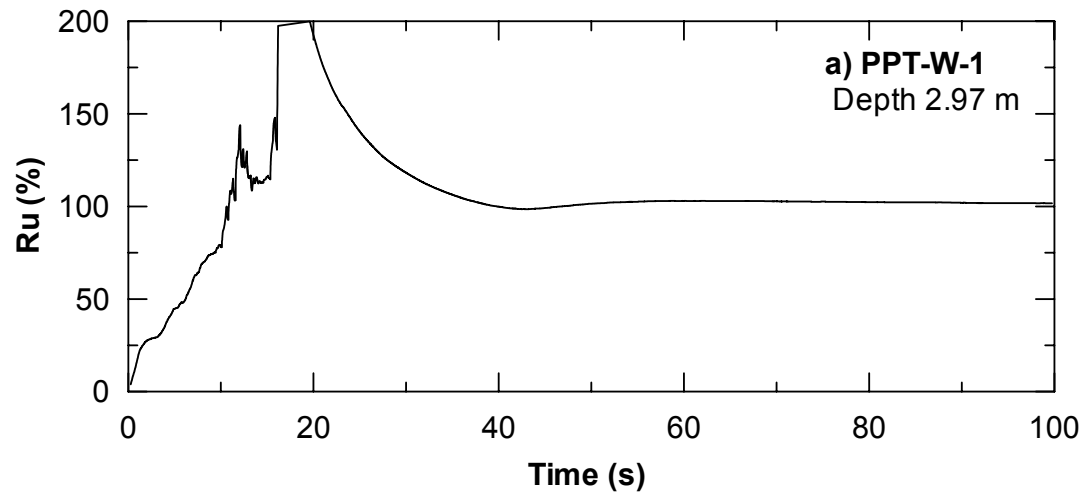
Figure 4.61   Excess Pore Pressure Ratio for (a) PPT -W-1, (b) PPT-W-2, and (c) PPT-W-3, 100s Duration

144
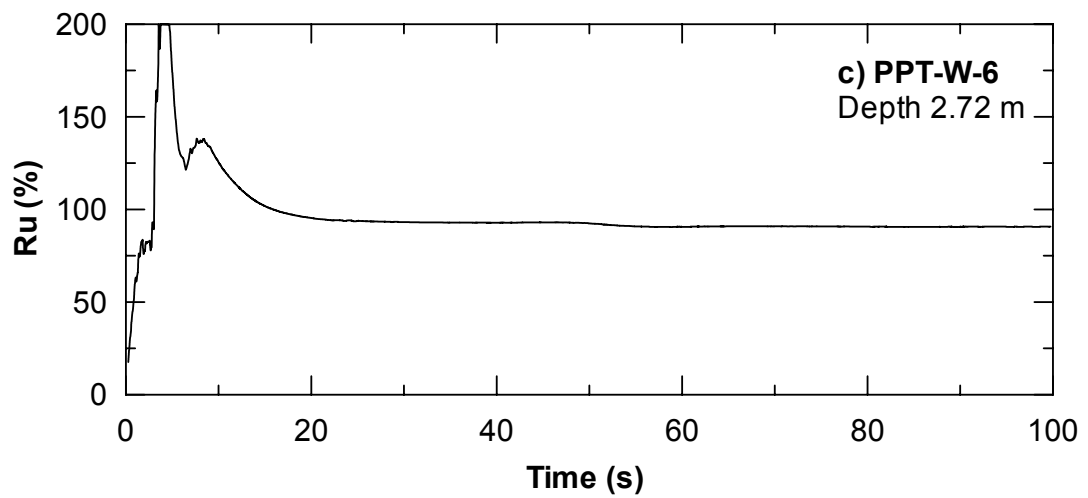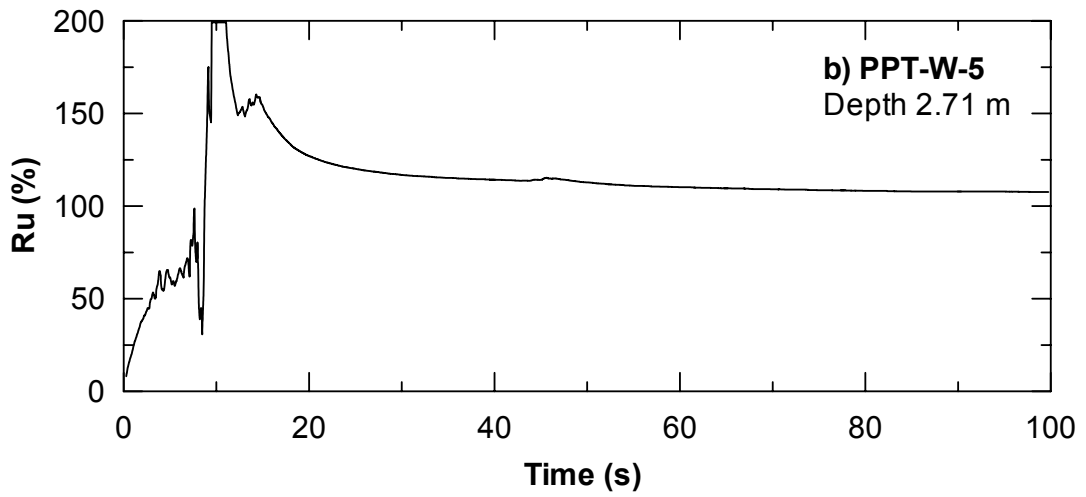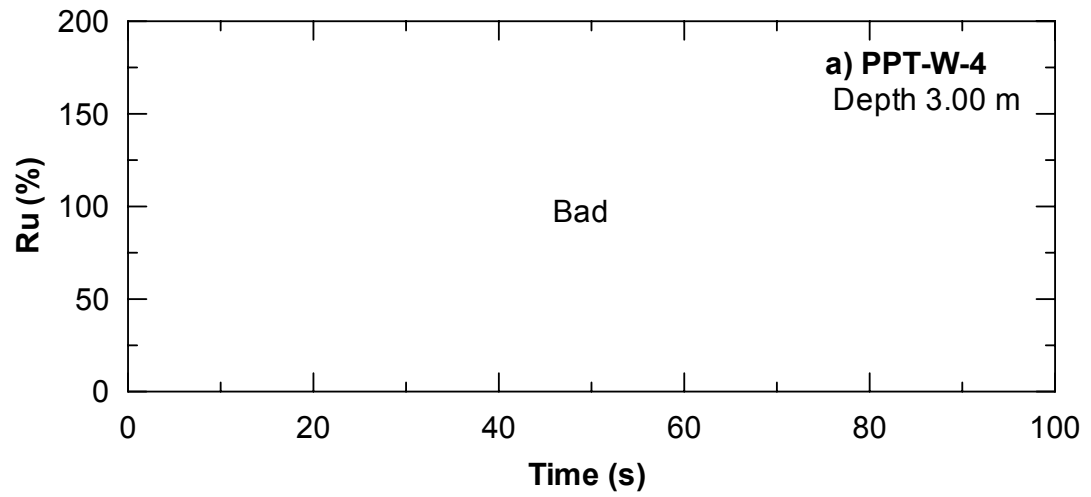
Figure 4.62   Excess Pore Pressure Ratio for (a) PPT -W-4, (b) PPT-W-5, and (c) PPT-W-6, 100s Duration
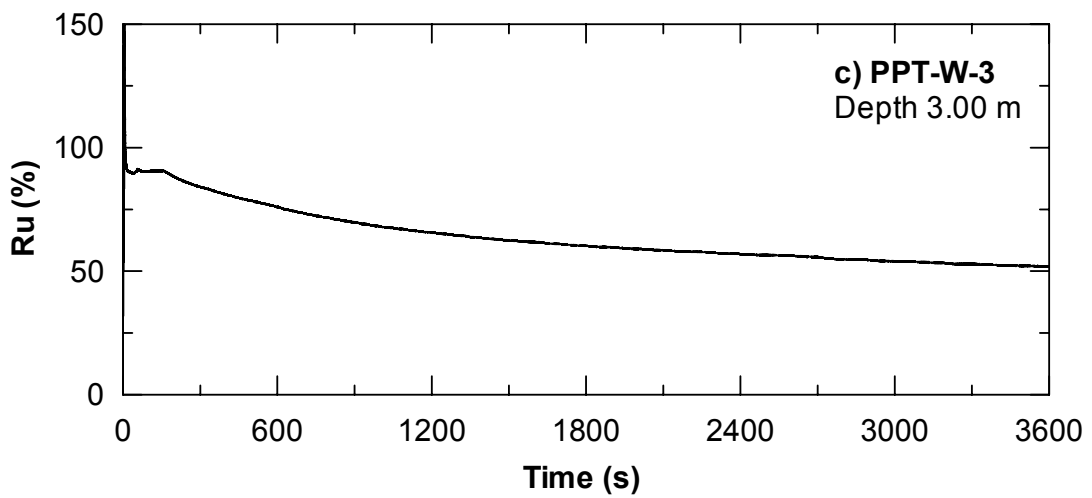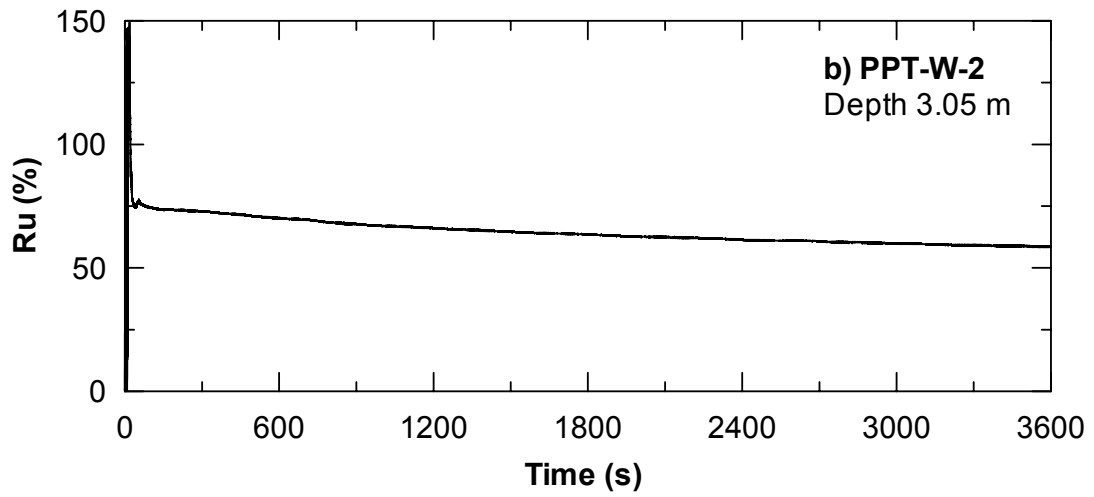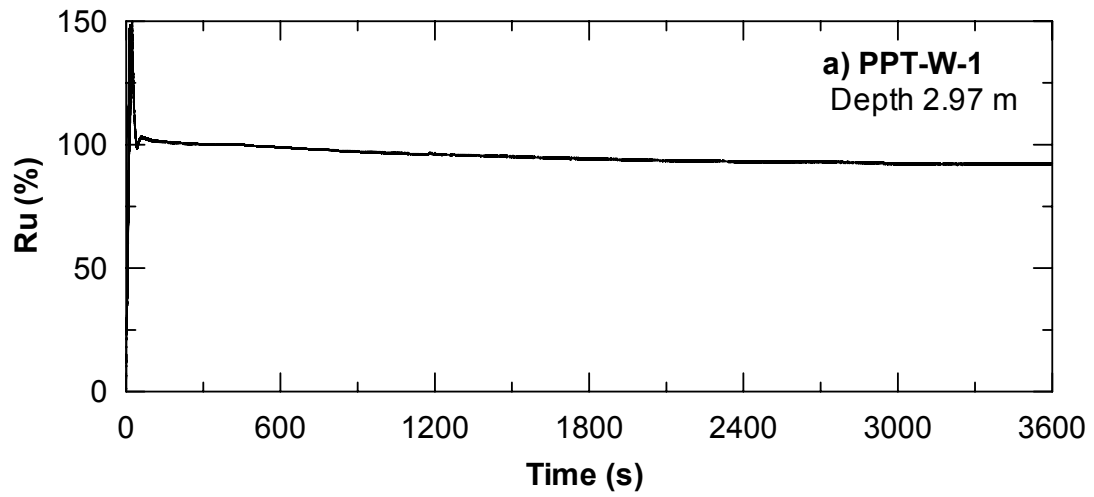
Figure 4.63   Excess Pore Water Pressure Ratio for (a) PPT-W-1, (b) PPT-W-2, and (c) PPT-W-3 , 3600s Duration
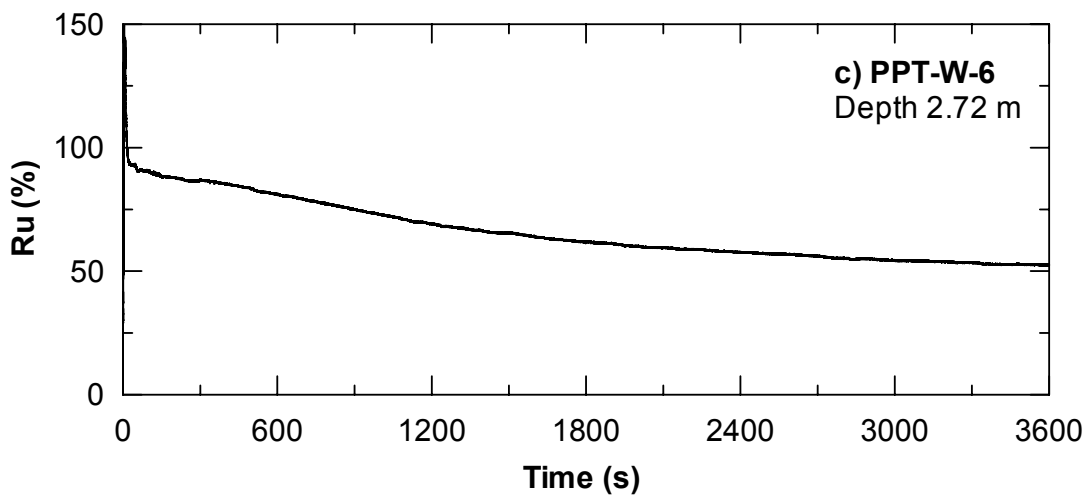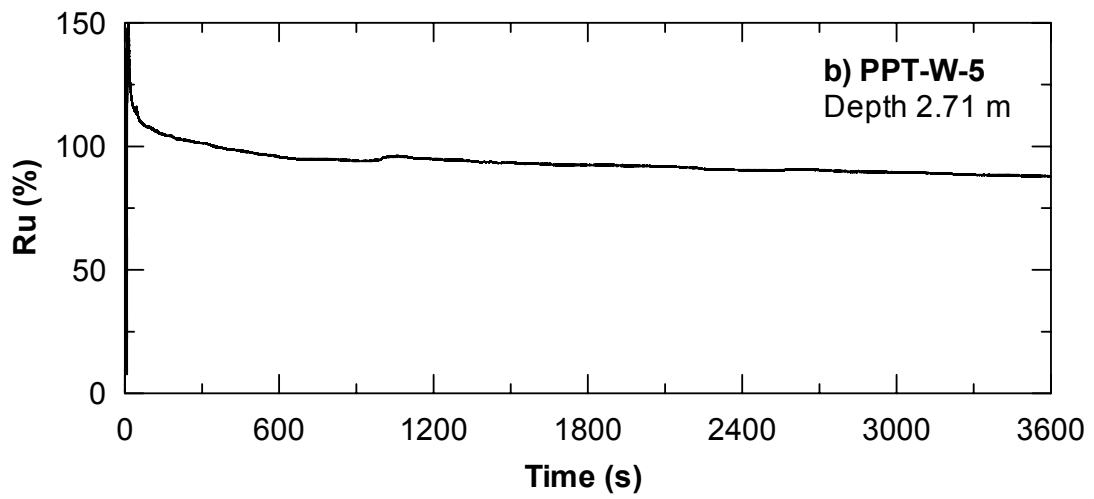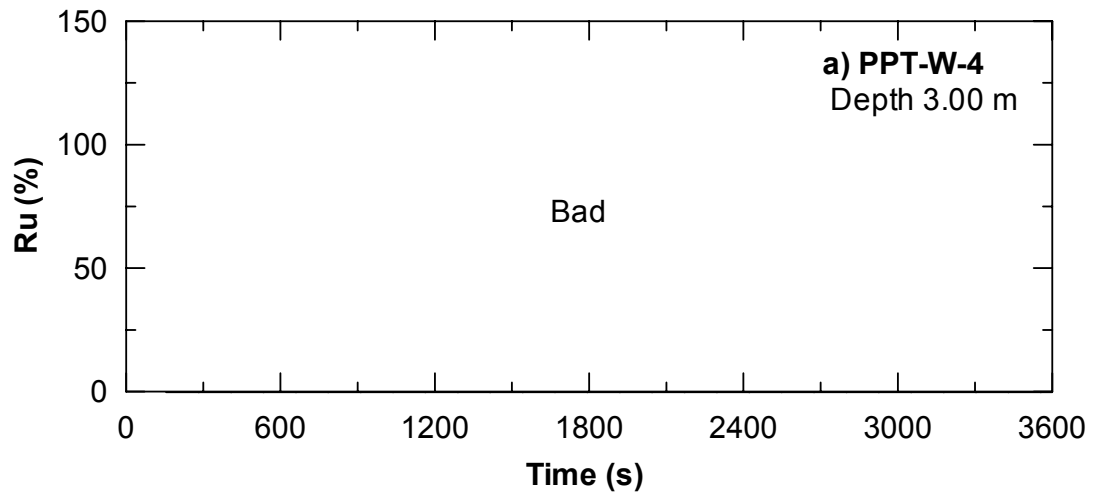
Figure 4.64   Excess Pore Water Pressure Ratio for (a) PPT-W-4, (b) PPT-W-5, and (c) PPT-W-6 , 3600s Duration
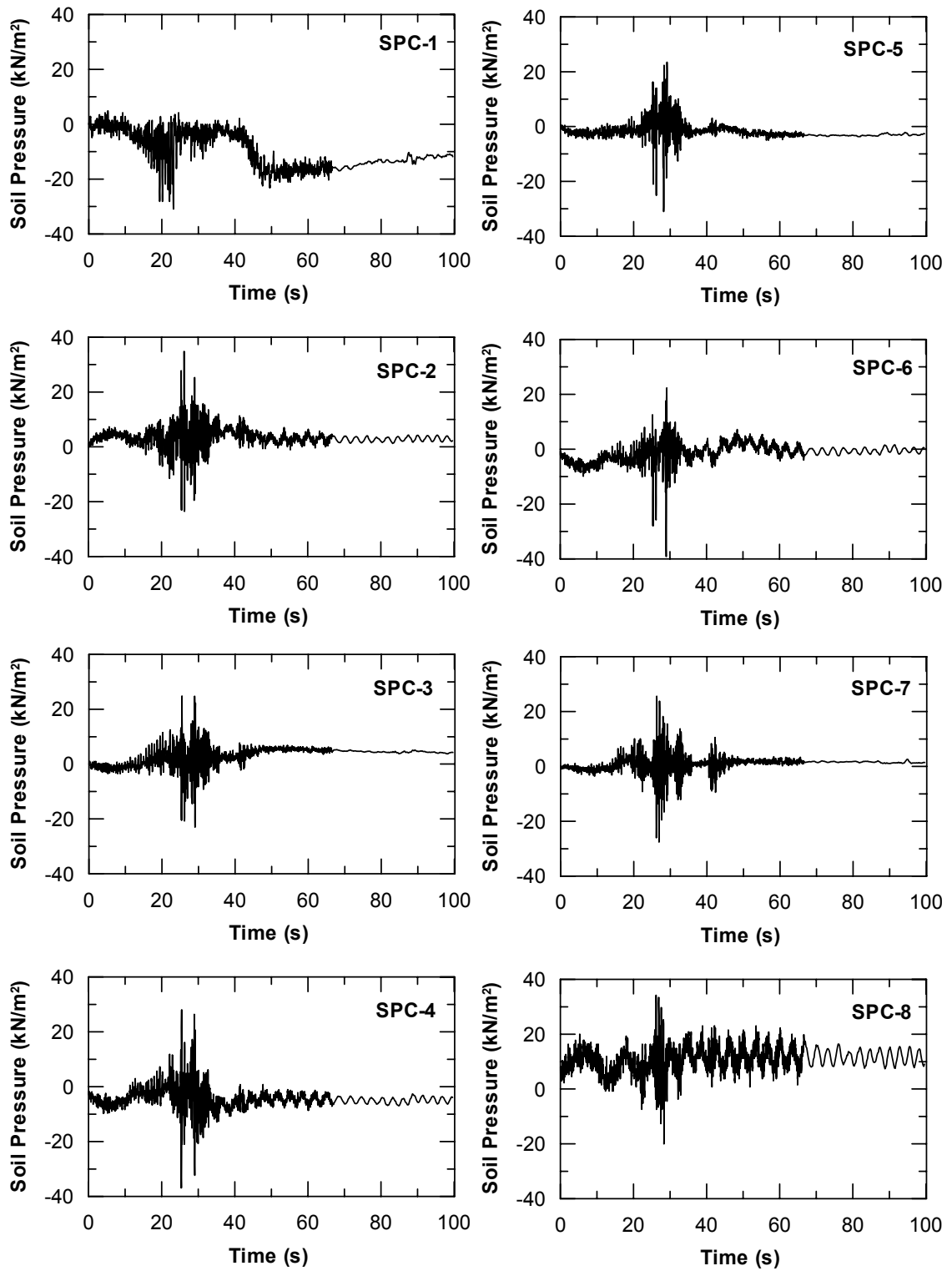
Figure 4.65   Response of Soil Pressure Cells for 4-Pile Group and 9-Pile Group

148
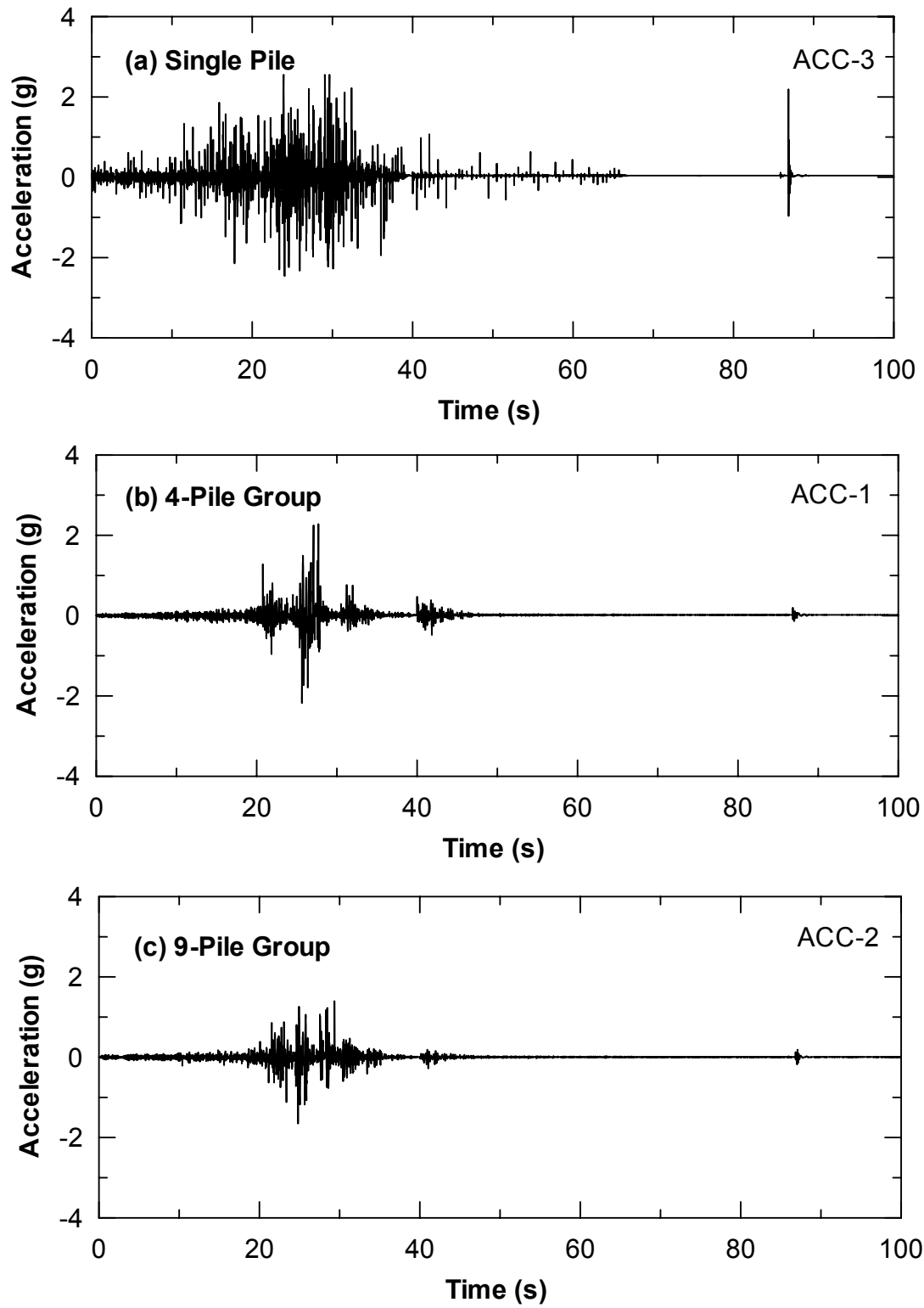
Figure 4.66   Acceleration Response at (a) Top of Single Pile, (b) Pile Cap of 4-Pile
Group, and (c) Pile Cap of 9-Pile Group

149
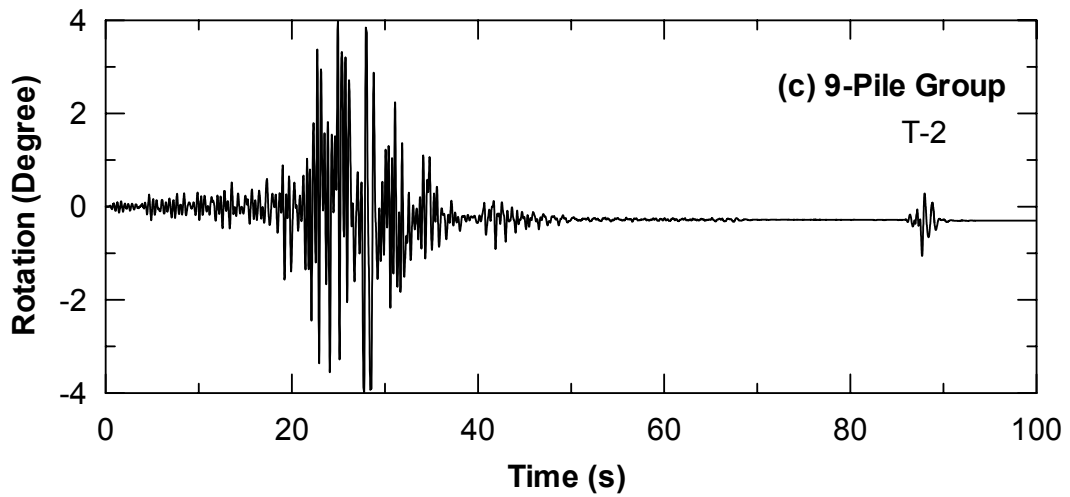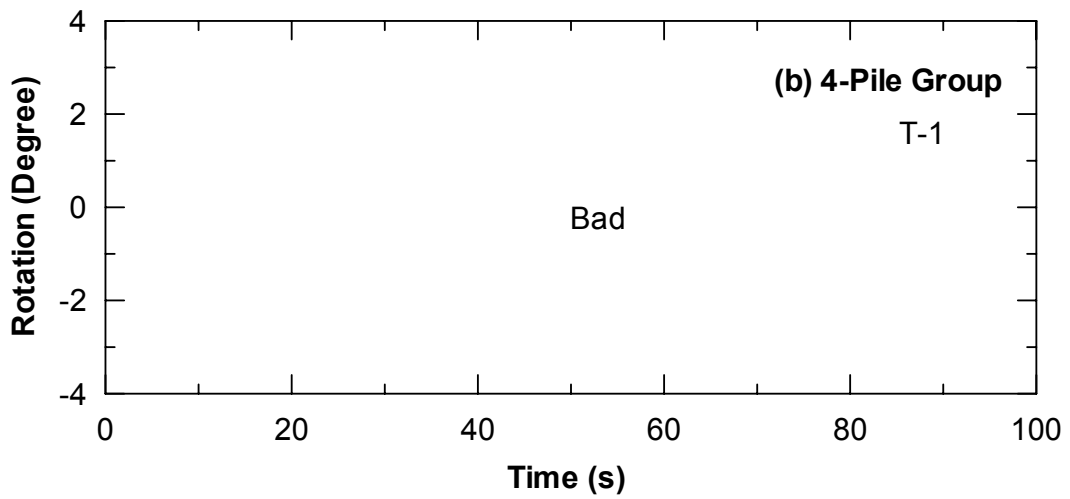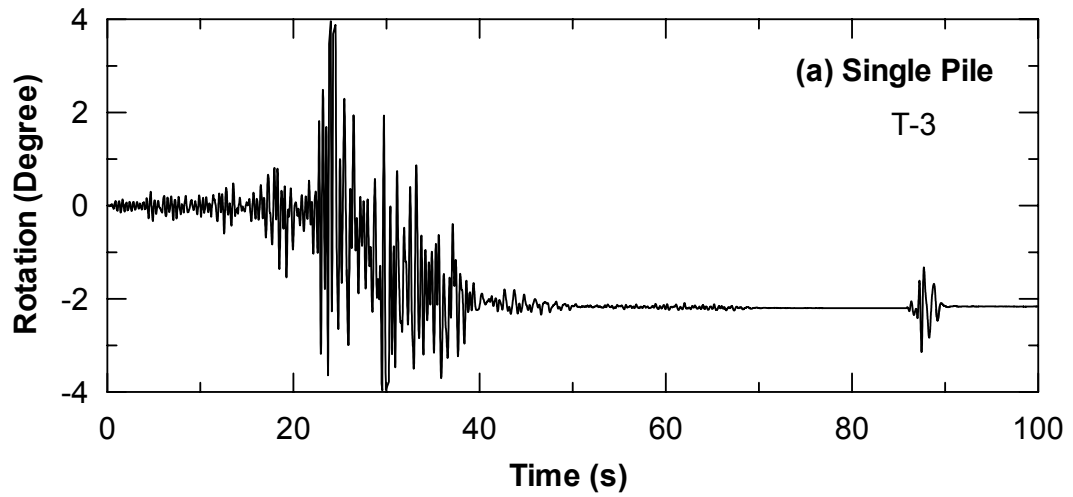
Figure 4.67   Rotation Response at (a) Top of Single Pile, (b) Pile Cap of 4-Pile, and (c) Pile Cap of 9-Pile Group
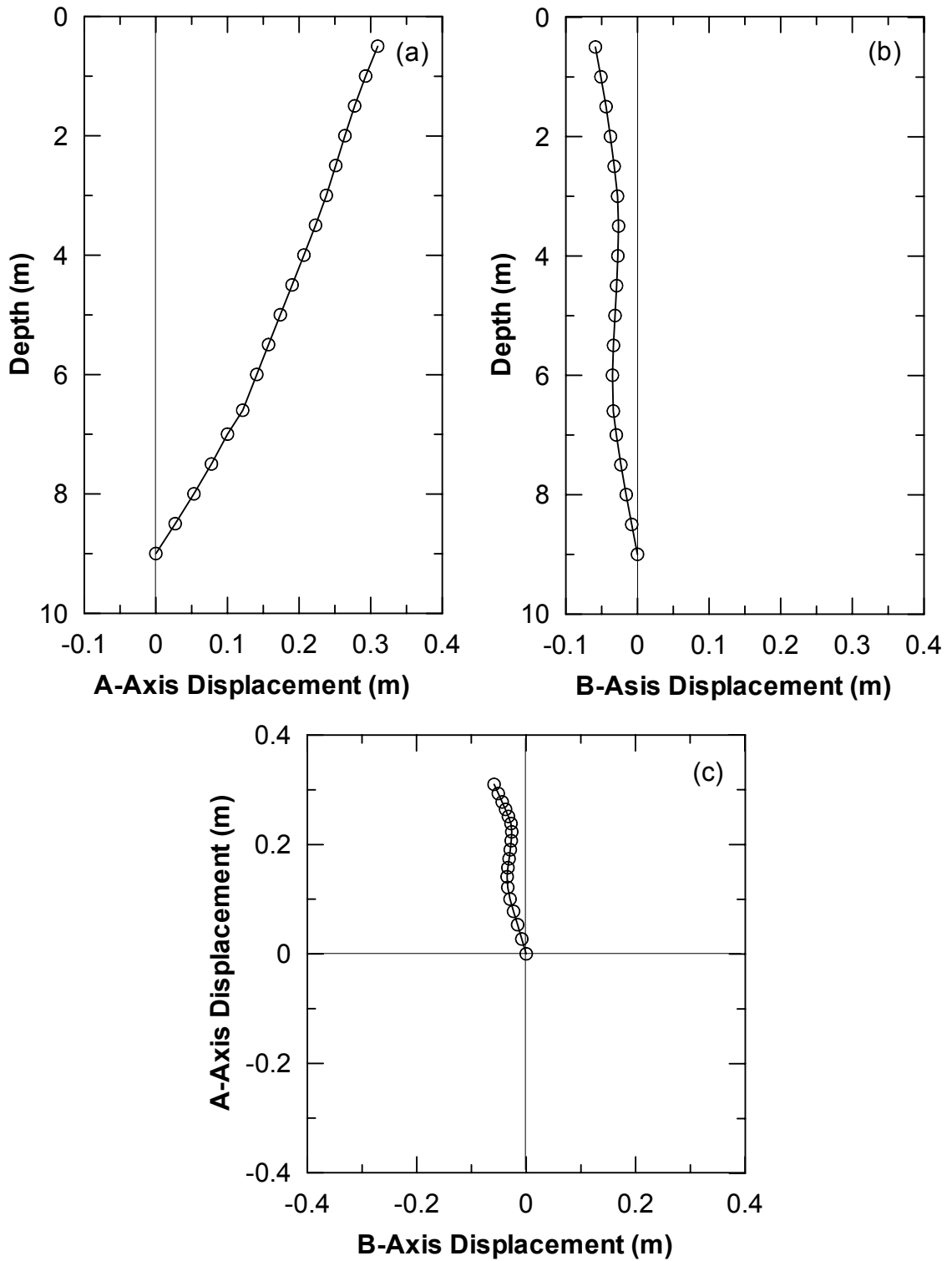
Figure 4.68   Soil Displacement from Inclinometer Casing S2 a) Section View A-Direction, b) Section View B-Direction, and c) Plan View
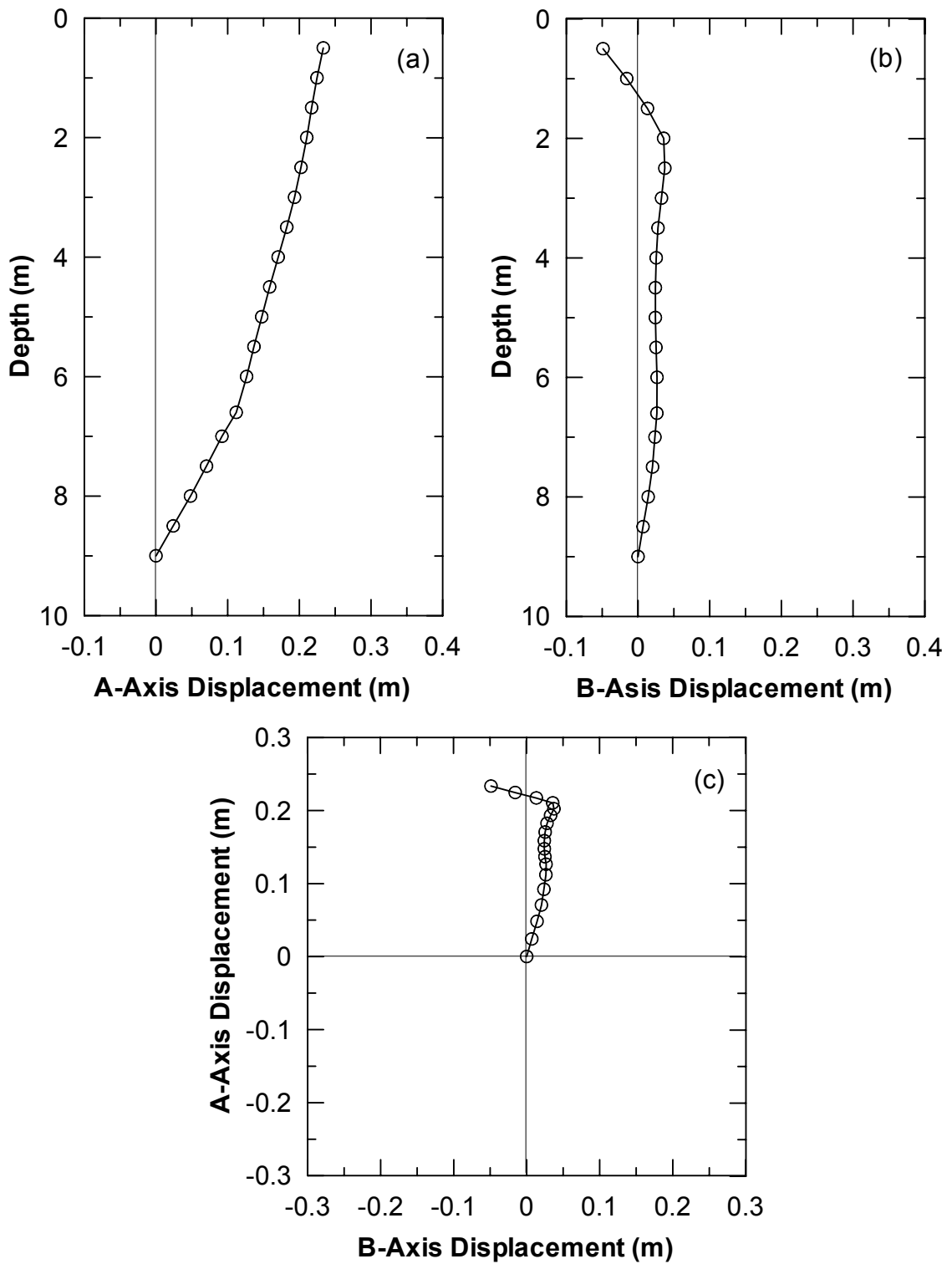
Figure 4.69   Soil Displacement from Inclinometer Casing S3 a) Section View A-Direction, b) Section View B-Direction, and c) Plan View
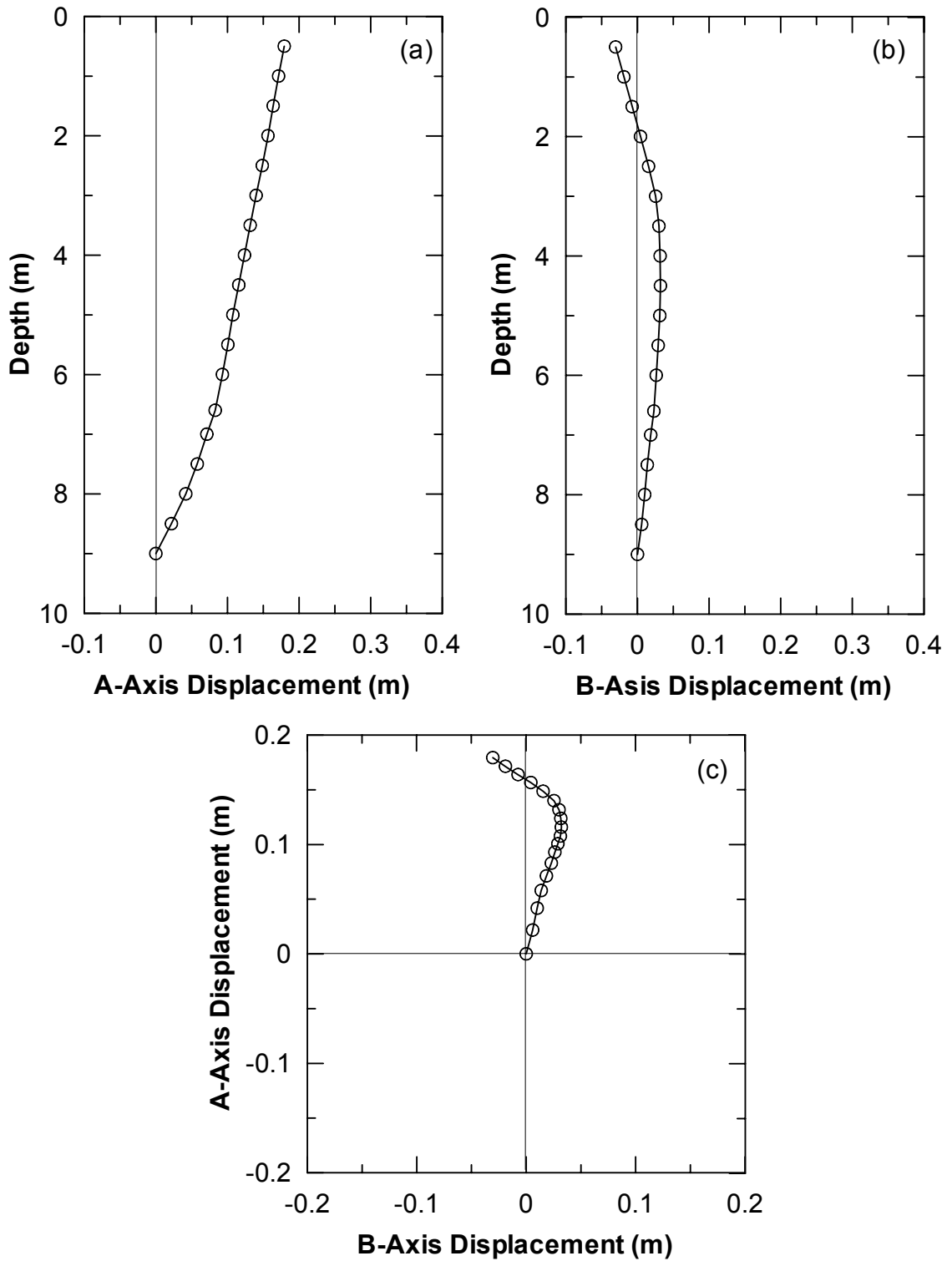
Figure 4.70   Soil Displacement from Inclinometer Casing S4 a) Section View A-Direction, b) Section View B-Direction, and c) Plan View

153
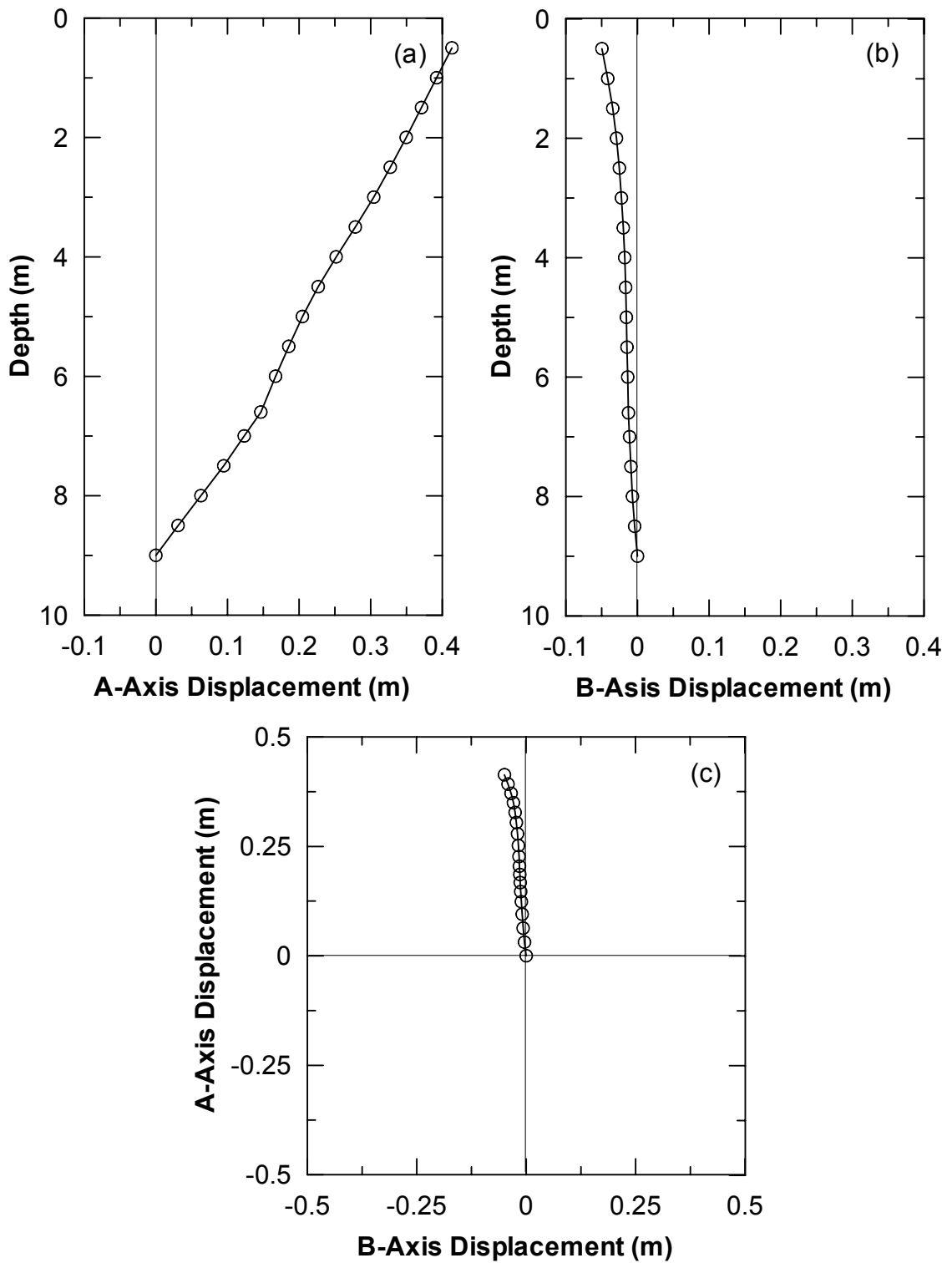
Figure 4.71   Soil Displacement from Inclinometer Casing S5 a) Section View A-
Direction, b) Section View B-Direction, and c) Plan View
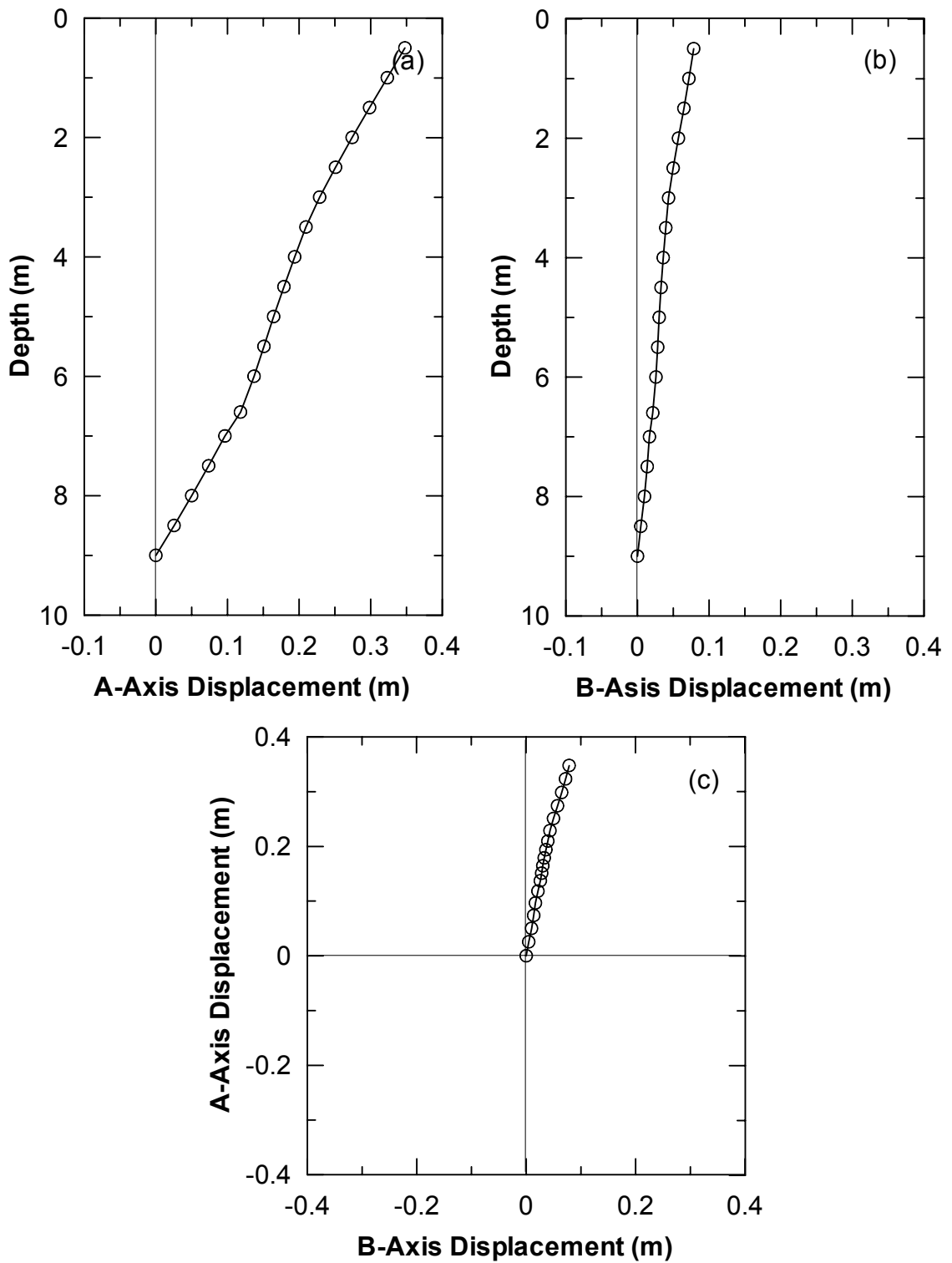
Figure 4.72   Soil Displacement from Inclinometer Casing S6 a) Section View A-Direction, b) Section View B-Direction, and c) Plan View
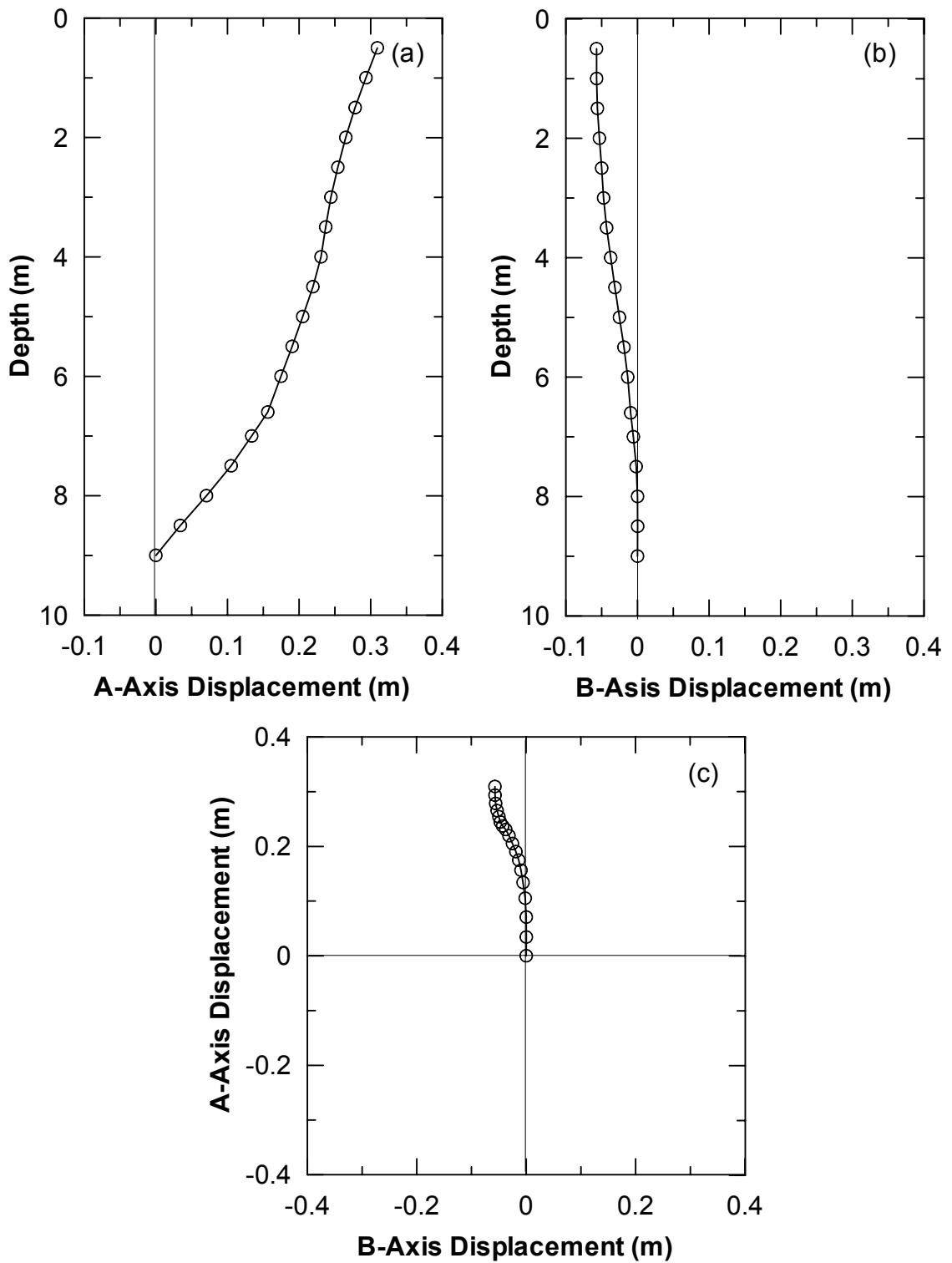
Figure 4.73   Soil Displacement from Inclinometer Casing S7 a) Section View A-Direction, b) Section View B-Direction, and c) Plan View

156
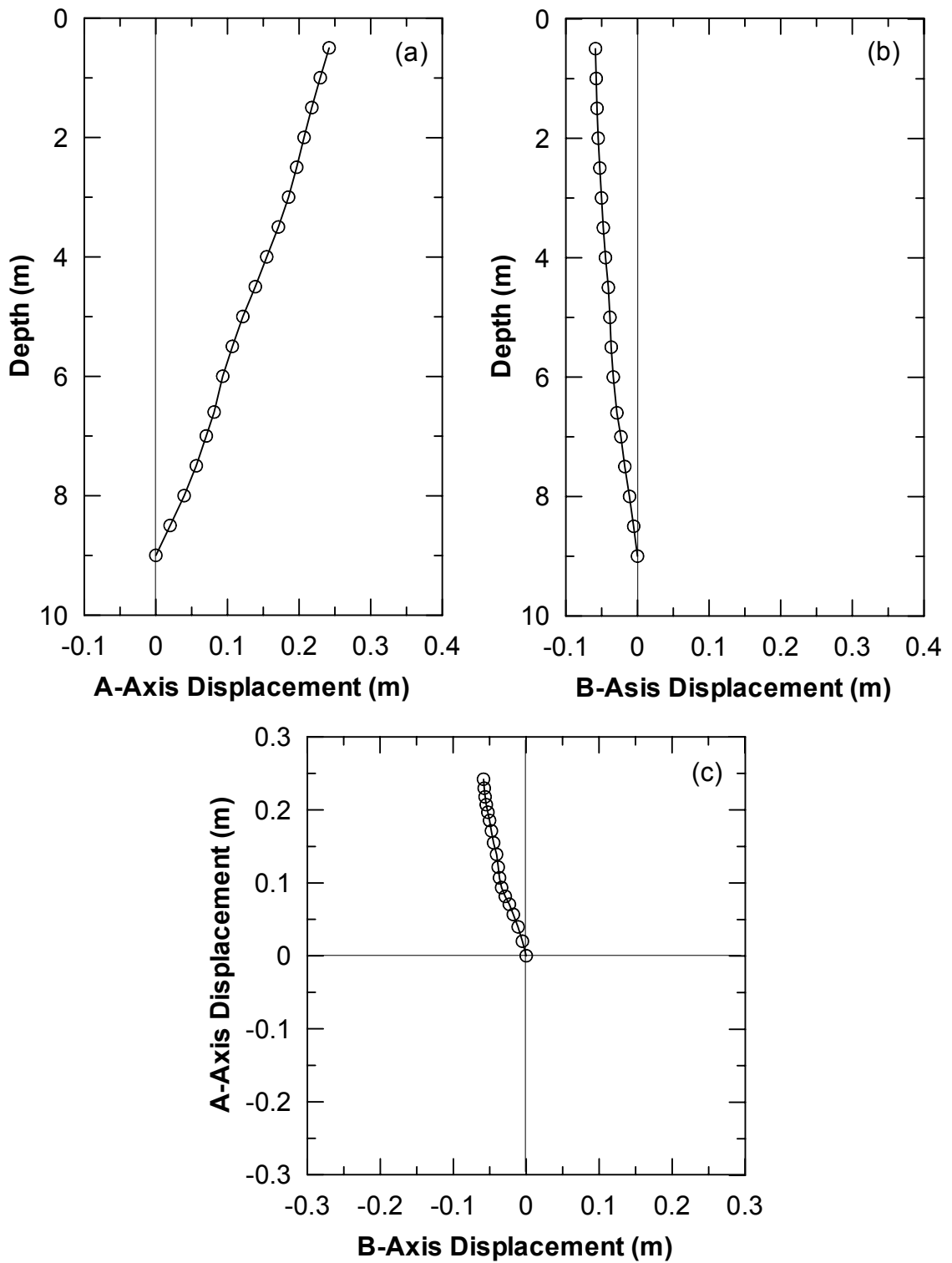
Figure 4.74   Soil Displacement from Inclinometer Casing S8 a) Section View A-Direction, b) Section View B-Direction, and c) Plan View
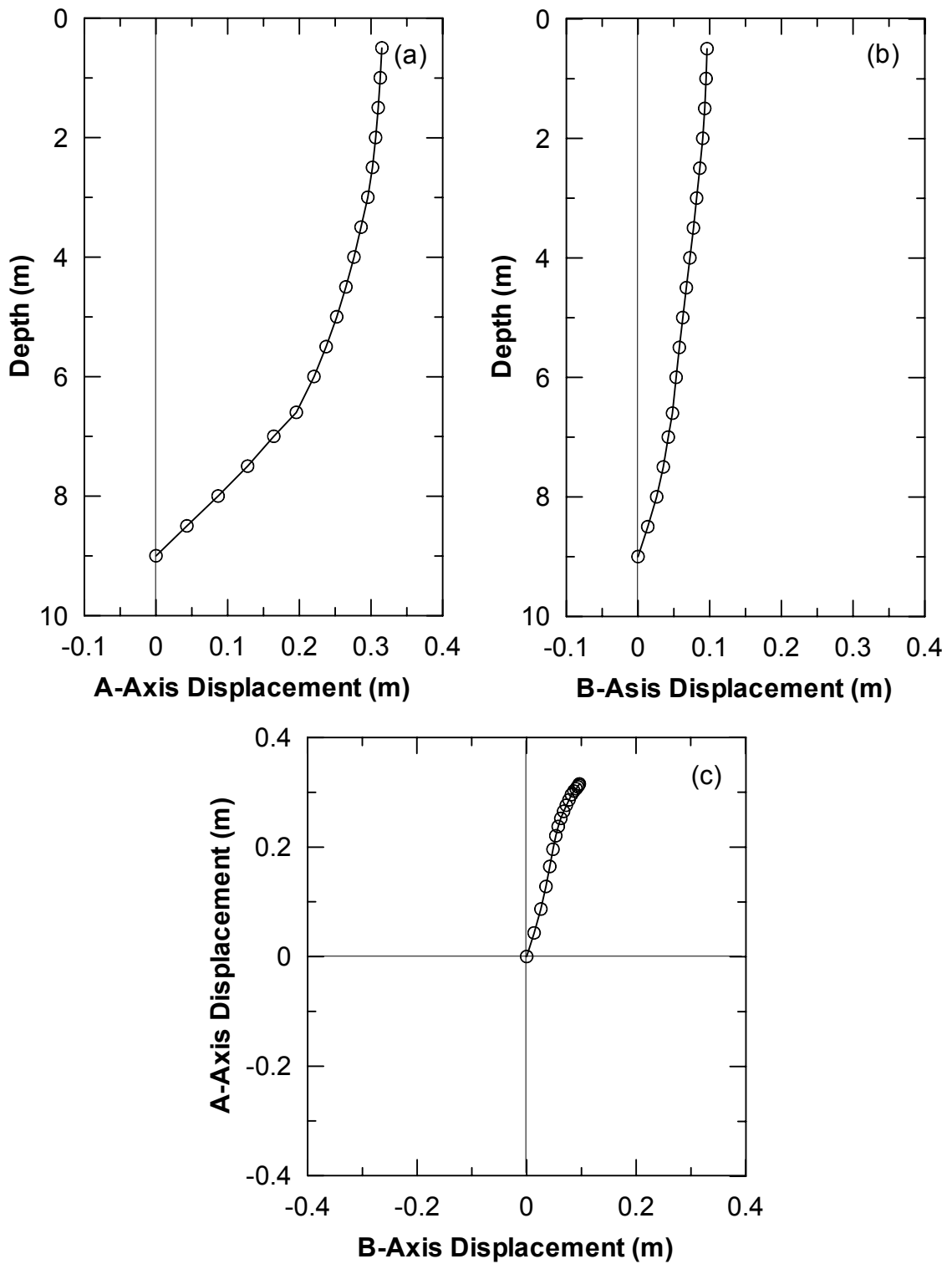
Figure 4.75   Soil Displacement from Inclinometer Casing S9 a) Section View A-Direction, b) Section View B-Direction, and c) Plan View

158
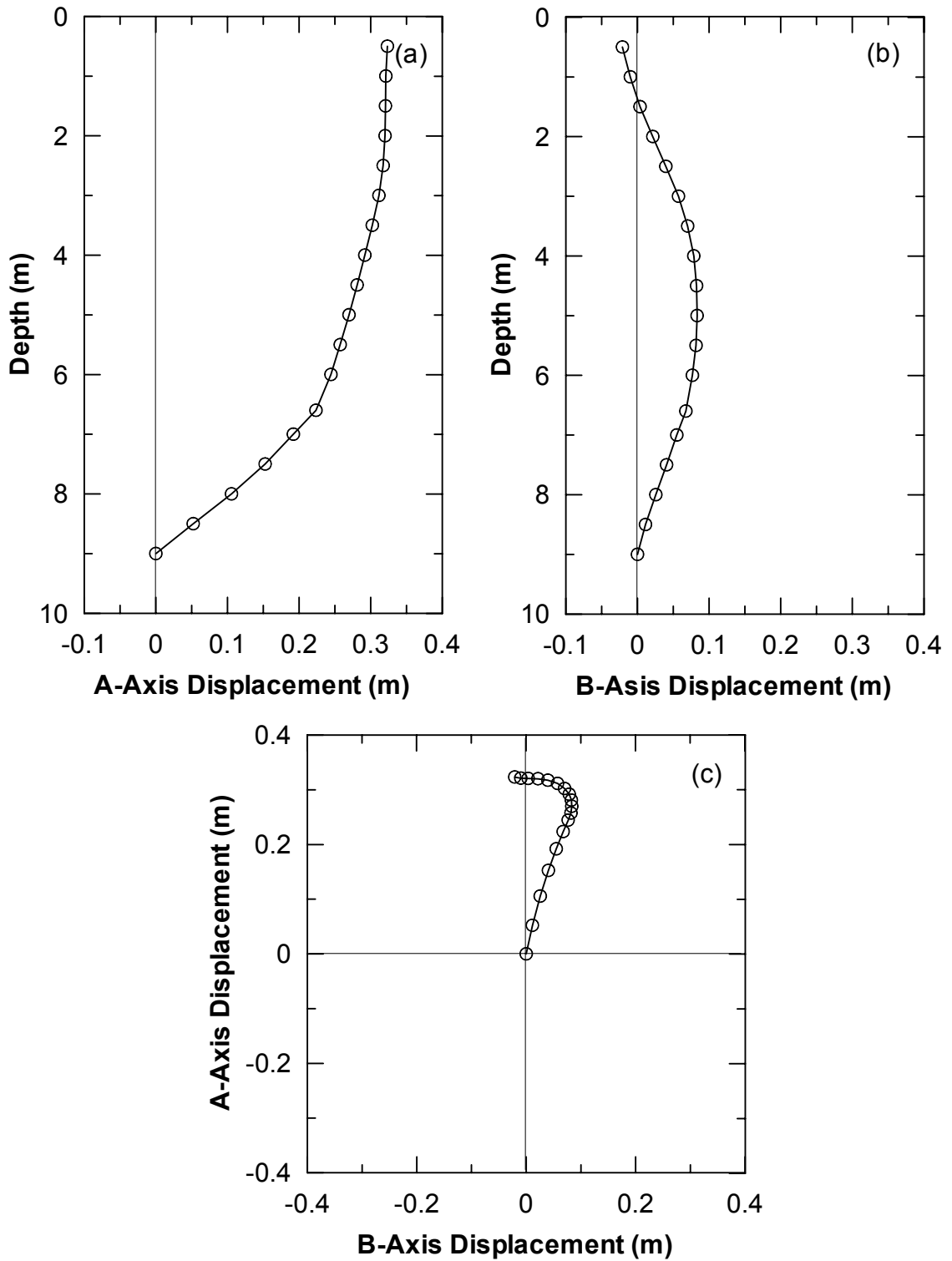
Figure 4.76   Soil Displacement from Inclinometer Casing S10 a) Section View A-Direction, b) Section View B-Direction, and c) Plan View

159
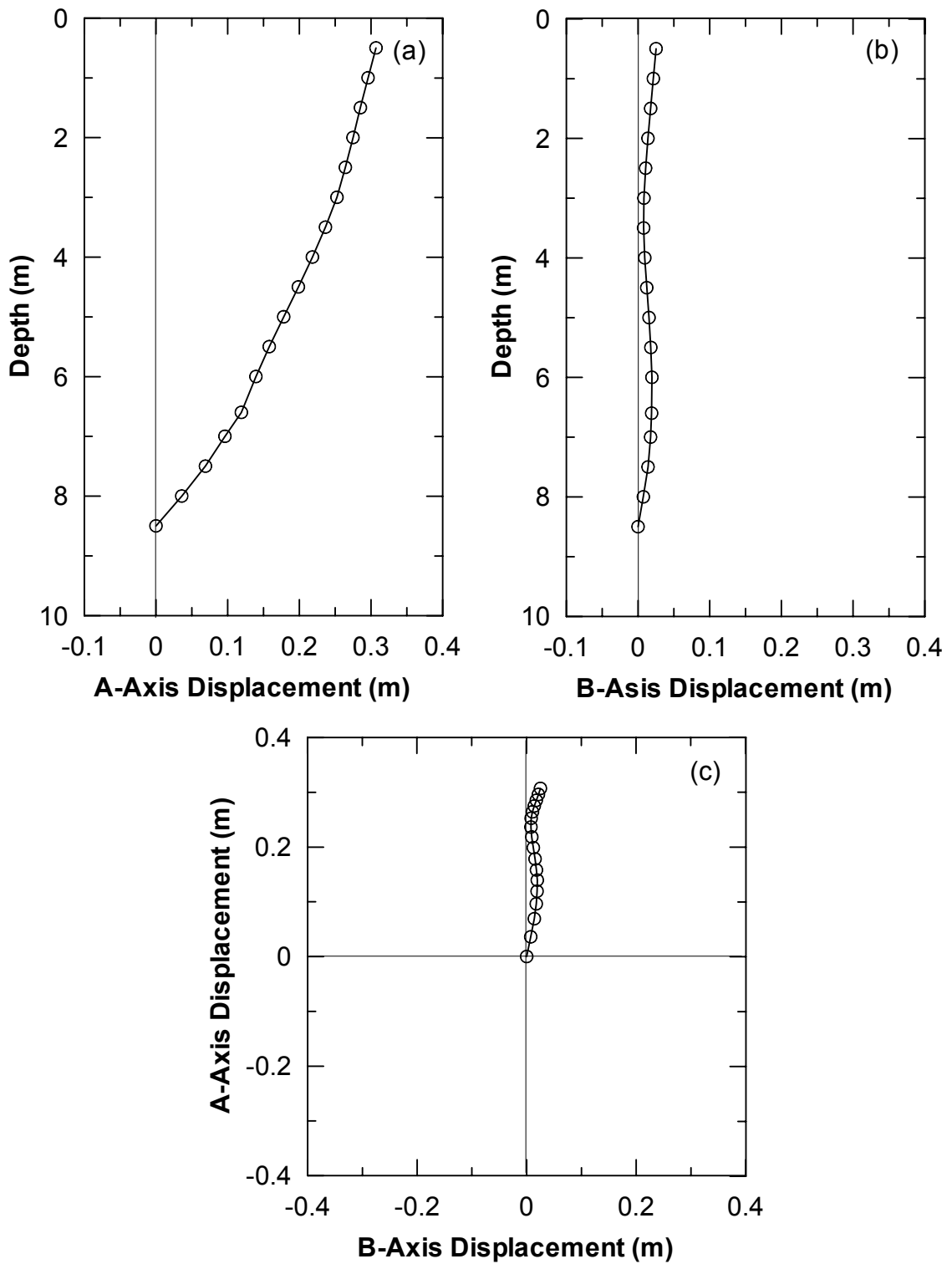
Figure 4.77   Soil Displacement from Inclinometer Casing S11 a) Section View A-Direction, b) Section View B-Direction, and c) Plan View
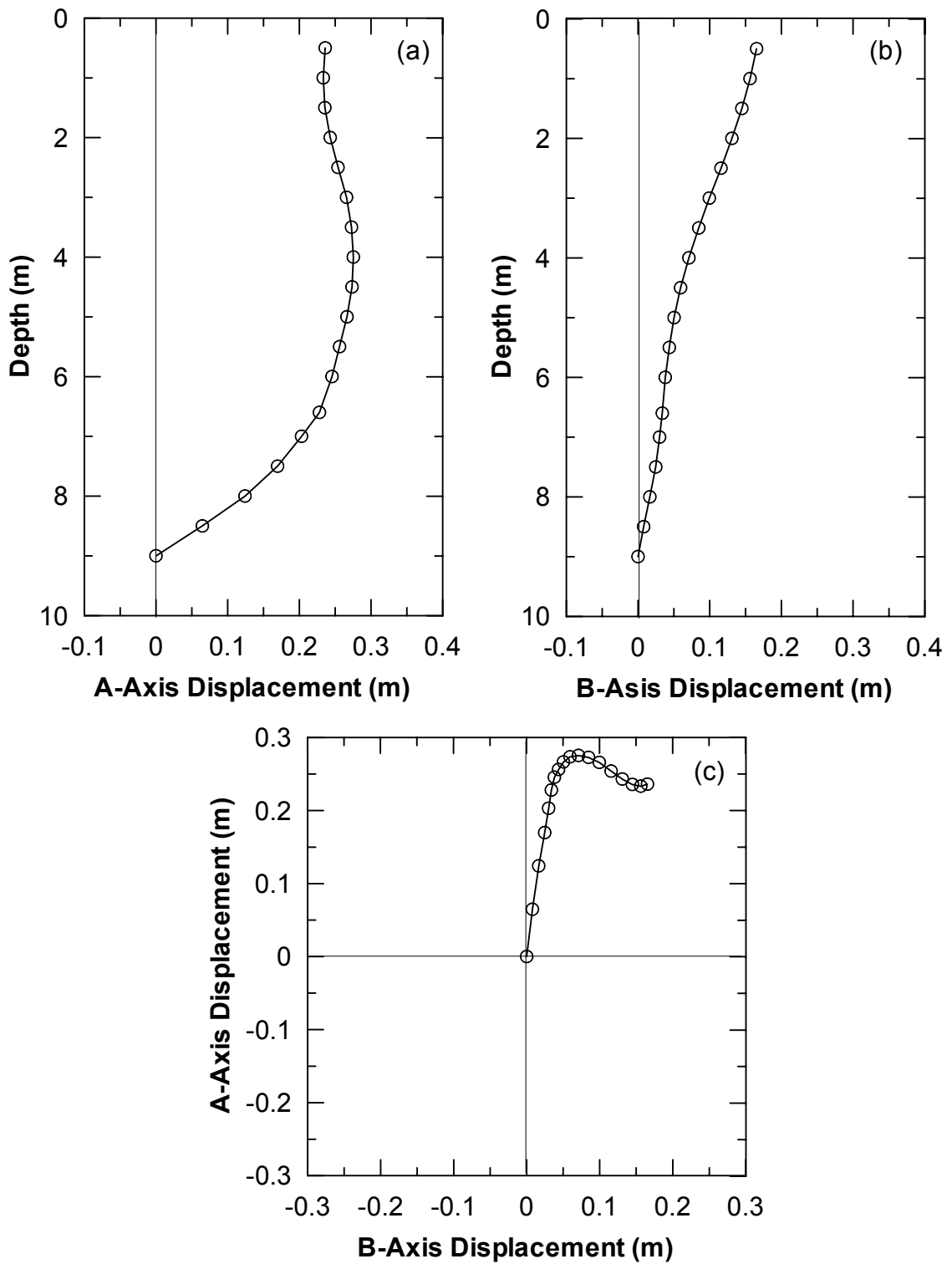
Figure 4.78   Soil Displacement from Inclinometer Casing S12 a) Section View A-Direction, b) Section View B-Direction, and c) Plan View
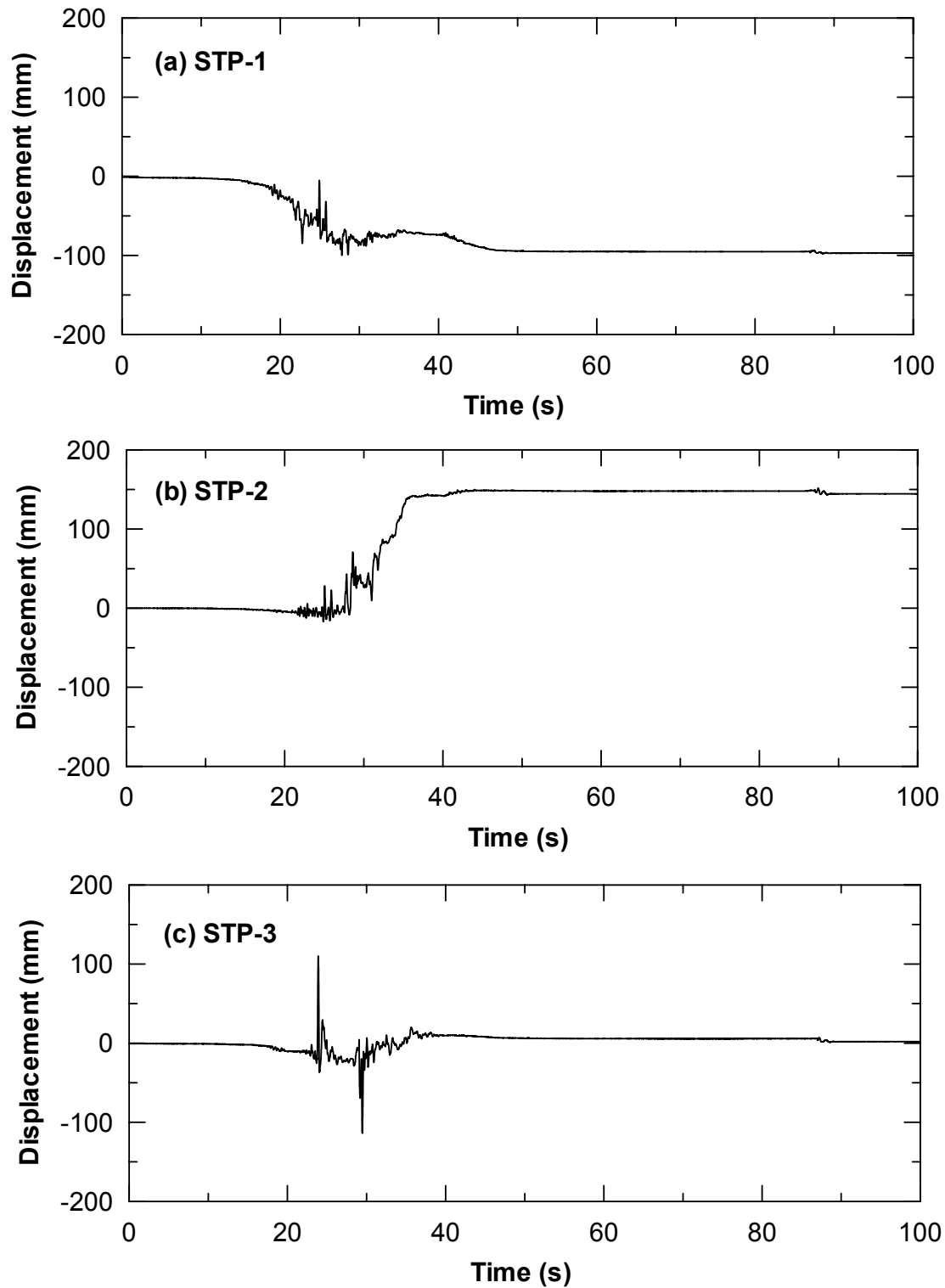
Figure 4.79   Relative Displacement between (a) S1 and 9-Pile Group, (b) S2 and 9-Pile Group, and (c) S7 and Single Pile
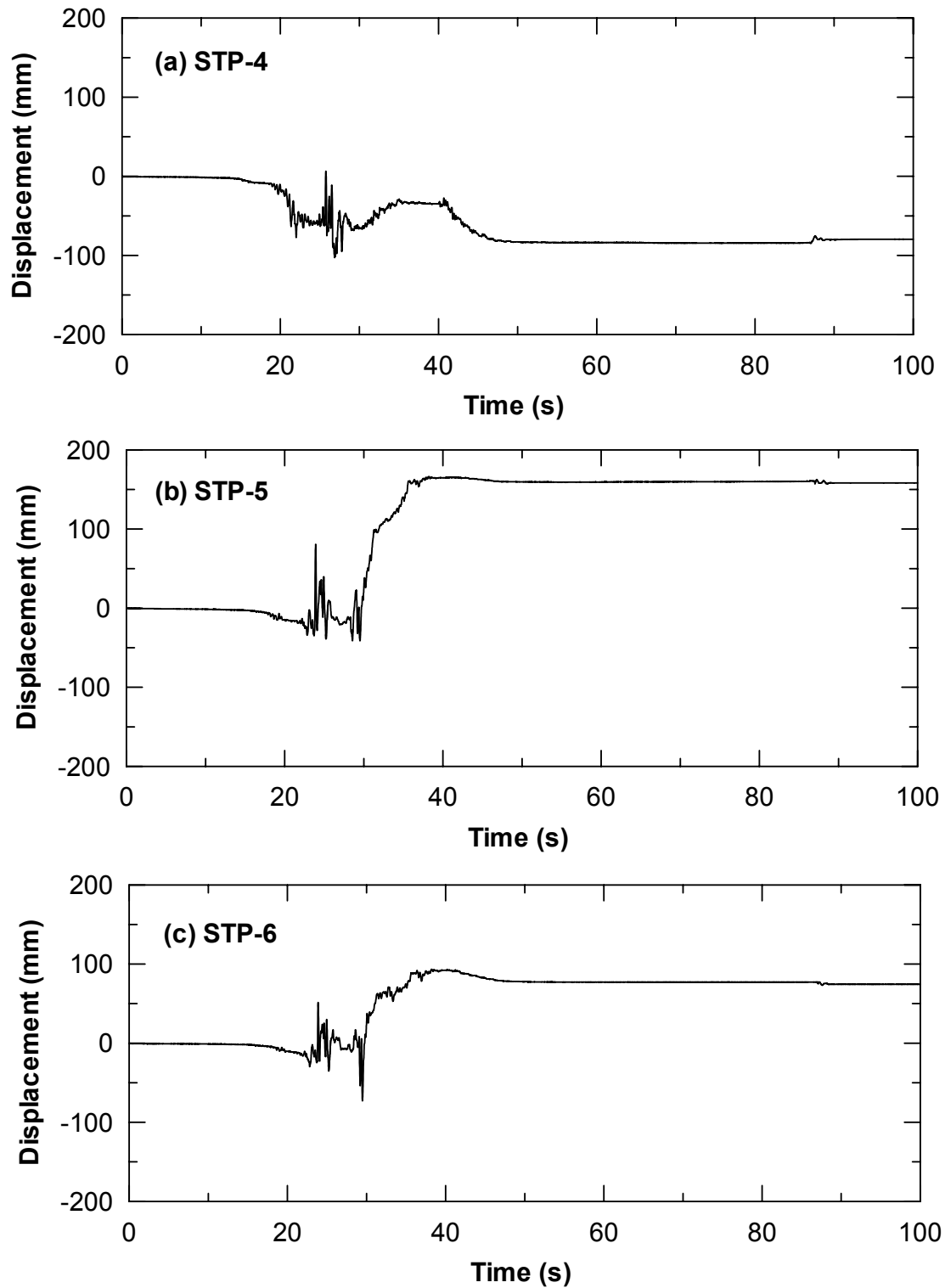
Figure 4.80   Relative Displacement between (a) S8 and 4-Pile Group, (b) S11 and W1
Pile, and (c) S11 and W2 Pile
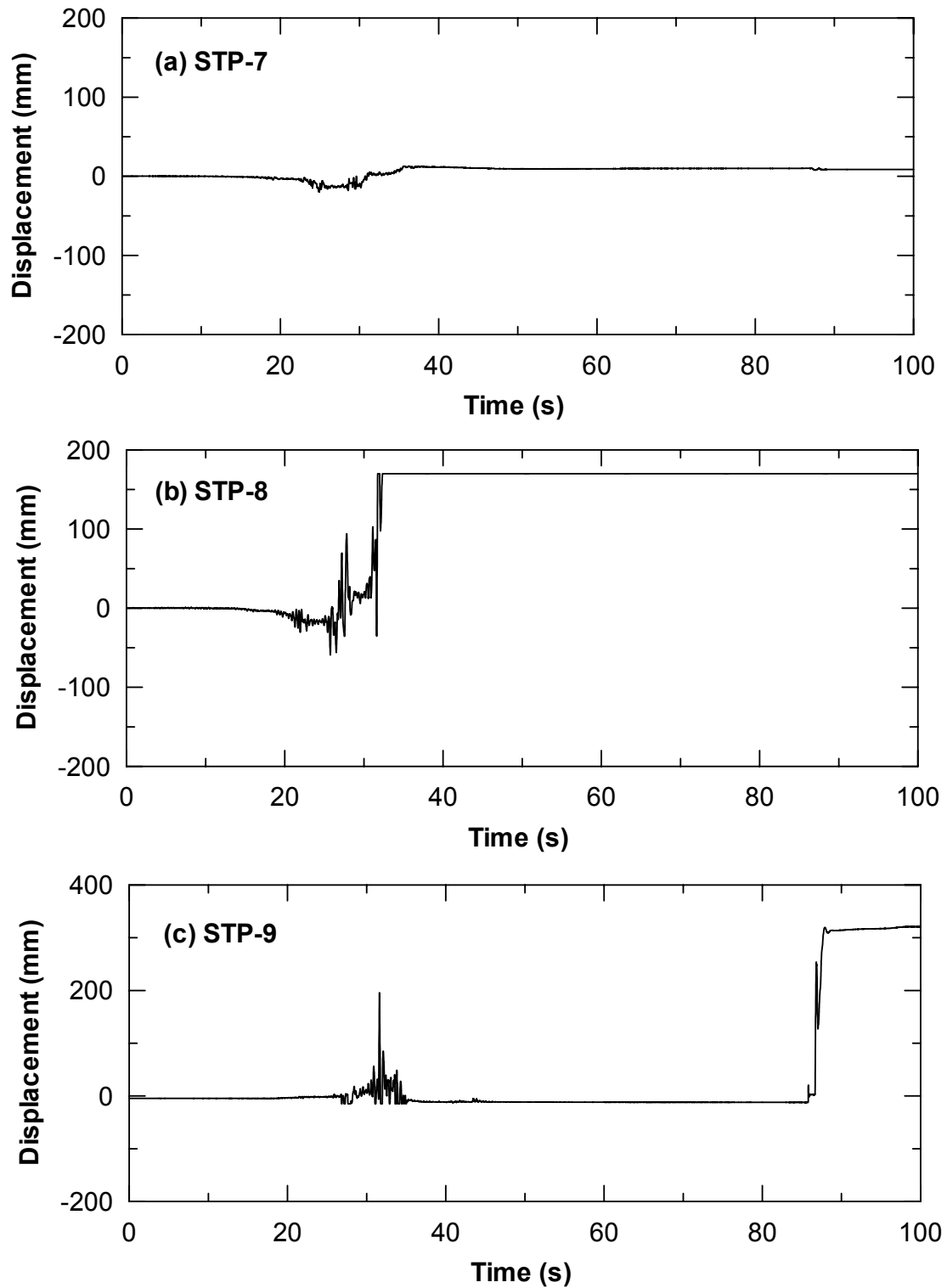
Figure 4.81   Relative Displacement between (a) Pile W1 and Pile W3, (b) 4-Pile
Group and Anchor Pile, and (c) Anchor Pile and Quay Wall
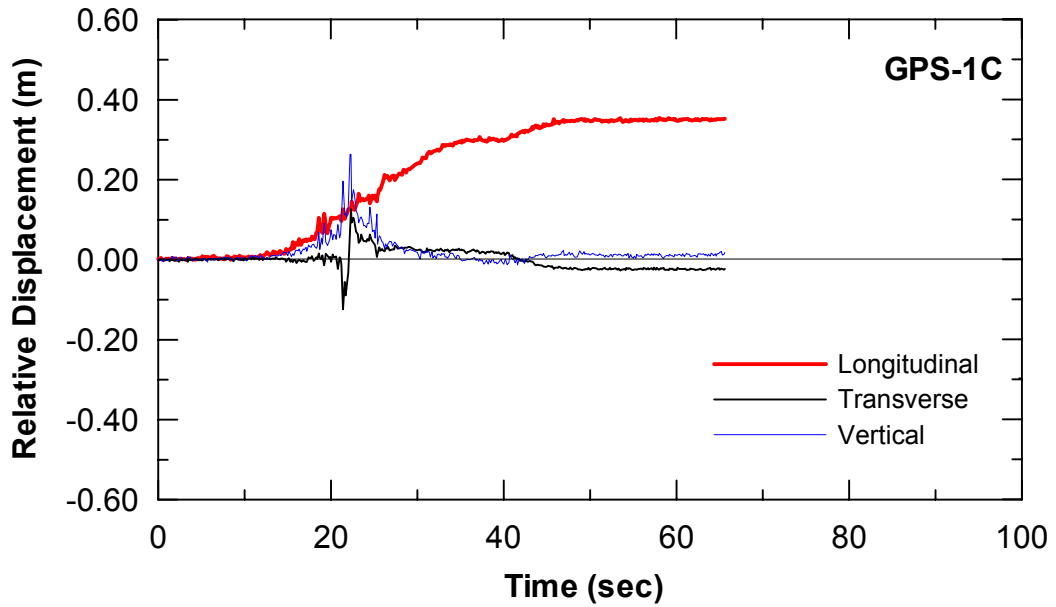
(a) Displacement Time-History
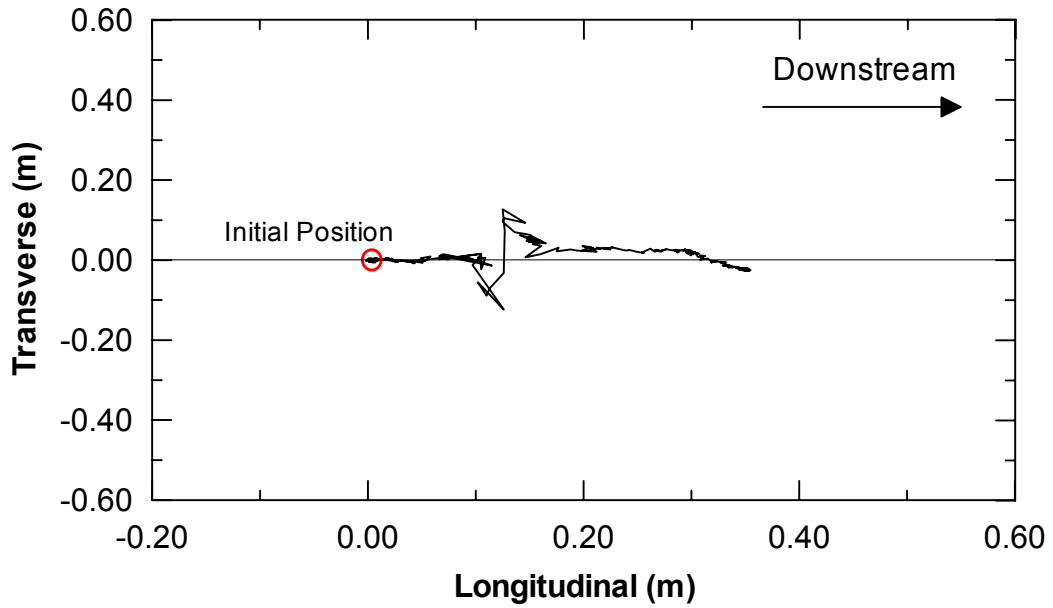
(b) Displacement Path

Figure 4.82 Global Positioning System Data of Unit 1C (1st Blast Test) (a) Displacement Time-History, and (b) Displacement Path , Data from Caltrans

165
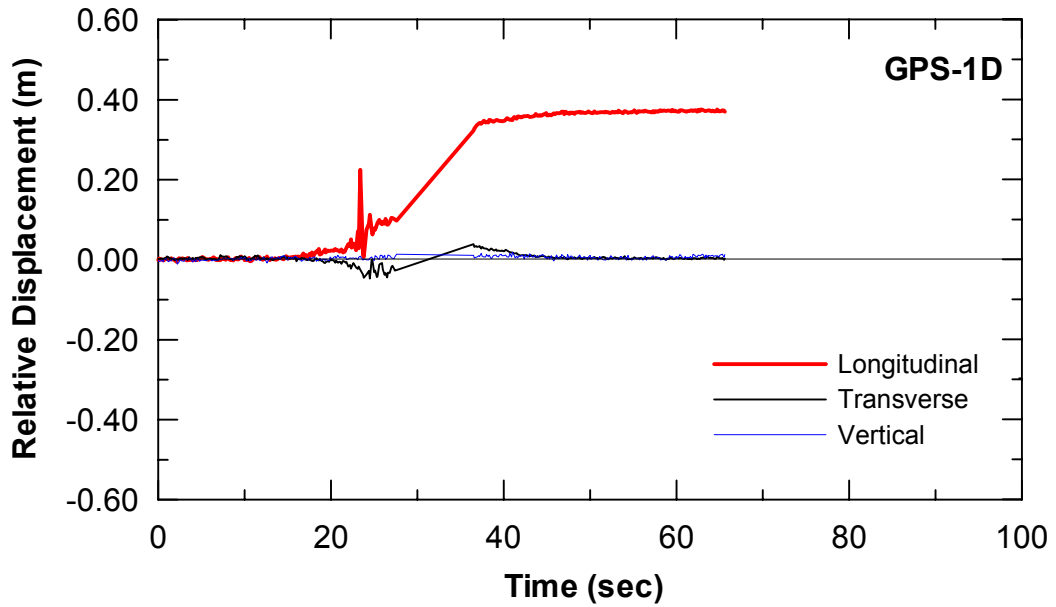
(a) Displacement Time-History
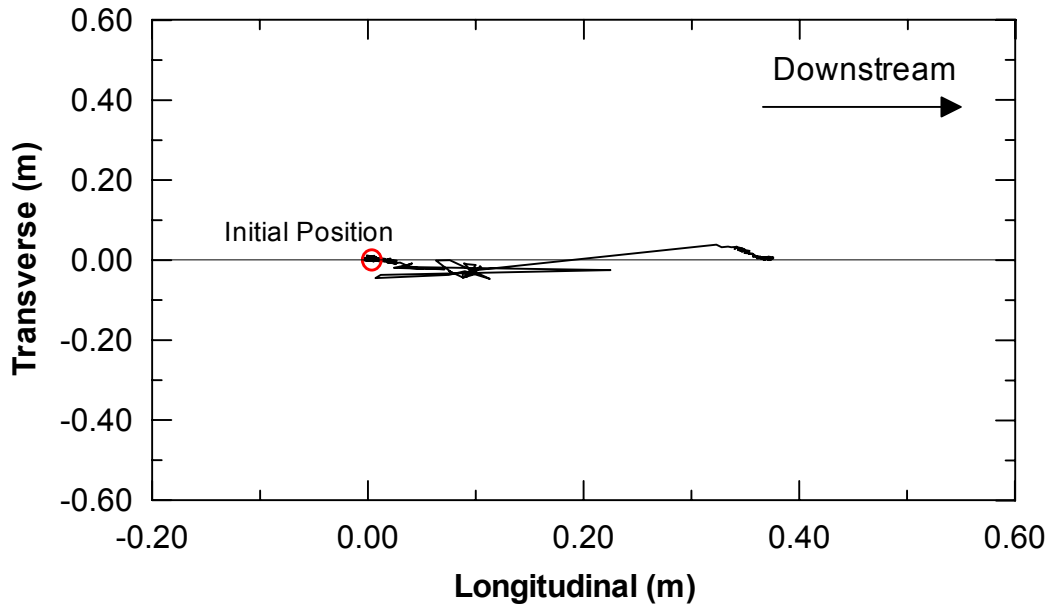
(b) Displacement Path

Figure 4.83   Global Positioning System Data of Unit 1D (1st Blast Test) (a) Displacement Time-History, and (b) Displacement Path, Data from Caltrans
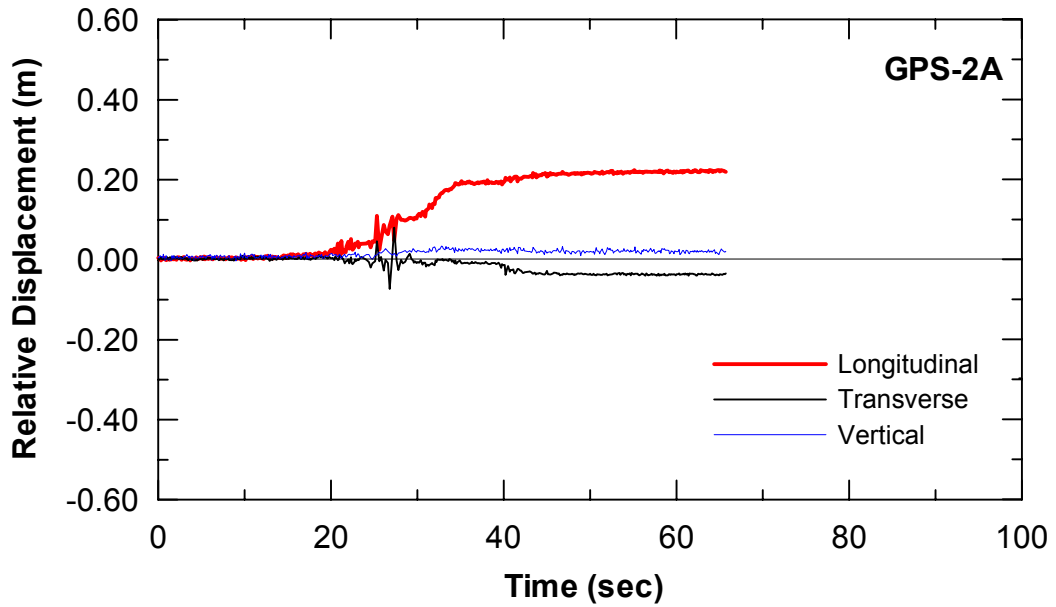
(a) Displacement Time-History
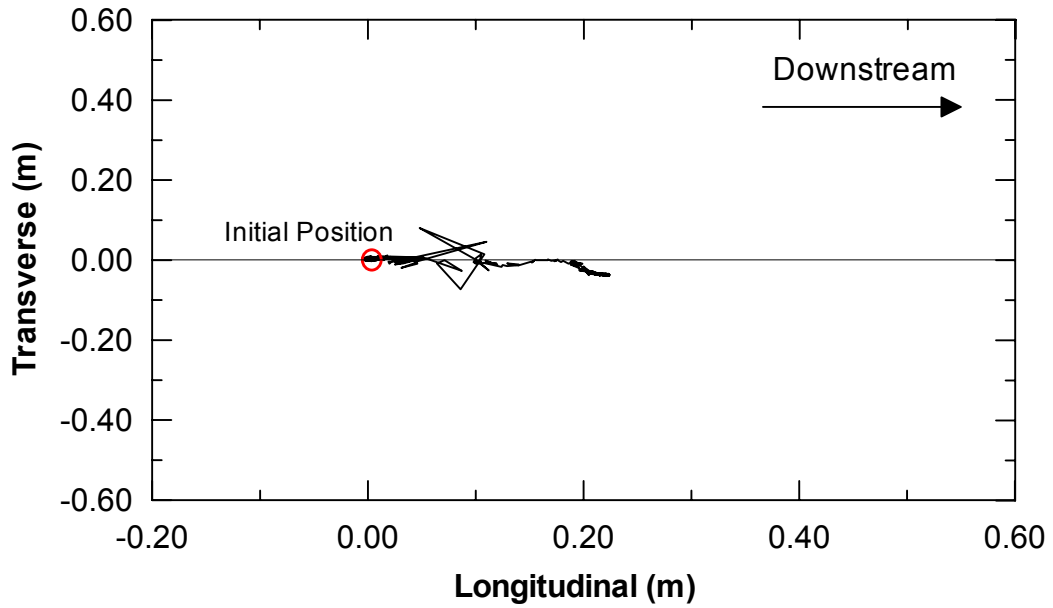
(b) Displacement Path

Figure 4.84   Global Positioning System Data of Unit 2A (1st Blast Test) (a)
Displacement Time-History, and (b) Displacement Path, Data from Caltrans
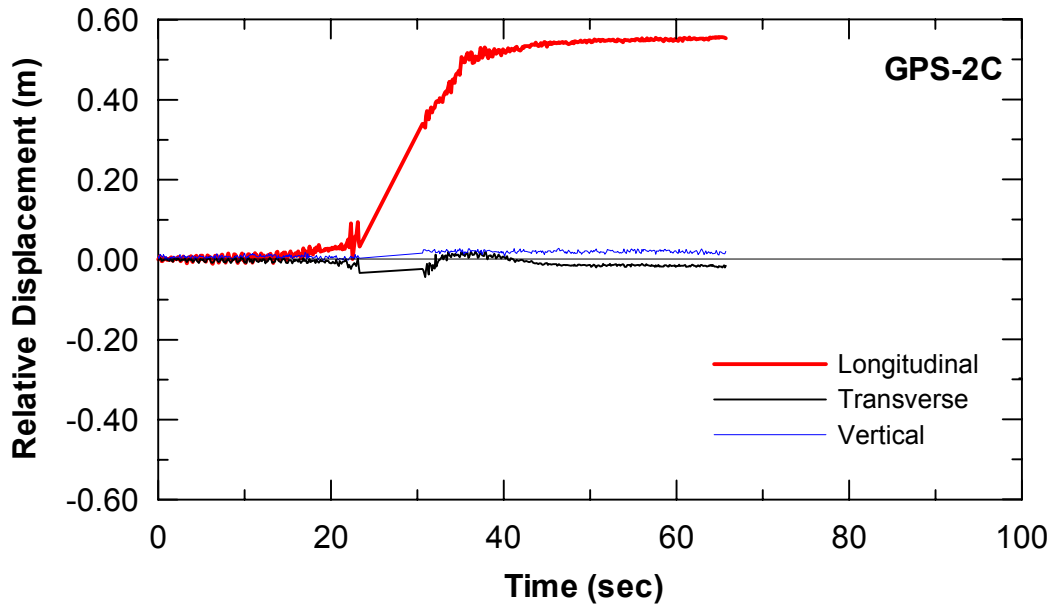
(a) Displacement Time-History
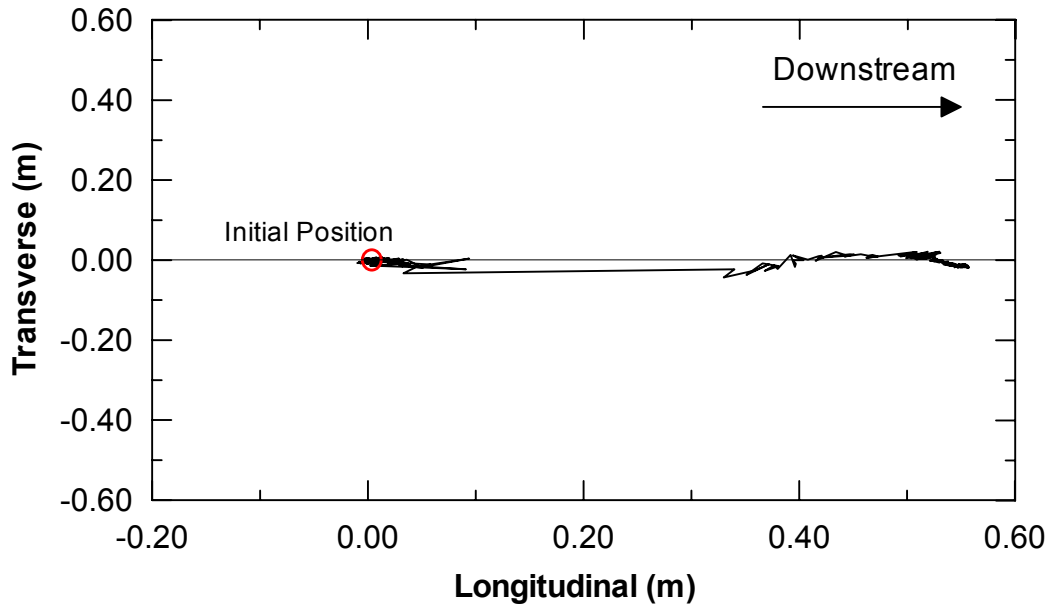
(b) Displacement Path

Figure 4.85   Global Positioning System Data of Unit 2C (1st Blast Test) (a) Displacement Time-History, and (b) Displacement Path, Data from Caltrans
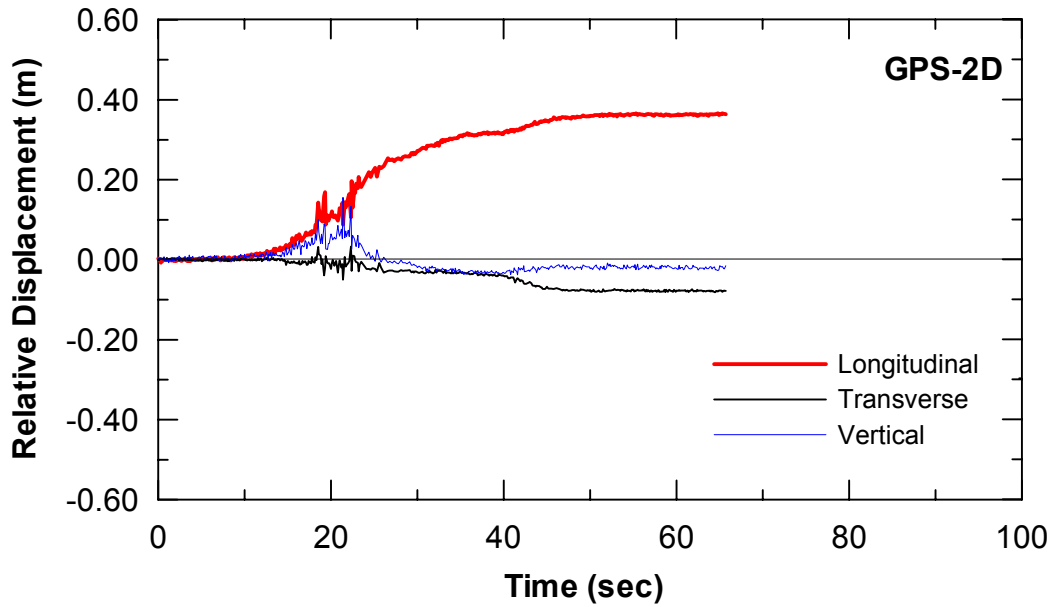
(a) Displacement Time-History
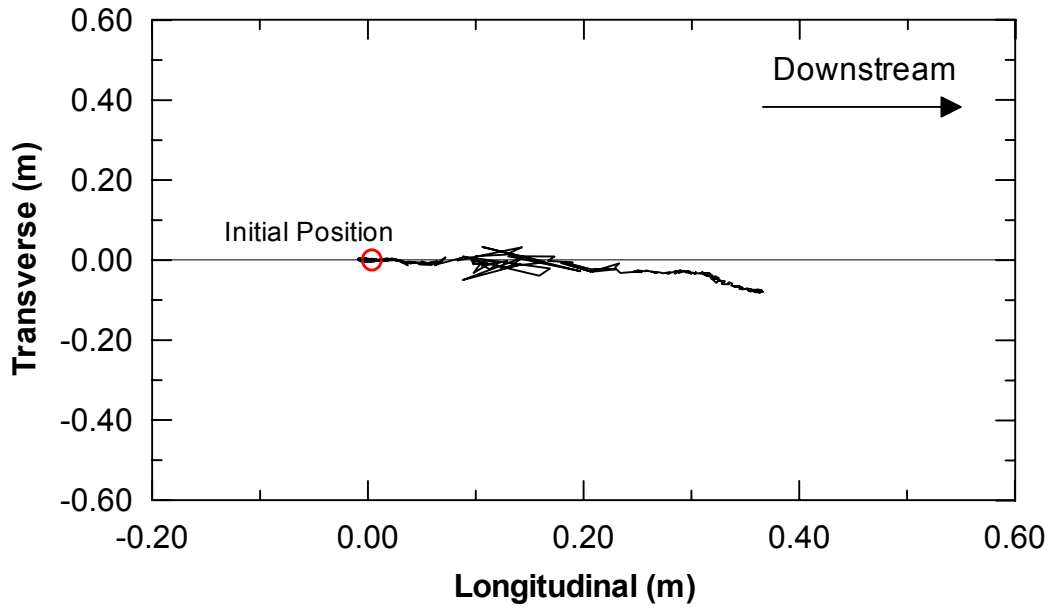
(b) Displacement Path

Figure 4.86   Global Positioning System Data of Unit 2D (1st Blast Test) (a) Displacement Time-History, and (b) Displacement Path, Data from Caltrans
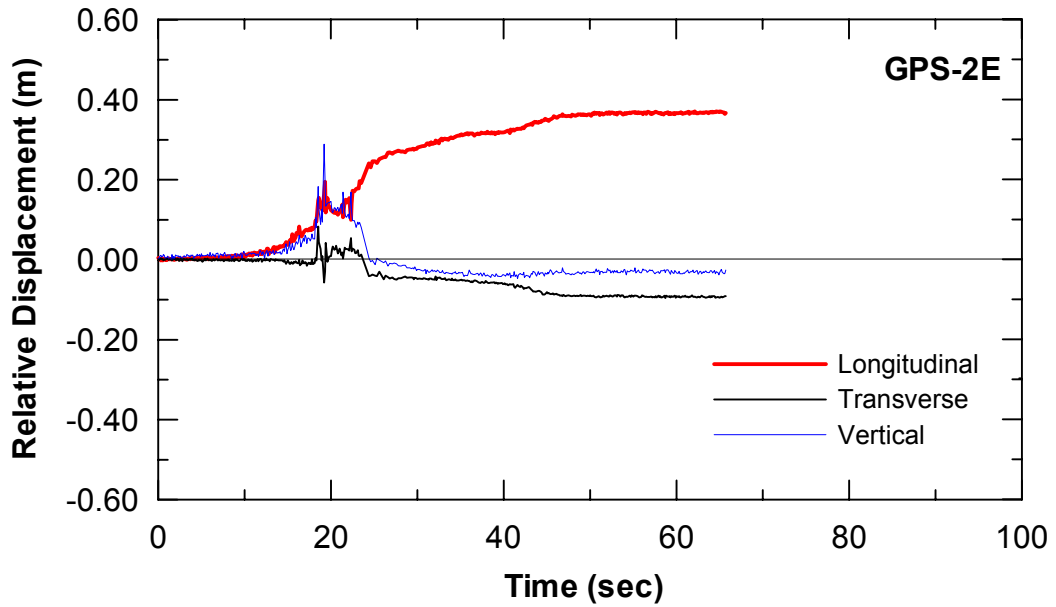
(a) Displacement Time-History
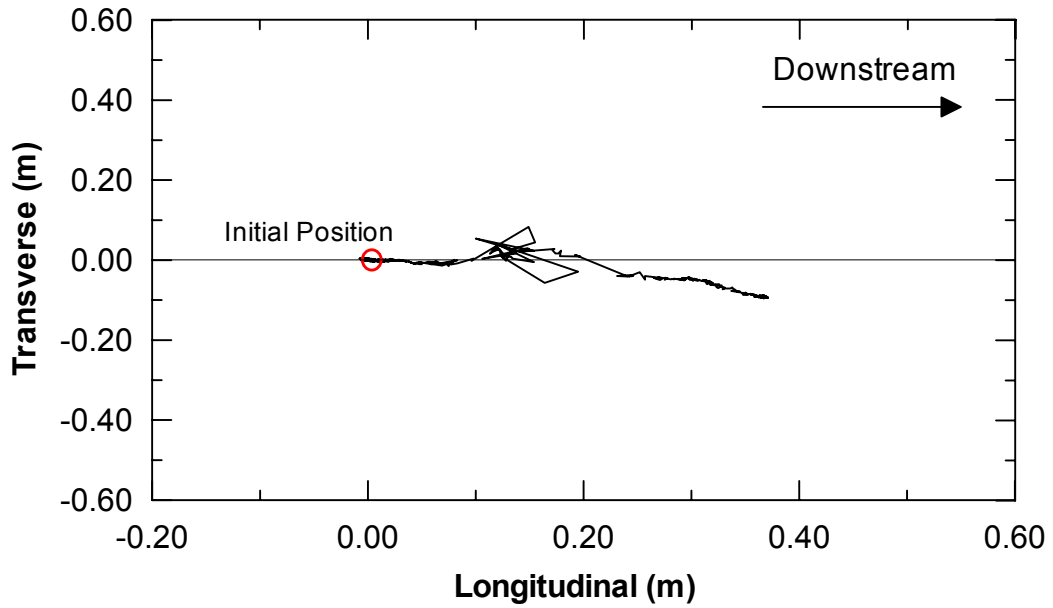
(b) Displacement Path

Figure 4.87   Global Positioning System Data of Unit 2E (1st Blast Test) (a) Displacement Time-History, and (b) Displacement Path, Data from Caltrans
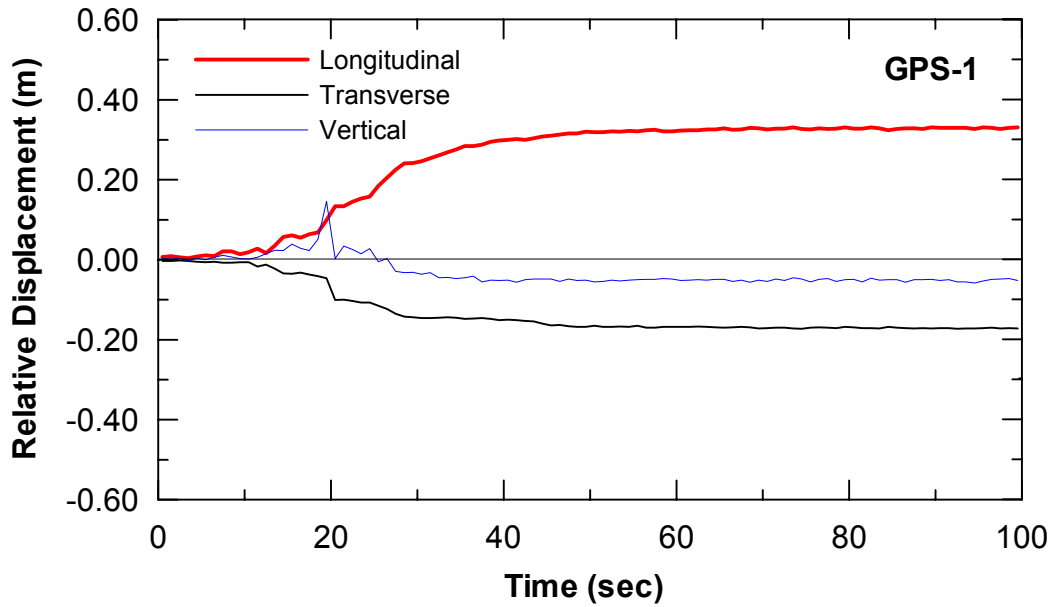
(a) Displacement Time-History
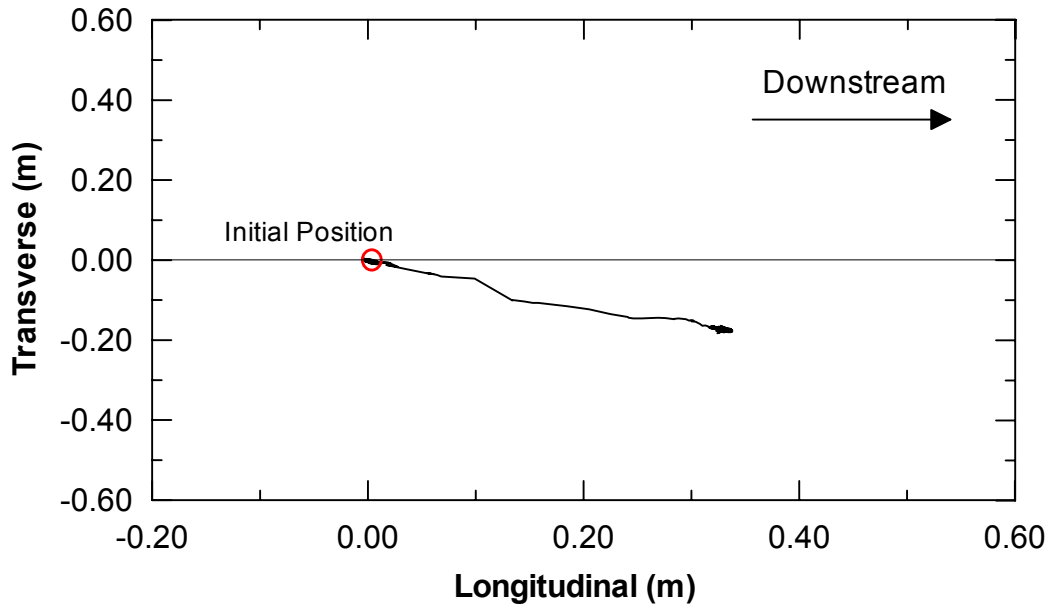
(b) Displacement Path

Figure 4.88   Global Positioning System Data of Unit 1 (1st Blast Test) (a) Displacement Time-History, and (b) Displacement Path, Data from WU
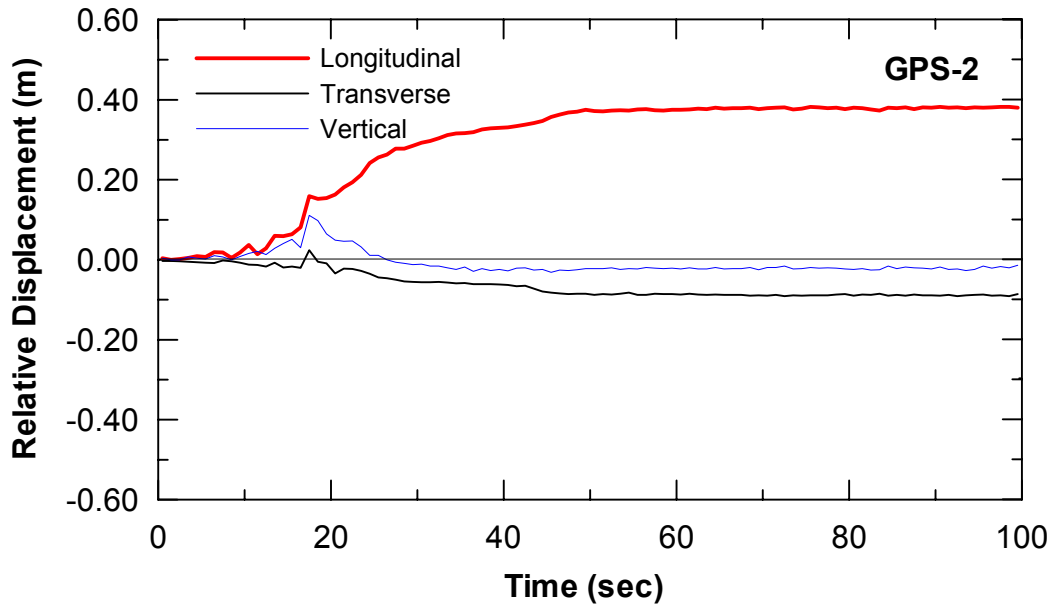
(a) Displacement Time-History
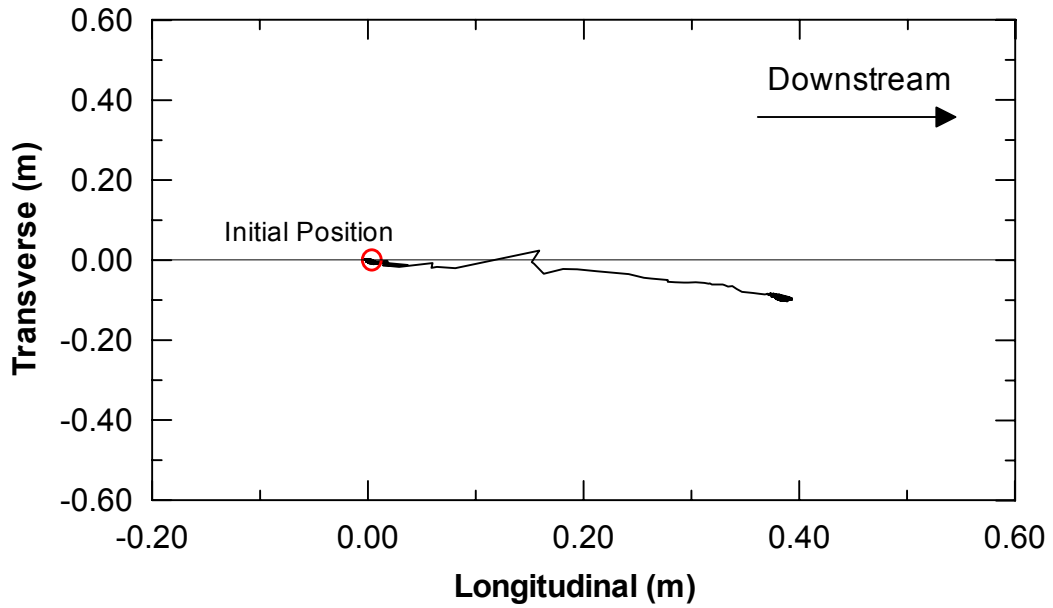
(b) Displacement Path

Figure 4.89   Global Positioning System Data of Unit 2 (1st Blast Test) (a)
Displacement Time-History, and (b) Displacement Path, Data from WU
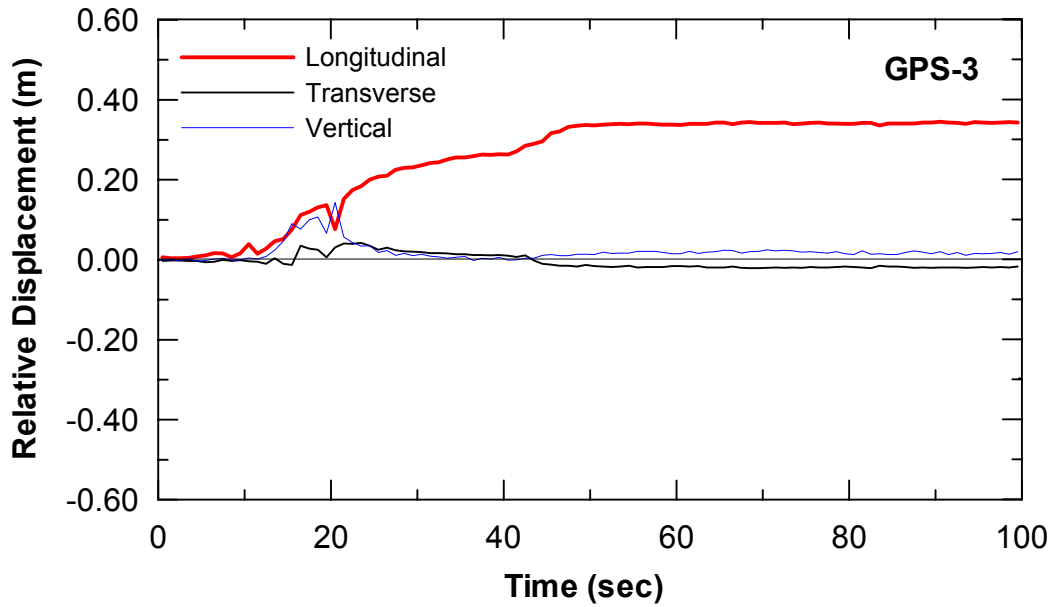
(a) Displacement Time-History
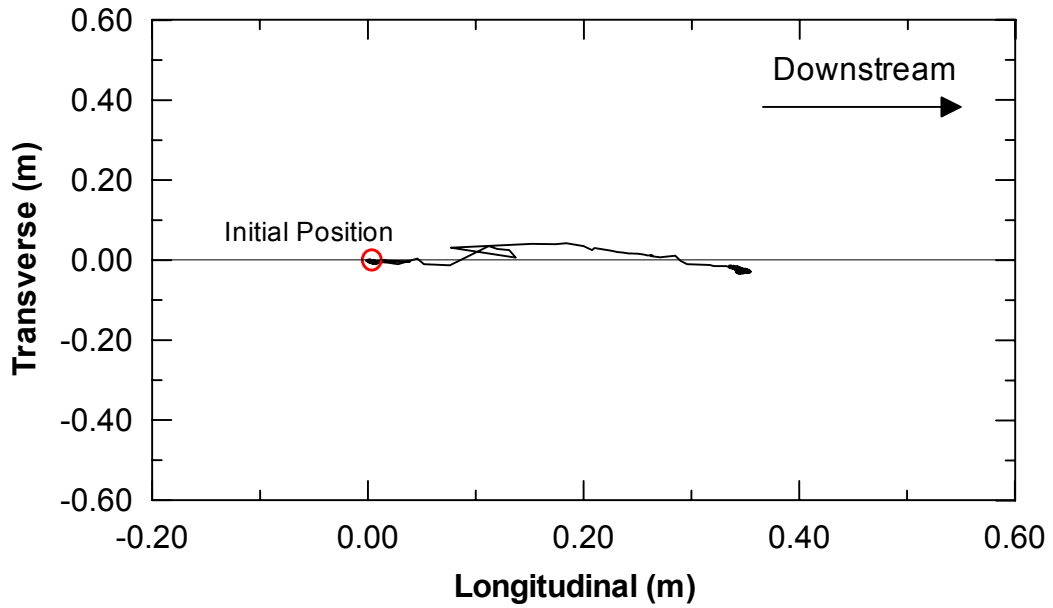
(b) Displacement Path

Figure 4.90 Global Positioning System Data of Unit 3 (1st Blast Test) (a) Displacement Time-History, and (b) Displacement Path, Data from WU
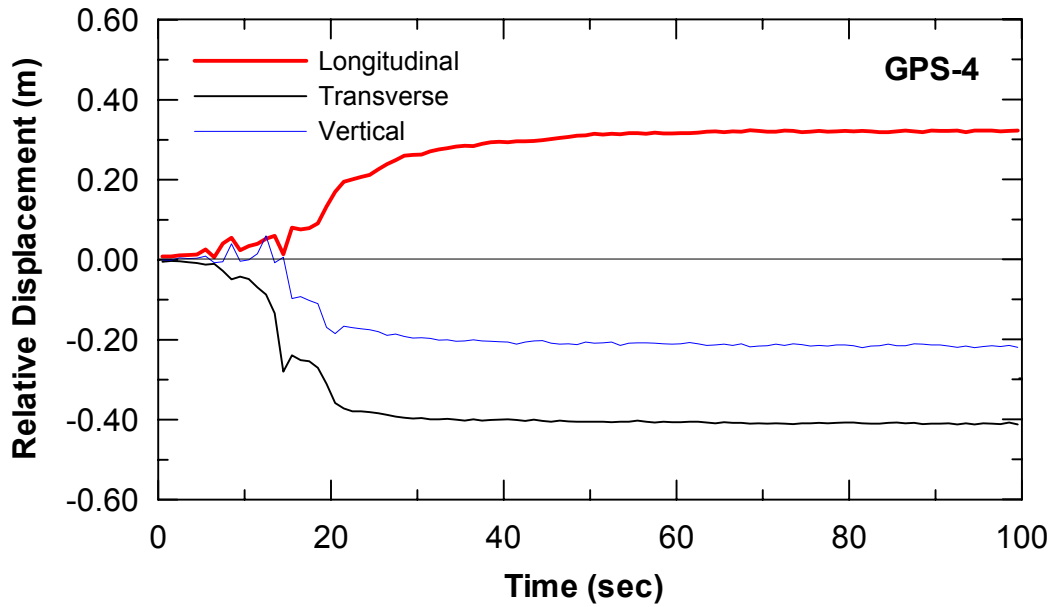
(a) Displacement Time-History
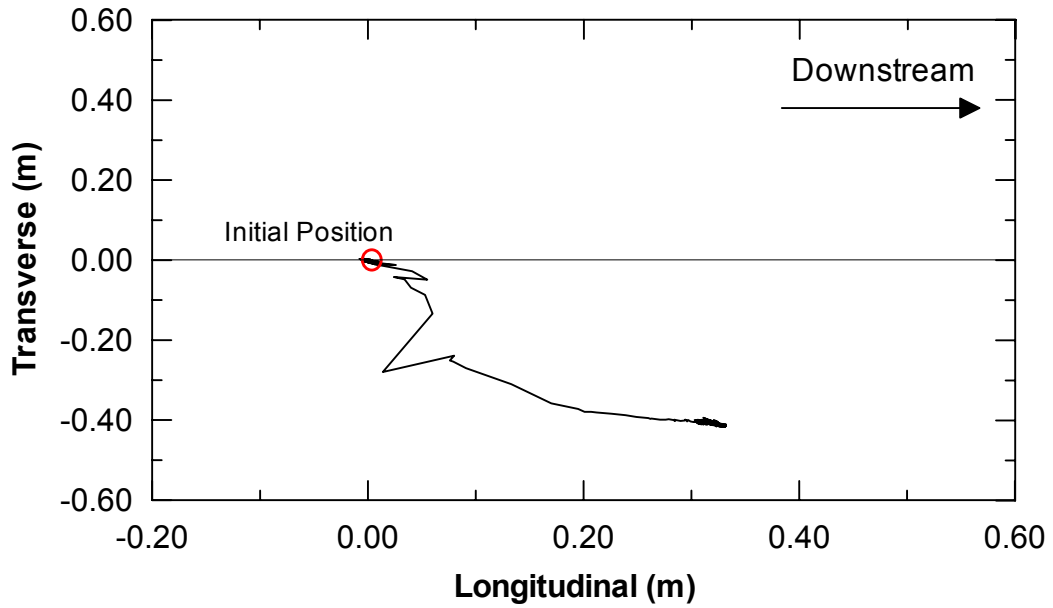
(b) Displacement Path

Figure 4.91   Global Positioning System Data of Unit 4 (1st Blast Test) (a) Displacement Time-History, and (b) Displacement Path, Data from WU
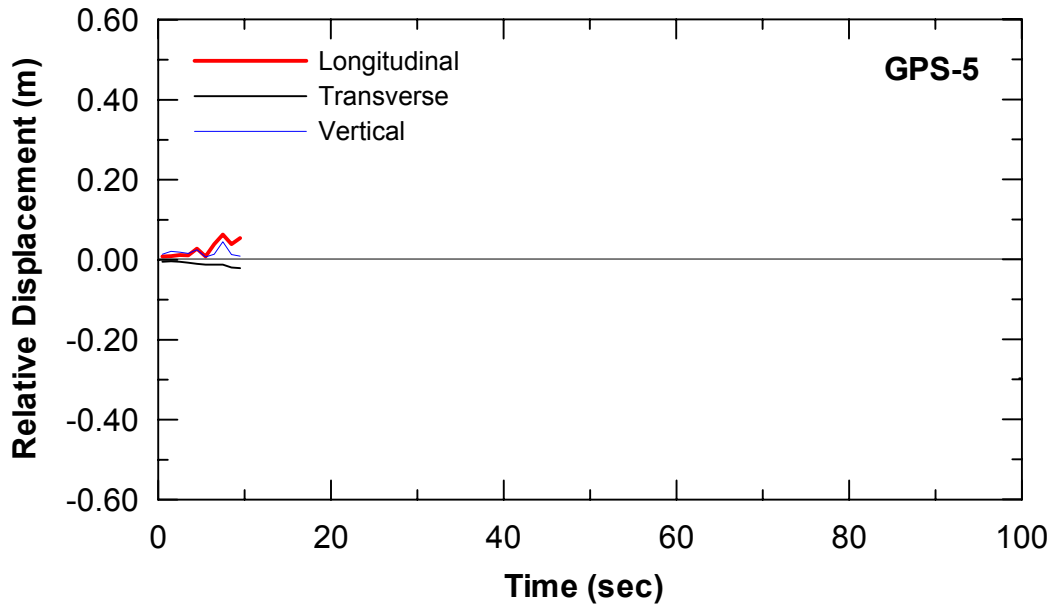
(a) Displacement Time-History
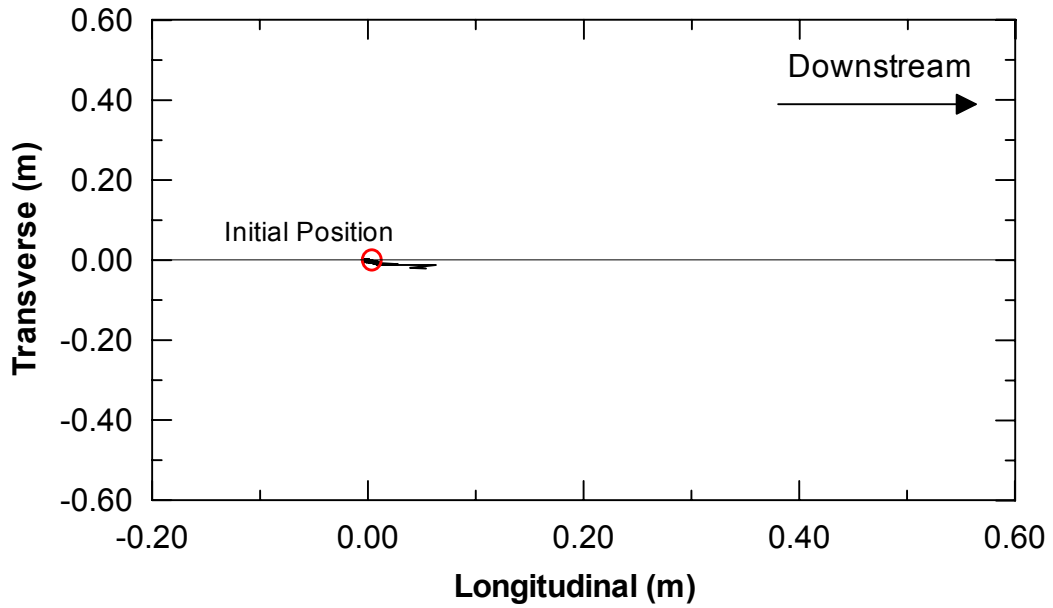
(b) Displacement Path

Figure 4.92   Global Positioning System Data of Unit 5 (1st Blast Test) (a) Displacement Time-History, and (b) Displacement Path, Data from WU
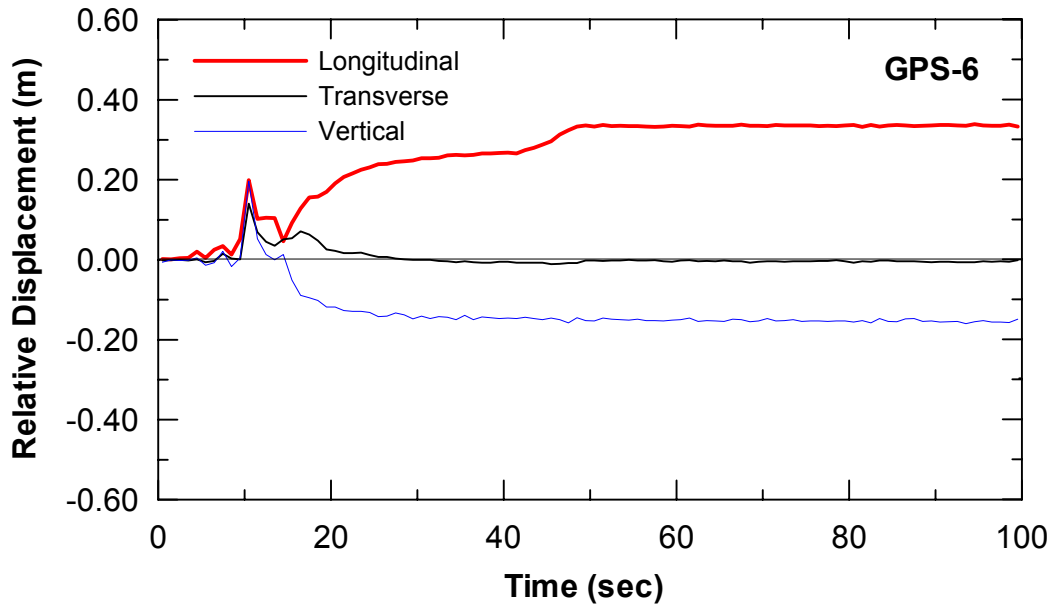
(a) Displacement Time-History
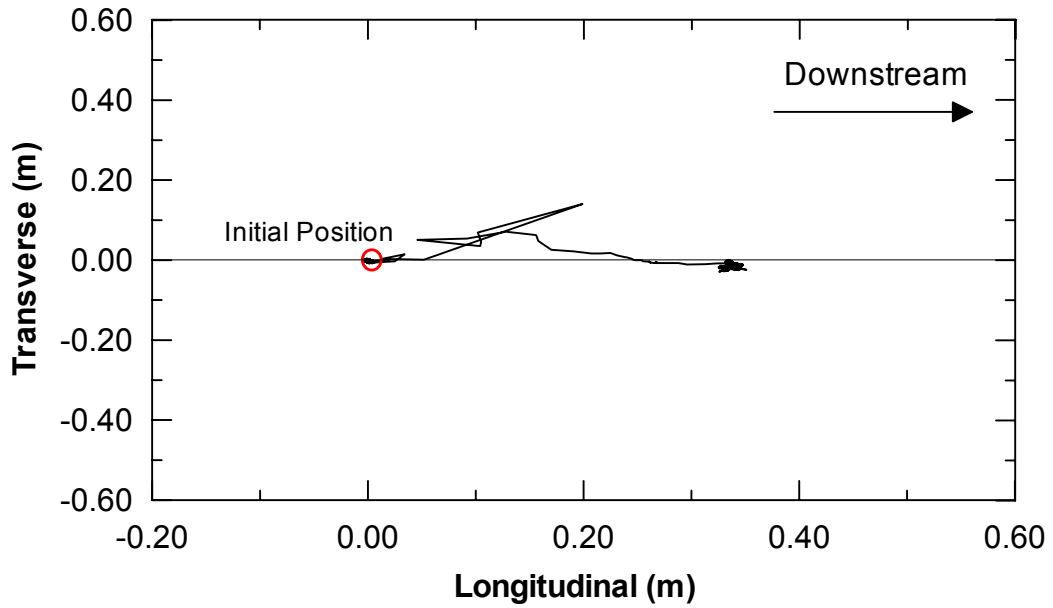
(b) Displacement Path

Figure 4.93   Global Positioning System Data of Unit 6 (1st Blast Test) (a) Displacement Time-History, and (b) Displacement Path, Data from WU
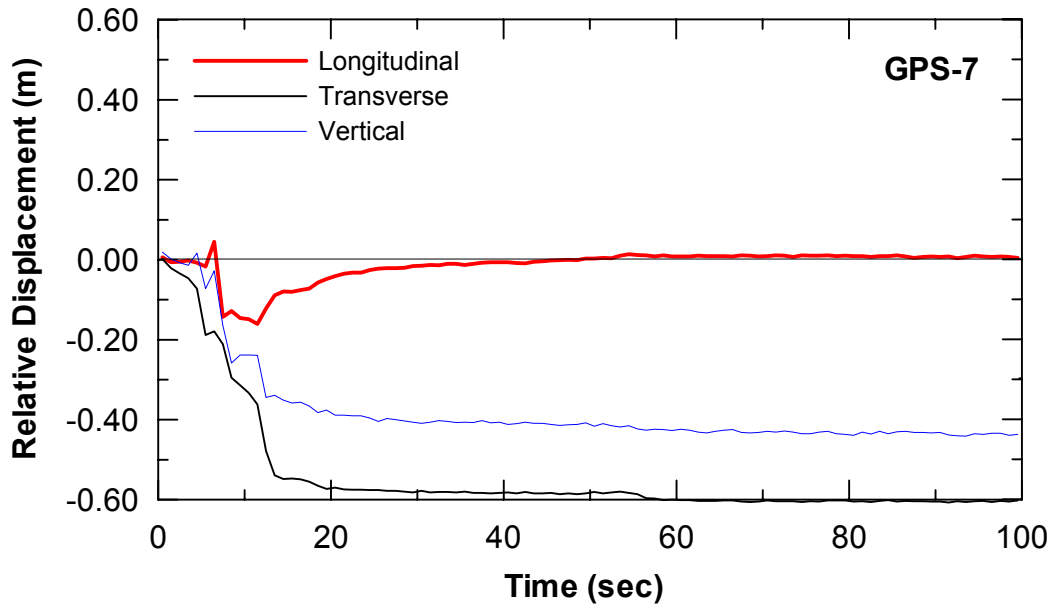
(a) Displacement Time-History
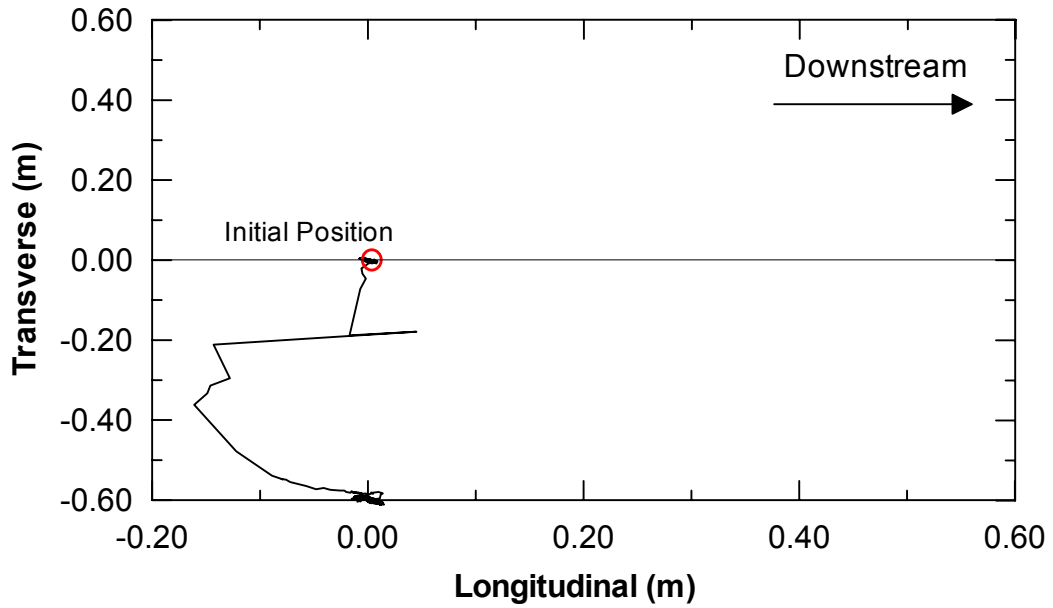
(b) Displacement Path

Figure 4.94   Global Positioning System Data of Unit 7 (1st Blast Test) (a) Displacement Time-History, and (b) Displacement Path, Data from WU
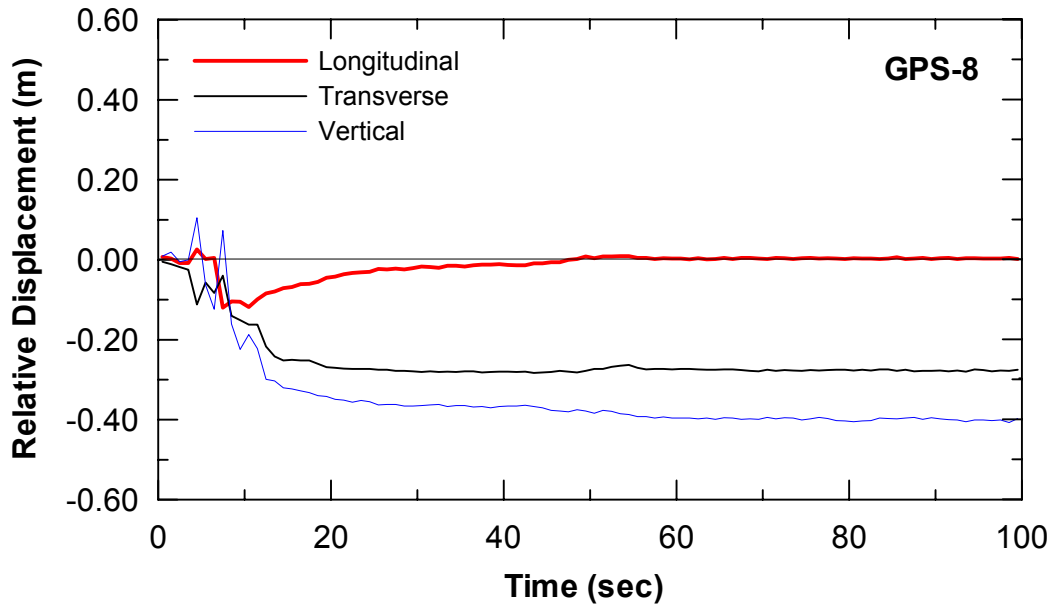
(a) Displacement Time-History
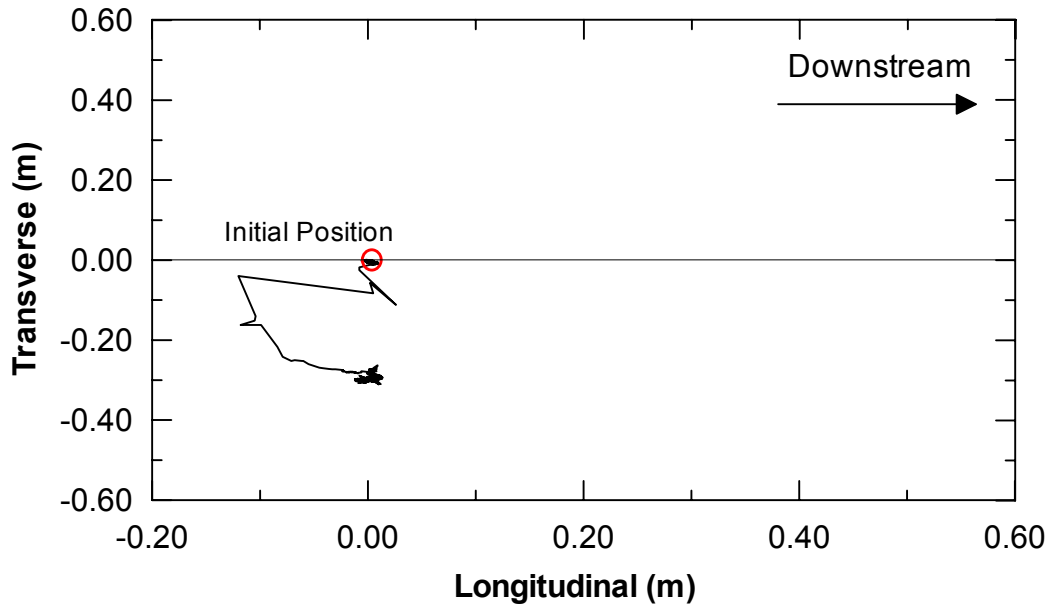
(b) Displacement Path

Figure 4.95   Global Positioning System Data of Unit 8 (1st Blast Test) (a) Displacement Time-History, and (b) Displacement Path, Data from WU
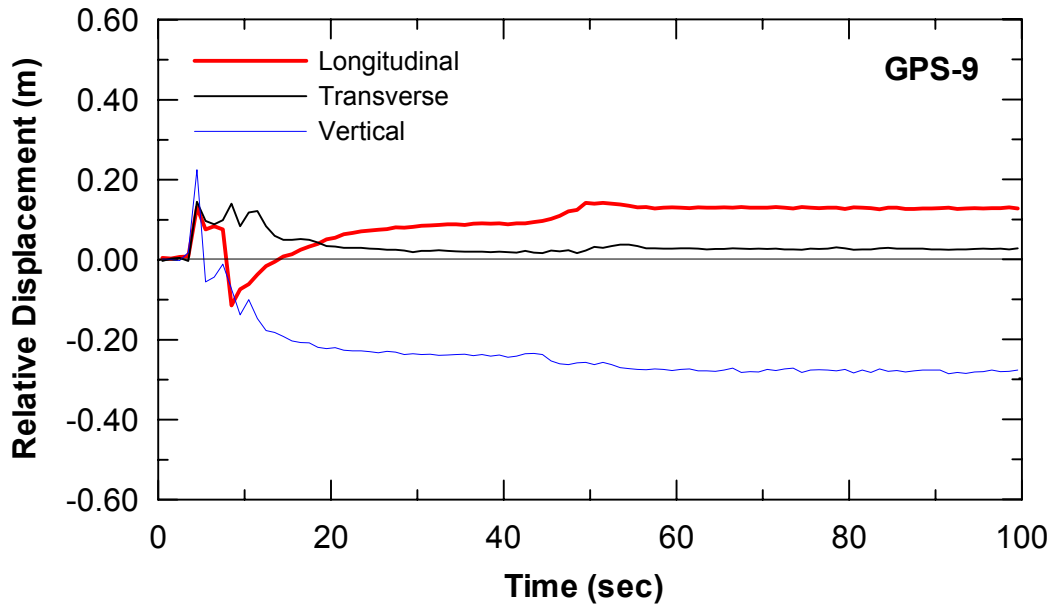
(a) Displacement Time-History
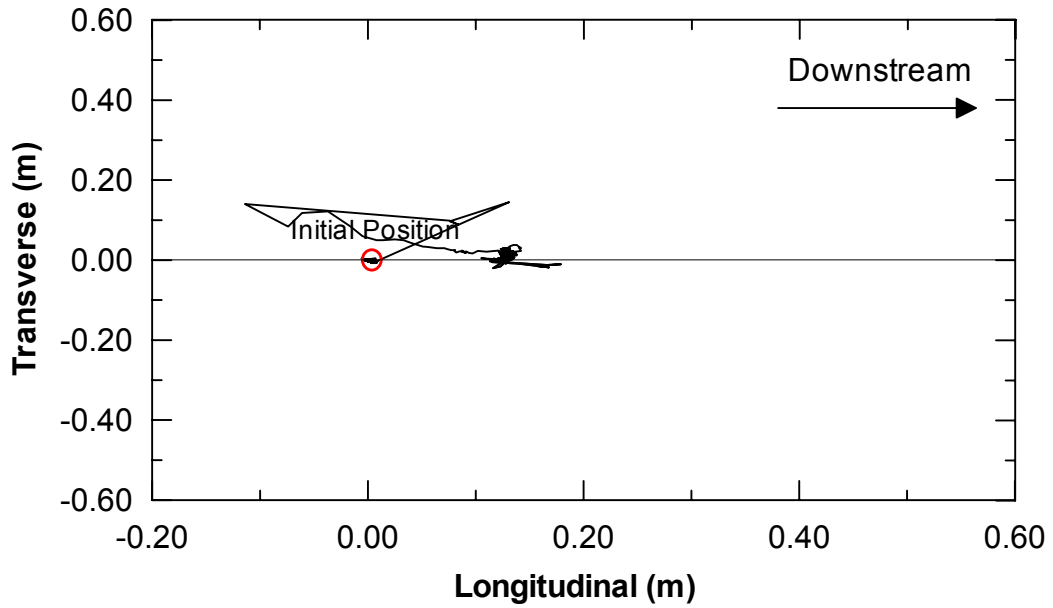
(b) Displacement Path

Figure 4.96   Global Positioning System Data of Unit 9 (1st Blast Test) (a) Displacement Time-History, and (b) Displacement Path, Data from WU
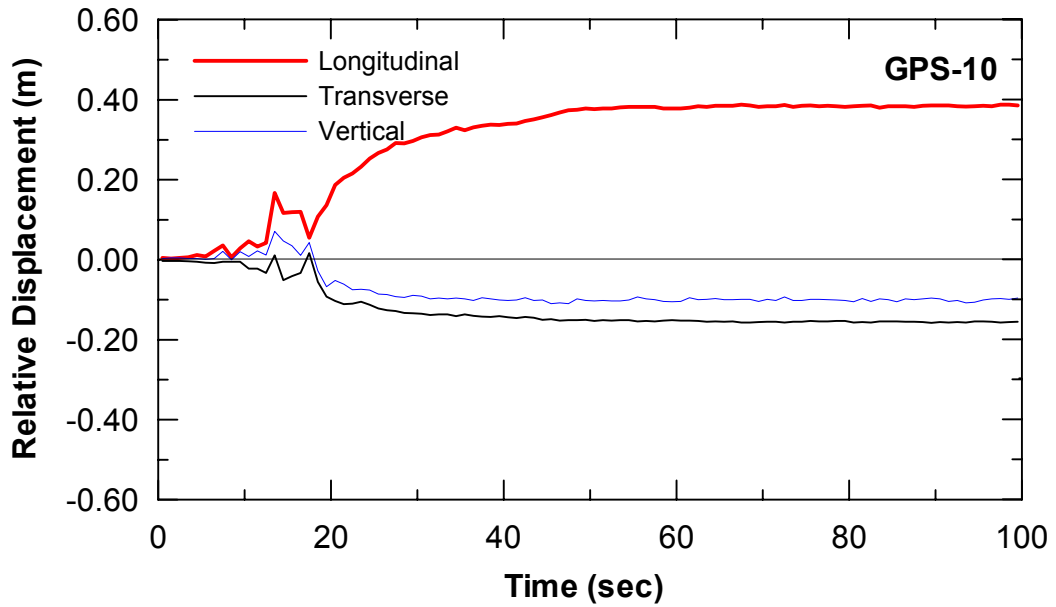
(a) Displacement Time-History
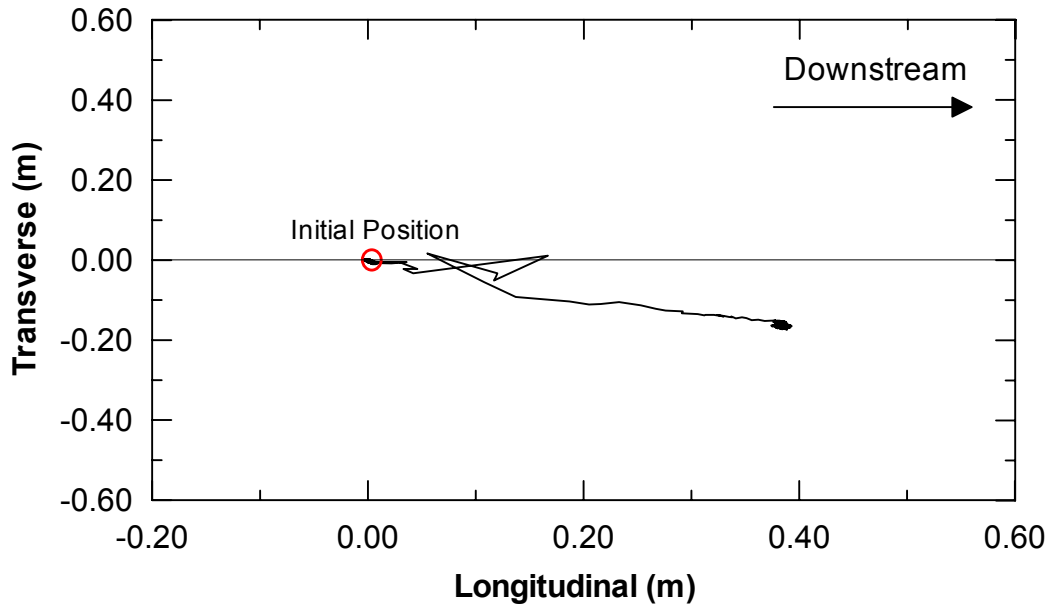
(b) Displacement Path

Figure 4.97   Global Positioning System Data of Unit 10 (1st Blast Test) (a)
Displacement Time-History, and (b) Displacement Path, Data from WU

180
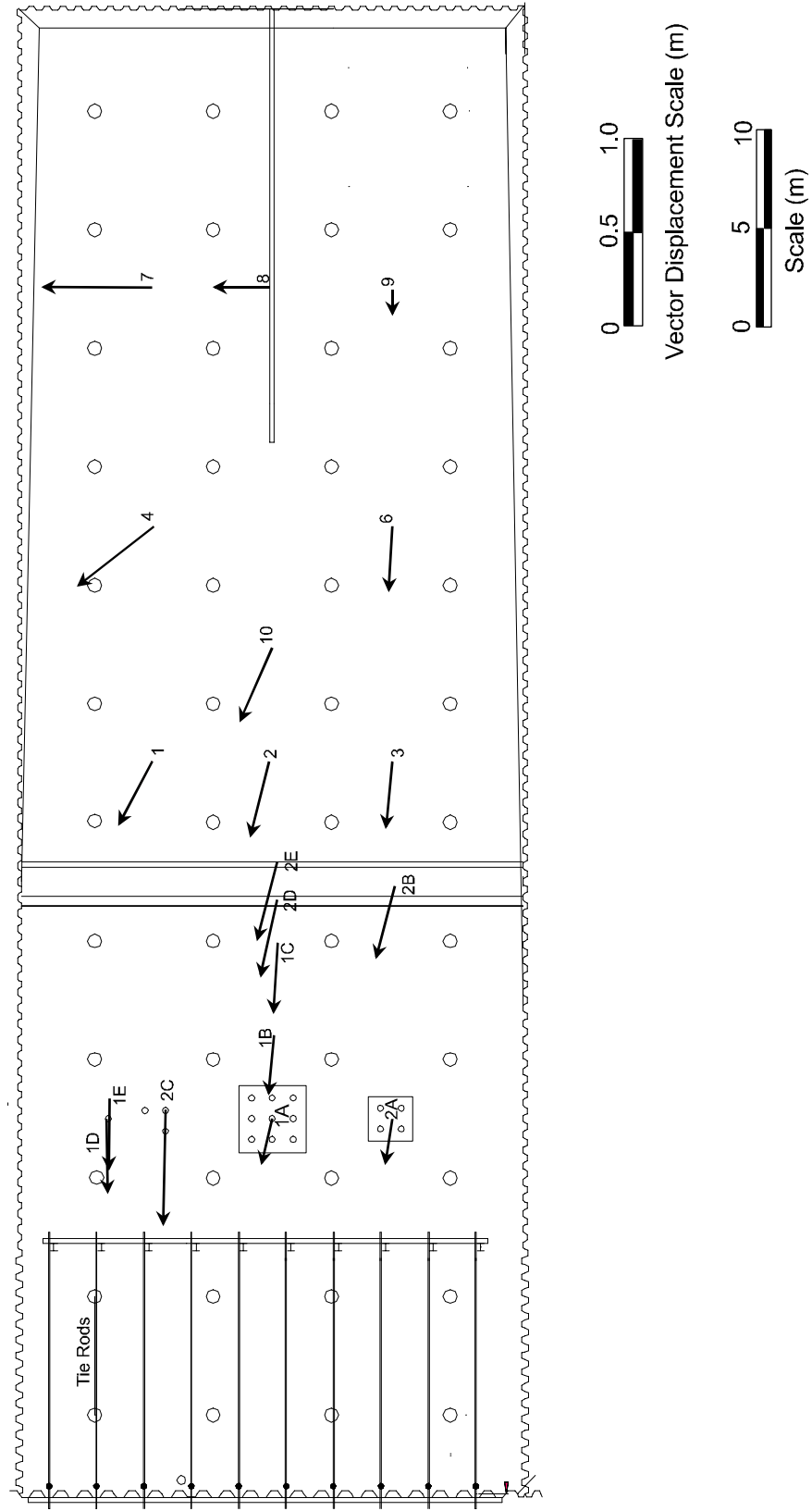
Figure 4.98   Vector Displacements in Horizontal Plane from GPS Data

181

Figure 4.99   Site Condition in the Vicinity of Pile Groups

Figure 4.100   Site Condition in the Vicinity of Single Piles

Figure 4.101   Movement of Quay Wall after the Test

Figure 4.102   Permanent Rotation of Single Piles

Figure 4.103   Settlement around 9-Pile Group after Blasting
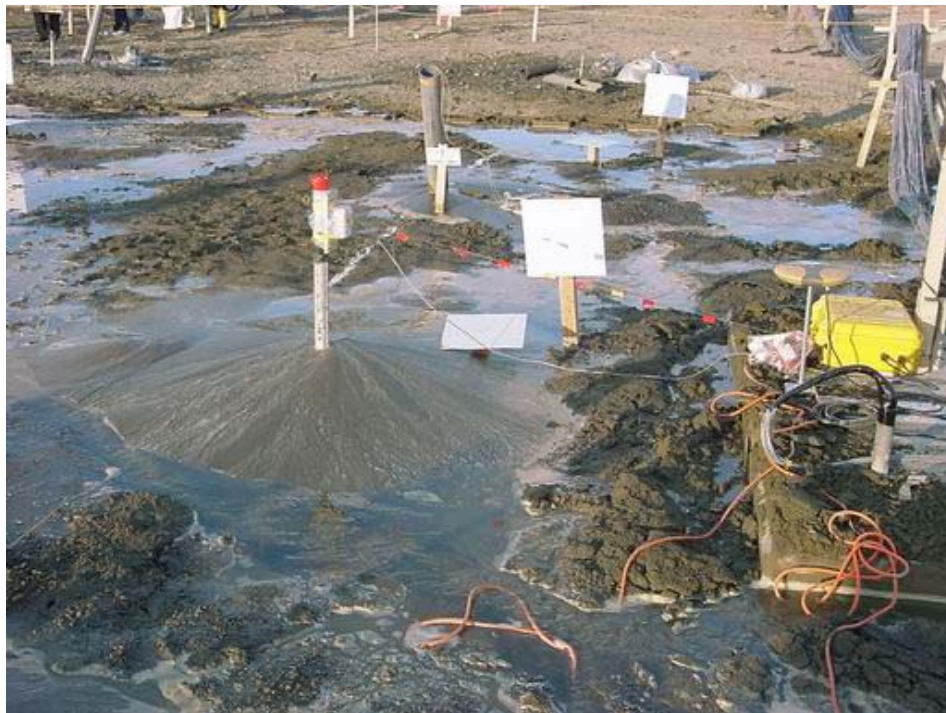
Figure 4.104   Sand Boil Following after Blasting in the Vicinity of 4-Pile Group

Figure 4.105   Sand Boils Following Blasting in Vicinity of Soil Embankment

Figure 4.106   Water Coming from Inclinometer Casing
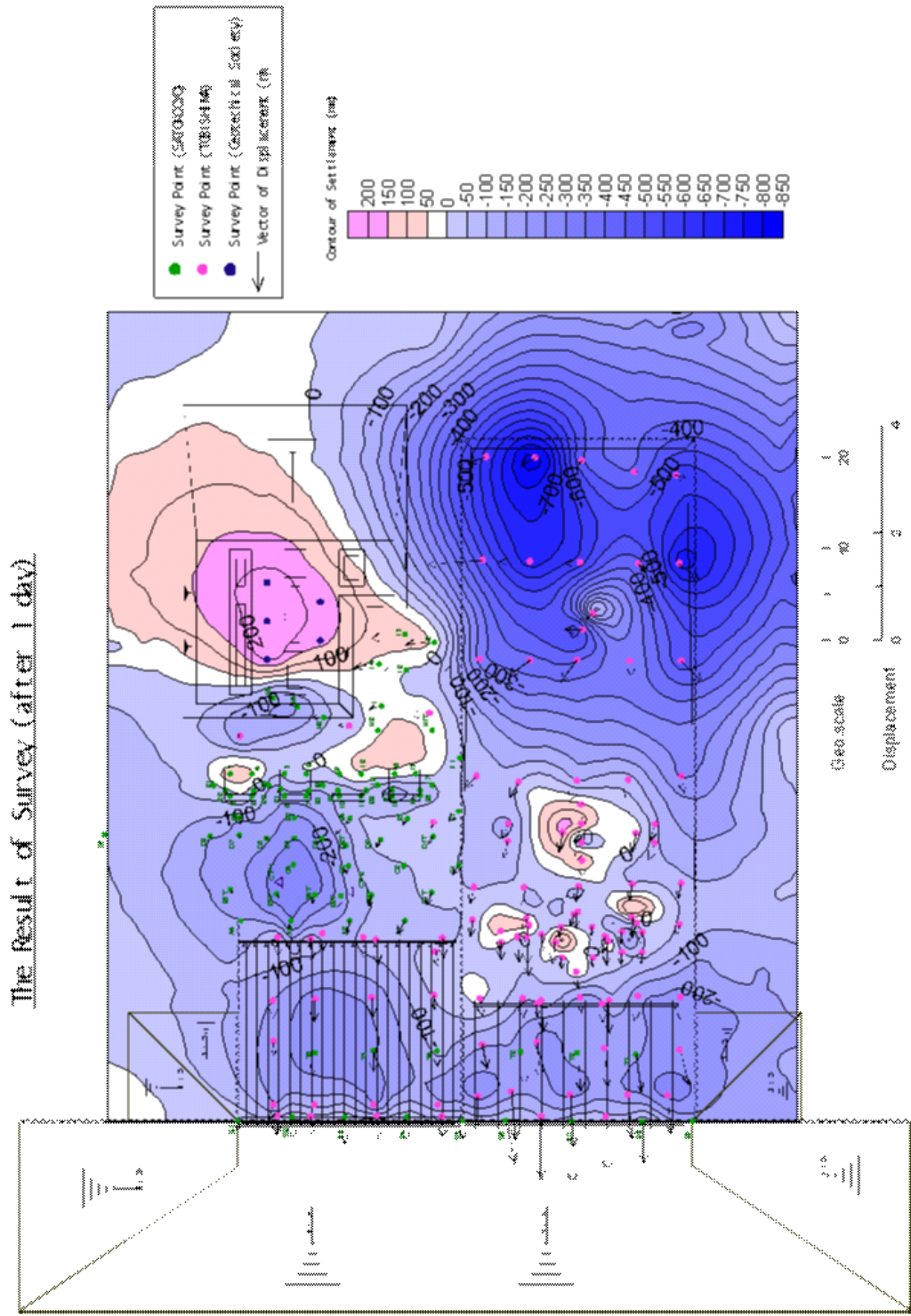
Figure 4.107 Vector Displacements and Settlement Contour 1 day after the Blast, Data from Sato Kogyo

5.   2nd Full-Scale Lateral Spreading Test

Based on the success of the November 2001 test, it was decided to carry out a second test in December while the test specimens and instrumentation were still in place. Therefore, the second lateral spreading test was performed with an attempt to induce additional ground deformations and further evaluate the performance of lifeline facilities subjected larger soil deformation.   In this chapter, the descriptions of test site and test set-up, as well as the test results for the 2nd full-scale lateral spreading experiment, are presented.   Furthermore, the investigation of connection of piles to pile caps after the experiment was discussed.

5.1   Site Description and Test Setup

The test site for the second lateral spreading test was significantly modified from the first one as presented in Figure 5.1. Overview of the test site is also shown in Figure 5.2 and Figure 5.3. The test site was approximately 30m wide by 40m long. The quay wall and sheet piles surrounding the test site were removed to allow the soil to move freely and thus provided larger displacement than the first test.   The waterway was excavated on one end of the test site to the elevation of -1.00m with the slope 1:2 and then filled with the water to the elevation of +1.00 m.   The ground surface was level for a distance of 7.5 m away from the edge of the waterway and then started to rise up with the embankment slope of 6% over a distance of 18.0m. The longitudinal gas pipeline was not included in the area of the 2nd test. It is noted that during the excavation of the water way, some ground movement had occurred and caused the soil settlement, gapping, and some surface cracks, in the areas of the pile groups and single pile as illustrated in Figure 5.4 and Figure 5.5.

Instrumentation of the lifeline utilities were essentially the same as the first experiment, which included strain gauges on the test specimens, pore pressure transducers, linear potentiometer, soil pressure cells, slope inclinometers, accelerometers, tiltmeters, and GPS units. The schematic diagram of the locations of those instruments is presented in Figure 5.6.

The blast holes were spaced at 6.0 m on centers in a regular grid pattern as presented in Figure 5.7. The charges were installed at depths of 4.0 m and 8.0 m below the design ground surface (El +3.00m). The amount of charges varied from 2 kg to 4 kg with the charges being smaller in the vicinity of specimens to prevent the damages to the instruments. Two additional rows of blast holes were drilled. One was located on the steep slope adjacent to the waterway with the amount of explosives ranging from 1to 3 kg. The purpose of these explosives was to create some movement at the slope toe prior to the primary blasting sequence such that the embankment soil behind it had a high potential to move freely with larger deformation once the primary blasting initiated. The other was located between the pipelines and pile as denoted as blast hole No. 7 to No.9. Three kilograms of explosives were installed at El. -3.00 m.

The weather condition for the second experiment was awful for the lateral spreading test due to the heavy snowfall with the snow thickness of about 0.50 m, and a new record of wind speed of 100 kph on the test day. The ground was frozen throughout the test site which would likely impede the global translation of the soil mass. In an attempt to mitigate this, jackhammers were used to break the frozen ground in the vicinity of test specimens to depths of approximately 20 to 30 cm below the ground surface.

The second test was carried out on December 14, 2001. The explosives on the steep slopes were detonated initially from S1 to S5. Approximately 15 second later, the primary sequence of blasting was started. The primary blast began with the back corner of the embankment denoted as blast hole No.1. Then, the blasting proceeded to the next holes of the same rows, then continued to the next row towards the waterway (i.e., from No.1 to No.17). The sequence of blasting is shown in Figure 5.7.

5.2   Test Results

In this section, the results from the 2nd full-scale lateral spreading experiment are presented. The results are presented in terms of additional amounts measured due to the movement of the soil which only occurred in the second test. The total responses of

those quantities which included the soil movements, strains in the piles and pipelines, as well as pile rotations, can be computed by summing those amounts from the first and second blast together.

5.2.2 Single Pile

The strain gauge data of the single pile are presented in Figure 5.9 to Figure 5.10. The strain profile of single pile is presented in Figure 5.11. Figure 5.12 presents cumulative moment of the pile due to the first and the second test in the same plot. The pile reached the yield moment after the second test at depths between 8 and 9.5 m. The moment along the pile was insignificant for the first 4m of a very loose sand layer which was highly susceptible to liquefaction.

The pore water pressure ratios nearby the single pile are presented in Figure 5.13 and Figure 5.14. The pore pressure ratios ranged between 30% and 70% immediately after the blast ceased and proceeded to drop below 20% one hour following the blast. The excess pore pressure ratios appeared to be much less than those measured during the first test. Two possible reasons can be explained. Firstly, the soil was less susceptible to liquefaction because some settlement took place after the first blast and caused the soil become denser. Secondly, frozen ground decreased the liquefaction potential.

The excess pore pressure ratios at a depth of 2 m were somewhat unusual between 5 and 20 seconds because they were negative (not presented in the plot). This might be due to the fact that transducer at this particular depth might not be fully saturated because it was left in the ground for a period of a month. The water table was possibly sometimes below the transducer level due to the fluctuation of the Pacific Ocean resulting in partially saturation of the transducer.

5.2.3 4-Pile Group

Individual strain gauge responses along instrumented piles in the 4-pile group are presented in Figure 5.15 through Figure 5.18. Strain gauges on the back side (downstream) of pile No.8 were damaged due to the blasting. Profiles of strain for pile No.7 and pile No.8 due to lateral spreading in the 2nd test are presented in Figure 5.19 and

Figure 5.20, respectively. The moment along the pile are presented in Figure 5.21 and Figure 5.22. The maximum moment for pile No.7 and No.8 was 44% and 70% of yield moment and occurred at depths approximately 9.0m below the ground surface.

The excess pore pressure ratios nearby the 4-pile group for durations of 100 seconds and 1 hour are presented in Figure 5.23 and Figure 5.24, respectively. The excess pore pressure ratios were approximately 50% immediately after the blast stopped. One hour after the blast, the pore water pressure ratios dropped to between 15 % and 30%. The transducer at depth of 2m showed negative excess pore pressure ratio as that occurred for the single pile which confirmed the possibility of partially saturation of the transducers at this particular depth. Again, the excess pore pressure ratios were much less than those occurred in the first blast. The possible reasons were already discussed in the single pile section.

5.2.4 9-Pile Group

Strain gauge data for instrumented piles in the 9-pile group are presented in Figure 5.25 through Figure 5.32. The time-history data for the pile No.4 and No.5 were lost due to the accidentally error in our data acquisition system. Fortunately, the residual strains of such piles were accessible. Strain profiles along individual piles are shown in Figure 5.33 through Figure 5.38. The moment distribution of each pile is presented in Figure 5.39 through Figure 5.44. The maximum moment ranged from about 50% to 60% of yield moment except for pile No.2 and No.4 for which the maximum moments were only 10% and 20% of yield moment, respectively. The lower moments along those two piles were likely due to the lower degree of fixity at pile tips because penetrated lengths of those piles into the dense soils were shorter.

The excess pore pressure ratios in the vicinity of the 9-pile group are presented in Figure 5.45 to Figure 5.48. Just the blast stopped, the excess pore pressure ratios ranged between 50% and 80%. One hour after the blast, the ratios dropped to between 10% and 55%. These ratios were lower than the first test, and therefore indicated the less degree of liquefaction.

190

5.2.5 Gas Pipeline in Transverse Direction (Pipeline Type A)

The strain gauge data along transverse gas-pipeline (pipeline A) are presented in Figure 5.49 and Figure 5.50. These were the additional strains measured in the 2nd test alone.   Figure 5.51 presents profiles of strain gauge along the top and the side of the pipeline. The maximum strains, which occurred at the top and the side of the pipeline, were approximately the same.

Figure 5.52 and Figure 5.53 present the data from pore pressure transducers installed between the middle of the pipeline A and B in several depths. Both transducers show the maximum excess pore pressure ratio ranging from 60% to 80% just after the blast stopped and then dropped to below 50% one hour after the blast.

5.2.6 Gas Pipeline in Transverse Direction (Pipeline Type B)

The data of strain gauges along the transverse electrical conduit are presented in Figure 5.54 and Figure 5.55. The profile of strain gauge on the top and the side of the pipeline are shown in Figure 5.56. The maximum strain occurred at about the middle of the pipeline as expected. The excess pore pressure ratios nearby this pipeline were already discussed in the previous section.

5.2.7 Results of Other Instruments

Other instruments that were not installed in the vicinity of the test specimens or inappropriate to incorporate in the above section were discussed separately in this section.

The data of soil pressure cells on the pile caps of the 4-pile group and the 9-pile group are presented in Figure 5.57. Considering the cells installed for the 9-pile group (SPC-1 to SPC-6), the soil pressures on the upstream side of the pile cap varied between 5 and 10 kN/m^2, while those on the downstream side were insignificant. This is because the gap on the downstream side of the pile cap was existed prior to the test. Furthermore, the soil on the downstream side moved towards the waterway resulting in loosing the contact between soil and the pile cap.

The results of accelerometers attached on the top of foundations are presented in Figure 5.58. Similar to the first test, acceleration at the pile head due to the effect of blasting decreased with increasing the foundation stiffness. The maximum acceleration occurred at the single pile, while the lowest acceleration was observed at the 9-pile group.

Figure 5.59 presents the tiltmeter data. The additional pile head rotation of the single pile (free head condition) due the movement occurred in the 2nd test alone was approximately 1.5 degree, and therefore the total rotation of the single pile was about 3.5 degree (2 degree from the first test). The rotation of the 9-pile group (fixed head condition) was again insignificant. The rotations of a group of WU single piles after the 2nd test were also crudely measured with ranging in values from 5.6^{o} to 6.3^{o}.

Profiles of soil displacement obtained from the inclinometer readings after the completion of the 2nd blast test are presented in Figure 5.60 through Figure 5.69. The summary of the movement at the ground surface of each location are summarized in Table 5.1. The displacements obtained from inclinometer data were generally slightly less than the actual soil displacement (i.e., compared to GPS data) because some rotations and displacements occurred at the tips of those casings. The movement of the soil ranged approximately from 9 to 43 cm. The soil between the foundation systems moved the most with an averages of 40 cm and the displacement tended to be smaller as moving away from the waterway.

The results of string activated linear potentiometers are presented in Figure 5.70 and Figure 5.73. A summary of relative movement is given in Table 5.2. The movements of the 4-pile group (19cm) and 9-pile group (17cm) were almost the same, while the movement of the single pile was approximately 10 cm more than the pile groups. The soil in front of the pile caps moved approximately the same amount as the pile caps. The soil on the downstream behind the 9- pile group moved 20 cm more than the pile cap.

The GPS data are presented in Figure 5.74 through Figure 5.83 Displacements in longitudinal, transverse, and vertical directions obtained at 1 minute and 20 hours following blasting are summarized in Table 5.3 and Table 5.4, respectively. No

horizontal creep was observed over 20 hours following blasting. Most of the horizontal displacement associated with the lateral spreading took placed within tens of seconds following the blast. Settlement about 4 cm was observed on the gas pipeline over a period of 20 hours. The vector displacements in horizontal plane throughout the test site are presented in Figure 5.84. The largest horizontal displacement was about 0.45 m occurring at a group of Waseda free head piles. The movement of the soil between two pile caps was 0.43m which was in good agreement with the inclinometer measurements.

The displacement measurements from GPS units were verified against linear potentiometer measurements in several locations as summarized in Table 5.5. Excellent agreement between measurements from GPS units and linear potentiometers were observed with the differences being within 1.4 cm, except at STP-3 where the measurements of GPS was 3.8 cm lower than that measured by linear potentiometer.

5.2.8 Overview of Site Condition after Testing

After the end of the test, some evidences of liquefaction were observed which included water coming out nearby the pile caps, from the inclinometer casings, as well as from the blast holes. However no sand boil was observed in any locations. Large settlement was observed in the downstream side of the pile cap as presented in Figure 5.85. Water was mainly coming out on the downstream side of the pile cap causing a small pond behind the pile caps as shown in the figure. Significant tilting of single piles was observed as presented in Figure 5.86. Figure 5.87 and Figure 5.88 show water coming out from a slope inclinometer casing and a blast hole, respectively. Figure 5.89 presents the locations of blast holes and inclinometer casings where water was observed. Some surface cracks were observed showing the movement of soil towards to waterway. Sketch of these cracks is shown in Figure 5.89. Based on the observation of site condition after the test as well as the test results from many instruments, the degree of the liquefaction for the second test was much less than that of the first test mainly due to the weather condition.

5.2.9 Survey of Movement after Testing

Prior to and after the test, the locations of specimens, inclinometer casings, and many references on soil surface were measured to determine the relative movements of those in x, y, and z direction due to the global translation of the soil mass. Figure 5.90 presents the vector movements of soil and specimens as well as the settlement contour one day following the test.

5.2.10 Investigation of Pile Cap Connection Condition

Soil around the pile caps was excavated to investigate the condition of connection between piles and pile caps. Figure 5.91 and Figure 5.92 show the connection conditions for 4-pile group and 9-pile group, respectively.   No any structural damage was observed for both connections though both pile groups experienced the total movements of almost 40 cm.

Table 5.1   Summary of Displacement at Ground Surface from Slope Inclinometer Data, 2nd Blast Test

Location	Displacement in A-Axis (m)	Displacement In B-Axis (m)	Total Vector (m)	Remarks
S1	-	-	-	Casing damaged.
S2	0.351	-0.033	0.353	
S3	0.143	0.066	0.157	
S4	0.136	-0.046	0.143	
S5	0.392	-0.076	0.400	
S6	0.429	0.025	0.430	
S7	0.218	-0.057	0.225	
S8	0.119	-0.015	0.120	
S9	0.091	0.038	0.098	
S10	0.090	-0.012	0.091	
S11	0.212	-0.001	0.212	

Table 5.2   Summary of Relative Displacements after 2nd Blast Test

Name	Location	Relative movement (m)	Interpretation	Remarks
STP-1	9-pile group and Inc. S1 (upstream)	0	Piles and soil had the same movement.	
STP-2	9-pile group and Inc. S2 (downstream)	0.196	Soil moved 196 mm more than piles.	
STP-3	Single pile and Inc. S7 (upstream)	0.038	Pile moved 38 mm more than pile.	
STP-4	4-pile group and Inc. S8 (upstream)	0.025	Soil moved 25 mm more than pile.	
STP-5	Single pile (W1) and Inc. S11 (upstream)	0.132	Pile moved 132 mm more than soil.	
STP-6	Single pile (W2) and Inc. S11 (upstream)	0.085	Pile moved 85 mm more than soil.	
STP-7	Single pile (W1) and Single pile (W3)	0.018	W3 moved 18 mm more than W1.	
STP-8	4-pile group	-0.187	4-pile group moved 187 mm.	
STP-9	9-Pile Group	-0.169	9-pile group moved 169 mm.	
STP-10	Single Pile	-0.285	Single pile moved 285 mm.	

Note: Refer to Figure 5.6 for a better understanding of the relative movements.

Table 5.3   Summary of GPS Data for 2nd Japan Blast Test, approximately 1.3 Minutes
Following Blasting (Data from Caltrans)

Location	Displacement (m)			Horizontal Displacement (m) (x-y plane)	Angle to Flow Direction (Degree)
	Longitudinal (x)	Transverse (y)	Vertical (z)		
1A	0.155	-0.022	0.009	0.157	8.06
1B	0.151	-0.017	0.066	0.151	6.34
1C	0.195	-0.048	0.015	0.201	13.81
1D	0.299	0.004	0.002	0.299	-0.70
1E	0.226	0.054	0.010	0.232	-13.37
2A	0.183	-0.012	0.009	0.184	3.83
2B	0.103	-0.039	0.028	0.110	20.98
2C	0.473	0.002	-0.019	0.473	-0.19
2D	0.170	-0.020	-0.107	0.171	6.71
2E	0.445	-0.018	-0.015	0.445	2.27

Table 5.4   Summary of GPS Data for 2nd Japan Blast Test, approximately 20 Hours
Following Blasting (Data from Caltrans)

Location	Displacement (m)			Horizontal Displacement (m) (x-y plane)	Angle to Flow Direction (Degree)
	Longitudinal (x)	Transverse (y)	Vertical (z)		
1A	0.149	-0.023	-0.001	0.151	8.76
1B	0.149	-0.016	0.047	0.150	6.24
1C	0.193	-0.034	-0.009	0.196	9.99
1D	0.296	0.011	-0.015	0.296	-2.17
1E	0.224	0.055	-0.012	0.230	-13.79
2A	0.171	-0.021	0.007	0.172	6.99
2B	0.104	-0.045	0.044	0.114	23.36
2C	0.475	0.005	-0.024	0.475	-0.57
2D	0.169	-0.022	-0.144	0.170	7.37
2E	0.459	-0.008	-0.022	0.459	1.00

Table 5.5   Verification of GPS Measurements with Data from Potentiometers

GPS Location	Potentiometer Location	GPS Measurement (m)	Potentiometer Measurement (m)
1A	STP-9	0.157	0.169
1D	STP-10	0.299	0.285
2A	STP-8	0.184	0.187
GPS 1A -1B	STP-1	0.006	0.000
GPS 1E -1D	STP-3	0.073	0.038
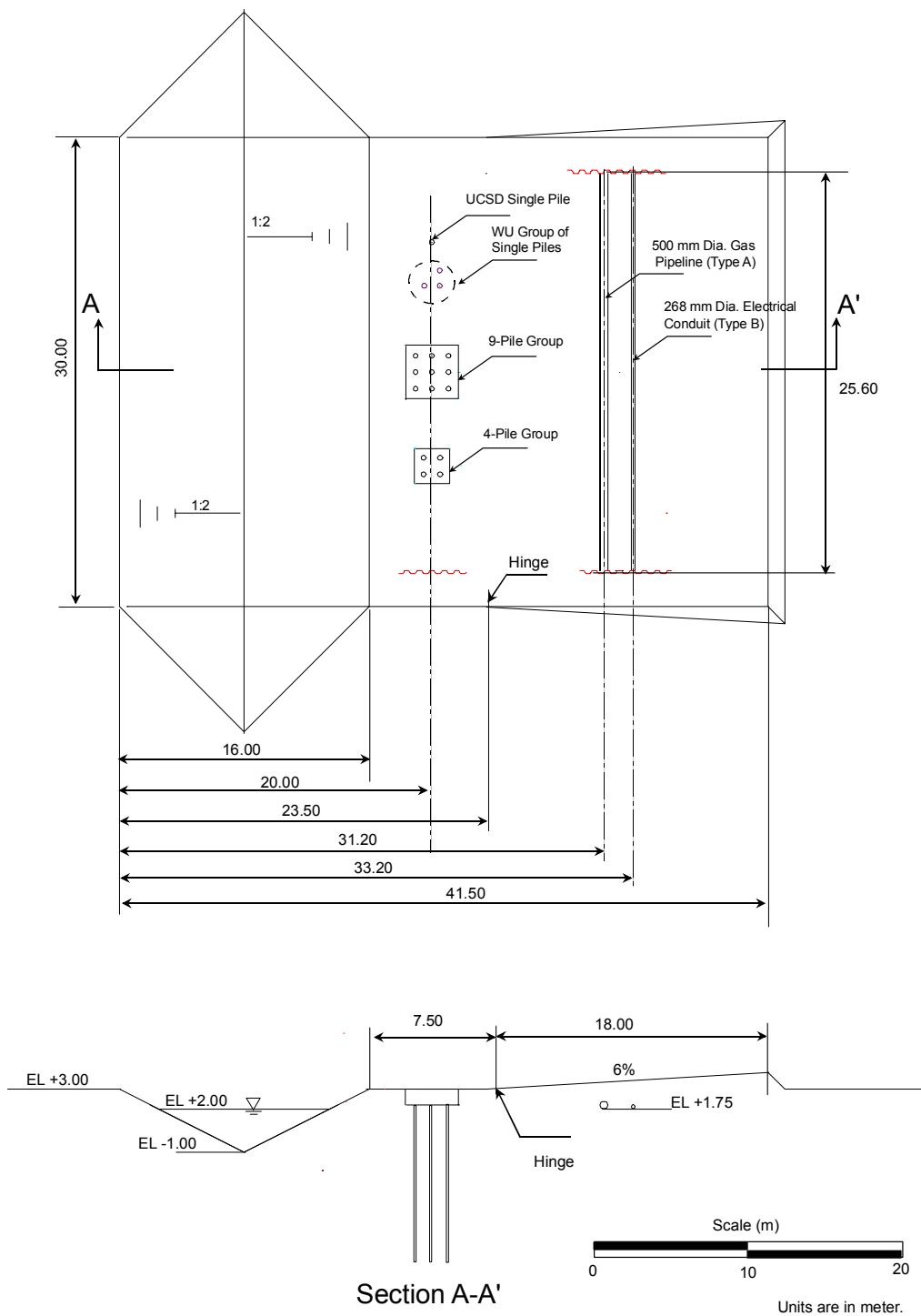
Figure 5.1 Test Site Layout for 2nd Japan Blast Test

Figure 5.2   Overview of Test Site (Front View), 2nd Japan Blast Test

Figure 5.3   Overview of Test Site (Side View), 2nd Japan Blast Test

Figure 5.4   Site Condition before 2nd Blast Test Showing Settlement and Gapping around 9-Pile Group

Figure 5.5   Site Condition before 2nd Blast Test Showing Gapping around Single Pile
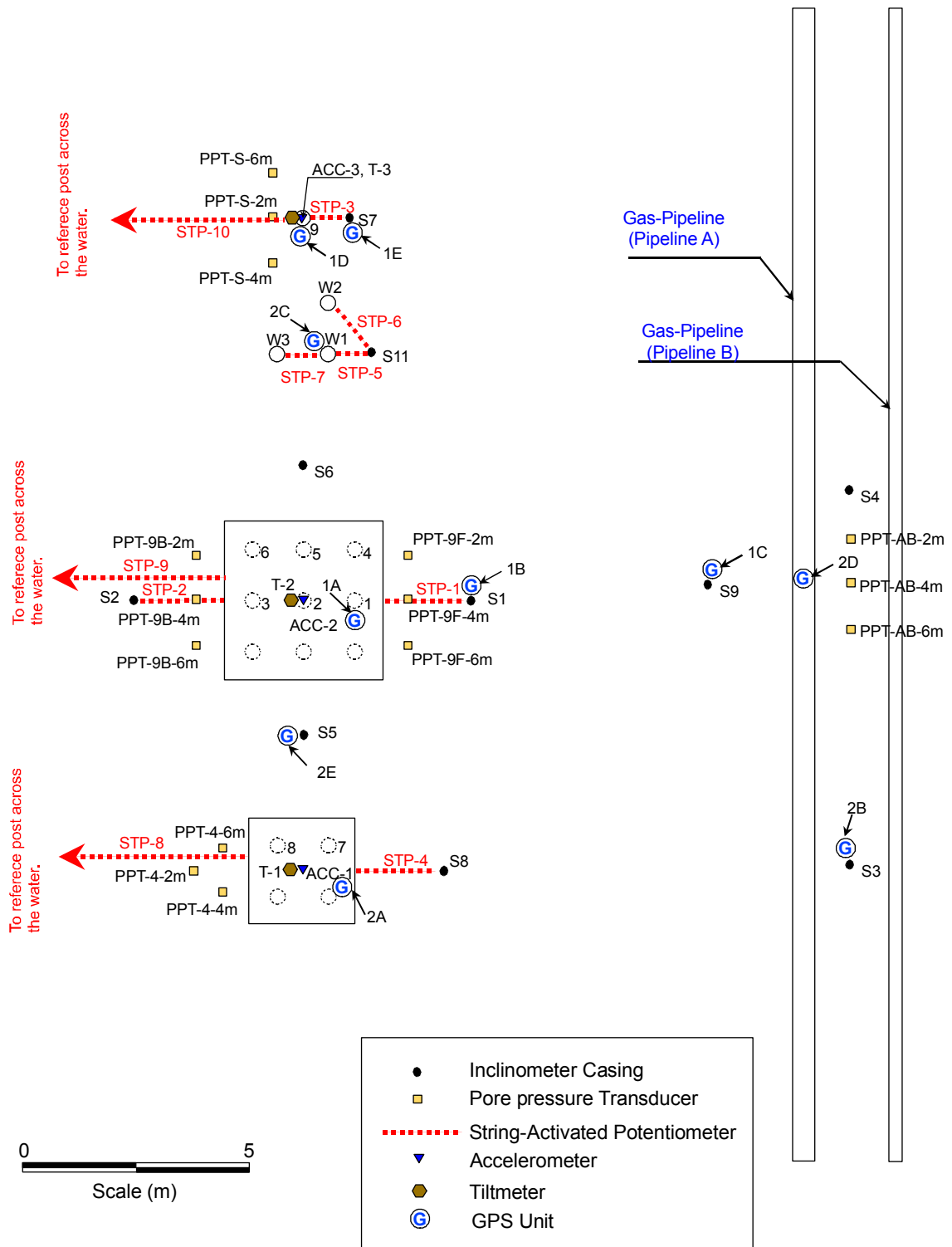
Figure 5.6 Schematic Diagram Showing Locations of Instruments nearby Pile and Pipeline Specimens, 2nd Blast Test

202

Figure 5.7 Locations of Blast Holes for 2nd Japan Blast Test

203

Figure 5.8   Bad Weather during 2nd Lateral Spreading Test
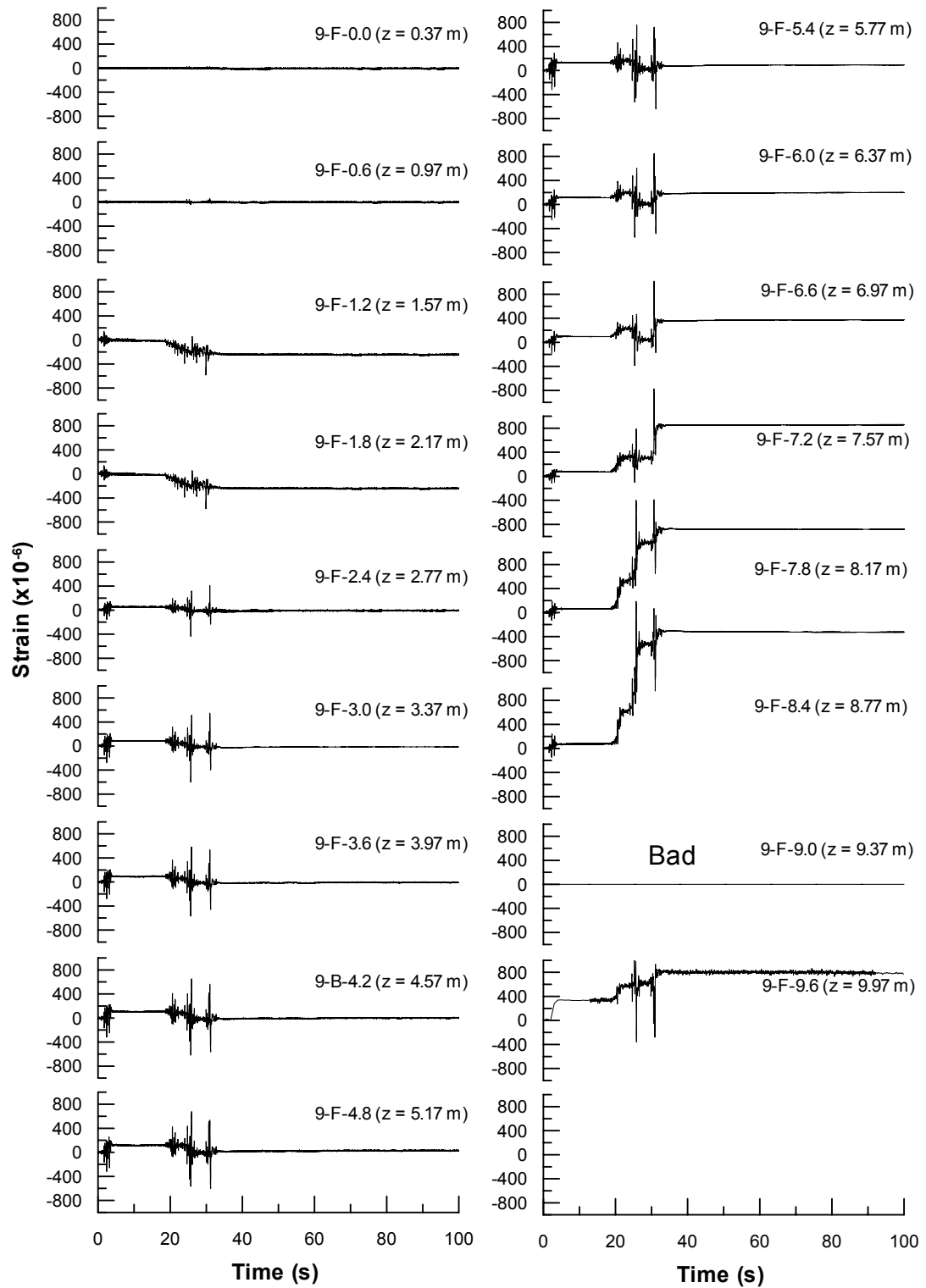
Figure 5.9 Strain Gauge Response along Single Pile (Pile No.9) at Front Side, 2nd Blast Test
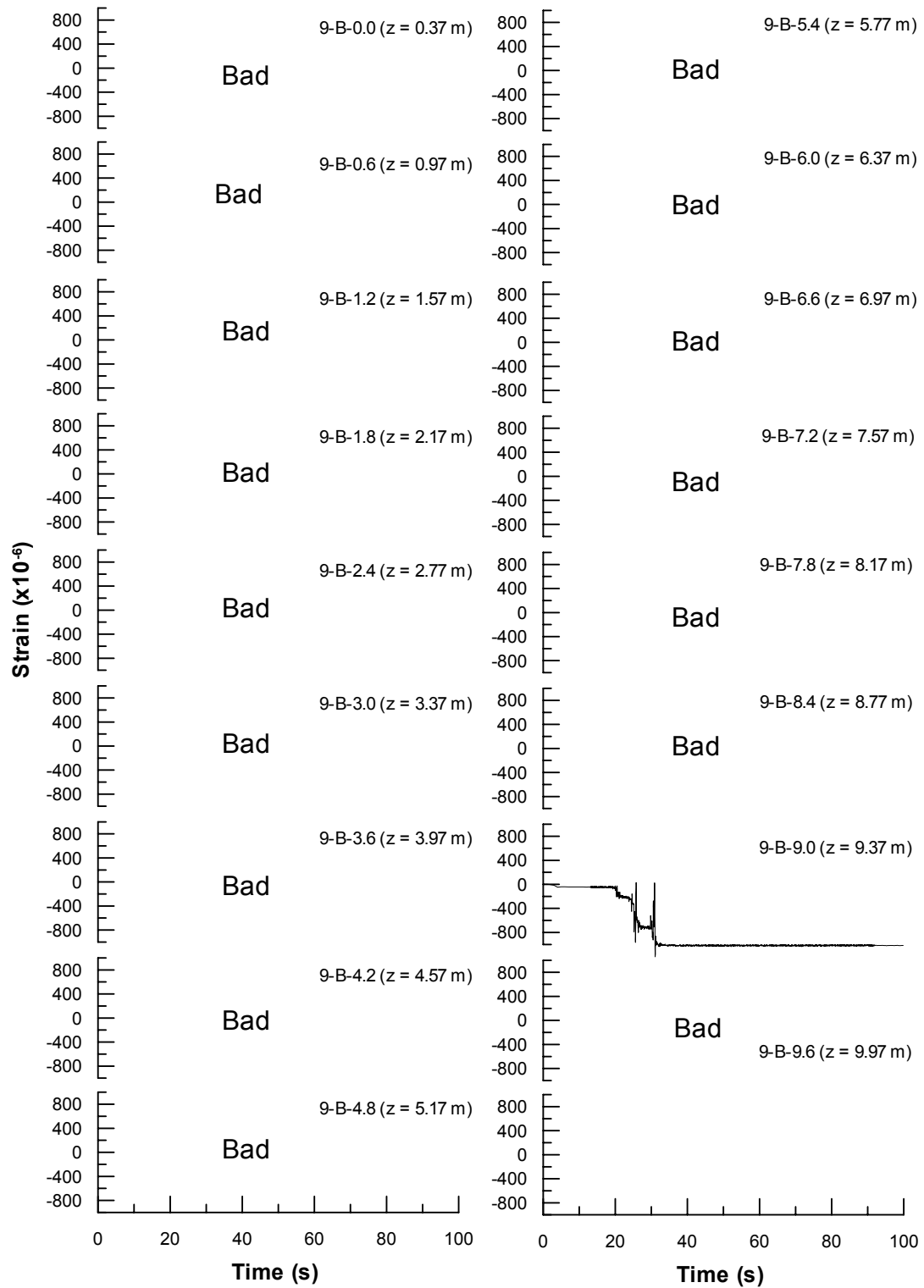
Figure 5.10 Strain Gauge Response along Single Pile (Pile No.9) at Back Side, 2nd Blast Test
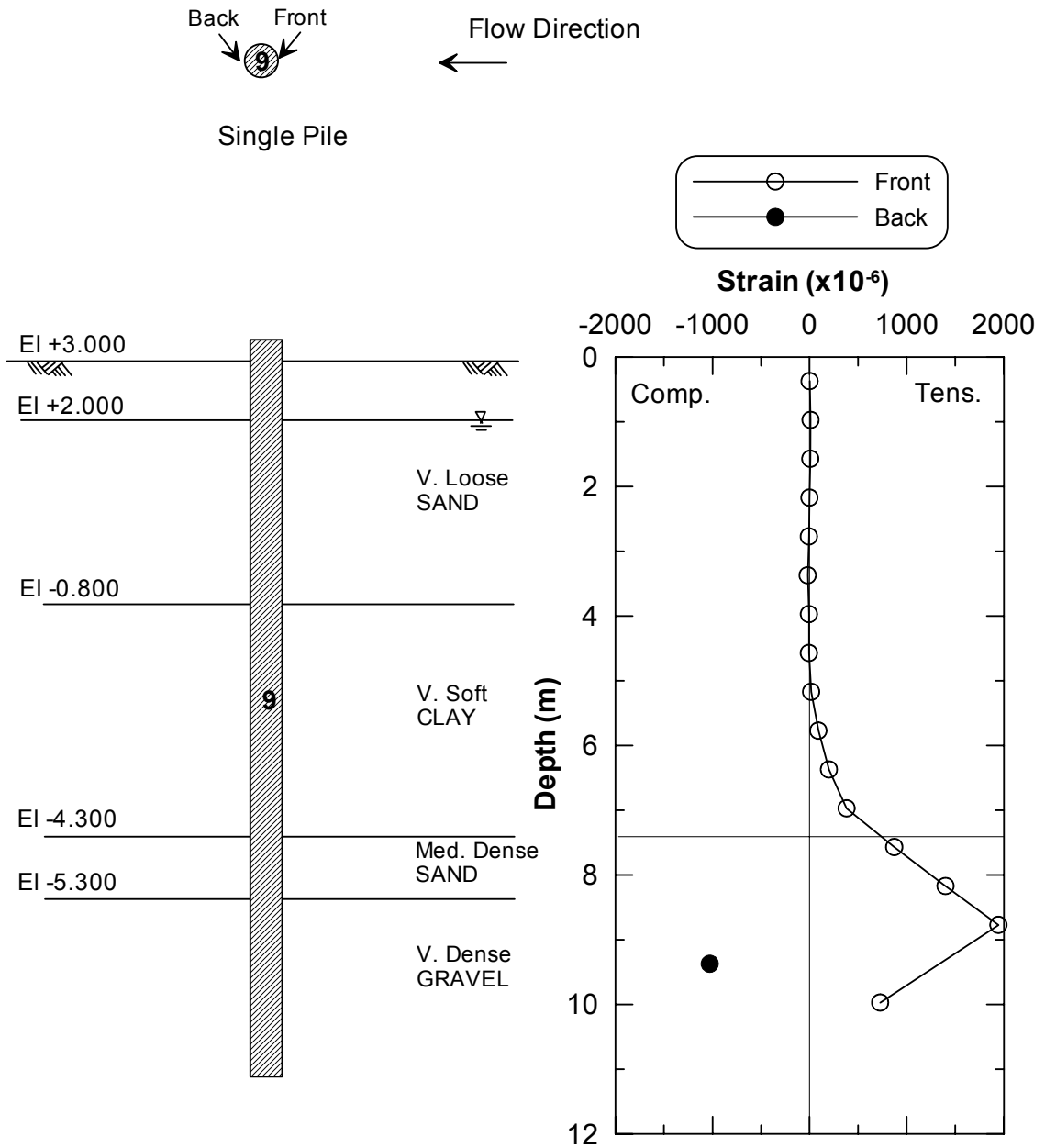
Figure 5.11 Profile of Residual Strain of Single Pile (Pile No.9) after 2nd Lateral Spreading
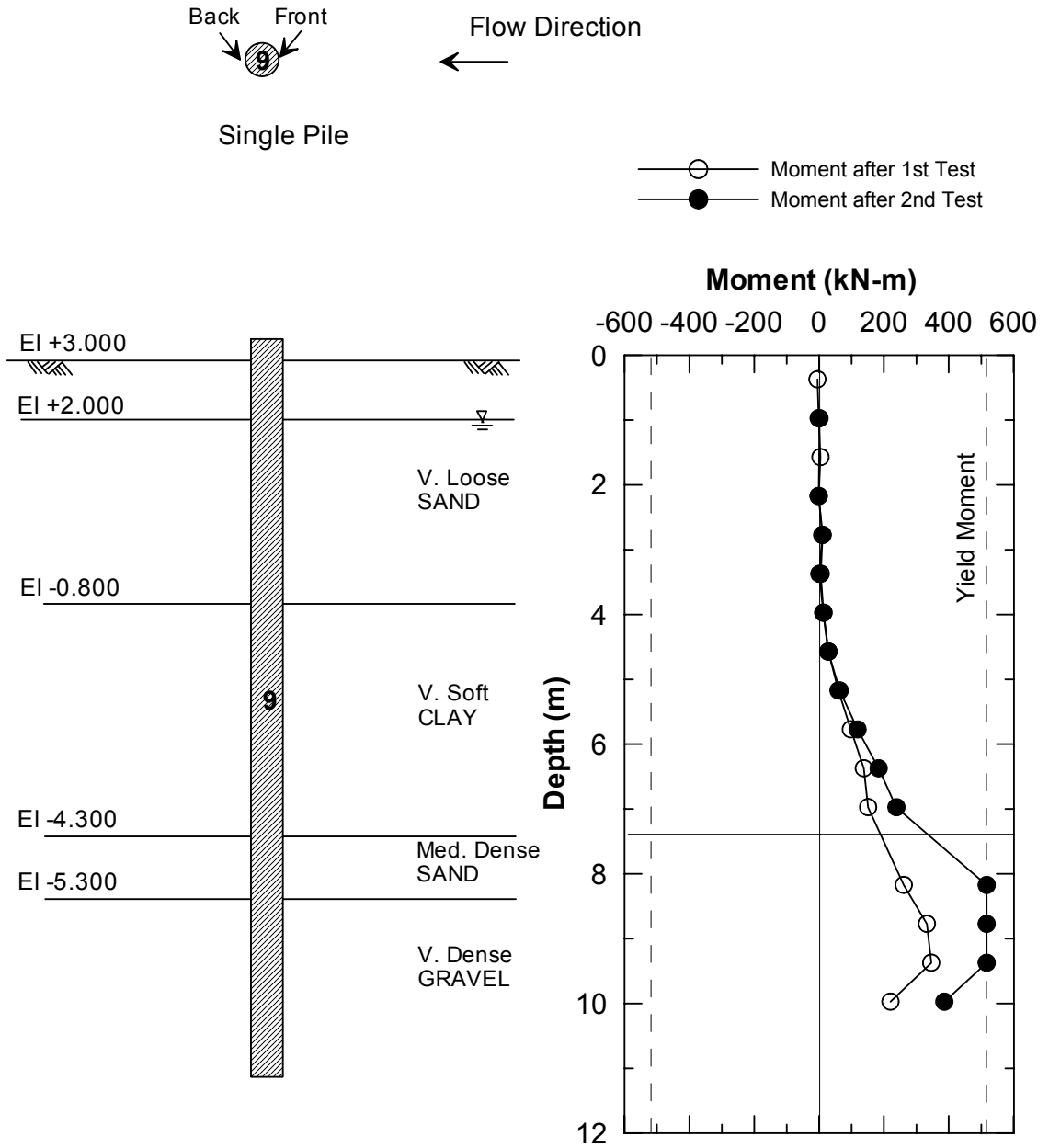
Figure 5.12 Moment Distribution along Single Pile (Pile No.9) after 2nd Lateral Spreading Test
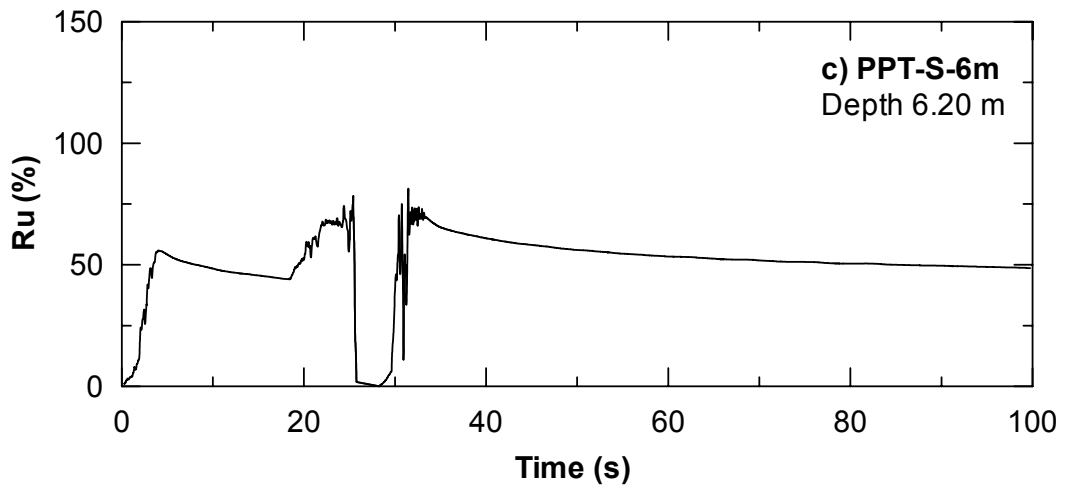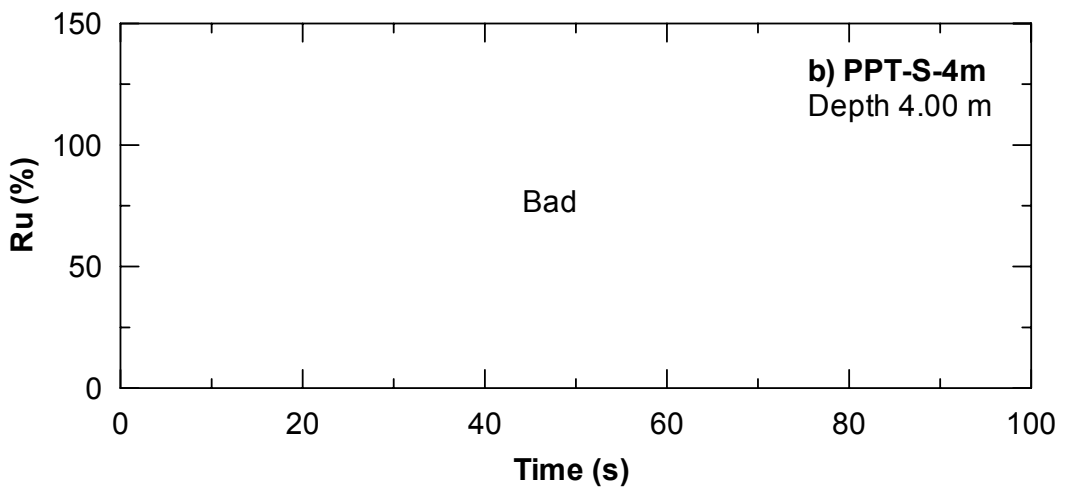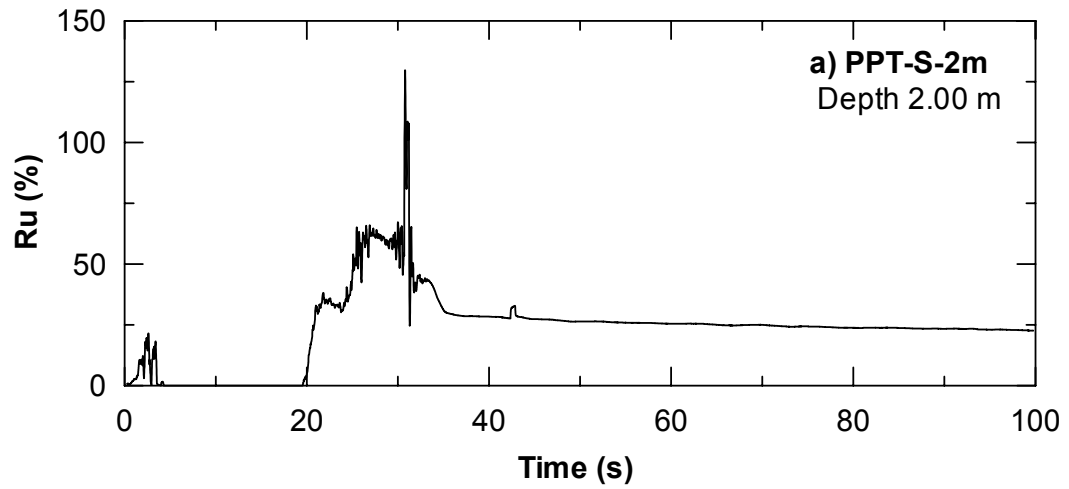
Figure 5.13   Excess Pore Water Pressure Ratios nearby Single Pile for (a) PPT-S-2m, (b) PPT-S-4m, and (c) PPT-S-6m, Duration of 100s (2nd Blast Test)
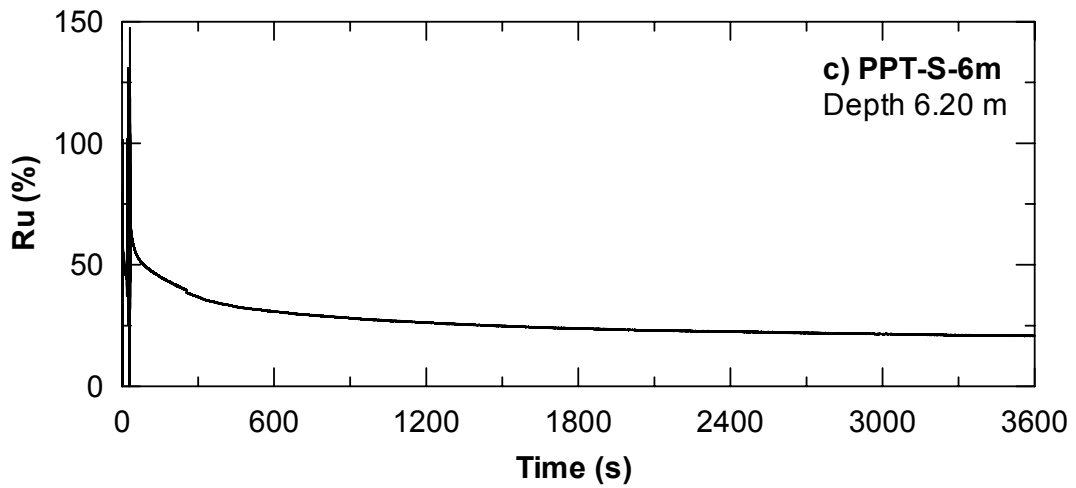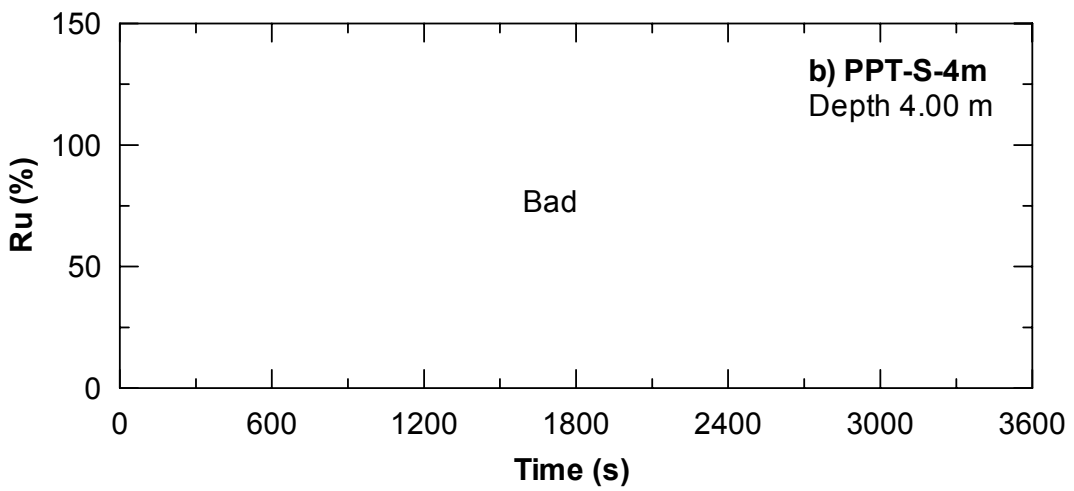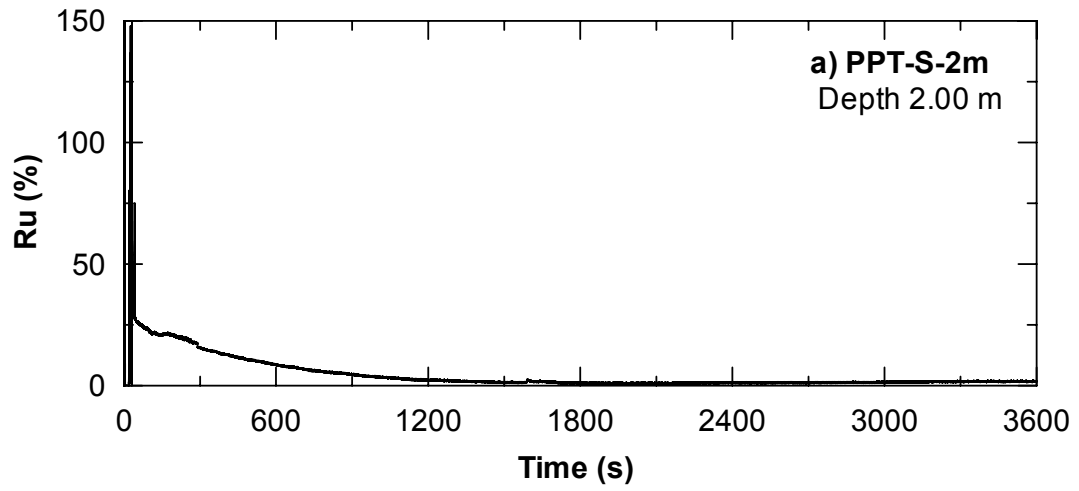
Figure 5.14   Excess Pore Water Pressure Ratios nearby Single Pile for (a) PPT-S-2m, (b) PPT-S-4m, and (c) PPT-S-6m, Duration of 3600s (2nd Blast Test)
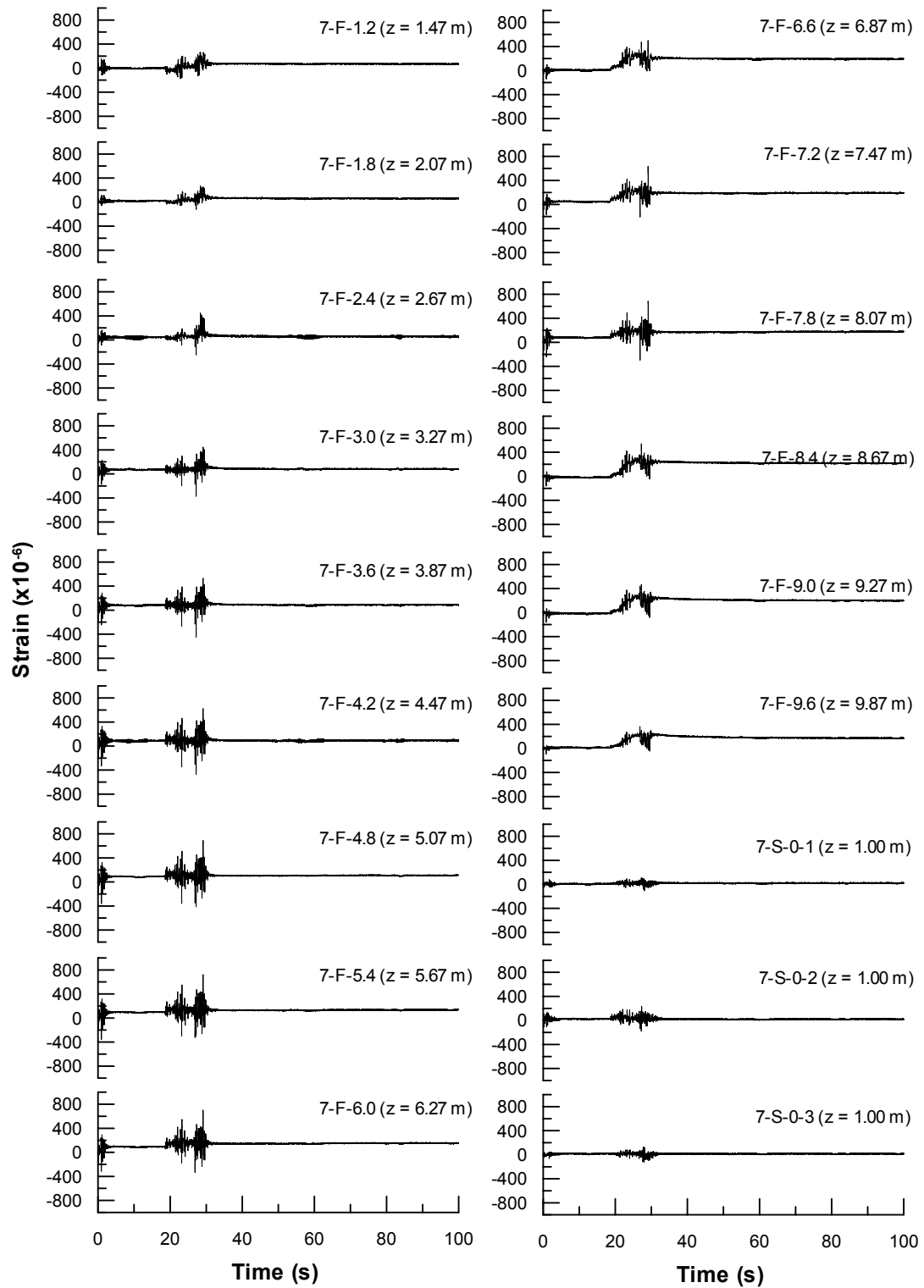
Figure 5.15 Strain Gauge Response along Steel Pipe Pile No.7 (Front Side) of 4-Pile Group, 2nd Blast Test
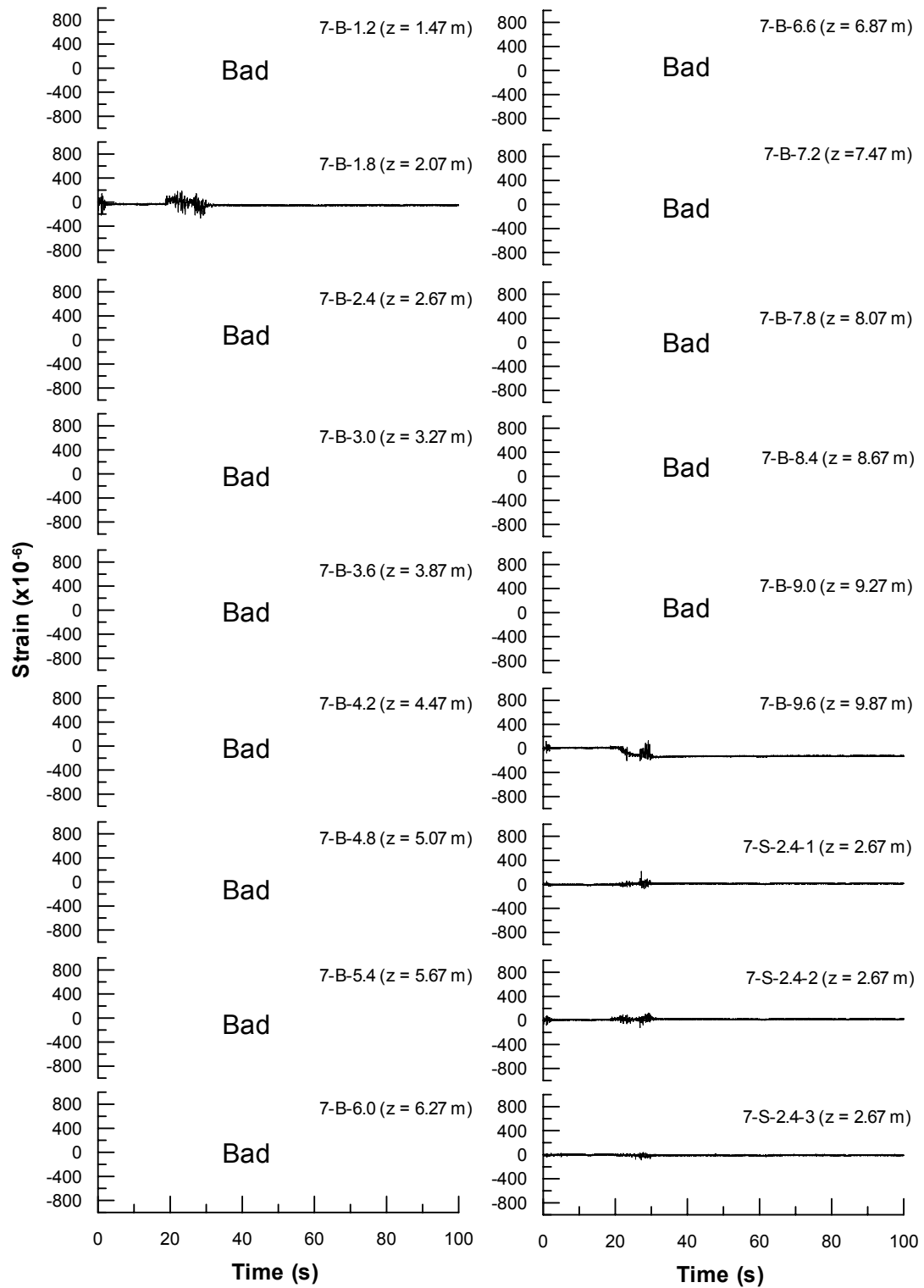
Figure 5.16 Strain Gauge Response along Steel Pipe Pile No.7 (Back Side) of 4-Pile Group , 2nd Blast Test
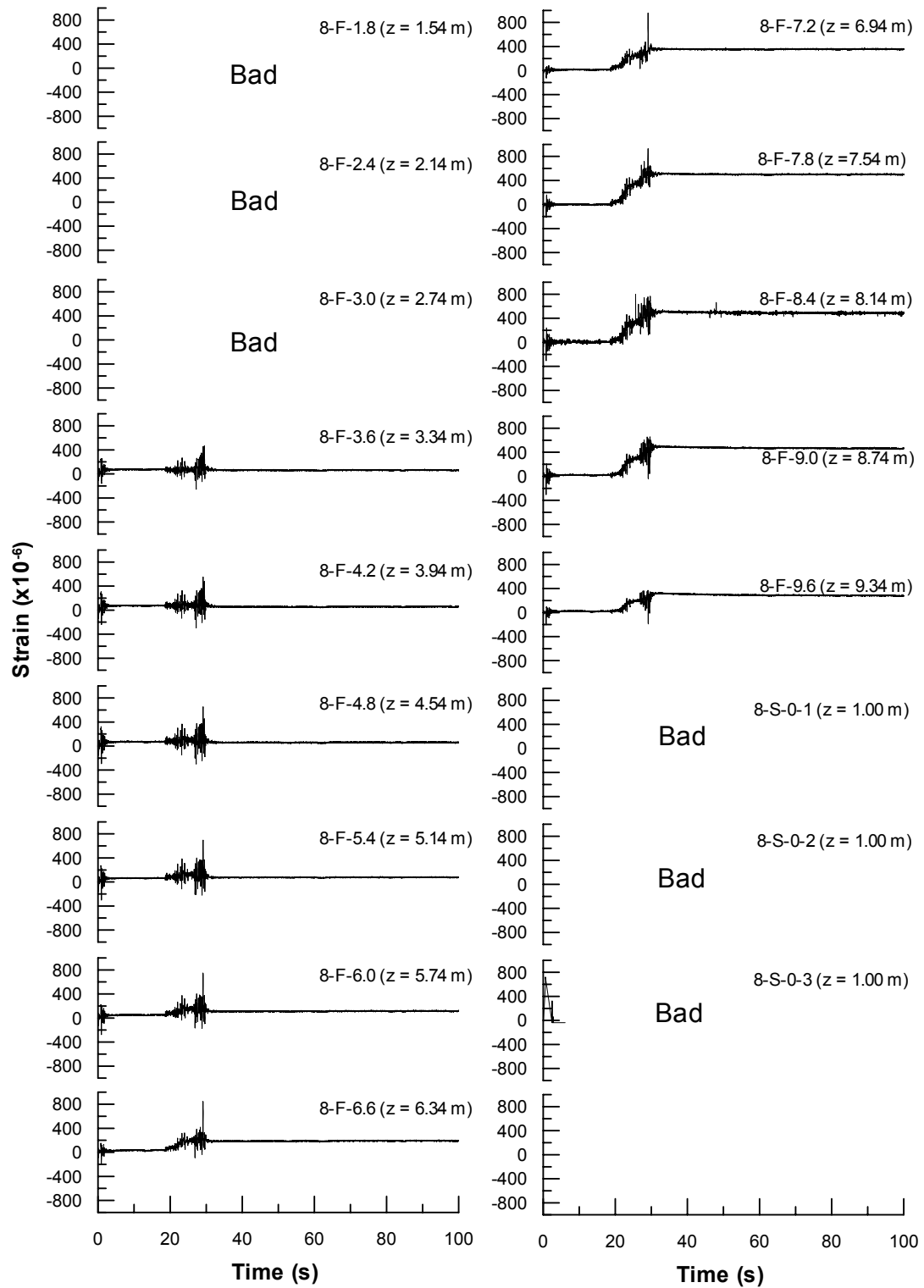
Figure 5.17 Strain Gauge Response along Steel Pipe Pile No.8 (Front Side) of 4-Pile Group , 2nd Blast Test
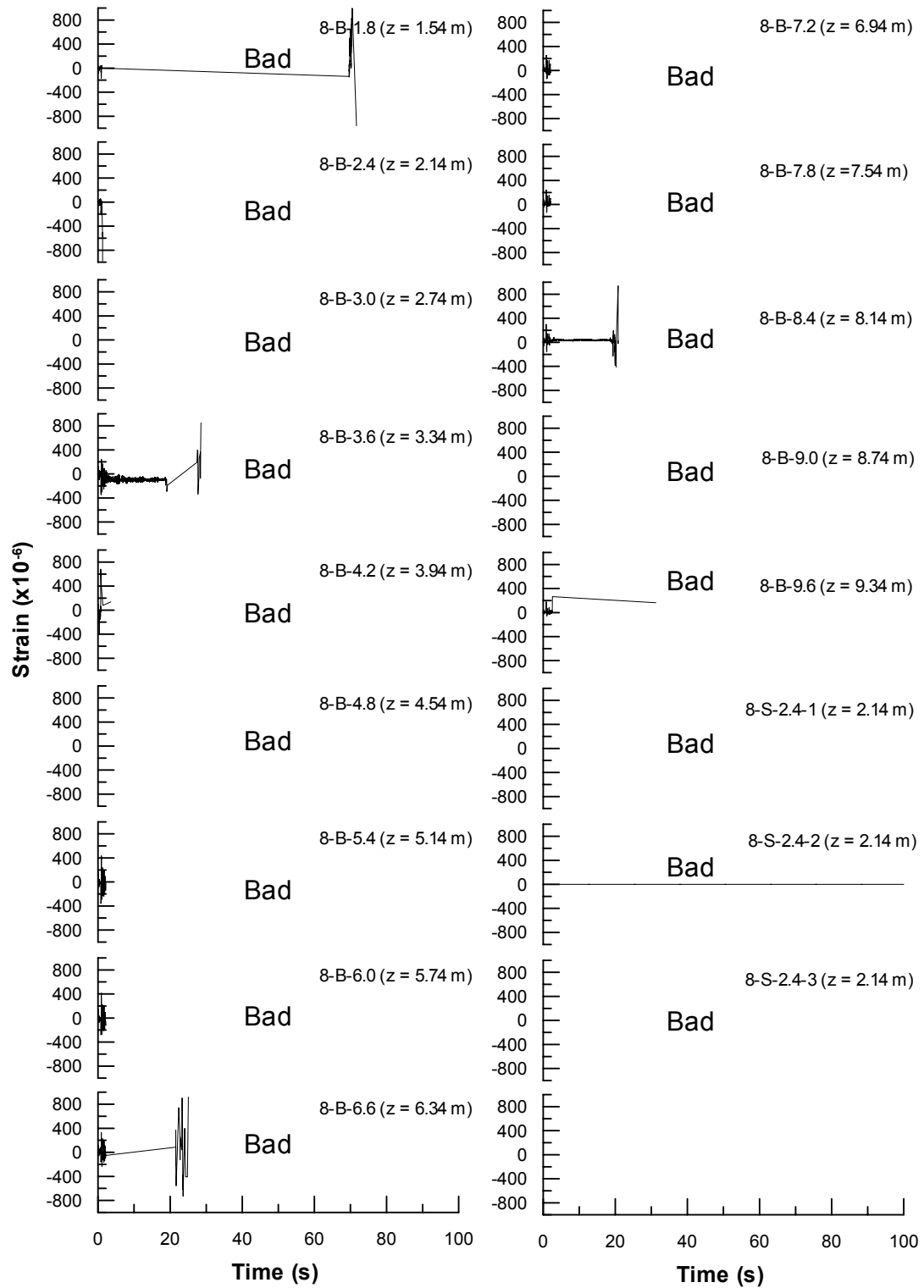
Figure 5.18 Strain Gauge Response along Steel Pipe Pile No.8 (Back Side) of 4-Pile Group , 2nd Blast Test
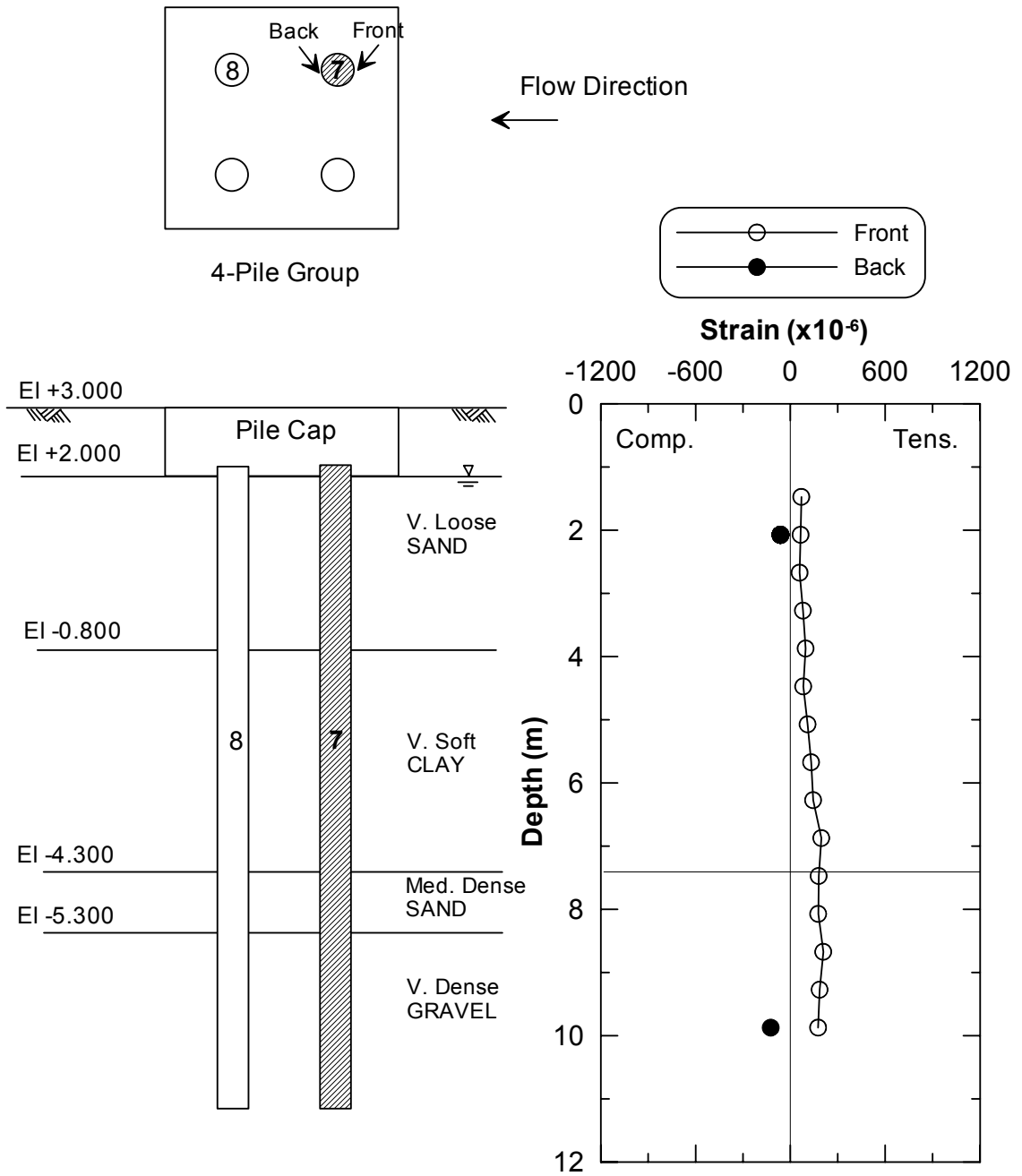
Figure 5.19 Profile of Residual Strain of 4-Pile Group (Pile No.7) after 2nd Lateral Spreading Test
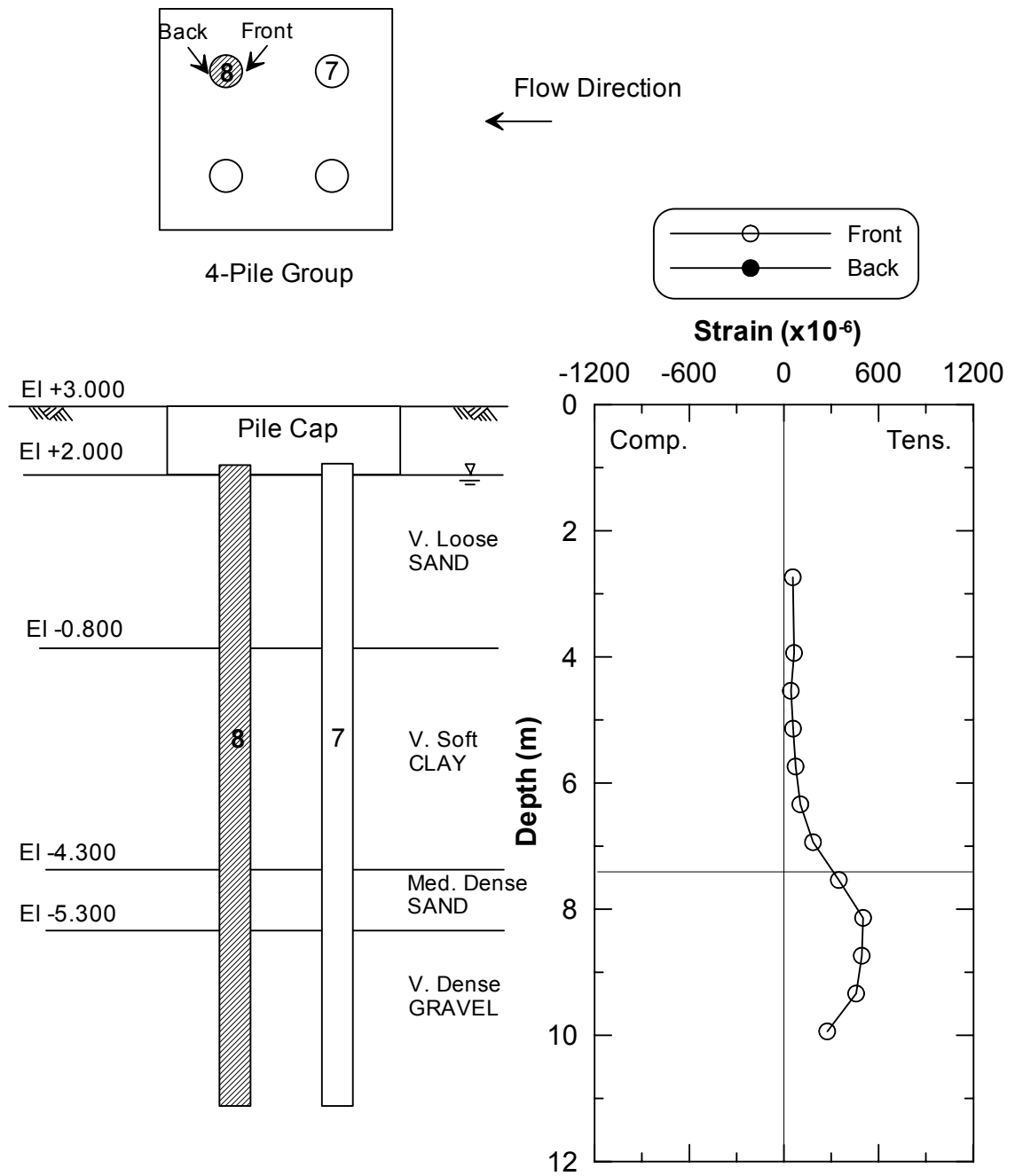
Figure 5.20 Profile of Residual Strain of 4-Pile Group (Pile No.8) after 2nd Lateral Spreading Test
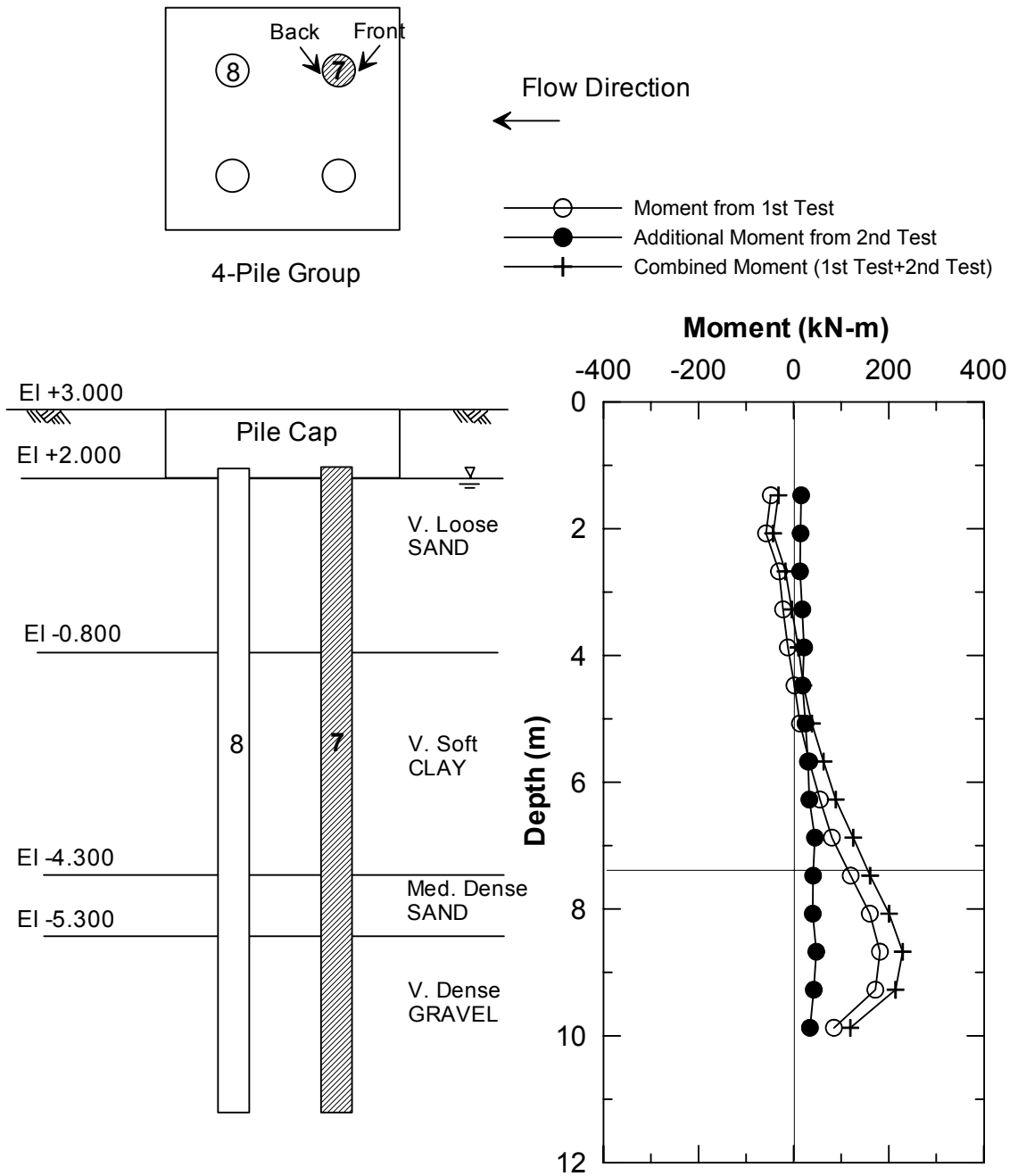
Figure 5.21 Moment Distribution along Pile No.7 of 4-Pile Group after 2nd Lateral Spreading Test
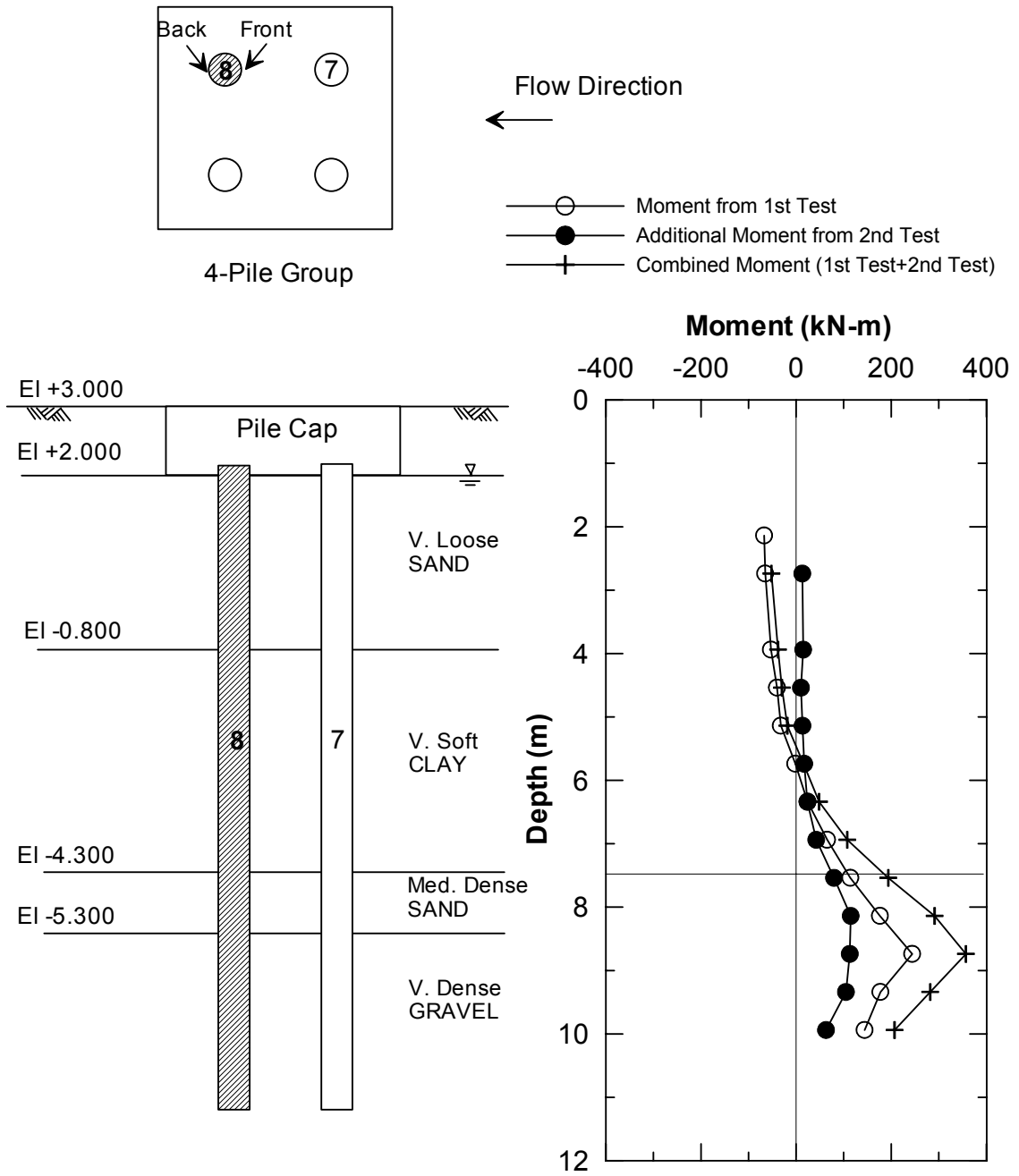
Figure 5.22 Moment Distribution along Pile No.8 of 4-Pile Group after 2nd Lateral Spreading Test

218
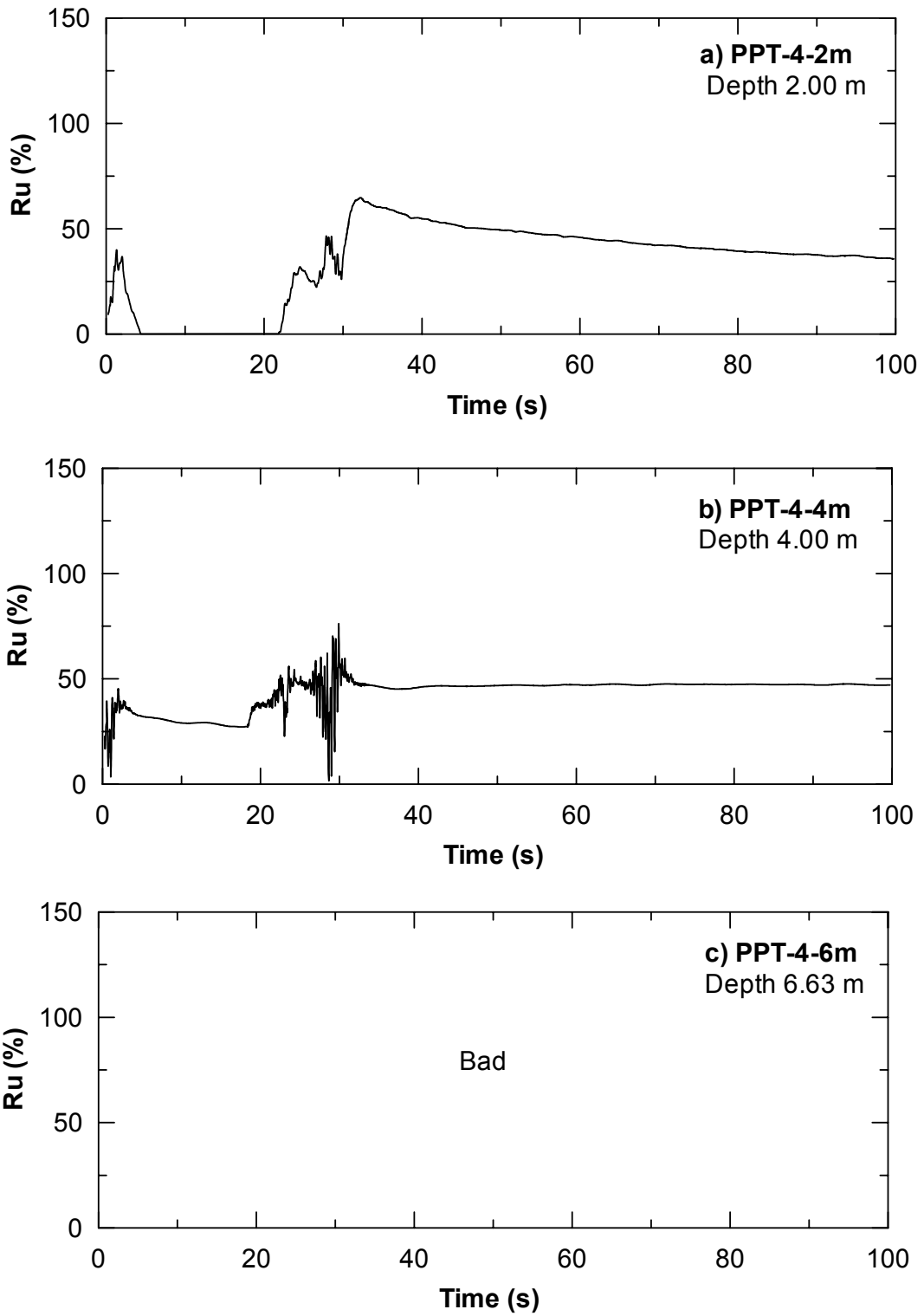
Figure 5.23   Excess Pore Water Pressure Ratios nearby 4-Pile Group for (a) PPT-4-2m (b) PPT-4-4m, and (c) PPT-4-6m, Duration of 100s (2nd Blast Test)
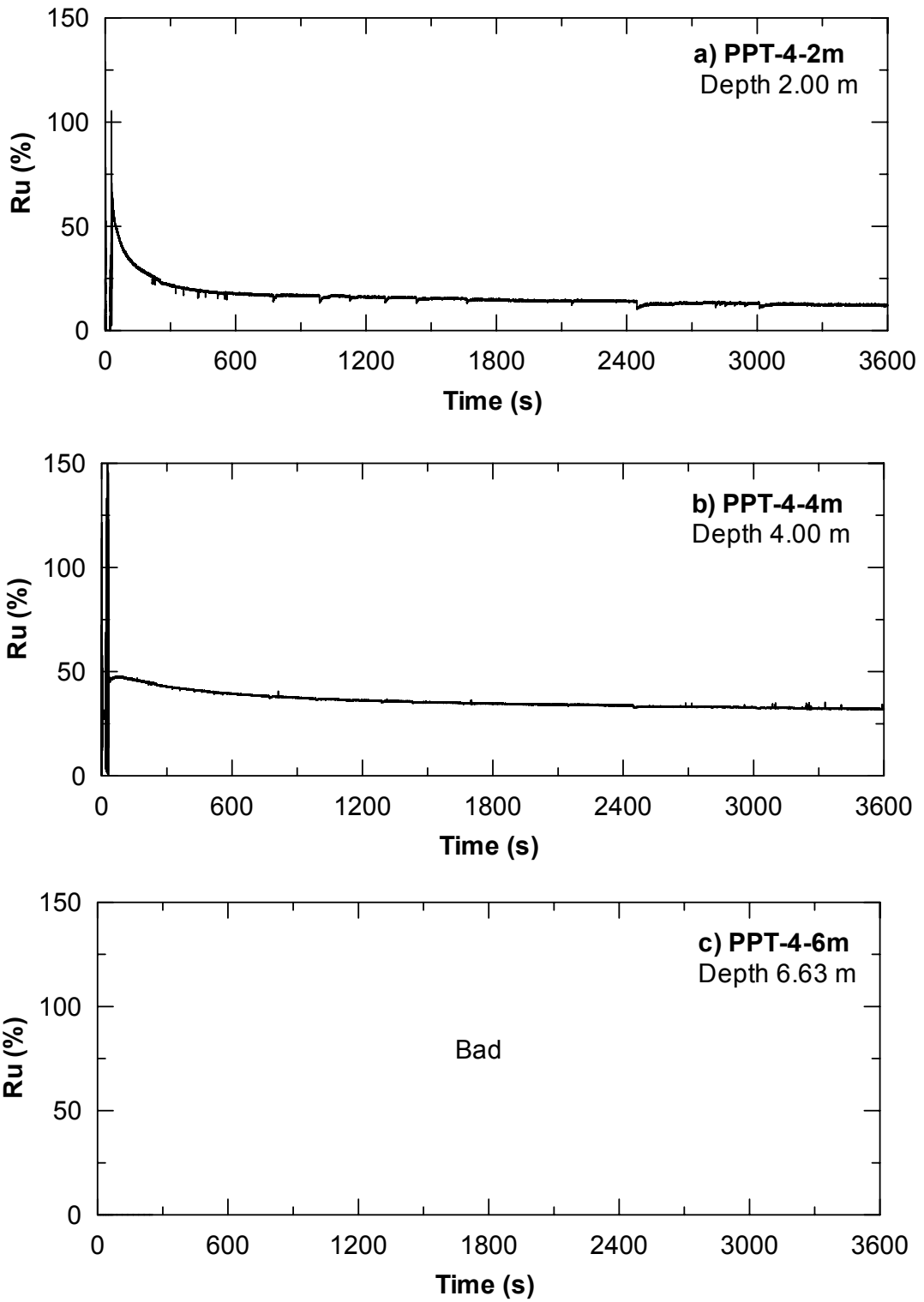
Figure 5.24 Excess Pore Water Pressure Ratios nearby 4-Pile Group for (a) PPT-4-2m (b) PPT-4-4m, and (c) PPT-4-6m, Duration of 3600s (2nd Blast Test)
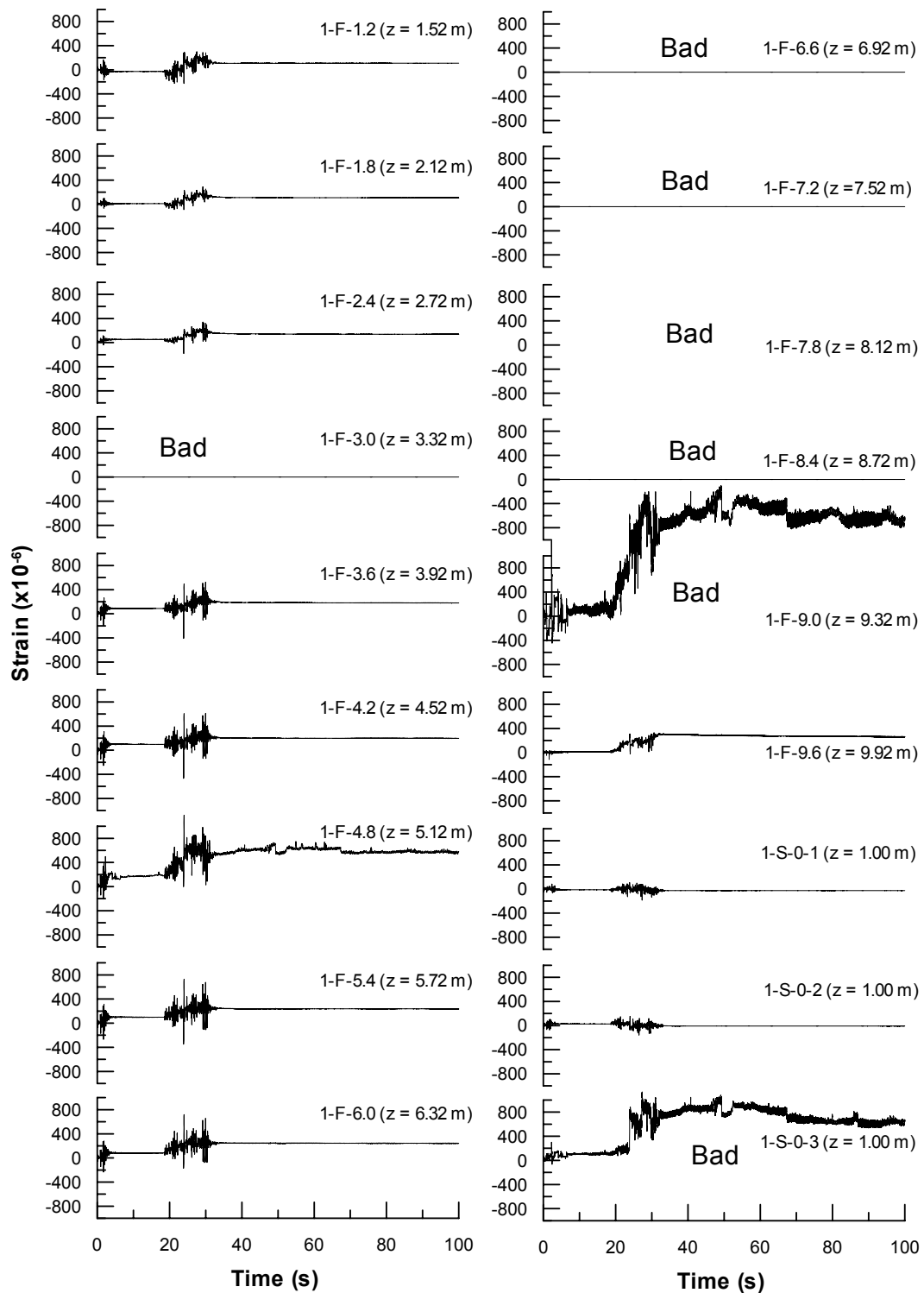
Figure 5.25 Strain Gauge Response along Steel Pipe Pile No.1 (Front Side) of 9-Pile Group, 2nd Blast Test

221
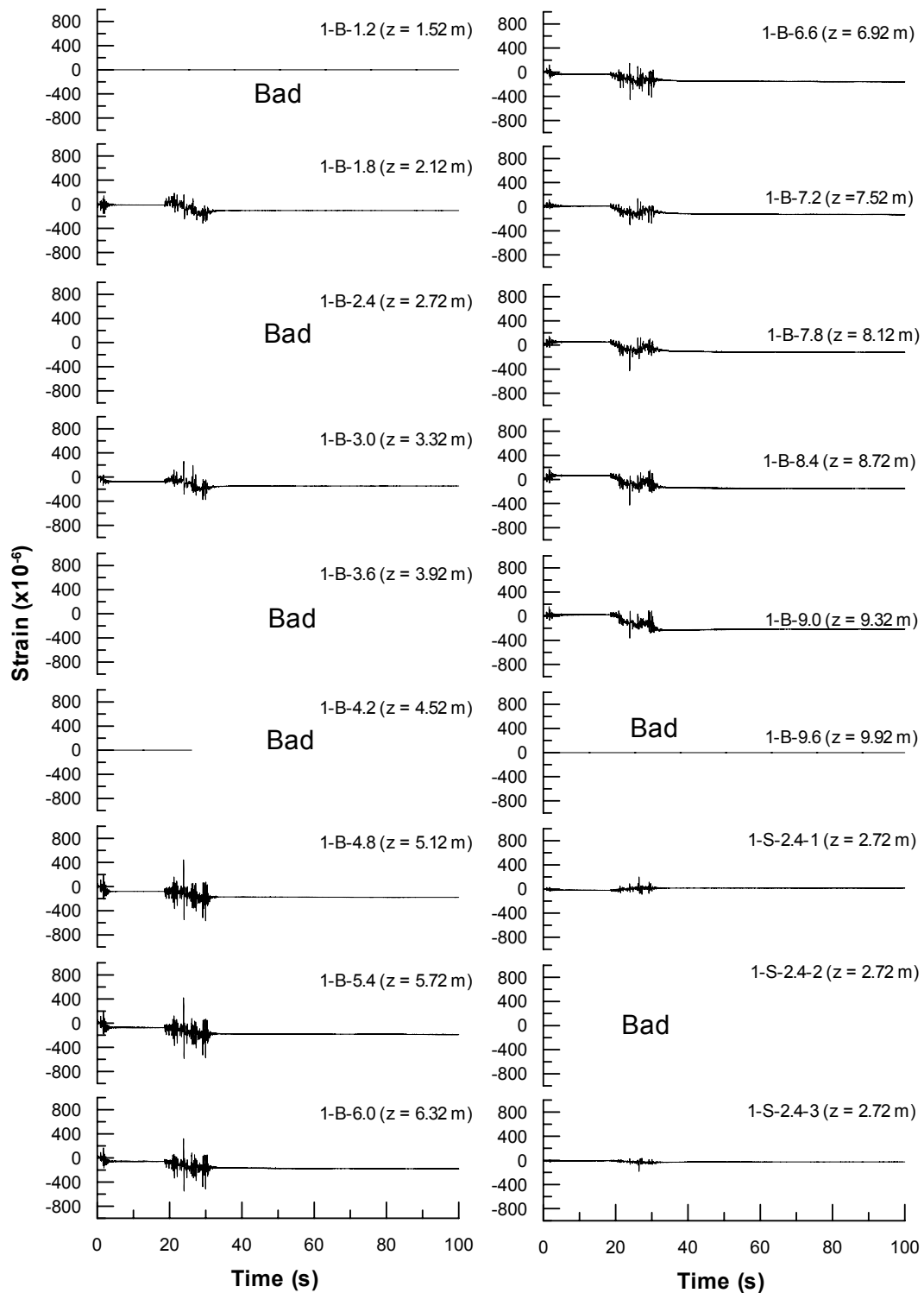
Figure 5.26 Strain Gauge Response along Steel Pipe Pile No.1 (Back Side) of 9-Pile Group, 2nd Blast Test
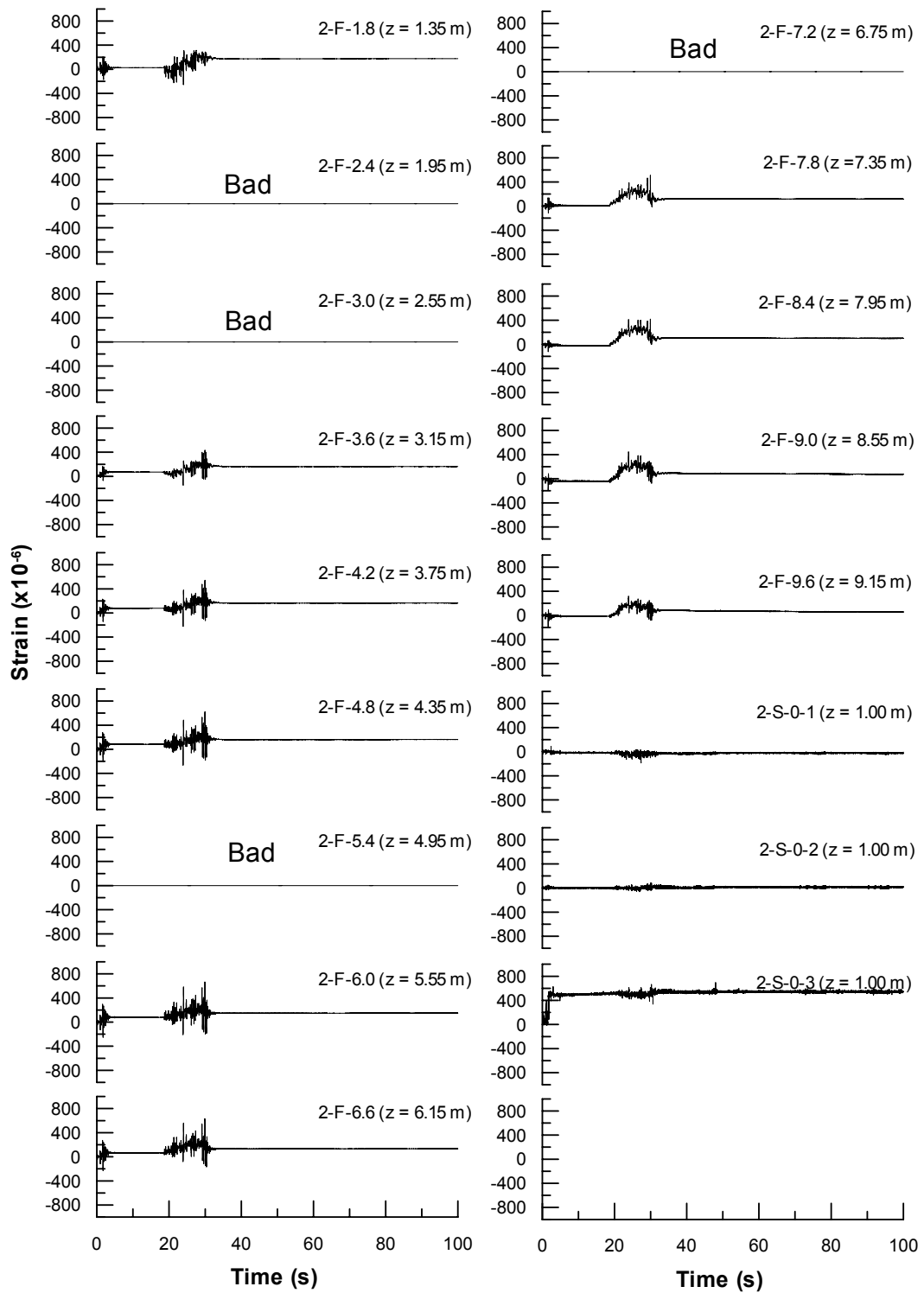
Figure 5.27 Strain Gauge Response along Steel Pipe Pile No.2 (Front Side) of 9-Pile Group, 2nd Blast Test

223
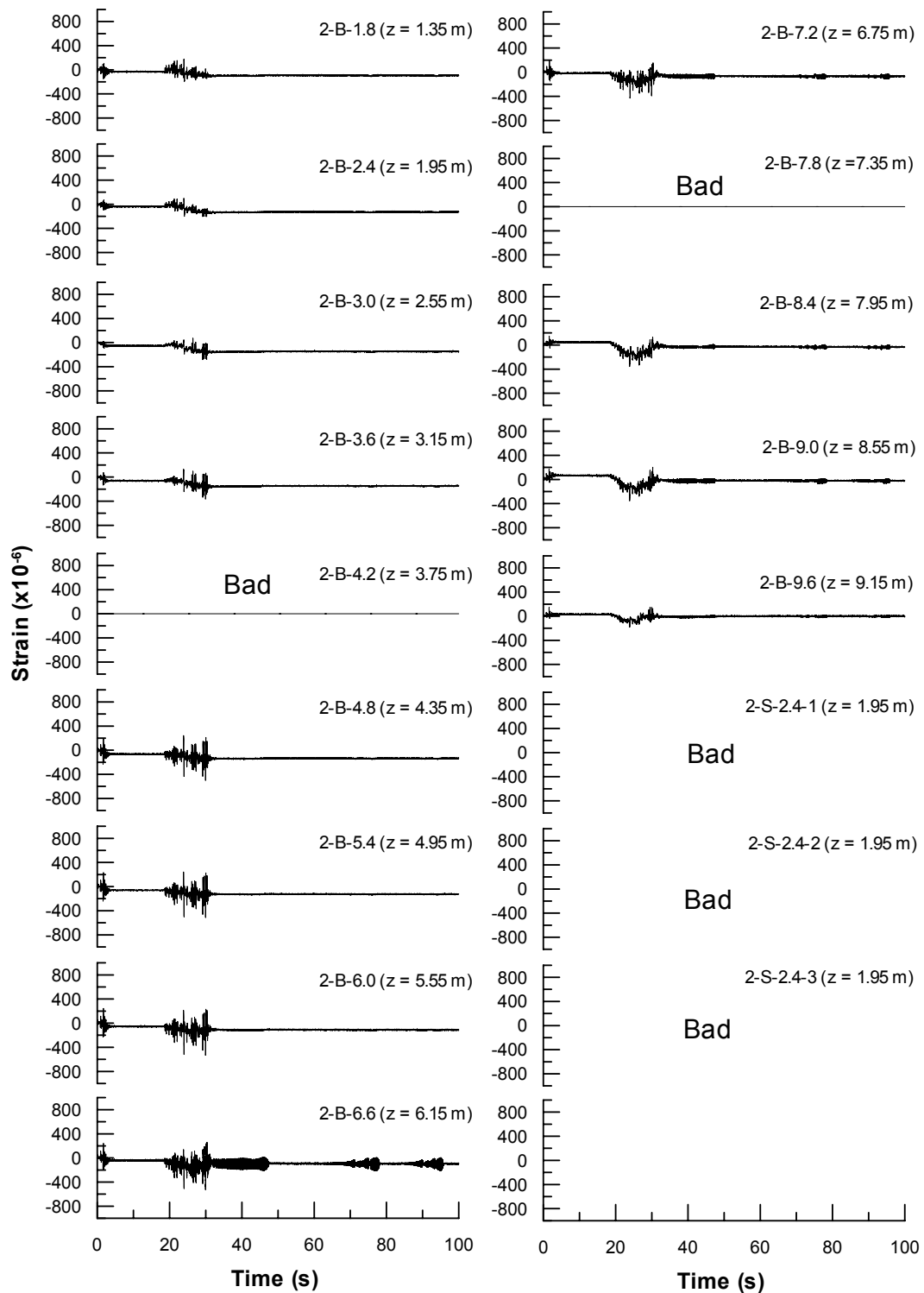
Figure 5.28 Strain Gauge Response along Steel Pipe Pile No.2 (Back Side) of 9-Pile Group, 2nd Blast Test

224
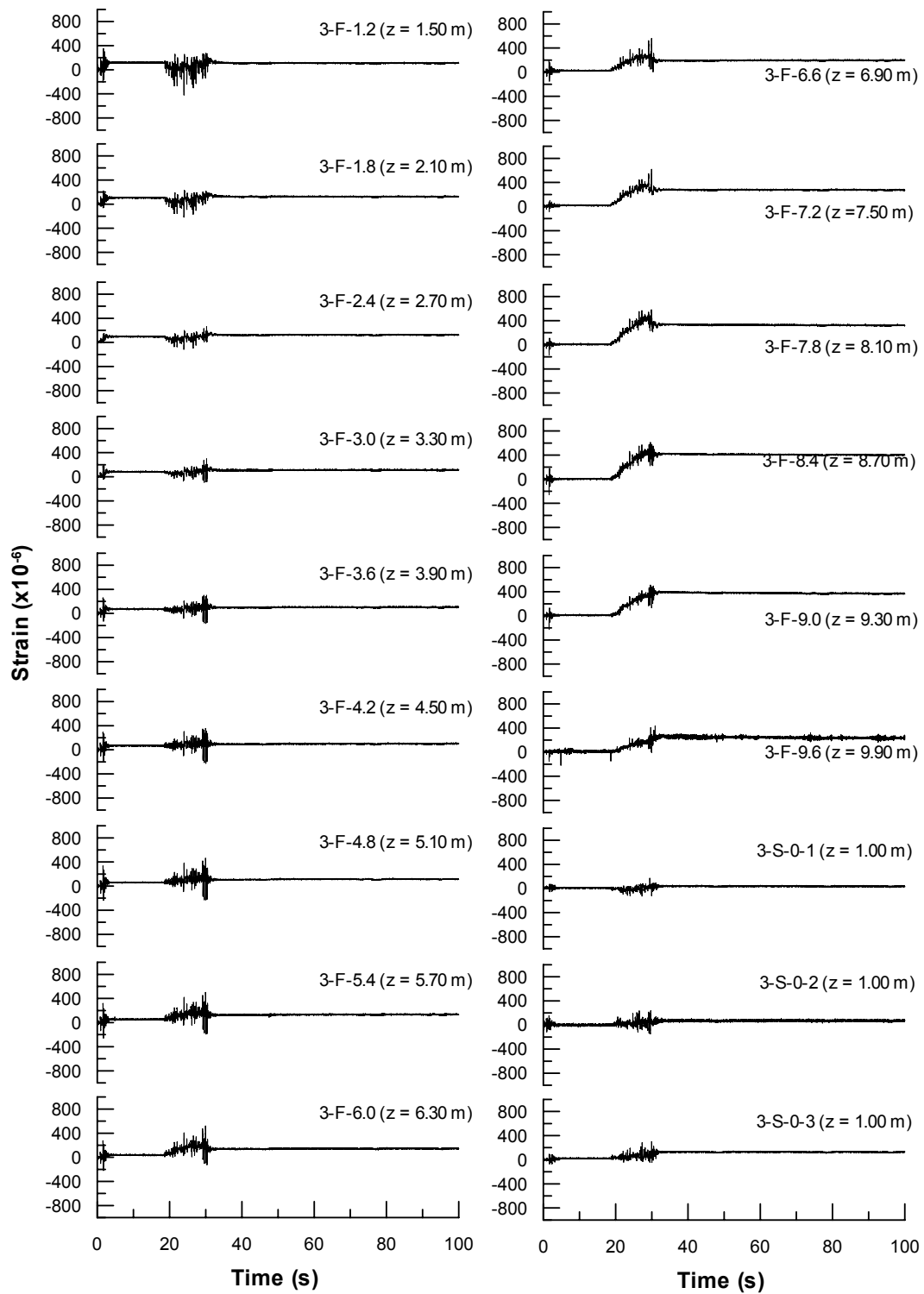
Figure 5.29 Strain Gauge Response along Steel Pipe Pile No.3 (Front Side) of 9-Pile Group , 2nd Blast Test
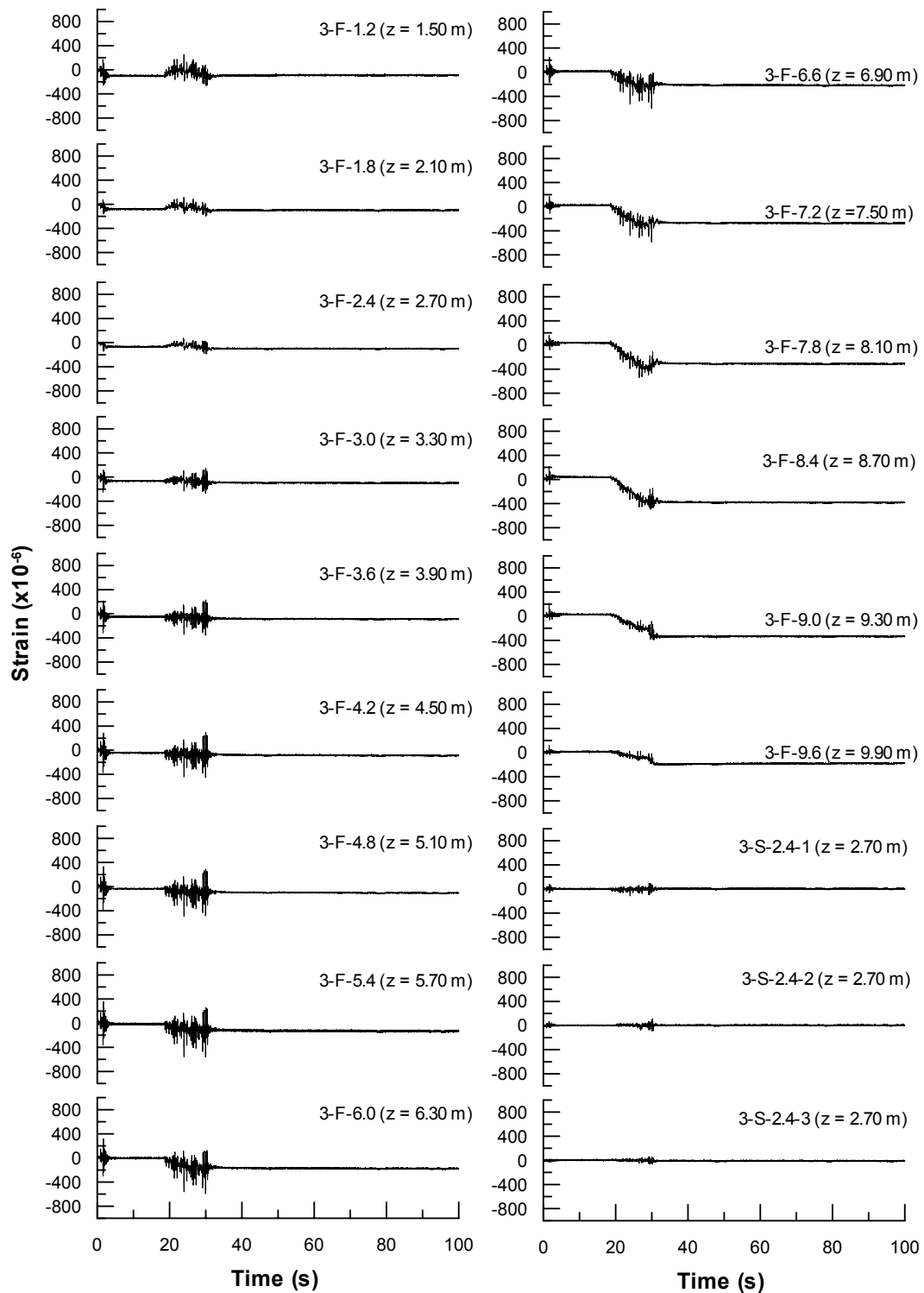
Figure 5.30 Strain Gauge Response along Steel Pipe Pile No.3 (Back Side) of 9-Pile Group, 2nd Blast Test
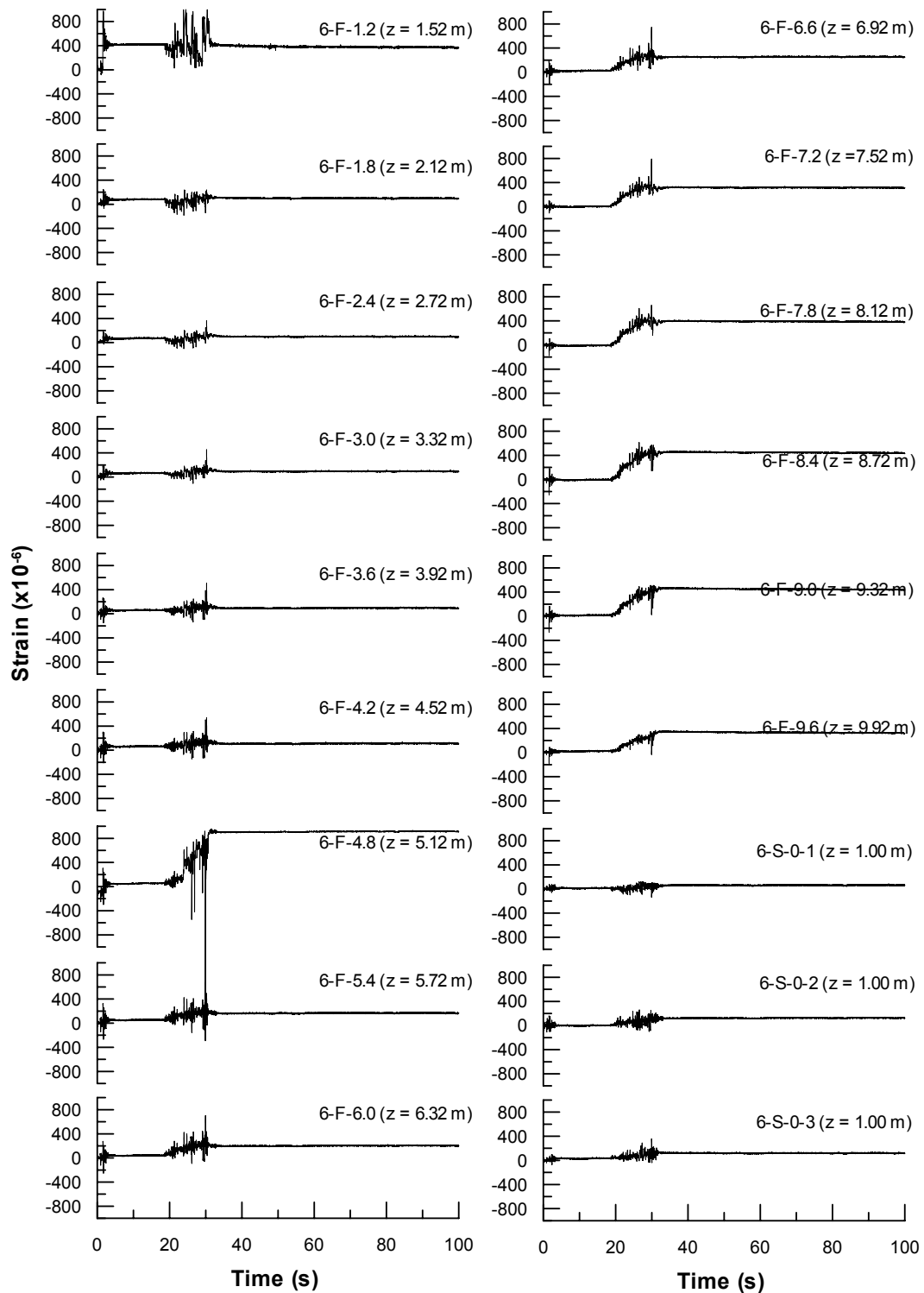
Figure 5.31 Strain Gauge Response along Steel Pipe Pile No.6 (Front Side) of 9-Pile Group, 2nd Blast Test

227
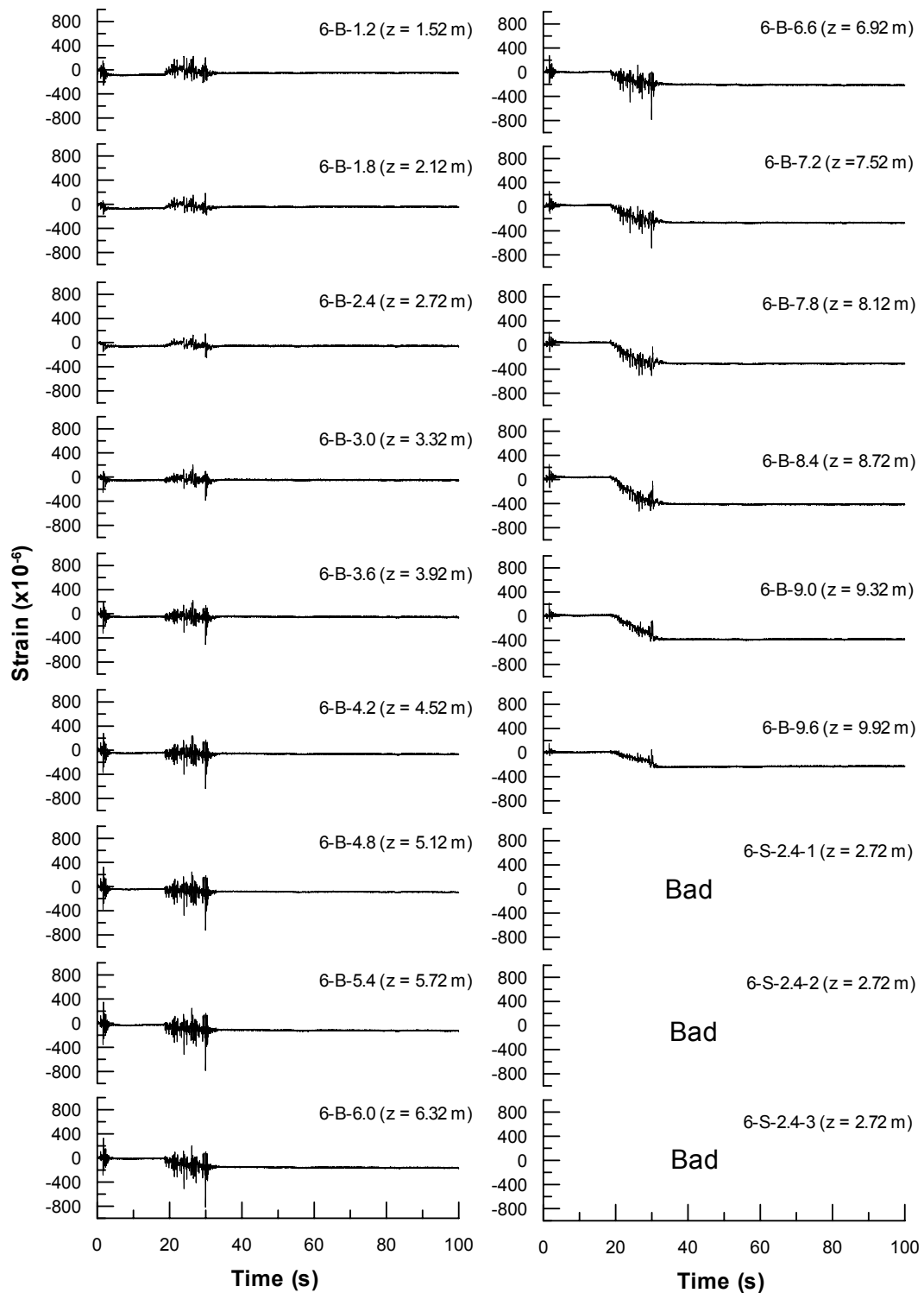
Figure 5.32 Strain Gauge Response along Steel Pipe Pile No.6 (Back Side) of 9-Pile Group, 2nd Blast Test
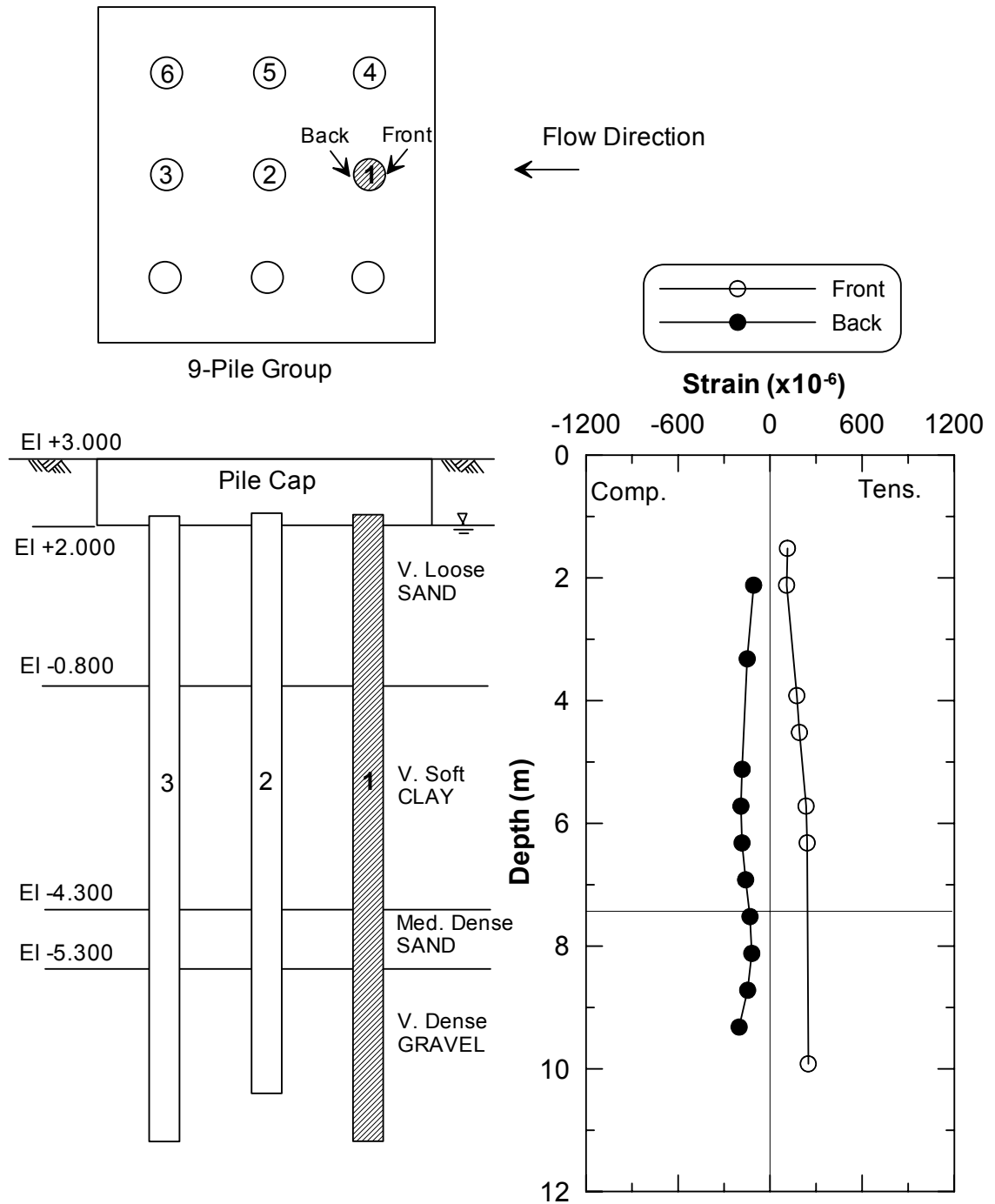
Figure 5.33 Profile of Residual Strain of 9-Pile Group (Pile No.1) after 2nd Lateral Spreading Test
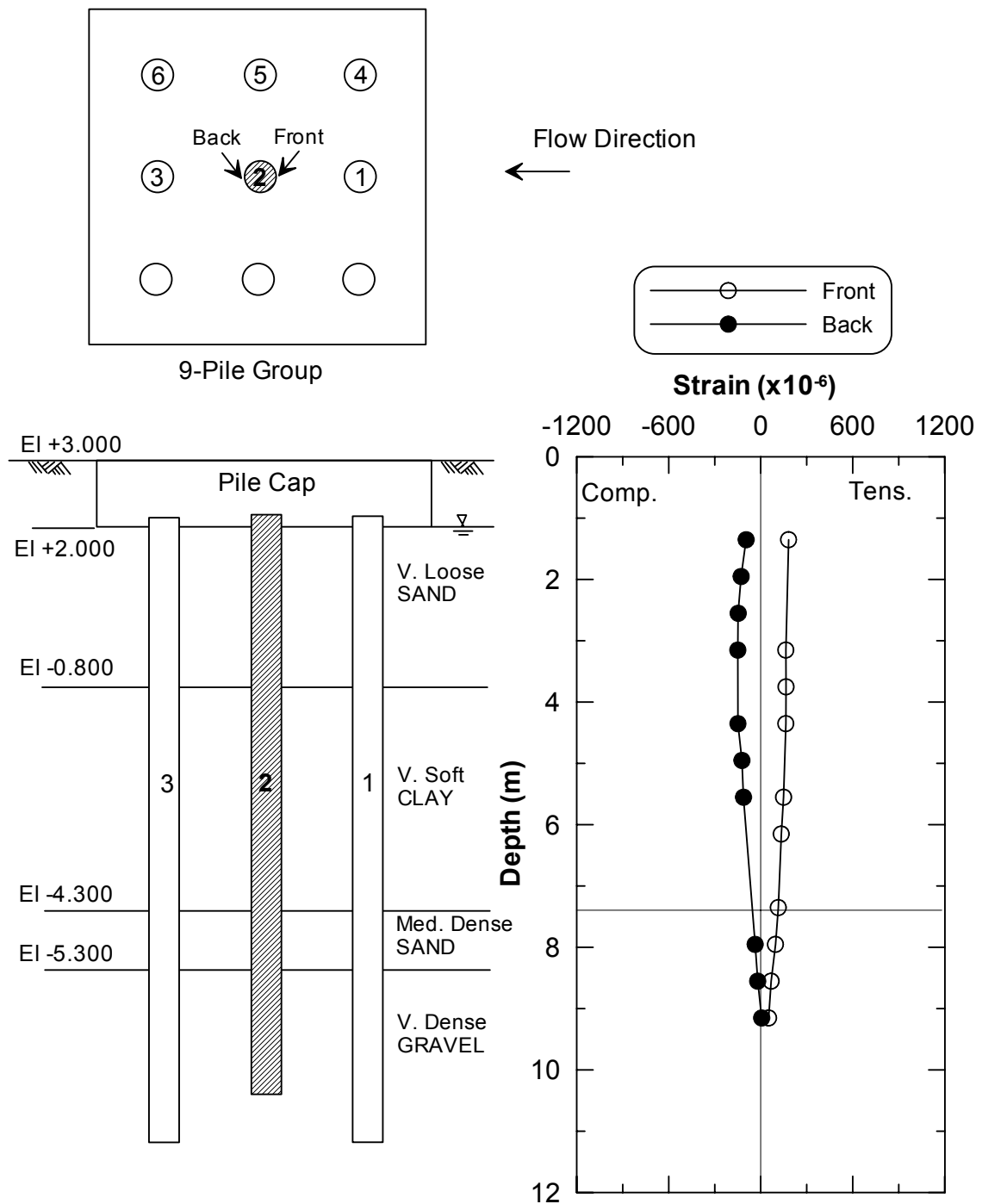
Figure 5.34 Profile of Residual Strain of 9-Pile Group (Pile No.2) after 2nd Lateral Spreading Test
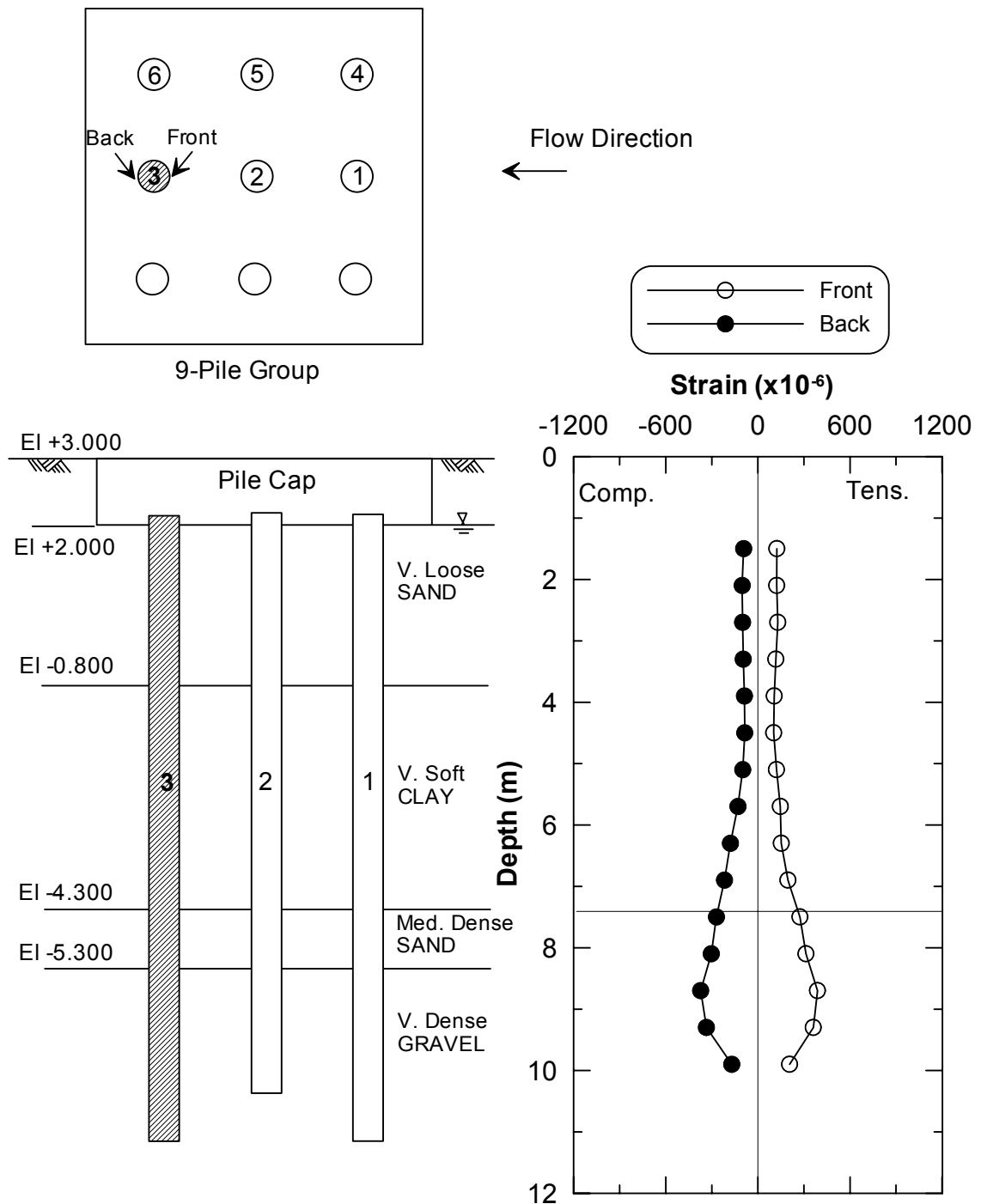
Figure 5.35 Profile of Residual Strain of 9-Pile Group (Pile No.3) after 2nd Lateral Spreading Test
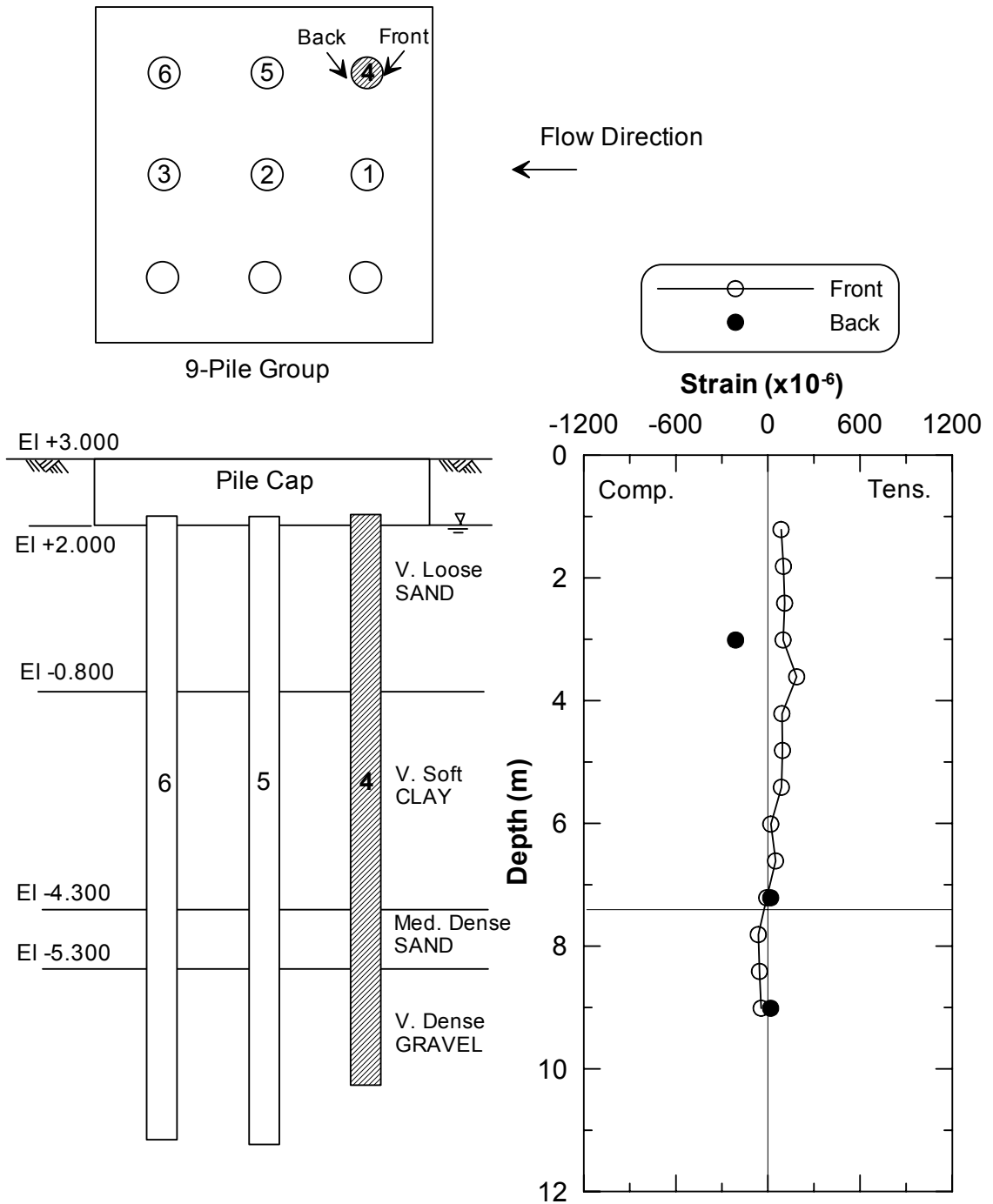
Figure 5.36 Profile of Residual Strain of 9-Pile Group (Pile No.4) after 2nd Lateral Spreading Test
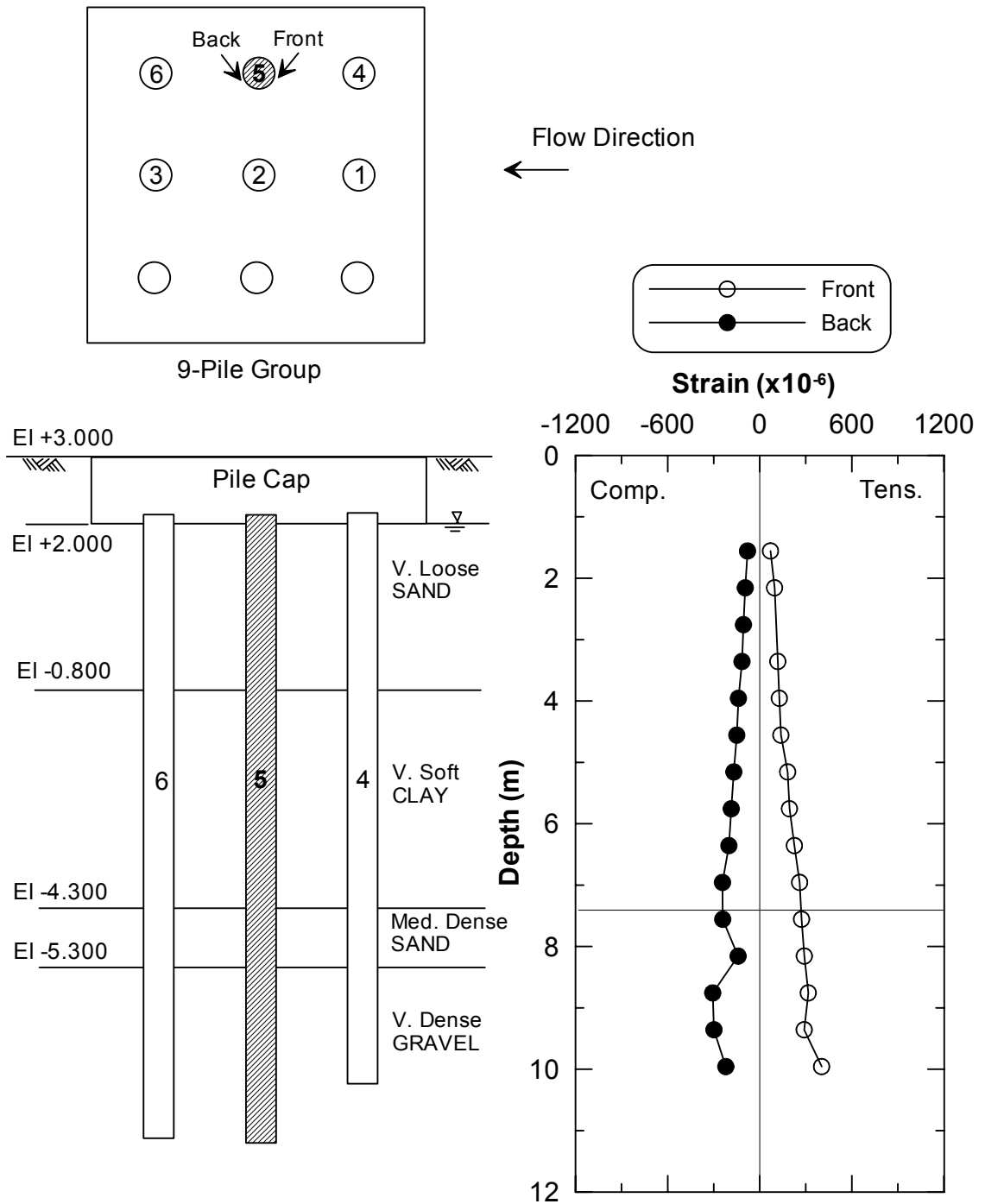
Figure 5.37 Profile of Residual Strain of 9-Pile Group (Pile No.5) after 2nd Lateral Spreading Test
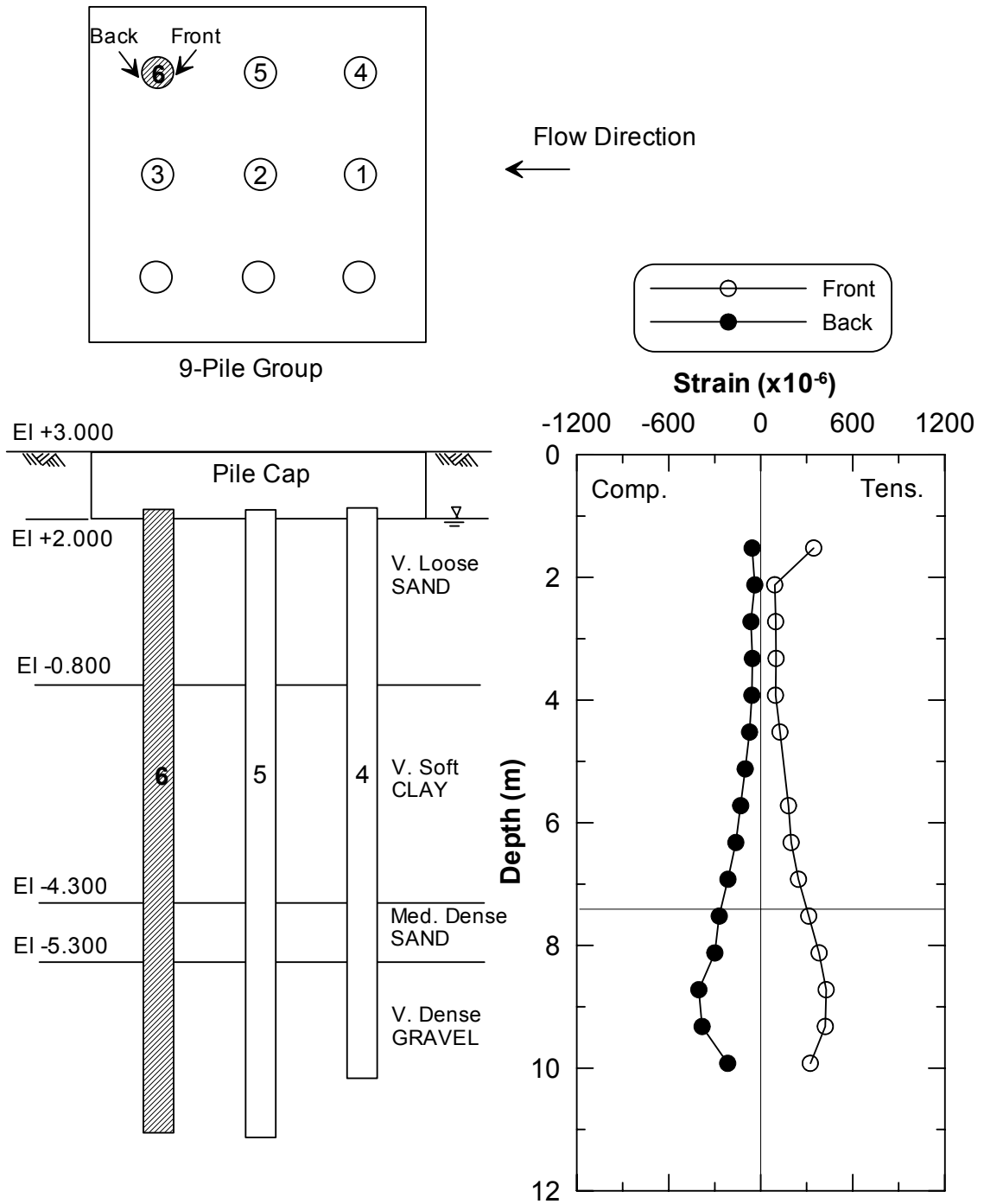
Figure 5.38 Profile of Residual Strain of 9-Pile Group (Pile No.6) after 2nd Lateral Spreading Test
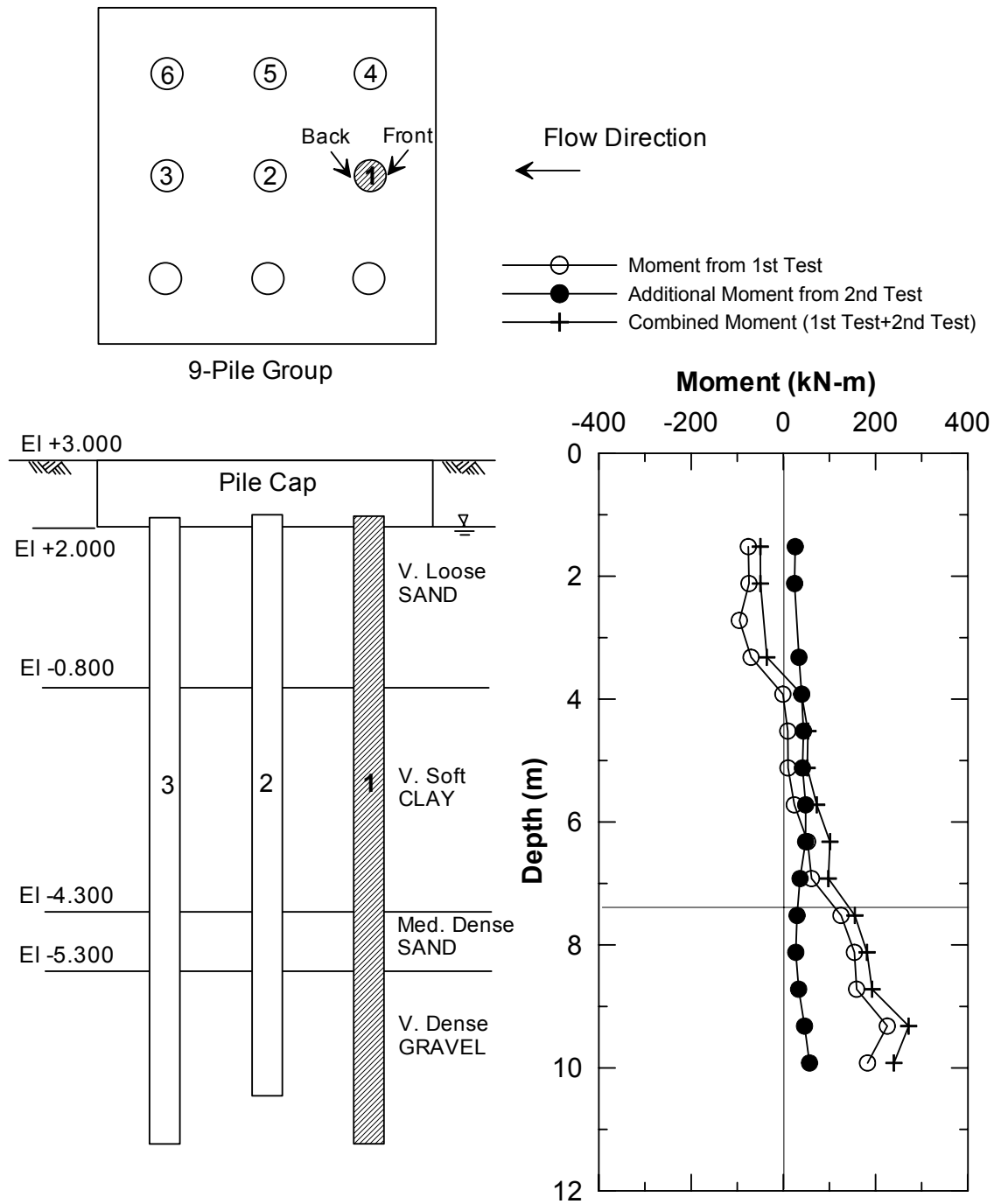
Figure 5.39 Moment Distribution along Pile No.1of 9-Pile Group after 2nd Lateral Spreading Test
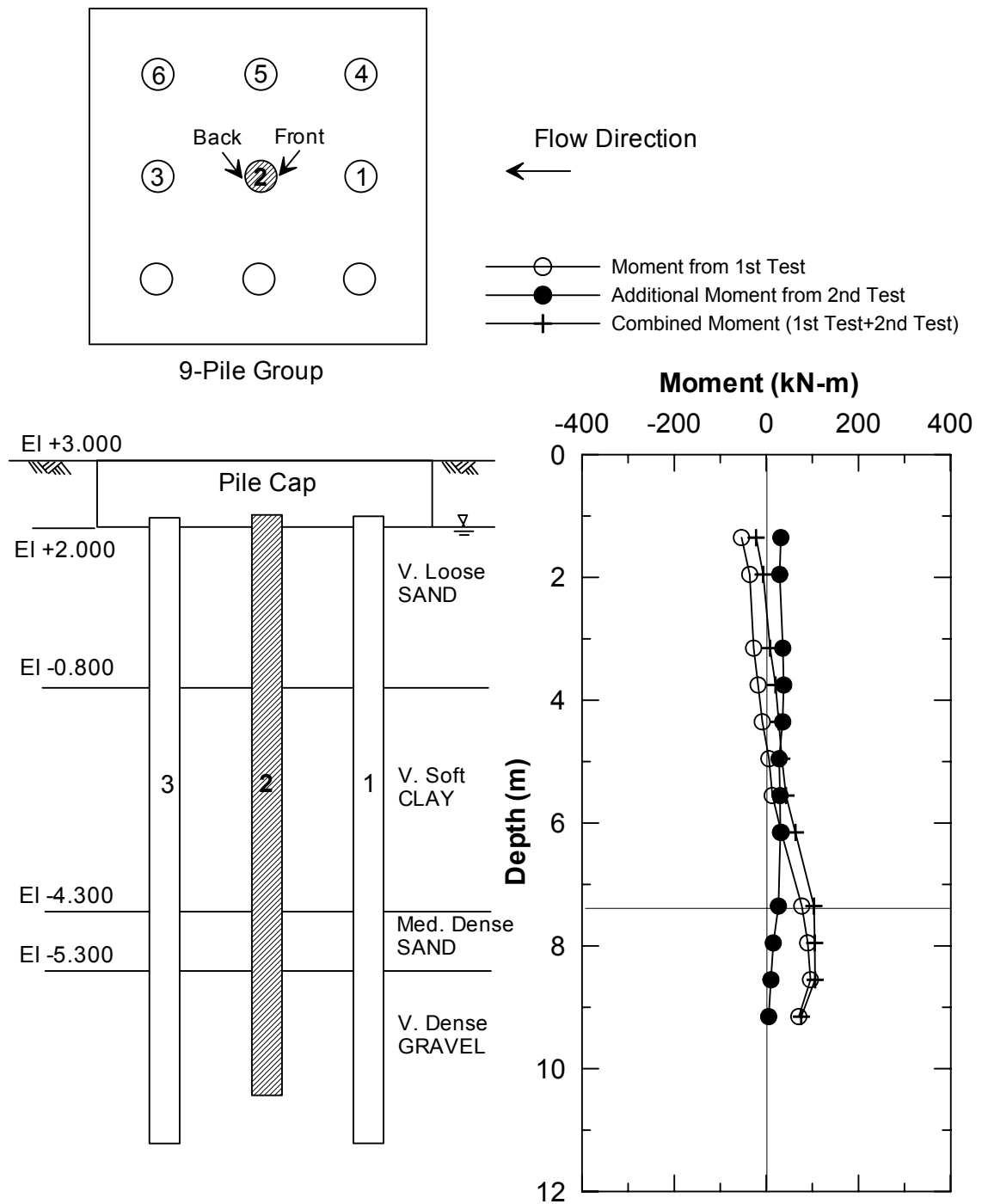
Figure 5.40 Moment Distribution along Pile No.2 of 9-Pile Group after 2nd Lateral Spreading Test
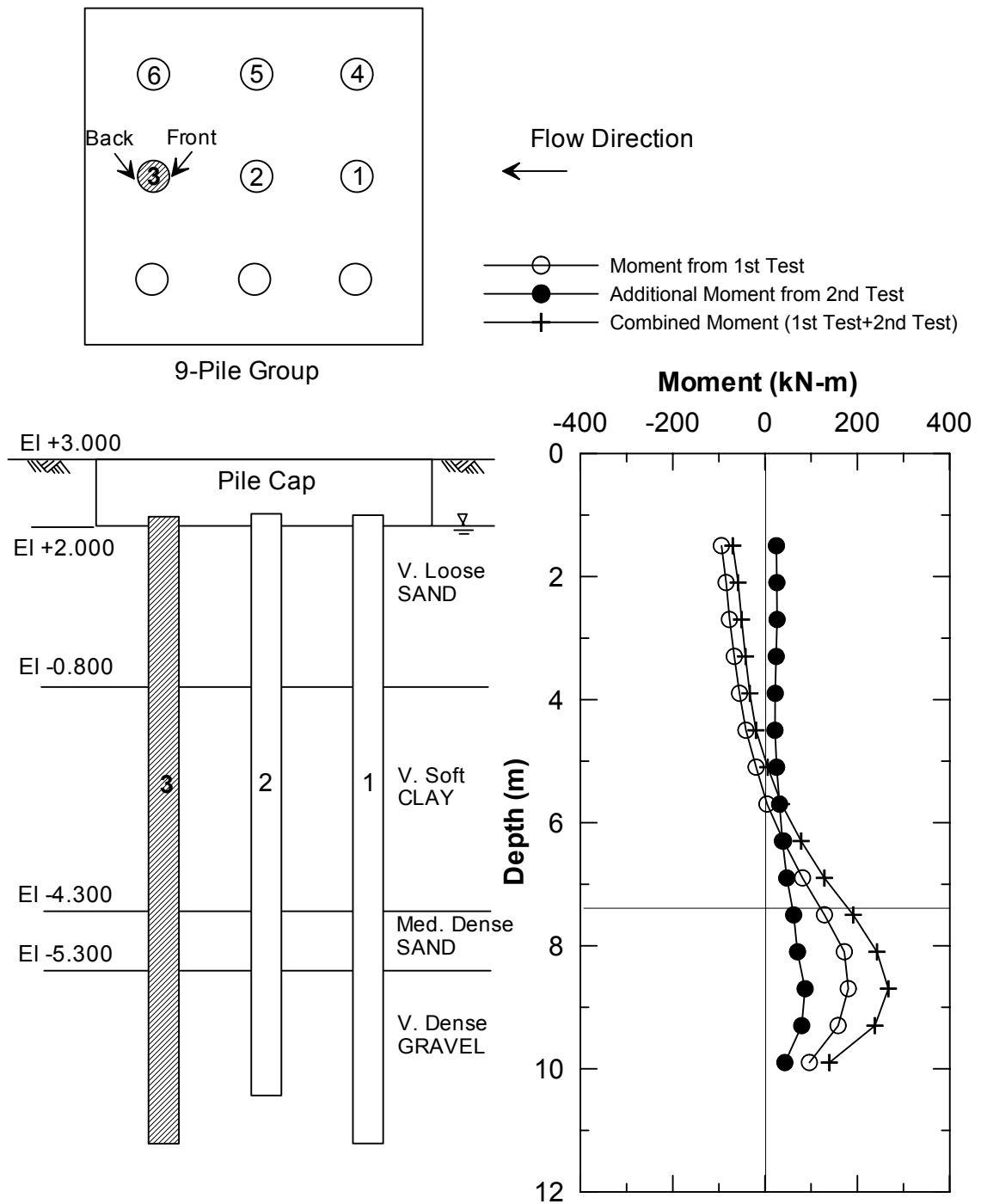
Figure 5.41 Moment Distribution along Pile No.3 of 9-Pile Group after 2nd Lateral Spreading Test
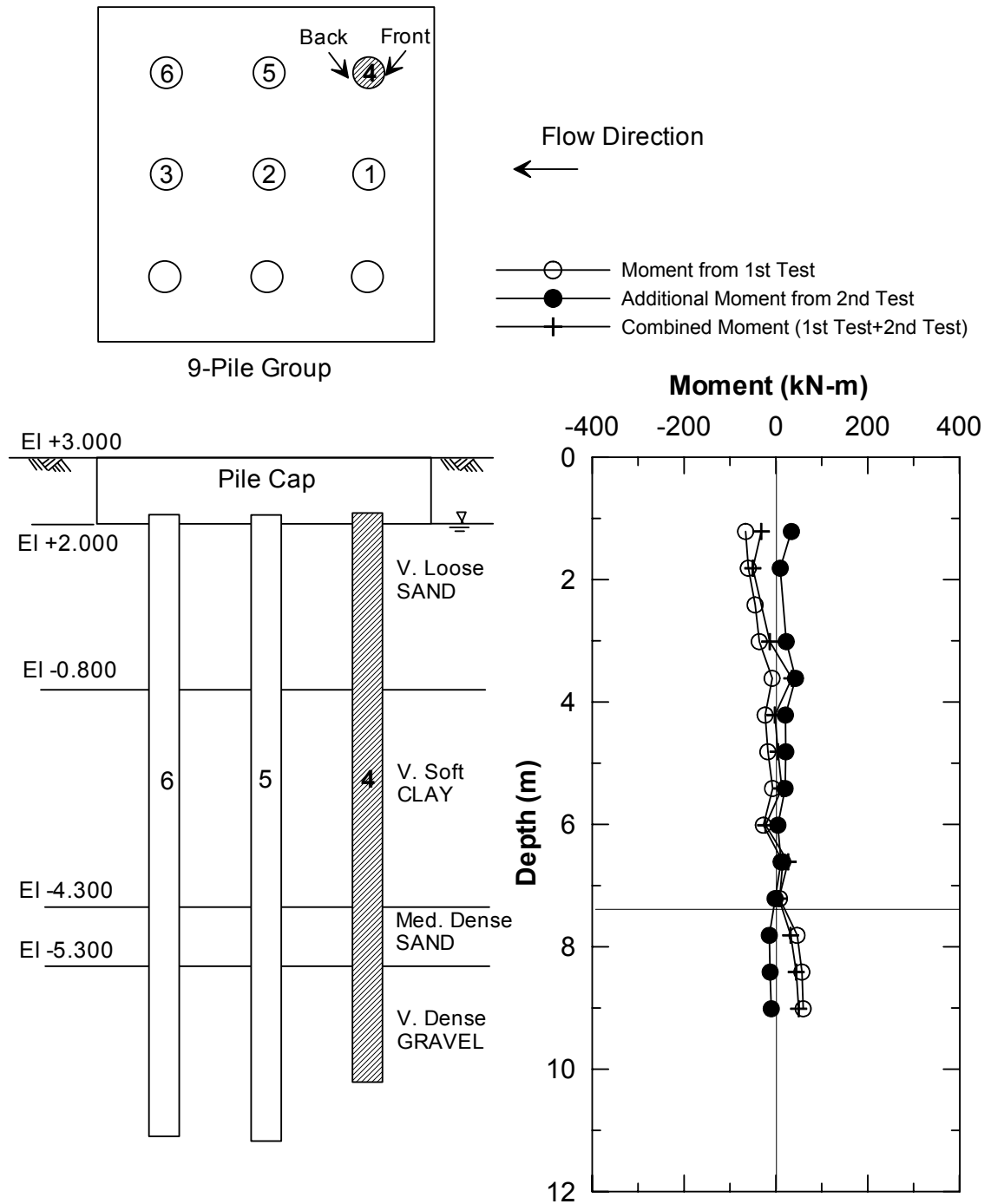
Figure 5.42 Moment Distribution along Pile No.4 of 9-Pile Group after 2nd Lateral Spreading Test
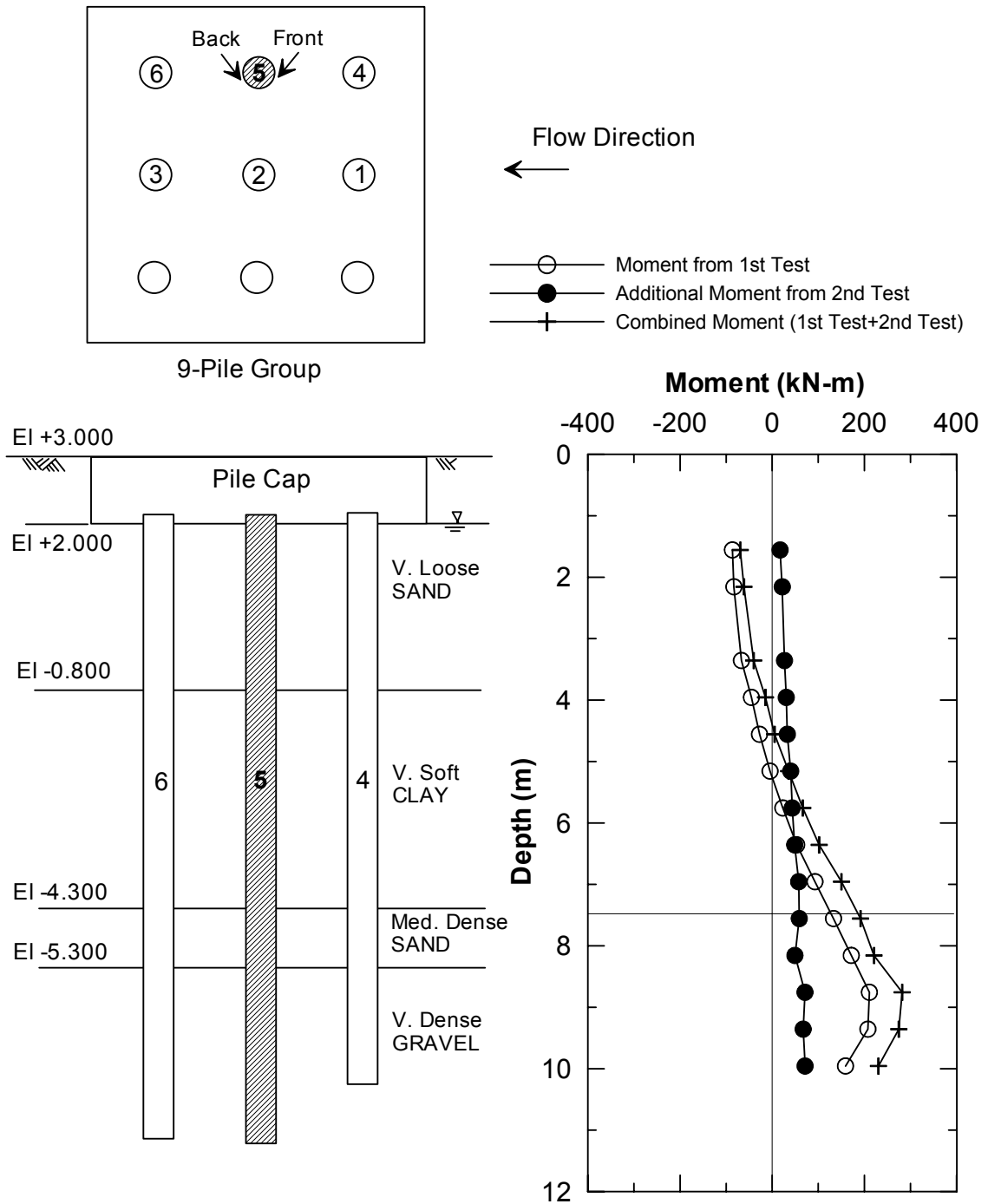
Figure 5.43 Moment Distribution along Pile No.5 of 9-Pile Group after 2nd Lateral Spreading Test
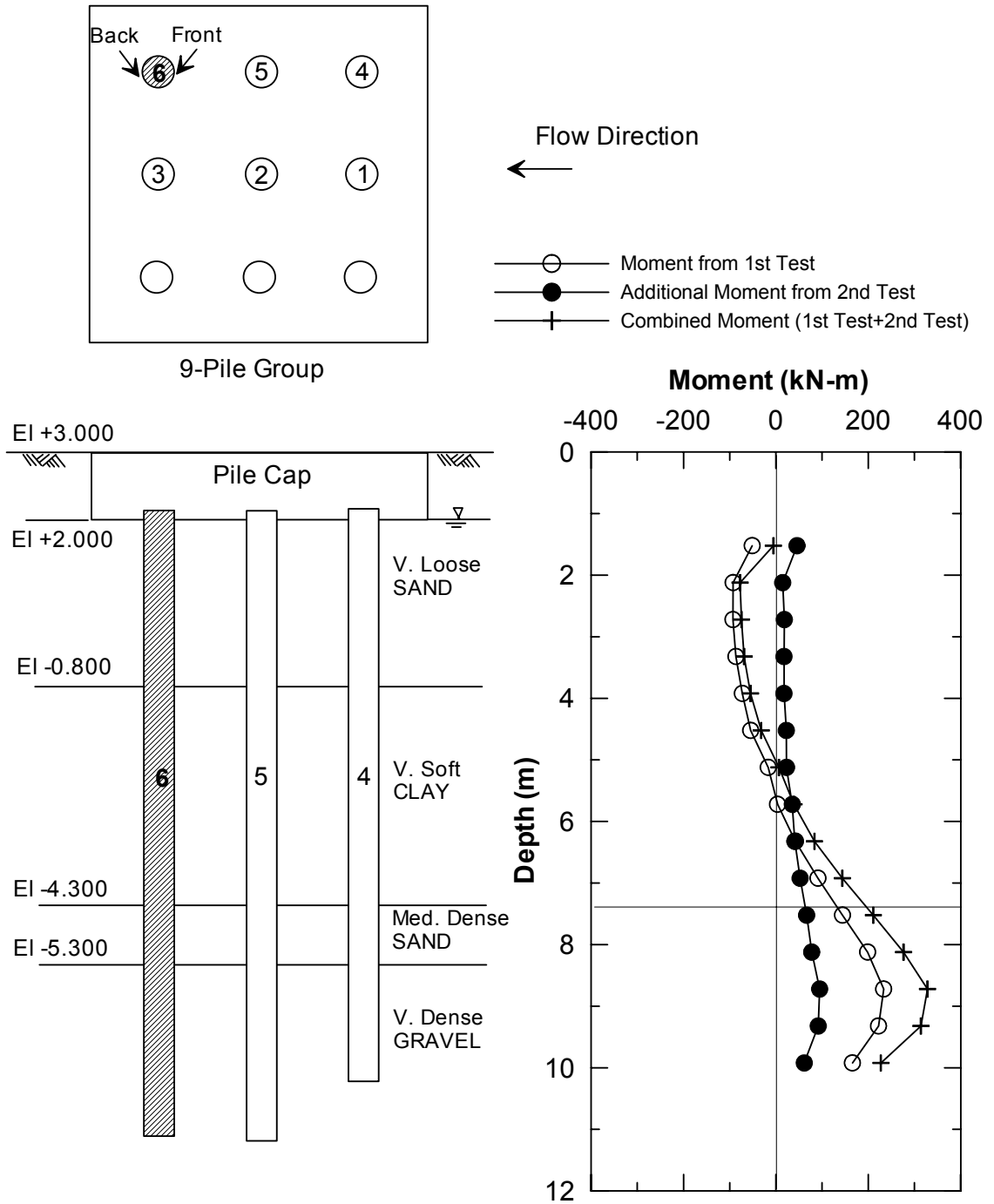
Figure 5.44 Moment Distribution along Pile No.6 of 9-Pile Group after 2nd Lateral Spreading Test
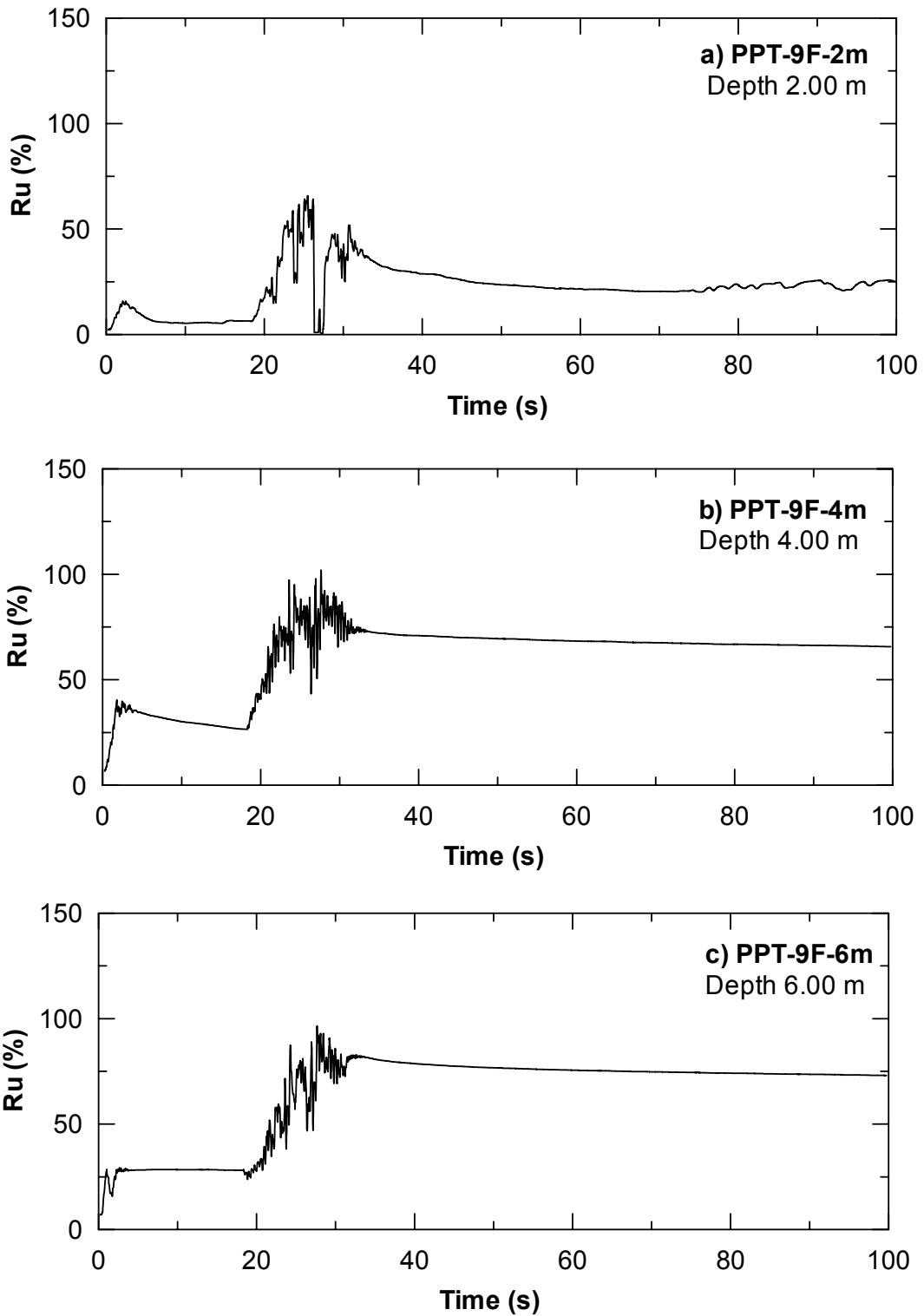
Figure 5.45   Excess Pore Water Pressure Ratios nearby 9-Pile Group (Front) for (a) PPT-9F-2m, (b) PPT-9F-4m, and (c) PPT-9F-6m, Duration of 100s (2nd Blast Test)
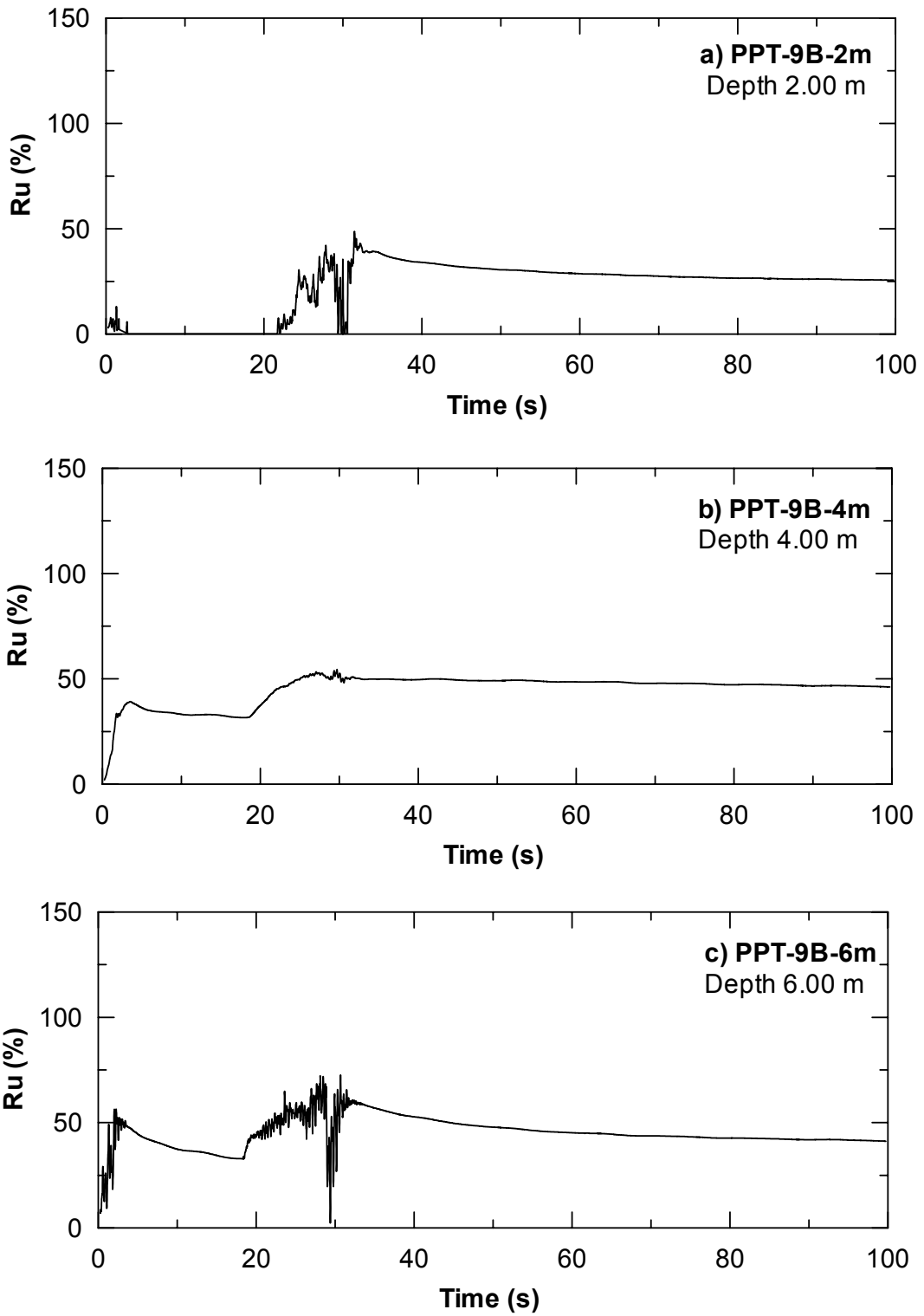
Figure 5.46   Excess Pore Water Pressure Ratios nearby 9-Pile Group (Back) for (a) PPT-9B-2m, (b) PPT-9B-4m, and (c) PPT-9B-6m, Duration of 100s (2nd Blast Test)
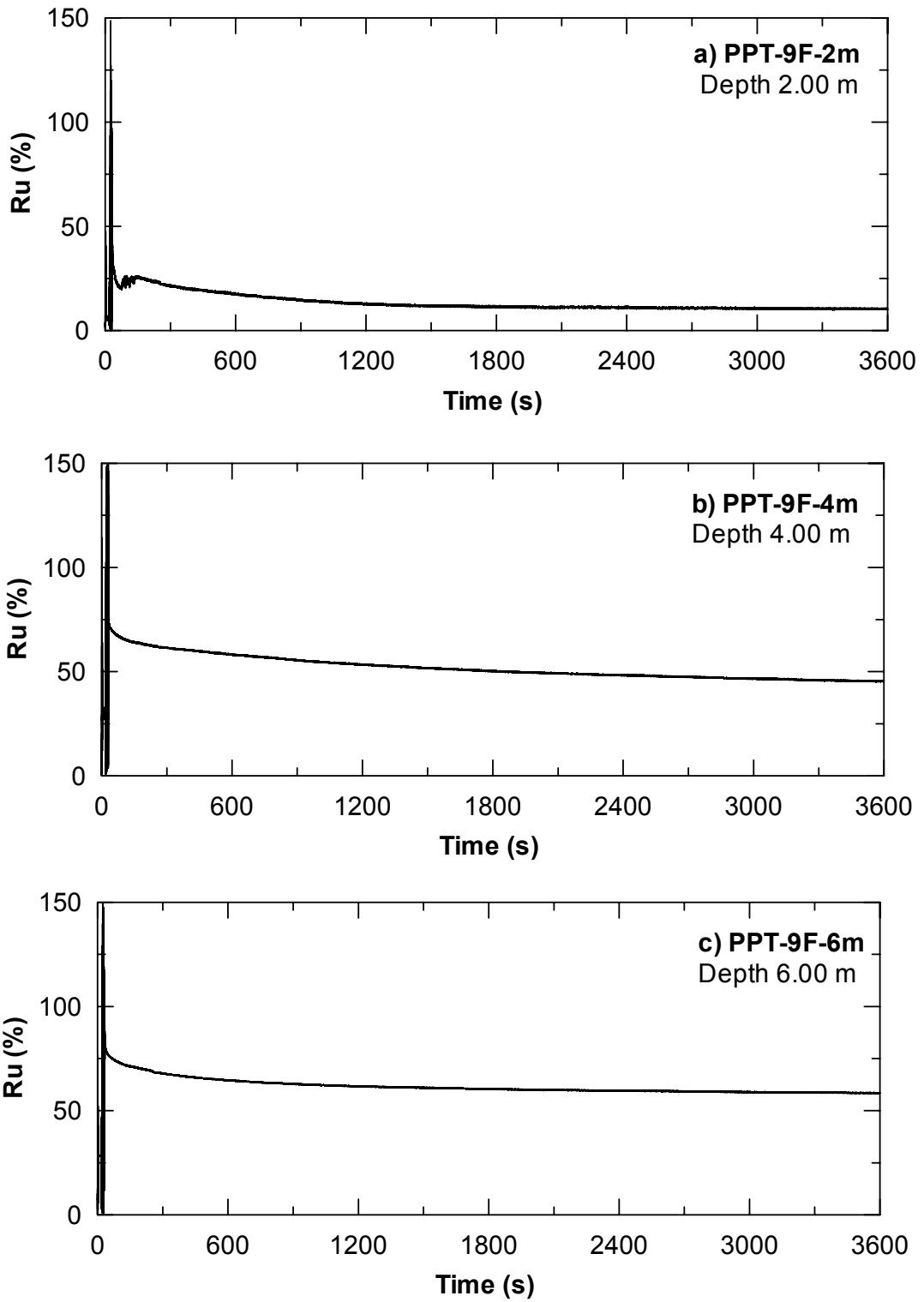
Figure 5.47   Excess Pore Water Pressure Ratios nearby 9-Pile Group (Front) for (a) PPT-9F-2m, (b) PPT-9F-4m, and (c) PPT-9F-6m, Duration of 3600s (2nd Blast Test)
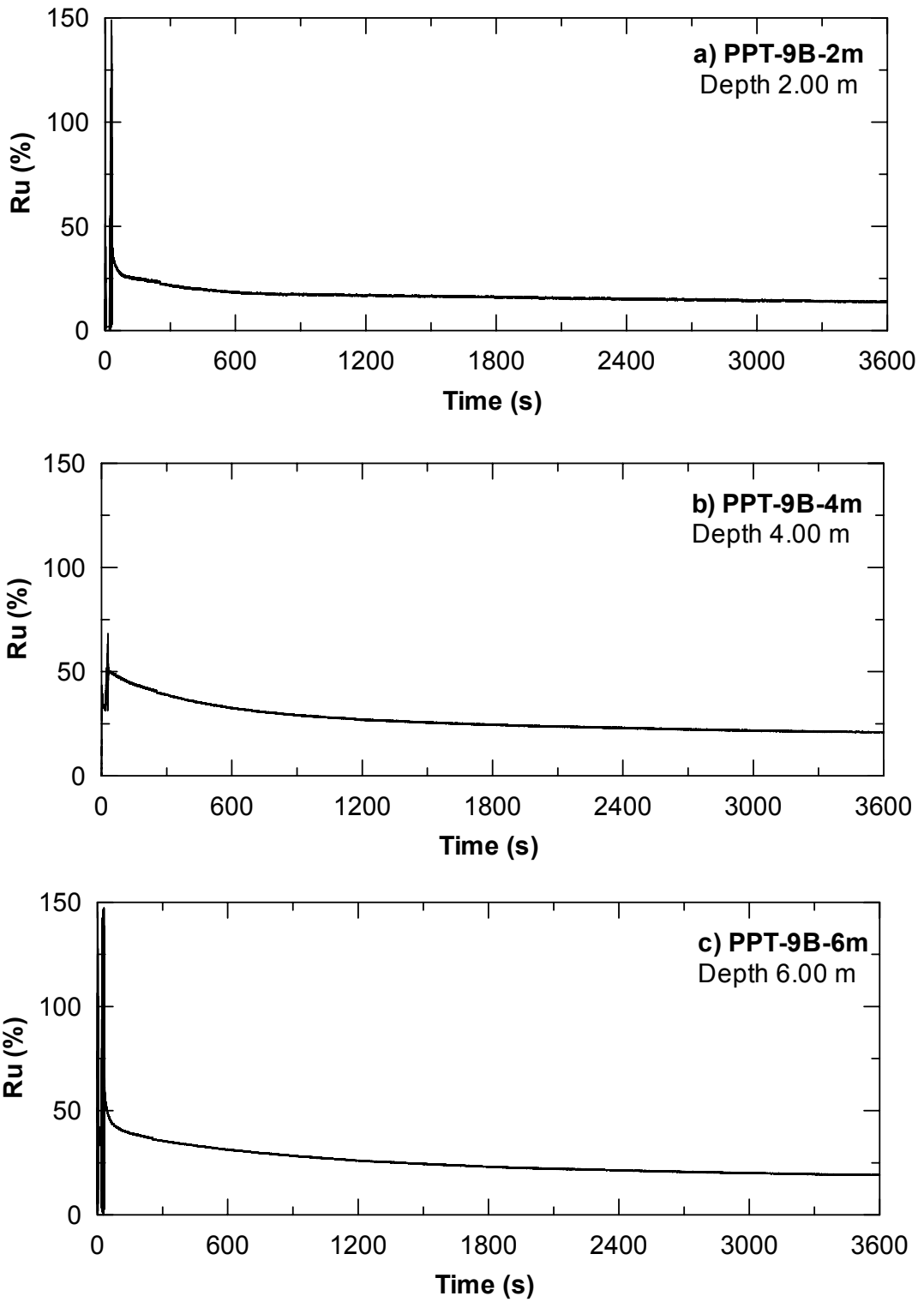
Figure 5.48   Excess Pore Water Pressure Ratios nearby 9-Pile Group (Back) for (a) PPT-9F-2m, (b) PPT-9F-4m, and (c) PPT-9F-6m, Duration of 3600s (2nd Blast Test)
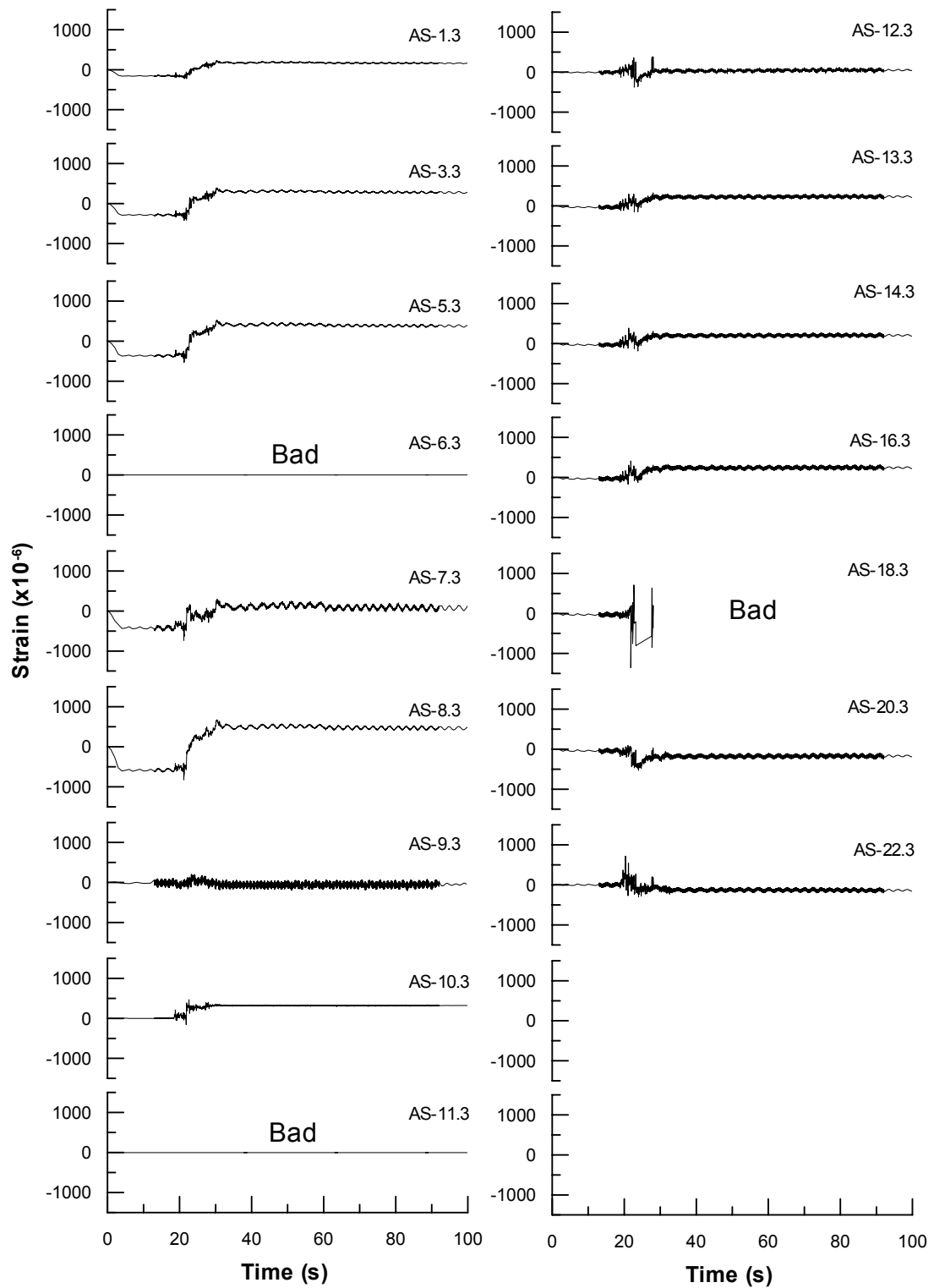
Figure 5.49   Strain Gauge Response along the Side of Transverse Gas Pipeline (Pipeline Type A), 2nd Blast Test

245
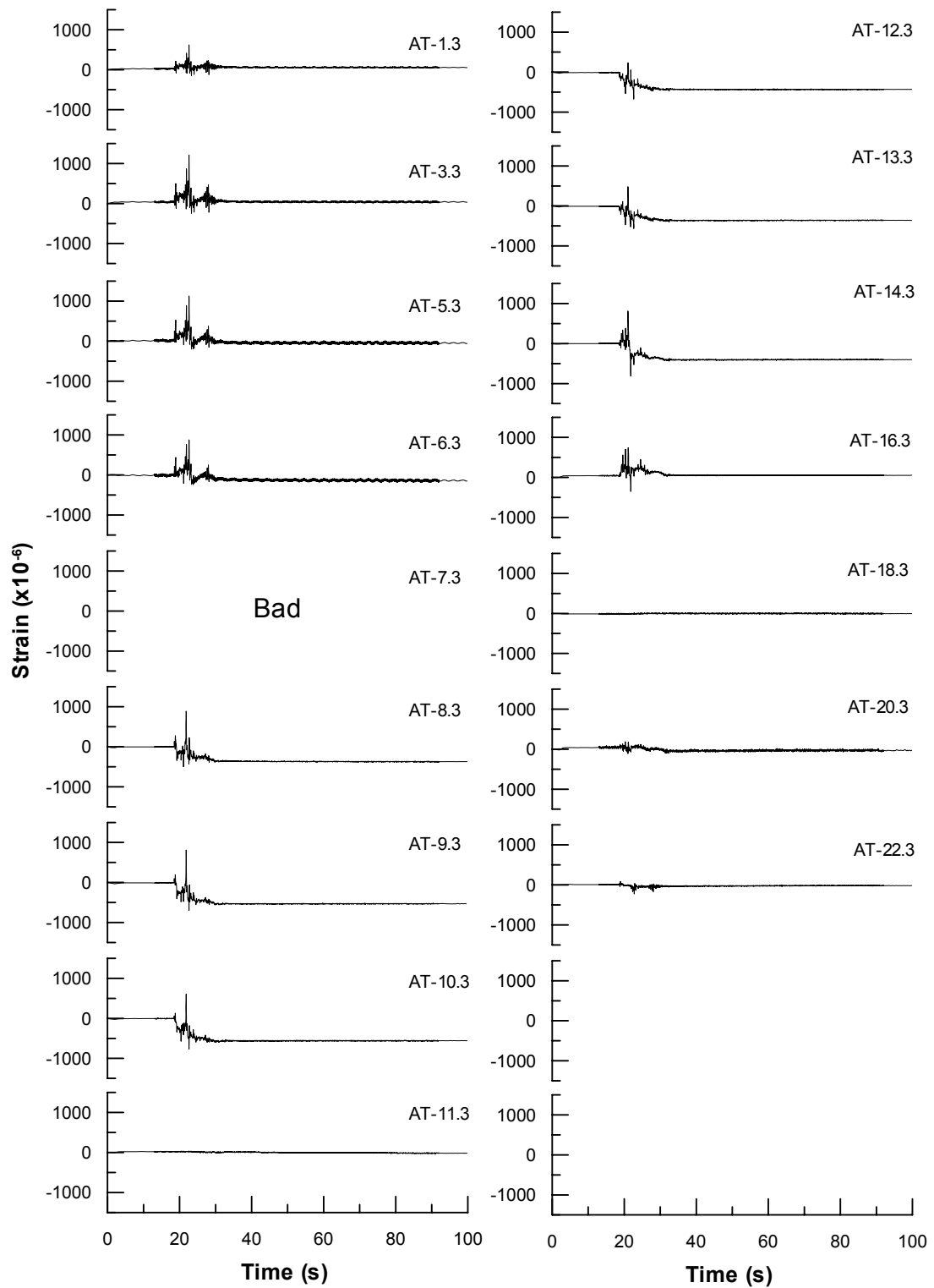
Figure 5.50   Strain Gauge Response along the Top of Transverse Gas Pipeline (Pipeline Type A), 2nd Blast Test

246
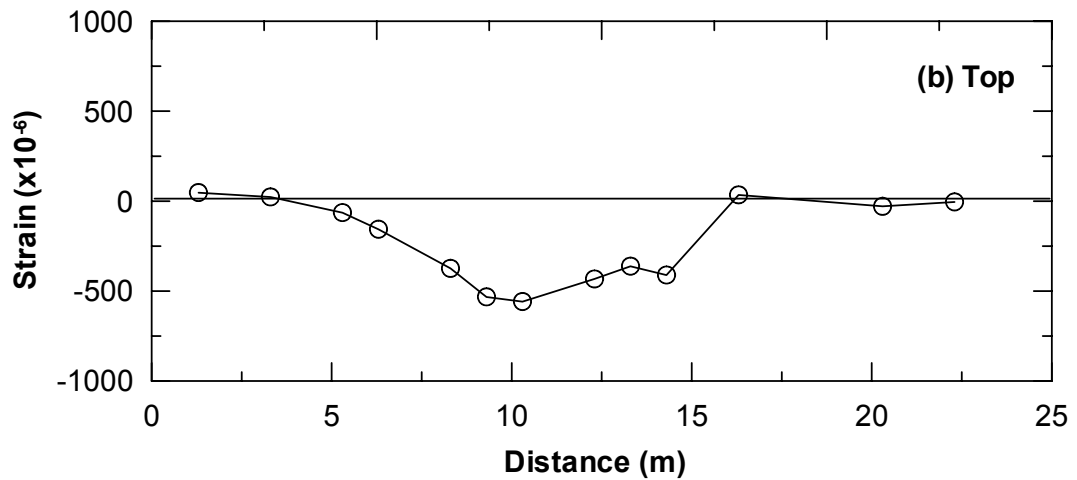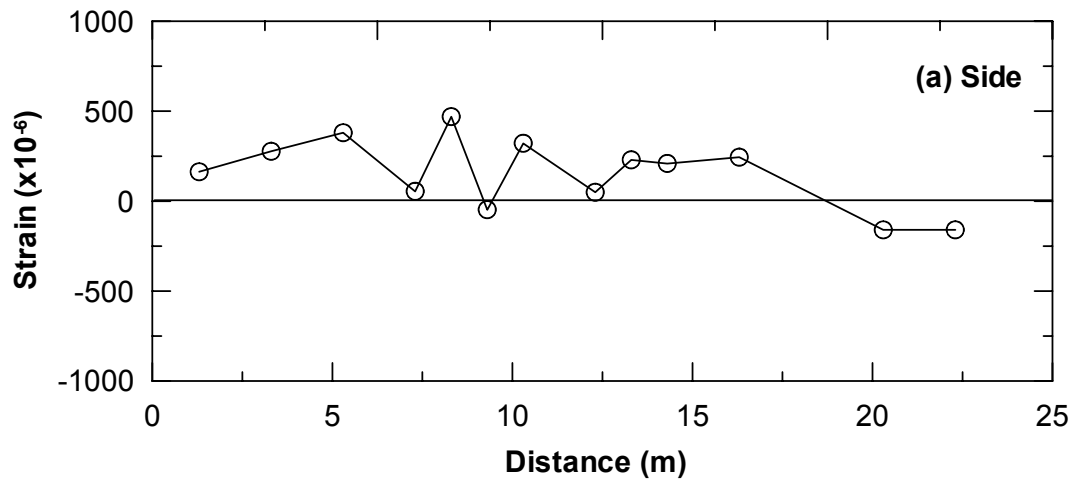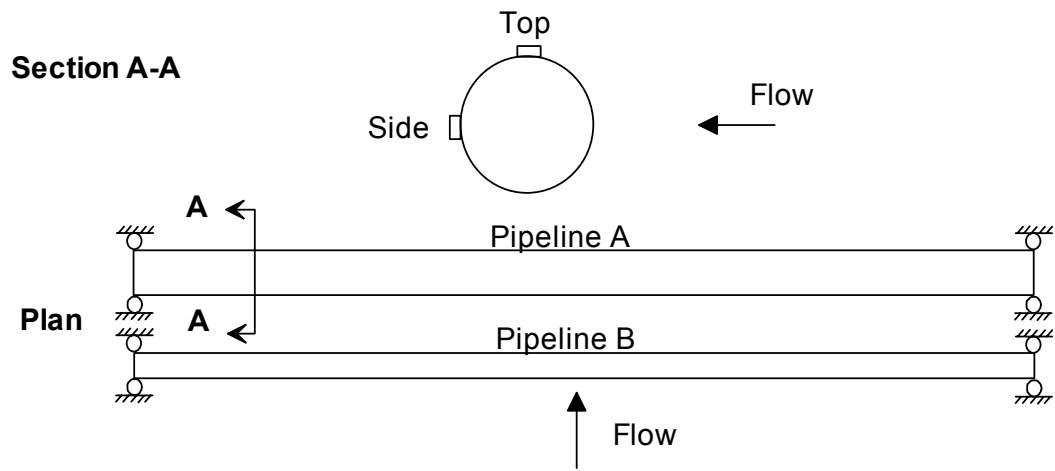
Figure 5.51 Profile of Residual Strain of Pipeline Type A at (a) Side of Pipeline, and (b) Top of Pipeline, 2nd Blast Test
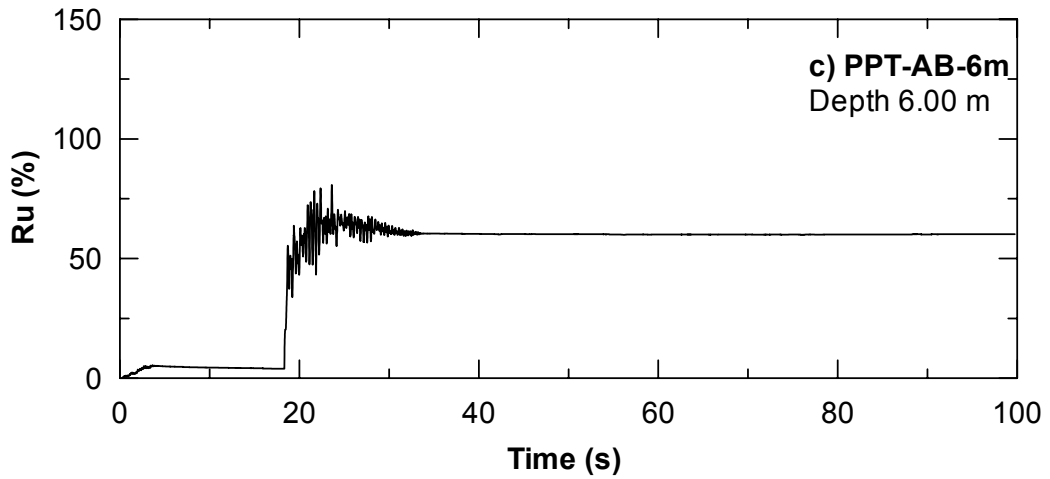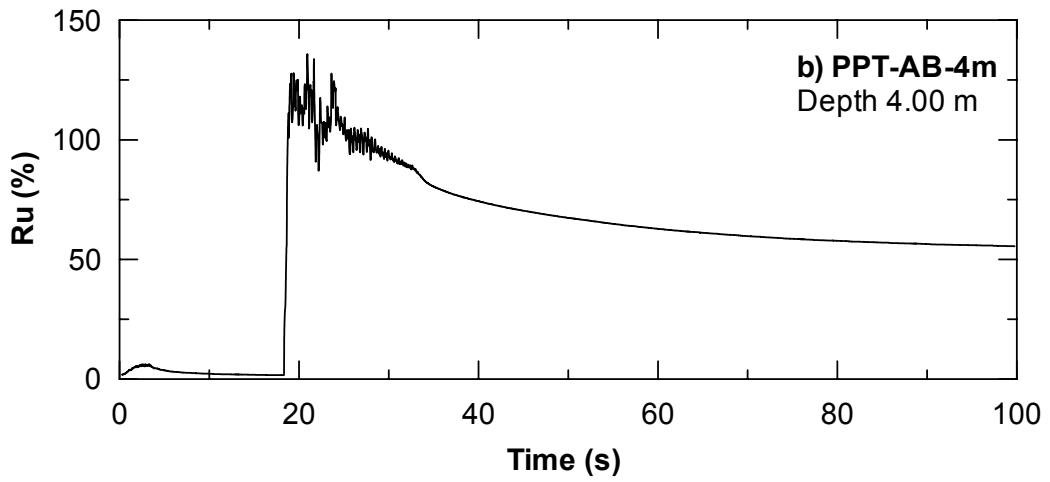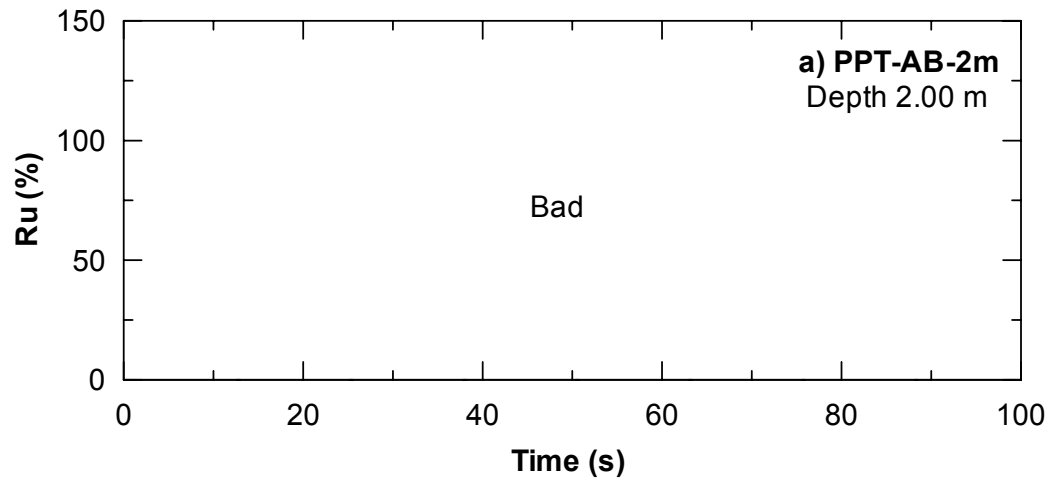
Figure 5.52   Excess Pore Water Pressure Ratios between Pipelines A and B for (a) PPT-AB-2m, (b) PPT-AB-4m, and (c) PPT-AB-6m, Duration of 100s (2nd Blast Test)
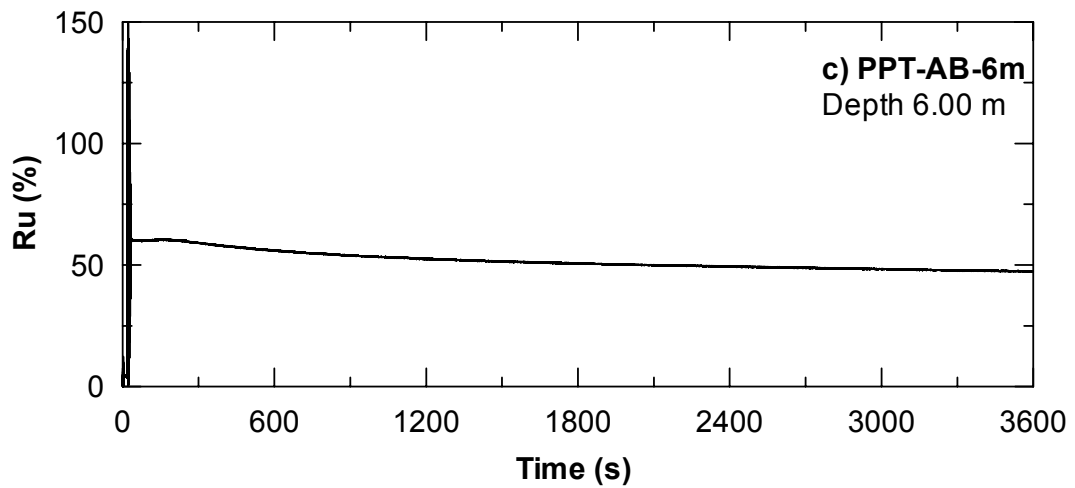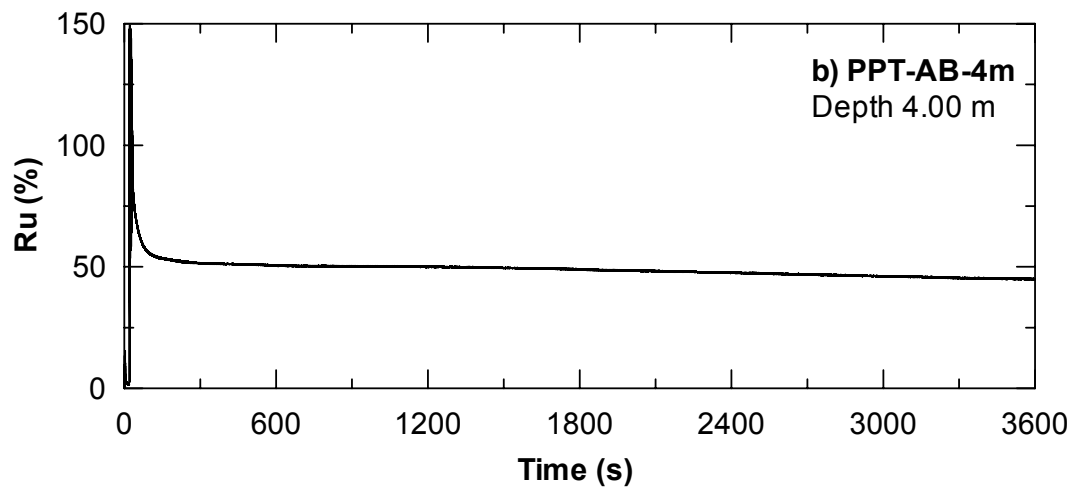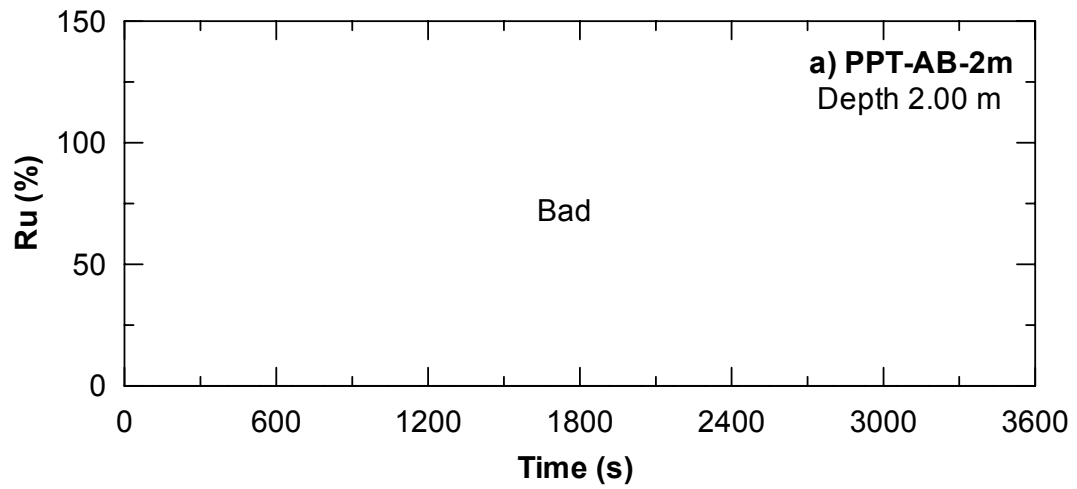
Figure 5.53   Excess Pore Water Pressure Ratios between Pipelines A and B for (a) PPT-AB-2m, (b) PPT-AB-4m, and (c) PPT-AB-6m, Duration of 3600s (2nd Blast Test)
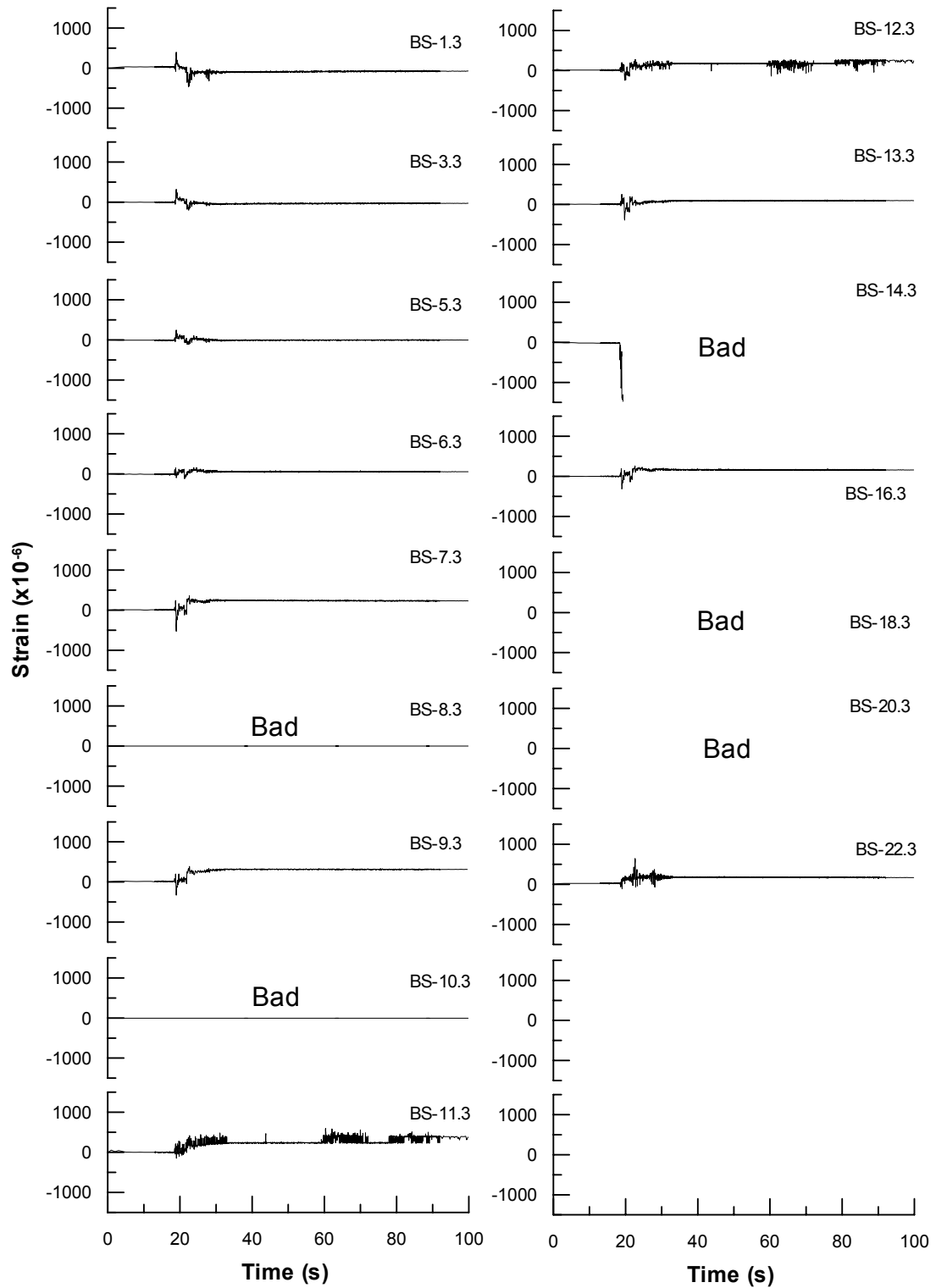
Figure 5.54   Strain Gauge Response along the Side of Transverse Electrical Conduit (Pipeline Type B), 2nd Blast Test
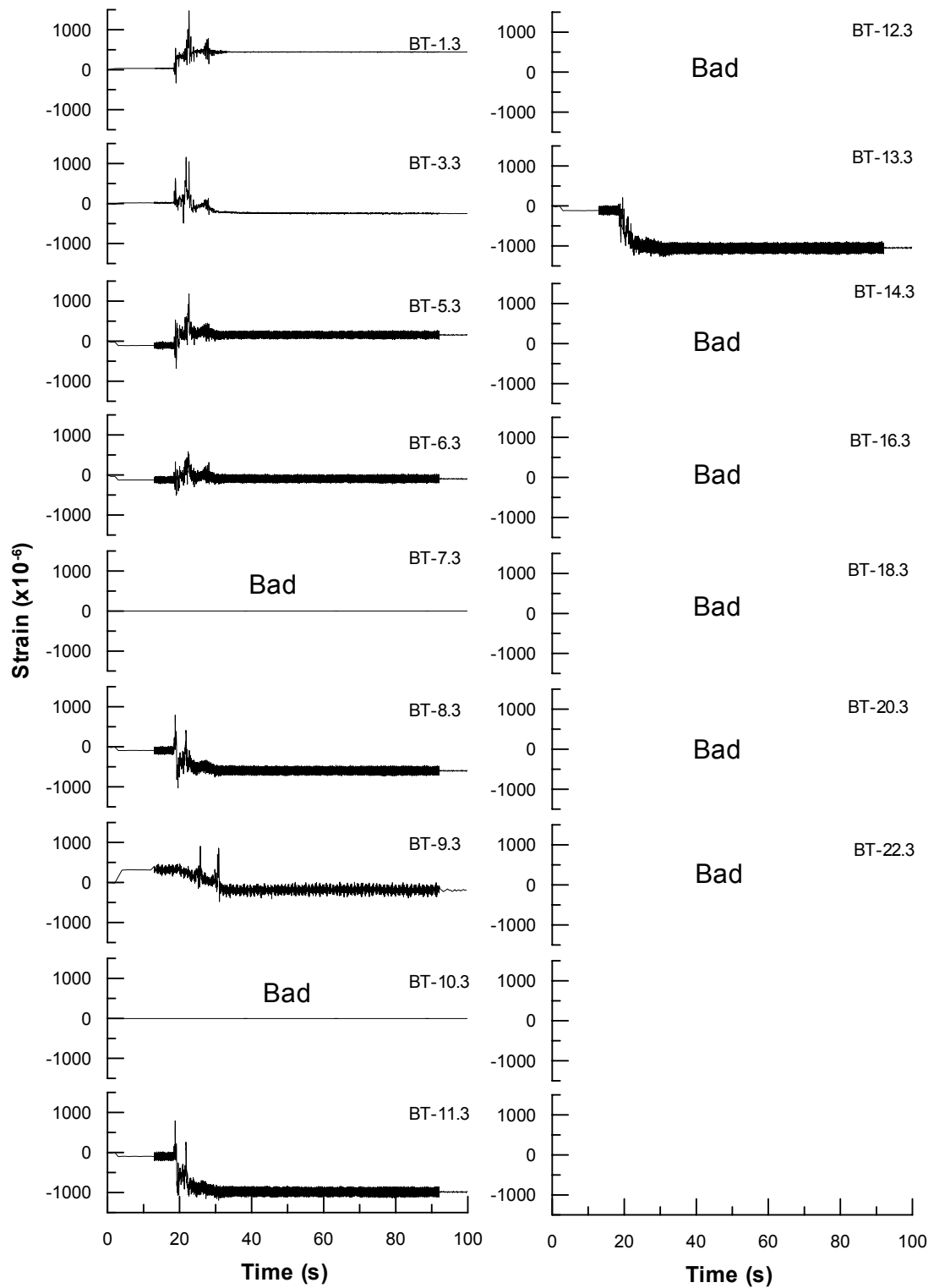
Figure 5.55   Strain Gauge Response along the Top of Transverse Electrical Conduit (Pipeline Type B), 2nd Blast Test

251
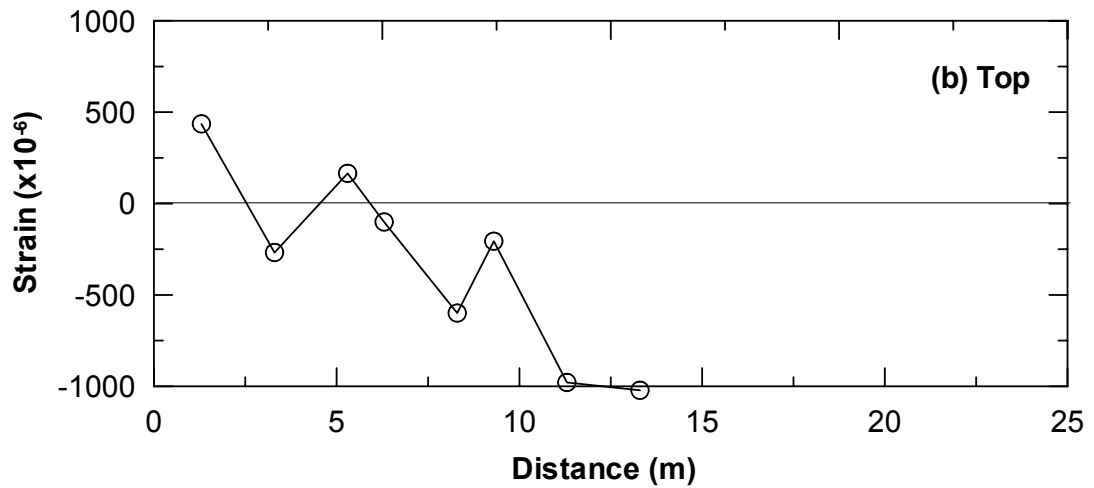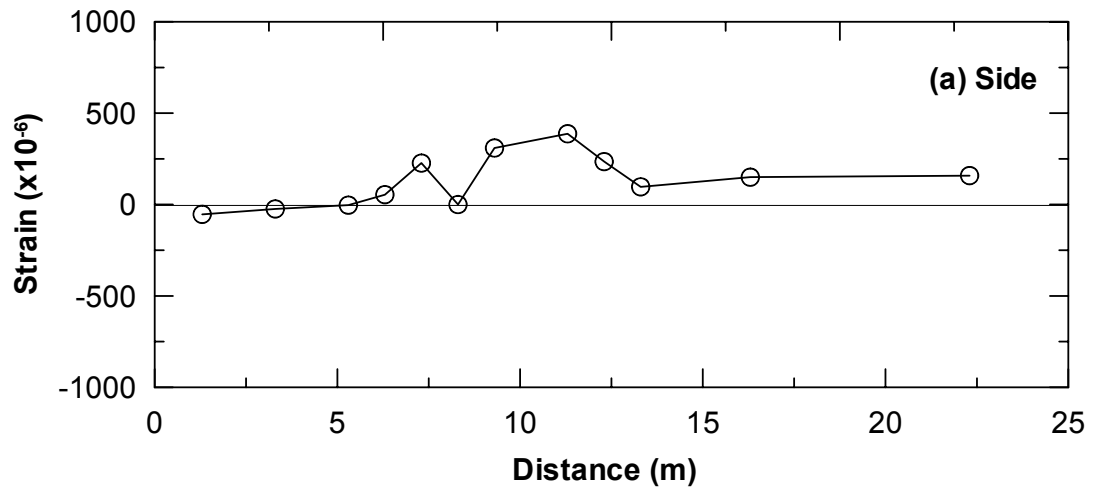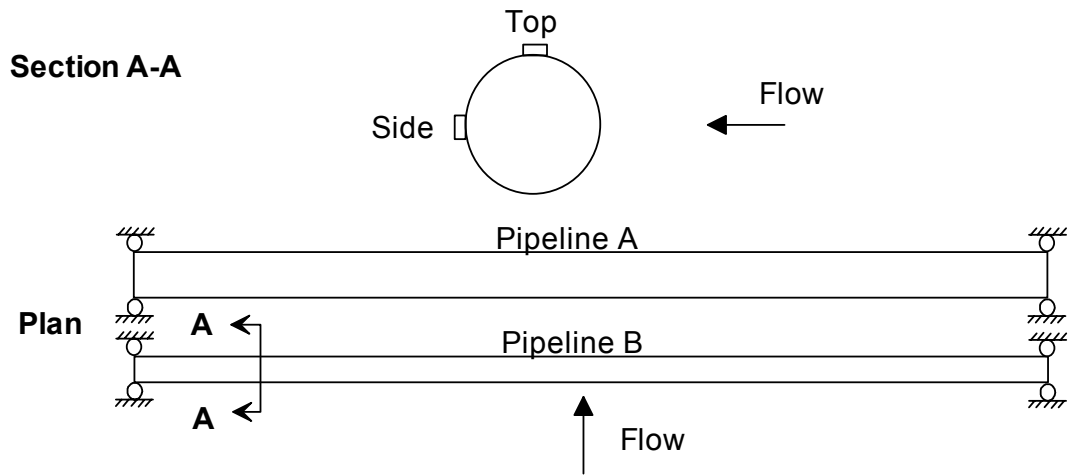
Figure 5.56   Profile of Residual Strain of Pipeline Type B at (a) Side of Pipeline, and (b) Top of Pipeline, 2nd Blast Test
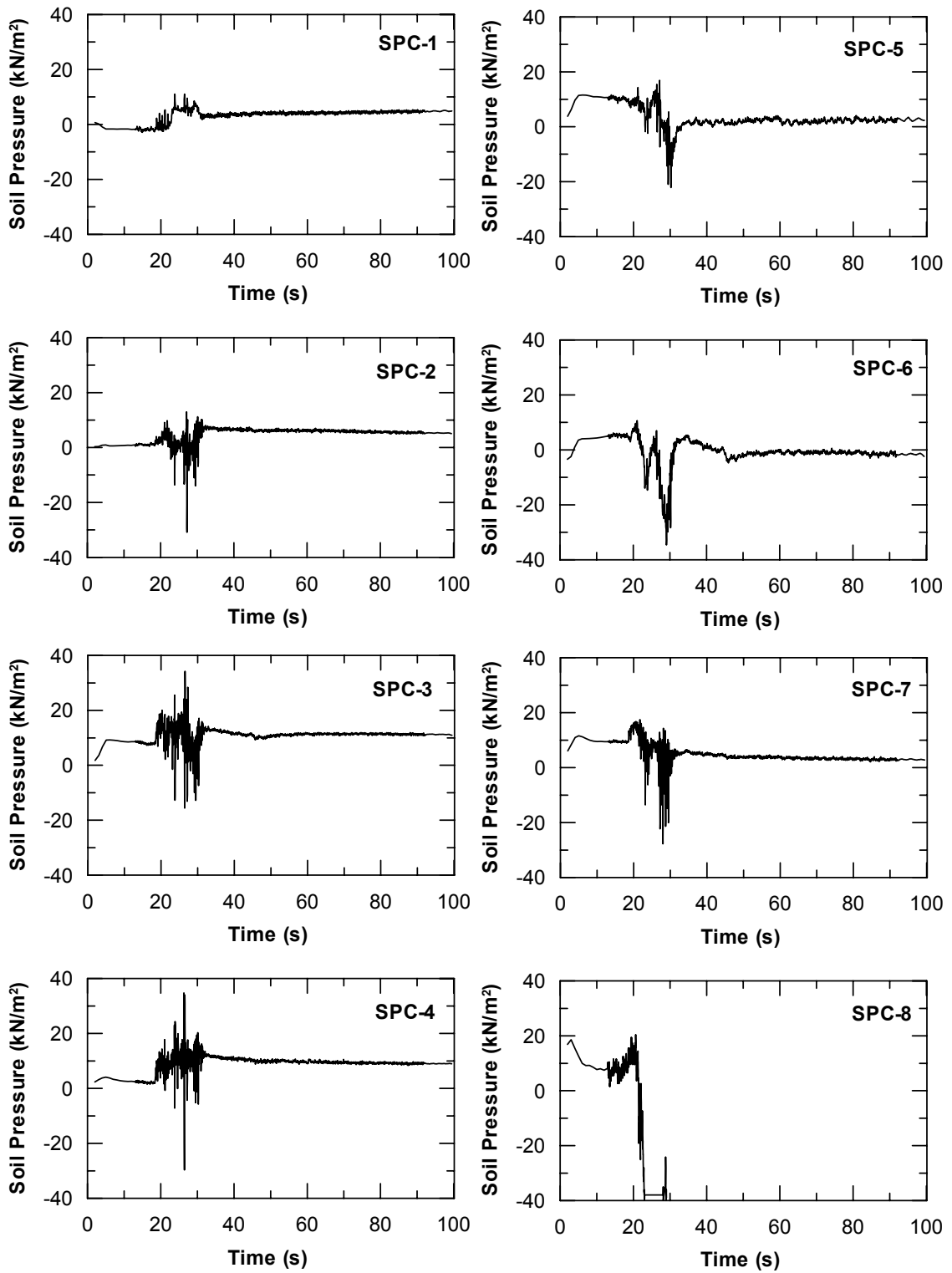
Figure 5.57   Response of Soil Pressure Cells for 4-Pile Group and 9-Pile Group, 2nd Blast Test

253
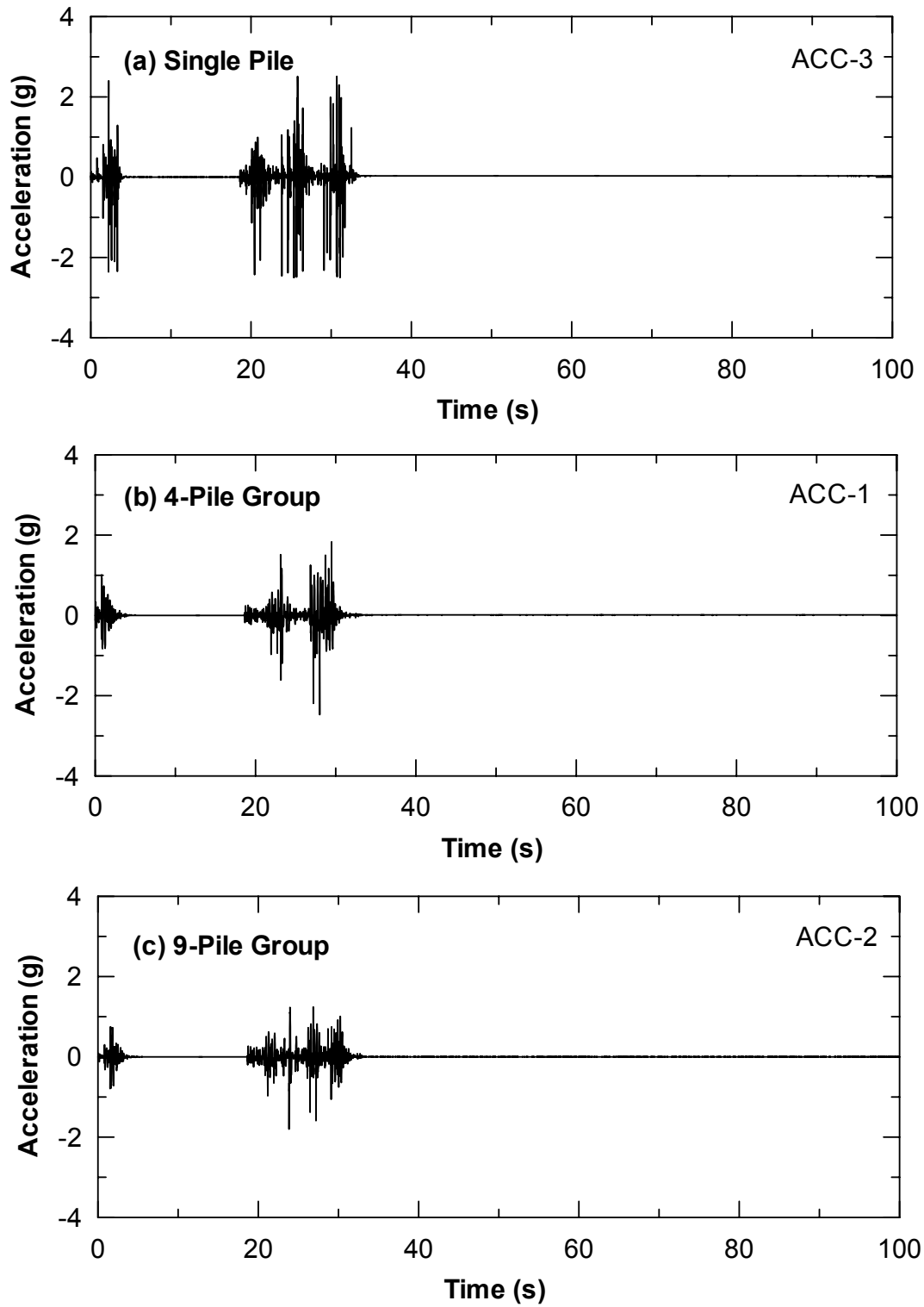
Figure 5.58 Acceleration Response at (a) Top of Single Pile, (b) Pile Cap of 4-Pile
Group, and (c) Pile Cap of 9-Pile Group, 2nd Blast Test
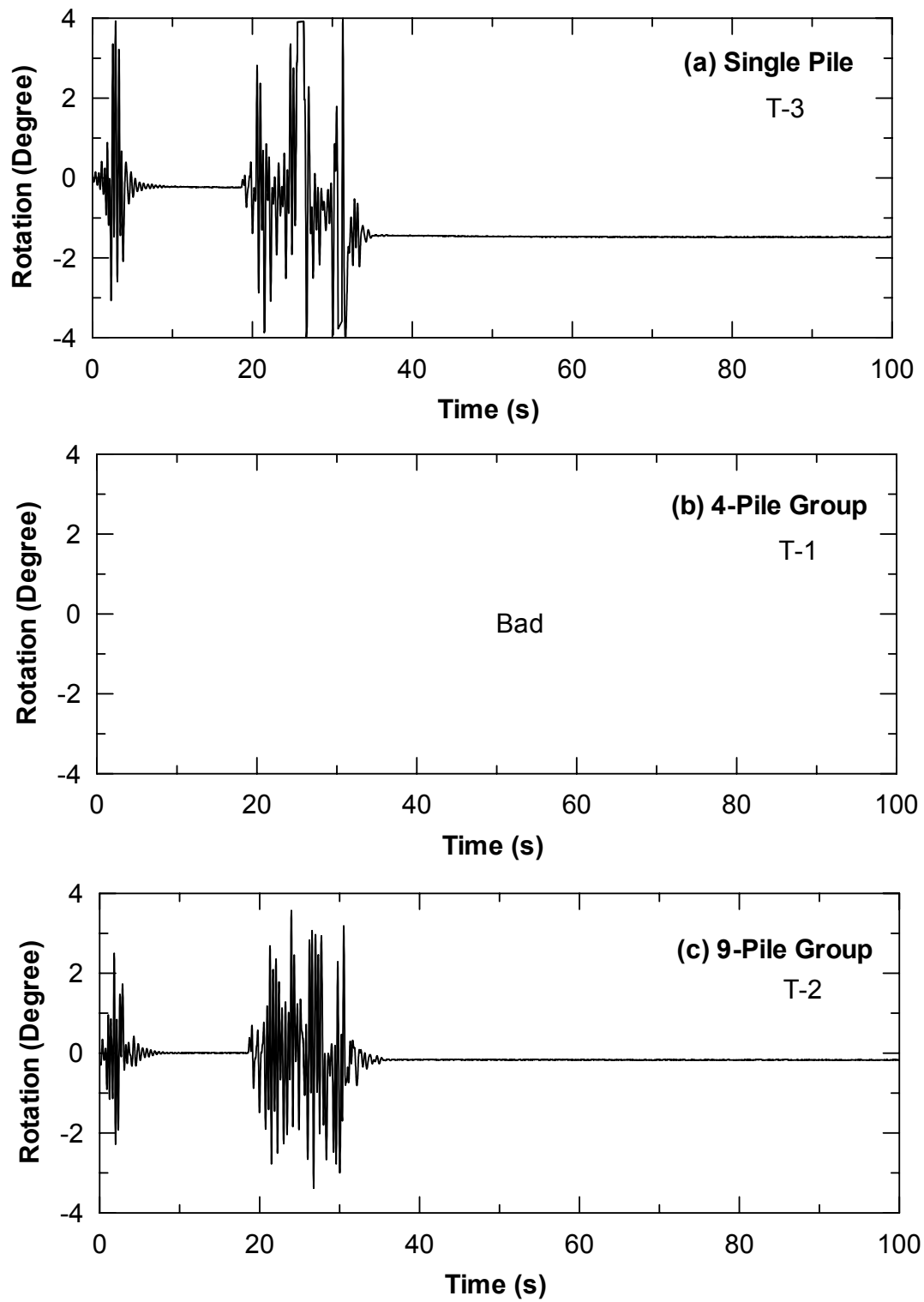
Figure 5.59   Rotation Response at (a) Top of Single Pile, (b) Pile Cap of 4-Pile, and (c) Pile Cap of 9-Pile Group, 2nd Blast Test
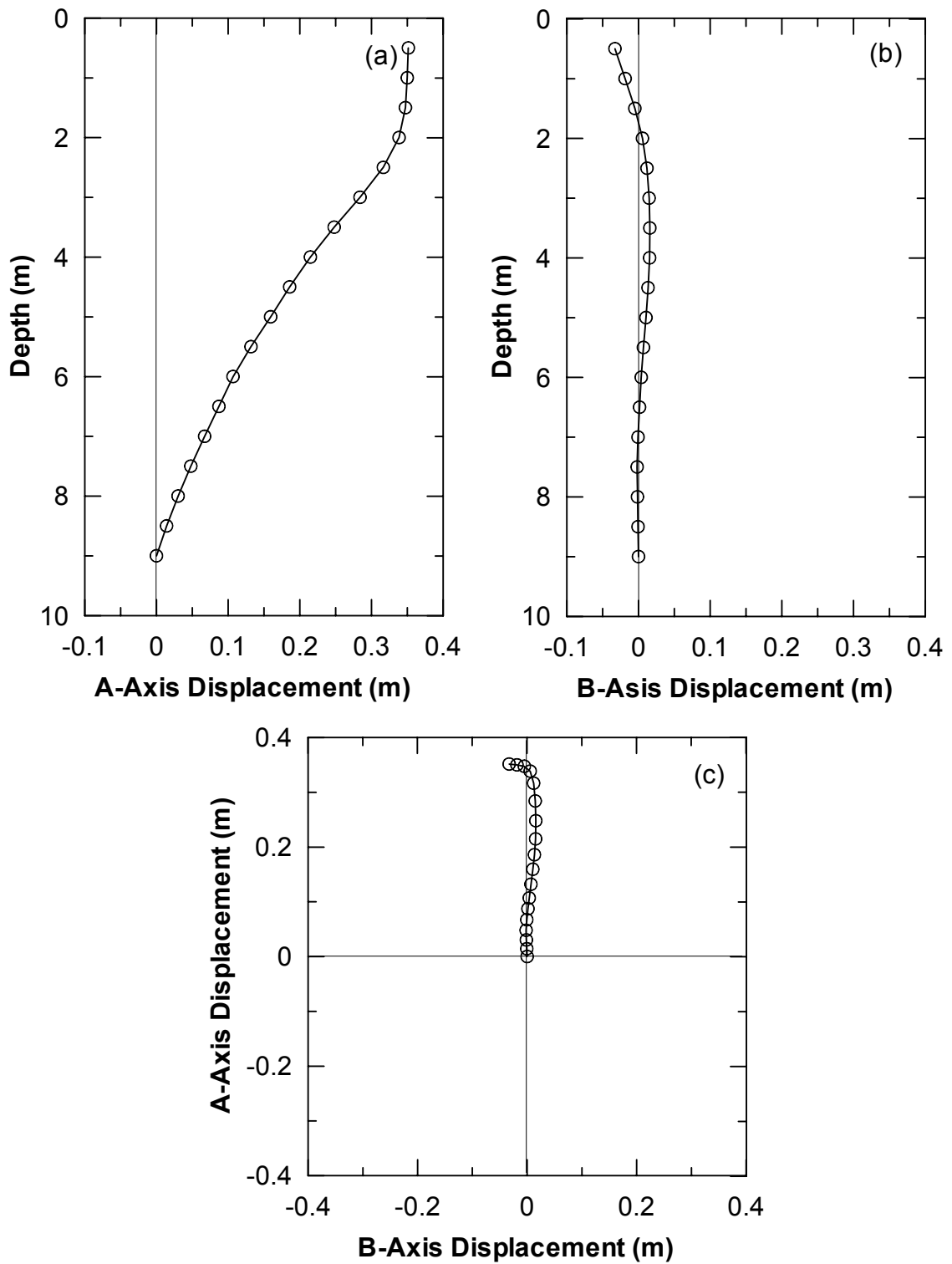
Figure 5.60 Soil Displacement from Inclinometer Casing S2 for 2nd Japan Blast Test
a) Section View A-Direction, b) Section View B-Direction, and c) Plan View

256
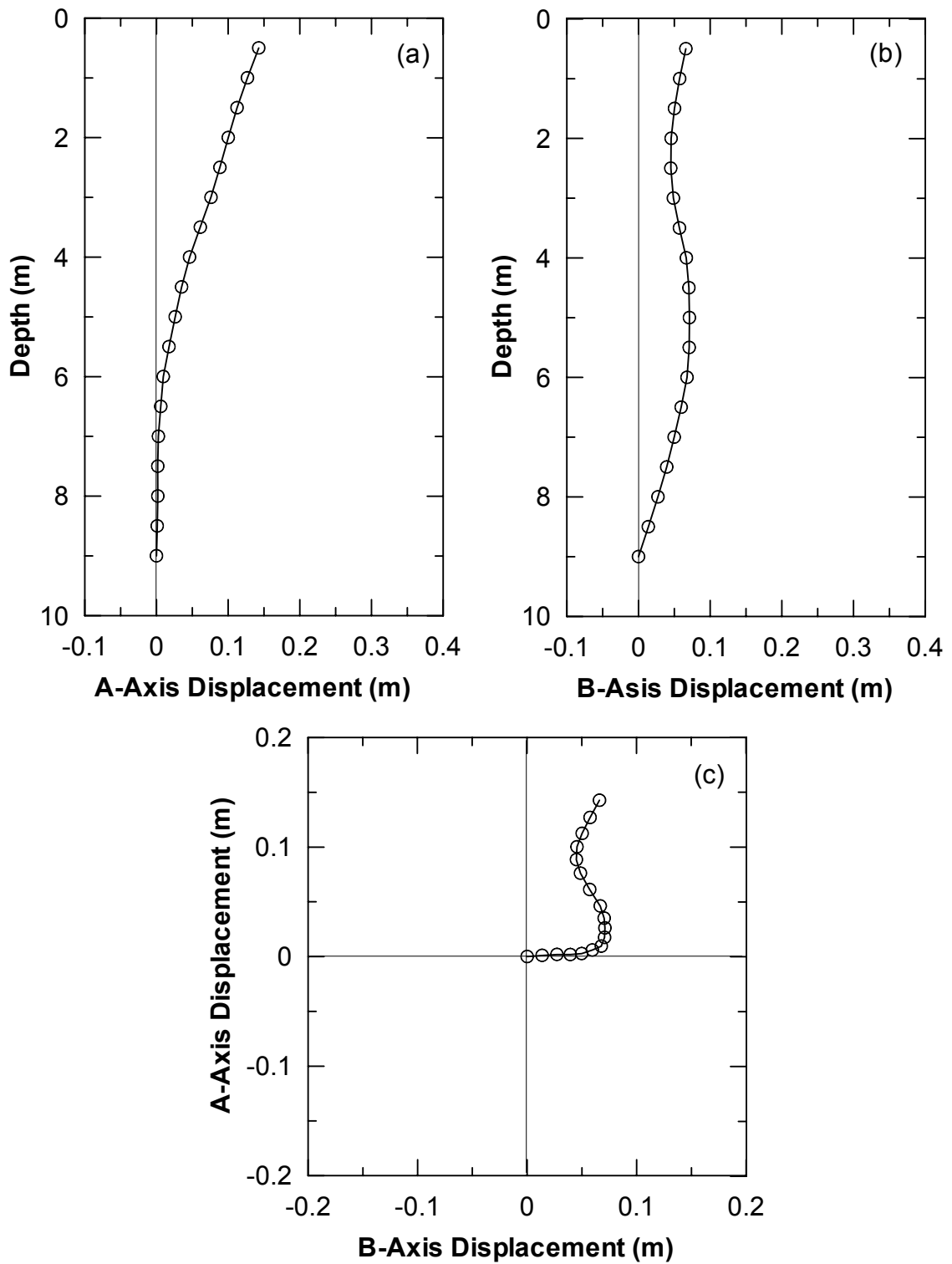
Figure 5.61   Soil Displacement from Inclinometer Casing S3 for 2nd Japan Blast Test
a) Section View A-Direction, b) Section View B-Direction, and c) Plan View

257
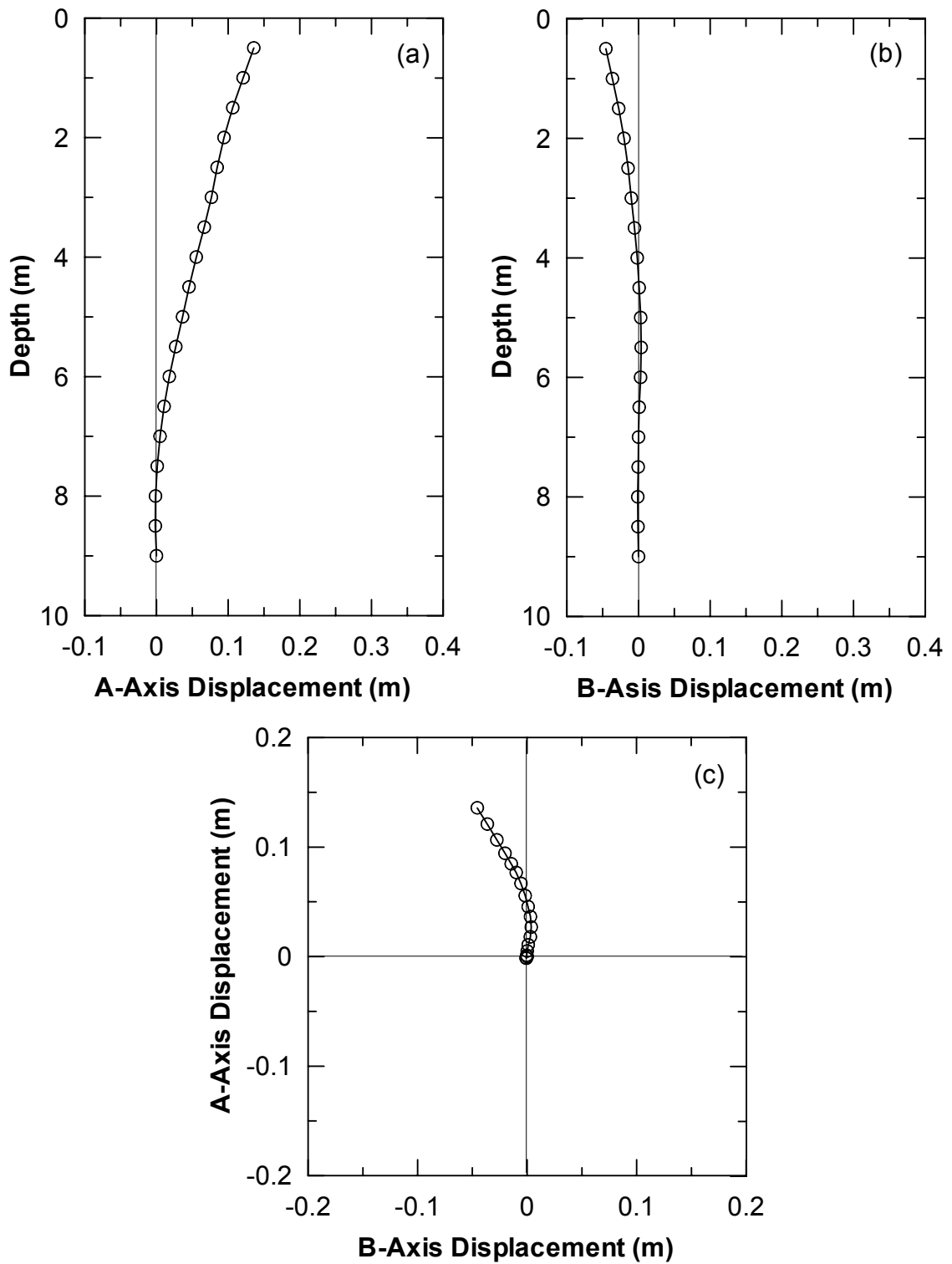
Figure 5.62   Soil Displacement from Inclinometer Casing S4 for 2nd Japan Blast Test
a) Section View A-Direction, b) Section View B-Direction, and c) Plan View
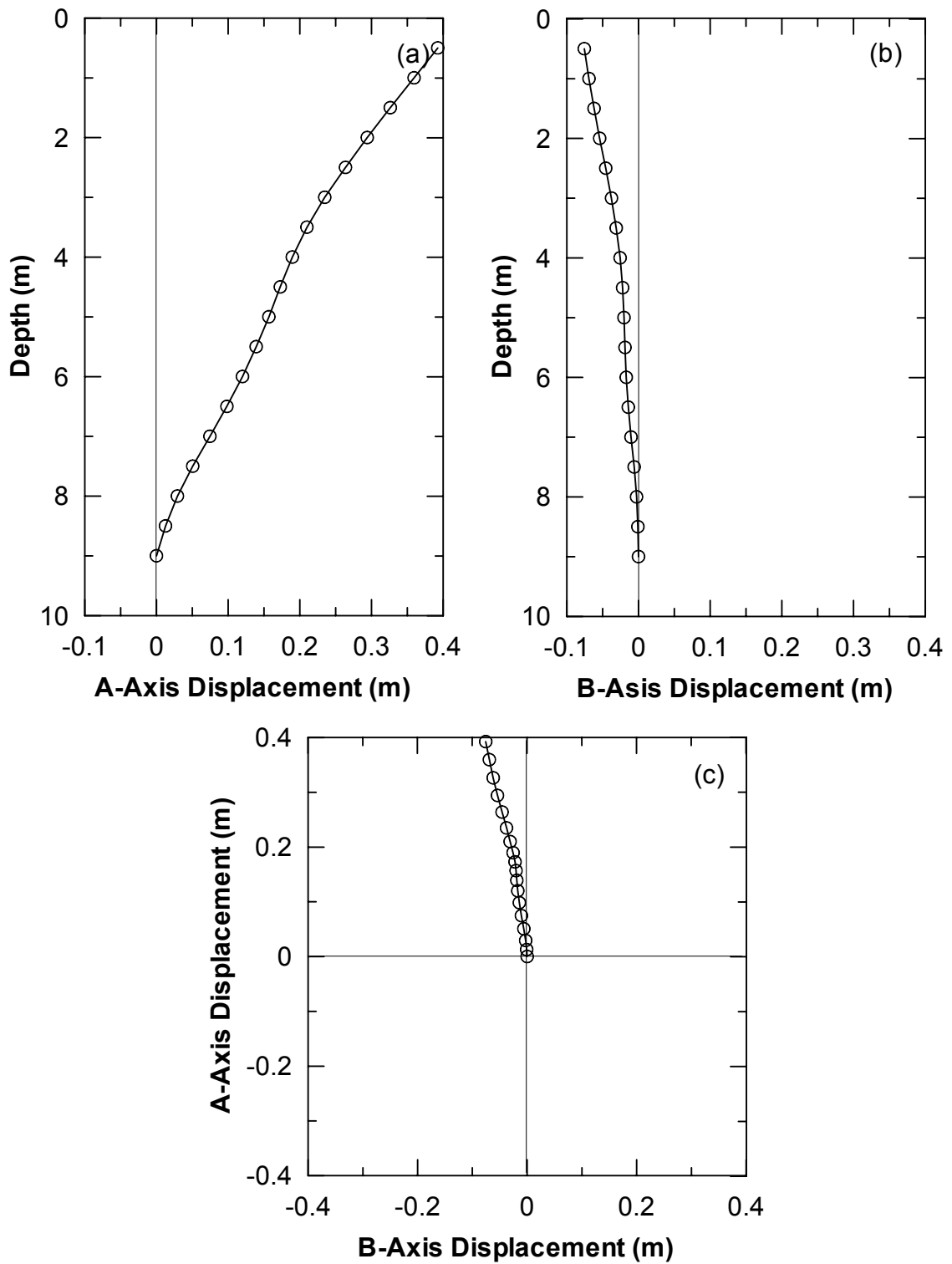
Figure 5.63   Soil Displacement from Inclinometer Casing S5 for 2nd Japan Blast Test
a) Section View A-Direction, b) Section View B-Direction, and c) Plan View
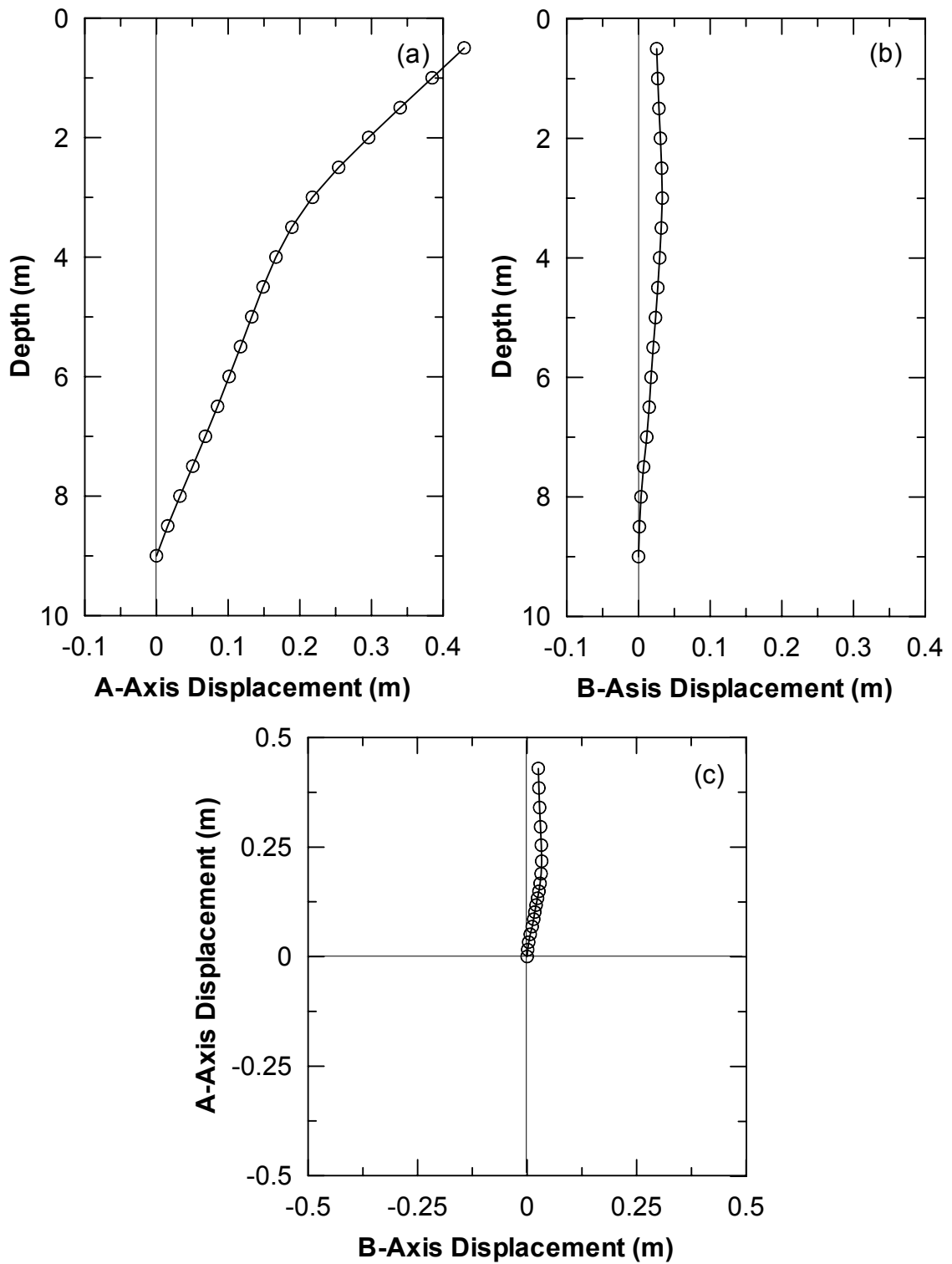
Figure 5.64   Soil Displacement from Inclinometer Casing S6 for 2nd Japan Blast Test
a) Section View A-Direction, b) Section View B-Direction, and c) Plan View

260
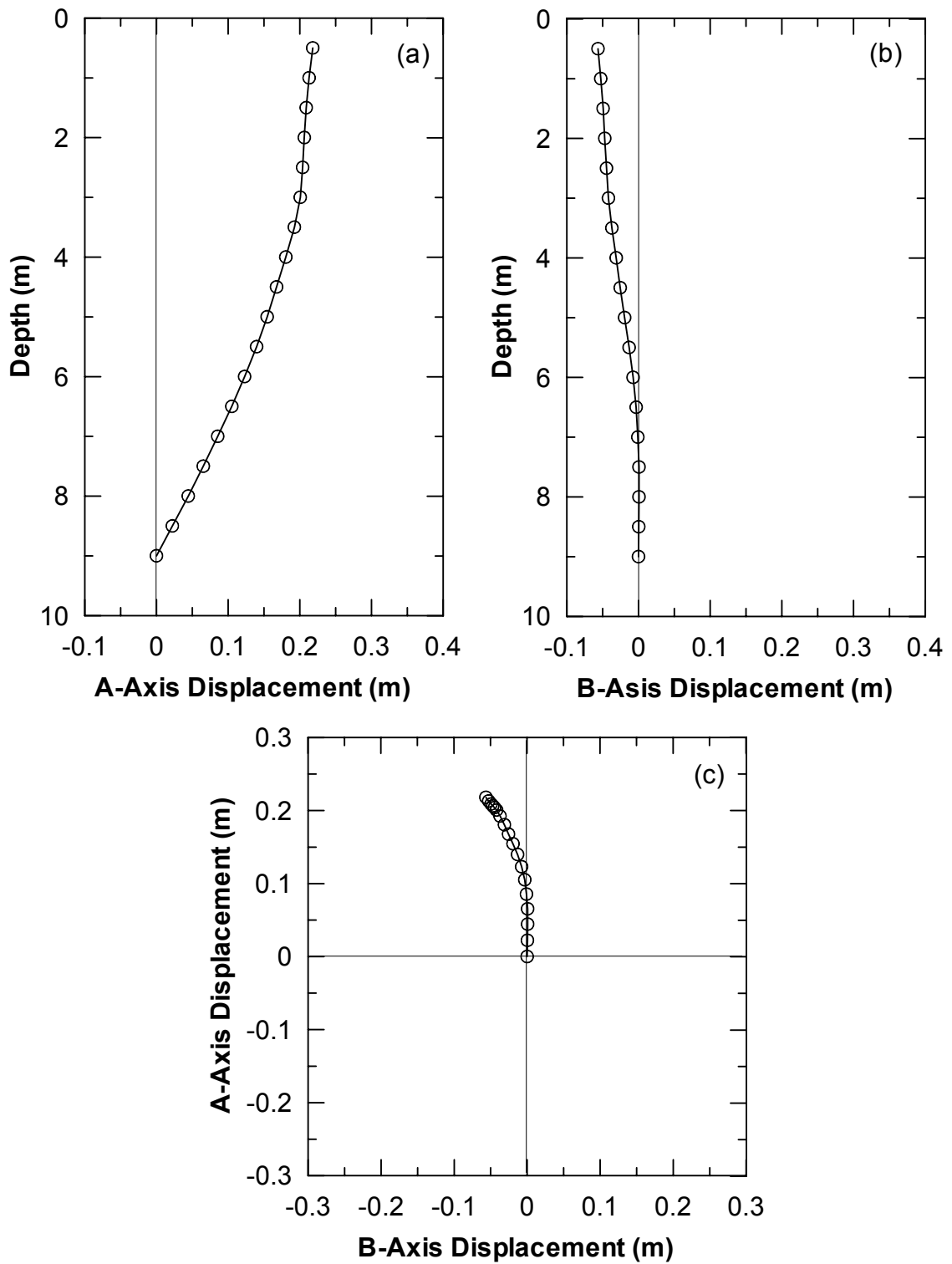
Figure 5.65   Soil Displacement from Inclinometer Casing S7 for 2nd Japan Blast Test
a) Section View A-Direction, b) Section View B-Direction, and c) Plan View

261
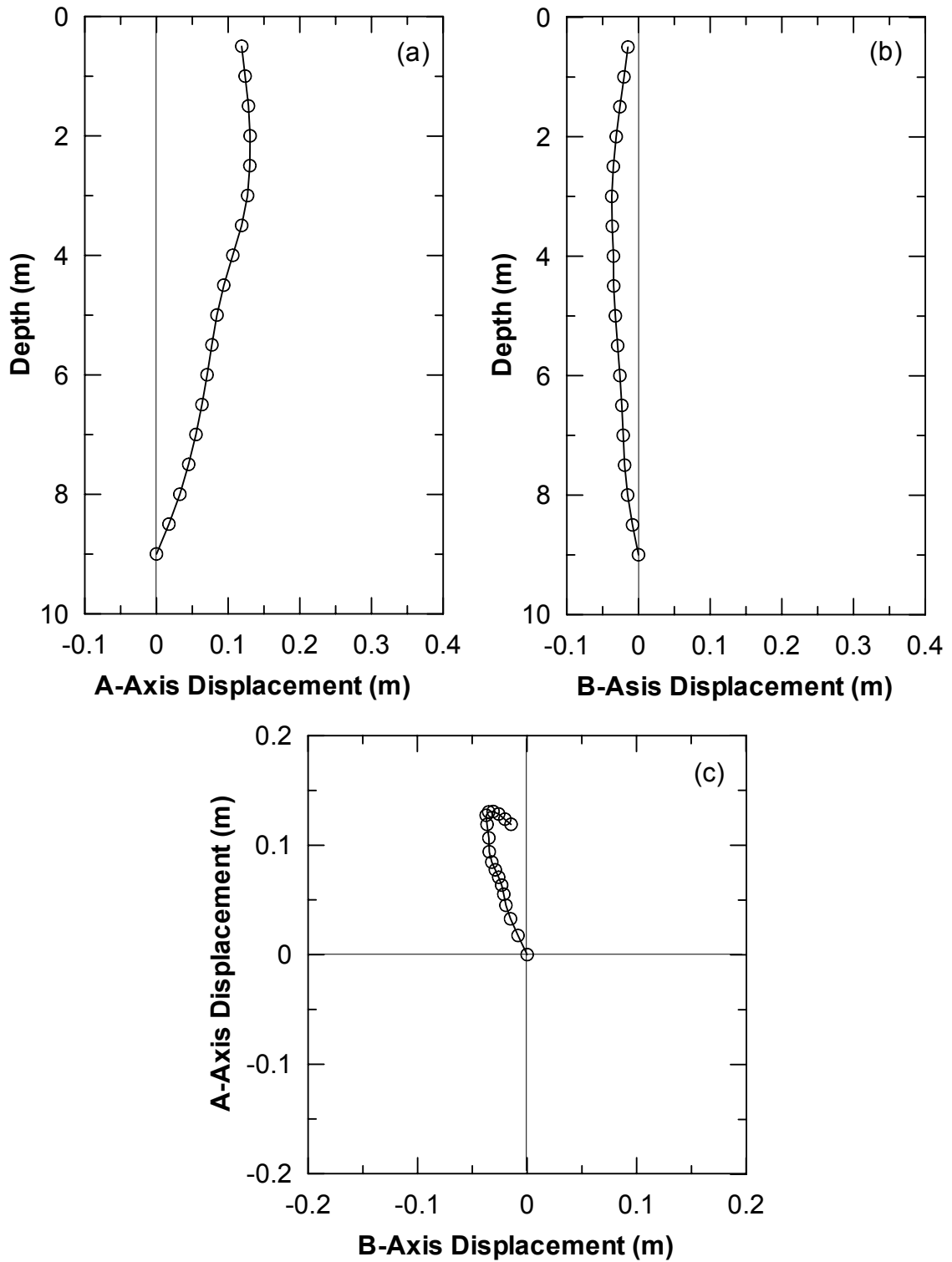
Figure 5.66 Soil Displacement from Inclinometer Casing S8 for 2nd Japan Blast Test
a) Section View A-Direction, b) Section View B-Direction, and c) Plan View
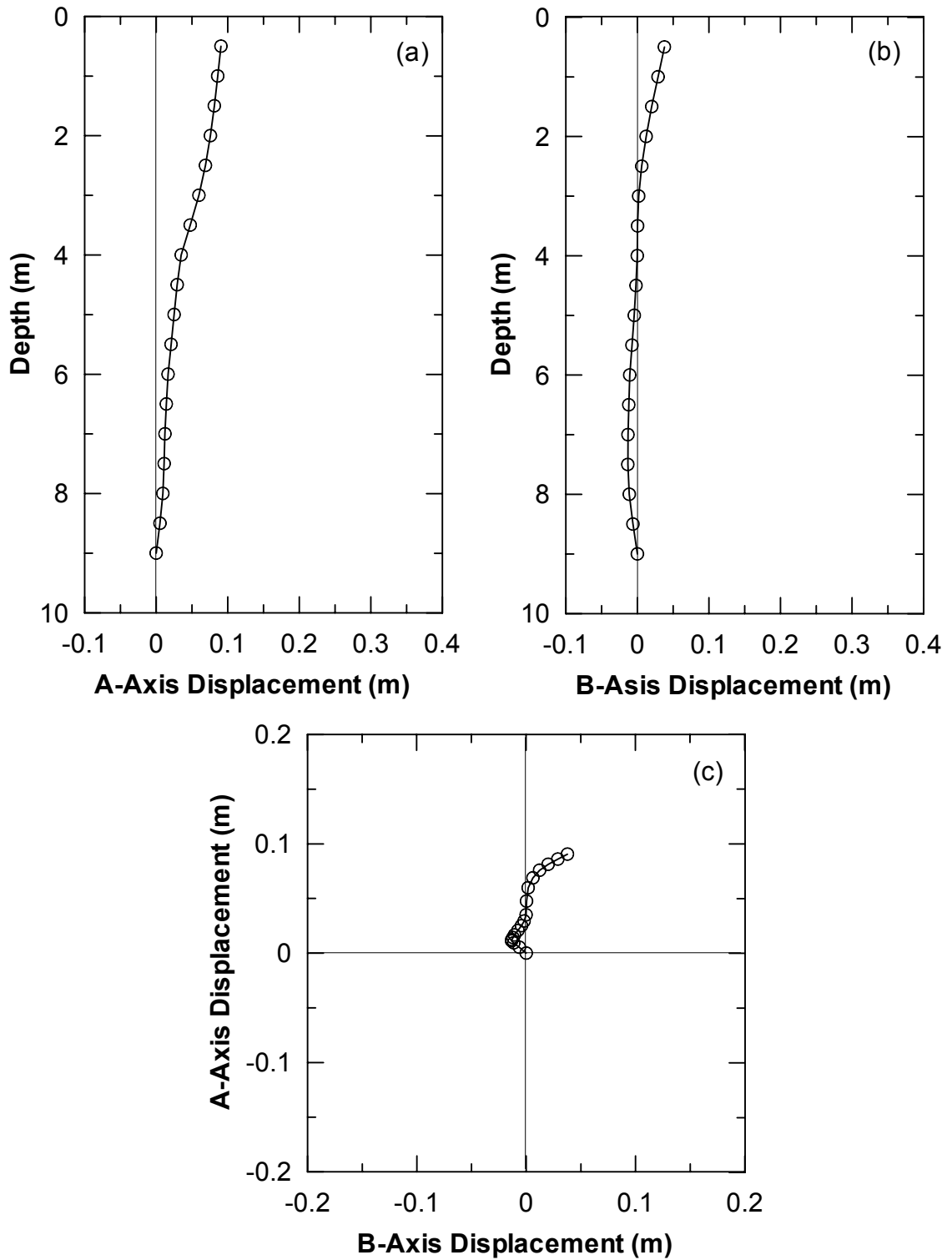
Figure 5.67   Soil Displacement from Inclinometer Casing S9 for 2nd Japan Blast Test
a) Section View A-Direction, b) Section View B-Direction, and c) Plan View
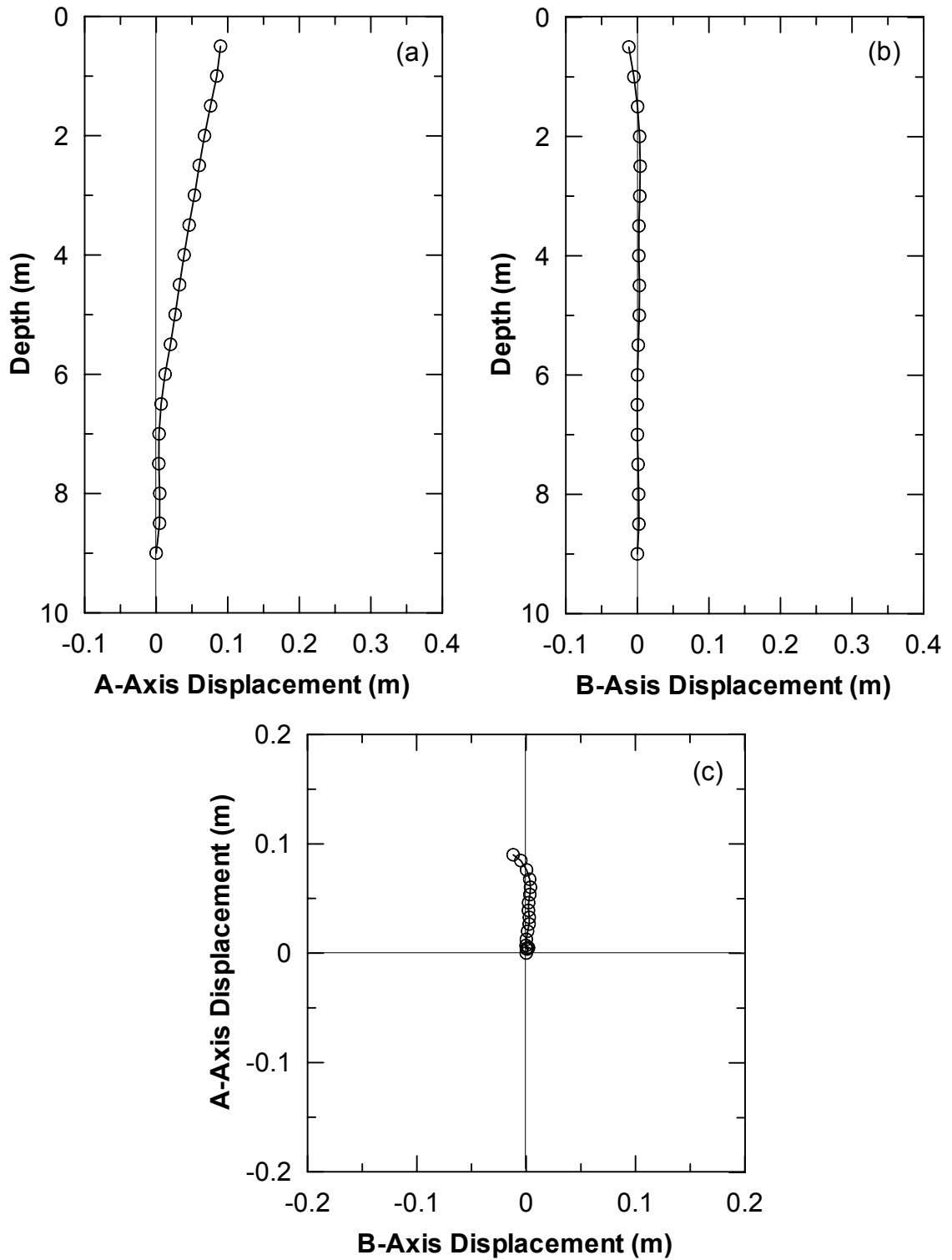
Figure 5.68   Soil Displacement from Inclinometer Casing S10 for 2nd Japan Blast Test   a) Section View A-Direction, b) Section View B-Direction, and c) Plan View
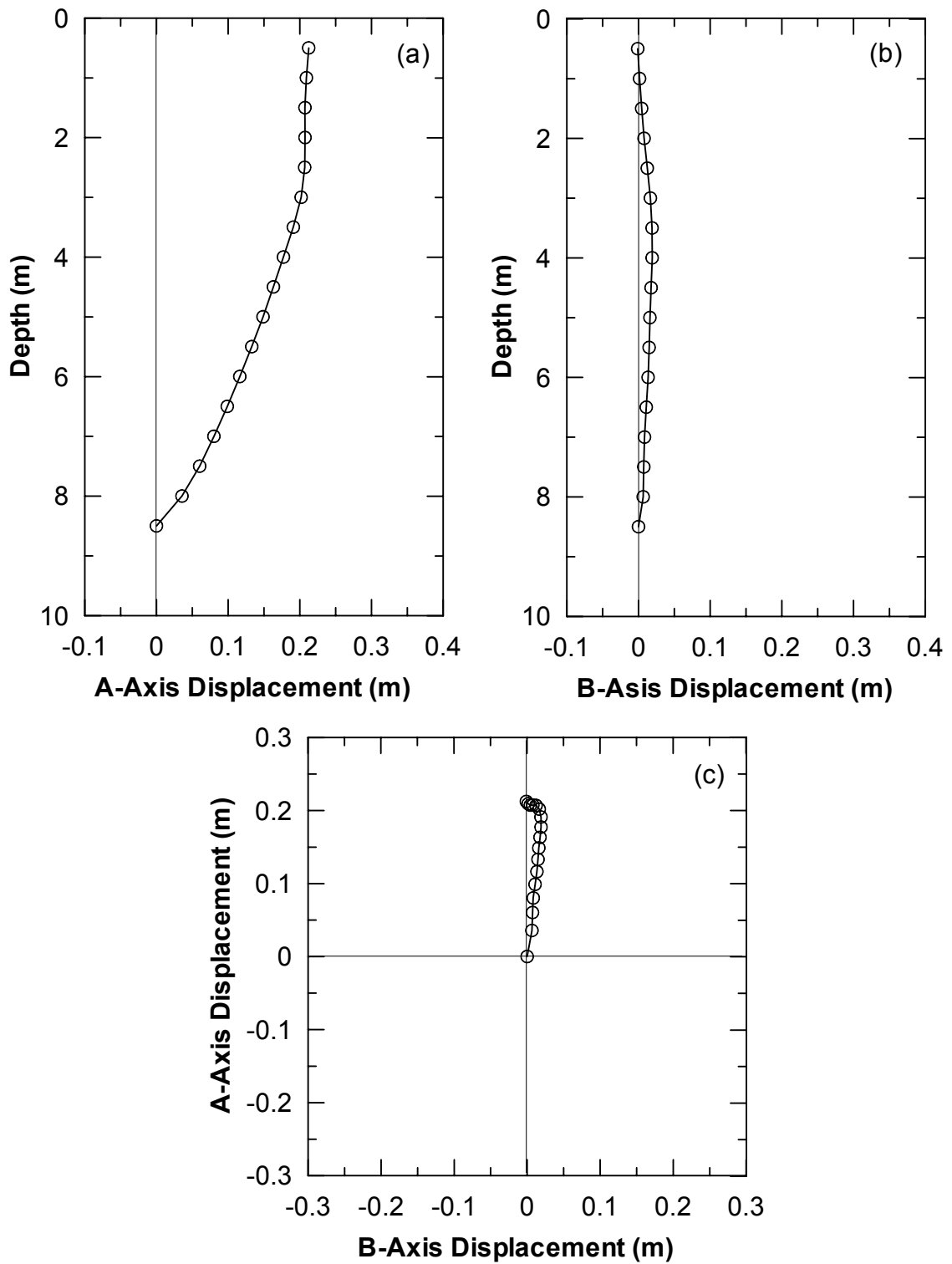
Figure 5.69   Soil Displacement from Inclinometer Casing S11 for 2nd Japan Blast Test
a) Section View A-Direction, b) Section View B-Direction, and c) Plan View
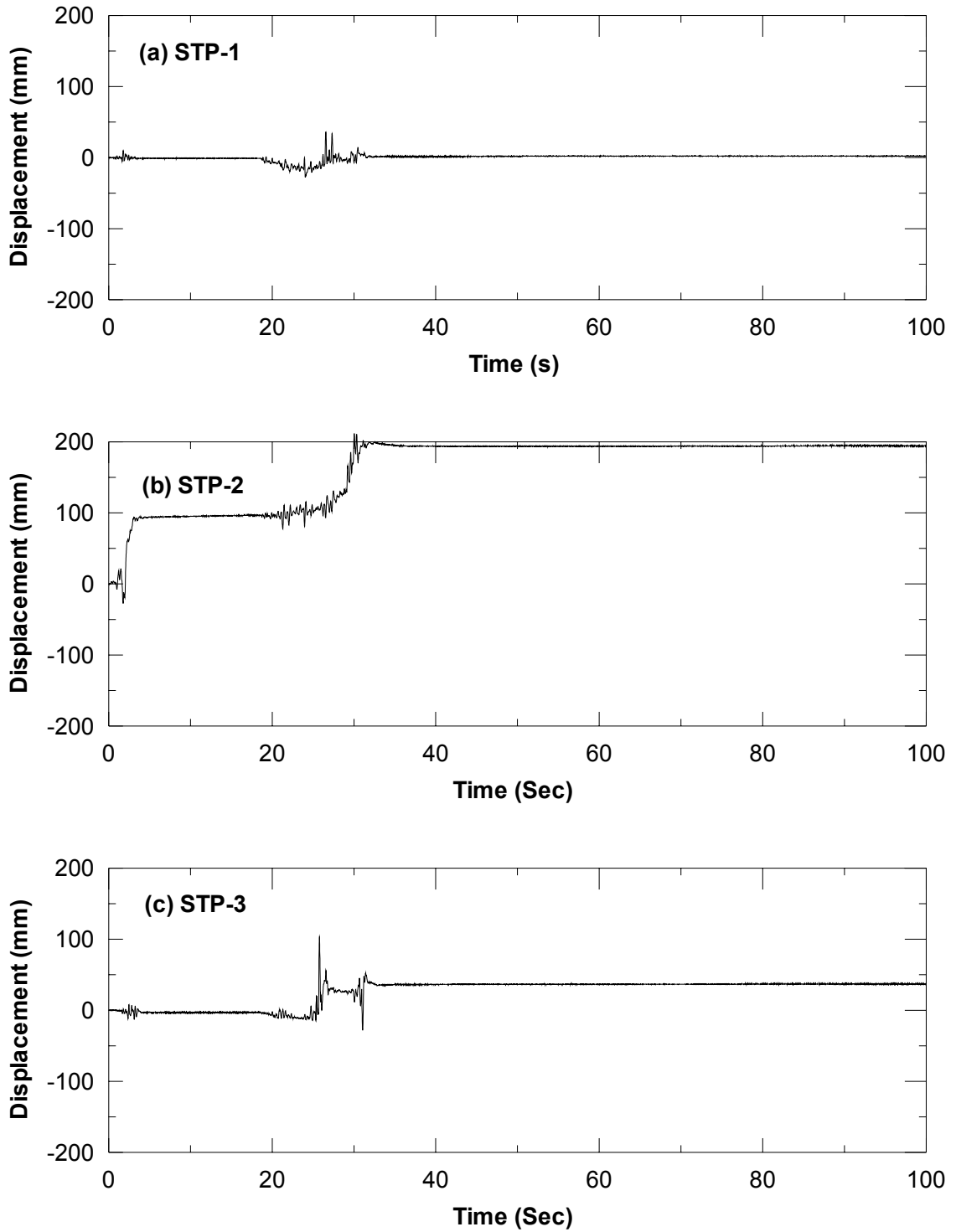
Figure 5.70   Relative Displacement between (a) S1 and 9-Pile Group, (b) S2 and 9-Pile Group, and (c) S7 and Single Pile, 2nd Blast Test
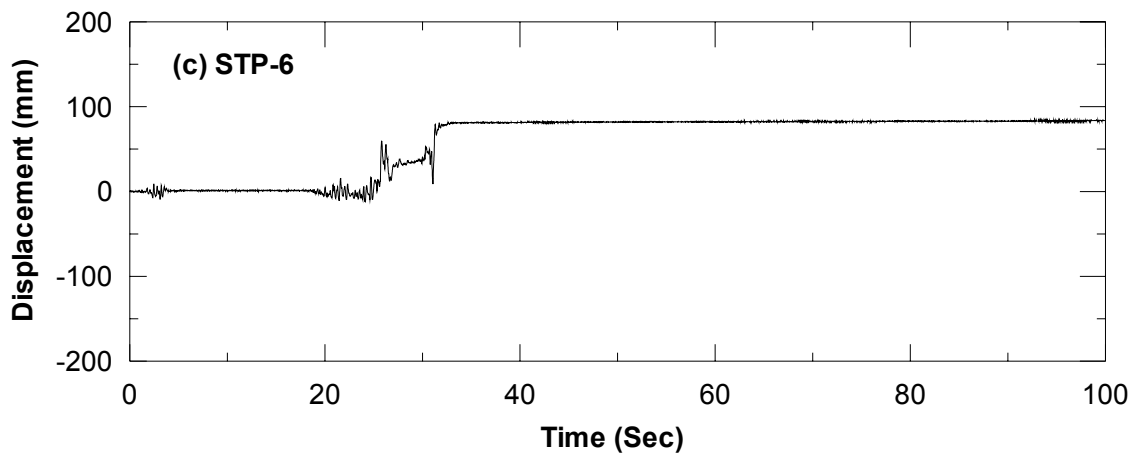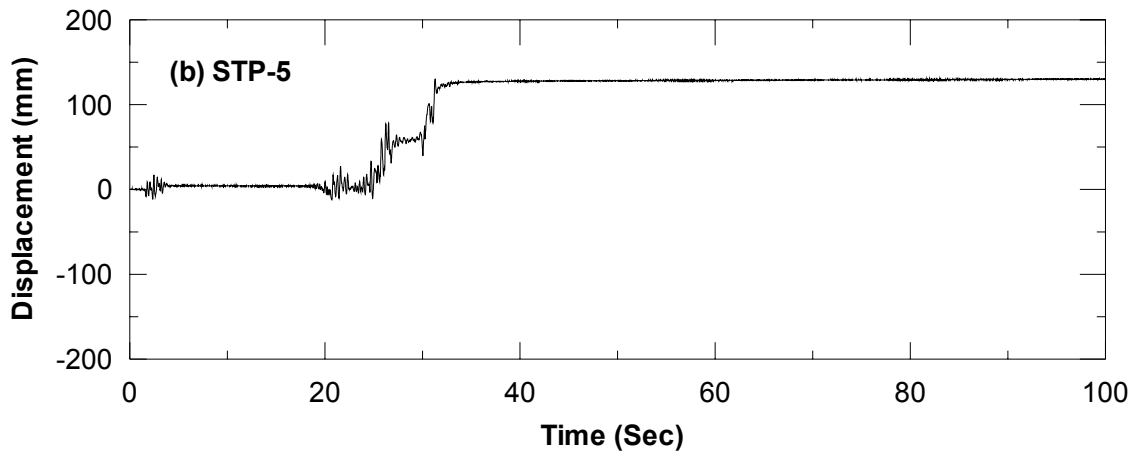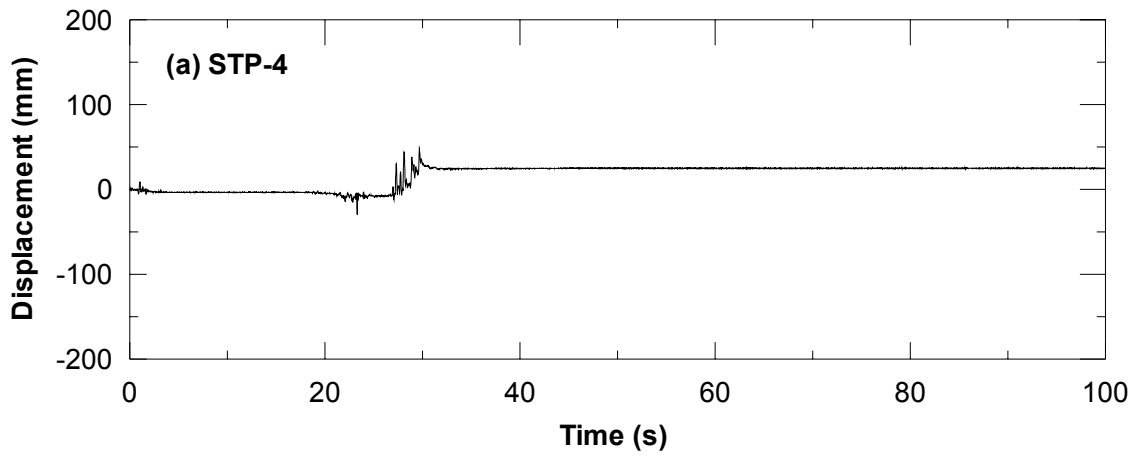
Figure 5.71   Relative Displacement between (a) S8 and 4-Pile Group, (b) S11 and W1 Pile, and (c) S11 and W2 Pile, 2nd Blast Test

267
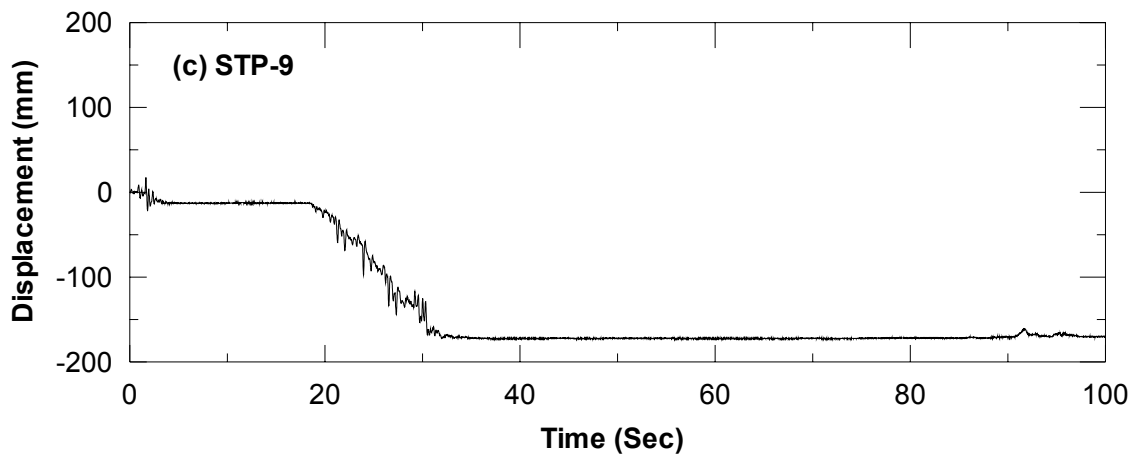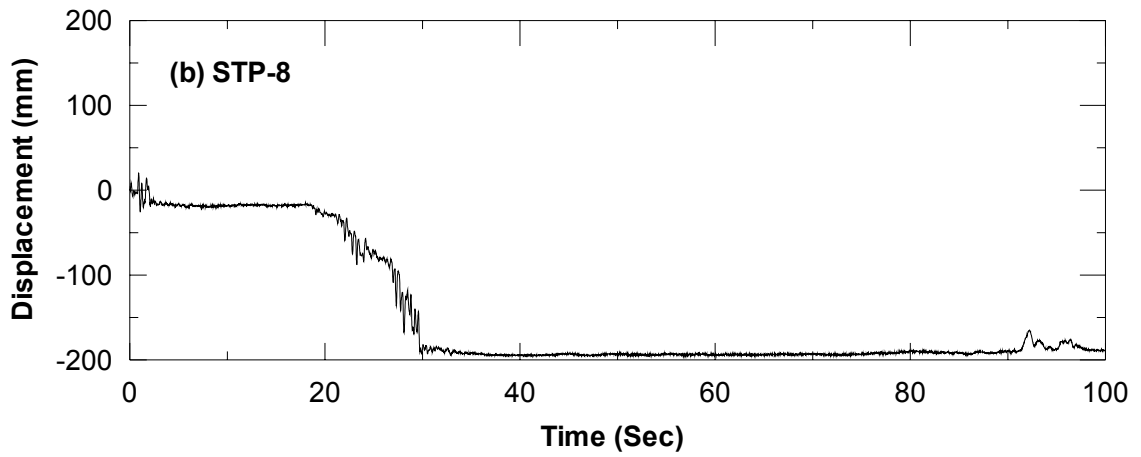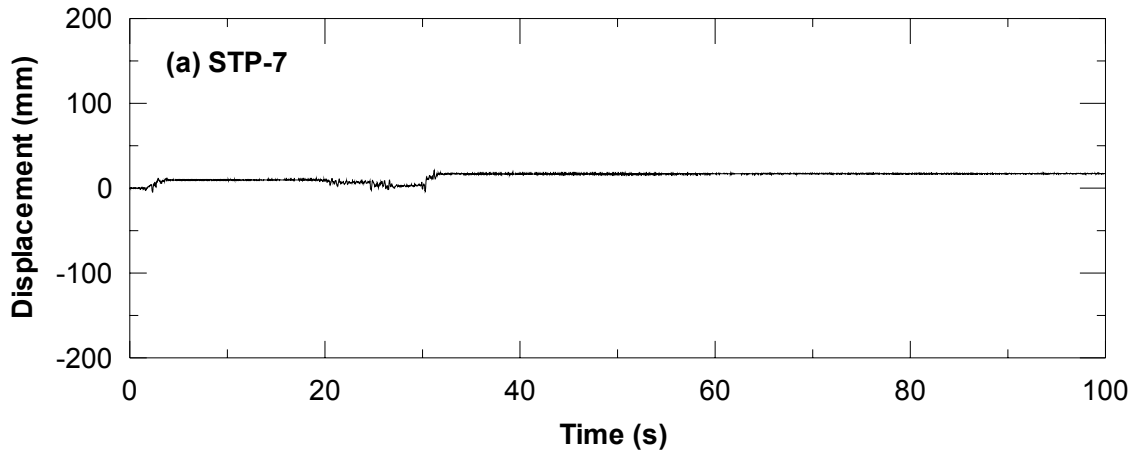
Figure 5.72   Relative Displacement between (a) Pile W1 and Pile W3, (b) 4-Pile Group and Reference Post, and (c) 9-Pile Group and Reference Post
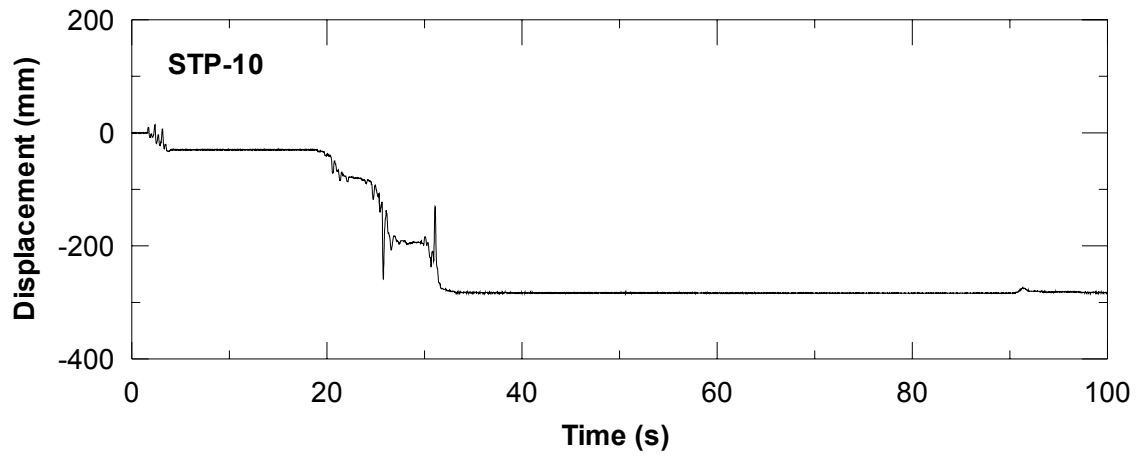
Figure 5.73   Relative Displacement between Single Pile and Reference Post
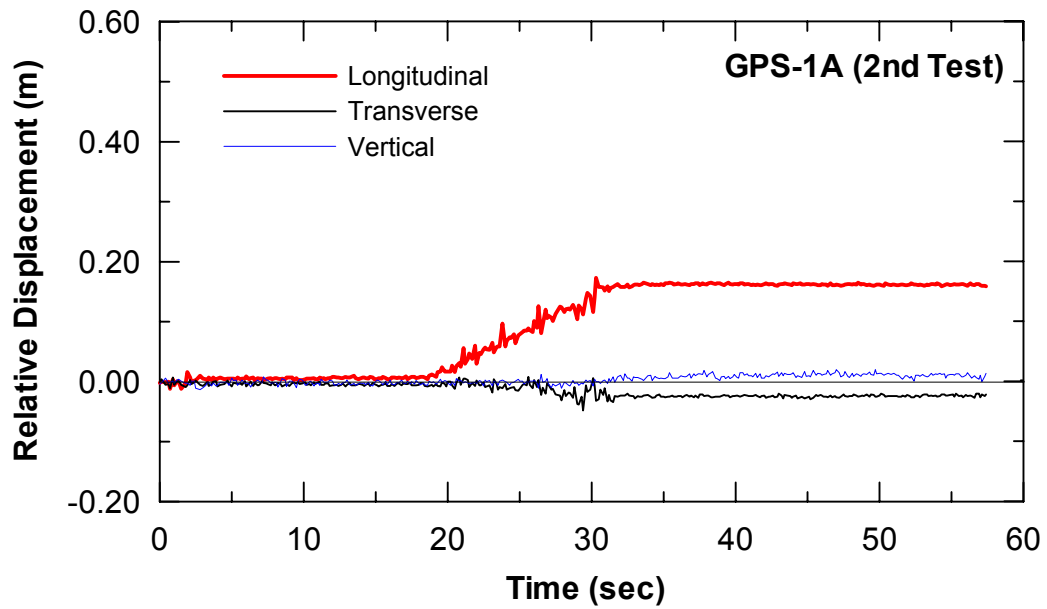
(a) Displacement Time-History
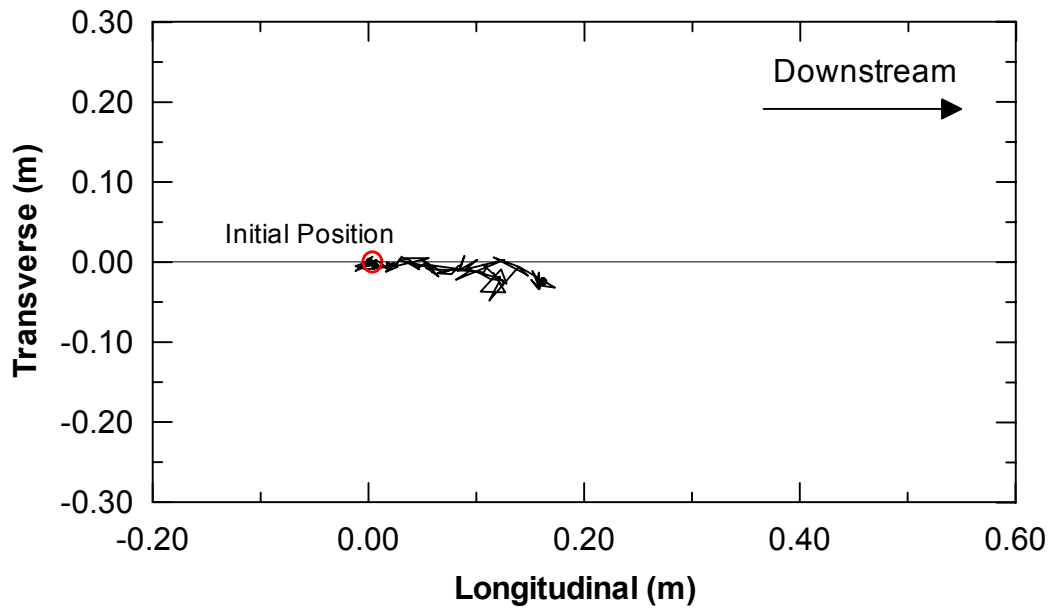
(b) Displacement Path

Figure 5.74   Global Positioning System Data of Unit 1A (2nd Blast Test) (a) Displacement Time-History, and (b) Displacement Path, Data from Caltrans
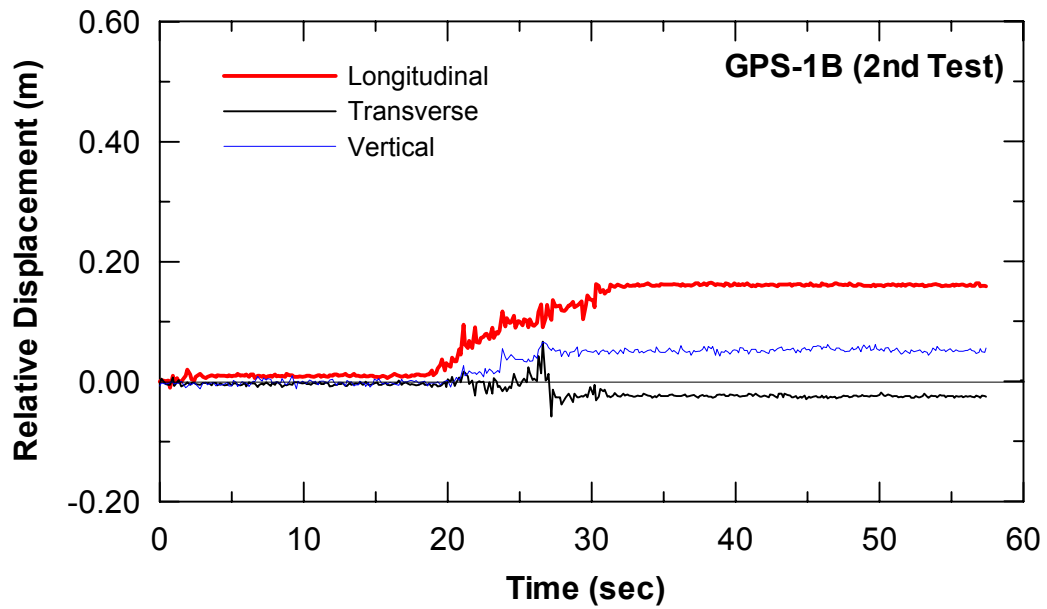
(a) Displacement Time-History
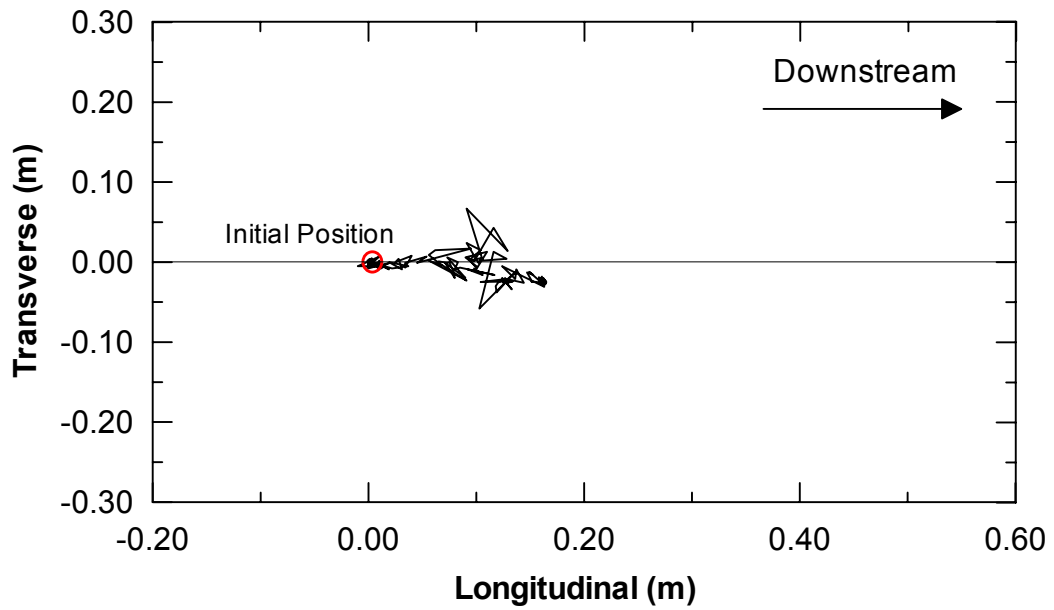
(b) Displacement Path

Figure 5.75 Global Positioning System Data of Unit 1B (2nd Blast Test) (a) Displacement Time-History, and (b) Displacement Path, Data from Caltrans
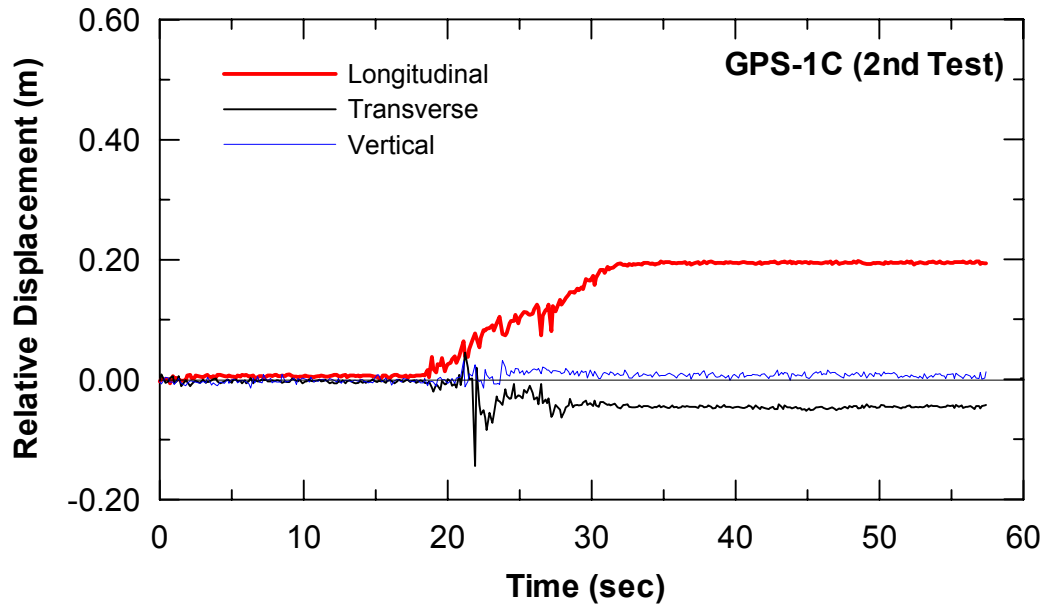
(a) Displacement Time-History
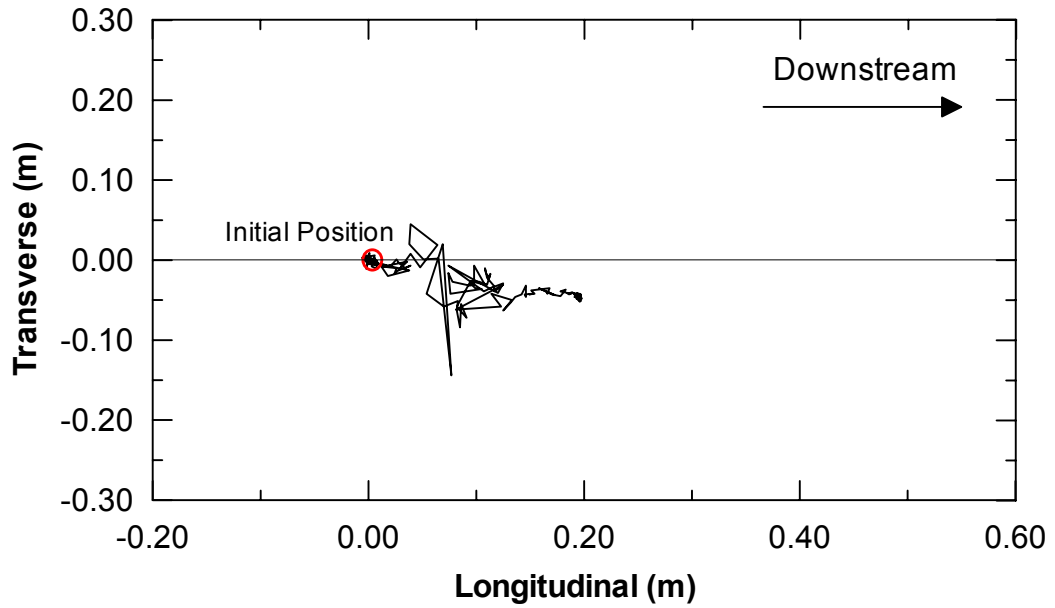
(b) Displacement Path

Figure 5.76 Global Positioning System Data of Unit 1C (2nd Blast Test) (a) Displacement Time-History, and (b) Displacement Path, Data from Caltrans
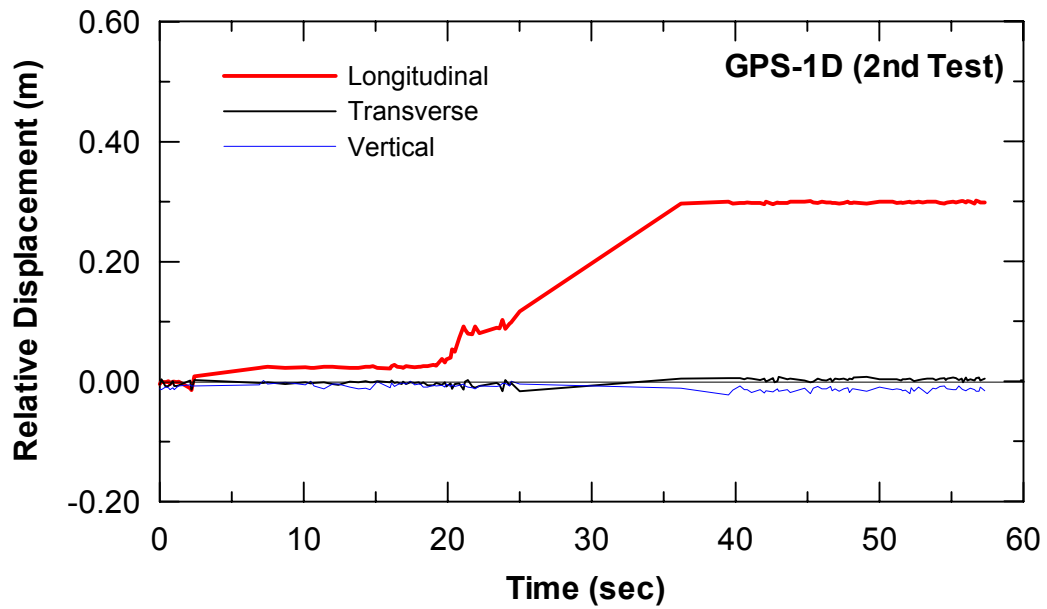
(a) Displacement Time-History
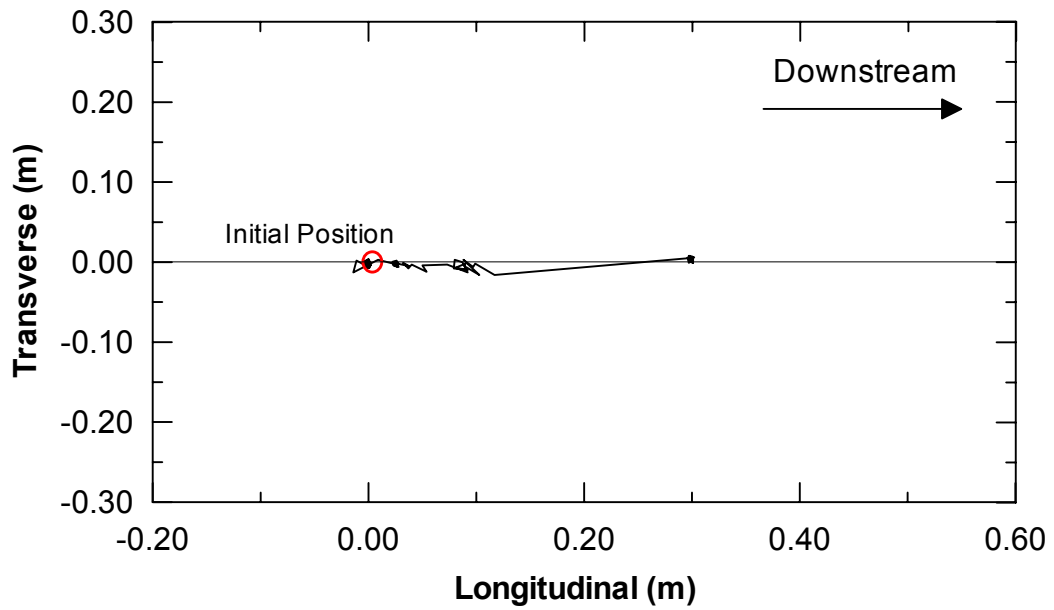
(b) Displacement Path

Figure 5.77   Global Positioning System Data of Unit 1D (2nd Blast Test) (a) Displacement Time-History, and (b) Displacement Path, Data from Caltrans
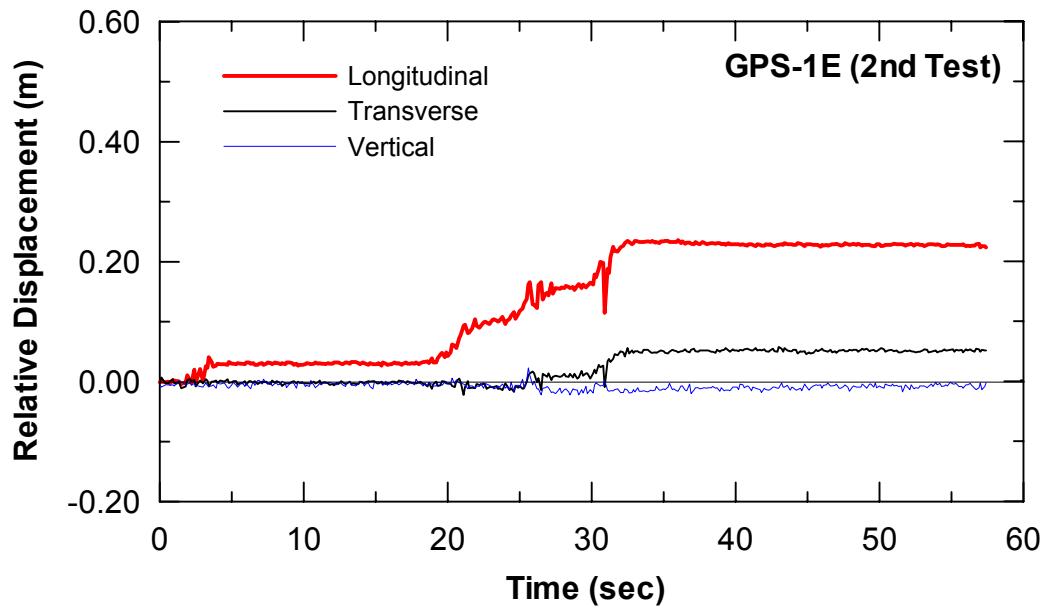
(a) Displacement Time-History
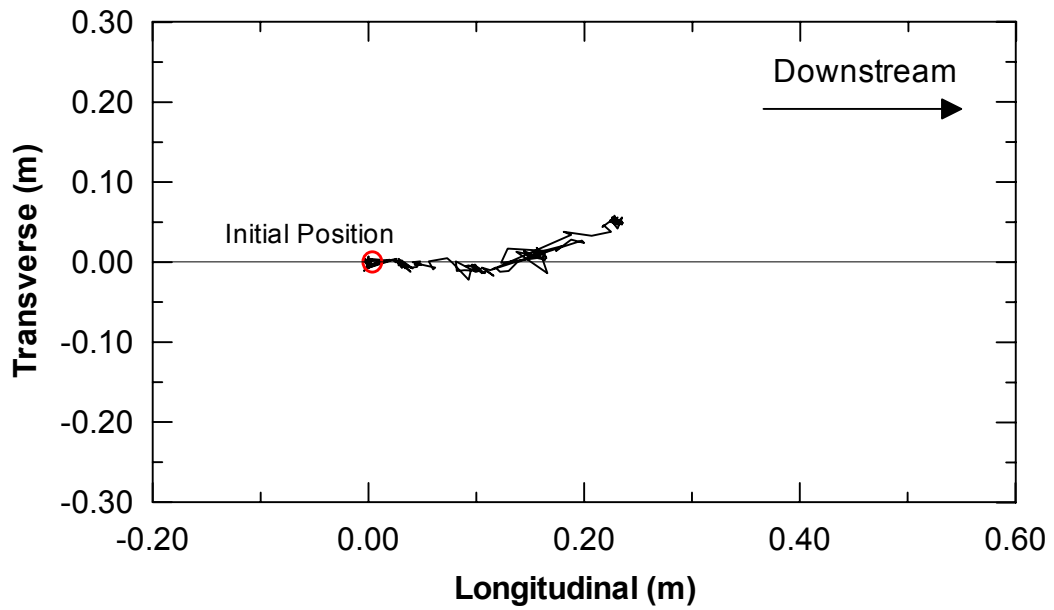
(b) Displacement Path

Figure 5.78   Global Positioning System Data of Unit 1E (2nd Blast Test) (a) Displacement Time-History, and (b) Displacement Path, Data from Caltrans
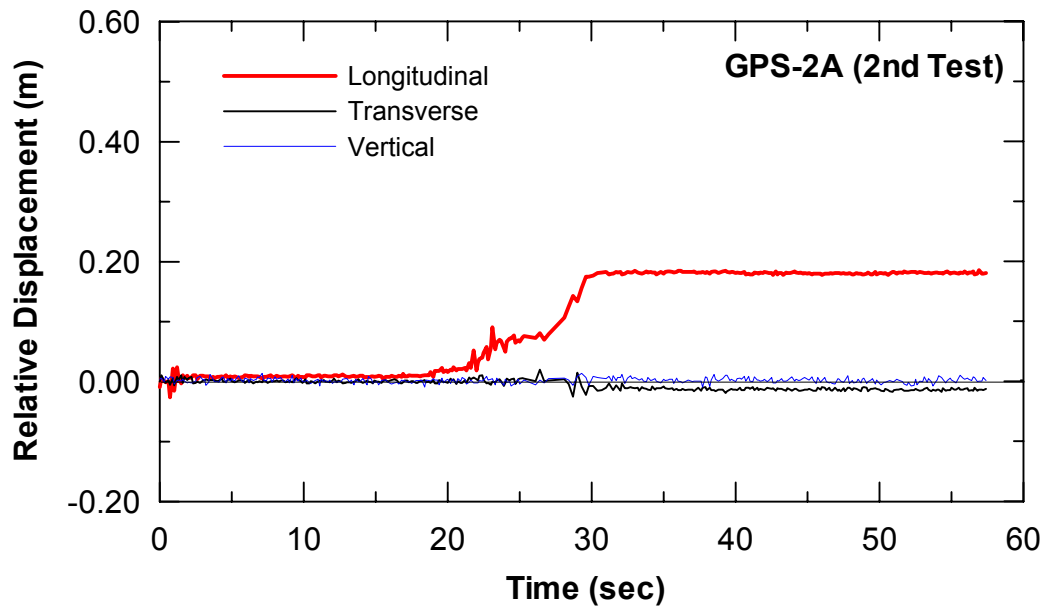
(a) Displacement Time-History
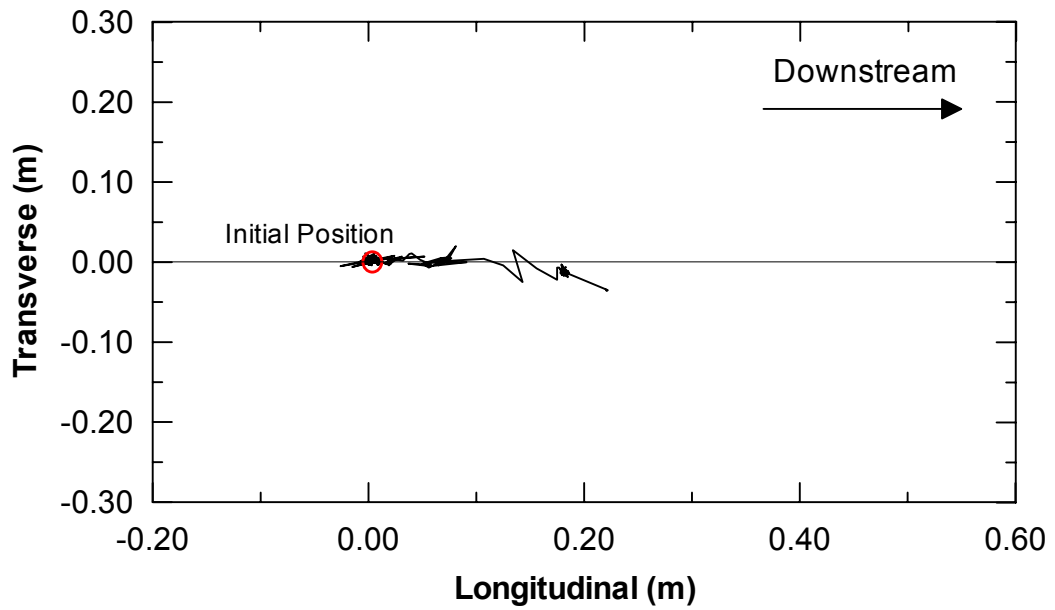
(b) Displacement Path

Figure 5.79 Global Positioning System Data of Unit 2A (2nd Blast Test) (a) Displacement Time-History, and (b) Displacement Path, Data from Caltrans

275
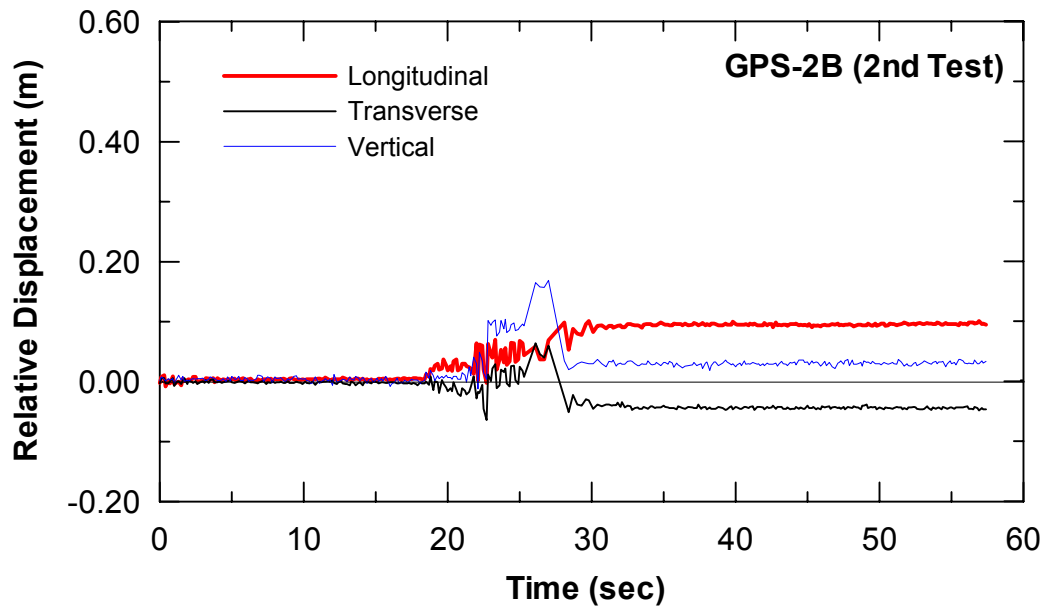
(a) Displacement Time-History
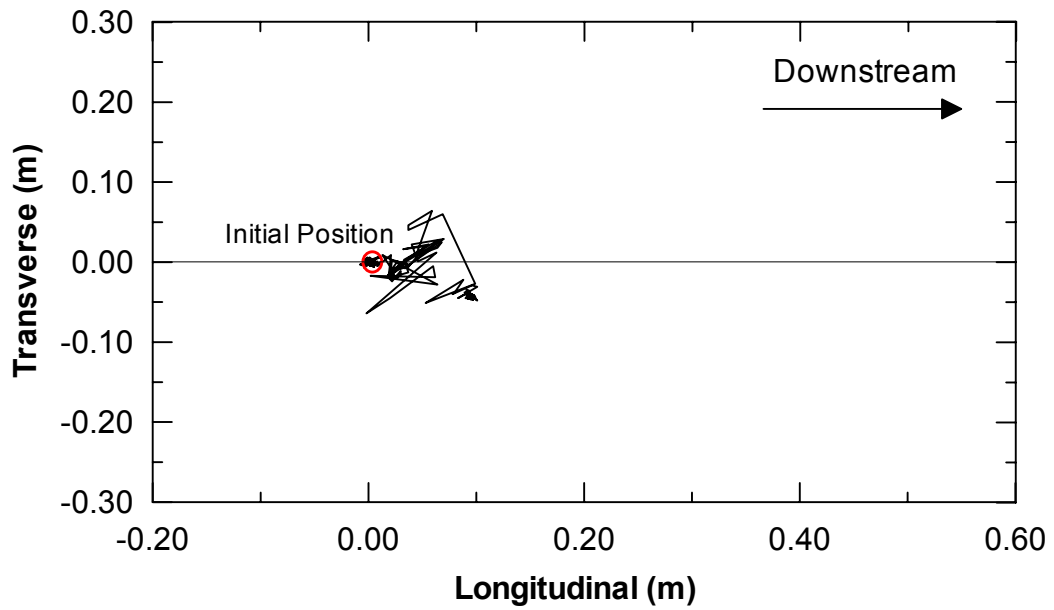
(b) Displacement Path

Figure 5.80   Global Positioning System Data of Unit 2B (2nd Blast Test) (a) Displacement Time-History, and (b) Displacement Path, Data from Caltrans
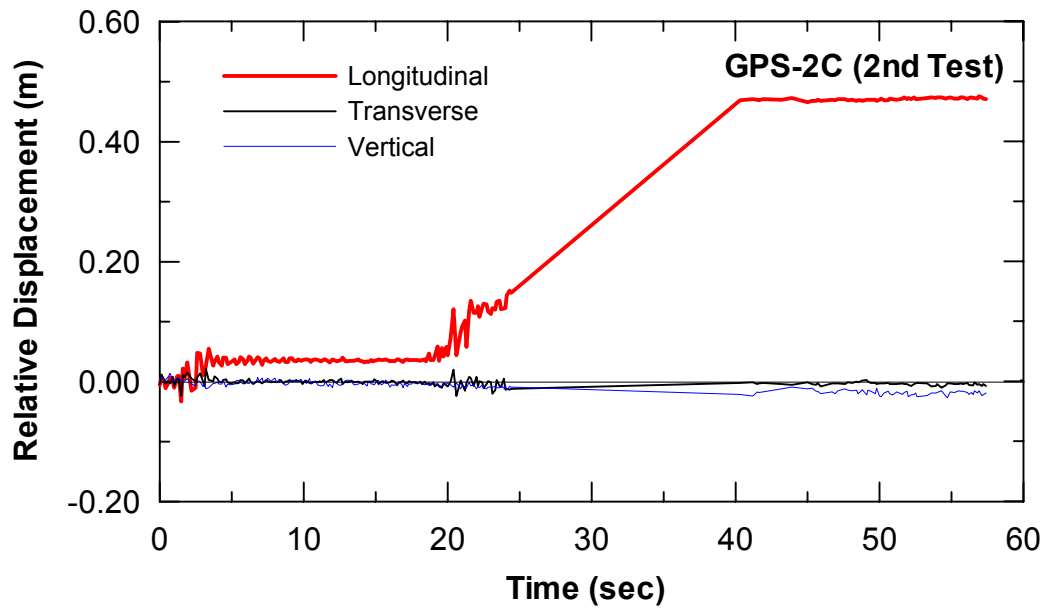
(a) Displacement Time-History
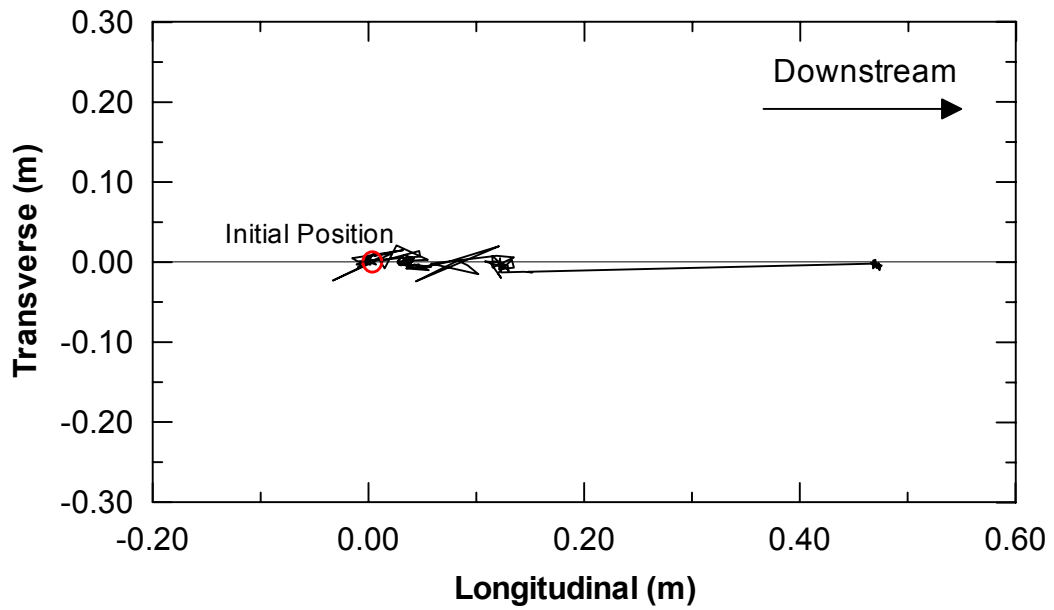
(b) Displacement Path

Figure 5.81   Global Positioning System Data of Unit 2C (2nd Blast Test) (a)
Displacement Time-History, and (b) Displacement Path, Data from Caltrans
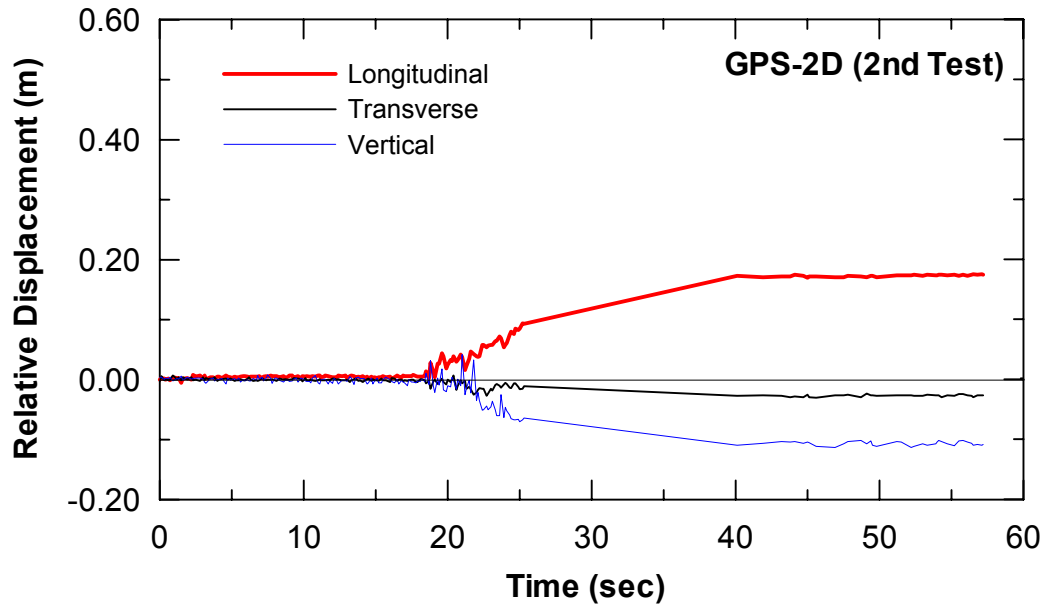
(a) Displacement Time-History
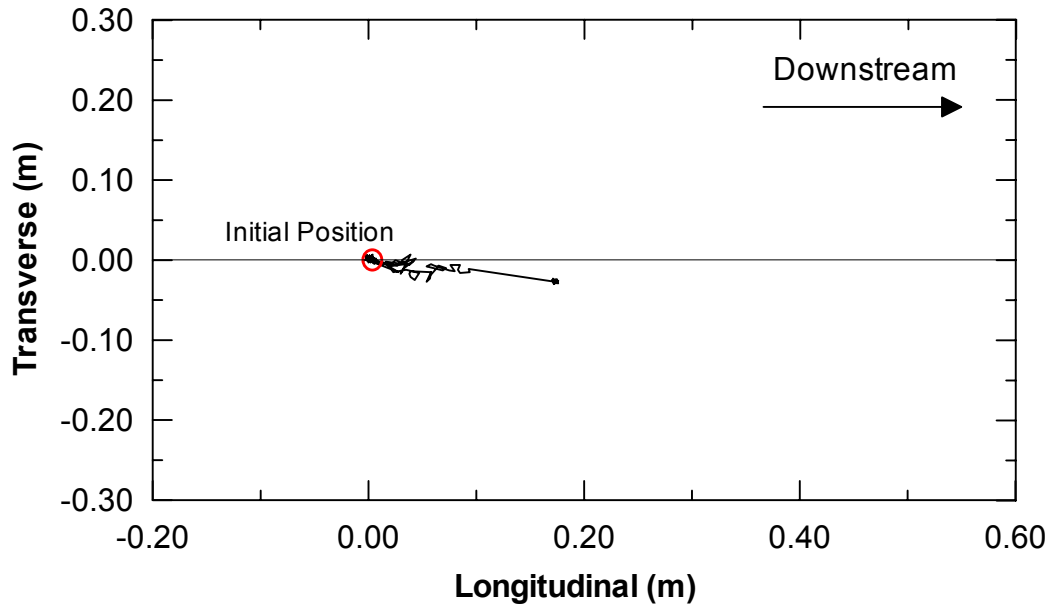
(b) Displacement Path

Figure 5.82 Global Positioning System Data of Unit 2D (2nd Blast Test) (a) Displacement Time-History, and (b) Displacement Path, Data from Caltrans
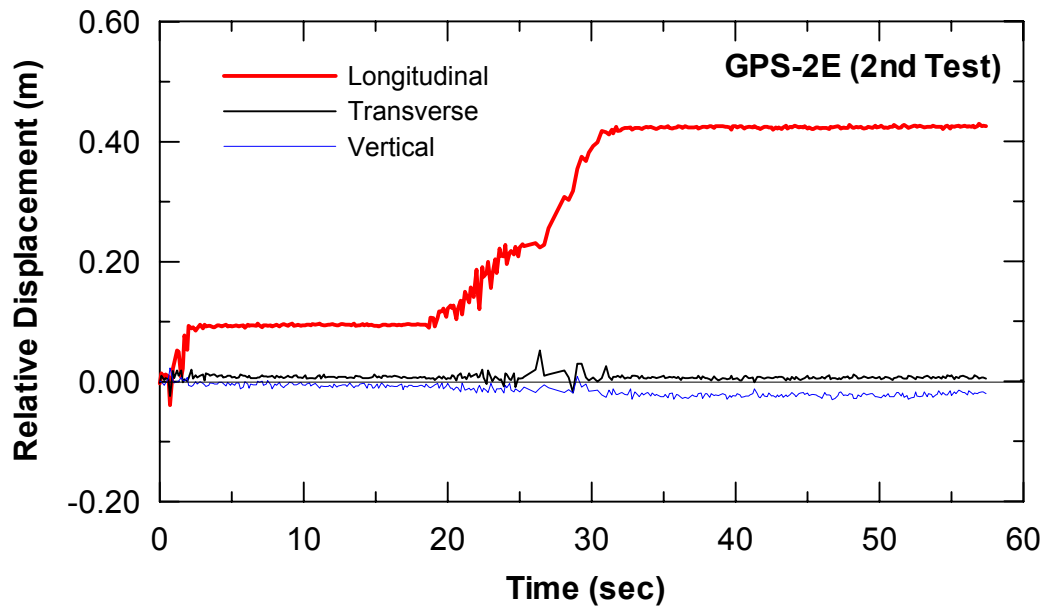
(a) Displacement Time-History
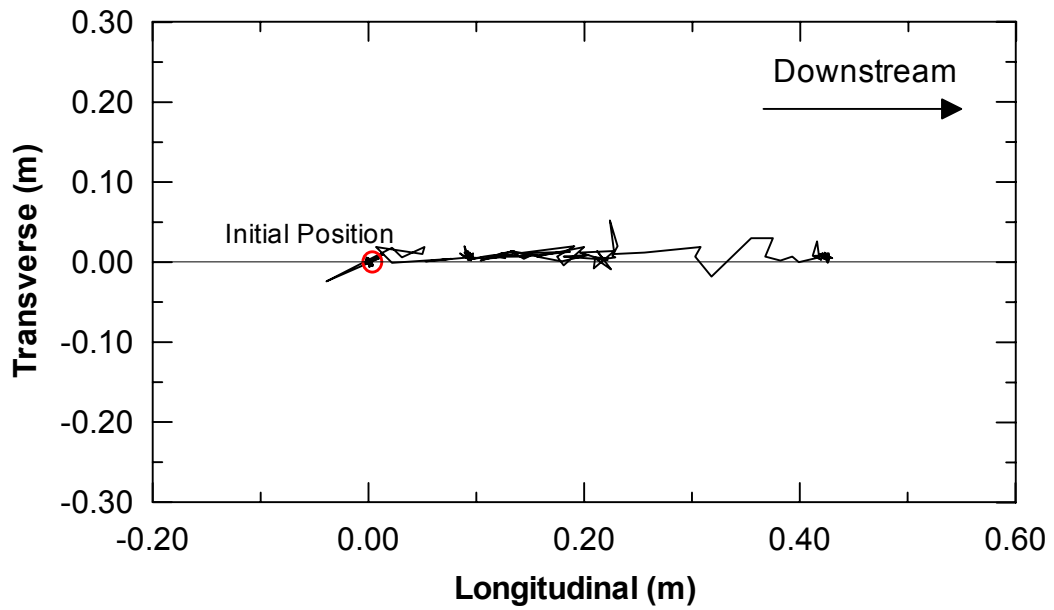
(b) Displacement Path

Figure 5.83   Global Positioning System Data of Unit 2E (2nd Blast Test) (a) Displacement Time-History, and (b) Displacement Path, Data from Caltrans
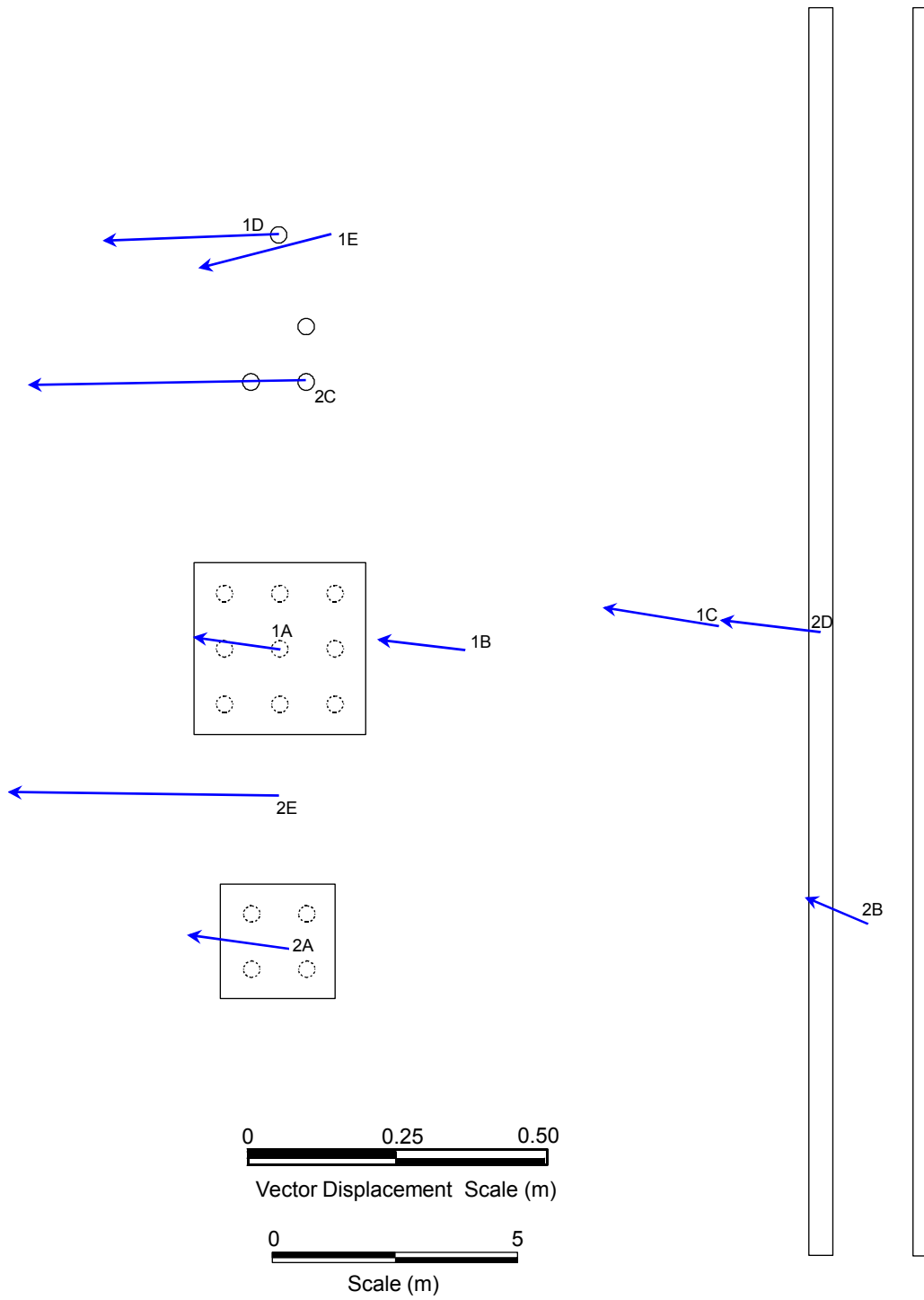
Figure 5.84   Vector Displacements in Horizontal Plane from GPS Data (2nd Blast Test)

280

Figure 5.85   Settlement and Water Pond on Downstream Side of Pile Groups

Figure 5.86   Tilting of Group of Single Piles
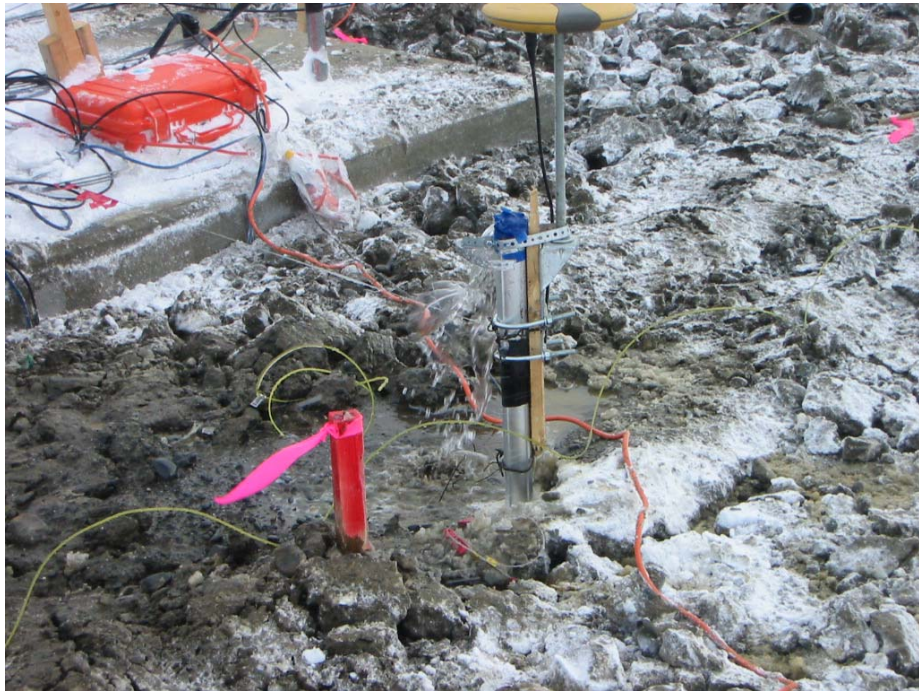
Figure 5.87   Water Coming out from Inclinometer Casing following Blasting

Figure 5.88   Water Coming from Inclinometer Casing
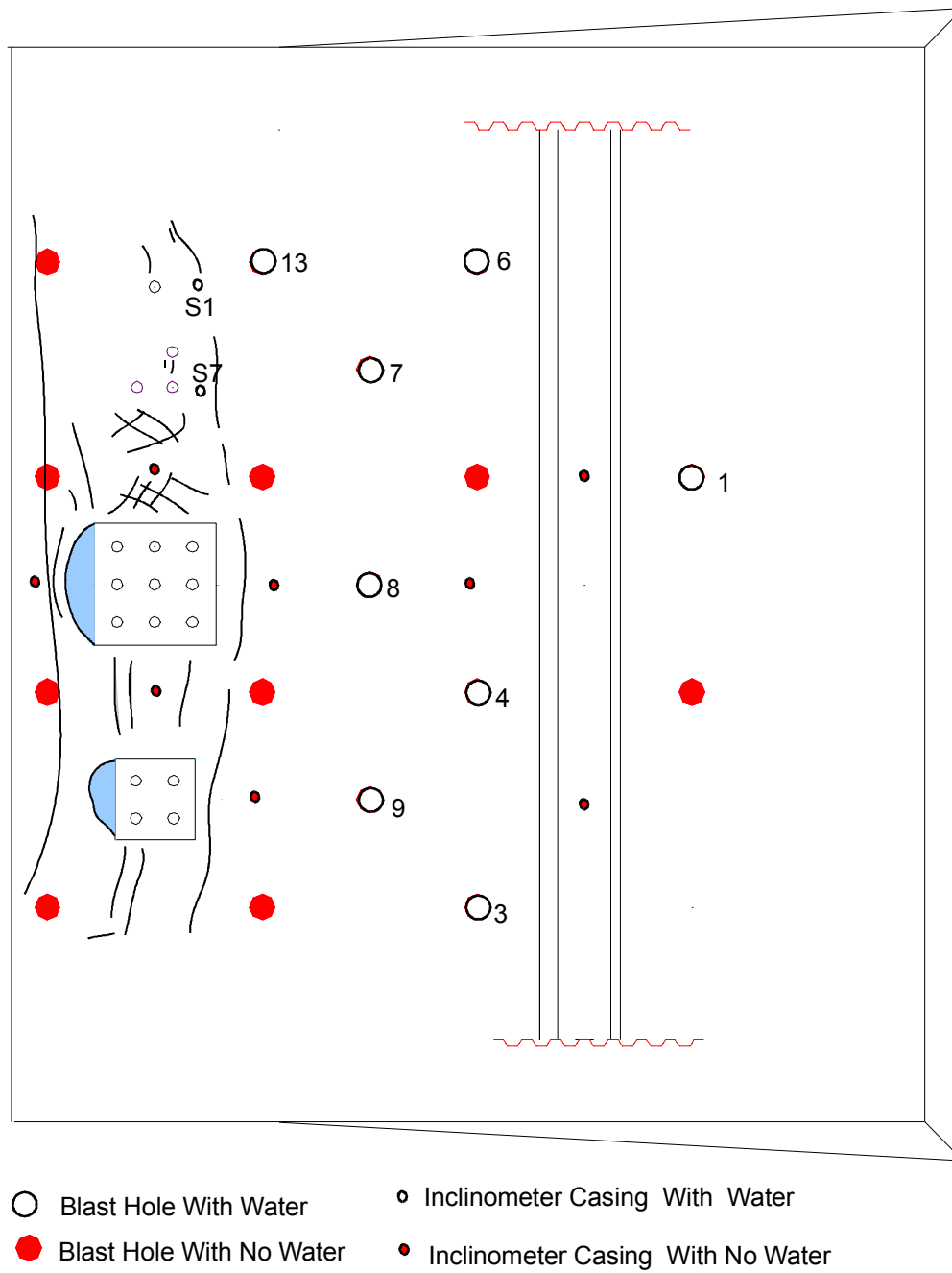
Figure 5.89   Sketch of Surface Cracks with Diagram of Liquefaction Evidence
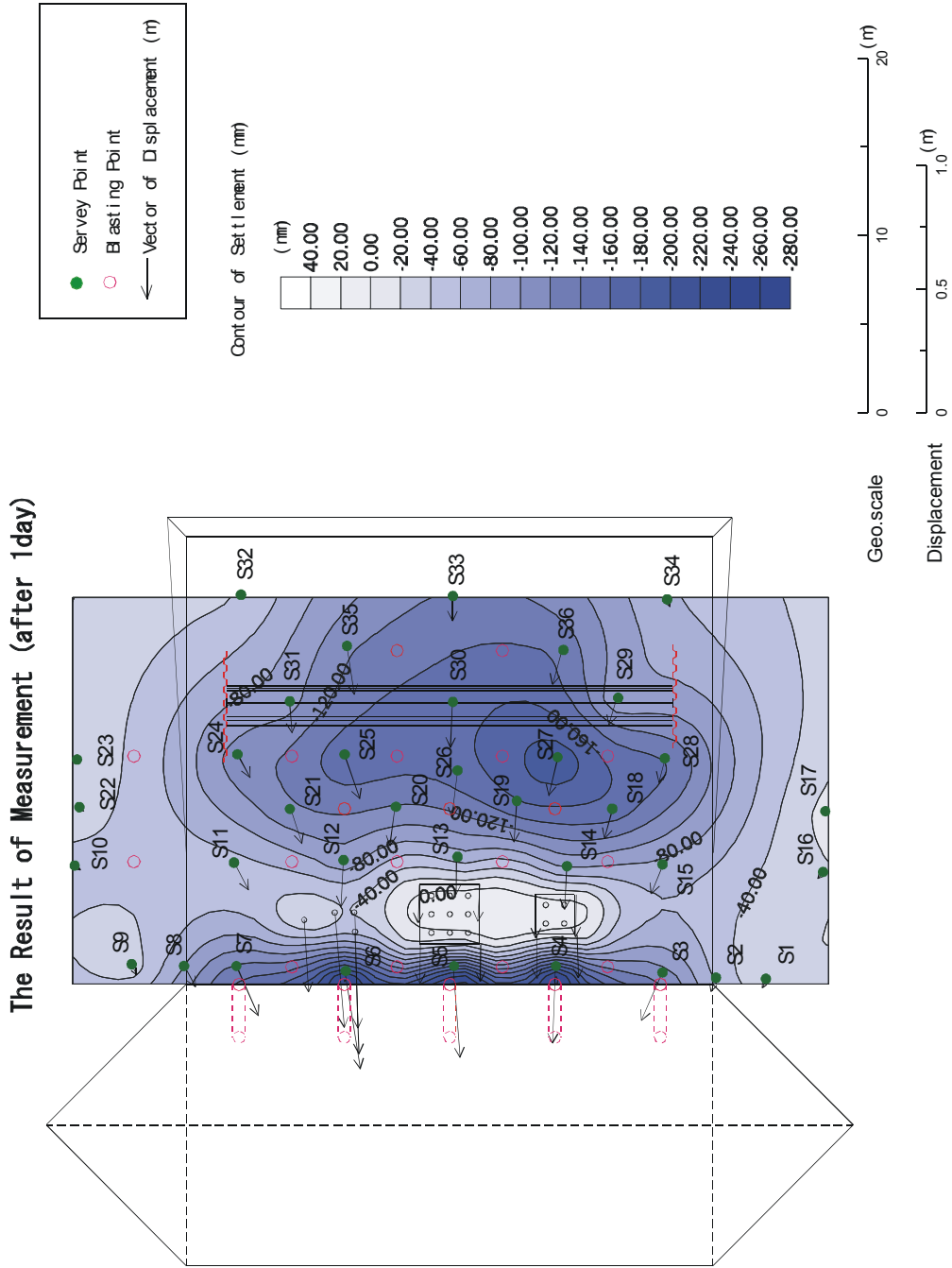
Figure 5.90   Vector Displacements and Settlement Contour from Survey Data, 2nd Blast Test, Data from Sato Kogyo

284

Figure 5.91   Condition of Piles to Pile Cap Connection of 4-Pile Group after Lateral Spread

Figure 5.92   Condition of Piles to Pile Cap Connection of 9-Pile Group after Lateral Spread

6. References

Abdoun, T. Dobry, R., and O-Rourke, T. D. (1997). "Centrifuge and numerical modeling of soil-pile interaction during earthquake induced soil liquefaction and lateral spreading," *Observation and Modeling in Numerical Analysis and Model Tests in Dynamic Soil-Structure Interaction Problems, Geotechnical Special Publication No. 64*, ASCE, New York, pp.64-70.

Ashford, S. A., Rollins, K. M., Bradford, S. C., Weaver, T. J., and Baez, J. I. (2000). "Liquefaction mitigation using stone columns around deep foundations: fill-scale test results," *Soil Mechanics 2000, Transportation Research Record No. 1736*, TRB, Washington D.C., pp.110-118.

Bardet, J. P., and Kapusker, M. (1993). "Liquefaction sand boils in San Francisco during 1989 Loma Prieta earthquake." *J. Geotech. Engrg., ASCE*, Vol. 119, No.3, March, pp. 543-562.

Bartlett, S. F. and Youd, T. L. (1992b). "Empirical analysis of horizontal ground displacement generated by liquefaction-induced lateral spreads." *Tech. Rep. NCEER-92-0021*, National Center for Earthquake Engineering Research, Buffalo, N.Y., M. Hamada and T.D. O'Rourke (eds.), August 17.

Clough, G. W., Martin, J. R., II, and Chameau, J. L. (1994). "The geotechnical aspects." *Practical Lessons from the Loma Prieta Earthquake*, National Research Council, National Academy Press, Washington, D.C., pp. 29-63.

Hamada, M., and O'Rourke, T., Editors. (1992). *Case Studies of Liquefaction and Lifeline Performance During Past Earthquakes, Report No. NCEER-92-0001, Vol.1*, National Center for Earthquake Engineering Research, Buffalo, N.Y.

O'Rouke, T. D. (1996). "Lessons learned for lifeline engineering from major urban earthquakes," Proceedings, *Eleventh World Conference on Earthquake Engineering*, Elsevier Science Ltd., 18 p.

O'Rouke, M. J., and Pease, J. W. (1992). "Large ground deformations and their effects on lifeline facilities: 1989 Loma Prieta earthquake." *Case Studies of Liquefaction and Lifeline Performance During Past Earthqakes, Volume 2*: United States Case Studies, Tech. Rep. NCEER-92-0002, M. Hamada and T.D. O'Rourke (eds.), February 17, 85 pages.

Seed, H. B. (1987). "Design problems in soil liquefaction." *J. Geotech. Engrg*., ASCE, Vol. 113, No. 8, August, pp. 827-845.

Tokida, K., Iwasaki, H., Matsumoto, H., and Hamasa, T. (1993). "Liquefaction potential and drag force acting on piles in flowing soils," Soil *Dynamic and Earthquake Engineering*, Computational Mechanics, South Hampton, England, pp. 349-364.

Turner, L. L., (2002). *Measurements of Lateral Spread Using a Real Time Kinematic Global Positioning System*, California Department of Transportation Division of New Technology &Research, April 2002, 94 pages..

Youd, T. L., and Hoose, S. N. (1976). "Liquefaction during 1906 San Francisco Earthquake." *J. Geotech. Engrg. Div*., ASCE, Vol. 102, No. GT5, May, pp. 425-439.